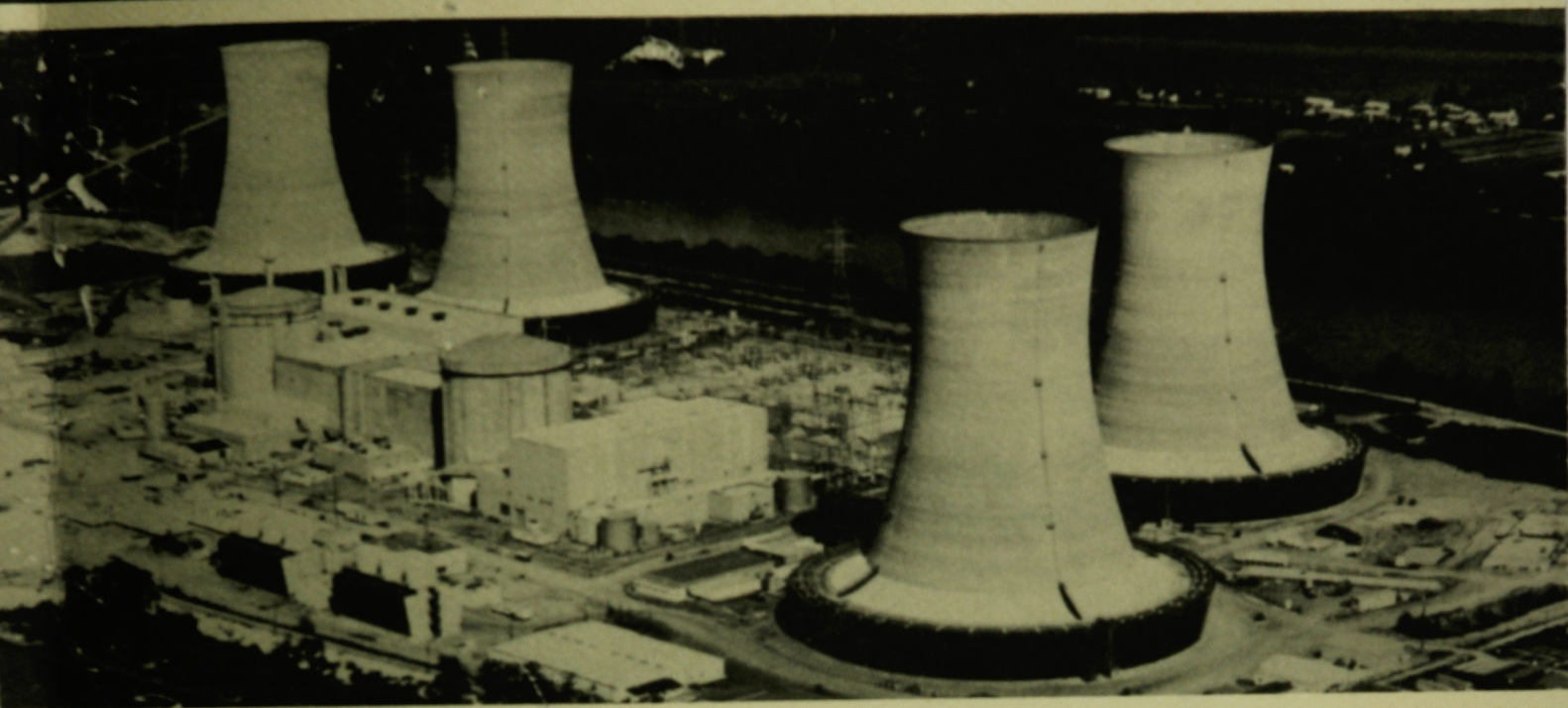


071
82382

CI



This is an informal report intended for use as a preliminary or working document

GEND

General Public Utilities • Electric Power Research Institute • U.S. Nuclear Regulatory Commission • U.S. Department of Energy

TEST DATA REPORT FOR QUARTER SCALE NUPAC 125-B RAIL CASK MODEL

LOAN COPY

"S REPORT MAY BE RECALLED
FOR TWO WEEKS. PLEASE
TURN PROMPTLY TO:

INEL TECHNICAL LIBRARY

M. M. Warrant
B. J. Joseph

Prepared for the
U.S. Department of Energy
Three Mile Island Operations Office
Under Contract No. DE-AC07-76ID01570

TL1208

DISCLAIMER

This book was prepared as an account of work sponsored by an agency of the United States Government. Neither the United States Government nor any agency thereof, nor any of their employees, makes any warranty, express or implied, or assumes any legal liability or responsibility for the accuracy, completeness, or usefulness of any information, apparatus, product or process disclosed, or represents that its use would not infringe privately owned rights. References herein to any specific commercial product, process, or service by trade name, trademark, manufacturer, or otherwise, does not necessarily constitute or imply its endorsement, recommendation, or favoring by the United States Government or any agency thereof. The views and opinions of authors expressed herein do not necessarily state or reflect those of the United States Government or any agency thereof.

TEST DATA REPORT FOR QUARTER SCALE
NUPAC 125-B RAIL CASK MODEL

M. M. Warrant
B. J. Joseph

February 26, 1987

Sandia National Laboratories
Albuquerque, New Mexico 87185

Prepared for the
U.S. Department of Energy
Idaho Operations Office
Under DOE Contract No. DE-AC07-76ID01570

Test Data Report for Quarter Scale NuPac 125-B Rail Cask Model

**M. M. Warrant
B. J. Joseph
Transportation Systems Technology
and Analysis Division
Sandia National Laboratories
Albuquerque, NM 87185**

Abstract

This report describes the testing conducted and presents the data obtained by Sandia National Laboratories on a quarter scale model of the NuPac 125-B Rail Cask. Three 30-ft free-fall impact tests and two 40-in. free-fall drops onto a puncture bar were performed. The 30-ft drop tests consisted of one end drop onto the bottom impact limiter, an oblique drop onto the closure-end impact limiter, and a flat drop onto both impact limiters on the exterior of the package. The 40-in. puncture tests were directed at the centers of the side and closure end of the package. The five tests were conducted to verify the structural adequacy of the package for the hypothetical accident conditions specified in 10CFR71 and to define the accident damage as initial conditions for the thermal, shielding, and criticality analyses.

Acknowledgments

The authors are indebted to a number of people who, directly and indirectly, have contributed to the program. They acknowledge with special thanks Steven A. Porter, the NuPac Test Engineer; David Bronowski, the Sandia Technical Aide and Test Coordinator; and Larry Sanchez and Randy Longenbaugh, who performed thermal analyses.

These tests were supported by the staff of several departments within Sandia National Laboratories. The work, assistance, and cooperation of the following are greatly appreciated: P. C. McKey and the staff of Mechanical Processing Division C, 7485; the staff of Track and Cables Division 7535, especially D. M. Gutierrez, R. Davis, and W. D. Jacoby; the staff of Remote Areas Maintenance and Test Support Division 7818; W. B. Leisher of Physical Standards Division 7241 (formerly Test Measurements and Precision Centrifuge Division 7545); M. W. Hancock of Motion Picture-Video Services Division 3153; and C. Holland of Photometrics and Optical Development Division 7556.

Contents

ABBREVIATIONS AND ACRONYMS	14
GLOSSARY	15
1. SCOPE.....	17
2. INTRODUCTION.....	18
2.1 Organizational Interfaces and Responsibilities	18
2.2 Test Requirements	19
2.2.1 Initial Test Conditions	19
2.2.2 Tests Conducted on the NuPac 125-B Quarter Scale Model	19
2.2.3 Summary of Test Requirements	20
2.3 Test Procedures	21
2.4 Description of the Quarter Scale Model	21
2.5 Coordinate System for NuPac 125-B Quarter Scale Model and Location of Instrumentation	30
2.6 Aerial Cable Facility, Sandia National Laboratories, Albuquerque, NM	31
2.7 Photometrics and Photographic Coverage.....	33
3. INITIAL EXAMINATION	35
3.1 Leak Test	35
3.2 Disassembly	35
3.2.1 Receipt of Model and Removal of Overpacks	35
3.2.2 Removal of Outer Vessel Lid.....	35
3.2.3 Removal of Inner Vessel.....	35
3.2.4 Removal of Inner Vessel Lid	36
3.2.5 Removal of Upper Internal Impact Limiters	36
3.2.6 Removal of Canisters	36
3.2.7 Removal of Lower Internal Impact Limiters.....	36
3.3 X-Radiography.....	36
3.4 Inspection	36
4. INSTRUMENTATION	39
4.1 Gage Characteristics.....	39
4.2 Calibration	39
4.3 Installation	39
5. 30-FT BOTTOM END DROP TEST	41
5.1 Assembly of Inner Vessel	41
5.2 Leak Testing of Inner Vessel	42
5.3 Assembly of Outer Vessel.....	42
5.4 Leak Testing of Outer Vessel	43
5.5 Assembly of Overpacks.....	44
5.6 Chilling.....	44
5.7 Bottom End Drop Test Procedure.....	49
5.8 Photometrics Data.....	55
5.9 Visual Observations.....	55
5.10 Data Acquisition System Information.....	58

Contents (continued)

6.	30-FT OBLIQUE DROP TEST.....	59
6.1	Chilling.....	59
6.2	Oblique Drop Test Procedure.....	60
6.3	Photometrics Data.....	66
6.4	Visual Observations.....	66
6.5	Data Acquisition System Information.....	66
7.	INTERMEDIATE POST-TEST EXAMINATION.....	68
7.1	Heating.....	68
7.2	Removal of Overpacks.....	68
7.3	Leak Testing of Outer Vessel.....	68
7.4	Removal of Outer Vessel Lid.....	68
7.5	Removal of Inner Vessel.....	70
7.6	Leak Testing of Inner Vessel.....	70
7.7	Removal of Inner Vessel Lid.....	70
7.8	Removal of Upper Internal Impact Limiters.....	72
7.9	Removal of Canisters.....	75
7.10	Removal of Lower Internal Impact Limiters.....	75
7.11	Inspection.....	75
7.11.1	Intermediate Inspection of Cask Body.....	80
7.11.2	Intermediate Inspection of Inner Vessel.....	80
7.11.3	Intermediate Inspection of Canisters.....	80
7.11.4	Intermediate Inspection of Cask Lid, Cask Bottom, and Inner Vessel Lid.....	81
7.11.5	Intermediate Inspection of Internal Impact Limiters.....	81
8.	INTERMEDIATE INSTRUMENTATION.....	82
8.1	Removal of Entran Accelerometers From Outer Vessel.....	82
8.2	Characteristics of Endevco Accelerometers.....	82
8.3	Intermediate Calibration of Accelerometers.....	82
8.3.1	Entran Accelerometers.....	82
8.3.2	Endevco Accelerometers.....	82
8.4	Intermediate Installation of Accelerometers.....	84
9.	30-FT SIDE DROP TEST.....	85
9.1	Assembly of Inner Vessel.....	85
9.2	Leak Testing of Inner Vessel.....	85
9.3	Assembly of Outer Vessel.....	85
9.4	Leak Testing of Outer Vessel.....	85
9.5	Assembly of Overpacks.....	86
9.6	Side Drop Test Procedure.....	86
9.7	Photometrics Data.....	87
9.8	Visual Observations.....	87
9.9	Data Acquisition System Information.....	87
10.	40-IN. SIDE PUNCTURE TEST.....	96
10.1	Puncture Bar.....	96
10.2	Side Puncture Test Procedure.....	97
10.3	Photometrics Data.....	100
10.4	Visual Observations.....	100
10.5	Data Acquisition System Information.....	102

Contents (continued)

11. 40-IN. CLOSURE END PUNCTURE TEST	103
11.1 Puncture Bar.....	103
11.2 Closure End Puncture Test Procedure.....	104
11.3 Photometrics Data.....	106
11.4 Visual Observations.....	106
11.5 Data Acquisition System Information.....	106
12. FINAL POST-TEST EXAMINATION	109
12.1 Removal of Overpacks.....	109
12.2 Leak Testing of Outer Vessel.....	109
12.3 Removal of Outer Vessel Lid.....	110
12.4 Removal of Inner Vessel.....	110
12.5 Leak Testing of Inner Vessel.....	111
12.6 Removal of Inner Vessel Lid.....	111
12.7 Removal of Upper Internal Impact Limiters.....	111
12.8 Removal of Canisters.....	115
12.9 Removal of Lower Internal Impact Limiters.....	115
12.10 X-Radiography.....	115
12.11 Inspection.....	120
12.11.1 Final Inspection of Cask Body.....	120
12.11.2 Final Inspection of Inner Vessel.....	125
12.11.3 Final Inspection of Canisters.....	125
12.11.4 Final Inspection of Cask Lid, Cask Bottom, and Inner Vessel Lid.....	125
12.11.5 Final Inspection of Internal Impact Limiters.....	125
12.11.6 Final Inspection of Overpacks.....	125
12.11.6.1 Inspection of Overpack Exteriors.....	125
12.11.6.2 Sectioning of Overpacks.....	125
12.12 Final Leak Testing of Outer Vessel Containment Boundary.....	136
12.13 Final Leak Testing of Inner Vessel Containment Boundary.....	136
12.14 Measurement of Lead Thickness in Area of Side Puncture.....	136
13. FINAL INSTRUMENTATION	138
13.1 Removal of Accelerometers From Outer Vessel.....	138
13.2 Final Calibration of Accelerometers.....	138
13.2.1 Entran Accelerometers.....	138
13.2.2 Endevco Accelerometers.....	138
14. TEST DATA EVALUATION	139
14.1 30-ft Bottom End Drop Test.....	139
14.1.1 Description of Test Events.....	139
14.1.2 Evaluation of Accelerometer and Strain Gage Data.....	139
14.2 30-ft Oblique Drop Test.....	139
14.2.1 Description of Test Events.....	139
14.2.2 Evaluation of Accelerometer and Strain Gage Data.....	139
14.3 Intermediate Inspection.....	140
14.3.1 Evaluation of Leakage Rate Measurements.....	140
14.3.2 Evaluation of Disassembly and Dimensional Inspection Data.....	140
14.4 Evaluation of Intermediate Instrumentation Data.....	140
14.5 30-ft Side Drop Test.....	140
14.5.1 Description of Test Events.....	140
14.5.2 Evaluation of Accelerometer and Strain Gage Data.....	140

Contents (continued)

14.6	40-in. Side Puncture Test	141
14.6.1	Description of Test Events	141
14.6.2	Evaluation of Accelerometer and Strain Gage Data	141
14.7	40-in. Closure End Puncture Test	141
14.7.1	Description of Test Events	141
14.7.2	Evaluation of Accelerometer and Strain Gage Data	141
14.8	Final Inspection	142
14.8.1	Evaluation of Leakage Rate Measurements	142
14.8.2	Evaluation of Disassembly and Dimensional Inspection Data	142
14.9	Evaluation of Final Instrumentation Data	142
REFERENCES		143
APPENDIX A—Initial Inspection Data		145
APPENDIX B1—Accelerometer and Strain Gage Data for the 30-ft Bottom End Drop Test Filtered at 1000 Hz		157
APPENDIX B2—Fast Fourier Transforms of Raw Accelerometer Data for the 30-ft Bottom End Drop Test		171
APPENDIX C1—Accelerometer and Strain Gage Data for the 30-ft Oblique Drop Test Filtered at 1000 Hz		181
APPENDIX C2—Fast Fourier Transforms of Raw Accelerometer Data for the 30-ft Oblique Drop Test		195
APPENDIX D1—Accelerometer and Strain Gage Data for the 30-ft Side Drop Test Filtered at 1000 Hz		205
APPENDIX D2—Fast Fourier Transforms of Raw Accelerometer Data for the 30-ft Side Drop Test		219
APPENDIX E1—Accelerometer and Strain Gage Data for the 40-in. Side Puncture Test Filtered at 1000 Hz		231
APPENDIX E2—Fast Fourier Transforms of Raw Accelerometer Data for the 40-in. Side Puncture Test		245
APPENDIX F1—Accelerometer and Strain Gage Data for the 40-in. Closure End Puncture Test Filtered at 1000 Hz		257
APPENDIX F2—Fast Fourier Transforms of Raw Accelerometer Data for the 40-in. Closure End Puncture Test		273

Note: See Appendix half-title pages for listing of figures and tables appearing in that Appendix.

Figures

2-1	Test Unit on Transport Skid	22
2-2	Outer Cask Body	22
2-3	Outer Cask Body With Lid Installed	23
2-4	Inner Vessel	23
2-5	Inner Vessel With Lid Installed	24
2-6	Canisters, Inner Vessel Upper Internal Impact Limiters/Shield Plugs, and Inner Vessel Lower Internal Impact Limiters	24
2-7	Overpacks With Attachment Bolts	25
2-8	Assembly Drawing of the Model	26
2-9	Drawing of the Model Inner Vessel	27
2-10	Drawing of the Model Outer Vessel	28
2-11	Drawing of the Model Overpacks	29
2-12	Coordinate System for NuPac 125-B Quarter Scale Model, and Transducer Locations and Orientations	30
2-13	Planned Relationship Between Inner Vessel Components and the Cask Coordinate System	31
2-14	Actual Relationships Among Inner Vessel, Inner Vessel Lid, and Outer Cask Body for Testing	31
2-15	Aerial Cable Facility at Sandia National Laboratories, Albuquerque, New Mexico	32
2-16	Mounting of Test Article on Aerial Cable Apparatus	32
2-17	Test Pad With Stadia Board	33
2-18	Typical Camera Locations	33
2-19	Typical Camera Setup	34
3-1	Removal of Cask Body Lid	35
3-2	X-Radiograph of Bottom End of Cask Body at 0°	37
3-3	Inspection of a Canister	38
4-1	Routing of Instrumentation Wires to Terminal Strips	40
4-2	Strain Gage SR4 Installed	40
5-1	Sketch of Inner Vessel Showing Cells and Alignment Pins	41
5-2	Inner Vessel Lid Bolts Being Torqued to 28 in.-lb	42
5-3	Synthetic Putty Plugging the Holes for Radiolysis Gases in the Bottom of the Inner Vessel	43
5-4	Inner Vessel Being Lowered Into the Outer Vessel	43
5-5	Plastic Bag Envelope Leak Test of the Outer Vessel	44
5-6	Leak Test of Outer Vessel Seal	44
5-7	Overpack Bolts Being Torqued to 70 in.-lb	45
5-8	Model Being Positioned in the Climatic Chamber	45
5-9	Thermocouple Attached to Model	46
5-10	Model Inside Climatic Chamber During Chilling Process	46
5-11	Cerablanket Insulation Covering the Model for the Time-to-Warm Calculation Verification Test	47
5-12	One-Dimensional Geometry Used for Transient Thermal Analysis of the Quarter Scale NuPac 125-B Cask	48
5-13	Temperature Response of the Quarter Scale NuPac 125-B Cask	49
5-14	Chilled Insulated Model Loaded on Truck for Transport to Drop Test Facility	50
5-15	NuPac 125-B Model Rigged for the 30-ft Bottom End Drop Test	50
5-16	Removal of Cerablanket Insulation	51
5-17	Drop Height and Orientation Verification Before the 30-ft Bottom End Drop Test	51
5-18	Sequential Photographs of the 30-ft Bottom End Drop Test	52
5-19	Orientation of Model for 30-ft Bottom End Drop Test	55

Note: See Appendix half-title pages for listing of figures and tables appearing in that Appendix.

Figures (continued)

5-20	NuPac 125-B Quarter Scale Model Immediately After 30-ft Bottom End Drop Test	55
5-21	Bottom Overpack Deformation After 30-ft Bottom End Drop Test	56
5-22	Measurements of Bottom Overpack "Dimple" Deformation After 30-ft Bottom End Drop Test	56
5-23	Measurements of Bottom Overpack "Mushroom" Deformation After 30-ft Bottom End Drop Test	56
5-24	Bottom Overpack Failed Weld After 30-ft Bottom End Drop Test	57
5-25	Weld Separation Around Inboard Seam of Bottom Overpack After 30-ft Bottom End Drop Test	57
5-26	Secondary Impact Damage to Top Overpack After 30-ft Bottom End Drop Test	58
5-27	Measurements of Secondary Impact Damage to Top Overpack After 30-ft Bottom End Drop Test	58
6-1	Inclinometer Reading for Cask Body Before 30-ft Oblique Drop Test	59
6-2	Positioning of Cooling Shroud Around Model	60
6-3	Model Installed in Cooling Shroud	60
6-4	Removal of Cooling Shroud	61
6-5	NuPac 125-B Model Rigged for the 30-ft Oblique Drop Test	61
6-6	NuPac 125-B Model Elevated to 30 ft Before the 30-ft Oblique Drop Test	61
6-7	Sequential Photographs of the 30-ft Oblique Drop Test	62
6-8	Orientation of Model for 30-ft Oblique Drop Test	65
6-9	NuPac 125-B Quarter Scale Model Immediately After the 30-ft Oblique Drop Test	66
6-10	Deformation of Top Overpack After 30-ft Oblique Drop Test	67
6-11	Measurement of Deformation Angle of Top Overpack After 30-ft Oblique Drop Test	67
7-1	Removal of the Overpacks	68
7-2	Condition of the Outer Vessel Closure During Intermediate Post-Test Examination	69
7-3	Cask Assembly After Removal of Outer Vessel Lid During Intermediate Post-Test Inspection	69
7-4	Close-up of Cask Assembly After Removal of Outer Vessel Lid During Intermediate Post-Test Inspection	70
7-5	Sketch of Inner Vessel Lid Bolts With Tightening Order	71
7-6	Removal of Inner Vessel Lid During Intermediate Post-Test Examination	71
7-7	Orientations of Upper Internal Impact Limiters After the 30-ft Oblique Drop Test	72
7-8	Upper Internal Impact Limiter Being Removed From Inner Vessel	72
7-9	Condition of Upper Internal Impact Limiter "A" After 30-ft Oblique Drop Test	73
7-10	Condition of Upper Internal Impact Limiter "B" After 30-ft Oblique Drop Test	73
7-11	Condition of Upper Internal Impact Limiter "C" After 30-ft Oblique Drop Test	73
7-12	Condition of Upper Internal Impact Limiter "D" After 30-ft Oblique Drop Test	73
7-13	Condition of Upper Internal Impact Limiter "E" After 30-ft Oblique Drop Test	74
7-14	Condition of Upper Internal Impact Limiter "F" After 30-ft Oblique Drop Test	74
7-15	Condition of Upper Internal Impact Limiter "G" After 30-ft Oblique Drop Test	74
7-16	Orientations of Canisters After 30-ft Oblique Drop Test	76
7-17	Condition of Lower Internal Impact Limiter "A" After 30-ft Oblique Drop Test	76
7-18	Condition of Lower Internal Impact Limiter "B" After 30-ft Oblique Drop Test	77
7-19	Condition of Lower Internal Impact Limiter "C" After 30-ft Oblique Drop Test	77
7-20	Condition of Lower Internal Impact Limiter "D" After 30-ft Oblique Drop Test	78
7-21	Condition of Lower Internal Impact Limiter "E" After 30-ft Oblique Drop Test	78
7-22	Condition of Lower Internal Impact Limiter "F" After 30-ft Oblique Drop Test	79
7-23	Condition of Lower Internal Impact Limiter "G" After 30-ft Oblique Drop Test	79
8-1	Centrifuge Used for Accelerometer Calibration at Ambient Temperature	83

Note: See Appendix half-title pages for listing of figures and tables appearing in that Appendix.

Figures (continued)

8-2	Mounting of an Accelerometer for Calibration in the Centrifuge	83
9-1	Model Being Lowered Into Overpack	86
9-2	Installation of the Upper Overpack	86
9-3	Model Rigged for 30-ft Side Drop Test	87
9-4	NuPac 125-B Model Elevated to 30 ft Before the 30-ft Side Drop Test	88
9-5	Sequential Photographs of the 30-ft Side Drop Test	88
9-6	Orientation of Model for 30-ft Side Drop Test	91
9-7	Basic Condition of Model After 30-ft Side Drop Test	91
9-8	Visual Inspection of Model After 30-ft Side Drop Test	92
9-9	Tear in Lower Overpack Shell After 30-ft Side Drop Test	92
9-10	Deformation of Lower Overpack After 30-ft Side Drop Test: End View	93
9-11	Deformation of Lower Overpack After 30-ft Side Drop Test: Side View	93
9-12	Deformation of Upper Overpack After 30-ft Side Drop Test: End View	94
9-13	Deformation of Upper Overpack After 30-ft Side Drop Test: Side View	94
9-14	Failure of the Weld Around the Foam Filling Hole Patch After 30-ft Side Drop Test	95
10-1	Puncture Bar for 40-in. Side Puncture Test	96
10-2	Verification of Puncture Bar Location and Distance From Model for 40-in. Side Puncture Test	97
10-3	NuPac 125-B Model Before 40-in. Side Puncture Test	97
10-4	Sequential Photographs of the 40-in. Side Puncture Test	98
10-5	Orientation of Model for 40-in. Side Puncture Test	100
10-6	Condition of the Model After the 40-in. Side Puncture Test	100
10-7	Width of Deformation From 40-in. Side Puncture Test	101
10-8	Depth of Deformation From 40-in. Side Puncture Test	101
10-9	Deformation of the Puncture Bar After the 40-in. Side Puncture Test: Front View	102
11-1	Puncture Bar for 40-in. Closure End Puncture Test	103
11-2	NuPac 125-B Model Rigged for 40-in. Closure End Puncture Test	104
11-3	Verification of Puncture Bar Location and Distance From Model for 40-in. Closure End Puncture Test	104
11-4	Sequential Photographs of the 40-in. Closure End Puncture Test	105
11-5	Orientation of Model for 40-in. Closure End Puncture Test	106
11-6	Condition of the Model After the 40-in. Closure End Puncture Test	106
11-7	Close-up of the Model and Puncture Bar After the 40-in. Closure End Puncture Test	107
11-8	Close-up of the Upper Overpack and Puncture Bar After Model Had Been Lifted Off the Bar Following the 40-in. Closure End Puncture Test	107
11-9	Deformed Area of Upper Overpack After the 40-in. Closure End Puncture Test	108
11-10	Deformation of the Puncture Bar After the 40-in. Closure End Puncture Test: Front View	108
12-1	Interior of Upper Overpack Showing Circular Mark Made by Puncture Bar During 40-in. Closure End Puncture Test	109
12-2	Condition of Outer Vessel Lid After 40-in. Closure End Puncture Test	110
12-3	Outer Vessel Lid and Cut Portion of Upper O-Ring	110
12-4	Orientation of Upper Internal Impact Limiters After 40-in. Closure End Puncture Test	111
12-5	Condition of Upper Internal Impact Limiter "A" After 40-in. Closure End Puncture Test	112
12-6	Condition of Upper Internal Impact Limiter "B" After 40-in. Closure End Puncture Test	112
12-7	Condition of Upper Internal Impact Limiter "C" After 40 in. Closure End Puncture Test	113
12-8	Condition of Upper Internal Impact Limiter "D" After 40-in. Closure End Puncture Test	113
12-9	Condition of Upper Internal Impact Limiter "E" After 40-in. Closure End Puncture Test	114

Note: See Appendix half-title pages for listing of figures and tables appearing in that Appendix.

Figures (continued)

12-10	Condition of Upper Internal Impact Limiter “F” After 40-in. Closure End Puncture Test	114
12-11	Condition of Upper Internal Impact Limiter “G” After 40-in. Closure End Puncture Test	115
12-12	Condition of Lower Internal Impact Limiter “A” After 40-in. Closure End Puncture Test	116
12-13	Condition of Lower Internal Impact Limiter “B” After 40-in. Closure End Puncture Test	116
12-14	Condition of Lower Internal Impact Limiter “C” After 40-in. Closure End Puncture Test	117
12-15	Condition of Lower Internal Impact Limiter “D” After 40-in. Closure End Puncture Test	117
12-16	Condition of Lower Internal Impact Limiter “E” After 40-in. Closure End Puncture Test	118
12-17	Condition of Lower Internal Impact Limiter “F” After 40-in. Closure End Puncture Test	118
12-18	Condition of Lower Internal Impact Limiter “G” After 40-in. Closure End Puncture Test	119
12-19	X-Ray Plate in Position for Examination of the Closure End of the Cask Body	119
12-20	X-Ray Plate in Position for Examination of the Bottom End of the Cask Body	120
12-21	X-Radiograph of Cask Bottom at 0° After Completion of Testing	121
12-22	X-Radiograph of Puncture Area Taken From Inside the Cask Body	122
12-23	X-Radiograph of Puncture Area: Side View at 270°	123
12-24	Top Overpack Exterior: End View	126
12-25	Top Overpack Exterior: Side View at 0°	126
12-26	Top Overpack Exterior: Side View at 90°	127
12-27	Top Overpack Interior	127
12-28	Bottom Overpack Exterior: End View	128
12-29	Bottom Overpack Exterior: Side View at 0°	128
12-30	Bottom Overpack Exterior: Side View at 90°	129
12-31	Bottom Overpack Interior	129
12-32	Top Overpack Measurements: Section Through Lifting Tabs	130
12-33	Top Overpack Measurements: Section Normal to Lifting Tabs	131
12-34	Bottom Overpack Measurements: Section Through Lifting Tabs	132
12-35	Bottom Overpack Measurements: Section Normal to Lifting Tabs	133
12-36	Sectioned Top Overpack: 0°–90°–180° View	134
12-37	Sectioned Top Overpack: 180°–270°–0° View	134
12-38	Sectioned Bottom Overpack: 180°–90°–0° View	135
12-39	Sectioned Bottom Overpack: 0°–270°–180° View	135
12-40	Section View of Hole Drilled for Measuring Shield Material Thickness	137

Tables

2-1	Test Requirements Matrix	20
2-2	Test Procedures	21
2-3	Procedures Used in Major Test Activities	21
2-4	Cameras Used to Record Photometric and Photographic Data	34
4-1	Characteristics of Entran Accelerometers	39
4-2	Characteristics of Micro-Measurements Strain Gages	39
4-3	Sensitivities of Entran Accelerometers at –20°F	39
4-4	Initial Installation Location of Accelerometers on Model	40
7-1	Rotations and Deformations of Upper Internal Impact Limiters After 30-ft Oblique Drop Test	75
7-2	Orientations of Canisters After 30-ft Oblique Drop Test	75
7-3	Differences Data for Cask Bore Straightness for the Intermediate Post-Test Inspection	80
7-4	Differences Data for Canister Diameters for the Intermediate Post-Test Inspection	80
7-5	Differences Data for Canister Straightness for the Intermediate Post-Test Inspection	80

Note: See Appendix half-title pages for listing of figures and tables appearing in that Appendix.

Tables (continued)

7-6	Amount of Crush for the Lower Internal Impact Limiters for the Intermediate Post-Test Inspection	81
7-7	Amount of Crush for the Upper Internal Impact Limiters for the Intermediate Post-Test Inspection	81
8-1	Characteristics of Endevco Accelerometers	82
8-2	Sensitivities of Entran Accelerometers at Ambient Temperature	82
8-3	Sensitivities of Endevco Accelerometers at Ambient Temperature	82
8-4	Intermediate Installation Location of Accelerometers on Model	84
10-1	Characteristics of Puncture Bar for Side Puncture Test	96
10-2	Characteristics of Micro-Measurements Strain Gages Used on Puncture Bar for Side Puncture Test	96
11-1	Characteristics of Puncture Bar for Closure End Puncture Test	103
11-2	Characteristics of Micro-Measurements Strain Gages Used on Puncture Bar for Closure End Puncture Test	103
12-1	Final Orientations of Upper Internal Impact Limiters	111
12-2	Final Orientations of Canisters	115
12-3	Differences Data for Cask Bore Diameter for the Final Post-Test Inspection	124
12-4	Differences Data for Cask Bore Straightness for the Final Post-Test Inspection	124
12-5	Differences Data for Canister Diameters for the Final Post-Test Inspection	125
13-1	Sensitivities of Entran Accelerometers at Ambient Temperature Before and After Final Three Tests	138
13-2	Sensitivities of Endevco Accelerometers at Ambient Temperature Before and After Final Three Tests	138

Note: See Appendix half-title pages for listing of figures and tables appearing in that Appendix.

Abbreviations and Acronyms

ANSI	American National Standards Institute	OCV	Outer containment vessel
DOE	US Department of Energy	PMI	Probable measurement inaccuracy
EG&G	EG&G Idaho, Inc.	QA	Quality assurance
fps	Frames per second	QAPP	Quality Assurance Program Plan
ICV	Inner containment vessel	R _B	Rockwell "B" scale for hardness
INEL	Idaho National Engineering Laboratory	R _A	Rockwell "A" scale for hardness
NBS	National Bureau of Standards	Sandia	Sandia National Laboratories
NP	Nuclear Packaging test procedure	TMI	Three Mile Island
NRC	US Nuclear Regulatory Commission	UNC	Unified National Coarse
NuPac	Nuclear Packaging, Inc.		

Glossary

CANISTERS. Containers loaded with fuel debris.

CASK BODY. See OUTER VESSEL.

CASK BORE. Internal cavity of cask body.

CONTAINMENT SYSTEM. The components of the packaging intended to retain the radioactive material during transport.

IMPACT LIMITERS. External impact limiters (also called OVERPACKS in this document) are attachments to each end of the cask body that consist of a polyurethane-foam-filled metal shell to provide protection from normal transport conditions and hypothetical accidents. Internal impact limiters consist of metallic honeycomb material to provide axial impact protection for the canisters.

INNER VESSEL. The inner containment vessel. Seven interconnected cells within the inner vessel are provided for seven payload canisters. Access to the cells is gained through the inner vessel lid.

INNER VESSEL TUBE BORES. The seven cylindrical cells that together form the inner vessel cavity.

LEAK TEST. Verification of the leak rate of a containment vessel or seal.

OUTER VESSEL. The outer containment vessel (also called CASK BODY in this document). The body of the cask, not including overpacks.

OVERPACKS. See IMPACT LIMITERS.

PACKAGE. The packaging together with its radioactive contents as presented for transport.

PACKAGING. The assembly of components necessary to ensure compliance with the packaging requirements of 10CFR71. It may consist of one or more receptacles, absorbent materials, spacing structures, thermal insulation, radiation shielding, and devices for cooling or absorbing mechanical shocks. The vehicle, tiedown system, and auxiliary equipment may be designated as part of the packaging. For the NuPac 125-B packaging, the components include the cask body, overpacks, inner containment vessel, internal impact limiters/shield plugs, and lids for the inner and outer vessels.

Test Data Report for Quarter Scale NuPac 125-B Rail Cask Model

1. Scope

This document presents the data obtained by Sandia National Laboratories (Sandia) during impact and puncture testing of the quarter scale model of the NuPac 125-B Cask. The data include the following:

- Inspection reports documenting the dimensions of the model inner vessel, outer vessel, canisters, and internal impact limiters
- Leak test measurements
- Temperature of the model just before the 30-ft bottom end and oblique drop tests
- Instrumentation calibration data
- Accelerometer and strain gage data
- Measurements of overpack and internal impact limiter deformations
- Individual frames from photometric footage of the tests
- Positive images from x-radiographs
- Documentary photographs of the tests and associated activities

The testing was performed to:

- (a) Verify that the package is structurally adequate to survive accidental drops of 30 ft in any orientation and accidental puncture events, without loss of either containment boundary
- (b) Provide test data on accelerations and strains to confirm analytic predictions that the package is adequate to resist all other structural provisions of normal and hypothetical accident conditions
- (c) Define hypothetical accident damage to the package as initial conditions for the hypothetical accident thermal event, shielding, and criticality analyses

Comparison of the test results with analytical predictions is presented in the Safety Analysis Report for the NuPac 125-B cask (Nuclear Packaging, 1986).

2. Introduction

The NuPac 125-B cask has been designed by Nuclear Packaging, Inc. (NuPac) under contract from EG&G Idaho, Inc. (EG&G). The cask is being used to transport up to seven canisters per shipment of Three Mile Island Unit 2 (TMI-2) fuel debris from the TMI site at Middletown, Pennsylvania, to the Idaho National Engineering Laboratory (INEL) at Idaho Falls, Idaho. The NuPac 125-B cask provides two levels of testable containment for the canisters: an inner vessel within an outer cask body. Polyurethane foam-filled impact limiters (also referred to as overpacks) are attached to each end of the outer cask.

2.1 Organizational Interfaces and Responsibilities

Early in the design process, NuPac held regular (monthly) meetings with the Nuclear Regulatory Commission (NRC), the certifying agency. NRC personnel encouraged scale-model testing of the cask. Planning meetings including NuPac, Sandia, and EG&G representatives were held in conjunction with the TMI-2 Core Shipment Technical Working Team meetings to (a) recommend tests to be performed, (b) decide which features of the cask should be modeled, and (c) determine the measurements to be taken pre- and post-test. Three 30-ft drop tests and one puncture test were proposed. The 30-ft drop tests were to consist of one end drop onto the bottom impact limiter, an oblique drop onto the closure-end impact limiter, and a flat drop onto the side of the package. The 40-in. puncture test was to be directed at the center of the side of the model.

Subsequent meetings that included NuPac, Sandia, EG&G, and NRC personnel expanded the scope of the tests. The NRC was particularly interested in (a) measurements of post-test deformations of the scale-model canisters and inner containment vessel, (b) measurements of leak rates of both inner and outer vessels, and (c) each test being conducted at the worst-case temperature and pressure of the cask determined by the structural analyses. Data from accelerometers and strain gages, while useful to check the analyses, were considered of secondary importance.

X-radiography and careful dimensional inspection of model components, and leak testing of both cask containment boundaries, were added to the test

program scope to address the concerns of the NRC. At the recommendation of Sandia, the thermal shield was included in the model design. At the request of NRC, a second puncture test directed at the center of the closure end of the model was added at the end of the test sequence.

The following program interfaces were established between Sandia, NuPac, and EG&G.

NuPac prepared the test plan, "Drop Test Requirements—Hypothetical Accident Conditions (Type "B") for Quarter Scale NuPac 125-B Rail Cask," DT-04, Rev. 0, January 24, 1985, with considerable input from Sandia. EG&G and Sandia reviewed the test plan, which was issued as a controlled document by NuPac. The tests were conducted in accordance with Rev. 2, April 8, 1985 (see Appendix 2.10.6 of Nuclear Packaging, 1986). DT-04 provided test performance parameters and acceptance criteria for test data, and criteria to determine whether the test article passed or failed each test. Sandia planned the tests and prepared test procedures to meet the requirements of DT-04. EG&G and NuPac reviewed the test procedures, which were later issued by Sandia as controlled documents.

NuPac provided the test article, striped the outside of the overpacks as described in DT-04, and identified the components so that the test article could be assembled in the same configuration for each test. Sandia performed inspections of the test article identified in DT-04 to document its measurements before testing began, after completion of the oblique drop test, and after completion of the drop and puncture tests. NuPac approved the inspection reports.

Sandia was responsible for conducting all tests and collecting and reducing data as specified in DT-04. NuPac was responsible for all engineering decisions relative to the integrity of the test article and its suitability for continued testing. "Quick-look" data from selected accelerometers and strain gages were available for inspection immediately following each test. Raw and filtered data from accelerometers and strain gages, inspection data sheets, documentary photographs, photometrics footage, and other information were provided to NuPac and EG&G as soon as possible after completion of a test.

NuPac was responsible for approving continuation or termination of the tests after visual examination of the test article, examination of the "quick-look"

data, and measurement of the containment vessel leak rates (if applicable). Quality Assurance representatives from Sandia and NuPac verified that test criteria and environmental conditions were satisfied before each test. Field changes to the test procedures required approval by Sandia and NuPac.

NuPac and EG&G reviewed the test data in draft form and provided comments for incorporation into the final test data report. NuPac interpreted the test data results and compared them with analytic predictions (Nuclear Packaging, 1986). Internal consistency of the data is evaluated in this test data report.

The test records package consisting of the data report, filled-out data sheets and test procedures forms, pre- and post-test inspection data, photographic records, and the raw and filtered data will be retained in Transportation System Development Department 6320, Sandia, in the project QA Coordinator's office. Duplicate copies have been provided to EG&G and NuPac. NuPac will retain the test hardware and a copy of the test records package for the duration of the useful life of the NuPac 125-B cask.

2.2 Test Requirements

Evaluation of the package design must address its adequacy both under normal conditions of transport and under hypothetical accident conditions specified by NRC in 10CFR71 (NRC, 1983). The tests reported in this test data report were performed in agreement with "Drop Test Requirements - Hypothetical Accident Conditions (Type "B") for Quarter Scale NuPac 125-B Rail Cask," DT-04, Revision 2, April 8, 1985 (see Appendix 2.10.6 of Nuclear Packaging, 1986). They address only the impact and puncture portions of the hypothetical accident conditions.

Evaluation for the hypothetical accident conditions is based on sequential application of the tests specified in 10CFR71.73, in the order indicated, to determine their cumulative effect on a package.

2.2.1 Initial Test Conditions

The initial conditions for the tests specified by 10CFR71.73 include:

- "The ambient air temperature before and after the tests must remain constant at that value between -29°C (-20°F) and $+38^{\circ}\text{C}$ (100°F) which is most unfavorable for the feature under consideration."

- "The initial internal pressure within the containment system must be the maximum normal operating pressure unless a lower internal pressure consistent with the ambient temperature assumed to precede and follow the tests is more unfavorable."

NuPac determined that ambient spring temperatures in Albuquerque provided sufficient initial temperatures for the 30-ft side drop test and puncture tests. The most unfavorable initial temperature for the 30-ft bottom end and oblique drop tests was calculated to be -20°F . Because the ambient air temperature could not be adjusted to -20°F , the model itself was chilled to a temperature above -40°F but below -20°F , and the bottom end and oblique drop tests were performed with the model at a temperature between -27°F and -19°F .

2.2.2 Tests Conducted on the NuPac 125-B Quarter Scale Model

The required impact tests include the following:

Free Drop—"A free drop of the specimen through a distance of nine m (30 ft) onto a flat, essentially unyielding, horizontal surface, striking the surface in a position for which maximum damage is expected."

Puncture—"A free drop of the specimen through a distance of one m (40 in.) in a position for which maximum damage is expected, onto the upper end of a solid, vertical, cylindrical, mild steel bar mounted on an essentially unyielding, horizontal surface. The bar must be 15 cm (six in.) in diameter, with the top horizontal and its edge rounded to a radius of not more than six mm (1/4 in.) and of a length as to cause maximum damage to the package, but not less than 20 cm (eight in.) long. The long axis of the bar must be vertical."

Three 30-ft drop tests were specified in DT-04, Rev. 2: an end drop onto the bottom impact limiter, an oblique drop onto the closure-end impact limiter, and a flat drop onto the side of the package. The flat end drop onto the bottom end was intended to determine the peak acceleration response of the lids and closure bolts and to qualify the internal impact limiters within the inner vessel cells. The oblique impact on the closure end was conducted at an angle intended to maximize cask body shell stresses. The side drop was intended to impart maximum loads to the inner vessel.

The 40-in. puncture tests were directed at the center of the side and closure ends of the package. The side puncture event was intended to verify the integrity of the cask side wall, and the end puncture event was intended to verify the integrity of the cask lid. Because the model was quarter scale, the puncture bars in the tests had quarter scale diameters (1.5 in. vs 6 in.) and radii (1/16 in. vs 1/4 in.). The puncture bar

lengths were specified by NuPac in DT-04 and were 9 in. and 11 in. for the side and closure end puncture tests, respectively.

2.2.3 Summary of Test Requirements

Table 2-1 summarizes the requirements for each test performed.

Table 2-1. Test Requirements Matrix

	Test Sequence				
	Bottom End Drop	Top Corner Drop	Side Drop	Side Puncture	End Puncture
TEST CONFIGURATION					
Impact End	Bottom	Top	Side	Side	Top
Orientation Angle (with respect to horizontal)	90° ± 1°	62.5° ± 1°	0° ± 1°	0° ± 1°	90° ± 1°
Drop Height	30 ft (+1, -0 in.)	30 ft (+1, -0 in.)	30 ft (+1, -0 in.)	40 in. (+0.25, -0 in.)	40 in. (+0.25, -0 in.)
PRETEST STEPS					
100% Visual Inspection	Yes	No	Yes	No	No
Dimensional Survey	Yes	No	Yes	No	No
Torque Lid Bolts	Yes	No	Yes	No	No
Leak Test	Yes	No	Yes	No	No
Install Overpacks	Yes	No	Yes	No	No
Chill to < -20°F	Yes	Yes	No	No	No
DROP STEPS					
Visual Inspection	Yes	Yes	Yes	Yes	Yes
Check Instrumentation	Yes	Yes	Yes	Yes	Yes
Check Outer Shell Temp	Yes	Yes	No	No	No
Drop	Yes	Yes	Yes	Yes	Yes
Document/Photos	Yes	Yes	Yes	Yes	Yes
POST-TEST STEPS					
Remove Overpacks	No	Yes	No	No	Yes
Leak Test	No	Yes	No	No	Yes
Inspect Lid Bolts	No	Yes	No	No	Yes
Disassemble and Visually Inspect	No	Yes	No	No	Yes
100% Visual Inspection	No	Yes	No	No	Yes
Dimensional Survey	No	Yes	No	No	Yes

2.3 Test Procedures

Procedures for all tests and related activities were prepared by Sandia and reviewed by EG&G and NuPac. The procedures defined the steps to be taken in performing the tests. They applied to instrumentation data collection, photometric and photographic coverage, test setup and performance, and documentation.

Activities described in the test procedures follow quality assurance procedures outlined in the Quality Assurance Program Plan (QAPP) for Organization 6000 (Sandia, 1984). The QAPP states the policies, assigns responsibilities, and provides descriptive procedures governing activities that affect the quality of products and services performed by Organization 6000 at Sandia National Laboratories.

The procedures used to test the NuPac 125-B Quarter Scale Model are listed in Table 2-2; procedures used for each major test activity are shown in Table 2-3.

Table 2-2. Test Procedures

Test Procedure Number	Title (NuPac 125-B)
NP-1	Quarter Scale Model Instrumentation Installation Procedure
NP-2	Quarter Scale Model Inspection Procedure
NP-3	Quarter Scale Model 30-ft Bottom End Drop Test Procedure
NP-4	Quarter Scale Model 30-ft Oblique Drop Test Procedure
NP-5	Quarter Scale Model 30-ft Side Drop Test Procedure
NP-6	Quarter Scale Model Side Puncture Test Procedure
NP-7	Quarter Scale Model Closure End Puncture Test Procedure
NP-8	Quarter Scale Model Assembly/Disassembly Procedure
NP-9	Quarter Scale Model Leak Test Procedure
NP-10	Quarter Scale Model Chilling Procedure
NP-11	Quarter Scale Model Impact Limiter Destructive Disassembly Procedure

Table 2-3. Procedures Used in Major Test Activities

Activity	Procedures Used
Initial examination	Leak test (NP-9), Disassemble (NP-8), Inspect (NP-2)
Instrument for tests	Instrument (NP-1)
30-ft bottom end drop test	Assemble (NP-8), Leak test (NP-9), Chill (NP-10), Bottom end drop (NP-3)
30-ft oblique drop test	Chill (NP-10), Oblique drop (NP-4)
Intermediate post-test examination	Heat (NP-10), Leak test (NP-9), Disassemble (NP-8), Inspect (NP-2)
30-ft side drop test	Assemble (NP-8), Leak test (NP-9), Side drop (NP-5)
40-in. side puncture test	Side puncture (NP-6)
40-in. closure end puncture test	Closure end puncture (NP-7)
Final post-test examination	Leak test (NP-9), Disassemble (NP-8), Inspect (NP-2), Impact limiter destructive disassembly (NP-11)

2.4 Description of the Quarter Scale Model

The assembled test unit is shown in Figure 2-1 on the transport skid. The unit consists of outer cask body and outer cask body lid, inner vessel and inner vessel lid, internal impact limiters/shield plugs, canisters, and overpacks. Total weight of the model and contents was 2830 lb.

The outer cask body and outer cask body assembled with its lid are shown in Figures 2-2 and 2-3, respectively. The inner vessel and inner vessel assembled with its lid and placed within the outer cask body are shown in Figures 2-4 and 2-5, respectively. Figure 2-6 shows the canisters, inner vessel upper internal impact limiters/shield plugs, and inner vessel lower internal impact limiters. Figure 2-7 shows the overpacks with their attachment bolts.

Fabrication drawings of the model appear in Figures 2-8 through 2-11. A thin thermal shield, consisting of wire wrapped around the cask body, covered by stainless steel sheet, is not shown in the drawings.

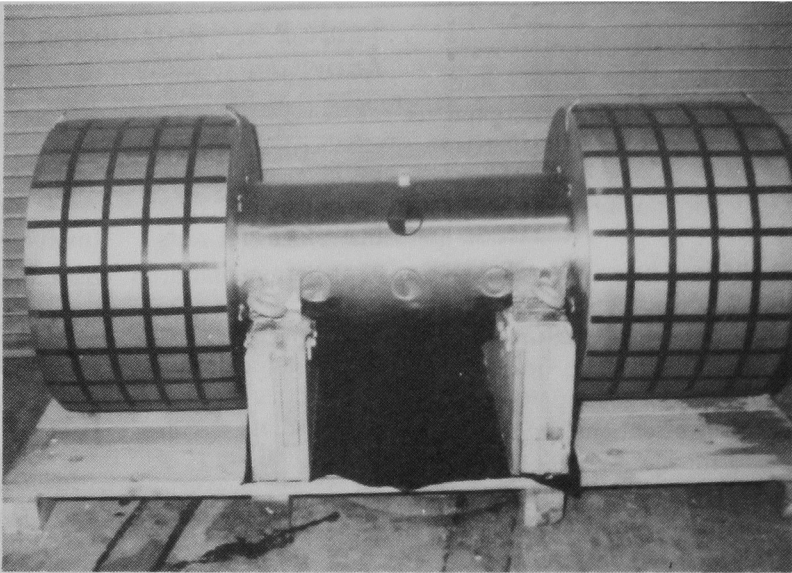


Figure 2-1. Test Unit on Transport Skid

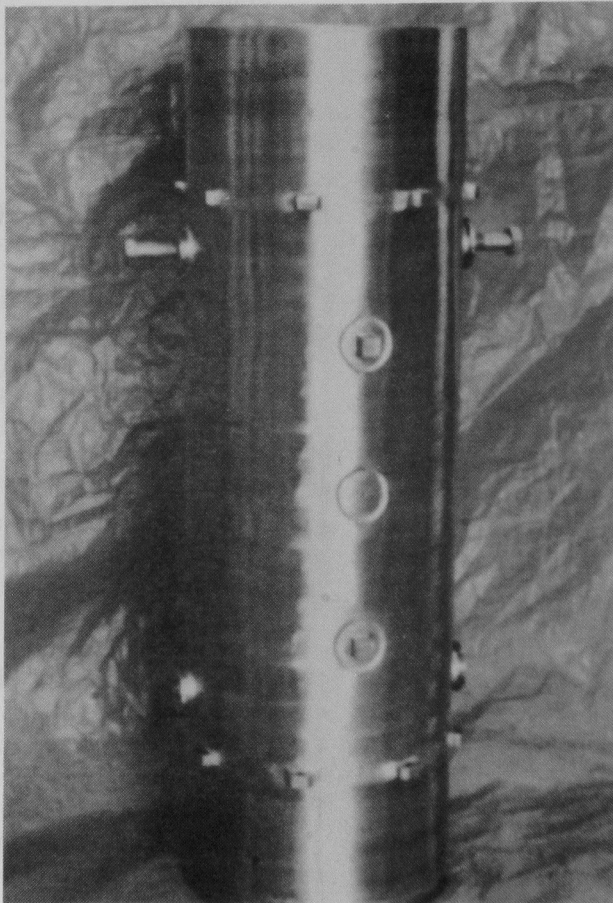


Figure 2-2. Outer Cask Body

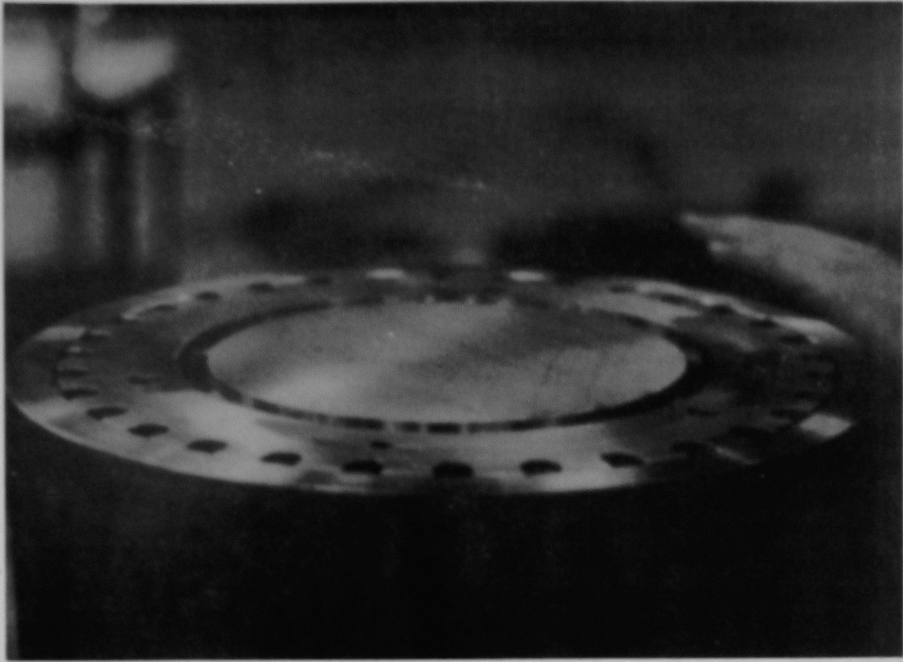


Figure 2-3. Outer Cask Body With Lid Installed

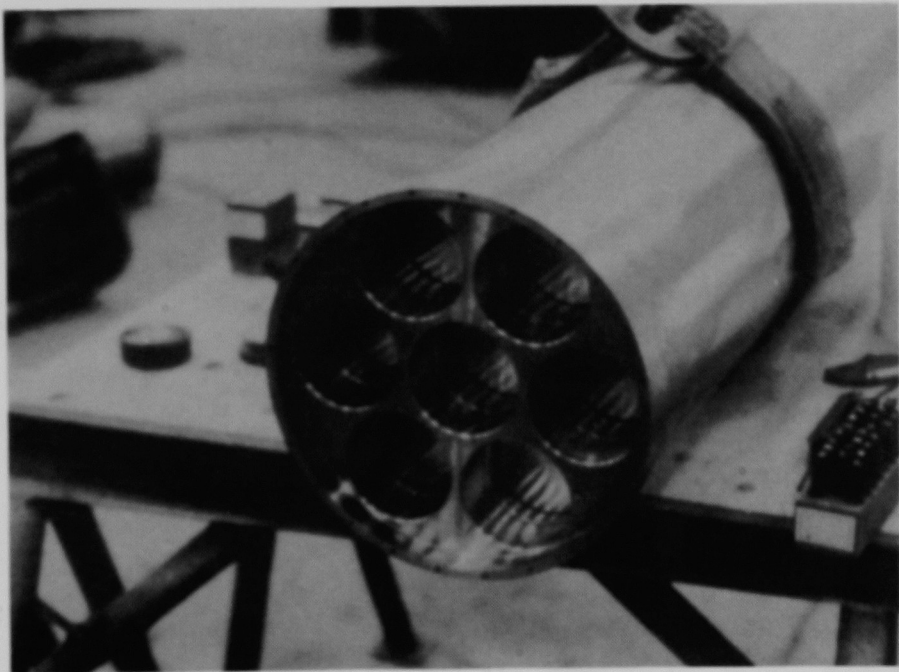


Figure 2-4. Inner Vessel

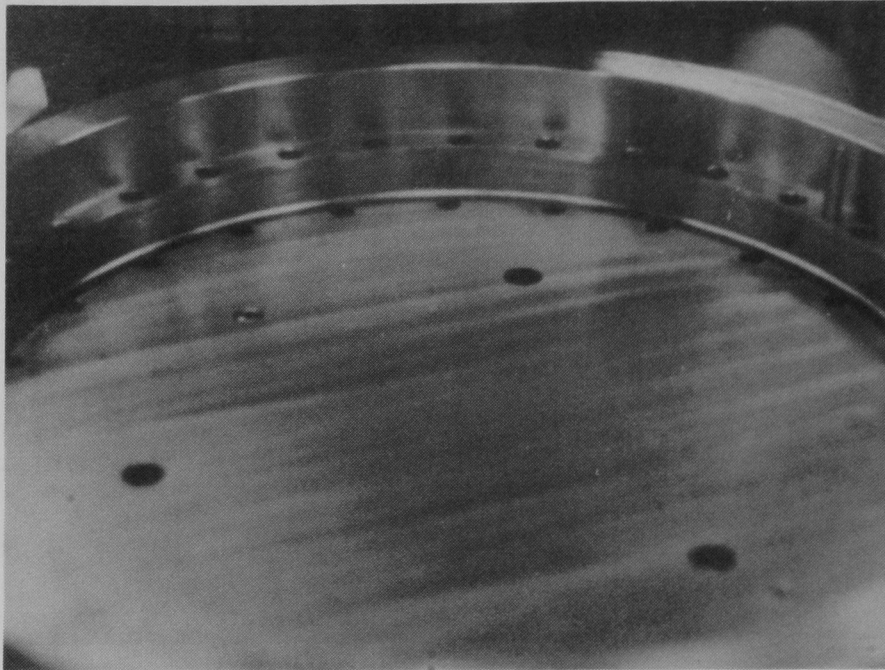


Figure 2-5. Inner Vessel With Lid Installed (placed within outer cask body)



Figure 2-6. Canisters (back row), Inner Vessel Upper Internal Impact Limiters/ Shield Plugs (middle row), and Inner Vessel Lower Internal Impact Limiters (front row)

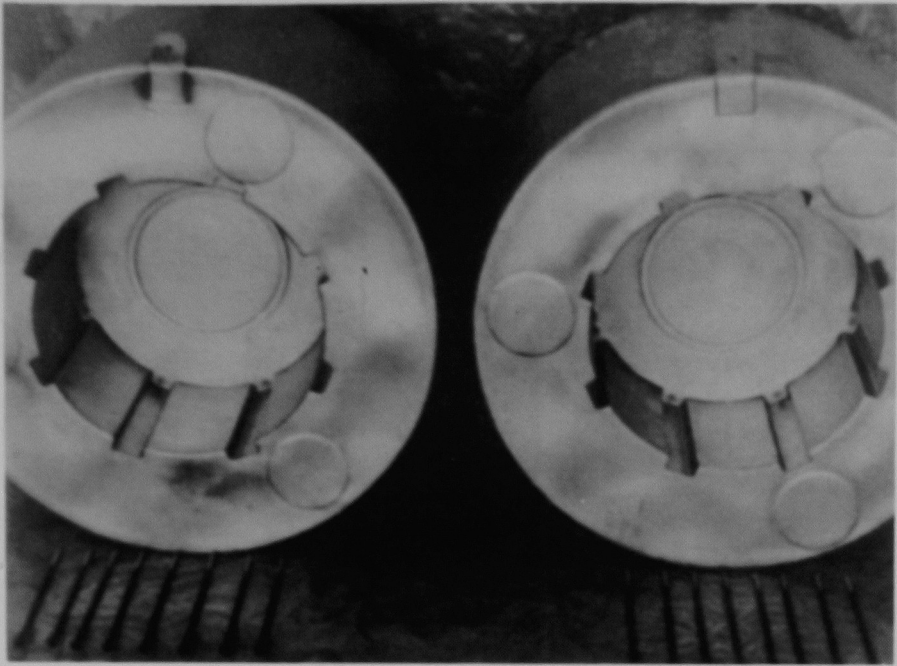
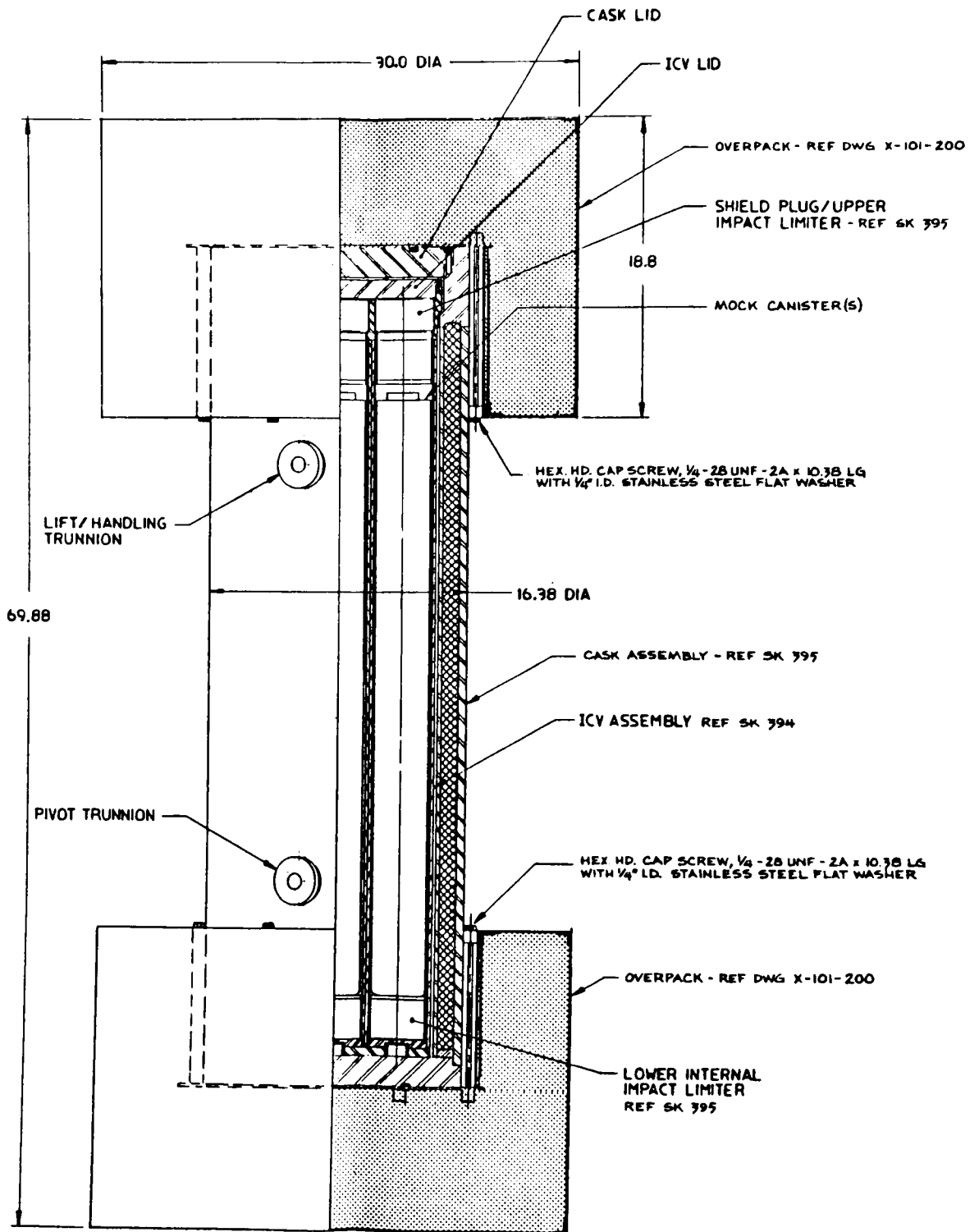


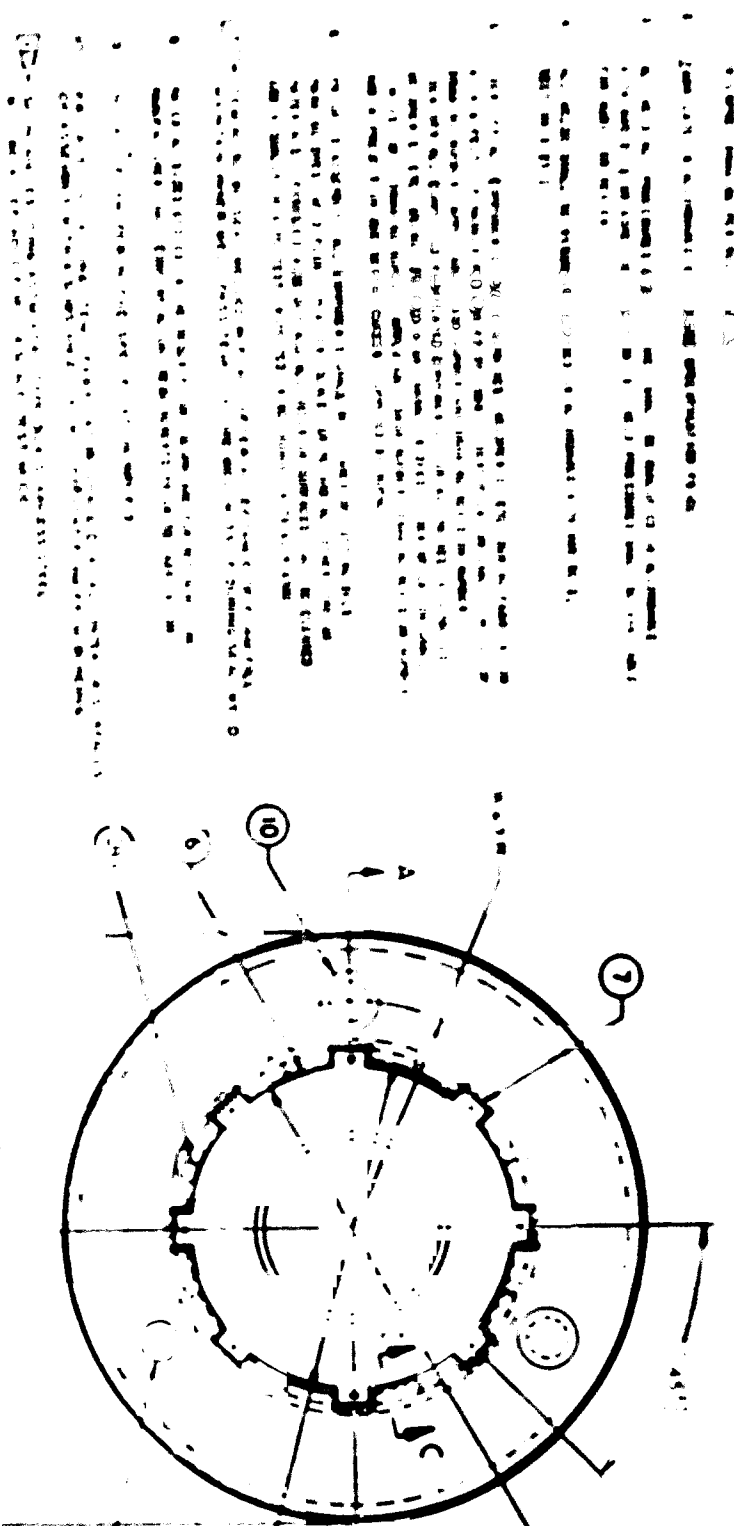
Figure 2-7. Overpacks With Attachment Bolts



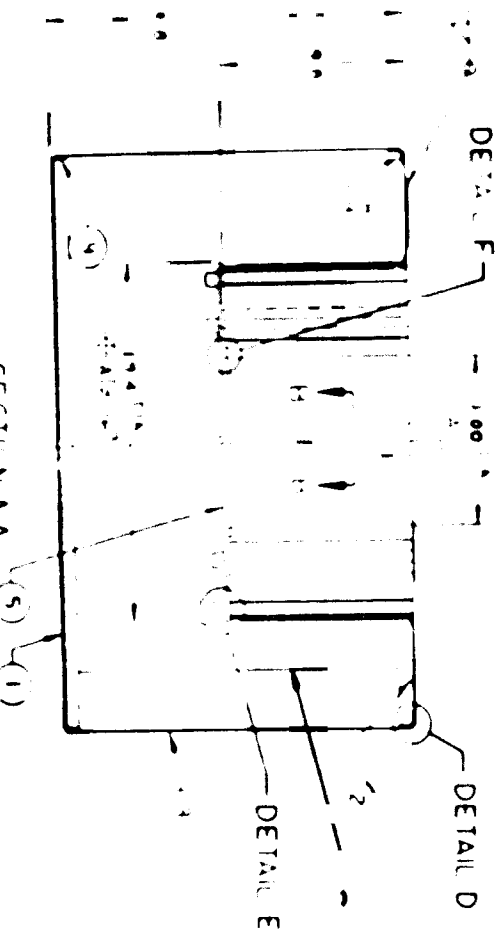
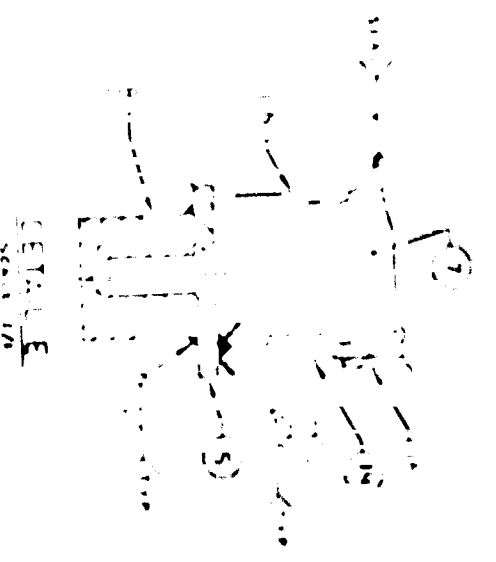
(A) ASSEMBLY

Figure 2-8. Assembly Drawing of the Model (NuPac Dwg No. SK-397) (from Nuclear Packaging, 1986)

ITEM 8
ITEM 9
ITEM 10
ITEM 11
ITEM 12



ALL ASSEMBLY



DETAIL D
SCALE 2

DETAIL F
SCALE 1/1

ITEM NO.	DESCRIPTION	QUANTITY	UNIT	REMARKS
1
2
3
4
5
6
7
8
9
10
11
12

Figure 2-11 Drawing of the Model Overpacks (Nuclear Power No. X 101 200) (from Nuclear Power Magazine 1950)

2.5 Coordinate System for NuPac 125-B Quarter Scale Model and Location of Instrumentation

Eight accelerometers and five strain rosettes were specified by DT-04.

Transducers were required to conform to the following requirements:

Strain Range:	3%
Accelerometer Range:	± 750 g's
Operating Temperature:	-40°F to $\pm 120^{\circ}\text{F}$
Frequency Response:	Flat within $\pm 10\%$ up to 5 kHz

Figure 2-12 shows the coordinate system used for the model, and the transducer locations and orientations with respect to this coordinate system. These transducer locations and orientations were used for all tests performed. Three additional accelerometers (A9, A10, A11) were installed on the mounting blocks opposite accelerometers A2, A5, and A8 after the oblique drop test.

The planned relationship between inner vessel components and the cask coordinate system is shown in Figure 2-13. The coordinate system shown in Figure 2-13 was described in the test plan and used for the dimensional inspection. Figure 2-14 shows the relationships among the inner vessel, the inner vessel lid, and the outer cask body when the model was assembled for testing. These components were marked and assembled as shown for each test conducted.

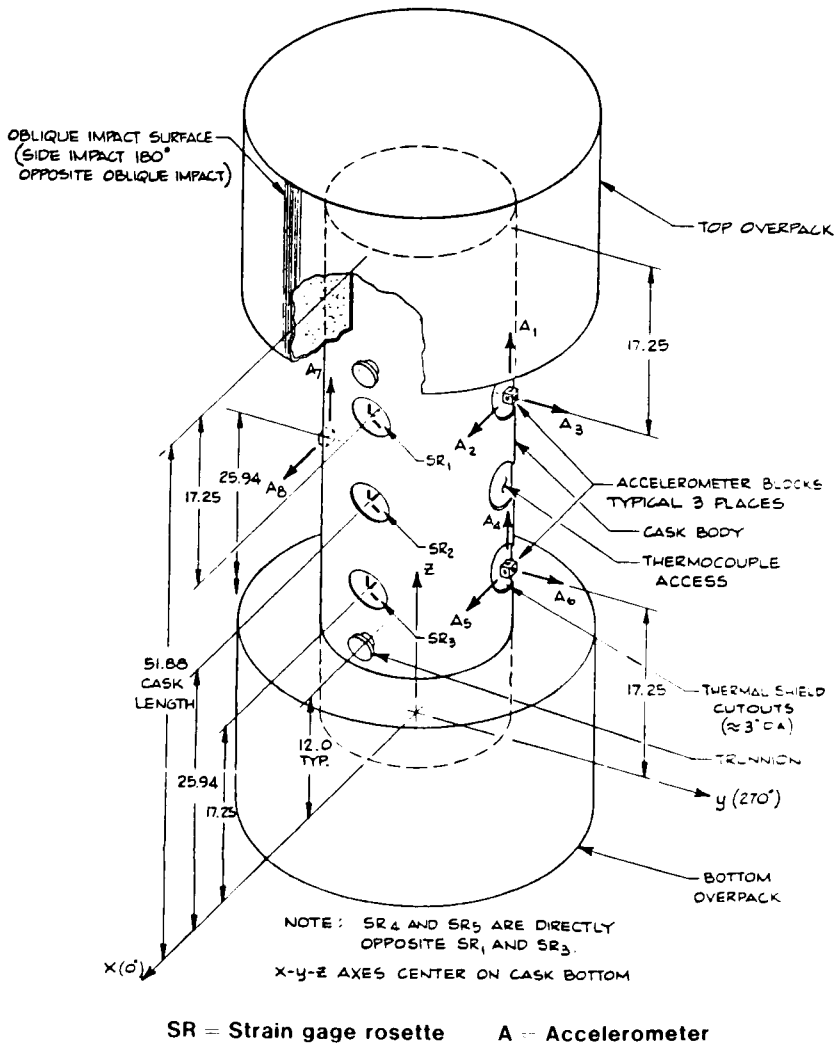


Figure 2-12. Coordinate System for NuPac 125-B Quarter Scale Model, and Transducer Locations and Orientations

2.6 Aerial Cable Facility, Sandia National Laboratories, Albuquerque, NM

The Aerial Cable Facility suspension mechanism consists of a wire rope cable suspended across a mountain canyon as illustrated in Figure 2-15. This load-bearing cable may be raised and lowered above the impact surface from 0 to 61 m (200 ft); the cable can support proportionally heavier loads at lower elevations. The load at 61 m (200 ft) is 1360 kg (3000 lb), whereas the load at 15 m (50 ft) is 4540 kg (10 000 lb).

The unyielding target is an extensively reinforced 2.4×10^5 -kg (5.3×10^5 -lb) mass of concrete and steel, ~6 m (20 ft) in diameter and 3.8 m (12.5 ft) deep, placed on top of tamped earth, faced with a 3×3 -m (10×10 -ft) slab of battleship armor plate, 7.6 to 12.7 cm (3 to 5 in.) thick. The steel facing is welded to the alloy steel-concrete reinforcing members and is grouted to the concrete plug with iron filings filled cement grout.

Two parallel wire rope cables were attached to the target and run vertically to a spreader beam mounted to the overhead cable as illustrated in Figure 2-16. The test unit was attached to a trolley with slider tubes that fit around the vertical cables. The trolley and test assembly were hoisted to the desired height. The test assembly was released by actuating guillotine cable cutters. The test assembly was then allowed to free fall to the impact target. The technique is repeatable, and impact can be determined accurately.

Figure 2-17 shows the test pad with stadia board. The pad has been swept and dampened in preparation for drop testing.

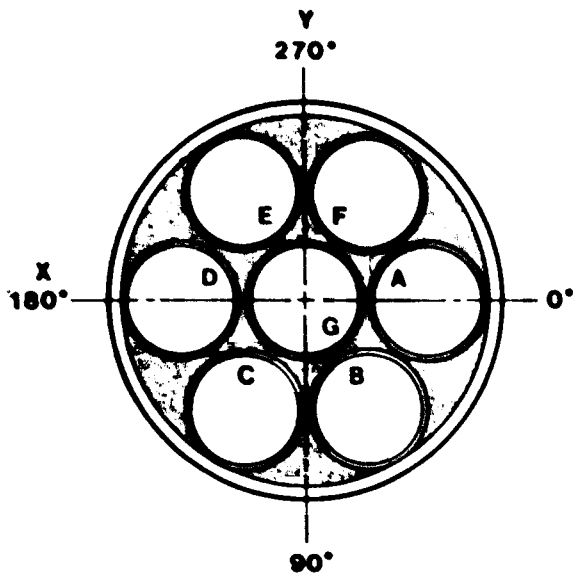


Figure 2-13. Planned Relationship Between Inner Vessel Components and the Cask Coordinate System

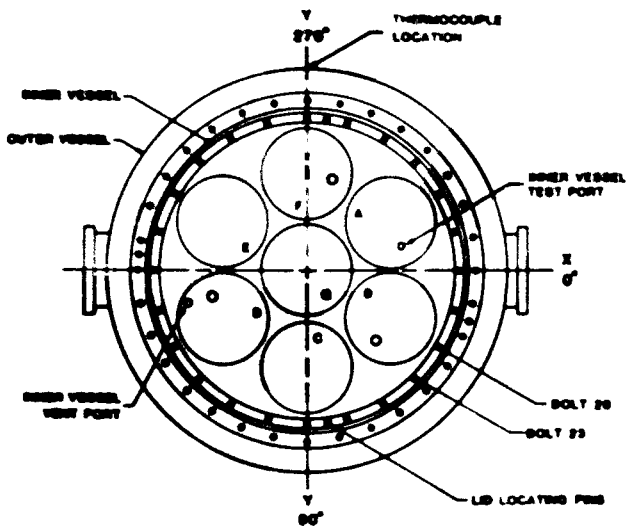


Figure 2-14. Actual Relationships Among Inner Vessel, Inner Vessel Lid, and Outer Cask Body for Testing

Aerial Cable Facility Description

MAIN SUSPENSION CABLE DIAMETER-3.175 cm (1.25 IN)
 CABLE CORE TYPE-FIBER
 BREAKING STRENGTH- 5.8×10^4 kg (126 000 LB)
 WEIGHT PER FOOT-1.19 kg (2.63 LB)
 HORIZONTAL DISTANCE BETWEEN CABLE SUPPORTS-823 M (2700 FT)
 VERTICAL DISTANCE MAXIMUM ABOVE GROUND ZERO-61 M (200 FT)
 LOAD RING HOISTING LINE DIAMETER-0.95 cm (0.375 IN.)
 CABLE STRENGTH-6818 kg (15 000)

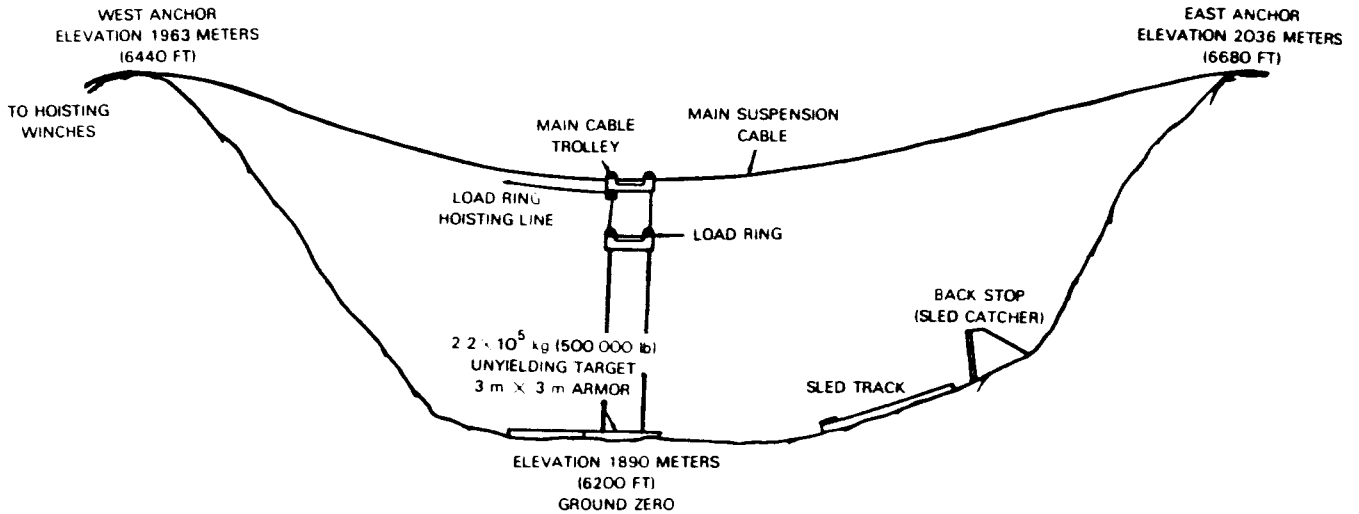


Figure 2-15. Aerial Cable Facility at Sandia National Laboratories, Albuquerque, New Mexico

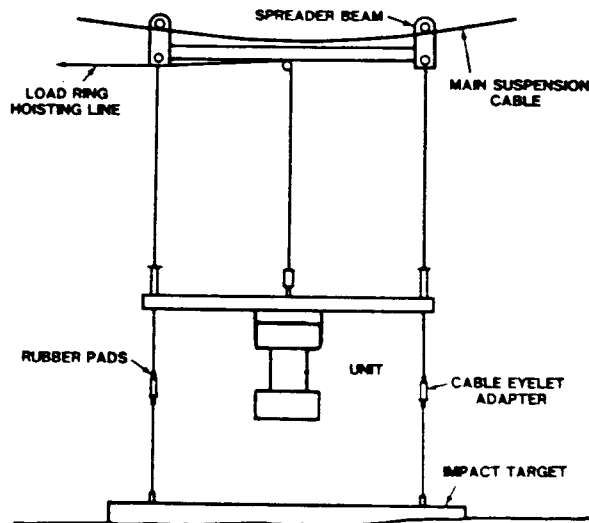


Figure 2-16. Mounting of Test Article on Aerial Cable Apparatus

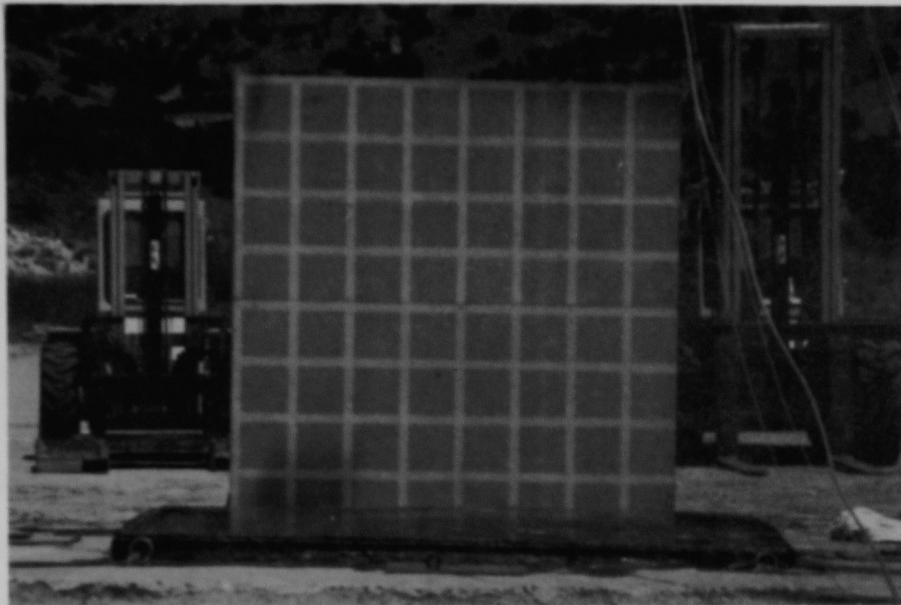
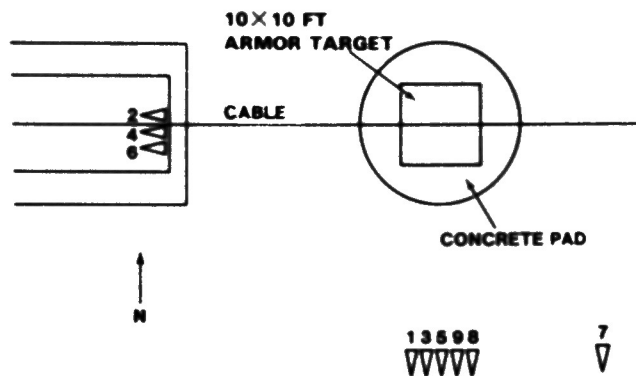


Figure 2-17. Test Pad With Stadia Board

2.7 Photometrics and Photographic Coverage

Photometrics and photographic data were recorded with the cameras listed in Table 2-4. The locations of the cameras with respect to the target are shown in Figure 2-18. Figure 2-19 shows some of the cameras used to document the tests.



Note: Numbers are explained in text.

Figure 2-18. Typical Camera Locations



Figure 2-19. Typical Camera Setup

Table 2-4. Cameras Used to Record Photometric and Photographic Data

No.	Camera Type	Lens (mm)	Camera Speed Setting (fps)
1	Video—color	17/102 zoom	video
2	Video—black and white	12.5/75 zoom	~ 500
3	2000 fps (16 mm)	254	~2000
4	2000 fps (16 mm)	2.8/105 zoom	~2000
5	400 fps (16 mm)	50	~ 400
6	400 fps (16 mm)	25	~ 400
7	24 fps real-time (16 mm)	12.5	24
8	Stills (35 mm)	80/200 zoom	5
9	150 fps (35 mm)	75/205 zoom	~ 150

Notes: See Figure 2-18 for typical camera locations.
fps = frames per second.

3. Initial Examination

3.1 Leak Test

The planned leak tests were not conducted when the cask and inner vessel arrived at Sandia because the O-ring seals had not been installed before the assembly was shipped.

3.2 Disassembly

3.2.1 Receipt of Model and Removal of Overpacks

The model was received in the horizontal orientation on a transport skid as shown in Figure 2-1. With the cask resting on the transport skid, the bolts attaching the overpacks to the cask were removed. The overpacks were then removed by sliding them horizontally from the ends of the cask. The eye bolts attached to trunnions on the sides of the cask were loosened to permit removal of the cask from the transport skid.

After lifting slings were attached to the eye bolts, the assembly was lifted in the horizontal orientation from the transport skid by a forklift. The cask was lowered, and wood blocking was placed under the ends of the cask. The lifting slings were repositioned, allowing the closure end to be raised until the cask was vertical. The cask was then lowered until the bottom end rested on the ground, and the lifting slings were removed.

3.2.2 Removal of Outer Vessel Lid

The lid bolts and vent plug on the lid of the cask were removed and eye bolts installed for the removal of the lid. After lifting slings were attached to the eye bolts, the lid was removed with a forklift, as shown in Figure 3-1. The O-ring grooves on the lid and sealing surface on the body of the cask were visually examined. There were no discernible marks or damage.



Figure 3-1. Removal of Cask Body Lid

3.2.3 Removal of Inner Vessel

Eye bolts were attached to the lid of the inner vessel, and the lifting slings were attached to the eye bolts and forklift. The inner vessel was pulled vertically from the cask and guided to prevent any scraping

of the sides of the two vessels. When the inner vessel neared the top of the cask, the lifting rate of the forklift was decreased so that the inner vessel would not swing against the sealing surface of the cask wall as it cleared the internal bore of the cavity. After the inner vessel cleared the top of the cask, the forklift was backed up, and the inner vessel was lowered in the vertical position. The slings and eye bolts were then removed from the lid of the inner vessel.

3.2.4 Removal of Inner Vessel Lid

The lid bolts and vent plug on the lid of the inner vessel were removed and eye bolts installed for the removal of the lid. After lifting slings were attached to the eye bolts, the lid was removed with a forklift. The O-ring grooves on the lid and sealing surface on the body of the inner vessel were visually examined. There were no discernible marks or damage.

3.2.5 Removal of Upper Internal Impact Limiters

Eye bolts were installed in the tapped holes in the upper impact limiters, which were lifted out by hand.

3.2.6 Removal of Canisters

Eye bolts were installed in the tapped holes in the canisters, and each canister was lifted out by hand.

3.2.7 Removal of Lower Internal Impact Limiters

Removal of the lower impact limiters was accomplished by attaching tape to the end of a wooden rod and reaching down into each of the cavities until the tape stuck to the individual impact limiters. The impact limiters were then slowly raised out of the vessel.

3.3 X-Radiography

X-radiography examination of the closure end of the cask body was accomplished by positioning the cask 32 ft 2 in. from the Linotron and then placing 8 × 10 in. x-ray plates 8 to 9 in. into the closure end of the cask body. After the exposure of the plate, the cask body was rotated 90° and another x-radiograph taken. None of these radiographs showed any anomalies.

The lower portion of the cask was x-radiographed by positioning 17 × 21-in. plates behind the body of the cask. After the exposure of the plate, the cask body was rotated 270° and another x-radiograph taken.

An anomaly ~3.75 in. up from the bottom (closed end) of the cask was observed on the 0° bottom x-ray plate, as shown in Figure 3-2.

3.4 Inspection

An initial inspection was performed to document the initial measurements of the cask components as the basis for determining the permanent deformations resulting from the tests. NuPac provided data sheets for the inspection that determined and defined where the measurements were to be made.

Before the model was inspected, all parts were thoroughly cleaned with methanol.

The inspection of the assembly was completed by the Mechanical Measurements Division at Sandia. Some model components exhibited relatively large deviations in diameters and straightnesses measured at different locations, compared to items usually inspected by the Mechanical Measurements Division. Nonstandard measurement methods had to be devised in some cases to measure these large deviations. Standard inspection equipment—such as micrometers, gage blocks, bore scopes, and dial indicators—was used to inspect the model. All equipment used had been certified by the National Bureau of Standards (NBS) and verified by Sandia QA. Figure 3-3 illustrates inspection of a canister.

After receiving the model, inspection personnel positioned individual parts on fixtures and marked the locations to be measured using permanent markers. This marking was required to facilitate the inspection process and assure repeatability of measurement locations for the three required inspections of the model. Tests were conducted to determine the accuracy and repeatability of the measurement techniques. The probable measurement inaccuracies (PMIs) for each inspection were recorded on the data sheets. Sandia and NuPac reviewed the PMIs before completion of the initial inspection and judged them to be acceptable.

The data from the initial inspection are contained in Appendix A.

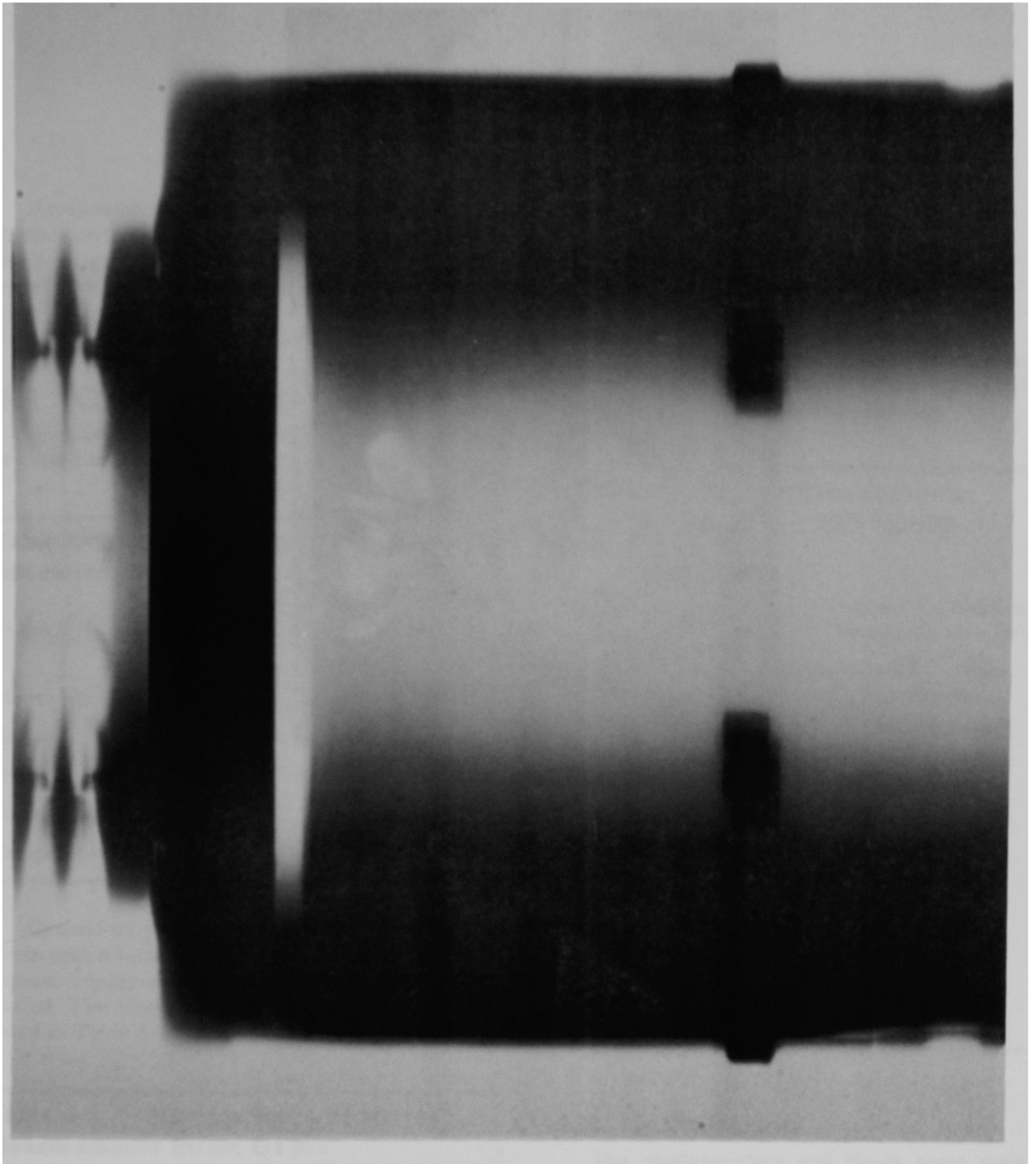


Figure 3-2. X-Radiograph of Bottom End of Cask Body at 0°

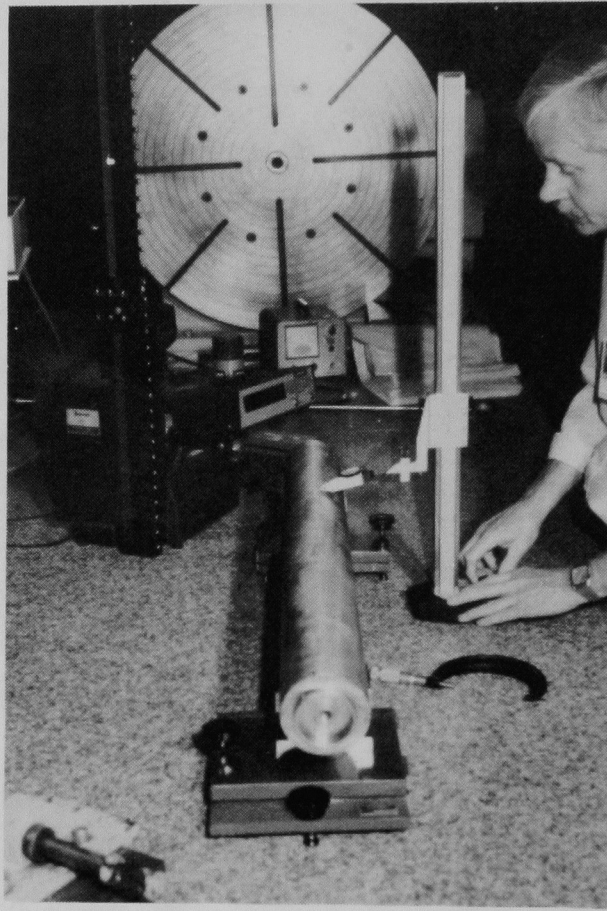


Figure 3-3. Inspection of a Canister

4. Instrumentation

Accelerometers and strain gage rosettes were used to measure accelerations and strains experienced by the package. The locations and orientations of the gages were defined by NuPac in DT-04. A total of eight Entran accelerometers and five strain gage rosettes were installed on the assembly (Figure 2-12).

4.1 Gage Characteristics

The characteristics of the Entran accelerometers are listed in Table 4-1.

Table 4-1. Characteristics of Entran Accelerometers

Type	Miniature Damped, (piezoresistive)
Model No.	EGANT-F-1000
Range	$\pm 1\ 000\ g's$
Over-range	$\pm 10\ 000\ g's$
Recommended Excitation	15.0 Vdc
Temperature Range	$-40^{\circ}F$ to $+250^{\circ}F$

General-purpose, stainless-steel, compensated strain gage rosettes, with fully encapsulated grids and exposed copper-coated integral solder tabs, were installed. The characteristics of the strain gages are listed in Table 4-2.

Table 4-2. Characteristics of Micro-Measurements Strain Gages

Gage Type	CEA-09-250UR-350
Strain Range	$\pm 5\%$
Temperature Range	$-100^{\circ}F$ to $+400^{\circ}F$

4.2 Calibration

Calibration of the Entran accelerometers was conducted by the Sandia Calibration Laboratory at $-20^{\circ}F$ on a shaker device. Measured sensitivities are given in Table 4-3 at an excitation of 15 V.

The test procedures used for the strain gage performance evaluation and gage factors for individual lots were supplied by the manufacturer.

Table 4-3. Sensitivities of Entran Accelerometers at $-20^{\circ}F$ (Model EGAXT-F-1000)

Serial Number	Initial Calibration Sensitivity at $-20^{\circ}F$ (mV/V/g)
21N50-A11-11	0.0165
21N50-A12-12	not measured
21N50-A13-13	0.0166
21N50-A14-14	0.0168
21N50-A15-15	0.0171
21N50-A16-16	0.0167
21N50-A17-17	0.0168
21N50-A18-18	0.0165
21N50-A21-21	0.0163
21N50-A22-22	0.0172

Note: Calibration performed on a shaker device.

4.3 Installation

The accelerometers and strain gages were installed on the model as specified in DT-04 and shown in Figure 2-12. Wires from the gages were routed to terminal strips attached to the model, as shown in Figure 4-1. All strain gage rosettes were oriented so that the "Z" gage was aligned with the z-axis of the

model, and the “Y” gage was aligned with the y-axis of the model. Figure 4-2 shows strain gage SR4 as installed on the model.

Table 4-4 lists initial installation location of each accelerometer.

Table 4-4. Initial Installation Location of Accelerometers on Model

Accelerometer Location	Accelerometer Serial Number
AZ1	21N50-A11-11
AX2	21N50-A21-21
AY3	21N50-A15-15
AZ4	21N50-A16-16
AX5	21N50-A18-18
AY6	21N50-A13-13
AZ7	21N50-A22-22
AX8	21N50-A17-17



Figure 4-1. Routing of Instrumentation Wires to Terminal Strips

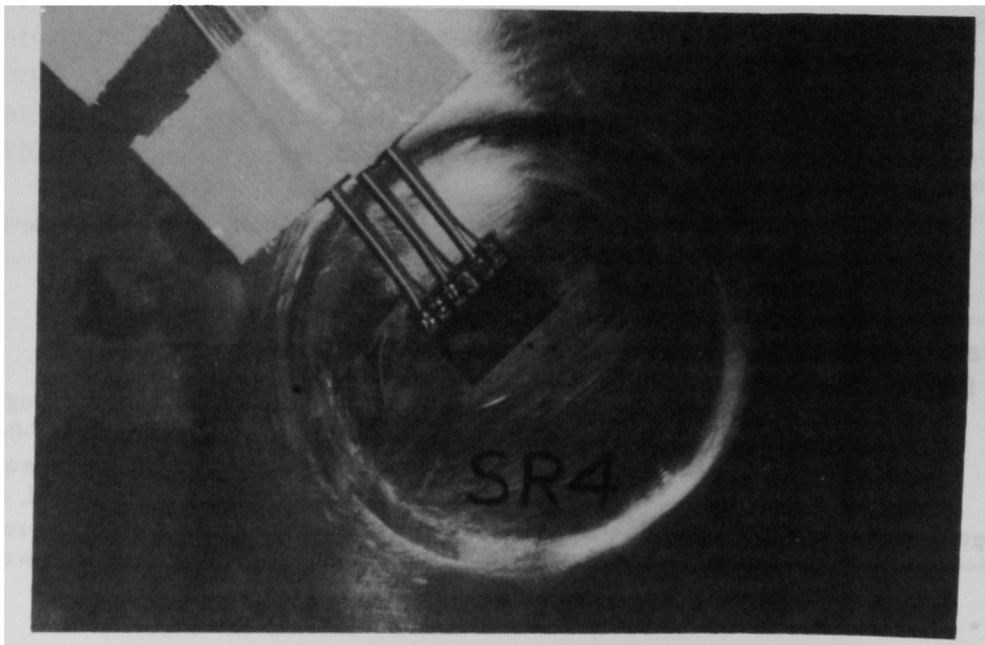


Figure 4-2. Strain Gage SR4 Installed

5. 30-ft Bottom End Drop Test

5.1 Assembly of Inner Vessel

The inner vessel was positioned vertically and thoroughly cleaned internally with rags dampened with methanol. Care was taken not to remove any marks used for the inspection process. It was believed that the removal of the lower impact limiters would be impossible after the drop tests unless the lower impact limiters were modified. Therefore, 1/2-13 UNC holes were drilled and tapped through the top stainless-steel plates of the impact limiters so that eye bolts could be attached to the impact limiters for their removal. The lower internal impact limiters were then cleaned with rags dampened with methanol.

The canisters, upper and lower internal impact limiters, and cells within the inner vessel had been marked by NuPac so that the model could be reassembled with all components in their initial locations and orientations. For example, the canister and upper and lower impact limiters belonging to cell A were marked with an "A" and the components oriented so that all scribed marks were aligned.

The interior surface of the inner vessel lid, the O-ring grooves on the inner vessel lid, and the O-rings were thoroughly cleaned with Kimwipes dampened with methanol. The O-rings were greased with Apiezon vacuum grease and installed in the grooves. After the sealing surface of the inner vessel was greased with Apiezon, the lid was positioned over the

alignment pins. Figure 5-1 shows the relationship of the inner vessel cells with the alignment pins. The lid was slowly lowered until the lower O-ring rested on top of the tapered region of the sealing surface bore. The lid was then forced down into position, and the bolts were installed and torqued to 28 in.-lb (Figure 5-2).

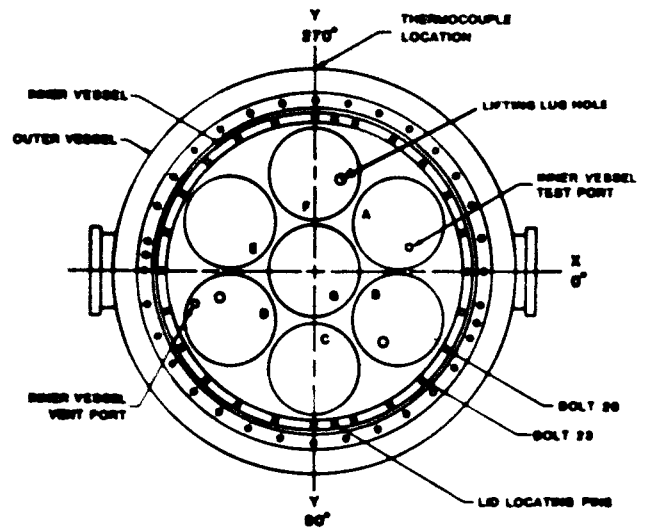


Figure 5-1. Sketch of Inner Vessel Showing Cells and Alignment Pins

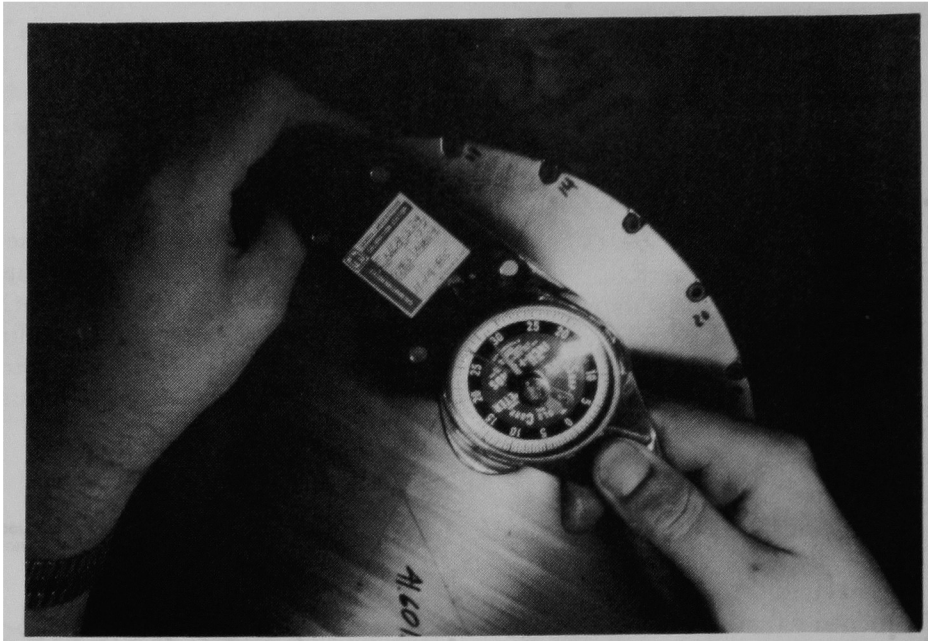


Figure 5-2. Inner Vessel Lid Bolts Being Torqued to 28 in.-lb

5.2 Leak Testing of Inner Vessel

The helium mass spectrometer leak detector was zeroed and calibrated according to the manufacturer's instructions and vented. Hardware was attached for leak testing of the inner vessel.

The test assembly was enclosed in a plastic bag envelope. The leak test hardware was attached to the vent port on the lid and the cavity evacuated to the standard operating pressure for the leak detector. The process of evacuating the vessel was very slow, probably because of outgassing from the cutting fluid used to drill and tap the holes in the lower internal impact limiters and from the adhesives used to bond the stainless-steel skins to the sides of the upper and lower impact limiters. The plastic bag envelope was pressurized with helium, and the leak detector was monitored. When the leak detector reading stabilized, the reading was recorded. This method is the A3.10.2 Pressurized Envelope procedure referenced in the ANSI leakage test standard (ANSI 14.5-1977). The helium leak rate for the inner vessel cavity was 9.0×10^{-9} cm³/s.

After the plastic bag envelope was removed from the inner vessel assembly, the leak test hardware was removed from the vent port and attached to the test port on the lid. The space between the O-rings was evacuated to the standard operating pressure for the leak detector. The inner vessel cavity was evacuated

and pressurized with helium. The leak detector was monitored, and the reading was recorded after it stabilized. The helium leak rate for the pair of inner vessel O-rings was 2.3×10^{-7} cm³/s.

5.3 Assembly of Outer Vessel

The interior surface of the outer vessel was only vacuumed out and wiped down with dry rags because cleaning solvents could remove the inspection markings. The exterior surface of the inner vessel was carefully cleaned with rags dampened with methanol. Seven holes in the bottom of the inner vessel for release of radiolysis gases in the full-scale cask were filled with synthetic putty (Figure 5-3). The inner vessel was lowered into the outer vessel (Figure 5-4) and rotated to ensure proper alignment.

The interior surface of the outer vessel lid, the O-ring grooves on the outer vessel lid, and the O-rings were thoroughly cleaned with Kimwipes dampened with methanol. The O-rings were greased with Apiezon vacuum grease and installed in the grooves. After the sealing surface of the outer vessel was greased with Apiezon, the lid was positioned over the alignment pins and slowly lowered until the lower O-ring rested on top of the tapered region of the sealing surface bore. The lid was then forced down into position, and the bolts were installed and torqued to 20 ft.-lb.

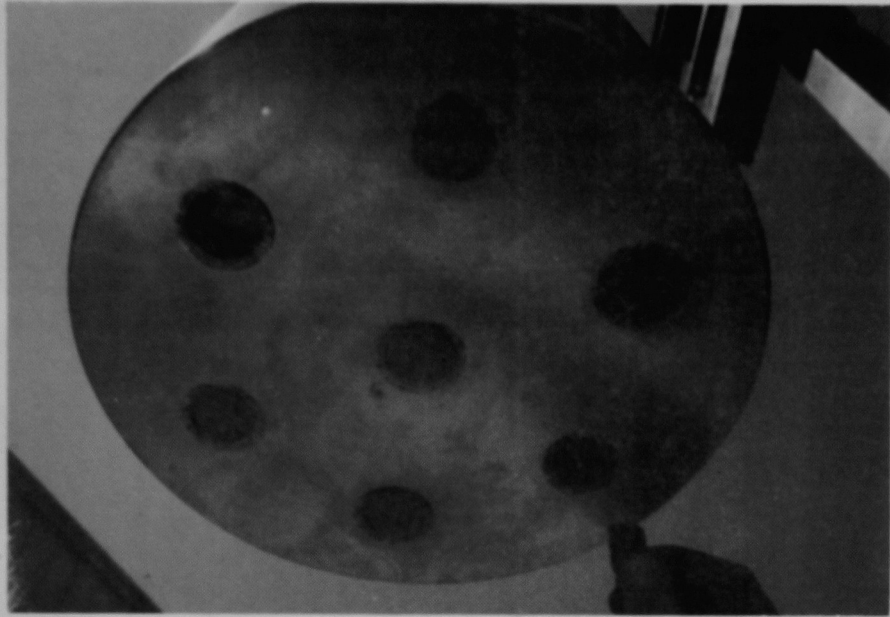


Figure 5-3. Synthetic Putty Plugging the Holes for Radiolysis Gases in the Bottom of the Inner Vessel



Figure 5-4. Inner Vessel Being Lowered Into the Outer Vessel

5.4 Leak Testing of Outer Vessel

The test assembly was enclosed in a plastic bag envelope as shown in Figure 5-5. The leak test hardware was attached to the vent port on the lid and the outer vessel cavity evacuated to the standard operating pressure for the leak detector. Here again, evacuation of the vessel was a very slow process, thought to be caused by outgassing. The interior surface of the outer vessel could not be thoroughly cleaned because of the inspection markings. The plastic bag envelope was pressurized with helium, and the leak detector was monitored. When the leak detector reading had stabilized, the reading was recorded. The helium leak rate for the outer vessel cavity was $3.5 \times 10^{-7} \text{ cm}^3/\text{s}$.

After the plastic bag envelope was removed from the outer vessel assembly, the leak test hardware was removed from the vent port and attached to the test port on the lid (Figure 5-6). The space between the O-rings on the outer vessel lid was evacuated to the standard operating pressure for the leak detector. The outer vessel cavity was evacuated and pressurized with helium. The leak detector was monitored, and the reading was recorded after it stabilized. The helium leak rate for the pair of outer vessel O-rings was $4.0 \times 10^{-8} \text{ cm}^3/\text{s}$.

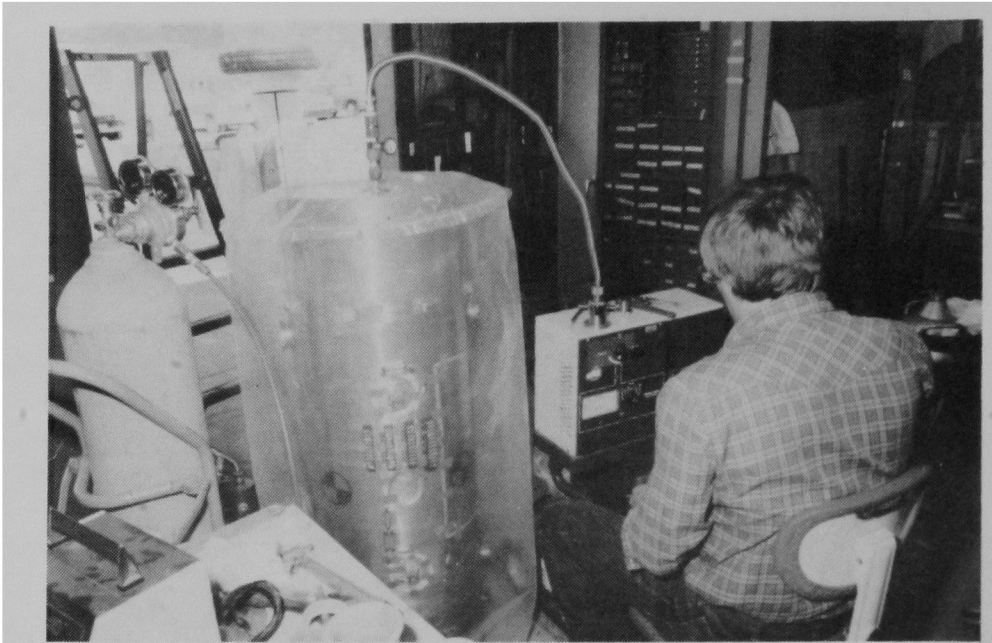


Figure 5-5. Plastic Bag Envelope Leak Test of the Outer Vessel

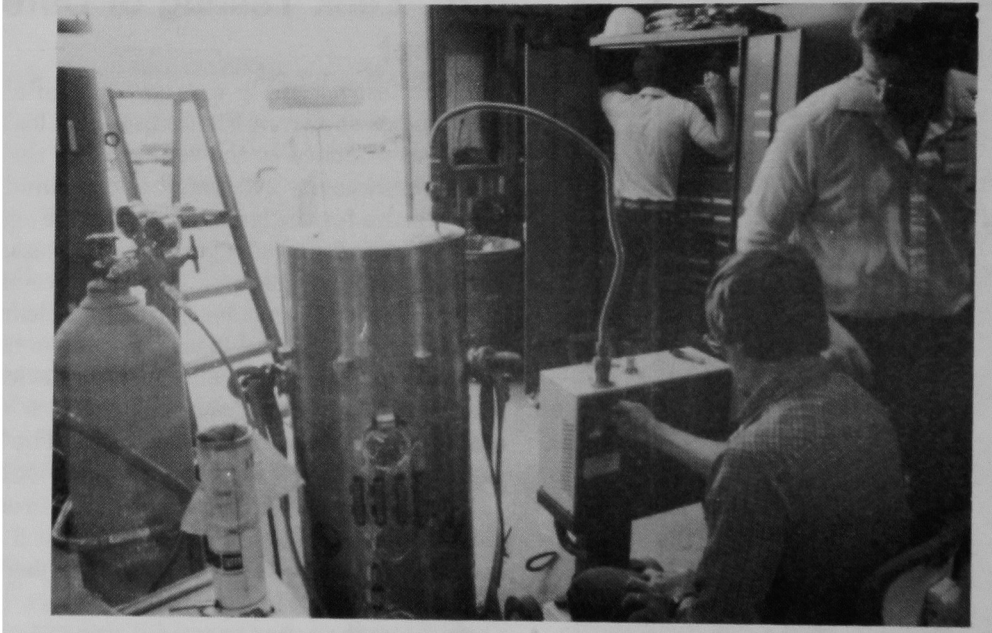


Figure 5-6. Leak Test of Outer Vessel Seal

5.5 Assembly of Overpacks

The model was positioned on the transport skid, and the overpacks were installed by sliding them horizontally onto the ends of the cask. After the overpacks were rotated to assure proper alignment, the bolts were installed and torqued to 70 in.-lb (Figure 5-7).

5.6 Chilling

The assembled cask was transported to the Sandia Shock and Climatic Division laboratory to be chilled. The cask and skid were positioned on a cart and placed inside a climatic chamber (Figure 5-8). The environmental temperature outside the climatic chamber was $\sim 68^{\circ}\text{F}$. Thermocouples inside the

chamber recorded the air temperature. One thermocouple was attached to the cask body at its midpoint, where the thermal shield had been ground away to expose the outer shell of the cask body (Figure 5-9). Two additional thermocouples were inserted into the small clearances between the thermal shield and the inner surfaces of the overpacks. The thermocouple attached to the cask body was covered with Cerablanket insulation to insulate it from the cold chamber air.

The thermocouple leads were routed through the wall of the climatic chamber and attached to temperature recorders. The chamber controls were adjusted to produce a -40°F environment. Figure 5-10 shows the model inside the climatic chamber during the chilling process.

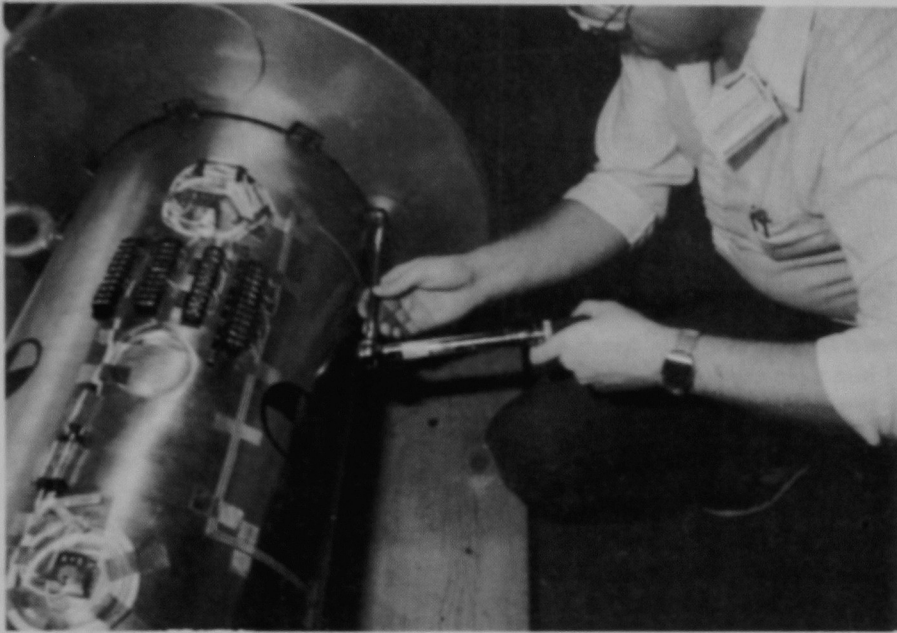


Figure 5-7. Overpack Bolts Being Torqued to 70 in.-lb



Figure 5-8. Model Being Positioned in the Climatic Chamber

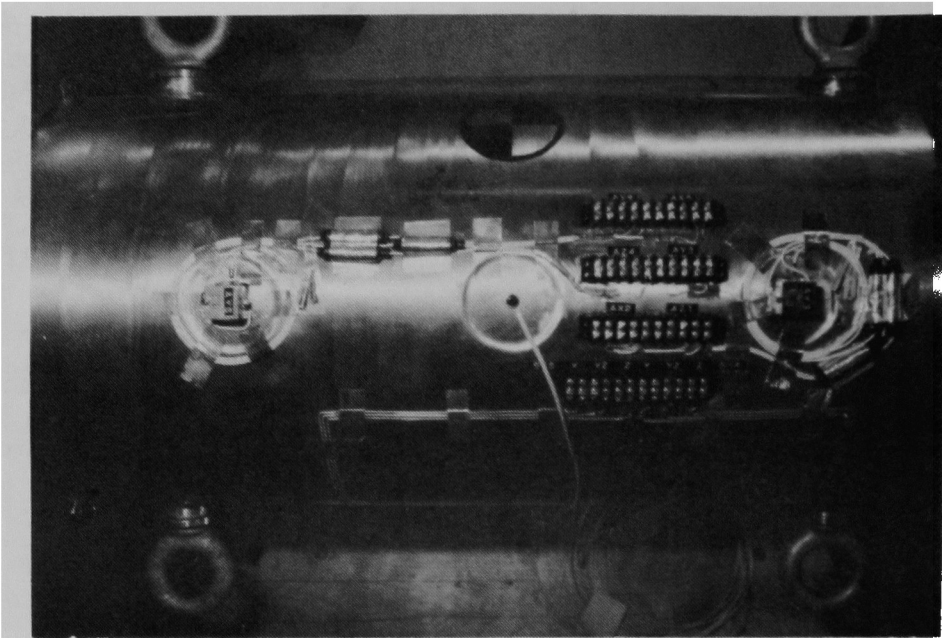


Figure 5-9. Thermocouple Attached to Model

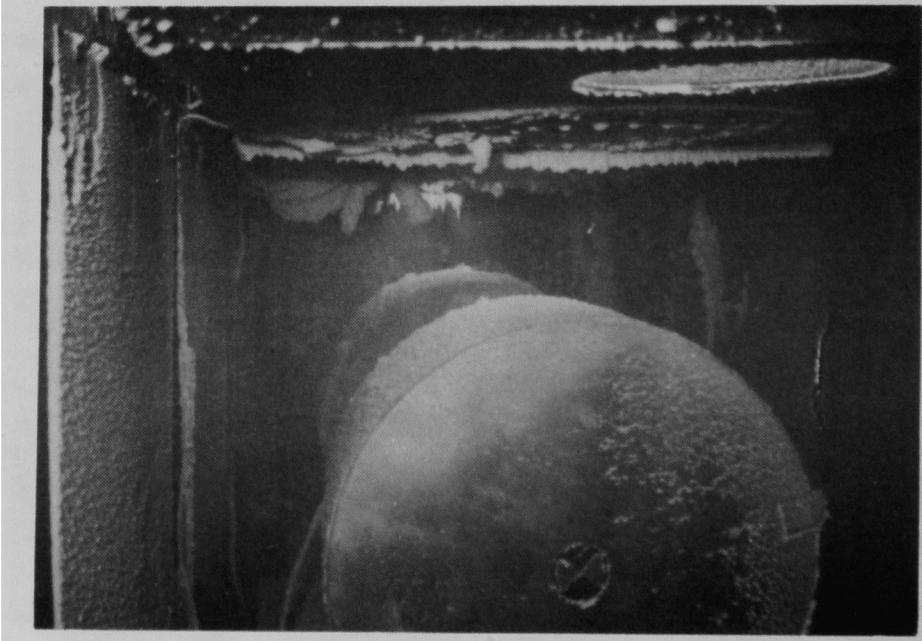


Figure 5-10. Model Inside Climatic Chamber During Chilling Process

For a thermally massive system with boundary conditions dictated by convective heat transfer, the temperature response is given by an equation exponential in form:

$$T_{\text{env}}(t) - T_s(t) = [T_{\text{env}}(t=0) - T_s(t=0)] \exp [(\ln 2/\tau_{1/2})t] \quad (1)$$

where

- T_s = surface temperature ($^{\circ}\text{F}$),
- T_{env} = temperature of the environment ($^{\circ}\text{F}$),
- $\tau_{1/2}$ = half-time constant (i.e., the time to reduce the initial temperature difference to half its value) (hr),
- t = elapsed time (hr).

A least-squares fit to the cool-down temperature data for the cask body thermocouple data using this equation resulted in a cool-down $t_{1/2}$ of 6.1 hr.

A second experiment was conducted to determine the rate at which the model would heat up without any insulation. A least-squares fit to the heat-up data using Eq (1) resulted in a $t_{1/2}$ for heat-up of 5.2 hr. The similarity between the $t_{1/2}$ values indicates that the convection coefficient for the heat-up phase is similar to that for the cool-down phase, and it is relatively constant over the applicable range of experimental test temperatures. Following this experiment, the model was returned to the climatic chamber and chilling continued.

A third experiment was conducted some 18 hr later to determine the rate of temperature rise if the model were insulated with Cerablanket. For this experiment, the entire model, including the overpacks, was covered with a layer of 1-in.-thick Cerablanket (Figure 5-11). The cask body itself was covered with two layers of the insulating blanket.

The temperature data for the model warming while covered with Cerablanket yielded a $t_{1/2}$ for heat-up of 30.8 hr. As expected, the heat-up half-time was much longer when the model was insulated.

After completion of the third experiment, the cask was again positioned inside the climatic chamber and the thermocouples were reattached. The Cerablanket insulation was removed from the cask and placed

inside the climatic chamber, and the chilling of the assembly was resumed.

The time behavior of the model surface temperature obtained from these experiments was used as input boundary conditions for modeling temperature behavior at other radial locations in the model, using the heat transfer code Q/TRAN (Rockenbach, 1984). The one-dimensional model used to approximate the geometry of the canisters, inner vessel, and cask body is shown in Figure 5-12. Nodes 1 through 16 represent points within the inner vessel and contents, which were approximated by redistributing the volume of sand (used to simulate the fuel debris), BISCO (neutron shielding material in the inner vessel), and stainless steel into equivalent one-dimensional rings. Node 17 is in the middle of the air gap between the inner vessel and cask body. Nodes 18 through 25 represent points within the cask body. The thermal shield is represented by Nodes 26 and 27.

Two modes of energy transfer were used in the thermal analysis: (1) conductive heat transfer within the solid regions of the cask and (2) thermal radiation between the surface of the inner vessel and the cask body. Convection between the inner vessel and cask body was not considered because of the small gap distance (0.125 in.). Thermal radiation between the inner vessel and the cask body was modeled by using enclosure theory for graybody surfaces.



Figure 5-11. Cerablanket Insulation Covering the Model for the Time-to-Warm Calculation Verification Test

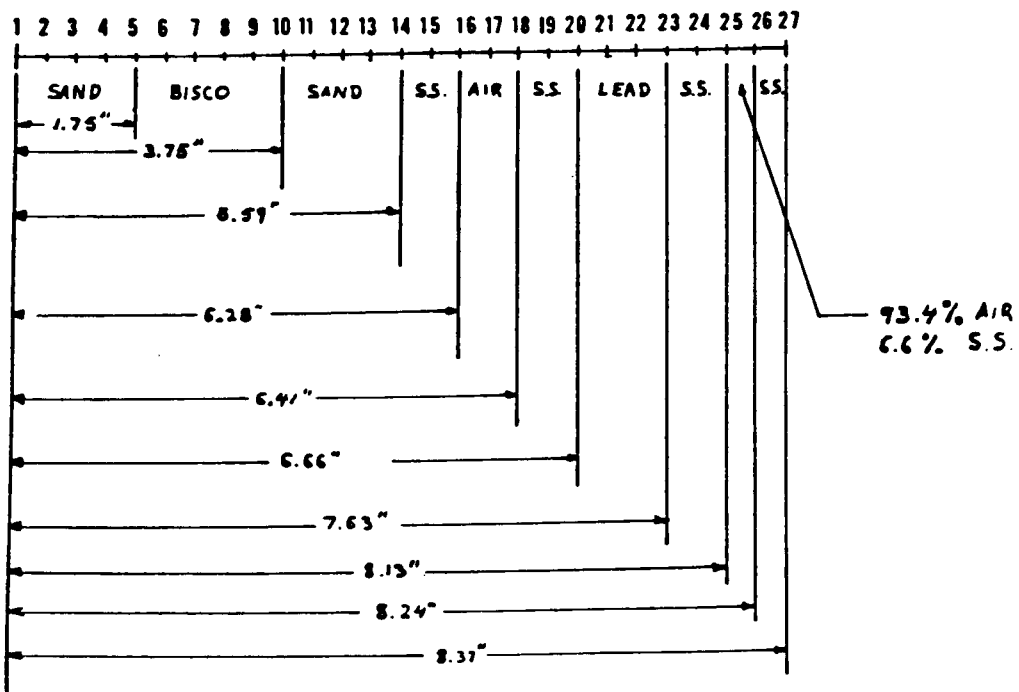


Figure 5-12. One-Dimensional Geometry Used for Transient Thermal Analysis of the Quarter Scale NuPac 125-B Cask

Experimental boundary conditions were used to control the surface temperature as a function of time. The boundary condition was applied to the outer surface at Node 27, even though experimentally the temperature was measured at Node 25. The calculations showed a temperature gradient across the thermal shield of $<0.5^{\circ}\text{F}$, which supports the choice of boundary condition.

The calculated temperatures at various radial locations for the model are plotted in Figure 5-13 for the entire chilling process. Three curves are shown: for Node 2 (close to the center of the model); for Node 16 (outer surface of inner vessel); and for Nodes 18, 25,

and 27 (cask body inner surface, outer surface, and thermal shield), which overlap on the figure. The innermost portions of the model were unaffected by fluctuations in external temperature that were of short duration. There was a very small temperature gradient across the cask body wall, including the thermal shield. However, there was a significant temperature gradient across the air gap between the inner vessel and the cask body. Therefore, the temperature response of the cask body, at least for short transient events, depends almost entirely on the surface temperature and not on the detailed modeling of the inner vessel.

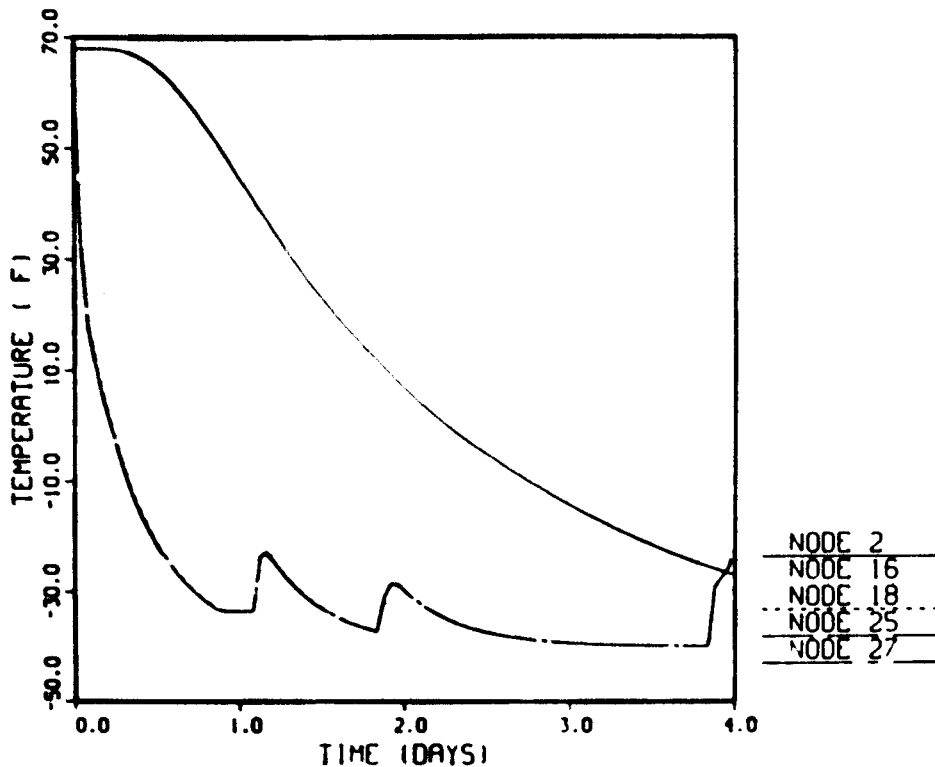


Figure 5-13. Temperature Response of the Quarter Scale NuPac 125-B Cask (see Figure 5-12 for node locations)

5.7 Bottom End Drop Test Procedure

The insulation blankets and the cart with the model were removed from the climatic chamber. The chilled insulation blankets were wrapped around and secured to the cask assembly, which was then placed on a truck (Figure 5-14) and transported to the drop test facility. There it was unloaded and placed on the unyielding target.

The rigging hardware, with guillotine cable cutters installed, was attached to the trolley on the overhead cable and to the eye bolts attached to the trunnions on the top portion of the cask body. Thermocouples were attached to the cask to record the temperature rise of the model while the final test

preparations were being completed. The unit was leveled by means of a turnbuckle in one of the rigging lines, and portions of the insulation blanket were removed for the attachment of the instrumentation cables.

The instrumentation cables were attached to the terminal strips and secured to a trunnion, and at the same time, the stadia boards were positioned, documentary photographs were taken, and the test procedure steps were verified and signed. Figure 5-15 shows the model rigged for the 30-ft bottom end drop test. After the data acquisition checkout was completed, the insulation blanket was removed (Figure 5-16). The thermocouples were removed and the assembly hoisted to the 30-ft drop height in final preparation for the test (Figure 5-17).



Figure 5-14. Chilled Insulated Model Loaded on Truck for Transport to Drop Test Facility

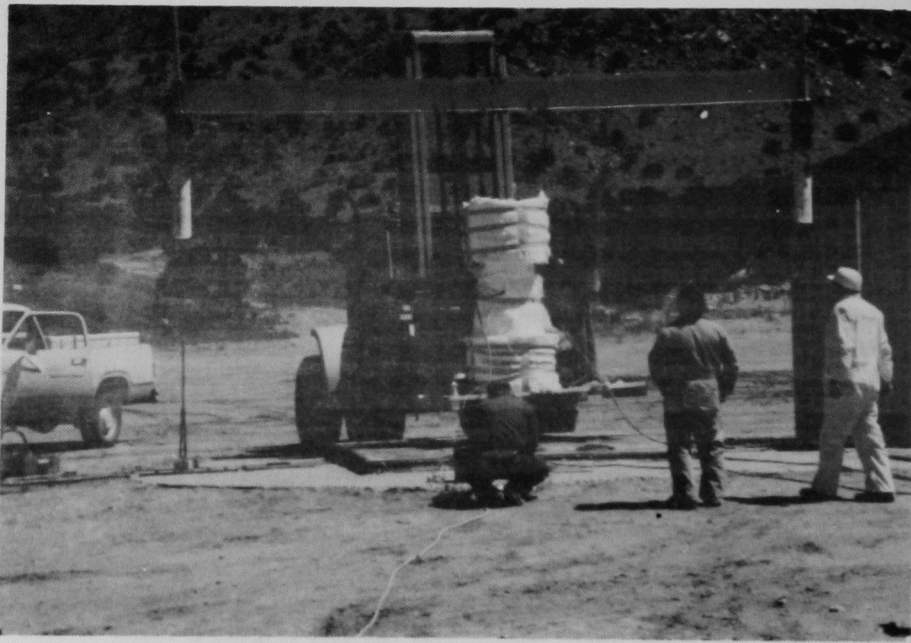


Figure 5-15. NuPac 125-B Model Rigged for the 30-ft Bottom End Drop Test



Figure 5-16. Removal of Cerablanket Insulation

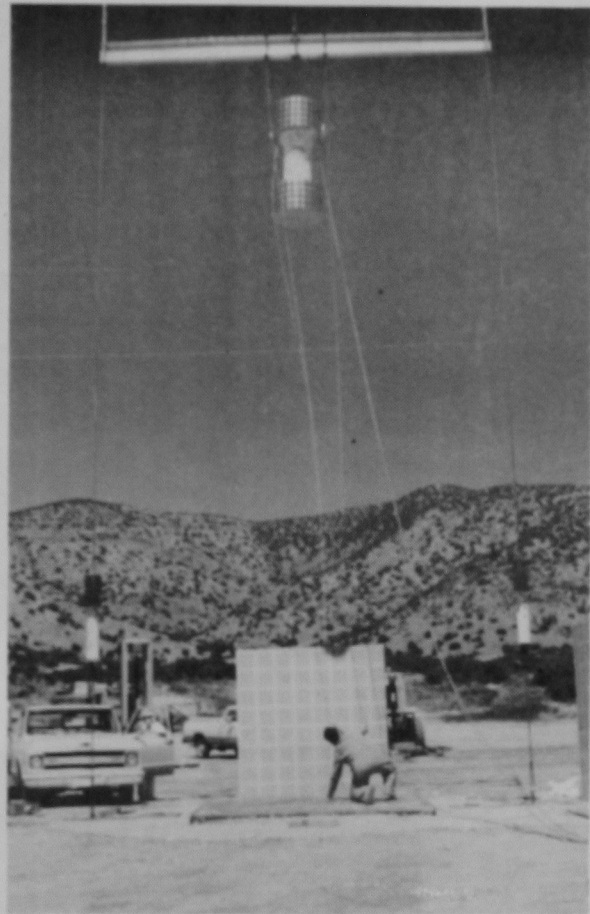


Figure 5-17. Drop Height and Orientation Verification Before the 30-ft Bottom End Drop Test

Approximately 4 hr after the unit had been removed from the climatic chamber, the guillotine cable cutters were actuated, and the model free fell to the impact target. Figure 5-18 shows the actual 30-ft bottom end drop test. Figure 5-19 shows the orientation of the tank when dropped.

A least squares fit to the model thermocouple data using Eq (1) resulted in a heat up $\tau_{1/2}$ of 30.5 hr while the model was insulated, at a maximum ambient temperature of 61°F. The insulation blanket was re-

moved from the model and the thermocouples were detached. The bottom end drop test was conducted 14 min later. The thermal model was used to predict temperatures in the model at the time of the test, using the heat-up $\tau_{1/2}$ of 5.2 hr determined in Section 5.6 for the uninsulated model. Temperatures in the model were calculated to range from -27°F (near the center) to -21°F (on the outer surface) at the time of the drop event.

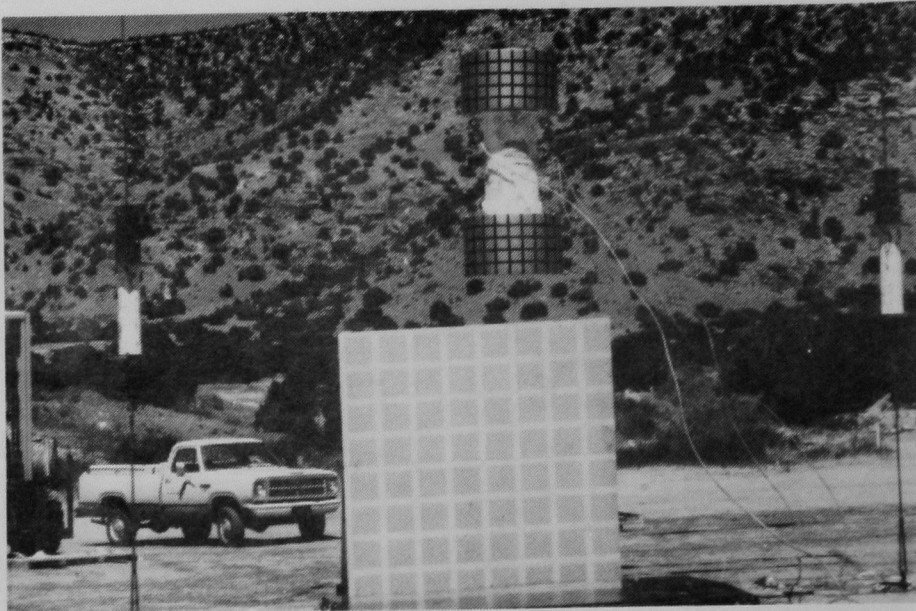


Figure 5-18. Sequential Photographs of the 30-ft Bottom End Drop Test

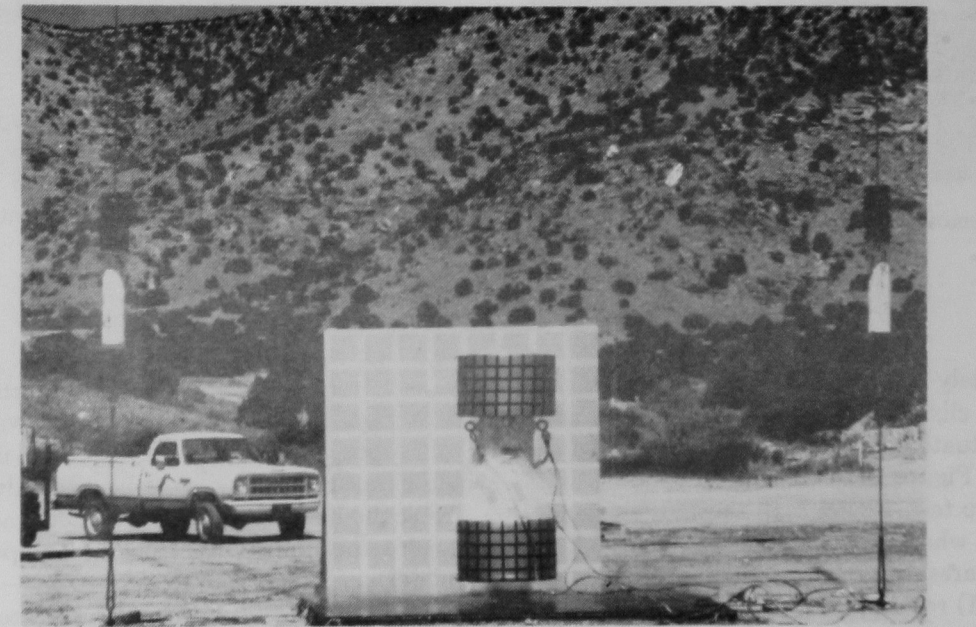


Figure 5-18. (continued)

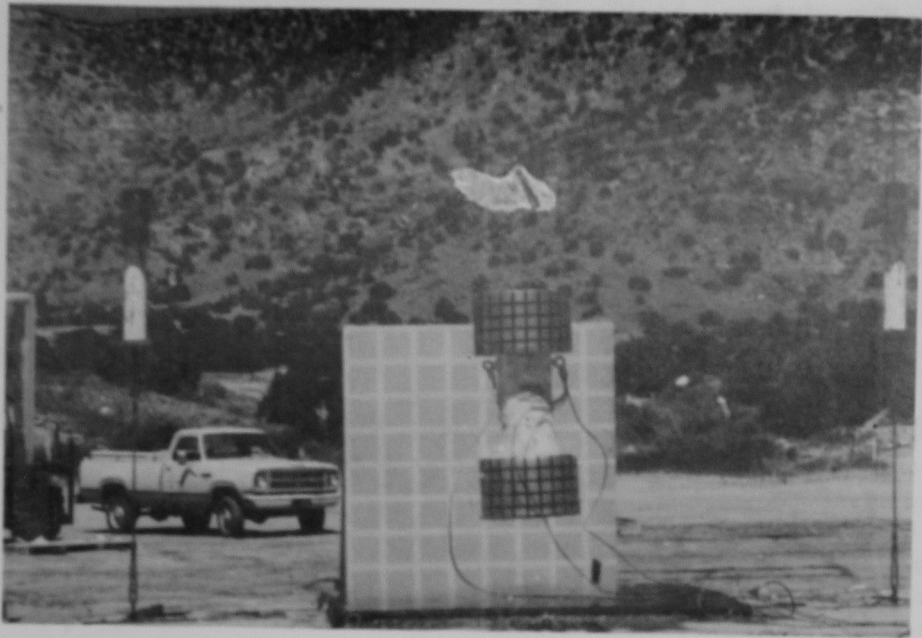


Figure 5-18. (continued)

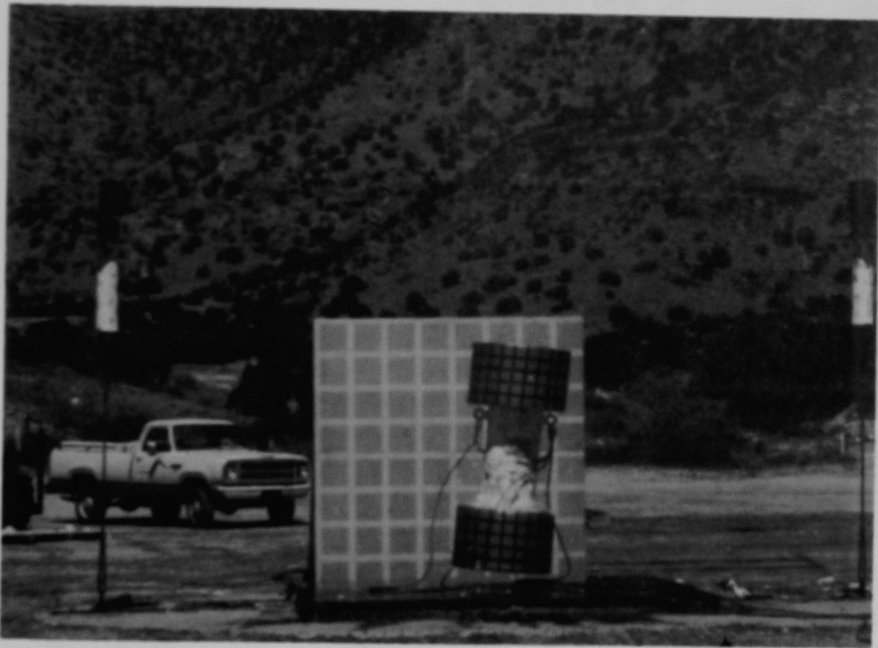


Figure 5-18. (continued)

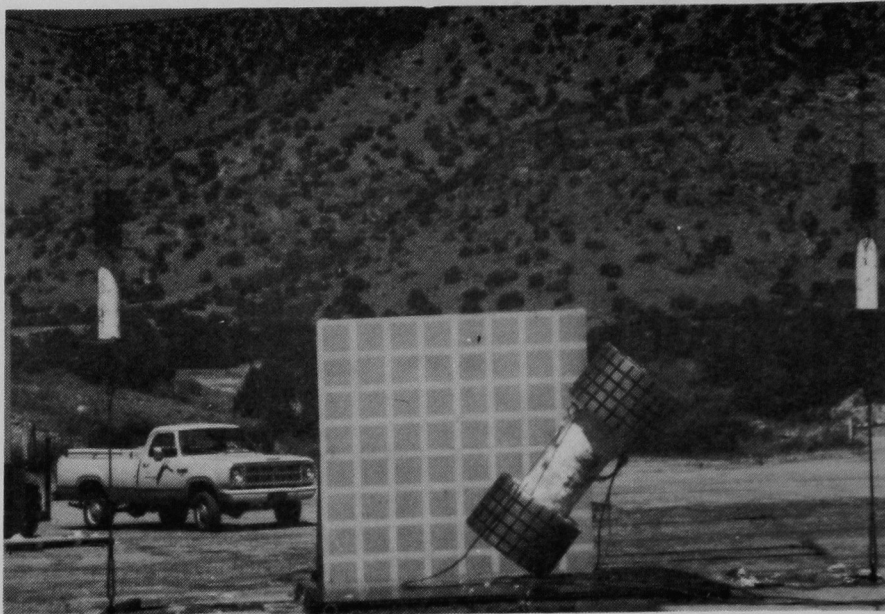


Figure 5-18. (continued)



Figure 5-18. (concluded)

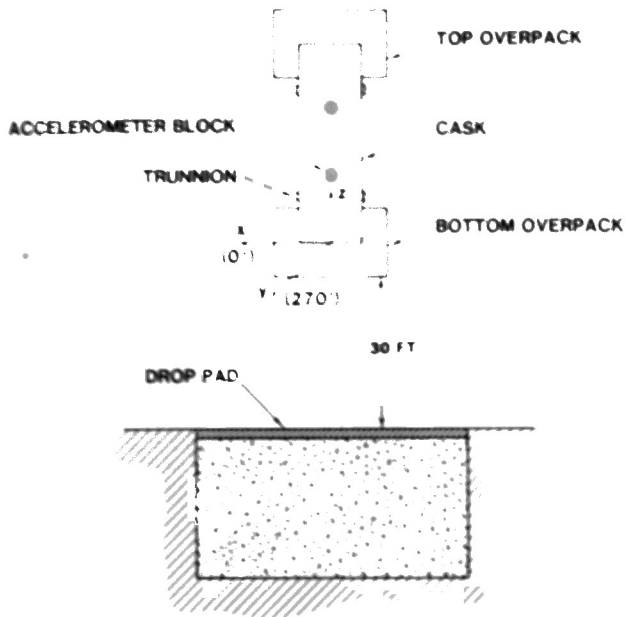


Figure 5-19. Orientation of Model for 30 ft Bottom End Drop Test (stadia board is behind model)

5.8 Photometrics Data

Photographs were made from one of the ~ 400 fps (frames per second), high speed, 16-mm cameras covering the test. The frame rate of the camera was determined by viewing the film, locating the frame at which impact occurred, and counting the frames near the impact frame with respect to the timing marks on the film. The frame rate for the camera was determined to be 383 fps. NuPac used 8 x 10 in. enlargements of these photographs to measure total overpack crush during impact.

5.9 Visual Observations

Figures 5-20 through 5-26 show the condition of the model after the test. The body of the cask appeared not to have been affected. Figures 5-21 through 5-23 show that the bottom impact limiter was deformed or "mushroomed"; Figures 5-24 and 5-25 show that the weld around the overpack bore diameter had partially failed. The surface of the impact limiter adjacent to the bore was deformed; however, there was no visible sign of exposed foam. The top overpack was damaged from the secondary impact of the model on the edge of the impact target (Figures 5-26 and 5-27).

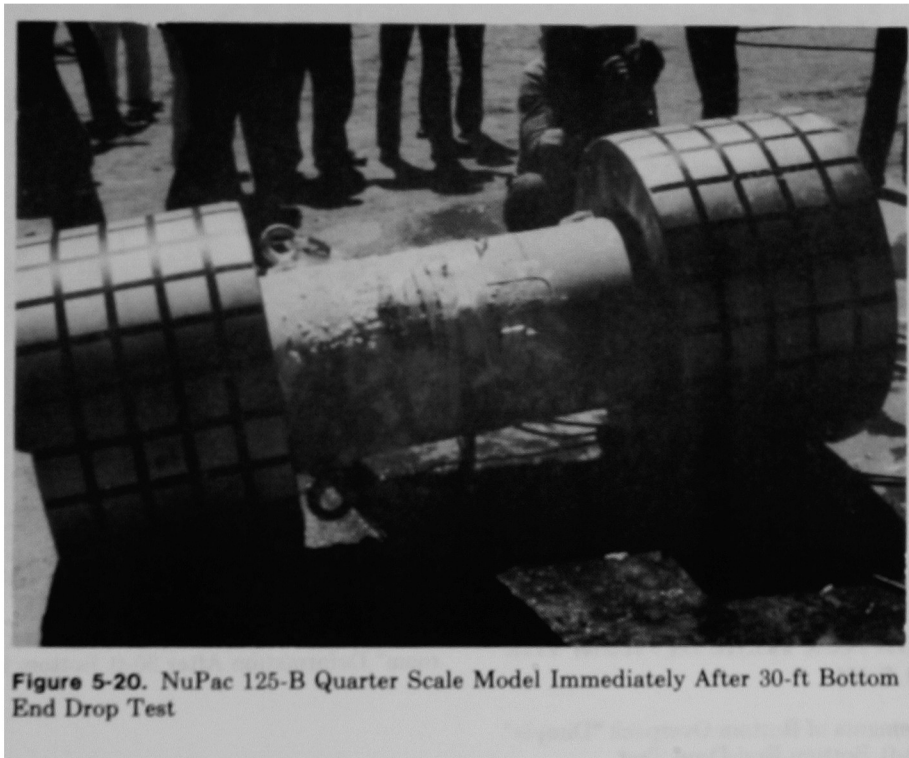


Figure 5-20. NuPac 125-B Quarter Scale Model Immediately After 30-ft Bottom End Drop Test

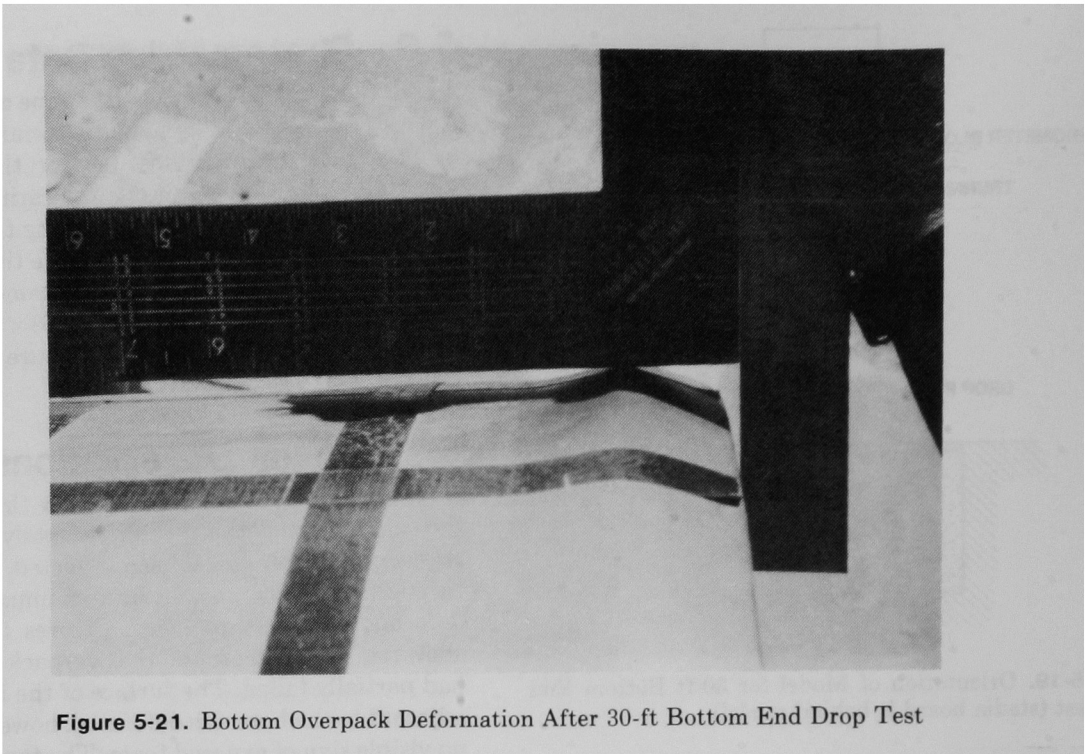
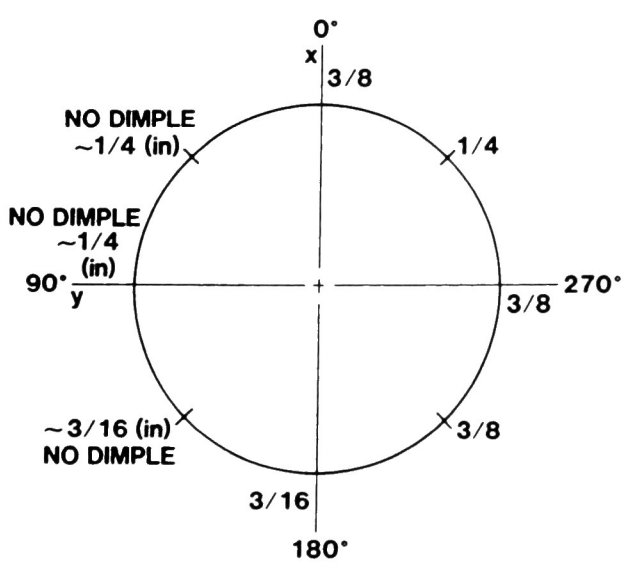


Figure 5-21. Bottom Overpack Deformation After 30-ft Bottom End Drop Test



NOTE: IMPACT LIMITER ~18-3/4 IN. HIGH. DIMPLES ON THE IMPACT END OF THE OVERPACK WERE IN FROM THE EDGE ~1.0 IN.

Figure 5-22. Measurements of Bottom Overpack "Dimple" Deformation After 30-ft Bottom End Drop Test

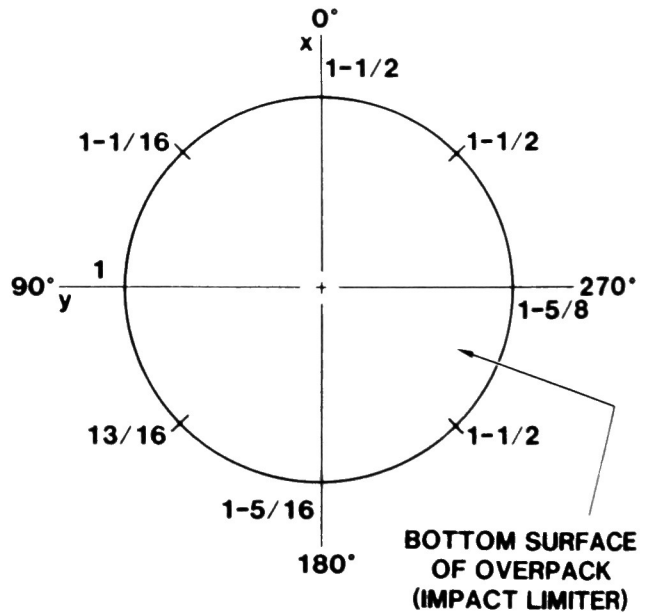


Figure 5-23. Measurements of Bottom Overpack "Mushroom" Deformation After 30-ft Bottom End Drop Test



Figure 5-24. Bottom Overpack Failed Weld After 30-ft Bottom End Drop Test

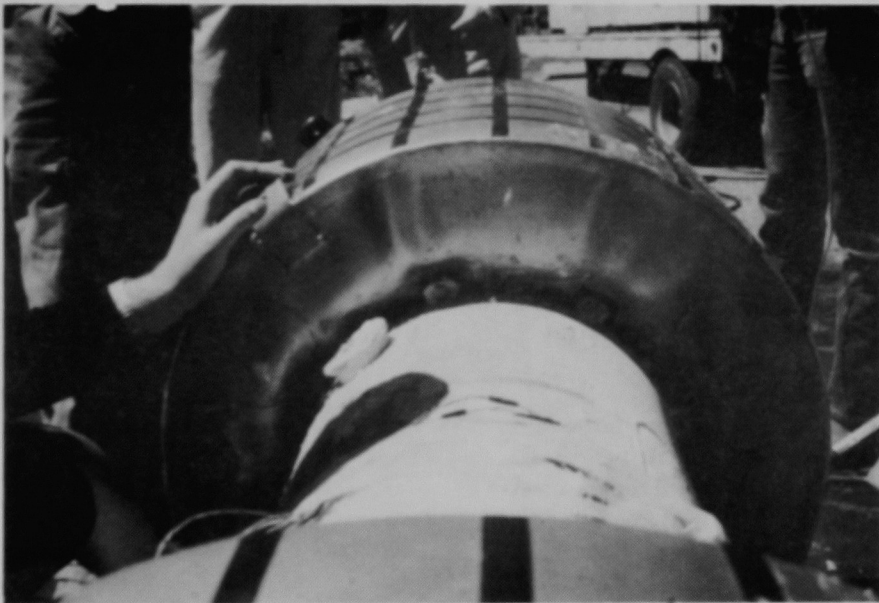


Figure 5-25. Weld Separation Around Inboard Seam of Bottom Overpack After 30-ft Bottom End Drop Test



Figure 5-26. Secondary Impact Damage to Top Overpack After 30-ft Bottom End Drop Test

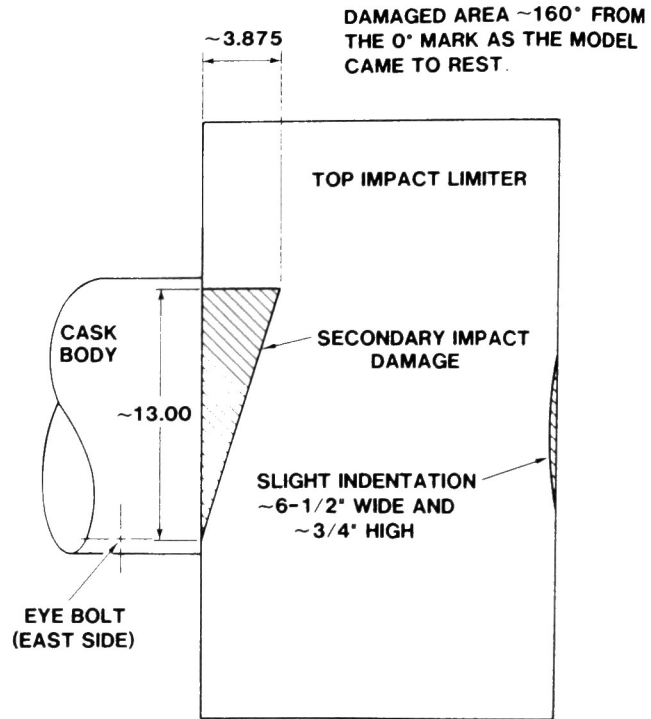


Figure 5-27. Measurements of Secondary Impact Damage to Top Overpack After 30-ft Bottom End Drop Test

5.10 Data Acquisition System Information

Accelerometer and strain gage data from the 30-ft bottom end drop test are contained in Appendix B1. The data were filtered at 1000 Hz, based on engineering judgment and the fast Fourier transforms of the unfiltered data (presented in Appendix B2), which give the frequency response of the model. The consistency and validity of the data are evaluated in Chapter 14.

6. 30-ft Oblique Drop Test

The cask was first rigged for the oblique drop test. The rigging hardware, with guillotine cable cutters installed, was attached to the trolley on the overhead cable and to the eye bolts attached to the trunnions on the bottom portion of the cask body. The unit was oriented by means of a turnbuckle in one of the rigging lines. The orientation was measured with an inclinometer and adjusted to obtain a 62° angle on the body and a $62^\circ 25'$ angle on the lower impact limiter (Figure 6-1).

6.1 Chilling

Thermocouples were attached to the cask to record the temperature of the model while the assembly was chilled for the test. The instrumentation cables

were attached to the terminal strips and secured to a trunnion. The cooling shroud was positioned around the model as shown in Figures 6-2 and 6-3. The thermocouples were routed through the wall of the cooling shroud and attached to a temperature recorder. The instrumentation cables and rigging cables were routed through the top of the shroud and all openings were sealed with Cerablanket. The shroud was connected to a controller, which was connected to a supply of liquid CO_2 . The controller was set at -40°F to chill the model overnight to the required temperature.

The supply of liquid CO_2 was disconnected the following morning at about 10:10 a.m. to allow the cask to warm while inside the cooling shroud from -40°F to a temperature between -25°F and -20°F for the oblique drop test.

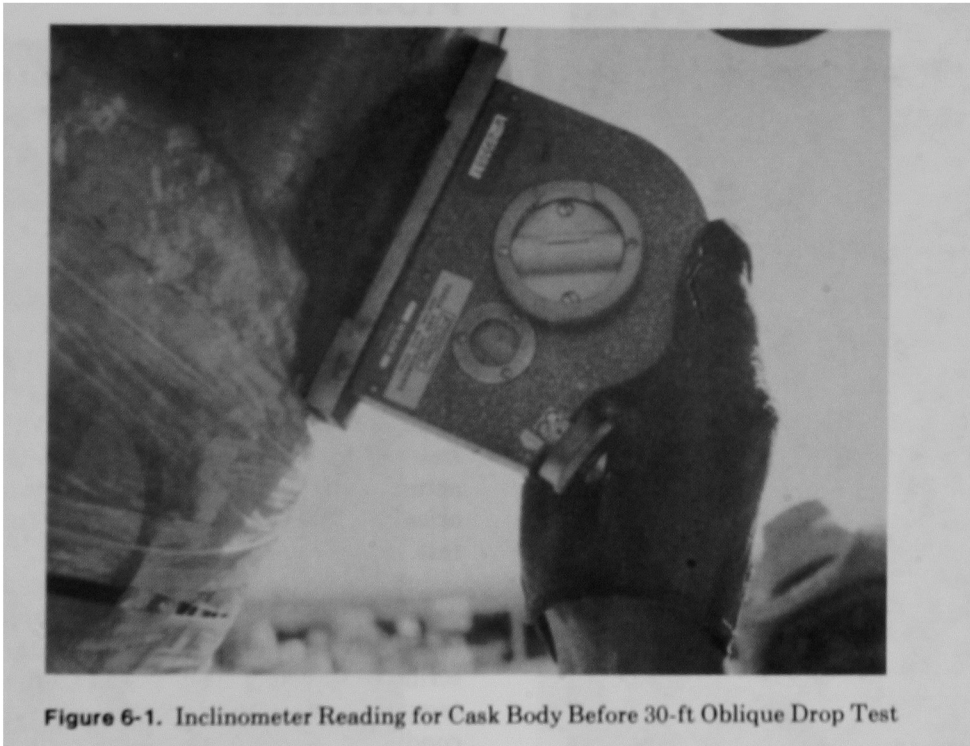


Figure 6-1. Inclinometer Reading for Cask Body Before 30-ft Oblique Drop Test



Figure 6-2. Positioning of Cooling Shroud Around Model

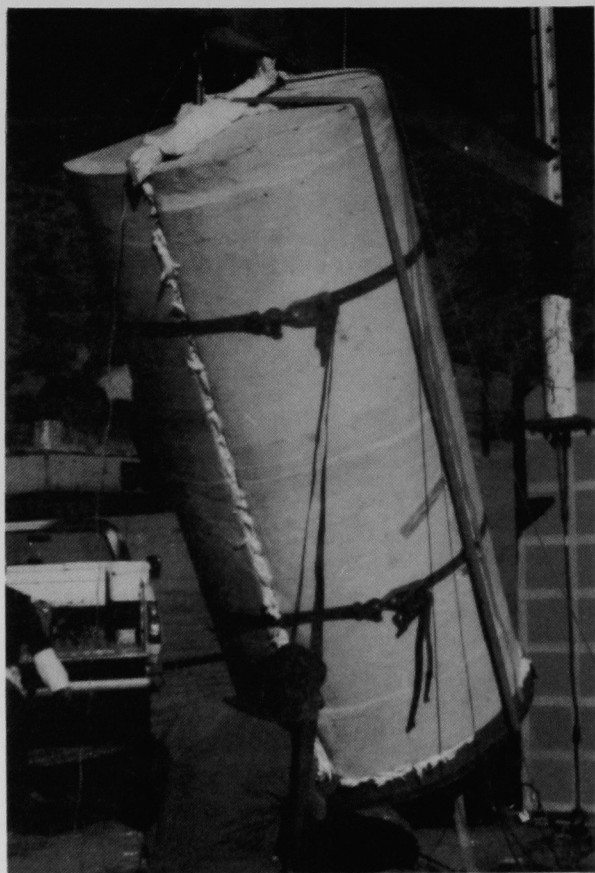


Figure 6-3. Model Installed in Cooling Shroud

6.2 Oblique Drop Test Procedure

The stadia boards were positioned, documentary photographs were taken, and the test procedure steps were verified and signed. After the data acquisition checkout was completed, the cooling shroud was removed (Figure 6-4). Figure 6-5 shows the model rigged for the 30-ft oblique drop test. The thermocouples were removed and the assembly hoisted to the 30-ft drop height in final preparation for the test (Figure 6-6).

Approximately 19 min after the unit had been removed from the cooling shroud, or 9 min after the thermocouples had been removed at the test site, the guillotine cable cutters were actuated, and the model free fell to the impact target. Figure 6-7 shows the actual 30-ft oblique drop test. Figure 6-8 shows the orientation of the model for the 30-ft oblique drop test.

A least-squares fit to the heat-up temperature data for the cask body thermocouple using Eq (1) resulted in a $\tau_{1/2}$ of 18.5 hr. The thermal model described in Section 5.6 was run to predict the model temperatures at the time the oblique drop test was conducted. Surface boundary conditions were determined by using a heat-up $\tau_{1/2}$ of 5.2 hr before the model was placed in the cooling shroud, a cool-down $\tau_{1/2}$ of 6.1 hr for forced convective cooling in the

shroud, and a heat-up $\tau_{1/2}$ of 18.5 hr while the model was inside the shroud after the coolant was disconnected. A higher heat-up $\tau_{1/2}$ of 4.0 hr was conservatively assumed for the 19-min period while the model

was outside the shroud and exposed to the sun. The ambient temperature was $\sim 75^\circ\text{F}$. Calculated model temperatures ranged from -26°F near the model center to -19°F on the surface.



Figure 6-4. Removal of Cooling Shroud

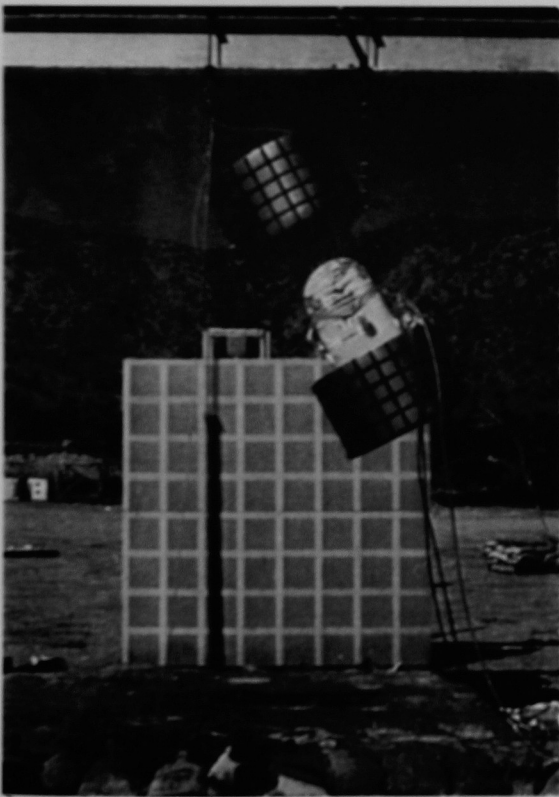


Figure 6-5. NuPac 125-B Model Rigged for the 30-ft Oblique Drop Test

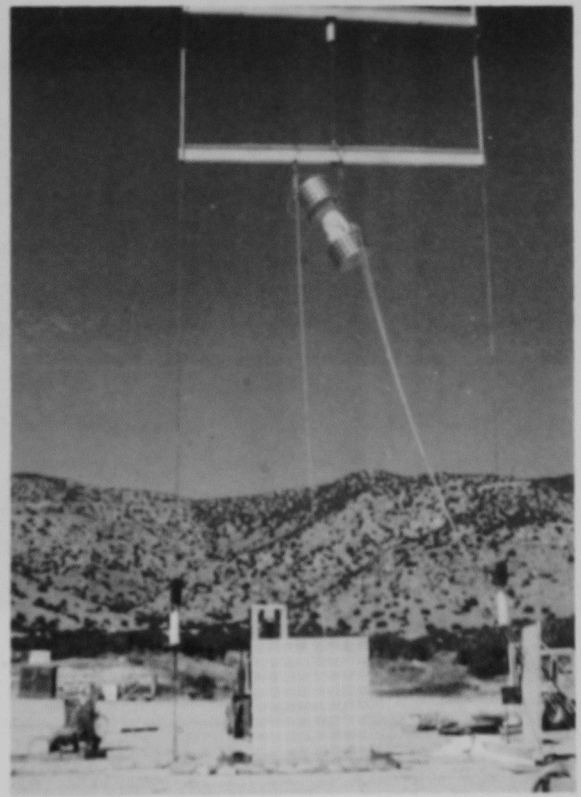


Figure 6-6. NuPac 125-B Model Elevated to 30 ft Before the 30-ft Oblique Drop Test

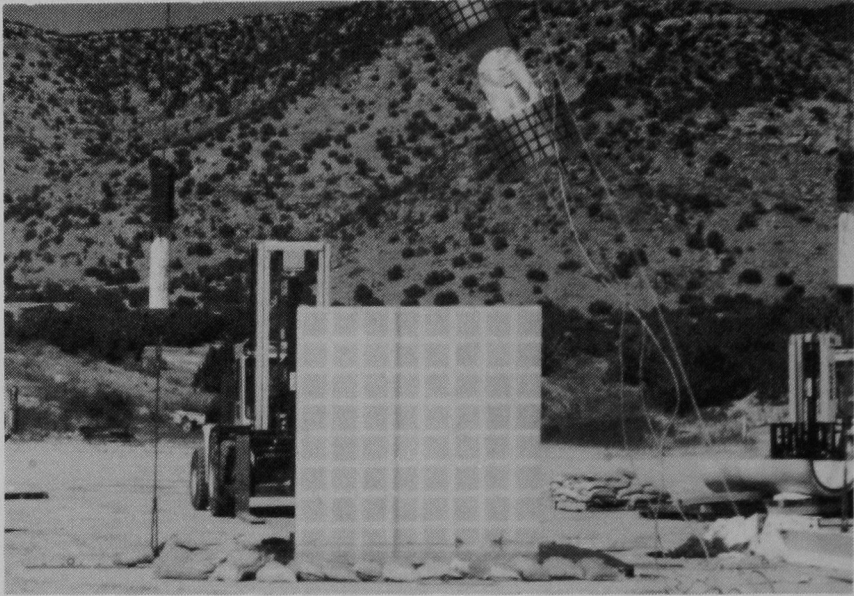


Figure 6-7. Sequential Photographs of the 30-ft Oblique Drop Test

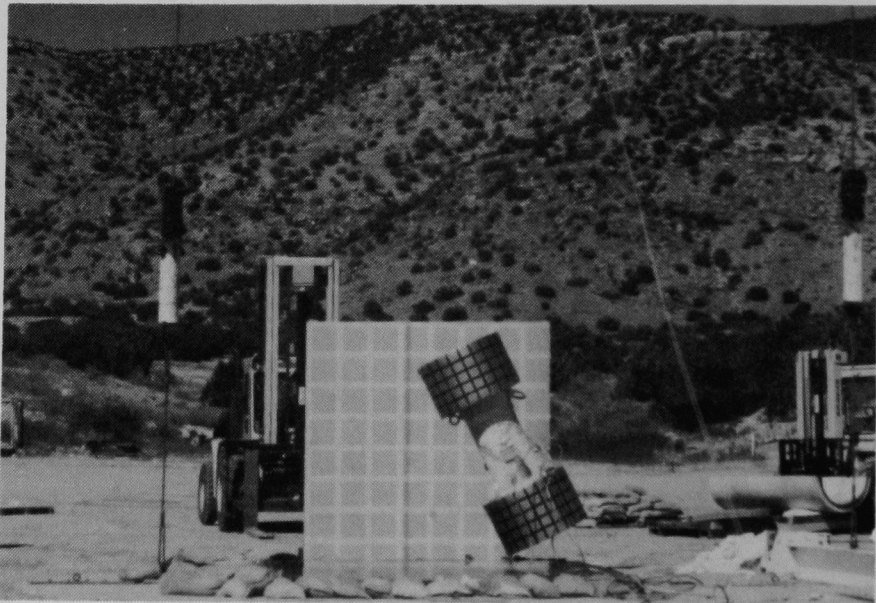


Figure 6-7. (continued)

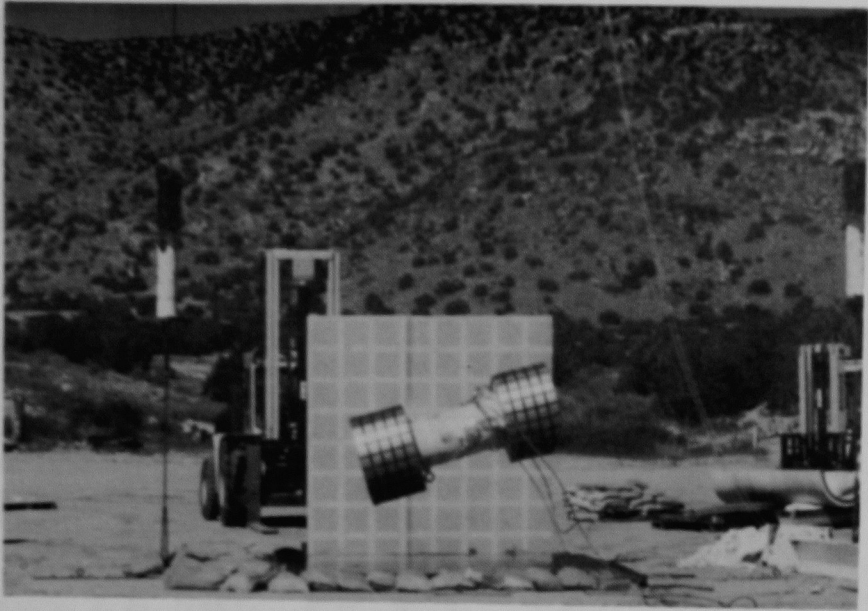


Figure 6-7. (continued)

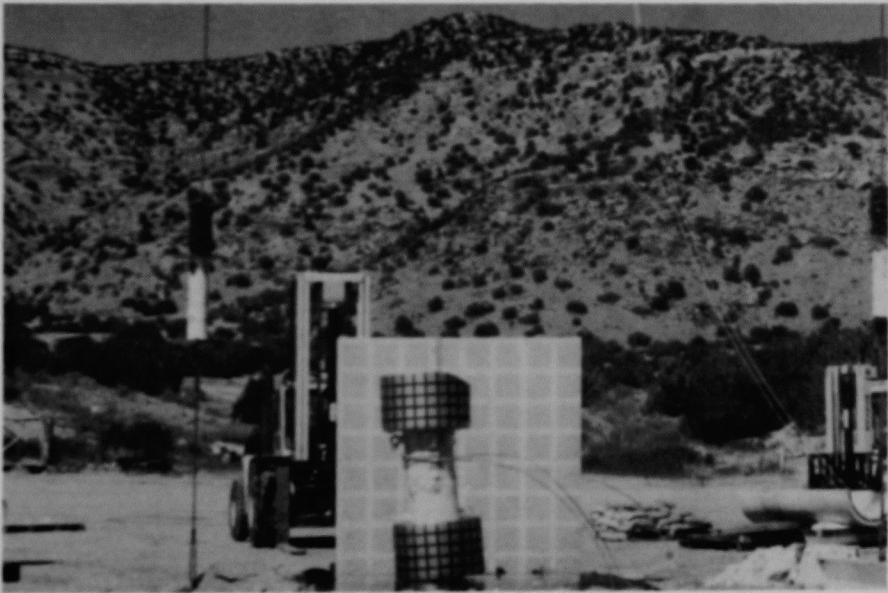


Figure 6-7. (continued)

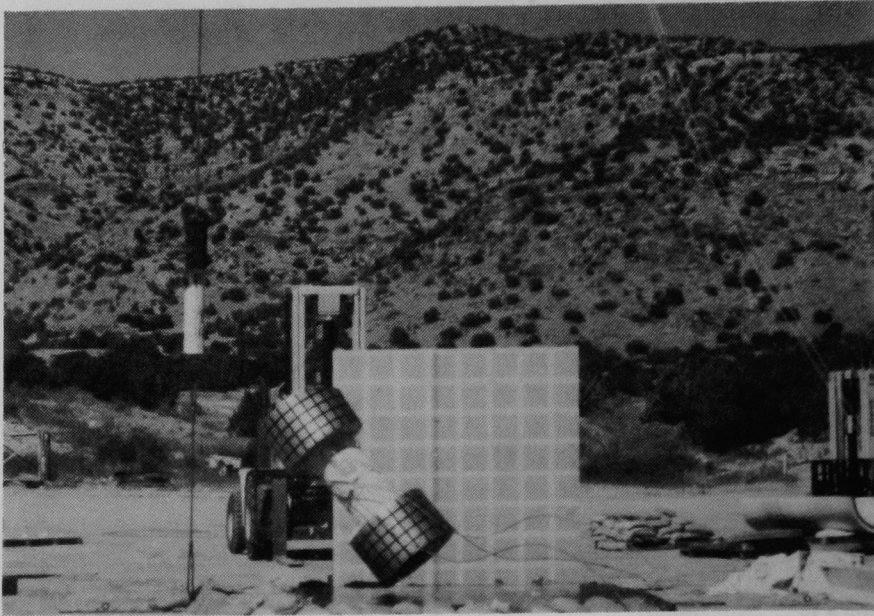


Figure 6-7. (continued)

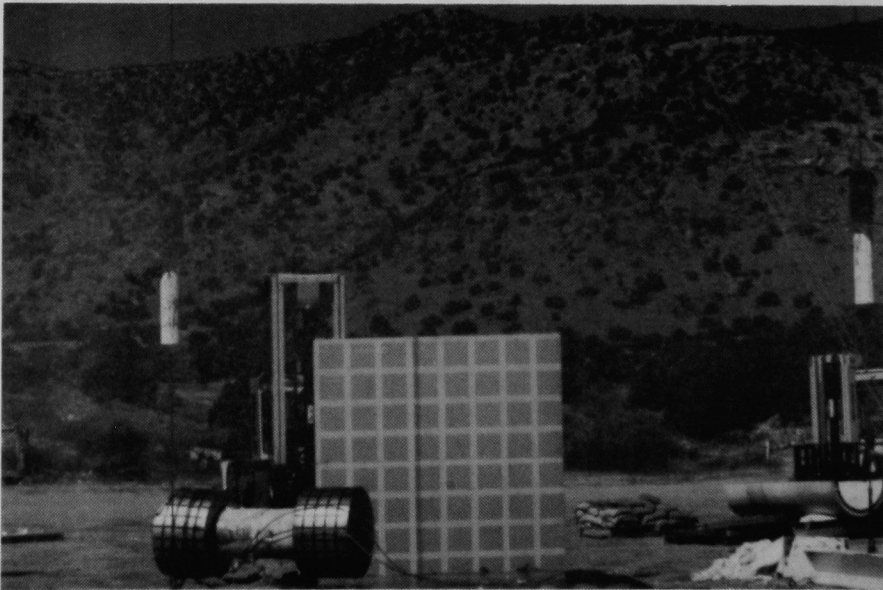


Figure 6-7. (continued)

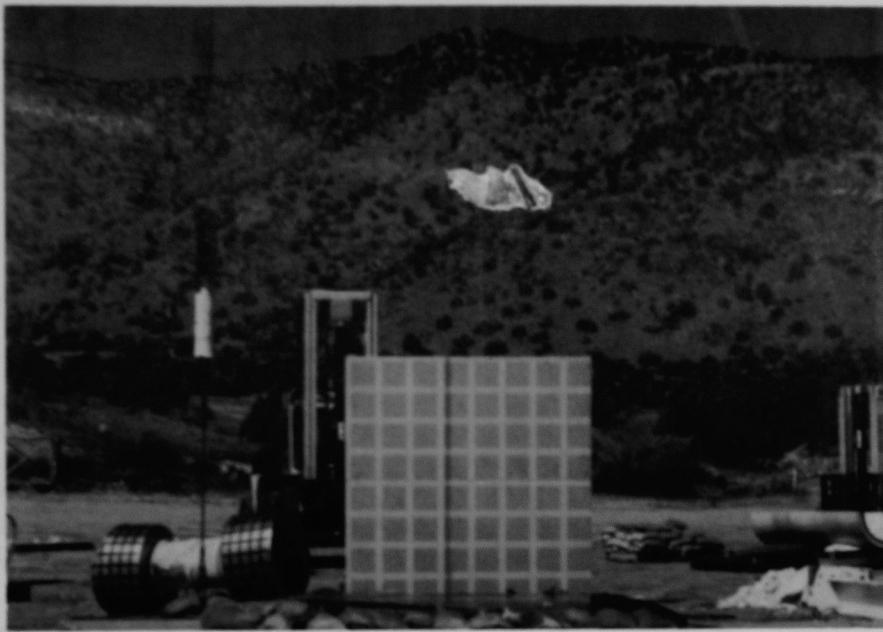


Figure 6-7. (concluded)

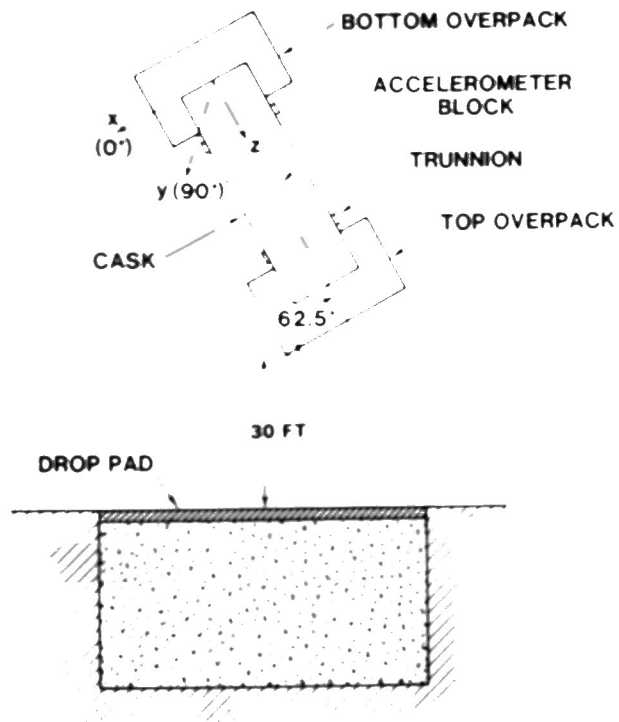


Figure 6-8. Orientation of Model for 30 ft Oblique Drop Test (stadia board is behind model)

6.3 Photometrics Data

Photographs were made from one of the ~400-fps, high-speed, 16-mm cameras covering the test. The frame rate of the camera was determined by viewing the film, locating the frame at which impact occurred, and counting the frames with respect to the timing marks on the film. The frame rate for the camera was determined to be 390 fps. NuPac used 8×10-in. enlargements to measure total overpack crush.

6.4 Visual Observations

Figures 6-9 through 6-11 show the results of the test. The body of the cask appeared not to have been affected. The top impact limiter was deformed (Figures 6-10 and 6-11), and the weld around the bore diameter partially failed. The surface of the impact

limiter adjacent to the bore was deformed; however, there was no visible sign of exposed foam. Two bolts attaching the bottom overpack to the cask had failed. They were on the opposite end of the cask from the impact end.

6.5 Data Acquisition System Information

Accelerometer and strain gage data from the 30-ft oblique drop test are contained in Appendix C1. The data were filtered at 1000 Hz. Fast Fourier transforms of the unfiltered data (presented in Appendix C2) give the frequency response of the model.

The consistency and validity of the data are evaluated in Chapter 14.

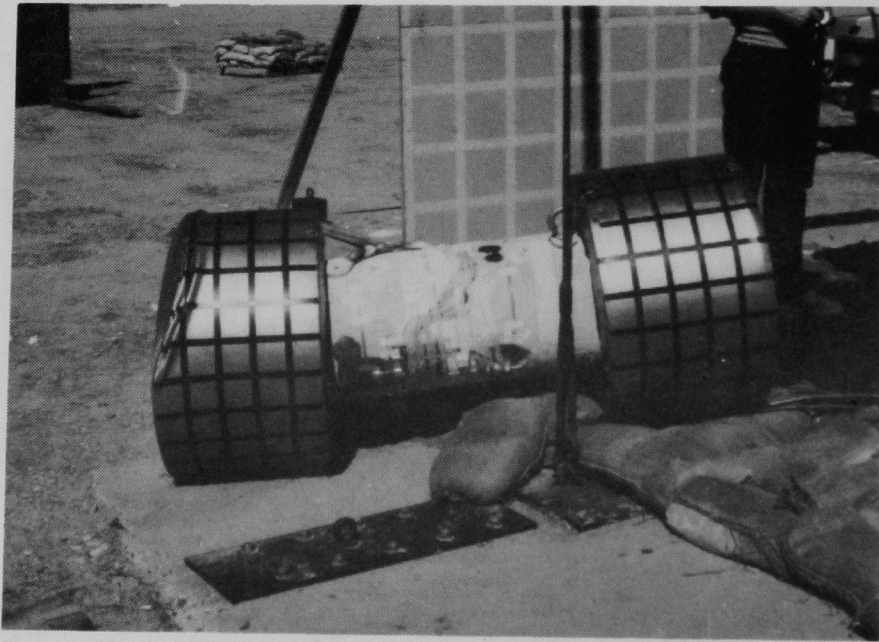


Figure 6-9. NuPac 125-B Quarter Scale Model Immediately After the 30-ft Oblique Drop Test



Figure 6-10. Deformation of Top Overpack After 30-ft Oblique Drop Test



Figure 6-11. Measurement of Deformation Angle of Top Overpack After 30-ft Oblique Drop Test

7. Intermediate Post-Test Examination

7.1 Heating

After the oblique drop test was completed, the assembly was positioned on the transport skid, returned to the laboratory, and covered with a plastic tent. A heat controller set at 100°F was connected to warm the cask to ~80°F.

7.2 Removal of Overpacks

The model was lifted from the transport skid. The overpacks were removed from the cask body by removing the bolts attaching them to the cask and sliding the overpacks horizontally from the ends of the cask (Figure 7-1).

7.3 Leak Testing of Outer Vessel

The test assembly was enclosed in a plastic bag envelope. After the leak test hardware was attached to the vent port on the lid, the outer vessel cavity was evacuated, which was a very slow process. Verification of the outer vessel cavity leak rate was deferred to the final post-test examination.

After the plastic bag envelope was removed from the outer vessel assembly, the leak test hardware was transferred from the vent port to the test port on the lid. The space between the O-rings on the outer vessel lid was evacuated to the standard operating pressure for the leak detector. The outer vessel cavity was evacuated and pressurized with helium. The leak detector was monitored, and the reading was recorded after it stabilized. The helium leak rate for the pair of outer vessel O-rings was 4.5×10^{-7} cm³/s.

7.4 Removal of Outer Vessel Lid

The lid bolt torques were checked, and all were unchanged within ± 2 ft-lb. The lid bolts and vent plug on the lid of the cask were removed and eye bolts installed for removal of the lid. Lifting slings were attached to the eye bolts, and the lid was removed with a forklift. The O-rings and sealing surface of the outer vessel lid were visually examined. The outermost or upper O-ring had been cut all around, and a small amount of the outer surface had been removed and pushed up (Figure 7-2). The inner (lower) O-ring was intact. The sealing surface on the outer vessel was

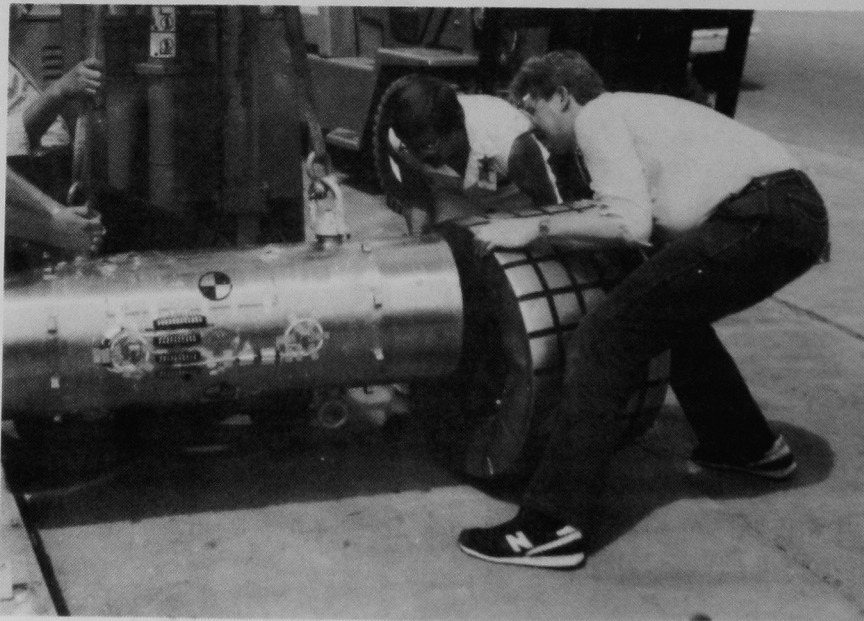


Figure 7-1. Removal of the Overpacks

scratched, which occurred either on installation or removal of the lid.

Figures 7-3 and 7-4 show the inner vessel inside the outer vessel after removal of the outer vessel lid

The orientation of the lifting holes and vent port of the inner vessel lid with respect to the alignment pins for the outer vessel lid show very little, if any, change from the initial orientation (Figure 2-14)

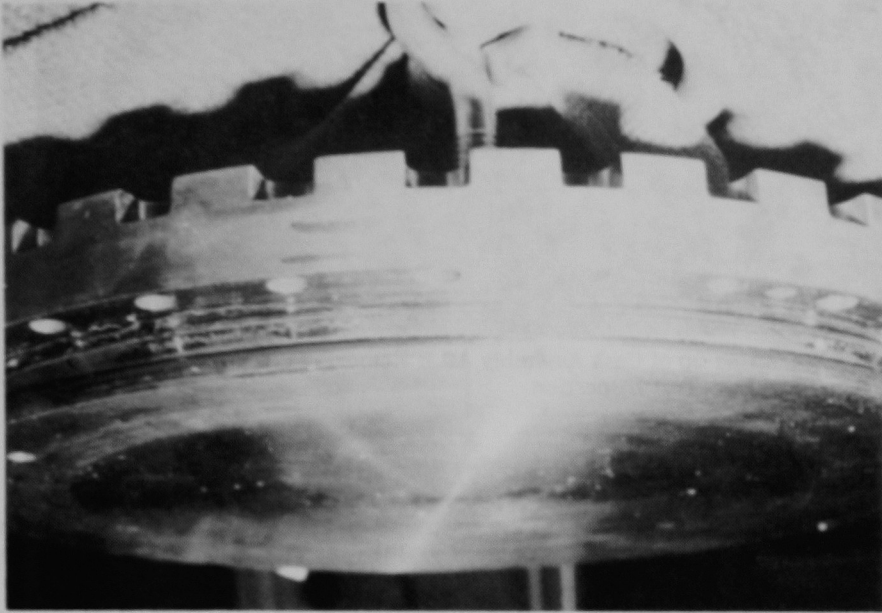


Figure 7-2. Condition of the Outer Vessel Closure During Intermediate Post-Test Examination

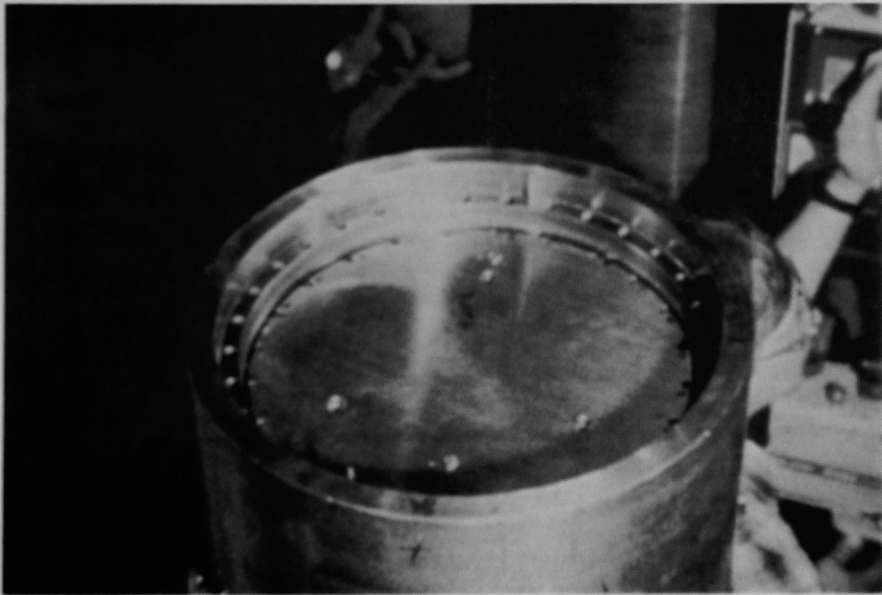


Figure 7-3. Cask Assembly After Removal of Outer Vessel Lid During Intermediate Post-Test Inspection

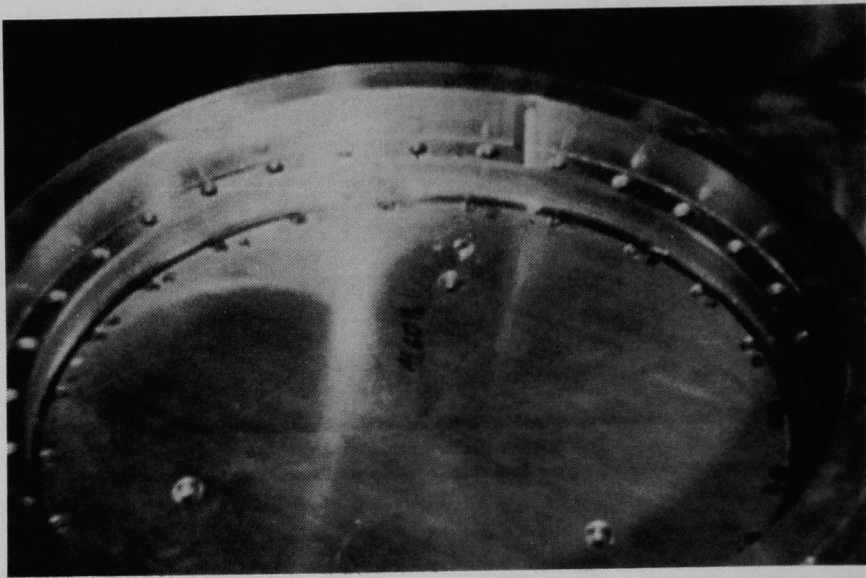


Figure 7-4. Close-up of Cask Assembly After Removal of Outer Vessel Lid During Intermediate Post-Test Inspection

7.5 Removal of Inner Vessel

Eye bolts were attached to the lid of the inner vessel, and the lifting slings were attached to the eye bolts and forklift. To prevent scraping the sides of the two vessels, the inner vessel was pulled vertically from the cask and guided as it rose. When the inner vessel neared the top of the cask, the lifting rate of the forklift was decreased to prevent the inner vessel from swinging against the sealing surface of the cask. After the inner vessel cleared the top of the cask, the forklift was backed up, and the inner vessel was lowered in the vertical position. The slings and eye bolts were then removed from the lid of the inner vessel.

7.6 Leak Testing of Inner Vessel

After the leak test hardware was attached to the vent port on the lid, the inner vessel cavity was evacuated, which was also a very slow process. Verification of the inner vessel cavity leak rate was deferred to the final post-test examination.

The leak test hardware was removed from the vent port and attached to the test port on the lid. The space between the O-rings on the inner vessel lid was evacuated to the standard operating pressure for the leak detector. The inner vessel cavity was evacuated and pressurized with helium. The leak detector was

monitored, and the reading was recorded after it stabilized. The helium leak rate for the pair of inner vessel O-rings was 1.1×10^{-7} cm³/s.

7.7 Removal of Inner Vessel Lid

When the lid bolt torques were checked, those for adjacent bolts 20 and 23 were found to be lower than their pre-test values. The number of turns to return the torques of those bolts to 28 in.-lb was measured to be 1/4 turn and 1/8 turn, respectively (see Section 14.3.2 for further discussion).

Figure 7-5 shows a sketch of the numbering scheme for the inner vessel lid bolts and the cask coordinate system. Bolts 20 and 23 were located on the impact side of the model for the oblique drop test and for the secondary impact in the bottom end drop test.

The lid bolts and vent plug on the lid of the cask were removed and eye bolts installed for removal of the lid. Lifting slings were attached to the eye bolts, and the lid was removed with a forklift (Figure 7-6). When the O-rings and sealing surface were visually examined, the O-rings were found to be intact. However, the sealing surface on the inner vessel was scratched, which occurred either on installation or removal of the lid.

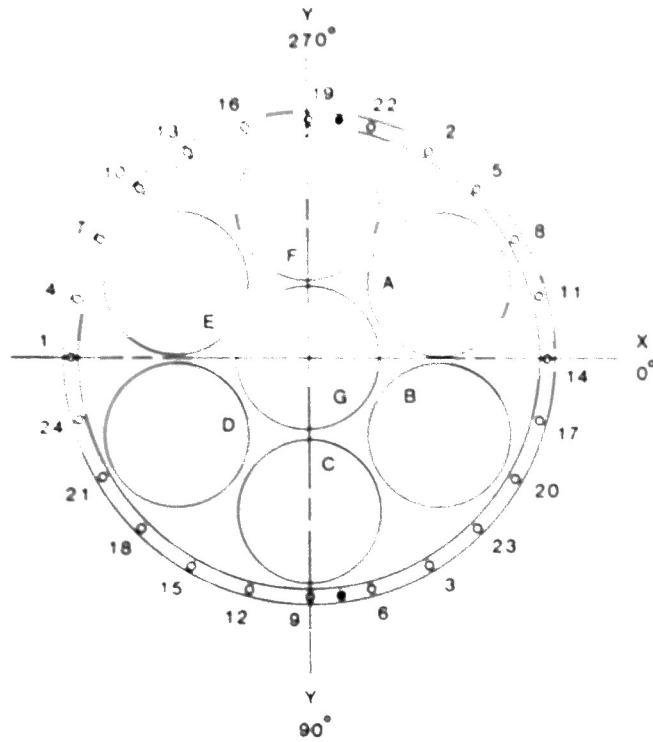


Figure 7-5. Sketch of Inner Vessel Lid Bolts With Tightening Order

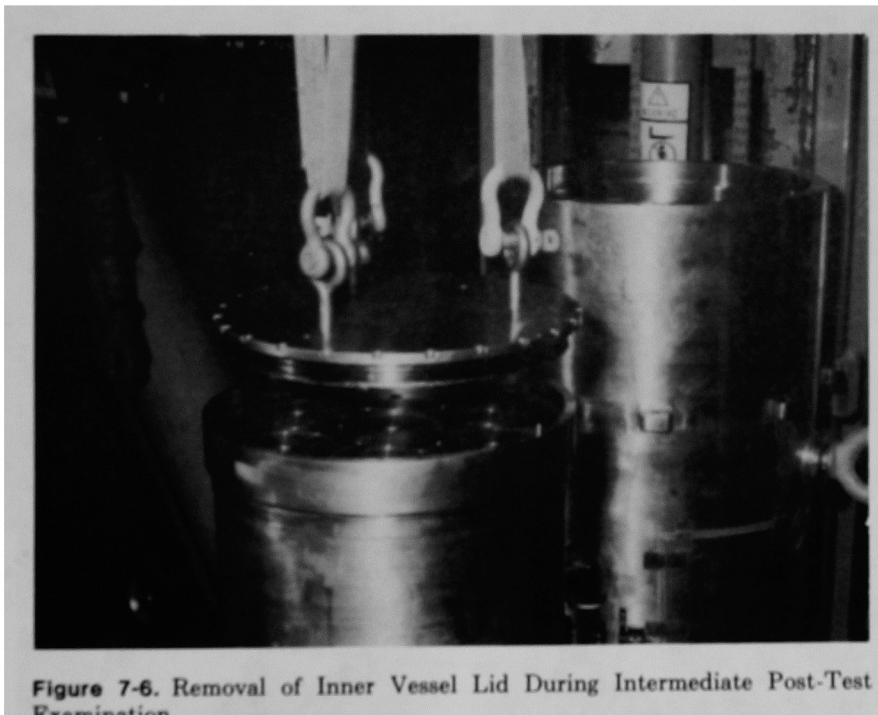


Figure 7-6. Removal of Inner Vessel Lid During Intermediate Post-Test Examination

7.8 Removal of Upper Internal Impact Limiters

The orientations of the upper internal impact limiters were documented and are shown in Figure 7-7 and Table 7-1. Eye bolts were installed in the tapped

holes in the upper impact limiters, and each impact limiter was lifted out by hand (Figure 7-8). The condition of each of the upper internal impact limiters is shown in Figures 7-9 through 7-15. The deformations are described in Table 7-1.

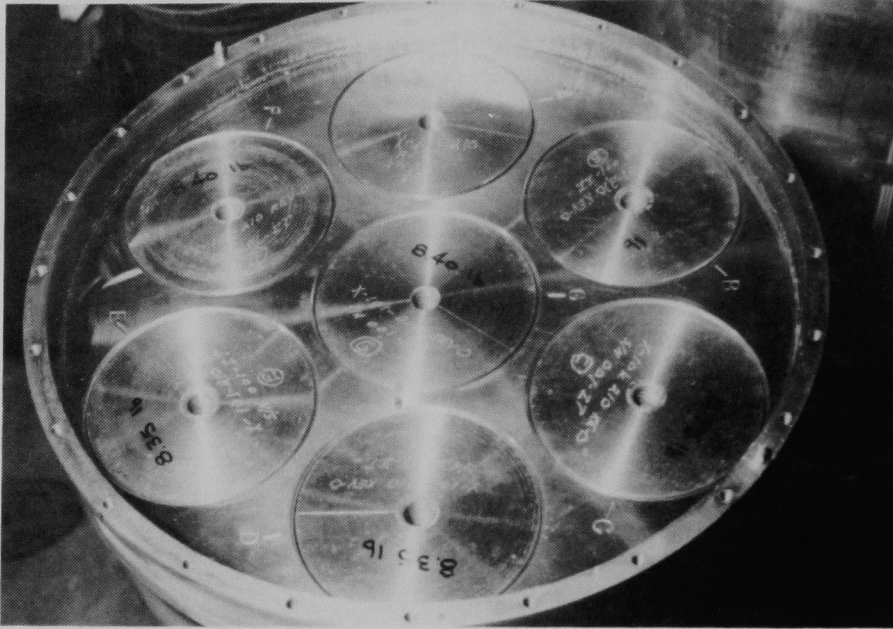


Figure 7-7. Orientations of Upper Internal Impact Limiters After the 30-ft Oblique Drop Test



Figure 7-8. Upper Internal Impact Limiter Being Removed From Inner Vessel

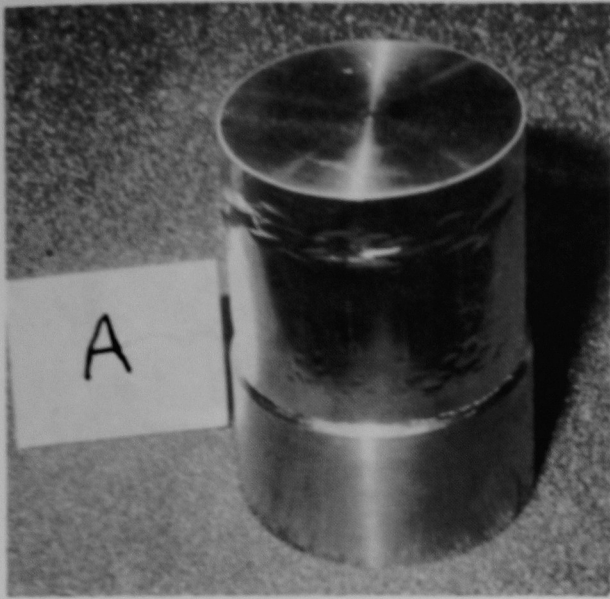


Figure 7-9. Condition of Upper Internal Impact Limiter "A" After 30-ft Oblique Drop Test

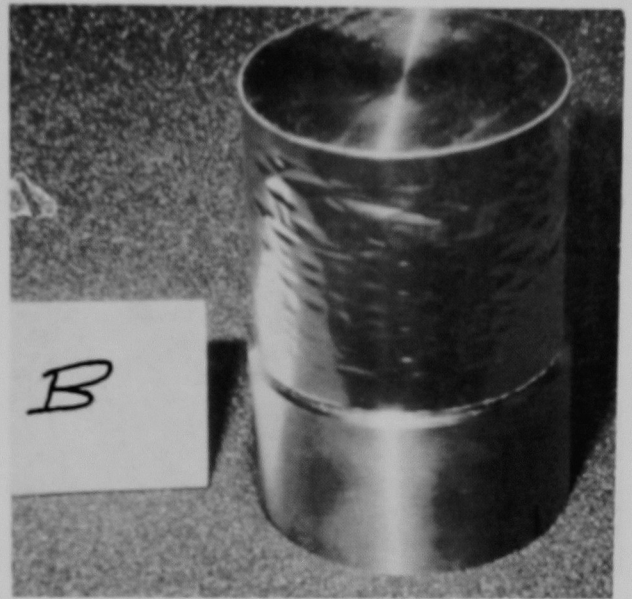


Figure 7-10. Condition of Upper Internal Impact Limiter "B" After 30-ft Oblique Drop Test

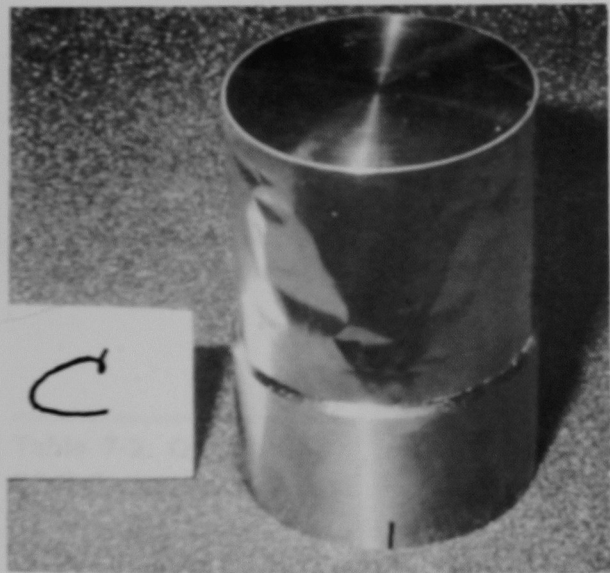


Figure 7-11. Condition of Upper Internal Impact Limiter "C" After 30-ft Oblique Drop Test



Figure 7-12. Condition of Upper Internal Impact Limiter "D" After 30-ft Oblique Drop Test



Figure 7-13. Condition of Upper Internal Impact Limiter "E" After 30-ft Oblique Drop Test



Figure 7-14. Condition of Upper Internal Impact Limiter "F" After 30-ft Oblique Drop Test



Figure 7-15. Condition of Upper Internal Impact Limiter "G" After 30-ft Oblique Drop Test

Table 7-1. Rotations and Deformations of Upper Internal Impact Limiters After 30-ft Oblique Drop Test

Impact Limiter	Rotation	Deformation
A	~30° clockwise	Deformation ~3/4 in. up from the bottom, ~3/4 around
B	~5° counterclockwise	Rippled skin ~3/4 around, all the way up the sides
C	~5° counterclockwise	Large ripples ~3/4 around, all the way up the sides
D	~10° clockwise	Deformation ~1/2×3/4-in. band; skin was pulled away ~3/4 in. down over the bottom
E	~5° clockwise	Skin was pushed under adhesive joint and rippled all around; major deformation ~1/2 to 3/4 in. up from the bottom
F	~30° clockwise	Large ripples all around, all the way up, ~1/2 in. from the bottom
G	~30° clockwise	Very large ripples all around

7.9 Removal of Canisters

The orientations of the canisters were documented and are shown in Figure 7-16 and Table 7-2. Eye bolts were installed in the tapped holes, and each canister was lifted out by hand. The canisters appeared intact and unaffected by the tests.

Table 7-2. Orientations of Canisters After 30-ft Oblique Drop Test

Canister	Orientation
A	No rotation
B	No rotation
C	2° - 3° clockwise
D	3° - 4° clockwise
E	~25° counterclockwise
F	~25° counterclockwise
G	~15° clockwise

7.10 Removal of Lower Internal Impact Limiters

During the dynamic tests, the honeycomb had been pushed through the 1/2-13 UNC holes drilled and tapped through the top of the impact limiters. As a result, removal of the individual impact limiters was difficult. It was, however, accomplished by attaching a tap to the end of a tube and reaching down into each of the cavities until the tap stuck into the impact limiter. The honeycomb was tapped, and the impact limiter was lifted out of the vessel by slowly raising the tube. The condition of each of the lower internal impact limiters is shown in Figures 7-17 through 7-23.

7.11 Inspection

The intermediate inspection of the assembly was completed by personnel from the Mechanical Measurements Division at Sandia National Laboratories who had performed the initial inspection. The measurements were taken from the locations previously marked and used to determine the probable measurement inaccuracy (PMI) (Appendix A).

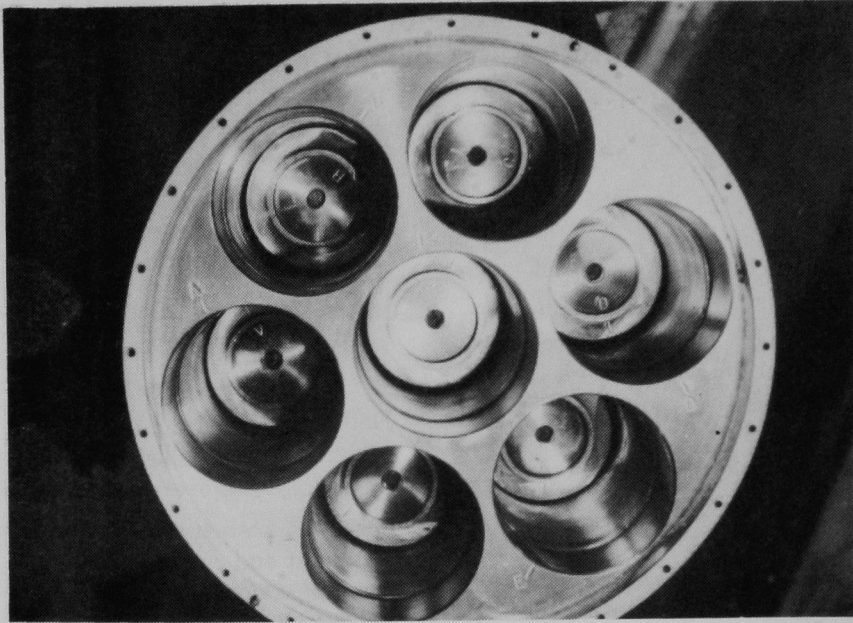


Figure 7-16. Orientations of Canisters After 30-ft Oblique Drop Test

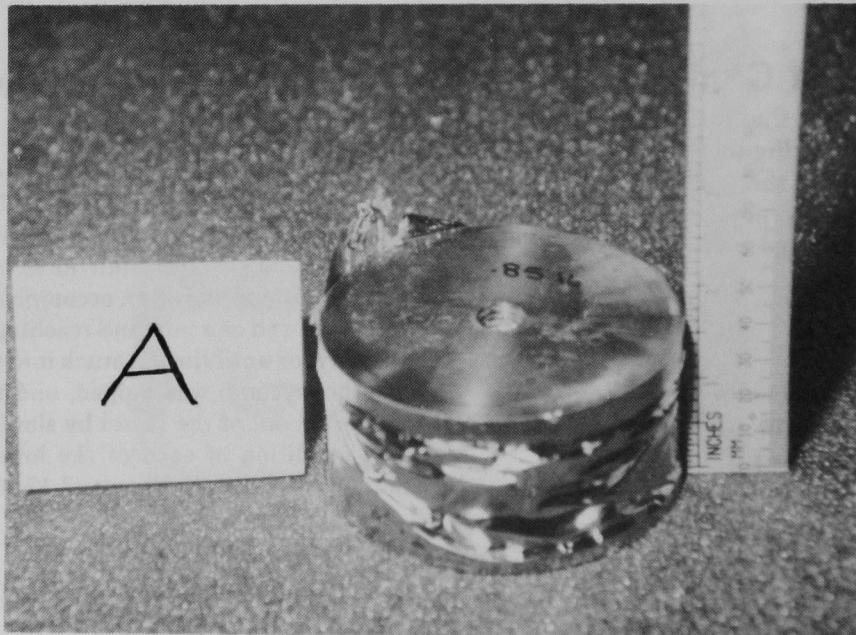


Figure 7-17. Condition of Lower Internal Impact Limiter "A" After 30-ft Oblique Drop Test



Figure 7-18. Condition of Lower Internal Impact Limiter "B" After 30-ft Oblique Drop Test



Figure 7-19. Condition of Lower Internal Impact Limiter "C" After 30-ft Oblique Drop Test



Figure 7-20. Condition of Lower Internal Impact Limiter "D" After 30-ft Oblique Drop Test



Figure 7-21. Condition of Lower Internal Impact Limiter "E" After 30-ft Oblique Drop Test



Figure 7-22. Condition of Lower Internal Impact Limiter "F" After 30-ft Oblique Drop Test

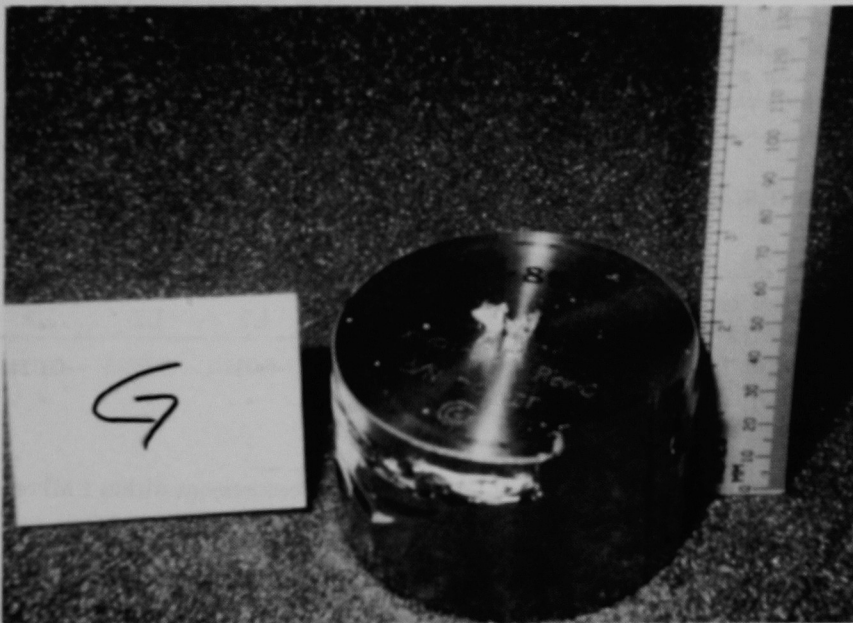


Figure 7-23. Condition of Lower Internal Impact Limiter "G" After 30-ft Oblique Drop Test

7.11.1 Intermediate Inspection of Cask Body

The measurements of the cask bore diameter showed no differences outside the PMI. The differences data for straightness measurements did show several changes in the cask bore. Differences greater than the PMI of ± 0.005 in. are listed in Table 7-3.

Table 7-3. Differences Data (in.) for Cask Bore Straightness for the Intermediate Post-Test Inspection

Tangential Location	Longitudinal Location					Orientation (°)
	L1	L2	L3	L4	L5	
D1	*	*	+0.006	*	*	270
D2	*	*	*	*	-0.006	315
D3	*	*	*	*	*	0
D4	*	*	*	-0.006	-0.007	45
D5	*	*	*	-0.006	-0.011	90
D6	*	*	*	*	*	135
D7	*	*	*	*	*	180
D8	*	*	*	*	*	225

Notes: *Measurement within PMI of ± 0.005 in.

Difference measurement = initial measurement minus current measurement. The sign has been adjusted to be positive for a change away from the center and negative for a change toward the center.

7.11.2 Intermediate Inspection of Inner Vessel

There were no measured differences exceeding the PMI for either the diameter or the straightness of the inner vessel exterior. None of the diametrical or straightness measurements for the inner vessel tube bores differed significantly from their original measurements.

7.11.3 Intermediate Inspection of Canisters

There were several diametrical measurements of the canisters that exceeded the PMI of ± 0.002 in. These are shown in Table 7-4.

Table 7-4. Differences Data (in.) for Canister Diameters for the Intermediate Post-Test Inspection

Tangential Location	Longitudinal Location				
	L1	L2	L3	L4	L5
D2e	*	*	*	+0.003	+0.005
D2g	*	+0.003	+0.004	+0.003	*

Notes: *Measurement within PMI of ± 0.002 in.

Difference measurement = initial measurement minus current measurement. The sign has been adjusted to be positive for a change radially outward and negative for a change radially inward.

Significant differences in straightness of the canisters are listed in Table 7-5. The large difference measurements for D2a appear to have been the result of a systematic sign error for either the initial or intermediate straightness measurements at that location. This hypothesis was verified at the final post-test inspection (see Section 12.11.3).

Table 7-5. Differences Data (in.) for Canister Straightness for the Intermediate Post-Test Inspection

Tangential Location	Longitudinal Location				
	L1	L2	L3	L4	L5
D2a	-0.0190	-0.0235	-0.0245	-0.0285	-0.0160
D2g	*	*	*	+0.003	*

Notes: *Measurement within PMI of ± 0.002 in.

Difference measurement = initial measurement minus current measurement. The sign has been adjusted to be positive for a change away from the center and negative for a change toward the center.

7.11.4 Intermediate Inspection of Cask Lid, Cask Bottom, and Inner Vessel Lid

There were no difference measurements exceeding the PMI of ± 0.002 in. for the cask lid, cask bottom, or inner vessel lid.

7.11.5 Intermediate Inspection of Internal Impact Limiters

The lengths of the upper and lower internal impact limiters were measured. The amount of crush of each impact limiter is given in Table 7-6 for the lower internal impact limiters and in Table 7-7 for the upper internal impact limiters.

Table 7-6. Amount of Crush (in.) for the Lower Internal Impact Limiters for the Intermediate Post-Test Inspection

Impact Limiter	Tangential Location			
	L1	L2	L3	L4
A	0.992	0.989	1.005	1.009
B	0.555	0.558	0.556	0.556
C	0.504	0.495	0.499	0.508
D	0.872	0.882	0.915	0.904
E	1.239	1.244	1.232	1.241
F	0.701	0.713	0.704	0.696
G	0.756	0.768	0.752	0.740

Note: Measurement within PMI of ± 0.002 in.

Table 7-7. Amount of Crush (in.) for the Upper Internal Impact Limiters for the Intermediate Post-Test Inspection

Impact Limiter	Tangential Location			
	L1	L2	L3	L4
A	0.005	0.003	0.005	0.020
B	0.013	0.008	•	0.003
C	0.004	•	•	0.003
D	0.089	0.077	0.070	0.076
E	0.237	0.241	0.234	0.230
F	0.007	0.081	0.072	0.069
G	0.005	0.013	0.018	0.010

*Measurement within PMI of ± 0.002 in.

8. Intermediate Instrumentation

8.1 Removal of Entran Accelerometers From Outer Vessel

The accelerometers installed for the initial drop tests were removed to prevent damage during inspection and to be calibrated for the tests conducted at ambient temperatures.

8.2 Characteristics of Endevco Accelerometers

Undamped Endevco accelerometers were added to the instrumentation installed on the model to obtain elastic body response in addition to the rigid body response measured by the Entran accelerometers (described in Section 4.1). The characteristics of the Endevco accelerometers are listed in Table 8-1.

Table 8-1. Characteristics of Endevco Accelerometers

Type	Piezoresistive
Model No.	2264A-5KR
Range	$\pm 5\,000\text{ g's}$
Over-range	$\pm 10\,000\text{ g's}$
Recommended Excitation	10.0 Vdc
Temperature Range	0°F to +150°F

8.3 Intermediate Calibration of Accelerometers

8.3.1 Entran Accelerometers

The Entran accelerometers used for the initial drop tests were calibrated on a centrifuge at ambient temperature as shown in Figures 8-1 and 8-2. Measured sensitivities are given in Table 8-2.

8.3.2 Endevco Accelerometers

The three Endevco accelerometers added to the model for the side drop test were calibrated as described in Section 8.3.1. Measured sensitivities are given in Table 8-3.

Table 8-2. Sensitivities of Entran Accelerometers at Ambient Temperature (Model EGAXT-F-1000)

Serial Number	Intermediate Calibration Sensitivity (mV/V/g)
21N50-A11-11	0.0172973
21N50-A12-12	0.0159721
21N50-A13-13	0.0180970
21N50-A14-14	0.0178023
21N50-A15-15	0.0182961
21N50-A16-16	0.0183473
21N50-A17-17	0.0182097
21N50-A18-18	0.0186624
21N50-A21-21	0.0185984
21N50-A22-22	0.0142827

Note: Calibration performed on a centrifuge at 15-V excitation. Accuracy of sensitivity measurement is estimated at $\pm 3\%$ to 4% .

Table 8-3. Sensitivities of Endevco Accelerometers at Ambient Temperature (Model 2264-5KR)

Serial Number	Intermediate Calibration Sensitivity (mV/V/g)
BN09B	0.0090163
BN17B	0.0106626
BK76B	0.0098656

Note: Calibration performed on a centrifuge at 10-V excitation. Accuracy of sensitivity measurement is estimated at $\pm 3\%$ to 4% .

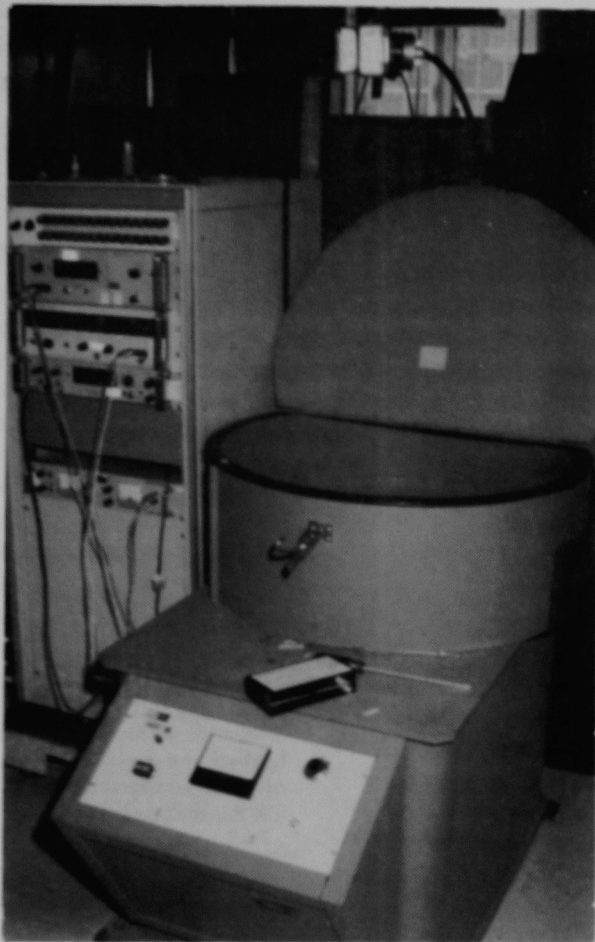


Figure 8-1. Centrifuge Used for Accelerometer Calibration at Ambient Temperature

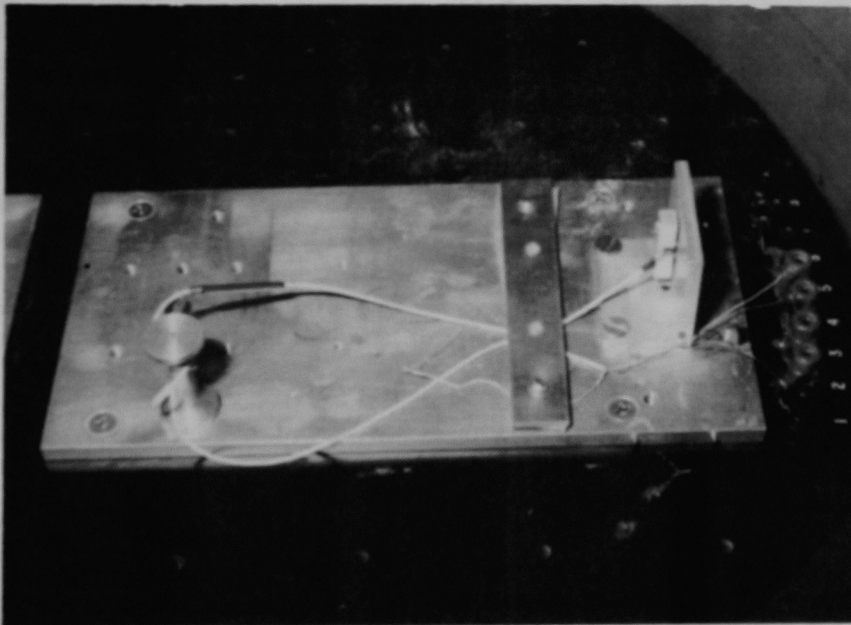


Figure 8-2. Mounting of an Accelerometer for Calibration in the Centrifuge

8.4 Intermediate Installation of Accelerometers

The Entran accelerometers were installed on the model as specified by DT-04 and shown in Figure 2-12. Because the Endevco accelerometers required two 4-40 UNC cap screws for mounting, two 4-40 UNC holes were drilled and tapped into the accelerometer mounting blocks opposite accelerometers A2, A5, and A8. The Instrumentation Installation Procedure was revised, and the accelerometers were installed. Table 8-4 lists the location of each accelerometer at the intermediate installation.

Table 8-4. Intermediate Installation Location of Accelerometers on Model

Accelerometer Location	Accelerometer Serial Number
AZ1	21N50-A11-11
AX2	21N50-A21-21
AY3	21N50-A15-15
AZ4	21N50-A16-16
AX5	21N50-A18-18
AY6	21N50-A12-12*
AZ7	21N50-A14-14*
AX8	21N50-A17-17
AX9	BN09B
AX10	BN17B
AX11	BK76B

*These accelerometers replace the ones used for the 30-ft bottom end and oblique drop tests. The recalibration of the original accelerometers (21N50-A13-13 and 21N50-A22-22) showed unacceptable responses.

9. 30-ft Side Drop Test

9.1 Assembly of Inner Vessel

The inner vessel was positioned vertically and cleaned internally with rags dampened with methanol. Care was taken not to remove any marks used for the inspection process. The lower internal impact limiters were also cleaned with rags dampened with methanol. Because the honeycomb was deformed, each lower internal impact limiter had to be pushed down into its corresponding cell with a tube.

The canisters and upper internal impact limiters were cleaned with rags dampened with methanol. Five bolts were installed in the tapped holes in the canisters and upper internal impact limiters, and each was lowered into its cell. Each component was returned to its initial location and orientation by aligning the scribed marks.

The scratches on the sealing surface of the inner vessel and the scratches and gouges around the O-ring grooves on the inner vessel lid were sanded. The interior surface of the inner vessel lid, the O-ring grooves on the inner vessel lid, and the O-rings were thoroughly cleaned with Kimwipes dampened with methanol. The O-rings were then greased with Apiezon vacuum grease and installed in the grooves. After the sealing surface of the inner vessel was greased with Apiezon, the lid was positioned over the alignment pins and slowly lowered until the lower O-ring rested on top of the tapered region of the sealing surface bore. The lid was then forced down into position, and the bolts were installed and torqued to 25 in.-lb.

9.2 Leak Testing of Inner Vessel

After the helium mass spectrometer leak detector was zeroed and calibrated according to the manufacturer's instructions and vented, hardware was attached for leak testing the O-ring seals of the inner vessel lid.

The leak test hardware was attached to the test port on the lid, and the space between the O-rings was evacuated to the standard operating pressure for the leak detector. The inner vessel cavity was evacuated and pressurized with helium. The leak detector was monitored, and the reading was recorded after it stabilized. There was no detectable helium leak rate for the pair of inner vessel O-rings to a sensitivity of 1.0×10^{-7} cm³/s.

9.3 Assembly of Outer Vessel

The outer vessel was positioned vertically. Its interior surface was only vacuumed out and wiped down with dry rags because cleaning solvents could remove the inspection markings. The exterior surface of the inner vessel was carefully cleaned with rags dampened with methanol. After eye bolts were attached to the lid of the inner vessel, the inner vessel was lifted over the outer vessel, lowered into the outer vessel, and rotated to ensure proper alignment.

The scratches on the sealing surface of the outer vessel and the scratches and gouges around the O-ring grooves on the outer vessel lid were sanded. The interior surface of the outer vessel lid, the O-ring grooves on the outer vessel lid, and the O-rings were thoroughly cleaned with Kimwipes dampened with methanol. The O-rings were then greased with Apiezon vacuum grease and installed in the grooves. After the sealing surface of the outer vessel was greased with Apiezon, the lid was positioned over the alignment pins and slowly lowered until the lower O-ring rested on top of the tapered region of the sealing surface bore. The lid was then forced down into position, and the bolts were installed and torqued to 20 ft.-lb.

9.4 Leak Testing of Outer Vessel

After the helium mass spectrometer leak detector was zeroed and calibrated according to the manufacturer's instructions and vented, hardware was attached for leak testing the O-ring seals of the outer vessel lid.

The leak test hardware was attached to the test port on the lid, and the space between the O-rings was evacuated to the standard operating pressure for the leak detector. The outer vessel cavity was evacuated and pressurized with helium. The leak detector was monitored, and the reading was recorded after it stabilized. There was no detectable helium leak rate for the pair of outer vessel O-rings to a sensitivity of 0.7×10^{-10} cm³/s.

9.5 Assembly of Overpacks

The lower overpack was positioned with the cavity for the cask outer vessel facing up. The cask was lifted and positioned over the overpack, which was rotated to assure proper alignment. Then the cask was lowered into position (Figure 9-1), and the overpack bolts were installed and torqued to 70 in.-lb.

The upper overpack was positioned on a forklift with the cavity for the cask outer vessel facing down. The overpack was lifted, positioned over the cask, and rotated to assure proper alignment. It was then lowered into position (Figure 9-2), and the overpack bolts were installed and torqued to 70 in.-lb.



Figure 9-1. Model Being Lowered Into Overpack

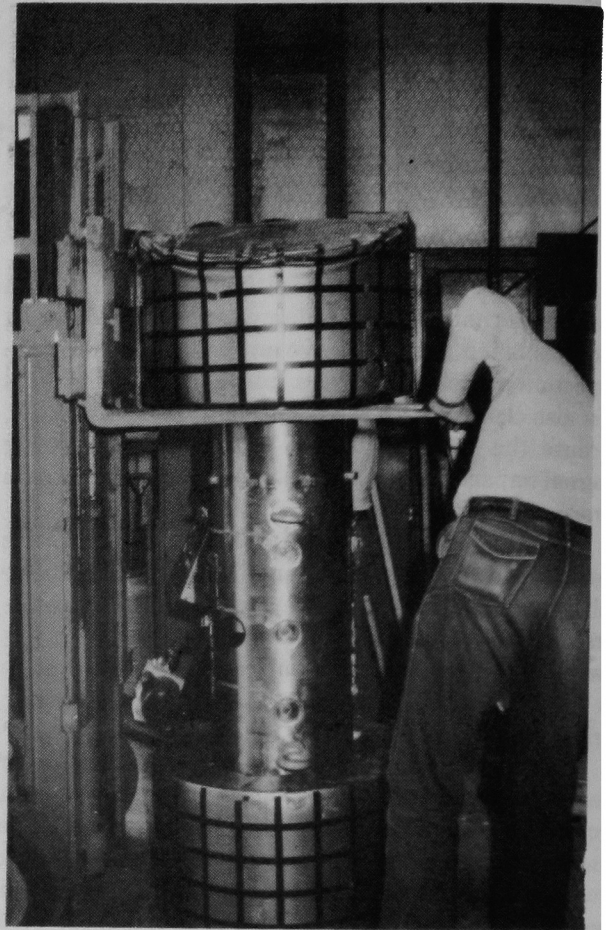


Figure 9-2. Installation of the Upper Overpack

9.6 Side Drop Test Procedure

The assembly was placed on a truck and transported to the drop test facility, where it was unloaded and placed on the unyielding target.

The rigging hardware, with guillotine cable cutters installed, was attached to the trolley on the overhead cable and to the eye bolts attached to the trunnions on the sides of the cask body. The unit was leveled by means of a turnbuckle in one of the rigging lines.

The instrumentation cables were attached to the terminal strips and secured to a trunnion. The stadia boards were positioned, documentary photographs

were taken, and the test procedure steps were verified and signed. Figure 9-3 shows the model rigged for the 30-ft side drop test. After the data acquisition check-out was completed, the assembly was hoisted to the 30-ft drop height in final preparation for the test (Figure 9-4).

After all of the test procedure steps were verified and signed, the guillotine cable cutters were actuated, and the model free fell to the impact target. The actual 30-ft side drop test and the orientation of the model for the test are shown in Figures 9-5 and 9-6, respectively.

9.7 Photometrics Data

Photographs were made from one of the ~2000-fps, high-speed, 16-mm cameras covering the test. The frame rate of the camera was determined by viewing the film, locating the frame at which impact occurred, and counting the frames near the impact frame with respect to the timing marks on the film. The frame rate for the camera was determined to be 1933.3 fps. NuPac used 8×10-in. enlargements of these photographs to determine total overpack crush.

9.8 Visual Observations

Figures 9-7 through 9-14 show the results of the test. The body of the cask appeared not to have been affected. Figures 9-7 and 9-8 show the basic condition of the model after the test. The lower overpack shell was torn (Figure 9-9), and the lower overpack was flattened or compressed (Figures 9-10 and 9-11). The upper overpack was deformed (Figures 9-12 and 9-13), and the weld around the foam filling hole patch partially tailed (Figure 9-14).

9.9 Data Acquisition System Information

Accelerometer and strain gage data from the 30-ft side drop test are contained in Appendix D1. The data were filtered at 1000 Hz. The fast Fourier transforms of the unfiltered data (presented in Appendix D2) give the frequency response of the model.

The consistency and validity of the data are evaluated in Chapter 14.

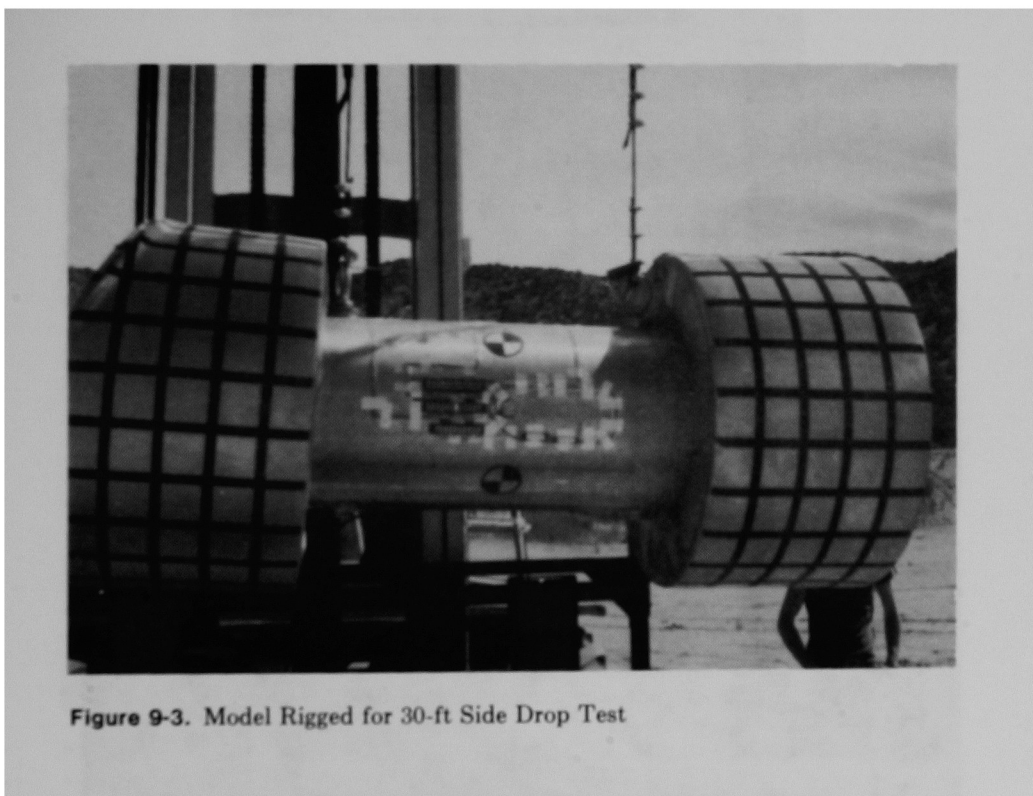


Figure 9-3. Model Rigged for 30-ft Side Drop Test

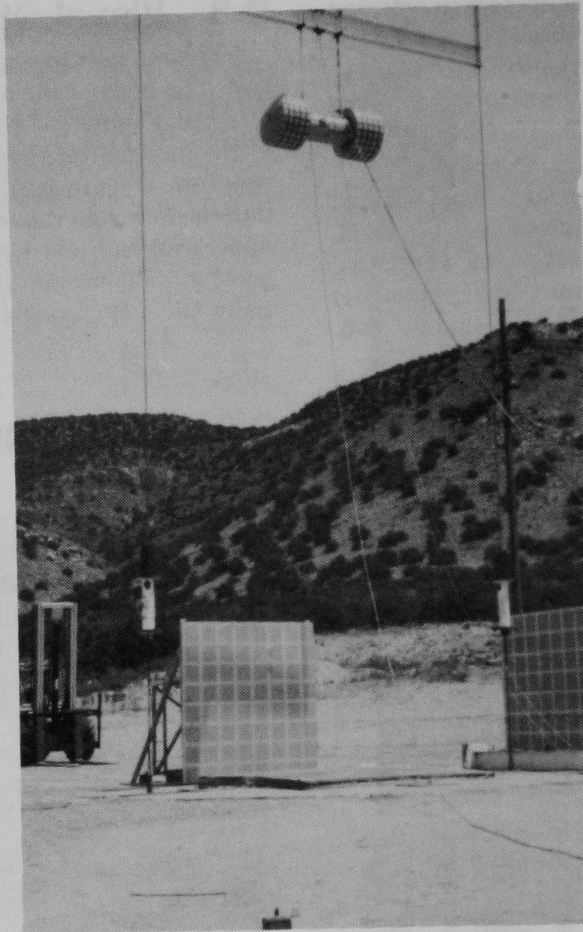


Figure 9-4. NuPac 125-B Model Elevated to 30 ft Before the 30-ft Side Drop Test

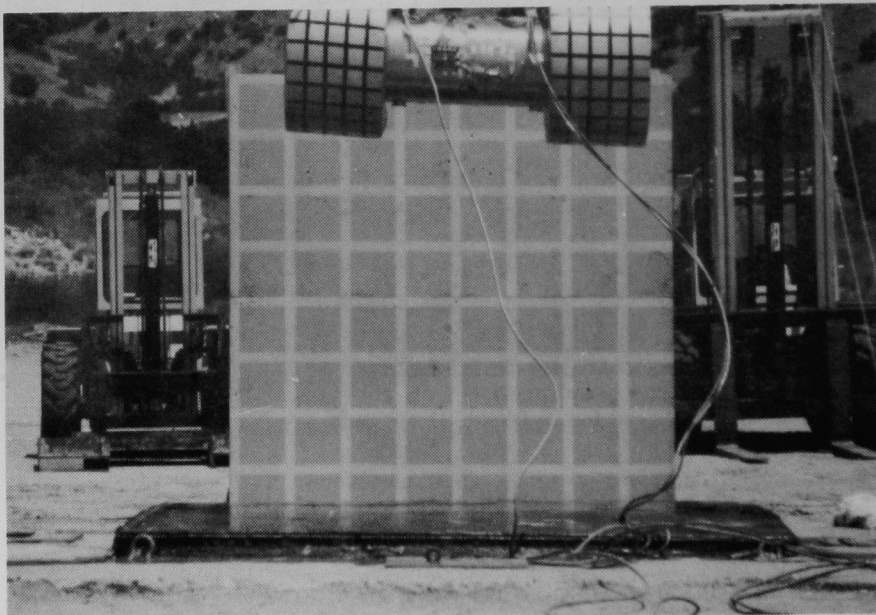


Figure 9-5. Sequential Photographs of the 30-ft Side Drop Test

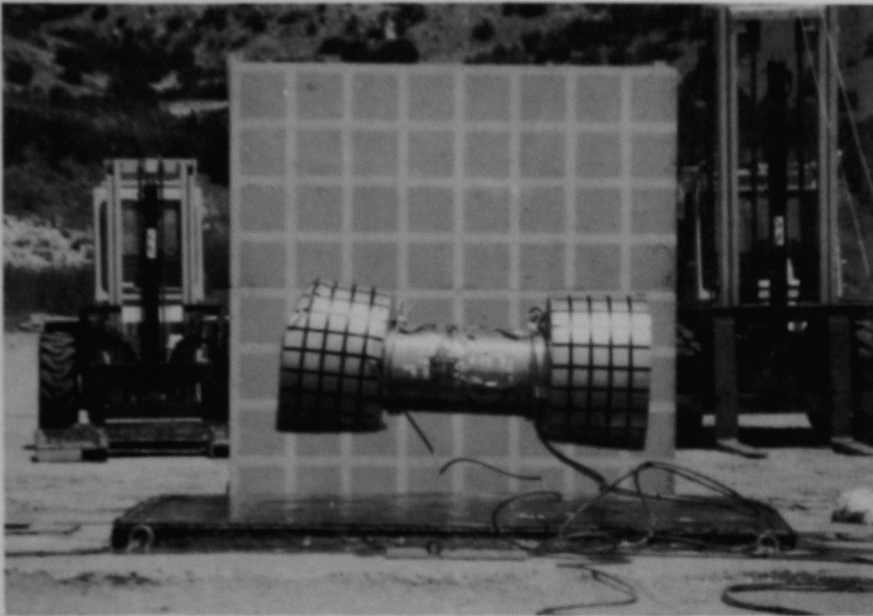


Figure 9-5. (continued)

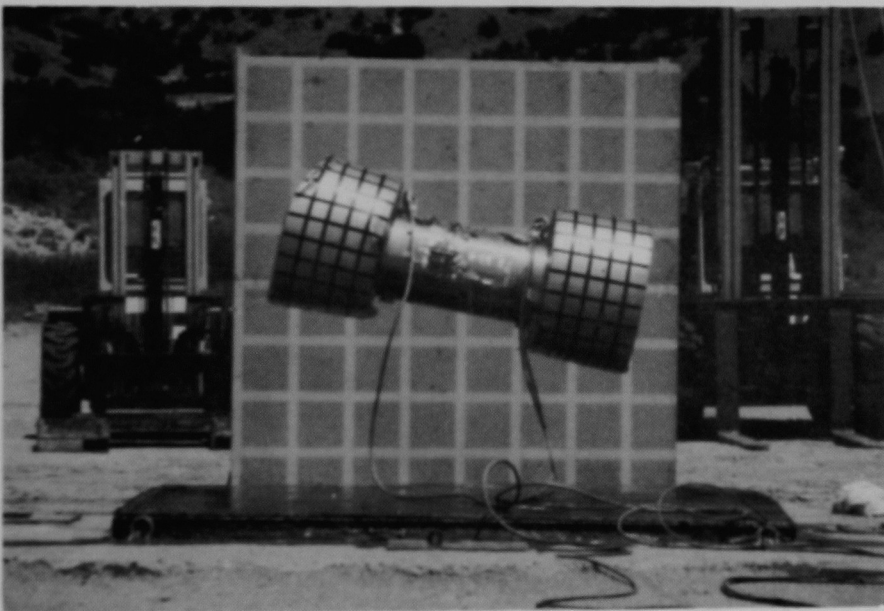


Figure 9-5. (continued)

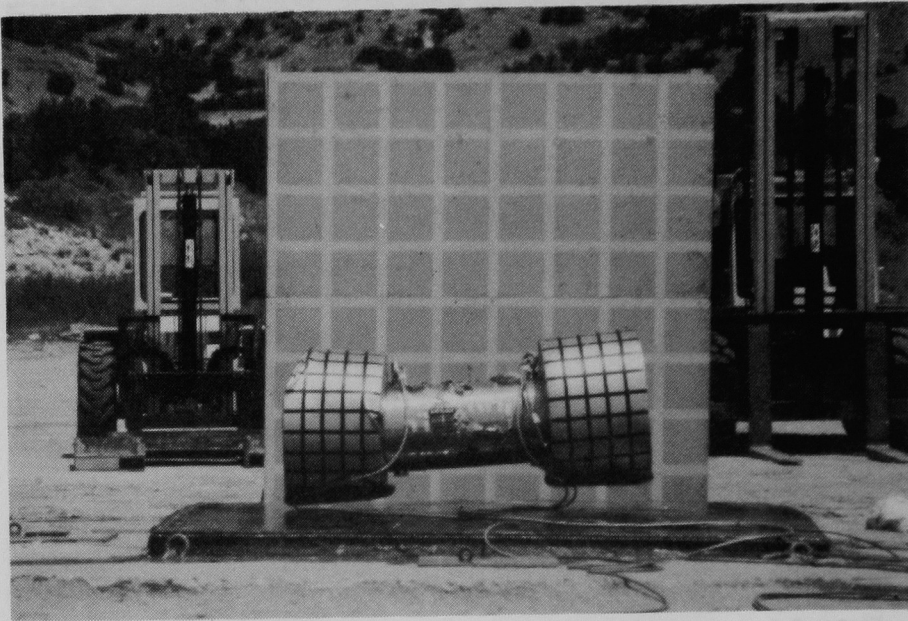


Figure 9-5. (continued)

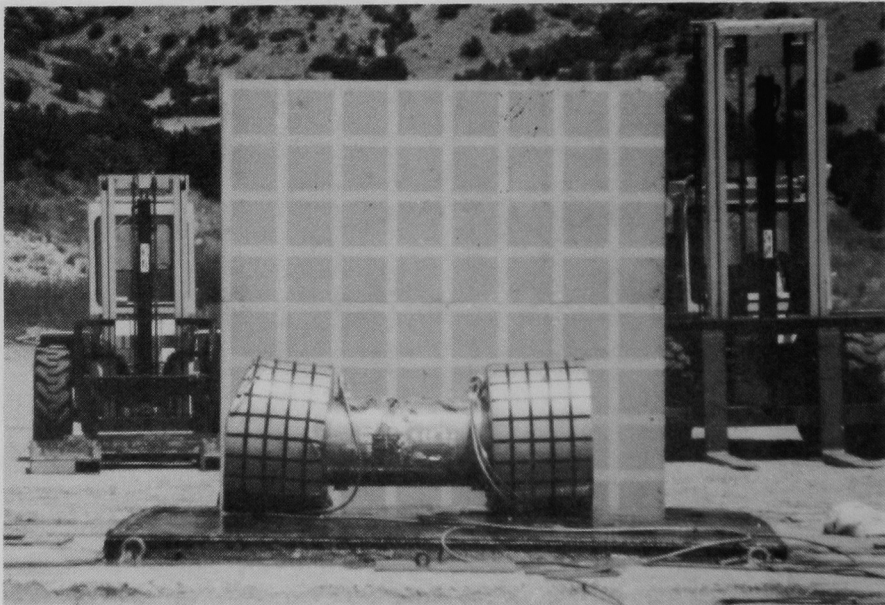


Figure 9-5. (concluded)

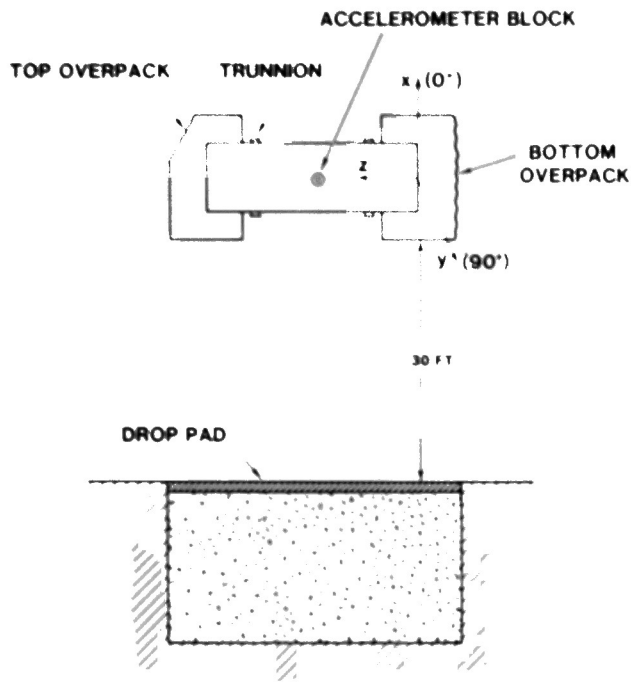


Figure 9-6. Orientation of Model for 30 ft Side Drop Test (stadia board is behind model)

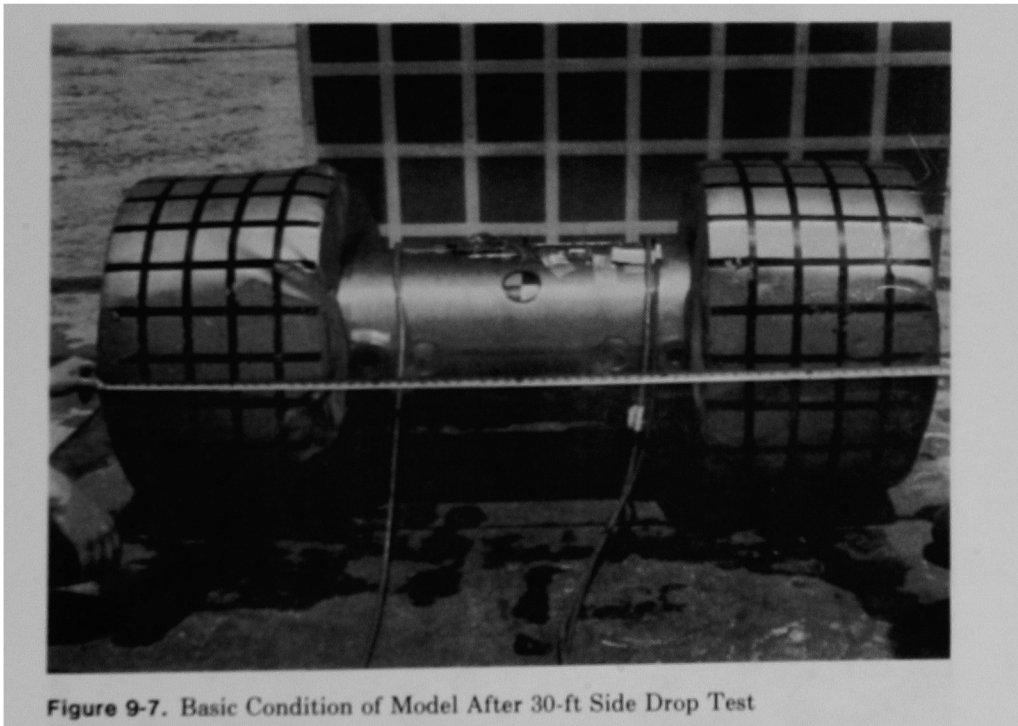


Figure 9-7. Basic Condition of Model After 30-ft Side Drop Test

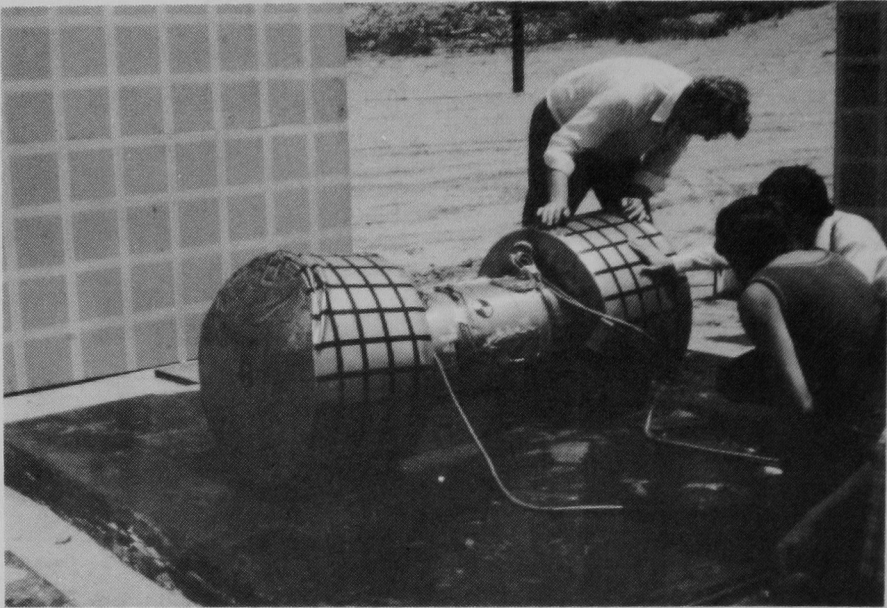


Figure 9-8. Visual Inspection of Model After 30-ft Side Drop Test

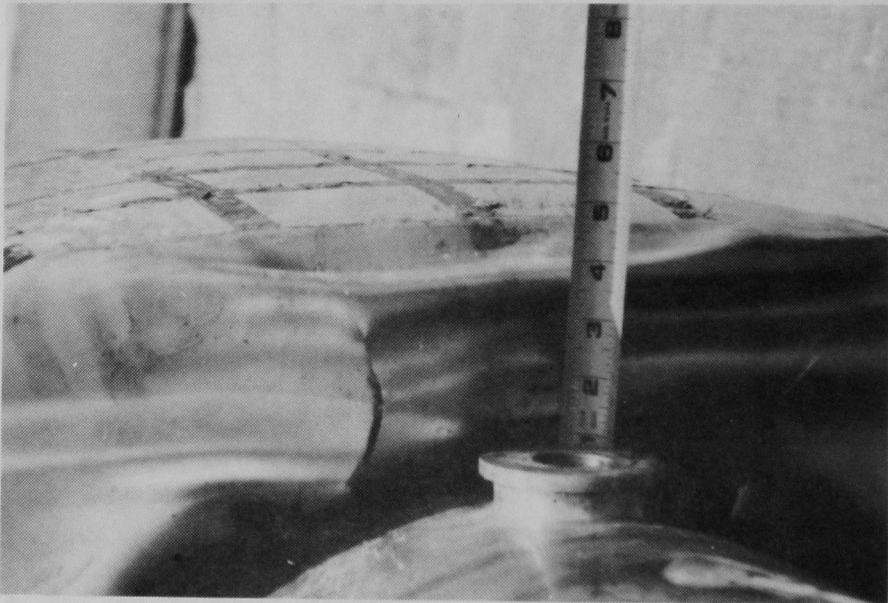


Figure 9-9. Tear in Lower Overpack Shell After 30-ft Side Drop Test



Figure 9-10. Deformation of Lower Overpack After 30-ft Side Drop Test: End View



Figure 9-11. Deformation of Lower Overpack After 30-ft Side Drop Test: Side View

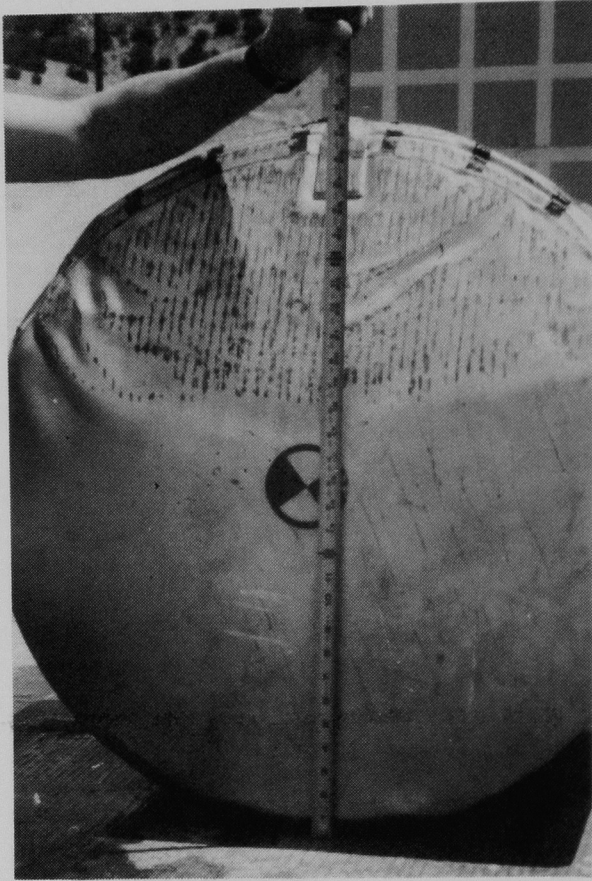


Figure 9-12. Deformation of Upper Overpack After 30-ft Side Drop Test: End View. (Upper part of deformation was caused by 30-ft oblique drop test.)

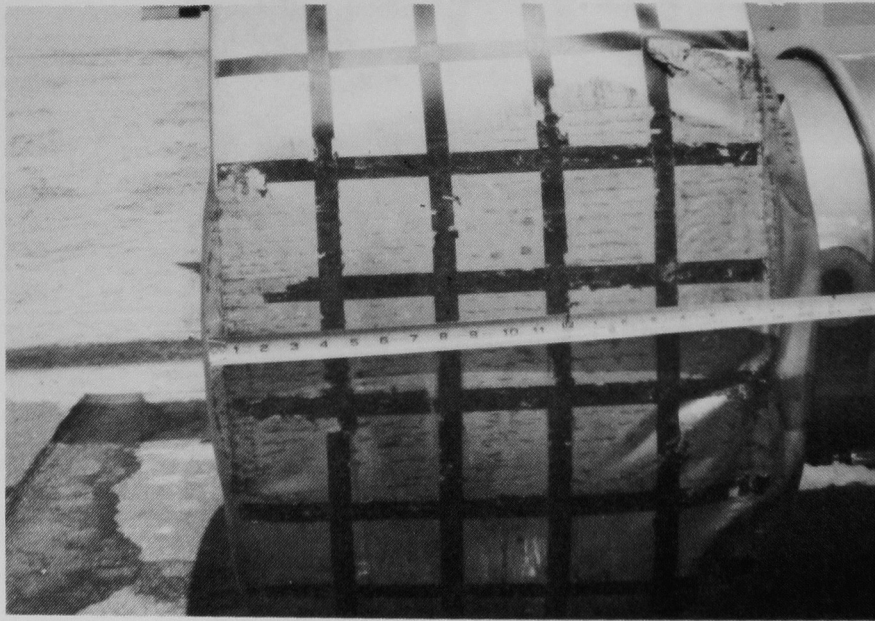


Figure 9-13. Deformation of Upper Overpack After 30-ft Side Drop Test: Side View



Figure 9-14. Failure of the Weld Around the Foam Filling Hole Patch After 30-ft Side Drop Test

10. 40-in. Side Puncture Test

10.1 Puncture Bar

A mild steel puncture bar was fabricated, instrumented, and calibrated for the test (Figure 10-1). Characteristics of the puncture bar are listed in Table 10-1.

Table 10-1. Characteristics of Puncture Bar for Side Puncture Test

Material	SAE 1018
Hardness	92.5-93.0 R _B
	55.9-57.00 R _A
Upper Radius	0.06 in.
Diameter	1.50 in.
Length	9.0 in.

General-purpose, mild-steel, compensated biaxial strain gages, with fully encapsulated grids and exposed copper-coated integral solder tabs, were installed on the puncture bar for the dynamic force analysis. Characteristics of these strain gages are listed in Table 10-2.

Table 10-2. Characteristics of Micro-Measurements Strain Gages Used on Puncture Bar for Side Puncture Test

Gage Type	CEA-06-125UT-350
Strain Range	$\pm 5\%$
Temperature Range	-100°F to +400°F

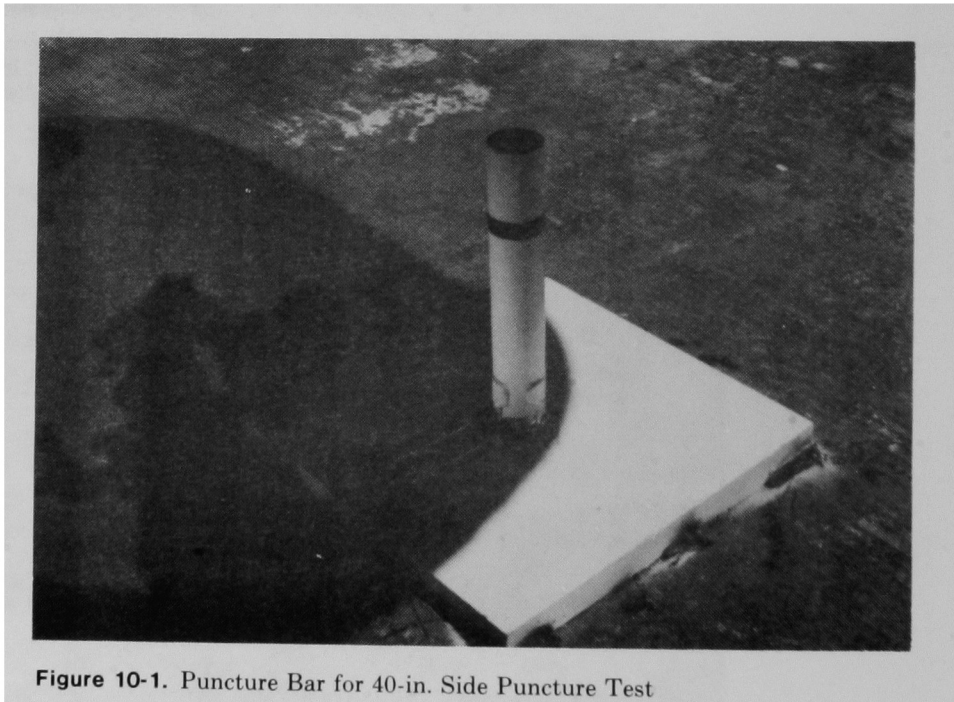


Figure 10-1. Puncture Bar for 40-in. Side Puncture Test

10.2 Side Puncture Test Procedure

The rigging hardware, with guillotine cable cutters installed, was attached to the trolley on the overhead cable and to the eye bolts attached to the trunnions on the sides of the cask body. The unit was leveled by means of a turnbuckle in one of the rigging lines.

The 9-in. puncture bar was positioned on the unyielding target. Puncture bar location and distance from the cask to the top of the puncture bar were verified (Figure 10-2). After the puncture bar base plate was welded to the target, instrumentation cables were attached to the terminal strips on the puncture bar base plate.

The instrumentation cables were attached to the terminal strips on the cask and secured to a trunnion. The stadia boards were positioned, documentary photographs were taken, and the test procedure steps were verified and signed. Figure 10-3 shows the model rigged for the 40-in. side puncture test.

After the test procedure steps were verified and signed, the guillotine cable cutters were actuated, and the model tree fell onto the puncture bar. The actual 40-in. side puncture test and orientation of the model for the test are shown in Figures 10-4 and 10-5, respectively.



Figure 10-2. Verification of Puncture Bar Location and Distance From Model for 40-in. Side Puncture Test

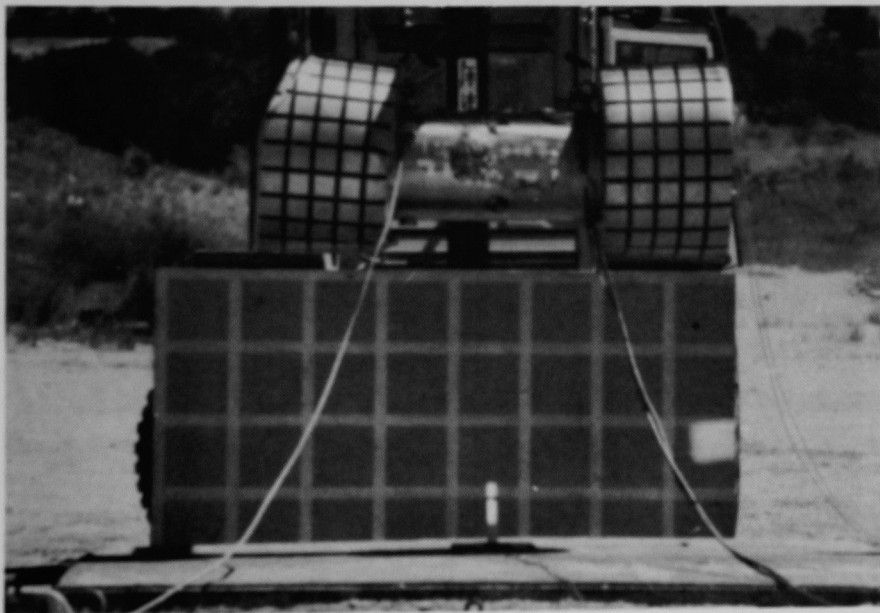


Figure 10-3. NuPac 125-B Model Before 40-in. Side Puncture Test

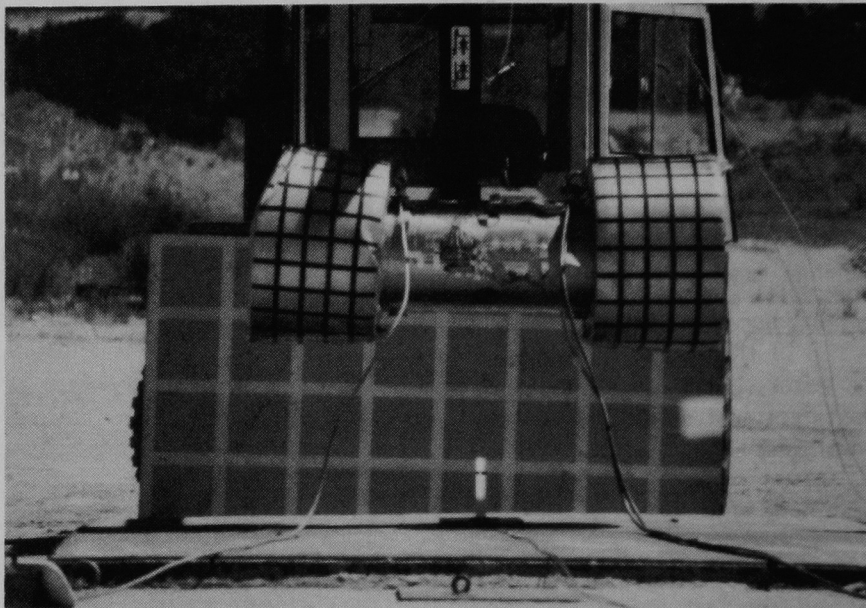


Figure 10-4. Sequential Photographs of the 40-in. Side Puncture Test

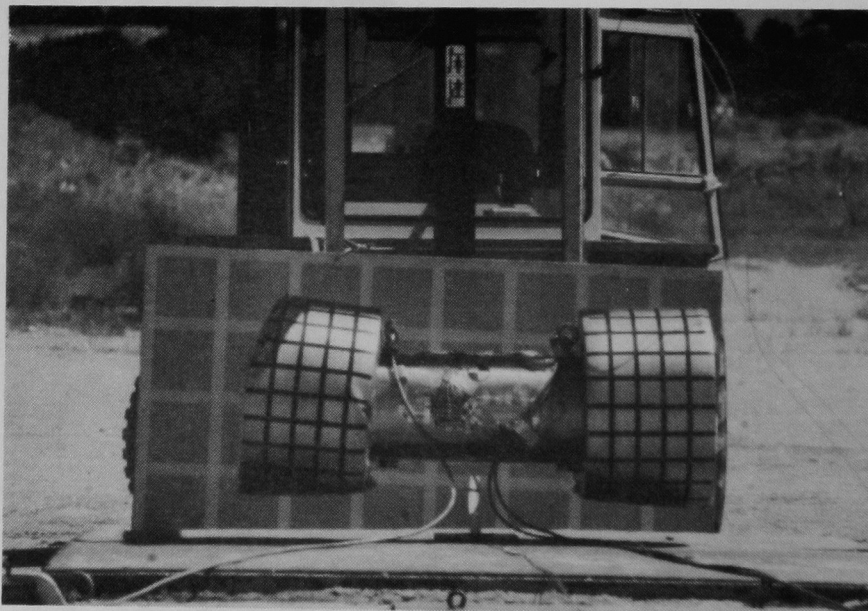


Figure 10-4. (continued)



Figure 10-4. (continued)

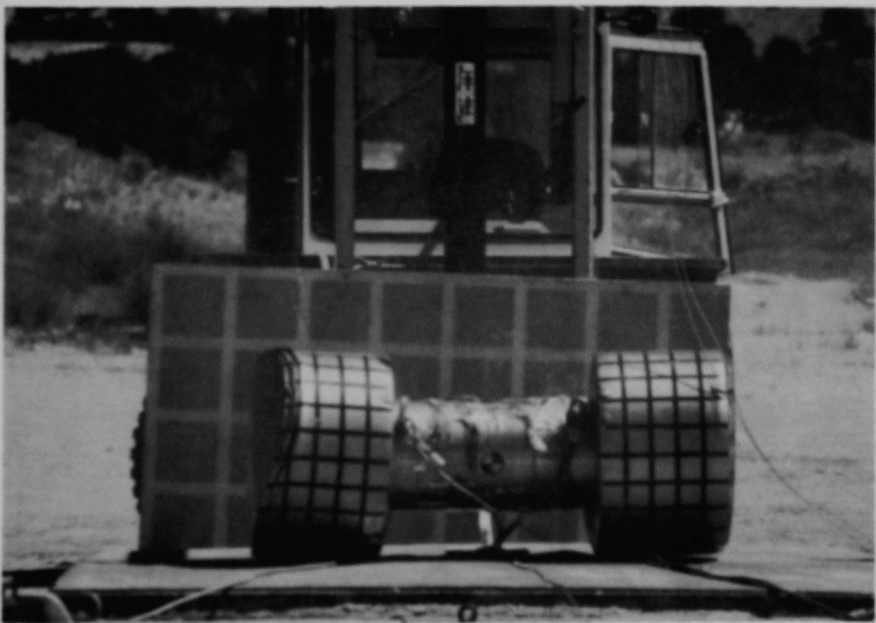


Figure 10-4. (concluded)

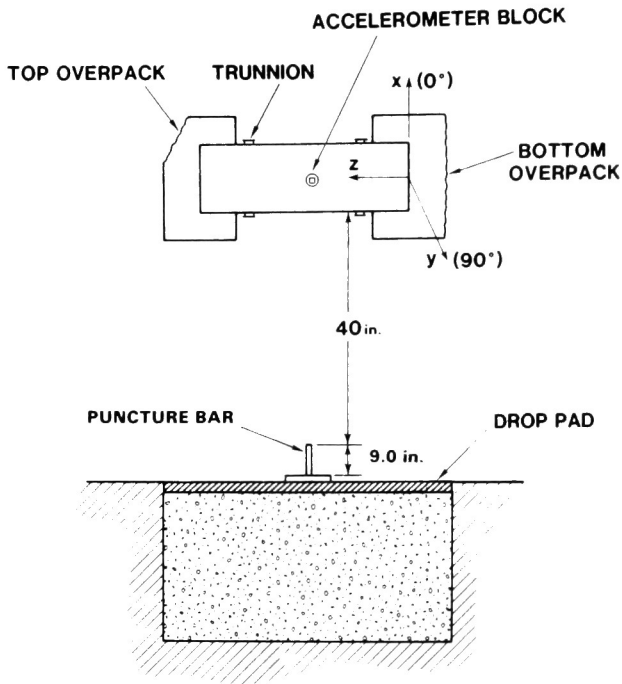


Figure 10-5. Orientation of Model for 40-in. Side Puncture Test (stadia board is behind model)

10.3 Photometrics Data

Photographs were made from one of the ~2000-fps, high-speed, 16-mm cameras covering the test. The frame rate of the camera was determined by viewing the film, locating the frame at which impact occurred, and counting the frames near the impact frame with respect to the timing marks on the film. The frame rate for the camera was determined to be 1900 fps.

10.4 Visual Observations

Figures 10-6 through 10-9 show the results of the test. The body of the cask was indented in the area of the puncture bar impact. Figures 10-7 and 10-8 show the width and depth of the deformed area. Figure 10-9 shows the deformation of the puncture bar caused by the test.

The thermal shield was torn near the area deformed by the puncture bar. The tear extended ~1/4 of the distance around the circumference of the indentation, on the closure end of the cask. The thermal shield also had a crack about 1/4 in. long, perpendicular to the tear and ~1/8 of the distance around the circumference of the indentation.

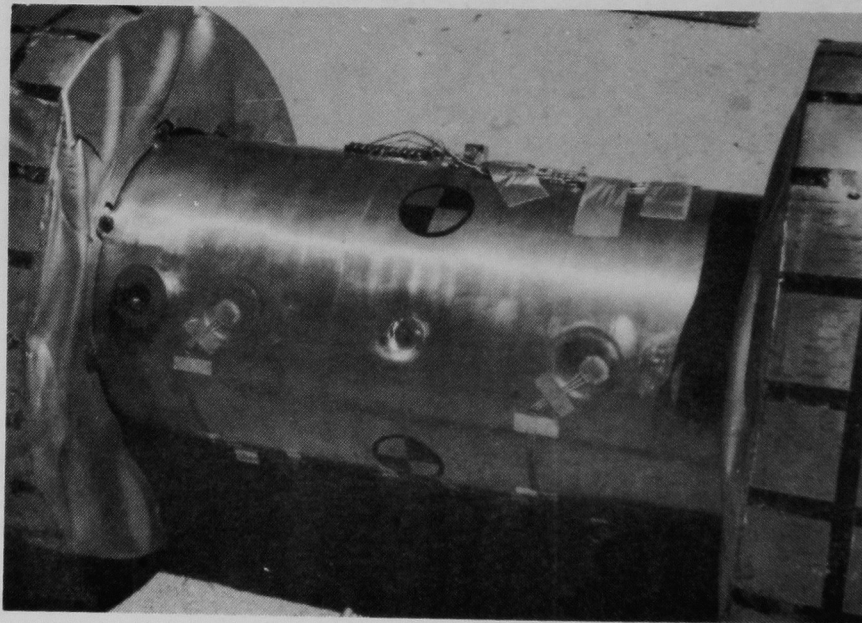


Figure 10-6. Condition of the Model After the 40-in. Side Puncture Test

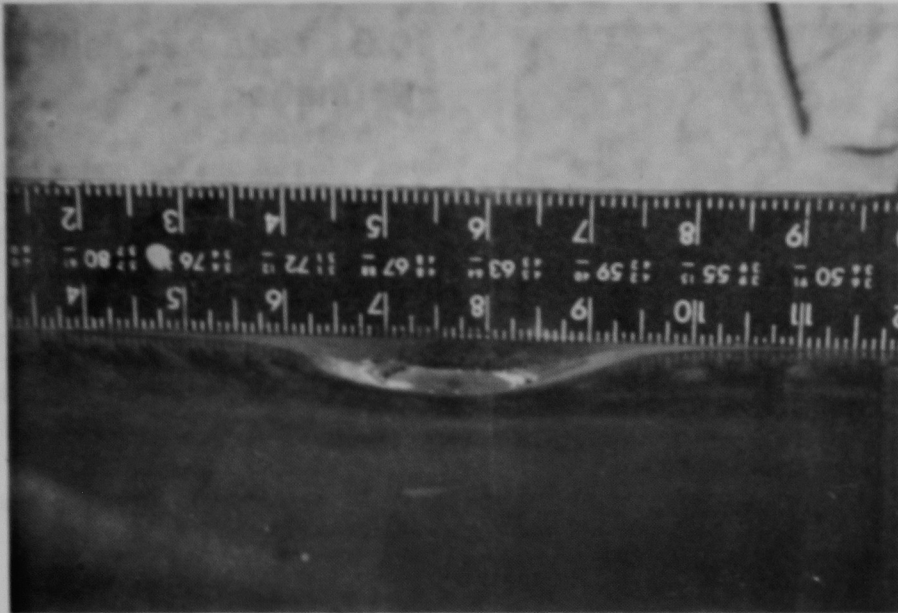


Figure 10-7. Width of Deformation From 40-in. Side Puncture Test

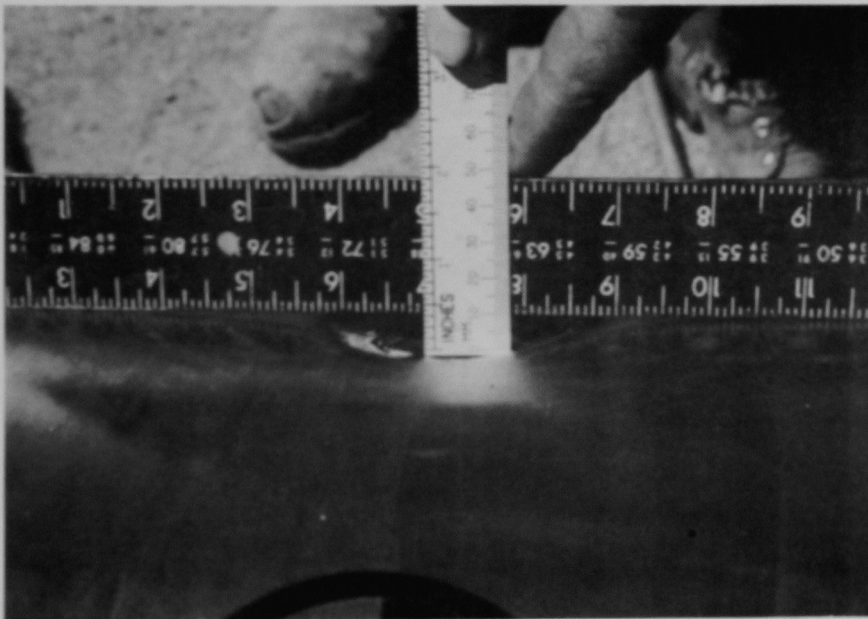


Figure 10-8. Depth of Deformation From 40-in. Side Puncture Test

10.5 Data Acquisition System Information

Accelerometer and strain gage data from the 40-in. side puncture test are contained in Appendix E1. The data were filtered at 1000 Hz. The fast Fourier transforms of the unfiltered data (presented in Appendix E2) give the frequency response of the model. Data from the strain gages located on the puncture bar are not presented. The signal saturated the instrumentation because the instrumentation calibration level used was much lower than the signal.

The consistency and validity of the data are evaluated in Chapter 14.

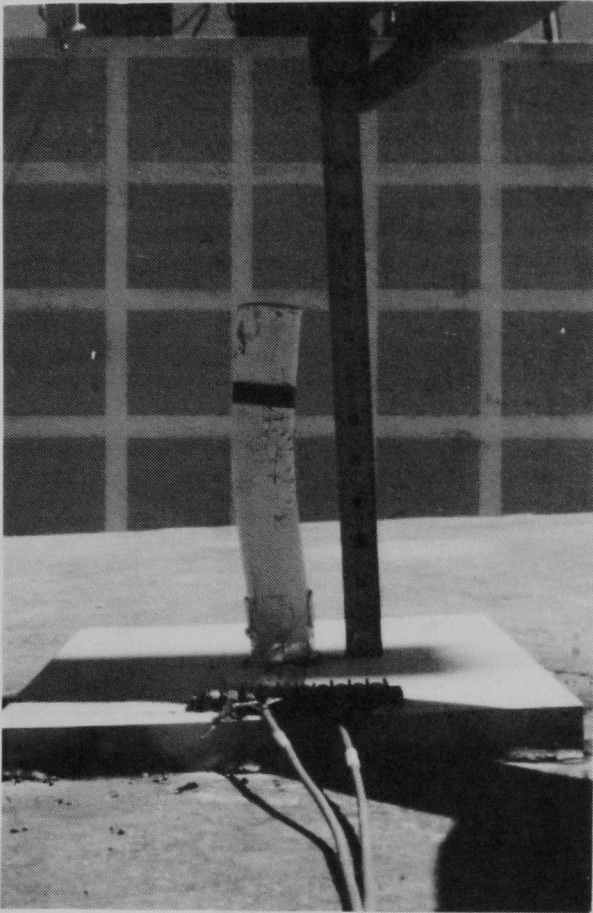


Figure 10-9. Deformation of the Puncture Bar After the 40-in. Side Puncture Test: Front View

11. 40-in. Closure End Puncture Test

11.1 Puncture Bar

A mild-steel puncture bar was fabricated, instrumented, and calibrated for the test as shown in Figure 11-1. Characteristics of the puncture bar are listed in Table 11-1.

General purpose, mild steel, compensated biaxial strain gages, with fully encapsulated grids and exposed copper coated integral solder tabs, were installed on the puncture bar for the dynamic force analysis. Characteristics of these strain gages are listed in Table 11-2.

Table 11-1. Characteristics of Puncture Bar for Closure End Puncture Test

Material	SAE 1018
Hardness	92.7-93.0 R _H 55.9-57.0 R _A
Upper Radius	0.06 in.
Diameter	1.50 in.
Length	11.0 in.

Table 11-2. Characteristics of Micro-Measurements Strain Gages Used on Puncture Bar for Closure End Puncture Test

Gage Type	CEA 06-125UT-350
Strain Range	± 5%
Temperature Range	-100°F to +400°F

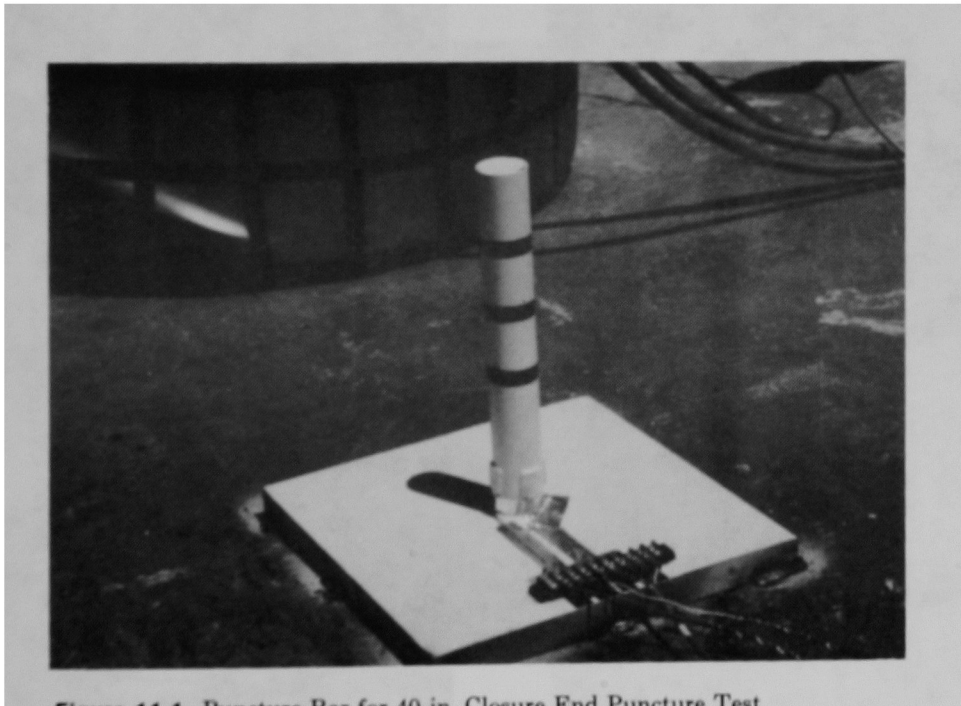


Figure 11-1. Puncture Bar for 40-in. Closure End Puncture Test

11.2 Closure End Puncture Test Procedure

The rigging hardware, with guillotine cable cutters installed, was attached to the trolley on the overhead cable and to the eye bolts attached to the trunnions on the bottom end of the cask body. The unit was leveled by means of a turnbuckle in one of the rigging lines.

The 11-in. puncture bar was positioned on the unyielding target. After the puncture bar base plate was welded to the target, instrumentation cables were attached to the terminal strips on the base plate.

The instrumentation cables were attached to the terminal strips on the cask and secured to a trunnion.

The stadia boards were positioned, documentary photographs taken, and the test procedure steps verified and signed. Figure 11-2 shows the model rigged for the 40-in. closure end puncture test. The puncture bar location and the distance from the cask to the top of the puncture bar were verified (Figure 11-3). After the data acquisition checkout was completed, the assembly was hoisted to the 40-in. drop height in final preparation for the test.

After the test procedure steps were verified and signed, the guillotine cable cutters were actuated, and the model free fell onto the puncture bar. The actual 40-in. closure end puncture test and the orientation of the model for the test are shown in Figures 11-4 and 11-5, respectively.

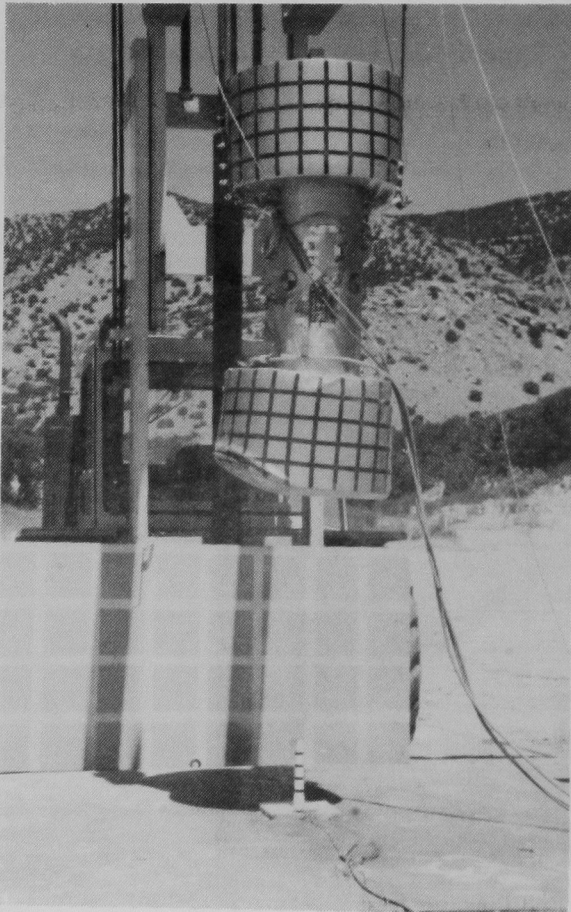


Figure 11-2. NuPac 125-B Model Rigged for 40-in. Closure End Puncture Test

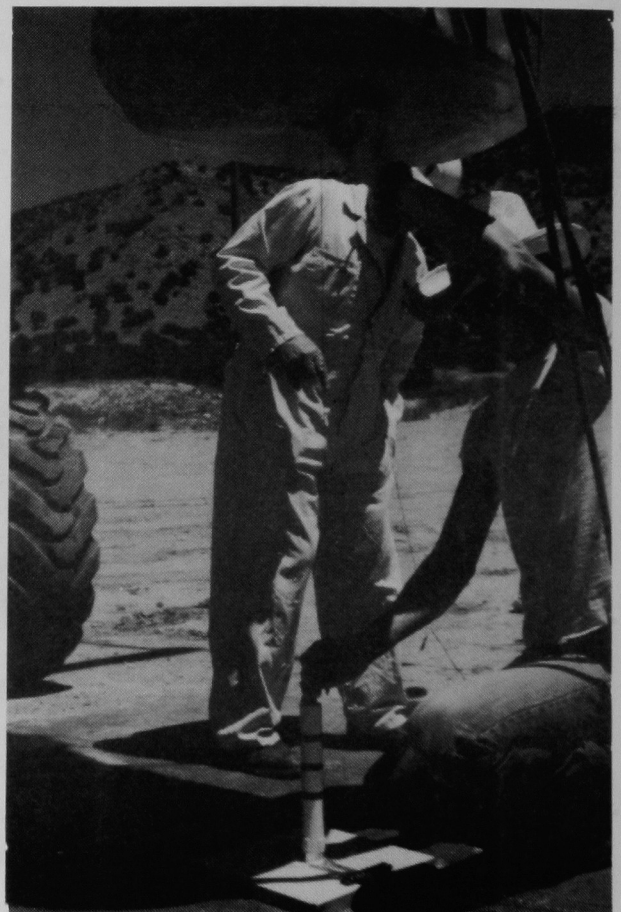


Figure 11-3. Verification of Puncture Bar Location and Distance From Model for 40-in. Closure End Puncture Test

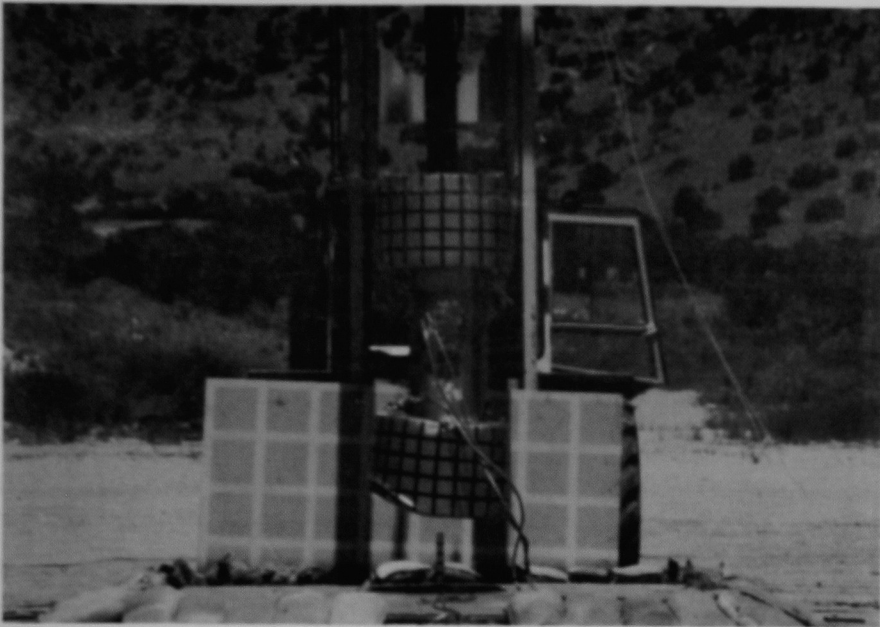


Figure 11-4. Sequential Photographs of the 40-in. Closure End Puncture Test

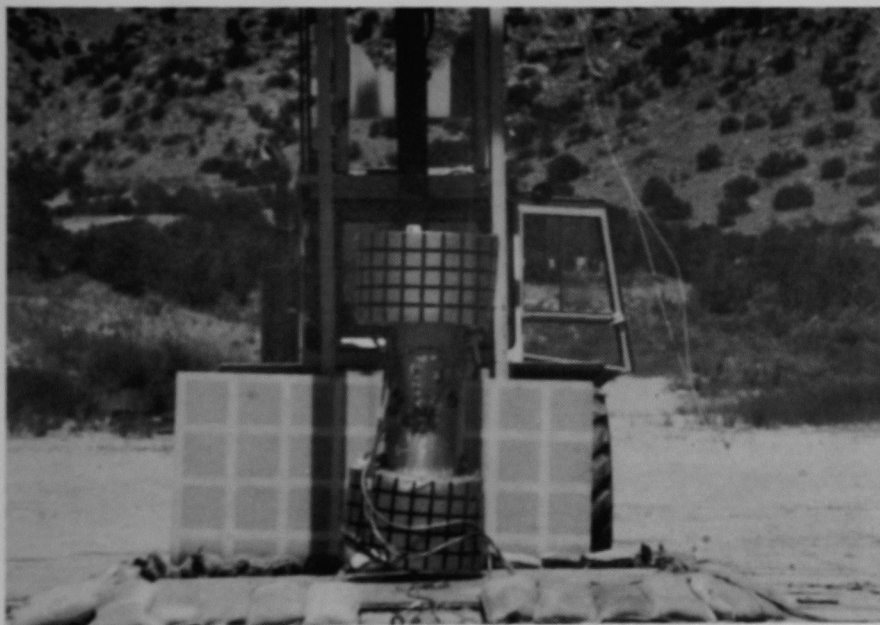


Figure 11-4. (concluded)

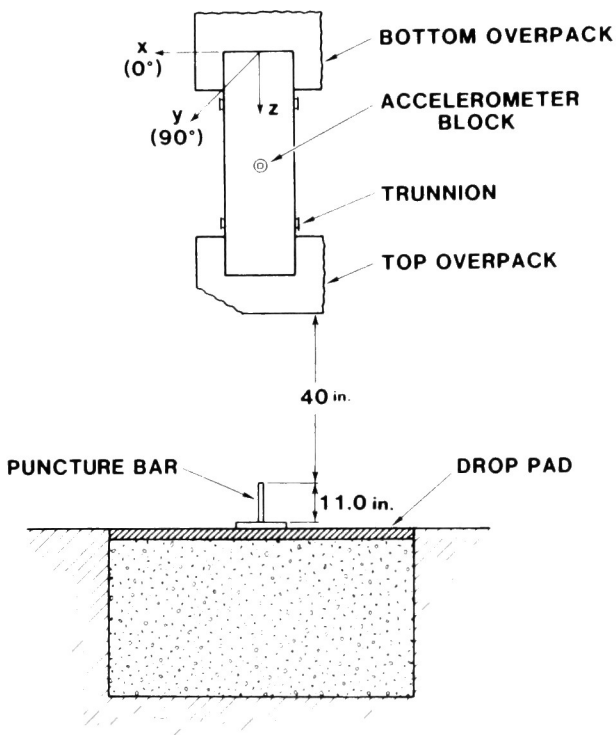


Figure 11-5. Orientation of Model for 40-in. Closure End Puncture Test (stadia board is behind model)

11.3 Photometrics Data

Photometrics data were obtained for this test. No photos from this footage were used, however, because effects on the model were obscured by the overpack during the puncture event.

11.4 Visual Observations

Figures 11-6 through 11-10 show the results of the test. Figure 11-9 shows the deformed area of the overpack, and Figure 11-10 shows the condition of the puncture bar.

11.5 Data Acquisition System Information

Accelerometer and strain gage data from the 40-in. closure end puncture test are contained in Appendix F1. Data from the strain gages on the puncture bar (Gage Nos. F1 and F2) are given at the end of Appendix F1. The data were filtered at 1000 Hz. The fast Fourier transforms of the unfiltered data (presented in Appendix F2) give the frequency response of the model.

The consistency and validity of the data are evaluated in Chapter 14.

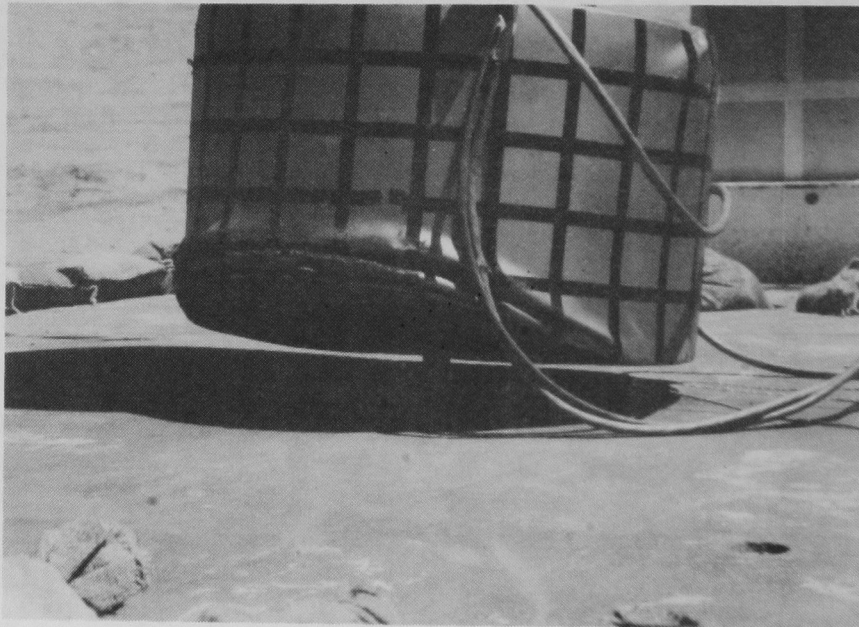


Figure 11-6. Condition of the Model After the 40-in. Closure End Puncture Test

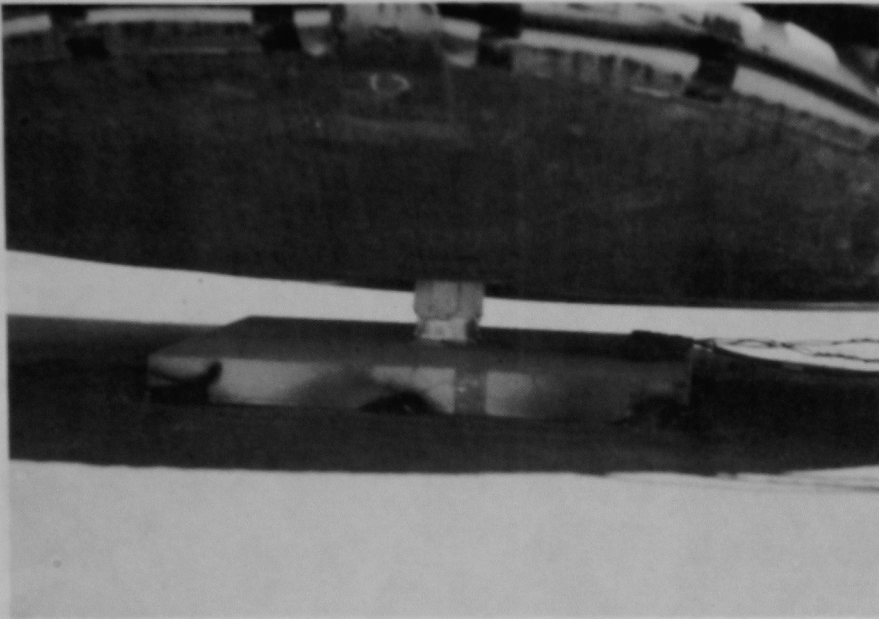


Figure 11-7. Close-up of the Model and Puncture Bar After the 40-in. Closure End Puncture Test



Figure 11-8. Close-up of the Upper Overpack and Puncture Bar After Model Had Been Lifted Off the Bar Following the 40-in. Closure End Puncture Test

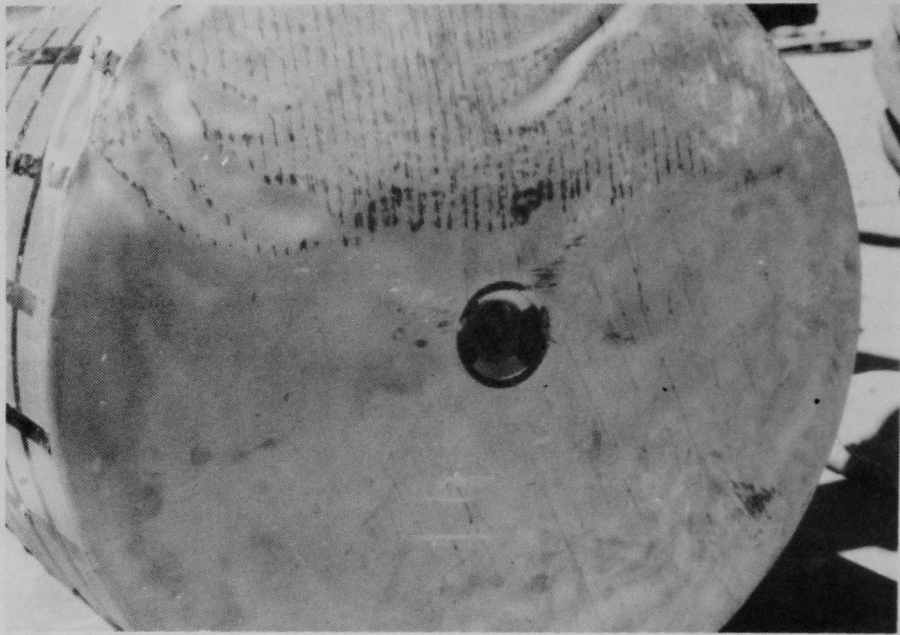


Figure 11-9. Deformed Area of Upper Overpack After the 40-in. Closure End Puncture Test

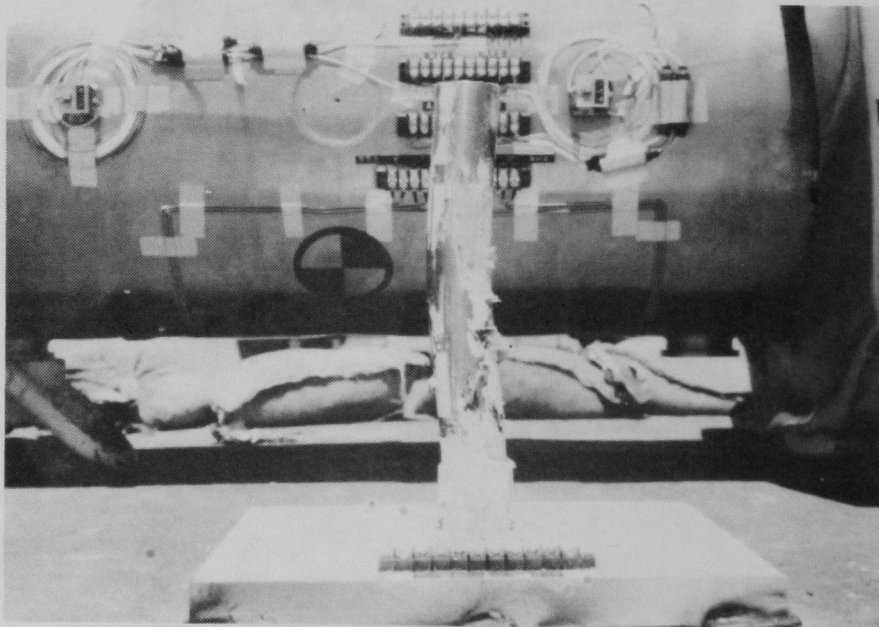


Figure 11-10. Deformation of the Puncture Bar After the 40-in. Closure End Puncture Test: Front View

12. Final Post-Test Examination

12.1 Removal of Overpacks

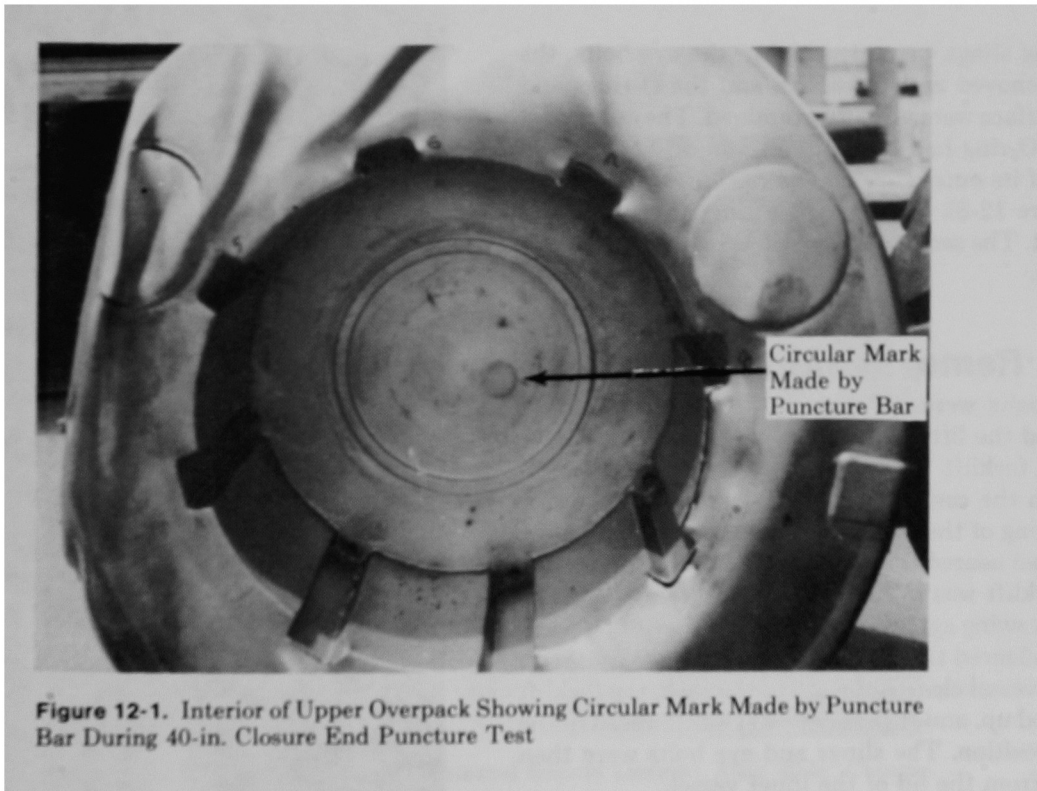
After the model was lifted off the transport skid, the overpacks were removed from the cask body by unfastening the bolts attaching them to the cask and sliding the overpacks horizontally from the ends of the cask. A circular mark caused by the closure end puncture test was visible on the top overpack (Figure 12-1), however the puncture bar had not penetrated through the overpack base plate. Figure 12-2 shows the condition of the outer vessel lid. A mark made by the puncture bar is barely visible between the 3- and 4-in. lines on the rule.

12.2 Leak Testing of Outer Vessel

The outer vessel containment boundary leak test was delayed until the inspection marks could be removed and the vessel thoroughly cleaned.

After the leak test hardware was attached to the test port on the outer vessel lid, the space between the O rings on the lid was evacuated to the standard operating pressure for the leak detector. The lid bolt torques were checked, and all were at their pre test values. The outer vessel cavity was evacuated and pressurized with helium. The leak detector was monitored, and the reading was recorded after it stabilized. There was no detectable helium leak rate for the pair of outer vessel O rings to a sensitivity of 5.5×10^{-10} cm^3/s .

The bolts on the lid of the cask were removed. The space between the O rings on the outer vessel lid remained evacuated to the standard operating pressure for the leak detector. The leak detector was monitored, and the reading was recorded after it stabilized. Even with the lid bolts removed, there was no detectable helium leak rate for the pair of outer vessel O-rings to a sensitivity of 1.4×10^{-8} cm^3/s .



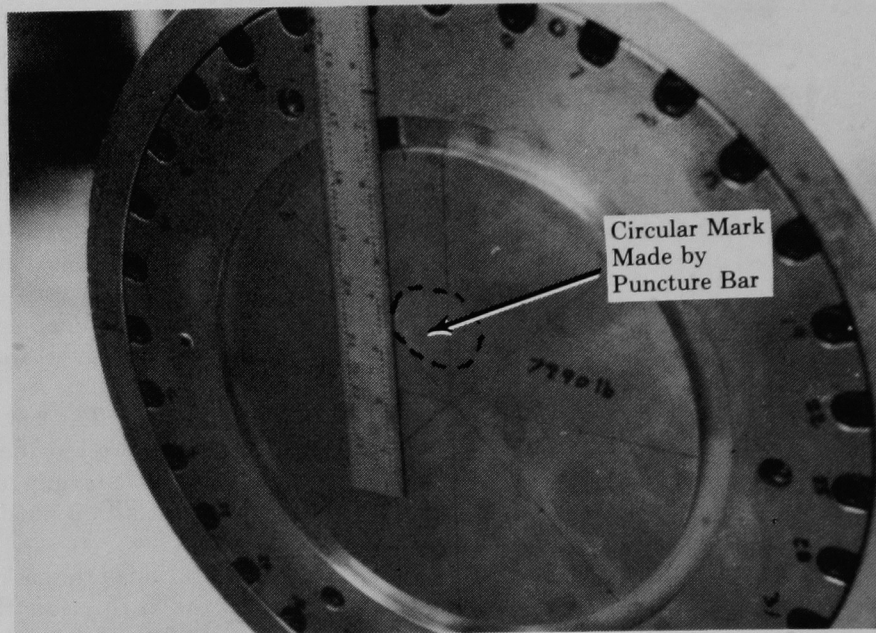


Figure 12-2. Condition of Outer Vessel Lid After 40-in. Closure End Puncture Test (A mark made by the puncture bar is visible between the 3- and 4-in. lines on the rule.)

12.3 Removal of Outer Vessel Lid

Lifting slings were attached to the eye bolts, the lid was removed with a forklift, and the O-rings and sealing surface were visually examined. The outermost or upper O-ring had been cut all around and a small amount of its outer surface removed from the assembly (Figure 12-3). However, the inner (lower) O-ring was intact. The sealing surface on the outer vessel was scratched.

12.4 Removal of Inner Vessel

Eye bolts were attached to the lid of the inner vessel, and the lifting slings were attached to the eye bolts and forklift. The inner vessel was pulled vertically from the cask and guided as it rose to prevent any scraping of the sides of the two vessels. When the inner vessel neared the top of the cask, the lifting rate of the forklift was decreased so that the inner vessel would not swing against the sealing surface of the cask wall as it cleared the internal bore of the cavity. After the inner vessel cleared the top of the cask, the forklift was backed up, and the inner vessel was lowered in the vertical position. The slings and eye bolts were then removed from the lid of the inner vessel.

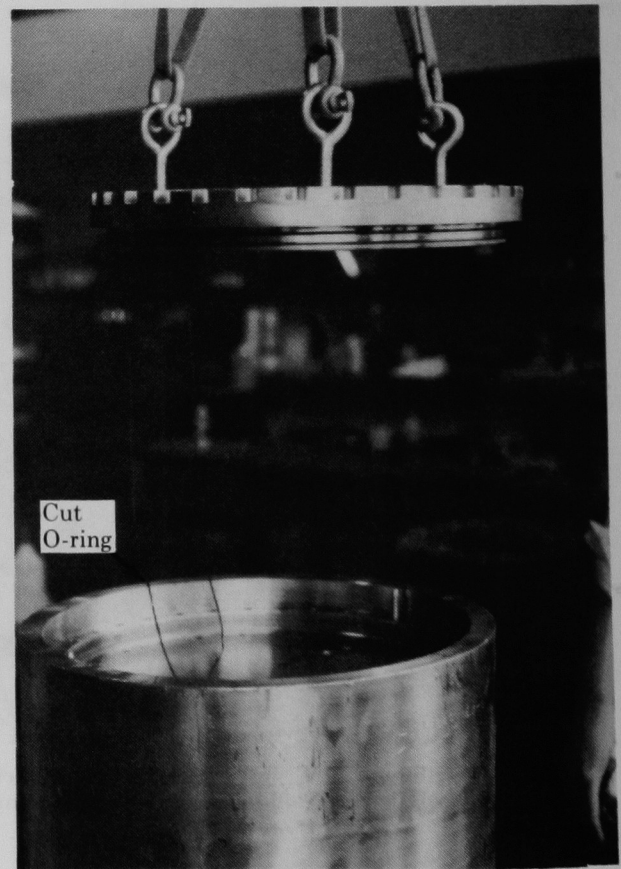


Figure 12-3. Outer Vessel Lid and Cut Portion of Upper O-Ring

12.5 Leak Testing of Inner Vessel

The inner vessel containment boundary leak test was delayed until the inspection marks could be removed and the vessel thoroughly cleaned.

After the leak test hardware was attached to the test port on the inner vessel lid, the space between the O-rings on the lid was evacuated to the standard operating pressure for the leak detector. However, the background reading was 2000 divisions, which is quite high. The inner vessel cavity was evacuated and pressurized with helium. The leak detector was monitored; the reading remained at the high background level. There was no detectable helium leak rate for the pair of inner vessel O-rings to a sensitivity of 5.2×10^{-10} cm³/s.

12.6 Removal of Inner Vessel Lid

The lid bolt torques were checked, and all were at their pre-test values. The bolts and vent plug on the lid of the cask were removed and eye bolts installed for removal of the lid. Lifting slings were attached to the eye bolts, the lid was removed with a forklift, and the O-rings and sealing surface were visually examined. The O-rings were intact. Once again, the sealing surface on the inner vessel was found to be scratched.

12.7 Removal of Upper Internal Impact Limiters

The orientations of the upper internal impact limiters were documented and are shown in Figure 12-4 and Table 12-1. After eye bolts were installed in the tapped holes in the upper impact limiters, each impact limiter was lifted out by hand. The cumulative damage to the upper internal limiters is shown in Figures 12-5 through 12-11.

Table 12-1. Final Orientations of Upper Internal Impact Limiters

Impact Limiter	Orientation
A	~5° clockwise
B	~5° counterclockwise
C	~5° clockwise
D	~2° counterclockwise
E	~10° clockwise
F	~2° clockwise
G	~10° counterclockwise

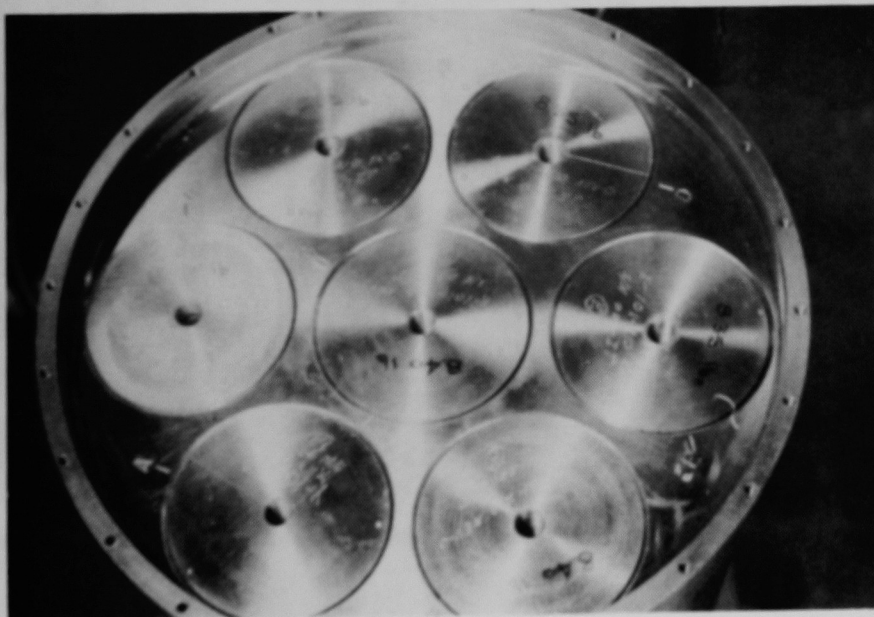


Figure 12-4. Orientation of Upper Internal Impact Limiters After 40-in. Closure End Puncture Test

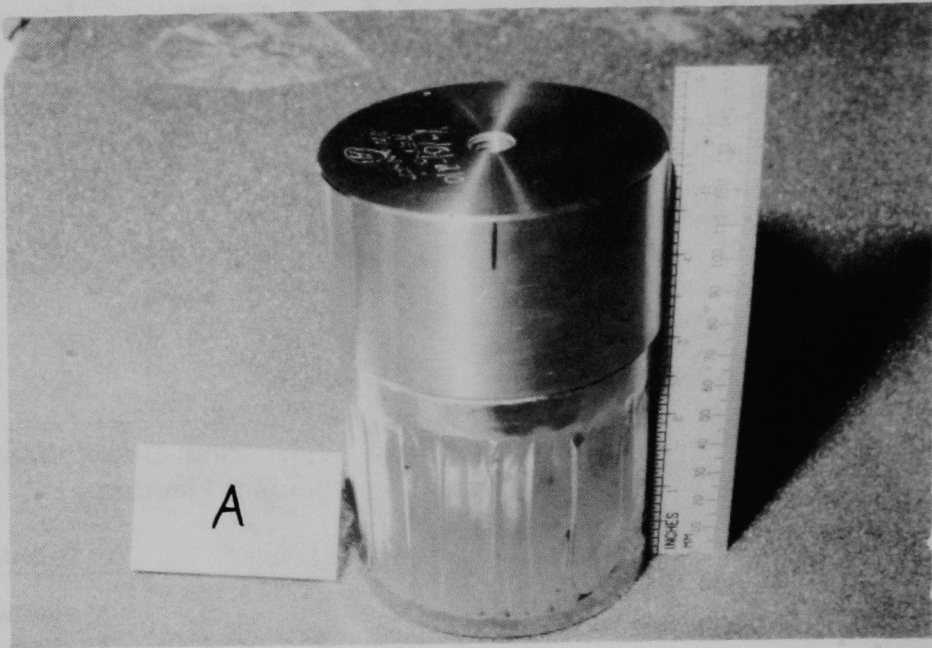


Figure 12-5. Condition of Upper Internal Impact Limiter "A" After 40-in. Closure End Puncture Test



Figure 12-6. Condition of Upper Internal Impact Limiter "B" After 40-in. Closure End Puncture Test

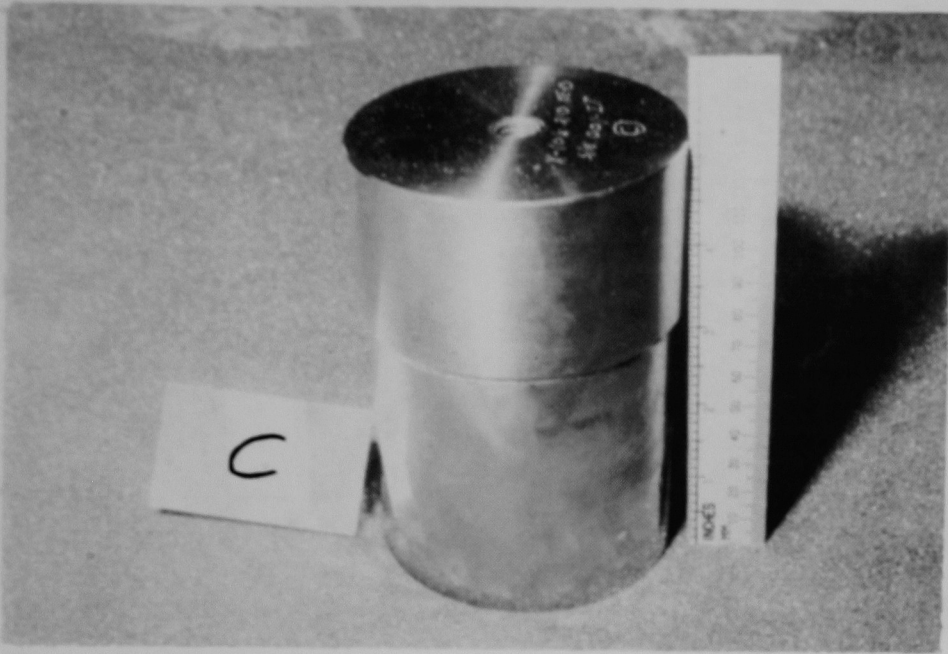


Figure 12-7. Condition of Upper Internal Impact Limiter "C" After 40-in. Closure End Puncture Test



Figure 12-8. Condition of Upper Internal Impact Limiter "D" After 40-in. Closure End Puncture Test



Figure 12-9. Condition of Upper Internal Impact Limiter "E" After 40-in. Closure End Puncture Test

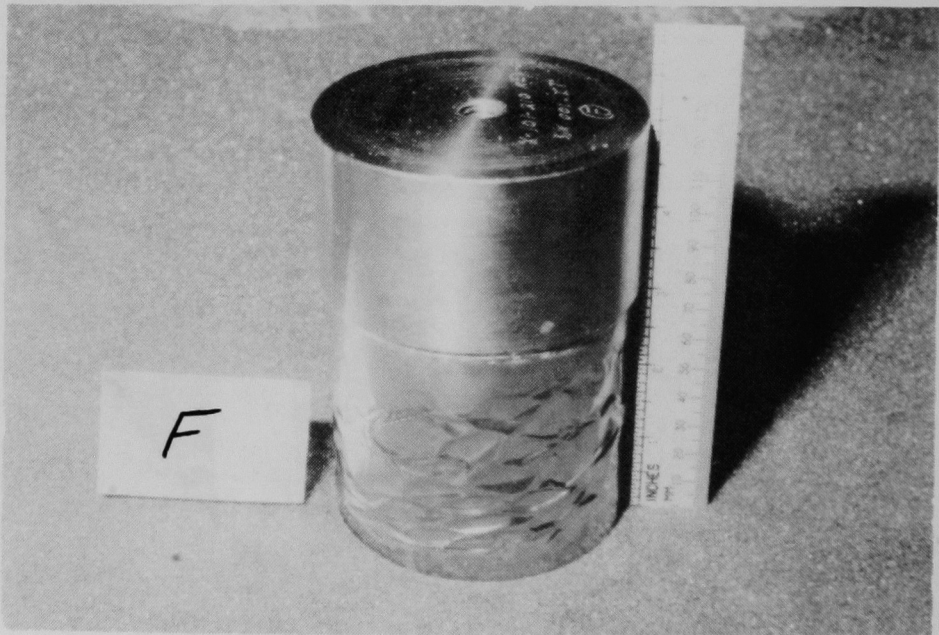


Figure 12-10. Condition of Upper Internal Impact Limiter "F" After 40-in. Closure End Puncture Test

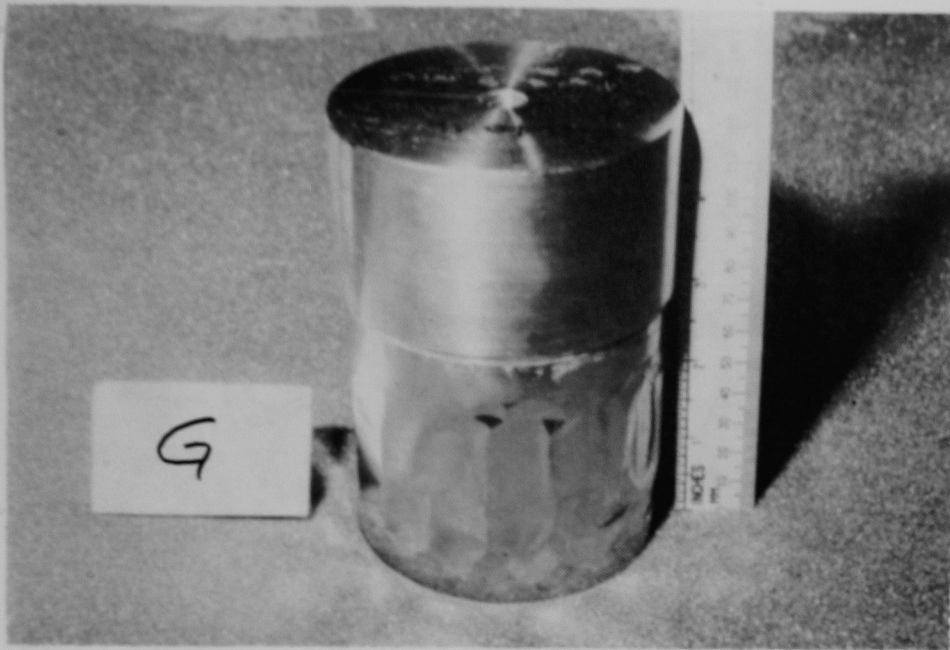


Figure 12-11. Condition of Upper Internal Impact Limiter "G" After 40-in. Closure End Puncture Test

12.8 Removal of Canisters

The orientations of the canisters were documented and are shown in Table 12-2. After eye bolts were installed in the tapped holes, each canister was lifted out by hand. The canisters appeared intact and unaffected by the tests.

Table 12-2. Final Orientations of Canisters

Canister	Orientation
A	~10° counterclockwise
B	~3° clockwise
C	~3° counterclockwise
D	~10° clockwise
E	~120° clockwise
F	~100° clockwise
G	~90° clockwise

12.9 Removal of Lower Internal Impact Limiters

Removal of the individual impact limiters was accomplished by attaching a tap to the end of a tube and reaching down into each of the cavities until the tap stuck into the impact limiter. The honeycomb was tapped, and by slowly raising the tube, the impact limiter was lifted out of the vessel. The cumulative damage to the impact limiters is shown in Figures 12-12 through 12-15.

12.10 X-Radiography

The x radiography of the closure end of the cask body was accomplished by positioning the cask 32 ft 2 in. from the Limitron and then placing 8 x 10 in. x ray plates 8 to 9 in. into the closure end of the cask body (Figure 12-19). After the plate was exposed, the cask body was rotated 90° and another x radiograph taken. No anomalies were observed for the closure end of the cask.



Figure 12-12. Condition of Lower Internal Impact Limiter "A" After 40-in. Closure End Puncture Test

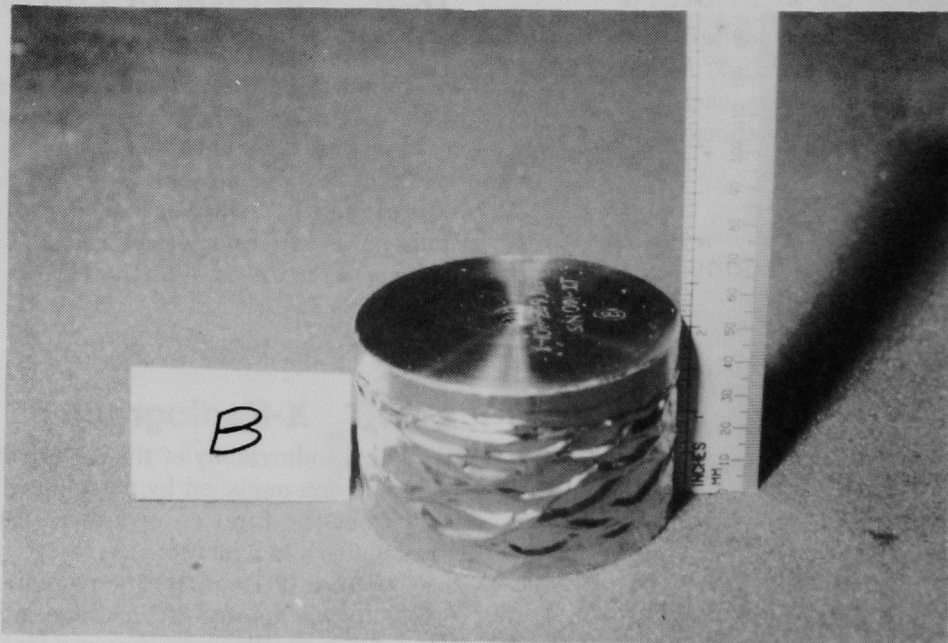


Figure 12-13. Condition of Lower Internal Impact Limiter "B" After 40-in. Closure End Puncture Test



Figure 12-14. Condition of Lower Internal Impact Limiter "C" After 40-in. Closure End Puncture Test



Figure 12-15. Condition of Lower Internal Impact Limiter "D" After 40-in. Closure End Puncture Test

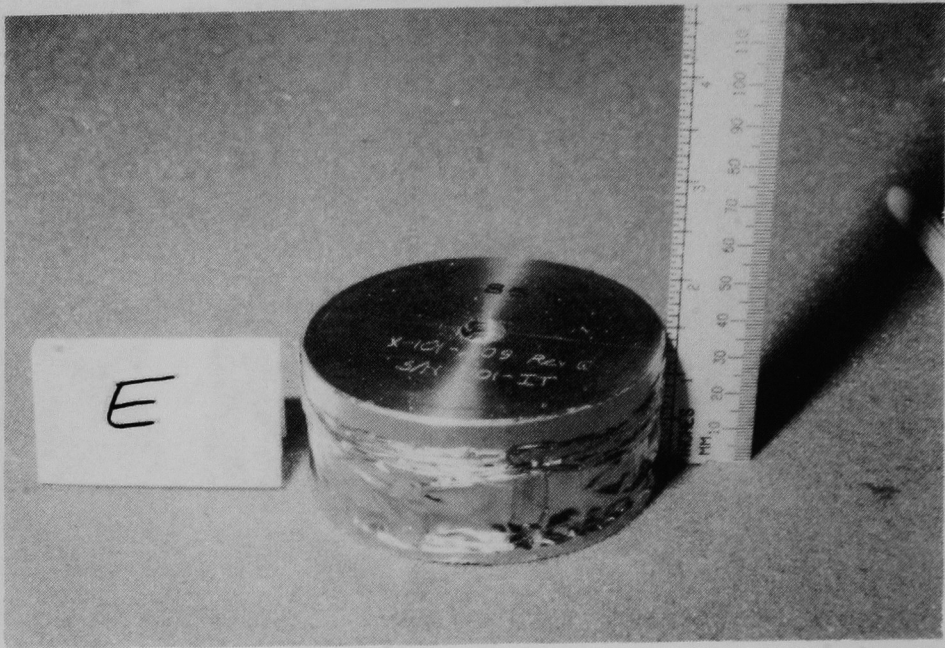


Figure 12-16. Condition of Lower Internal Impact Limiter "E" After 40-in. Closure End Puncture Test



Figure 12-17. Condition of Lower Internal Impact Limiter "F" After 40-in. Closure End Puncture Test



Figure 12-18. Condition of Lower Internal Impact Limiter "G" After 40-in. Closure End Puncture Test

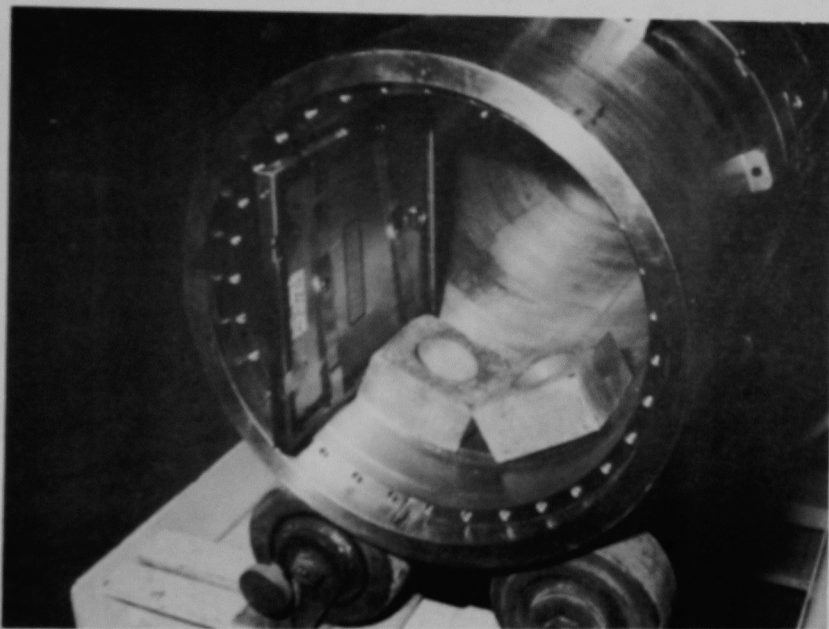


Figure 12-19. X-Ray Plate in Position for Examination of the Closure End of the Cask Body

The lower portion of the cask was x-radiographed by positioning 17×21-in. plates behind the body of the cask (Figure 12-20). After the plate was exposed, the cask body was rotated 90° and another x-radiograph taken.

An anomaly ~3.750 in. up from the bottom (closed end) of the cask was observed in the original x-radiography examination on the 0° bottom x-ray plate. As shown in Figure 12-21, the anomaly remained unchanged.

Two views of the cask side wall deformed by the puncture bar are shown in Figure 12-22 (x-radiograph taken inside the cask body) and Figure 12-23 (x-radiograph of the cask side wall). A side view of the indentation caused by the test can be seen at the top of Figure 12-23.

12.11 Inspection

Final inspection of the assembly was completed by the personnel from the Mechanical Measurements Division at Sandia National Laboratories who had performed the initial and intermediate inspections. The measurements were taken from the locations previously marked and used to determine the PMI (Appendix A).

12.11.1 Final Inspection of Cask Body

The measurements of the cask bore diameter showed many differences outside the PMI. Differences data for the cask bore diameter in excess of the PMI of ± 0.005 in. are listed in Table 12-3.

Location D3 is measured across the bore at the site of the trunnions, and the cask was dropped with trunnions down for both the side drop test and side puncture test. Therefore, the cask bore diameter decreased along the line of impact, most of all near the puncture location D3,L3. The cask bore ovalized outward at the other diameter locations (D1, D2, D4).

The differences data for straightness measurements also showed changes in the cask bore. Differences greater than the PMI of ± 0.005 in. are listed in Table 12-4.

Measurements taken at tangential locations D1, D5, D6, and D8 show a localized movement inward radially at these locations. Measurements taken at tangential locations D3 and D7 show a localized movement outward radially.

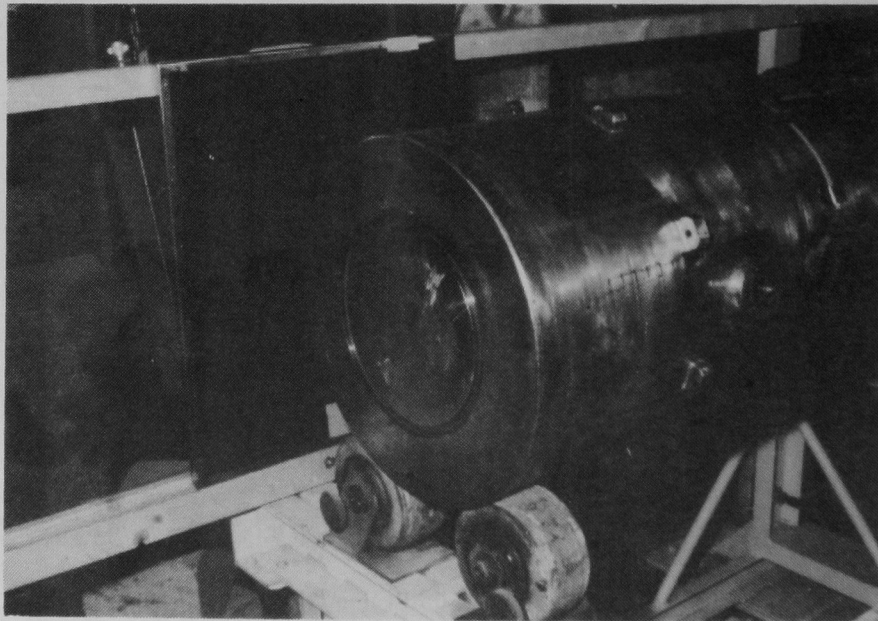


Figure 12-20. X-Ray Plate in Position for Examination of the Bottom End of the Cask Body

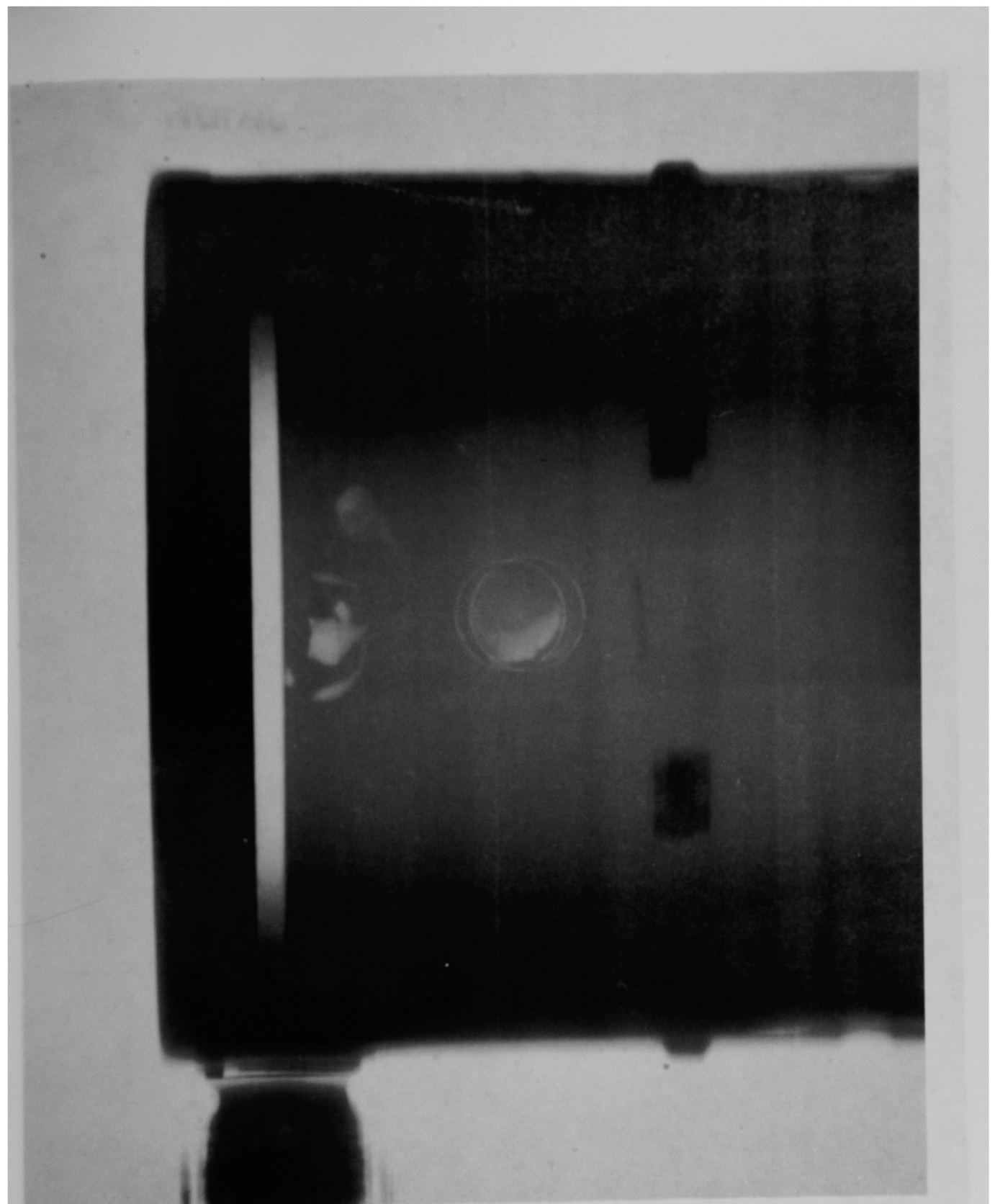


Figure 12-21. X-Radiograph of Cask Bottom at 0° After Completion of Testing

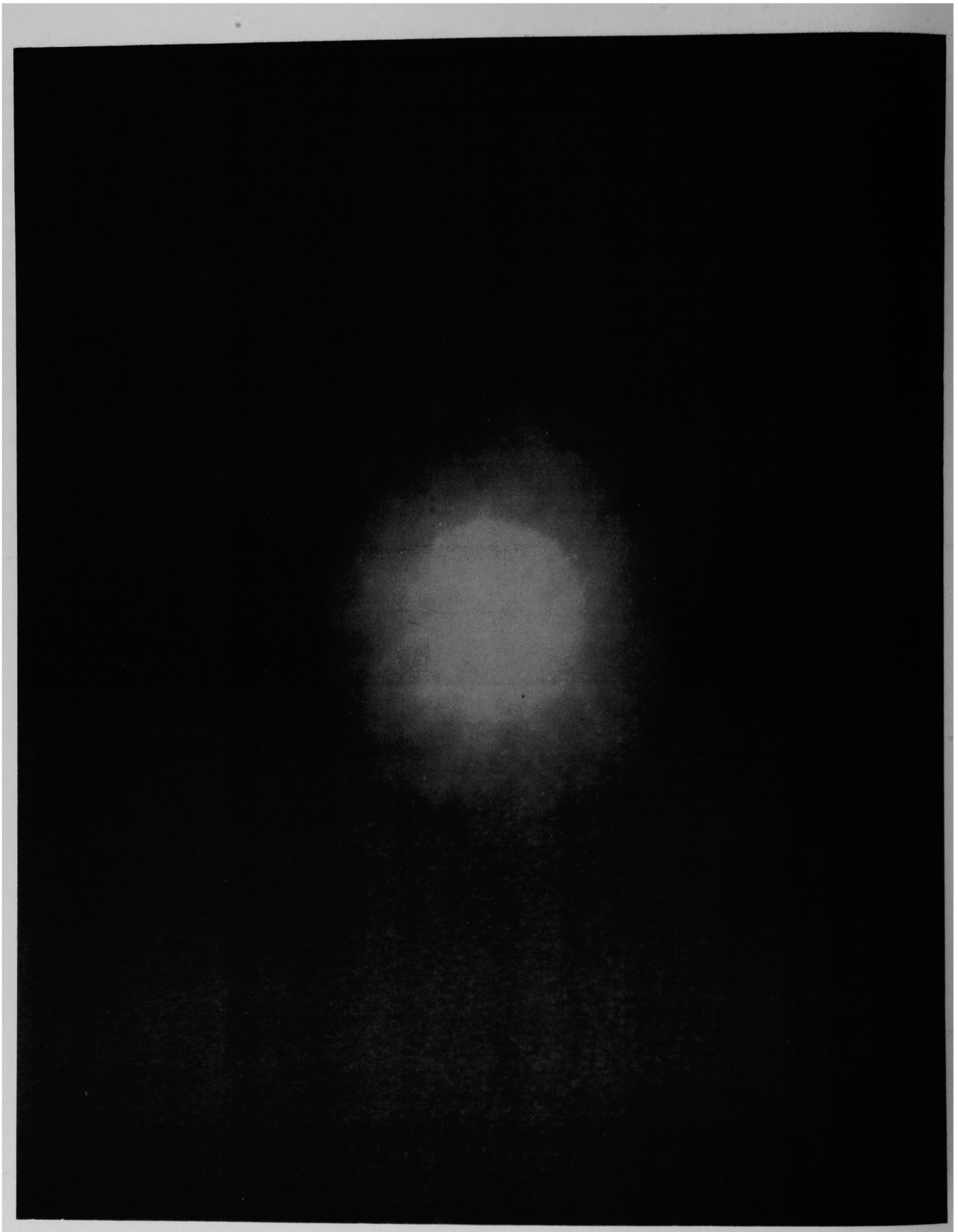


Figure 12-22. X-Radiograph of Puncture Area Taken From Inside the Cask Body

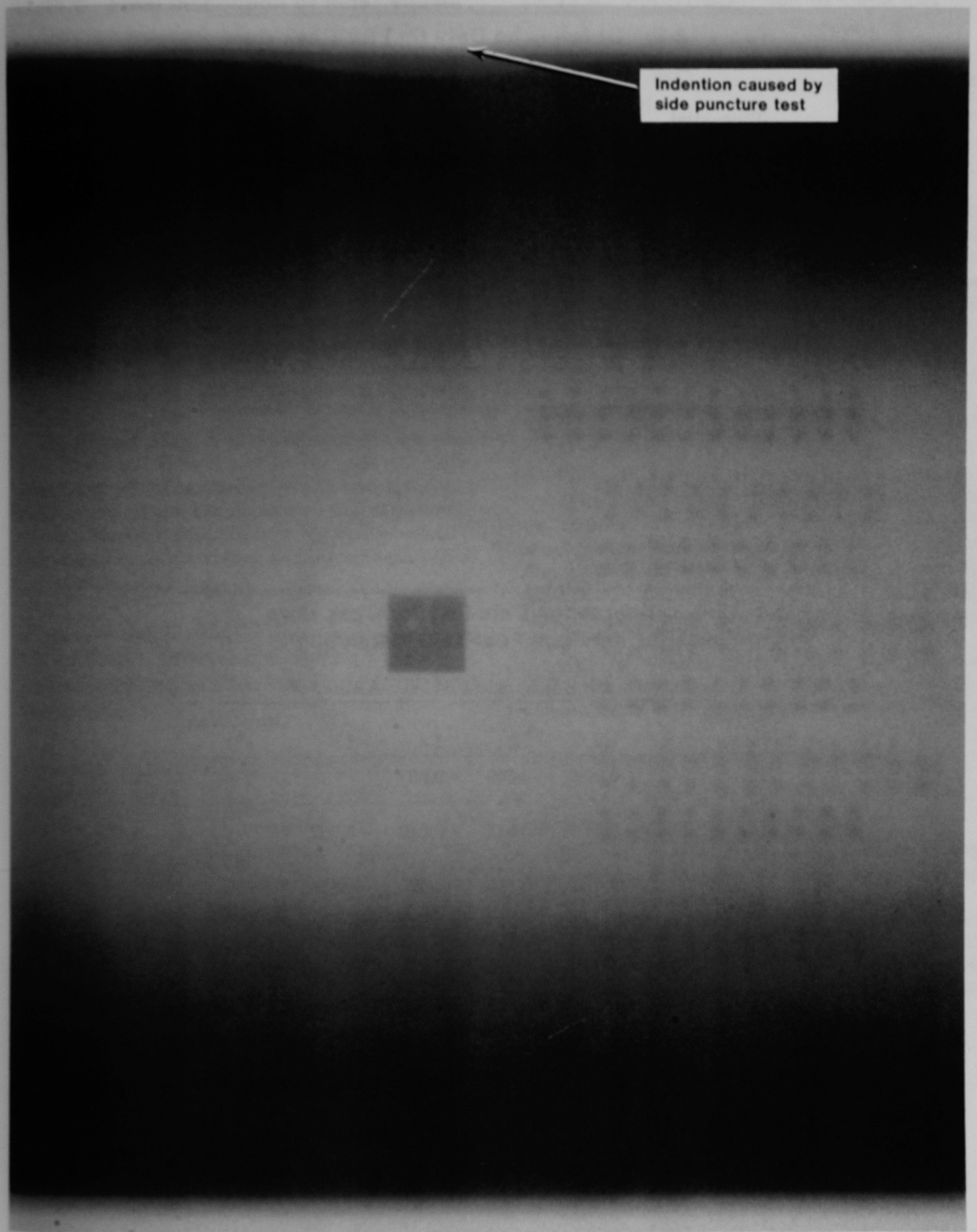


Figure 12-23. X-Radiograph of Puncture Area: Side View at 270°

Table 12-3. Differences Data (in.) for Cask Bore Diameter for the Final Post-Test Inspection

Tangential Location	Longitudinal Location					
	LS	L1	L2	L3	L4	L5
D1	*	+0.009	+0.022	+0.023	+0.023	+0.011
D2	*	*	+0.011	+0.028	*	*
D3	*	-0.009	-0.031	-0.121	-0.031	-0.010
D4	*	*	*	+0.028	*	*

Notes: *Measurement within PMI of ± 0.005 in.

Difference measurement = initial measurement minus current measurement. The sign has been adjusted to be positive for an increase in diameter and negative for a decrease in diameter.

Table 12-4. Differences Data (in.) for Cask Bore Straightness for the Final Post-Test Inspection

Tangential Location	Longitudinal Location					Orientation (°)
	L1	L2	L3	L4	L5	
D1	*	-0.008	-0.009	-0.007	*	270
D2	*	*	*	*	*	315
D3	*	+0.008	+0.011	+0.010	+0.007	0
D4	*	*	*			45
D5	*	-0.012	-0.113	-0.020	-0.017	90
D6	*	*	-0.029	-0.006	*	135
D7	*	+0.025	+0.115	+0.028	+0.011	180
D8	*	*	-0.024	-0.007	-0.006	225

Notes: *Measurement within PMI of ± 0.005 in.

Difference measurement = initial measurement minus current measurement. The sign has been adjusted to be positive for a change away from the center and negative for a change toward the center.

12.11.2 Final Inspection of Inner Vessel

Only one measured difference exceeded the PMI of ± 0.010 in. for either the diameter or the straightness of the inner vessel exterior, that was the diameter at location D3L3, which measured a slight increase (0.011 in.) in the inner vessel outer diameter. No difference measurements of the inner vessel tube bores exceeded the PMI.

12.11.3 Final Inspection of Canisters

Several difference measurements of the canisters exceeded the PMI of ± 0.002 in. (Table 12-5).

The canisters were slightly bulged outward. The measurements for D2g agree exactly with the difference measurements taken at the intermediate post-test inspection. However, the measurements for D2e have changed, particularly near the end of the canister.

In contrast to the intermediate post-test inspection (Section 7.11.3), no significant differences in straightness of the canisters were observed at the final post-test inspection. This finding verifies the assumption that the large change in straightness recorded for D2a at the intermediate post-test inspection involved a systematic sign error.

Table 12-5. Differences Data (in.) for Canister Diameters for the Final Post-Test Inspection

Tangential Location	Longitudinal Location				
	L1	L2	L3	L4	L5
D2e	•	•	- 0.004	•	•
D2g	•	+ 0.003	- 0.004	+ 0.003	•

Notes: *Measurement within PMI of ± 0.002 in.
 Difference measurement = initial measurement minus current measurement. Signs have been adjusted to be positive for an increase in diameter and negative for a decrease in diameter.

12.11.4 Final Inspection of Cask Lid, Cask Bottom, and Inner Vessel Lid

There were no difference measurements exceeding the PMI of ± 0.002 in. for the cask lid, cask bottom, or inner vessel lid.

12.11.5 Final Inspection of Internal Impact Limiters

The lengths of the upper and lower internal impact limiters were measured. The amount of crush of each impact limiter was the same within the PMI as the crush measured for the intermediate post-test inspection, with two exceptions. Upper impact limiter "D" was measured at two locations, L3 and L4, to have slightly less crush (by 0.003 to 0.004 in.) at the end of the test sequence than at the intermediate inspection.

12.11.6 Final Inspection of Overpacks

12.11.6.1 Inspection of Overpack Exteriors

After testing of the NuPac quarter scale model was complete, the exterior surfaces of the overpacks were measured and photographed to document their final condition. Figures 12-24 through 12-27 show the condition of the top overpack, while Figures 12-28 through 12-31 show the condition of the bottom overpack.

The major exterior deformations were measured before the sectioning of the individual overpacks. Figures 12-32 and 12-33 show the measurements of the top overpack, while Figures 12-34 and 12-35 show the measurements of the bottom overpack.

12.11.6.2 Sectioning of Overpacks

The overpacks were permanently marked through the center and around the exterior surface through areas where damage appeared to be maximal.

The overpacks were positioned on a hand saw and cut as indicated by the permanent marks. Figures 12-36 and 12-37 show the sectioned top overpack, while Figures 12-38 and 12-39 show the sectioned bottom overpack.

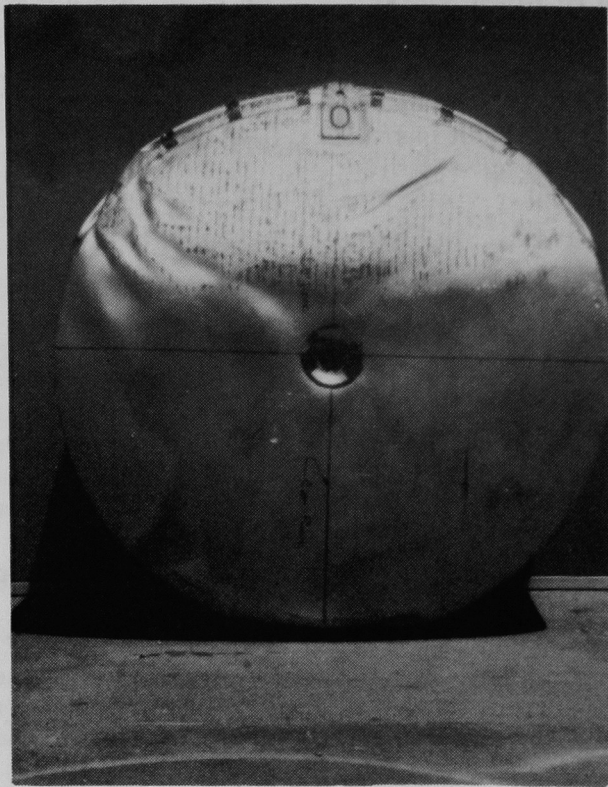


Figure 12-24. Top Overpack Exterior: End View

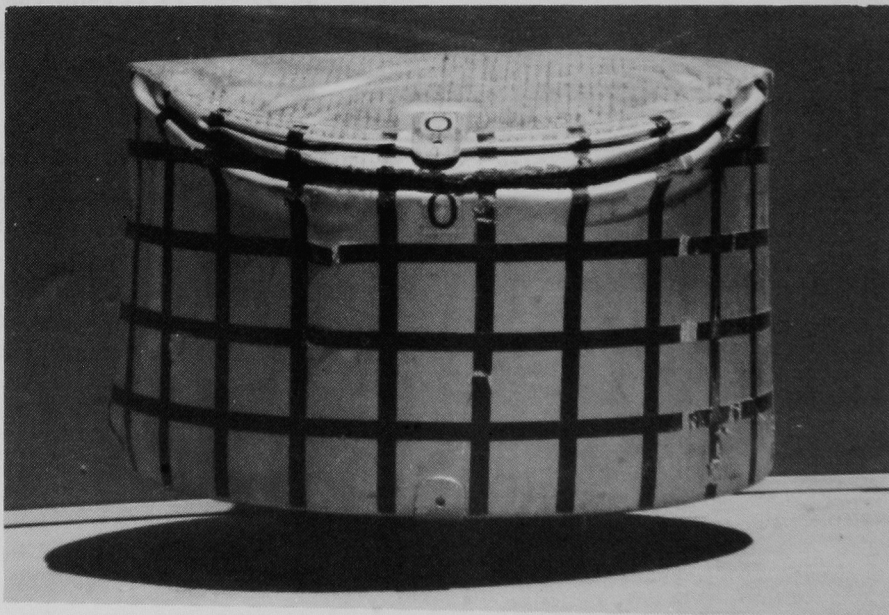


Figure 12-25. Top Overpack Exterior: Side View at 0°

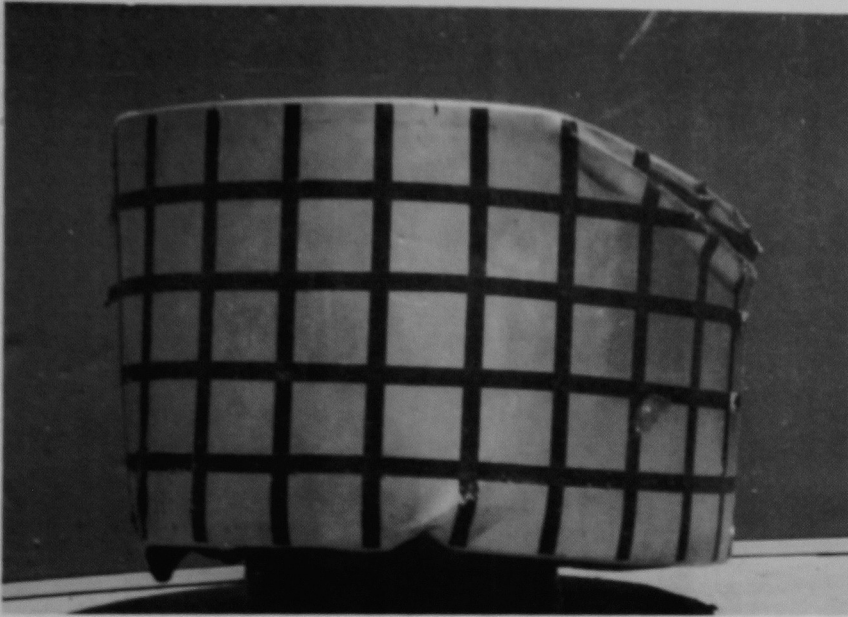


Figure 12-26. Top Overpack Exterior: Side View at 90°

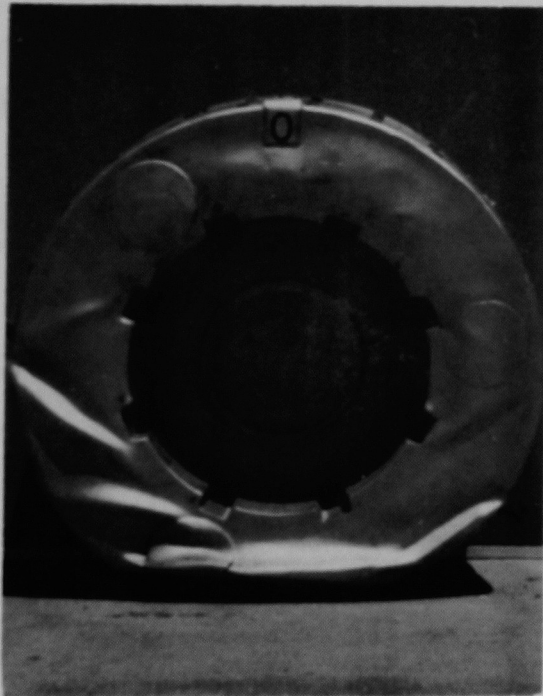


Figure 12-27. Top Overpack Interior

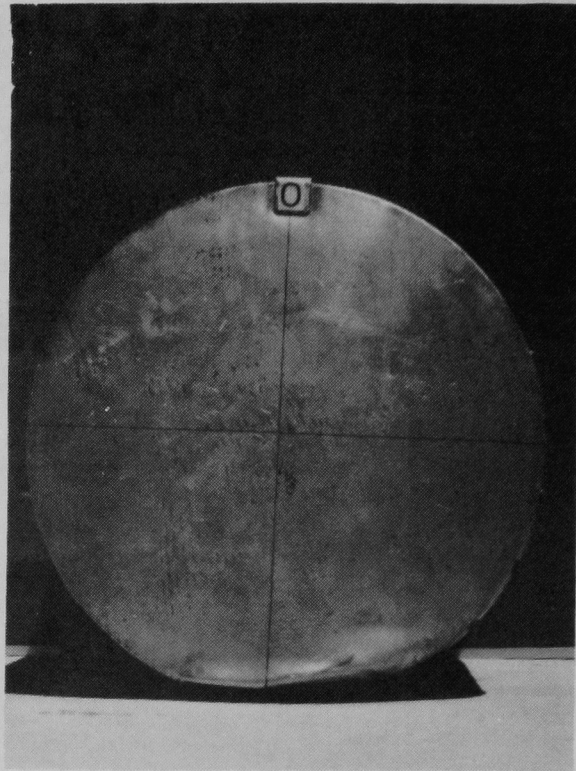


Figure 12-28. Bottom Overpack Exterior: End View

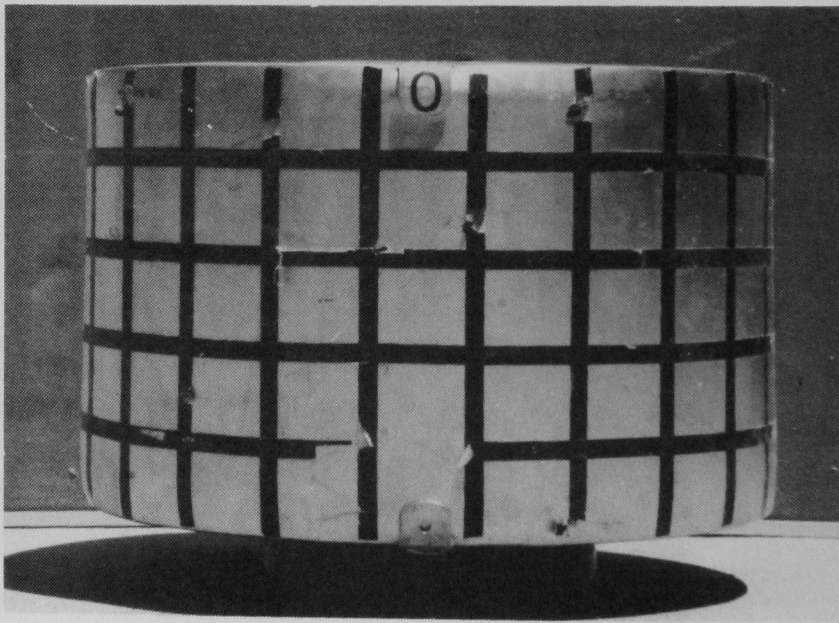


Figure 12-29. Bottom Overpack Exterior: Side View at 0°

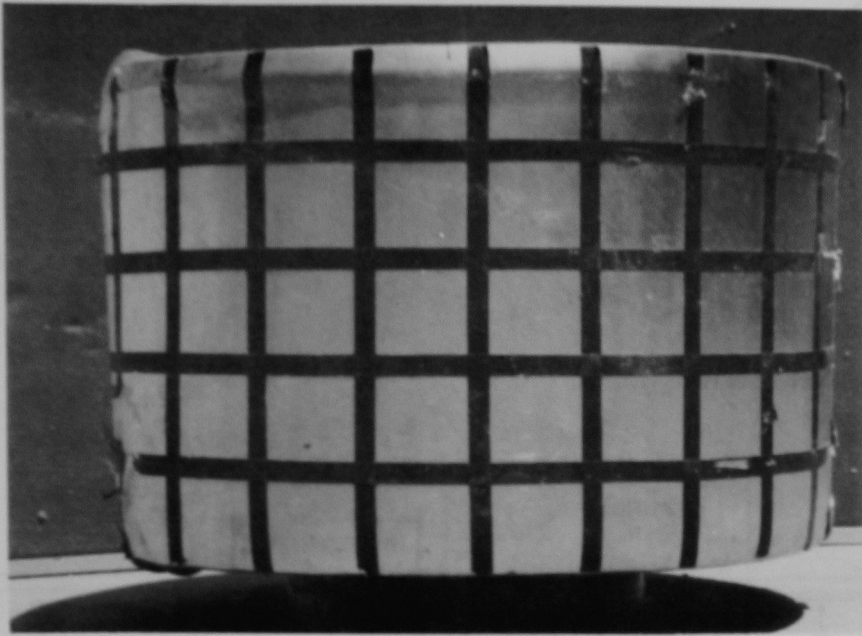
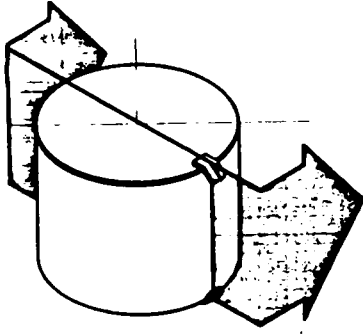


Figure 12-30. Bottom Overpack Exterior: Side View at 90°



Figure 12-31. Bottom Overpack Interior



SECTION THRU LIFTING TABS

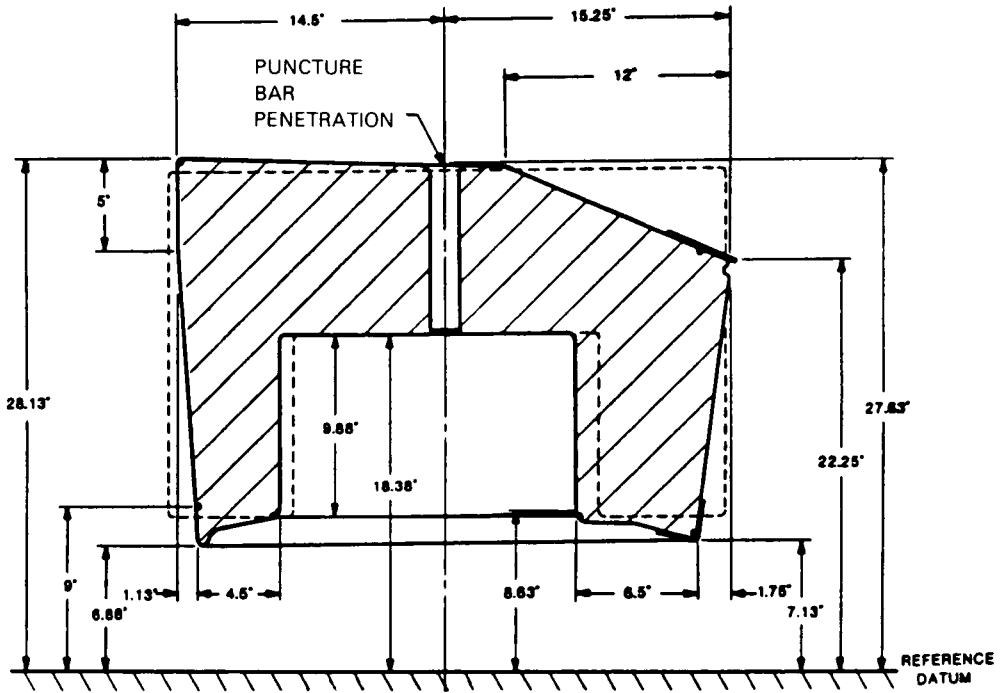
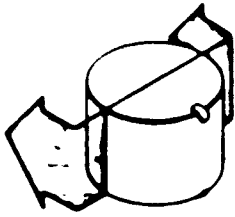


Figure 12-32. Top Overpack Measurements: Section Through Lifting Tabs



SECTION NORMAL TO LIFTING TABS (90° CCW)

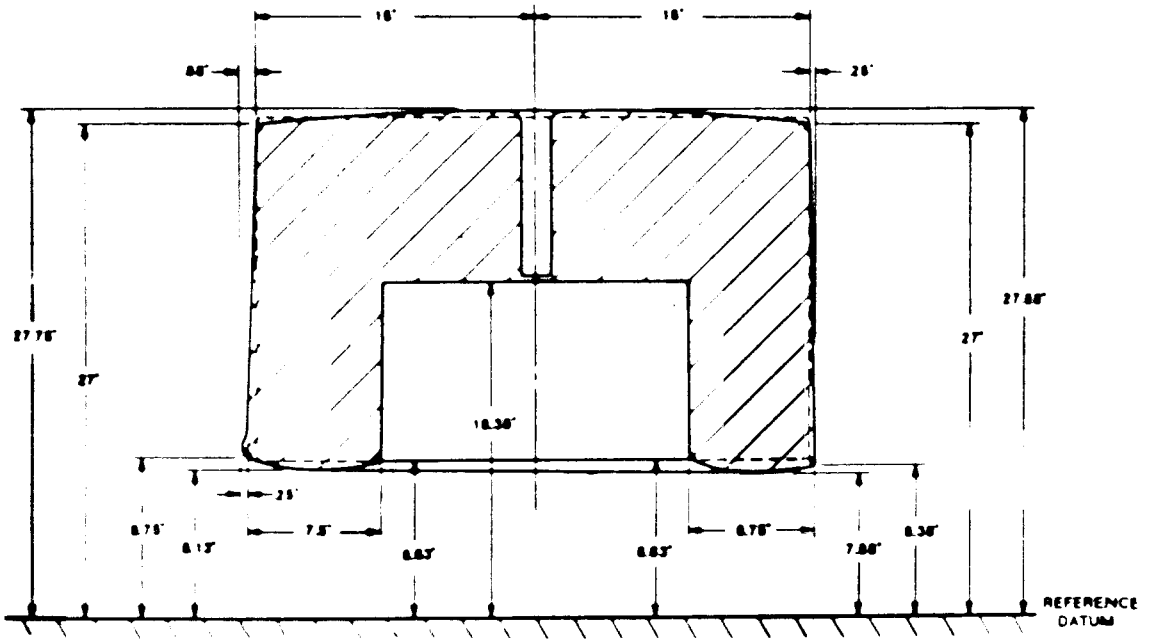
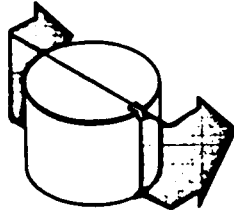


Figure 12-33. Top Overpack Measurements: Section Normal to Lifting Tabs (90° ccw)



SECTION THRU LIFTING TABS

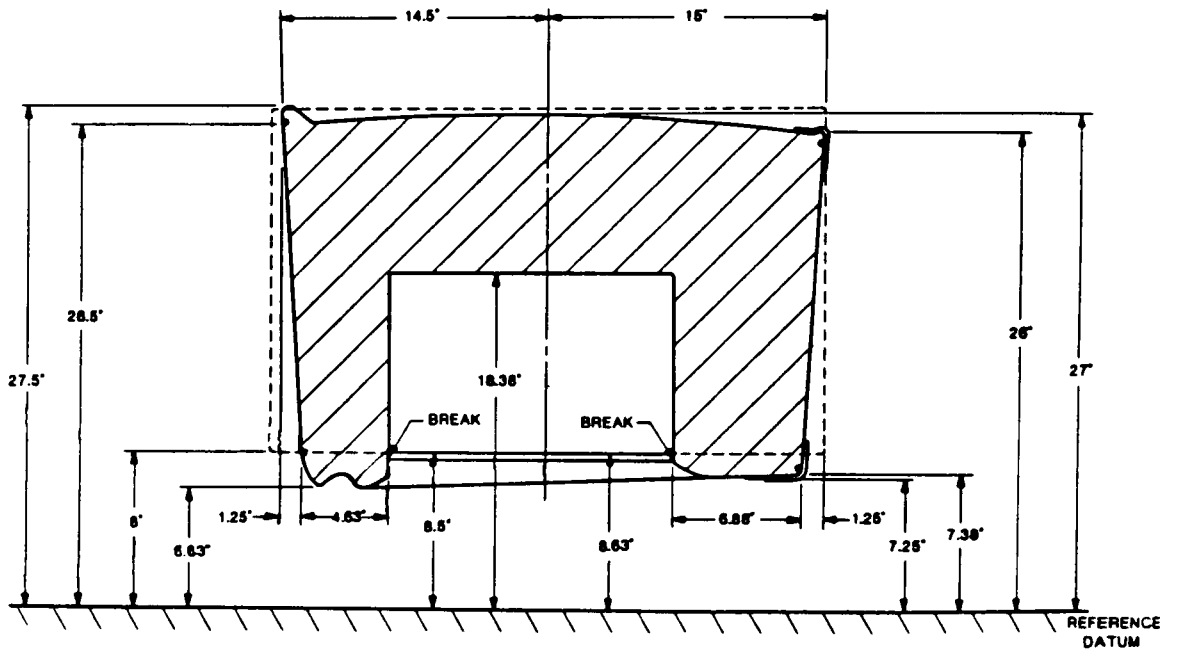


Figure 12-34. Bottom Overpack Measurements: Section Through Lifting Tabs

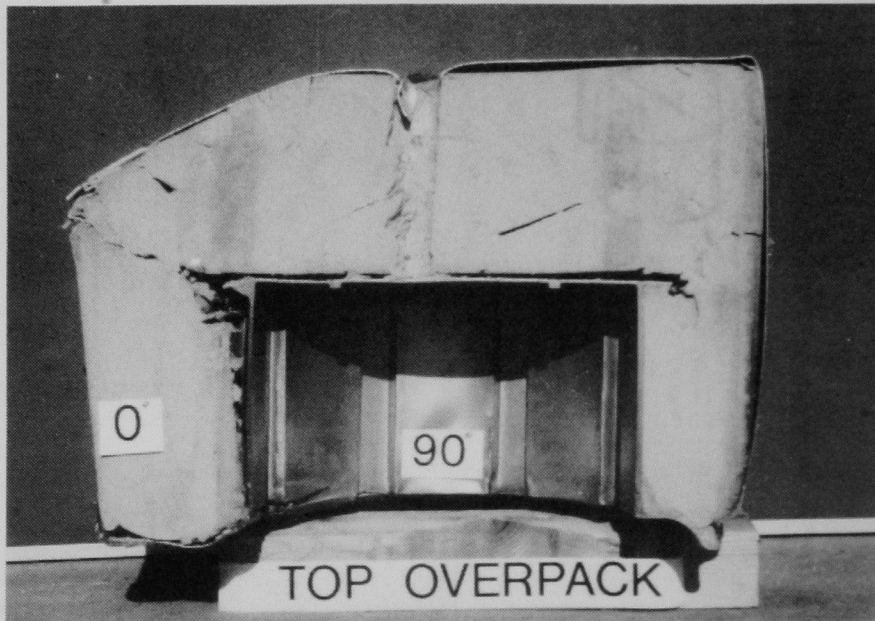


Figure 12-36. Sectioned Top Overpack: 0°-90°-180° View



Figure 12-37. Sectioned Top Overpack: 180°-270°-0° View



Figure 12-38. Sectioned Bottom Overpack: 180°-90°-0° View



Figure 12-39. Sectioned Bottom Overpack: 0°-270°-180° View

12.12 Final Leak Testing of Outer Vessel Containment Boundary

The outer vessel was disassembled, examined, inspected, and the x-radiography completed before reassembly for the final leak test to check the entire containment boundary of the outer vessel.

The cavity and lid of the outer vessel were cleaned as thoroughly as possible with methanol. The outer vessel was assembled with new O-rings and enclosed in a plastic bag envelope. The leak test hardware was attached to the vent port on the lid, and the outer vessel cavity was evacuated. Evacuation of the vessel was a very slow process because of the volume of the vessel and the possible presence of residual helium. The leak detector was monitored for 1 wk, during which time the readings gradually lowered until they stabilized. The plastic bag envelope was pressurized with helium, and the leak detector reading was recorded. There was no detectable helium leak rate for the outer vessel containment boundary to a sensitivity of 2.4×10^{-8} cm³/s.

12.13 Final Leak Testing of Inner Vessel Containment Boundary

The inner vessel was disassembled, examined, and inspected before reassembly for the final leak test to check the entire containment boundary of the inner vessel.

The cavity and lid of the inner vessel were cleaned as thoroughly as possible with methanol. The inner

vessel was assembled with new O-rings and enclosed in a plastic bag envelope. The leak test hardware was attached to the vent port on the lid, and the inner vessel cavity was evacuated. Evacuation of the inner vessel was also a slow process, taking several days to complete. The leak detector was monitored until the reading stabilized, the plastic bag envelope was pressurized with helium, and the leak detector reading was recorded. There was no detectable helium leak rate for the inner vessel containment boundary to a sensitivity of 7.3×10^{-10} cm³/s.

12.14 Measurement of Lead Thickness in Area of Side Puncture

A 0.375-in.-dia hole was drilled in the cask body at the puncture location through the 10-gage thermal shield, outer stainless-steel shell, and lead shielding (but not through the stainless-steel inner liner). The bar of a dial caliper was inserted into the hole, and the depth indicated on the dial was read. The hole depth was 1.195 in.

The thickness of the stainless-steel thermal shield and outer shell was then measured. A dental pick was inserted into the hole and used to locate the stainless-steel/lead junction. The bar of a dial caliper was inserted into the hole, and the depth from the outer surface of the thermal shield to the dental pick was measured. The stainless-steel thickness was 0.550 in.

Figure 12-40 shows a section view of the hole with measured thicknesses. The thickness of the lead shielding material is given by the hole depth minus the stainless-steel thickness, or 0.645 in.

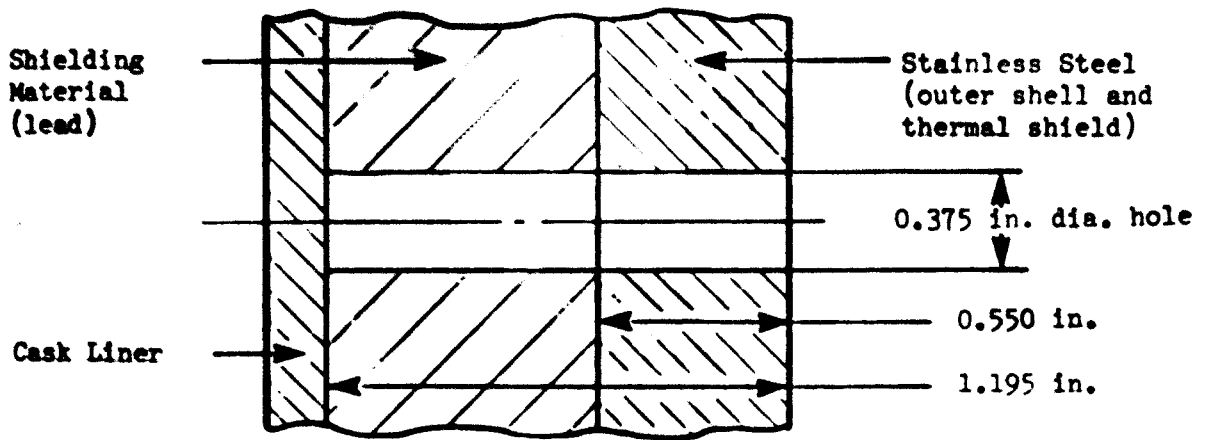


Figure 12-40. Section View of Hole Drilled for Measuring Shield Material Thickness

13. Final Instrumentation

13.1 Removal of Accelerometers From Outer Vessel

The Entran and Endevco accelerometers installed for the drop and puncture tests were removed to prevent damage during x-radiography and inspection of the outer vessel.

13.2 Final Calibration of Accelerometers

13.2.1 Entran Accelerometers

The Entran accelerometers used for the tests were calibrated on a centrifuge at ambient temperature to determine whether there were any differences in response from the previous calibration.

Measured sensitivities before and after the final three tests are given in Table 13-1.

13.2.2 Endevco Accelerometers

The Endevco accelerometers used for the tests were calibrated on a centrifuge at ambient temperature to determine whether there were any differences in response from the previous calibration.

Measured sensitivities before and after the final three tests are given in Table 13-2.

Table 13-1. Sensitivities of Entran Accelerometers at Ambient Temperature (Model EGAXT-F-1000) Before and After Final Three Tests

Serial Number	Intermediate Calibration Sensitivity (mV/V/g)	Final Calibration Sensitivity (mV/V/g)
21N50-A11-11	0.0172973	0.0167827
21N50-A12-12	0.0159721	0.0158868
21N50-A13-13*	0.0180970	not measured
21N50-A14-14	0.0178023	0.0177016
21N50-A15-15	0.0182961	0.0181520
21N50-A16-16	0.0183473	0.0183458
21N50-A17-17	0.0182097	0.0181835
21N50-A18-18	0.0186624	0.0187214
21N50-A21-21	0.0185984	0.0186890
21N50-A22-22*	0.0142827	not measured

Notes: Calibration performed on a centrifuge. Accuracy of sensitivity measurement is estimated at $\pm 3\%$ to 4% .

*These accelerometers were not used in the final three tests.

Table 13-2. Sensitivities of Endevco Accelerometers at Ambient Temperature (Model 2264-5KR) Before and After Final Three Tests

Serial Number	Intermediate Calibration Sensitivity (mV/V/g)	Final Calibration Sensitivity (mV/V/g)
BN09B	0.0090163	0.0090613
BN17B	0.0106626	0.0108099
BK76B	0.0098656	0.0098951

Notes: Calibration performed on a centrifuge. Accuracy of sensitivity measurement is estimated at $\pm 3\%$ to 4% .

14. Test Data Evaluation

This section summarizes the results of the tests and addresses internal consistency of the data, including accelerometer and strain gage data, leak test measurements, dimensional inspection, x-radiography, and visual observations. Incorrect or questionable data are identified where possible. Comparison of the test results with analytical predictions is presented in the Safety Analysis Report for the NuPac 125-B Cask (Nuclear Packaging, 1986).

14.1 30-ft Bottom End Drop Test

14.1.1 Description of Test Events

The model was dropped with its negative z-axis in the direction of motion (bottom end down) and the x- and y-axes in the plane perpendicular to the direction of motion. The model impacted almost flat onto the target, bounced once on the same end, rotated about its y-axis, bounced one more time on the overpack edge, then continued rotating about its y-axis, resulting in a final impact as the upper overpack hit the edge of the target (Figure 5-18). The "dimple" in the bottom overpack was confined to the surface defined by 0°-270°-180° axes.

14.1.2 Evaluation of Accelerometer and Strain Gage Data

Accelerations in the x- and y-directions should be zero or very small. The following relationships are found (Appendix B1):

- Accelerometers AZ1, AZ4, and AZ7 have the largest accelerations; their peak readings range from 189 to 205 g.
- Accelerometers AX2, AX5, and AX8 have very low readings, averaging close to zero.
- Accelerometers AY3 and AY6 have very low readings, averaging close to zero.

Spikes in some of the data traces were observed before impact. These spikes should not be considered as part of the impact data.

14.2 30-ft Oblique Drop Test

14.2.1 Description of Test Events

The model was dropped (lid end down) with its z-axis at an angle of ~62° with respect to the horizontal (28° with respect to the vertical). The y-axis was in the plane perpendicular to the plane of motion. The model impacted onto the target, rebounded, and rotated about its y-axis, hit the target with the lower overpack almost flat, bounced twice as it continued rotating, and finally impacted on its upper overpack outside the target area (Figure 6-7).

14.2.2 Evaluation of Accelerometer and Strain Gage Data

The accelerations in the x- and z-directions can be predicted from the impact angle, and the acceleration in the y-direction should be zero or very small. The following relationships are found (Appendix C1):

- Accelerometers A1Z, A4Z, and A7Z have the largest accelerations; their peak readings range from 87 to 93 g (average = 91 g).
- Accelerometers A2X, A5X, and A8X have the second largest accelerations; their peak readings range from 42 to 67 g (average = 52 g). Note that the sign of the data from accelerometer A8X is incorrect; all three accelerometers in the x-direction should have recorded a negative acceleration.
- Accelerometers A3Y and A6Y have very low readings, averaging close to zero.
- The impact angle with respect to the horizontal is given by $\sin\theta = a_z/a_T$

where a_z is the acceleration in the z-direction and a_T is the total acceleration. Calculation of the impact angle for each of the accelerometers in the z-direction yields an average angle of 62.5° with respect to the horizontal, verifying the impact orientation.

- The final impact had an acceleration along the z-axis ~30% that of the primary impact along the z-axis.

Spikes in some of the data traces were observed before impact. These spikes should not be considered as part of the impact data.

Strain gage SR5-Z has a high noise-to-signal ratio, much higher than the other strain gages. The data do not return to a reasonable level after the test. Data from this gage for the oblique drop test should be considered faulty and for subsequent tests may be questionable.

14.3 Intermediate Inspection

14.3.1 Evaluation of Leakage Rate Measurements

No degradation of the containment boundaries sufficient to cause an increase in leakage rates was observed.

14.3.2 Evaluation of Disassembly and Dimensional Inspection Data

Two of the bolts on the inner vessel lid, #20 and #23, were found to have torques less than their pre-test values at the intermediate post-test inspection (Section 7.7). These bolts are adjacent, located on the impact side of the model in the oblique drop test. They were also located on the impact side of the model for the final impact in the bottom end drop test after the model rebounded and overturned.

The upper internal impact limiters and canisters showed rotations as much as 25° to 30° from their initial orientations (Section 7.8). However, the inner vessel had not rotated appreciably with respect to the outer cask.

The dimensional inspection measurements (Section 7.11) showed several changes in outer cask bore straightness outside the PMI of ± 0.005 in. These changes in cask bore straightness would be unlikely to indicate important deformations in the cask bore because there were no changes in the cask bore diameter outside the PMI. The measurements are probably the result of a larger-than-expected PMI caused by the relatively large initial variations in dimensions of the cask.

Two of the canisters, "E" and "G," showed very small changes in their diameters at different points along their lengths at the D2 location. Because these canisters had rotated 25° and 15° from their initial orientations, no attempt is made to identify a physical cause for these diametrical changes. Relatively large changes were recorded for the straightness of canister "A" at tangential location D2, but these were found to be caused by a measurement sign error.

Differences were observed in the amount of crush of both the upper and lower internal impact limiters. These differences could have been caused by different canister weights, the orientations of the model in all of the impacts that occurred during the bottom end and oblique drop tests, and differences in strength of the honeycomb, which came from three different material lots, according to NuPac.

14.4 Evaluation of Intermediate Instrumentation Data

Accelerometers 21N50-A13-13 and 21N50-A22-22, located for the first two tests at positions AZ7 and AY6, respectively, did not recalibrate successfully (Section 8.4) and were replaced during intermediate instrumentation. These accelerometers could have been adversely affected by impacts experienced during the tests, by handling after the tests, or by other factors.

Data taken by these gages may be considered suspect. However, the acceleration data taken by these gages appear to be consistent with data from other gages having the same orientations.

14.5 30-ft Side Drop Test

14.5.1 Description of Test Events

The model was dropped with its negative x-axis in the direction of motion and the z- and y-axes in the plane perpendicular to the direction of motion. The model impacted almost flat onto the target, rebounded and then rotated about its y-axis, with the upper overpack reaching the maximum rebound height. The model then impacted on its lower overpack and again on its lid-end overpack (Figure 9-5).

14.5.2 Evaluation of Accelerometer and Strain Gage Data

Accelerations in the z- and y-directions should be zero or very small. The following relationships are found (Appendix D1):

- Accelerometers AZ1, AZ4, and AZ7 have very low readings, averaging close to zero.
- Accelerometers AX2, AX5, and AX8 have readings from 170 to 180 g (average = 176 g).
- Additional accelerometers AX9, AX10, and AX11 have data almost identical to accelerometers AX2, AX5, and AX8 (but of opposite sign because they were installed on the opposite side of the accelerometer blocks).

- Accelerometer AY3 has very low readings, averaging close to zero. The data from AY6 should be disregarded. During pre-test instrumentation checkout, balancing the signal from the AY6 channel was found to be impossible. The test engineer noted on the test procedure data sheet that AY6 data would be "bad." NuPac gave approval for the test, and it was conducted. The same problem occurred on the remaining two tests. Because the accelerometer recalibrated successfully, the problem was most likely with the instrumentation at the test site.

No spikes in the data were observed before impact for this test. Strain gage SR4-Z did not provide usable data. The data from the other two components of the strain gage rosette appear to be consistent with the data from corresponding components of SR5.

The strain gage data show residual strain in the model of 20 to 40 (in units of microstrain), indicating some permanent deformation. These data do not differentiate between inelastic behavior of the steel shells and movement of the lead that locks the shells in place in an ovalized configuration.

14.6 40-in. Side Puncture Test

14.6.1 Description of Test Events

The model was dropped with its negative x-axis in the direction of motion and the z- and y-axes in the plane perpendicular to the direction of motion. The model impacted almost horizontally onto the puncture bar, bounced, and hit the bar again in nearly the same location, began rotating about its z-axis, rolled off the bar, hit the target, and rolled off the target (Figure 10-4).

14.6.2 Evaluation of Accelerometer and Strain Gage Data

Accelerations in the z- and y-directions should be zero or very small. The following relationships are found (Appendix E1):

- Accelerometers AZ1, AZ4, and AZ7 have very low readings, averaging close to zero.
- Accelerometers AX2, AX5, and AX8 show a strong effect of the elastic body vibration of the model. The maximum accelerations measured by these accelerometers range from 102 to 89 g; the minimum accelerations range from 18 to 7 g. The average can be expressed as 53 ± 40 g. Both rigid body and elastic body responses are seen.

- Additional accelerometers AX9, AX10, and AX11 have data almost identical to accelerometers AX2, AX5, and AX8 (but of opposite sign because they were installed on the opposite side of the accelerometer blocks).
- Accelerometer AY3 has very low readings, averaging close to zero. The data from AY6 should be disregarded.

No spikes in the data for this test were observed before impact.

The data for gage SR4-Z appear consistent with the data from SR5-Z. The data from gage SR4-Z may be considered questionable, however, because of the bad data recorded from that gage for the side drop test.

The strain gages show residual strain after the side puncture test. Most of the residual strains are in the 20 to 50 microstrain range. Three gages show much higher residual strains: SR5-YZ at 120, SR4-Z at 220, and SR5-Z at 200, all in units of microstrain. Gages SR4 and SR5 were located on the model collinear with and equidistant from the puncture location. The large residual strains in these gages are consistent with the permanent deformation of the model found in the final post-test inspection (Section 12.11). These data do not differentiate between inelastic behavior of the steel shells and movement of the lead that locks the shells in place in an ovalized configuration.

Data from the strain gages located on the puncture bar are not presented. The signal saturated the instrumentation because the instrumentation calibration level used was lower than the signal.

14.7 40-in. Closure End Puncture Test

14.7.1 Description of Test Events

The model was dropped onto the puncture bar with its positive z-axis in the direction of motion (lid end down) and the x- and y-axes in the plane perpendicular to the direction of motion. The puncture bar penetrated through the lid-end overpack, but did not pierce the back plate on the overpack. The model remained upright, supported on the bar (Figure 11-4).

14.7.2 Evaluation of Accelerometer and Strain Gage Data

Accelerations in the x- and y-directions should be zero or very small. The following relationships are found (Appendix F1):

- Accelerometers AZ1, AZ4, and AZ7 have the largest accelerations; their peak readings range from 64 to 72 g (average = 68 g). The accelerometer data show a small shock upon initial impact of the puncture bar with the overpack shell and large shock upon impact with the lid.
- Accelerometers AX2, AX5, and AX8 have very low readings, averaging close to zero.
- Accelerometer AY3 has very low readings, averaging close to zero. The data from AY6 should be disregarded.

Zero time was set by the puncture bar data. The data from the accelerometers in the z-direction are consistent and show the following:

- A negative peak at $\sim +7$ ms
- A sharp positive peak of about the same amplitude at $\sim +9$ ms
- A sharp positive peak of about the same amplitude at $\sim +31$ ms
- A large negative peak at $\sim +62$ ms, with width ~ 10 ms (beginning at ~ 58 ms).

The data from the strain gages on the puncture bar show a relatively small force on the bar beginning at 0 ms and peaking at $\sim +6$ ms. This is followed at $\sim +58$ ms by a relatively large force on the bar.

Strain gages SR1-Z, SR2-Z, and SR3-Z on the model recorded appreciable strains at ~ 62 ms, with an event duration of ~ 10 ms, in agreement with the accelerometer data. All of the data for the strain gages on the model show sharp spikes at ~ 0 ms, with a much higher reading than the strain recorded at 62 ms. Some, but not all, of the strain gages recorded sharp spikes at $\sim +9$ ms.

The event at ~ 62 ms of ~ 10 ms duration can be attributed to the puncture bar striking the back plate of the impact limiter and forcing the plate against the outer cask lid. The puncture bar data indicate that the bar struck the overpack shell at 0 ms.

The sharp positive spikes in the accelerometer data occurring at $\sim +9$ and $\sim +31$ ms are questionable. The large spikes recorded from strain gages on

the cask body before 50 ms are not readily explained either, because they would have occurred before the puncture bar hit the cask body.

The noise-to-signal ratio in the SR4-Z data is unacceptable, and those data should be disregarded.

14.8 Final Inspection

14.8.1 Evaluation of Leakage Rate Measurements

No degradation of the containment boundaries sufficient to cause an increase in the leakage rates was observed.

14.8.2 Evaluation of Disassembly and Dimensional Inspection Data

The x-radiography examination of the outer vessel showed no observable changes in the location of the lead shielding, except in the puncture impact area.

The dimensional inspection measurements showed appreciable changes in the cask bore diameters, the largest change being 0.121 in. near the coordinates of the puncture on the outside of the outer vessel. The measurements show a distinct ovalizing of the outer vessel, with decreases in the diameters measured from the line of impact upwards, and increases in the other directions. Many changes in straightness outside the PMI were also observed.

Only one change in a measurement of the inner vessel exterior exceeded the PMI (Section 12.11). No changes in the inner vessel tube bores exceeded the PMI. Four different measurements for canister diameters exceeded the PMI, but only slightly.

The foam in both of the overpacks exhibited cracking and had at least one crack extending from a damaged surface through to the back plate (Section 12.11.6.2).

14.9 Evaluation of Final Instrumentation Data

All of the accelerometers recalibrated successfully.

References

ANSI N14.5-1977. American National Standards Institute, "American National Standard for Leakage Tests on Packages for Shipment of Radioactive Materials" (Washington, DC: American National Stds Inst, 1977).

NRC, 1983. US Nuclear Regulatory Commission, 10 CFR Part 71, "Rule to Achieve Compatibility with the Transport Regulations of the International Atomic Energy Agency (IAEA)." *Federal Register*, Friday, August 5, 1983, Vol. 48, No. 151, pp 35600-27; corrected Wednesday, August 24, 1983, Vol. 48, No. 165, pp 38449-50 (Washington, DC: US Nuclear Regulatory Commission).

Nuclear Packaging, 1986. Nuclear Packaging, Inc., "Safety Analysis Report for the NuPac 125-B Fuel Shipping Cask, Docket No. 71-9200," Rev 3 (Washington, DC: US NRC, February 1986).

Rockenbach, R. A., 1984. *Q/TRAN, Version 1.2 User's Manual* (Santa Ana, CA: PDA Engineering, Inc., May 1984).

Sandia, 1984. Sandia National Laboratories, "Quality Assurance Program Plan for Organization 6000, Energy Programs Vice Presidency" (Albuquerque, NM: Sandia National Laboratories, December 3, 1984).

APPENDIX A

Initial Inspection Data

Figures

A1	Cask Bore Inspection Geometry	146
A2	Inner Vessel External Inspection Geometry	147
A3	Inner Vessel Tube Bore Inspection Geometry	149
A4	Canister External Inspection Geometry	151
A5	Cask Lid, Cask Bottom, and Inner Vessel Lid Inspection Geometry	153

Tables

A1	Diametrical Measurements of the Cask Bore for the Initial Inspection	146
A2	Straightness Measurements of the Cask Bore for the Initial Inspection	147
A3	Diametrical Measurements of the Exterior of the Inner Vessel for the Initial Inspection	148
A4	Straightness Measurements of the Inner Vessel Outside Diameter for the Initial Inspection	148
A5	Diametrical Measurements of the Inner Vessel Tube Bores for the Initial Inspection	149
A6	Straightness Measurements of the Inner Vessel Tube Bores for the Initial Inspection	150
A7	Diametrical Measurements of the Canisters for the Initial Inspection	151
A8	Straightness Measurements of the Canisters for the Initial Inspection	152
A9	Flatness Measurements of the Cask Lid for the Initial Inspection	154
A10	Flatness Measurements of the Cask Bottom for the Initial Inspection	154
A11	Flatness Measurements of the Inner Vessel Lid for the Initial Inspection	154
A12	Length Measurements of the Upper Internal Impact Limiters	155
A13	Length Measurements of the Lower Internal Impact Limiters	155
A14	Weights of Major Model Components	155
A15	Weights of Internal Impact Limiters	156
A16	Weights of Canisters	156

A.1 Initial Inspection of Cask Body

Body

The internal cavity of the cask body (referred to as the cask bore) was inspected for straightness and diameter.

The diameter was measured at tangential locations D1 (between points D1 and D5), D2 (between points D2 and D6), D3 (between points D3 and D7), and D4 (between points D4 and D8), at each longitudinal location (Figure A1). The PMI was determined to be ± 0.005 in. The diametrical measurements for the initial inspection are listed in Table A1.

The straightness was measured at longitudinal locations L1 through L5 for each tangential location D1 through D8. Positive or negative values were recorded to indicate a point radially greater or less than Reference Datum "C" shown in Figure A1 at longitudinal reference locations "A" and "B." The PMI was determined to be ± 0.005 in. The straightness measurements for the initial inspection are listed in Table A2.

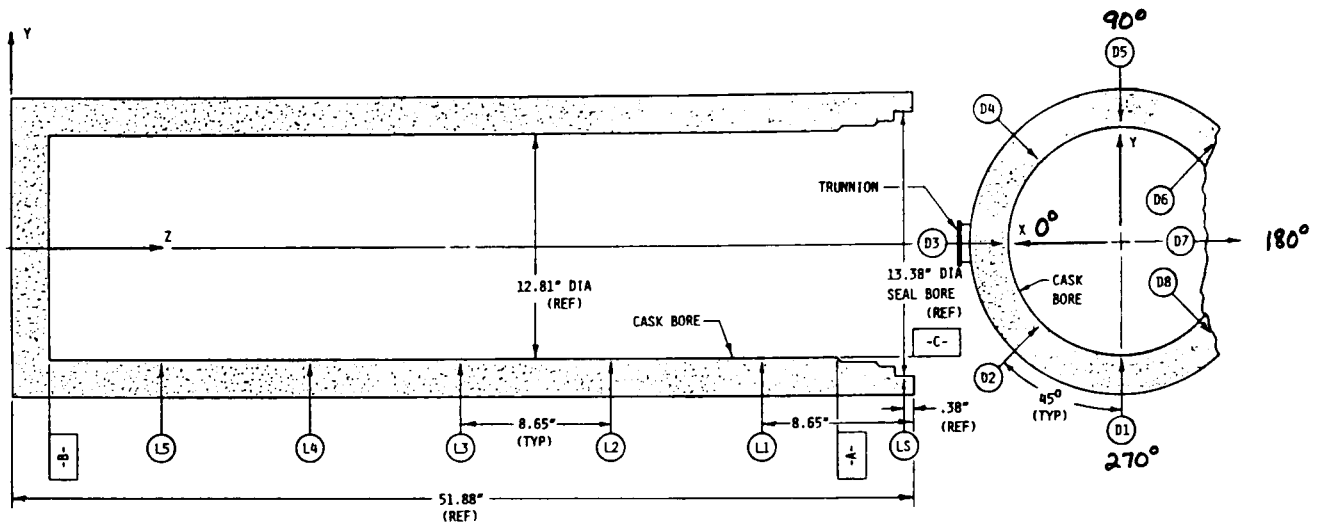


Figure A1. Cask Bore Inspection Geometry

Table A1. Diametrical Measurements (in.) of the Cask Bore for the Initial Inspection

Tangential Location	Longitudinal Location					
	LS	L1	L2	L3	L4	L5
D1	13.375	12.767	12.785	12.882	12.798	12.769
D2	13.376	12.799	12.809	12.784	12.823	12.835
D3	13.376	12.864	12.831	12.827	12.831	12.839
D4	13.375	12.783	12.788	12.770	12.770	12.785

Table A2. Straightness Measurements (In.) of the Cask Bore for the Initial Inspection

Tangential Location	Longitudinal Location				
	L1	L2	L3	L4	L5
D1	-0.016	-0.013	-0.038	-0.013	-0.004
D2	-0.018	-0.021	-0.013	-0.029	-0.028
D3	-0.054	-0.043	-0.041	-0.031	-0.028
D4	-0.019	-0.014	+0.001	-0.012	-0.021
D5	+0.003	-0.017	+0.009	-0.031	-0.011
D6	+0.016	+0.005	+0.018	-0.007	-0.027
D7	-0.021	+0.002	+0.002	-0.005	-0.012
D8	-0.009	-0.025	-0.031	-0.015	-0.022

A.2 Initial Inspection of Inner Vessel Exterior

The exterior of the inner vessel was inspected for straightness and diameter.

The diameter was measured at tangential locations D1 (between points D1 and D5), D2 (between points D2 and D6), D3 (between points D3 and D7), and D4 (between points D4 and D8), at each longitudinal location (Figure A2). The PMI was determined to be ± 0.010 in. The diametrical measurements for the initial inspection are listed in Table A3.

The straightness of the inner vessel outside diameter was measured at longitudinal locations L1 through L5 for each tangential location D1 through D8. Positive or negative values were recorded to indicate a point radially greater or less than Reference Datum "C" shown in Figure A2 at longitudinal reference locations "A" and "B." The PMI was determined to be ± 0.10 in. The straightness measurements for the initial inspection are listed in Table A4.

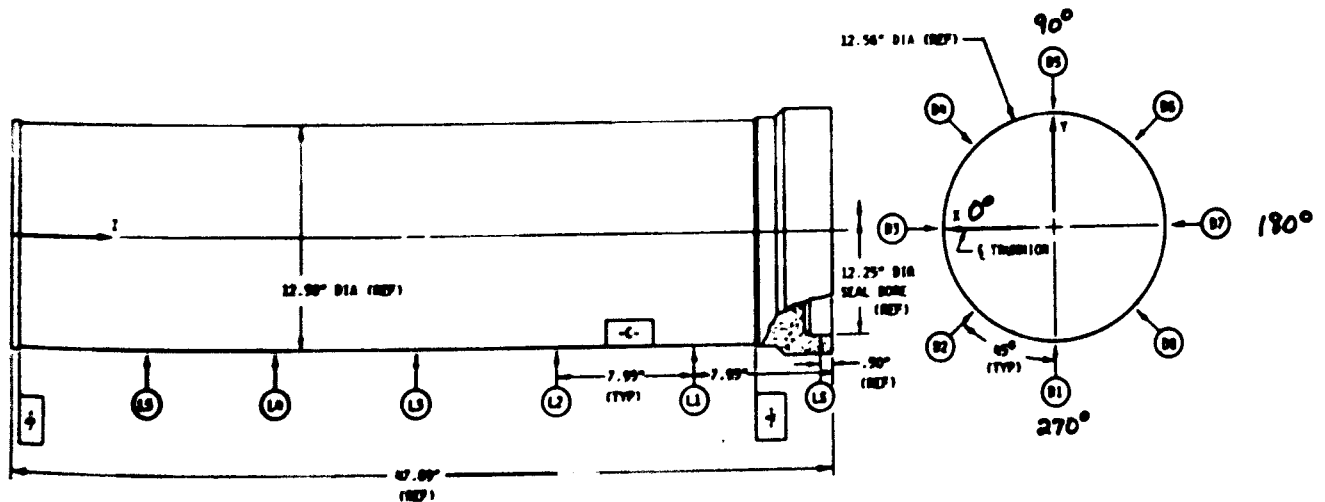


Figure A2. Inner Vessel External Inspection Geometry

Table A3. Diametrical Measurements (in.) of the Exterior of the Inner Vessel for the Initial Inspection

Tangential Location	Longitudinal Location					
	LS	L1	L2	L3	L4	L5
D1	12.253	12.518	12.532	12.532	12.535	12.521
D2	12.256	12.529	12.538	12.534	12.502	12.505
D3	12.256	12.495	12.553	12.524	12.483	12.463
D4	12.255	12.576	12.605	12.595	12.567	12.563

Table A4. Straightness Measurements (in.) of the Inner Vessel Outside Diameter for the Initial Inspection

Tangential Location	Longitudinal Location				
	L1	L2	L3	L4	L5
D1	+0.001	+0.007	+0.011	+0.012	+0.011
D2	+0.006	+0.003	+0.001	-0.002	+0.002
D3	-0.047	-0.014	-0.029	-0.045	-0.038
D4	+0.018	+0.027	+0.019	+0.009	+0.002
D5	-0.027	-0.011	-0.002	+0.009	+0.007
D6	-0.038	-0.019	-0.010	-0.021	-0.029
D7	+0.001	+0.037	+0.029	-0.002	-0.026
D8	+0.013	+0.032	+0.025	+0.004	-0.001

A.3 Initial Inspection of Inner Vessel Tube Bores

The internal cavities of the inner vessel (referred to as inner vessel tube bores) were inspected for straightness and diameters.

The diameter of each tube bore, labeled "a" through "g," was measured at tangential locations D1 (between points D1 and D5), D2 (between points D2 and D6), D3 (between points D3 and D7), and D4 (between points D4 and D8), at five evenly spaced longitudinal locations separated by 7.28 in. These locations were marked for subsequent inspections. The inner vessel tube bore inspection geometry is shown in Figure A3. The PMI was determined to be

± 0.005 in. The diametrical measurements for the initial inspection are listed in Table A5.

The straightness of the tube bore diameters was measured at longitudinal locations L1 through L5 for each tangential location D1 through D4 for each of the tube bores. Positive or negative values were recorded to indicate a point radially greater or less than the Reference Datum defined as the bore surface at the extreme ends of each bore length. In Figure A1, Reference Datum "C" is the tube bore, and reference locations "A" and "B" are the extreme ends of the tube bores. The PMI was determined to be ± 0.005 in.

The straightness measurements for the initial inspection are listed in Table A6.

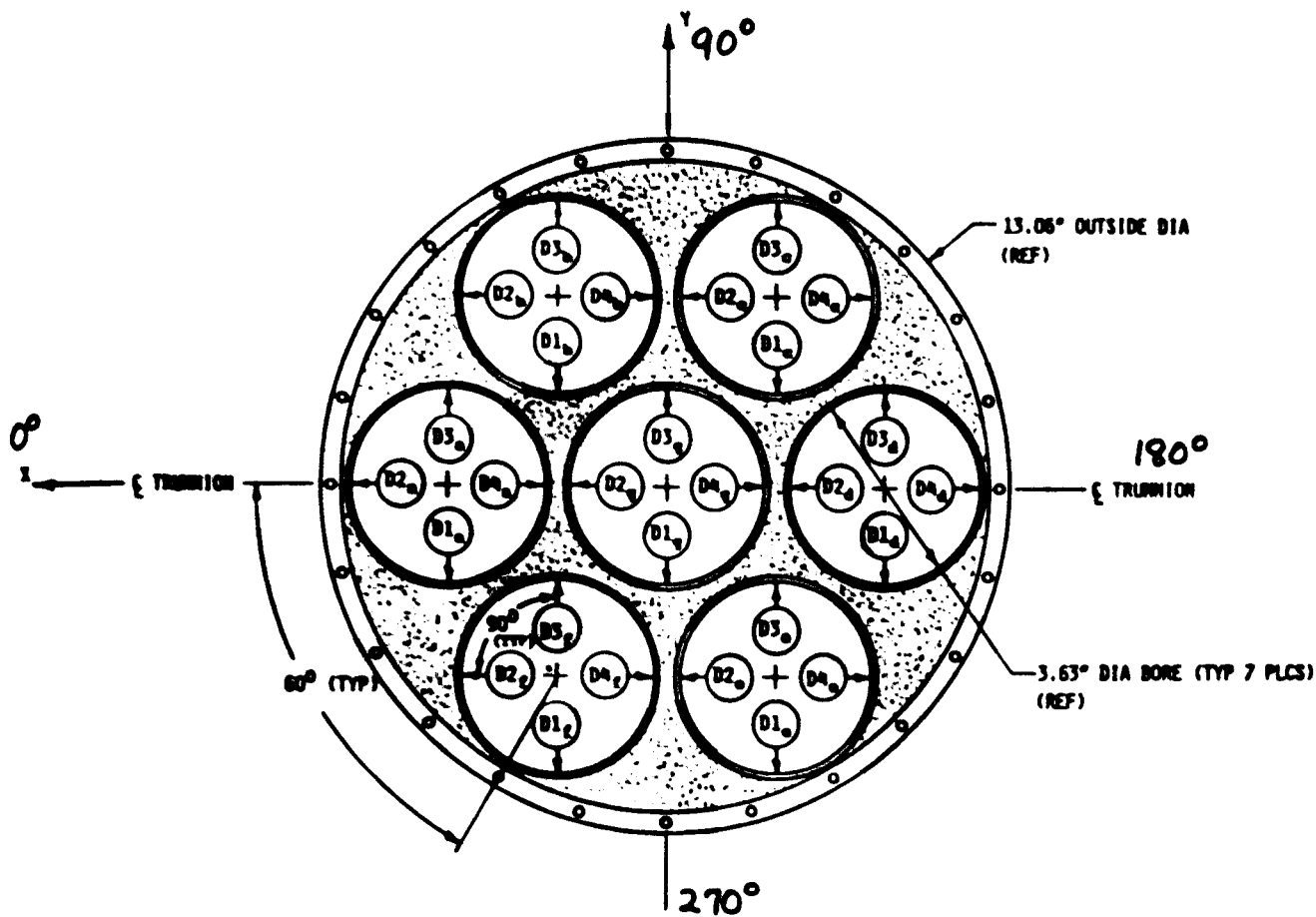


Figure A3. Inner Vessel Tube Bore Inspection Geometry (Viewed from Closure End)

Table A5. Diametrical Measurements (in.) of the Inner Vessel Tube Bores for the Initial Inspection

Tangential Location	Longitudinal Location				
	L1	L2	L3	L4	L5
D1a	3.673	3.682	3.688	3.692	3.691
D2a	3.563	3.563	3.556	3.523	3.541
D1b	3.620	3.622	3.623	3.622	3.609
D2b	3.642	3.634	3.629	3.639	3.649
D1c	3.607	3.603	3.595	3.594	3.600
D2c	3.656	3.656	3.667	3.668	3.658
D1d	3.648	3.640	3.634	3.640	3.655
D2d	3.605	3.620	3.624	3.617	3.593
D1e	3.616	3.611	3.607	3.608	3.602
D2e	3.643	3.645	3.645	3.650	3.653
D1f	3.629	3.617	3.615	3.618	3.614
D2f	3.633	3.646	3.648	3.646	3.650
D1g	3.633	3.635	3.635	3.636	3.636
D2g	3.638	3.636	3.635	3.634	3.634

Table A6. Straightness Measurements (in.) of the Inner Vessel Tube Bores for the Initial Inspection

Tangential Location	Longitudinal Location				
	L1	L2	L3	L4	L5
D1a	-0.013	-0.016	-0.019	-0.021	-0.022
D2a	+0.034	+0.018	+0.013	+0.039	+0.030
D3a	-0.028	-0.033	-0.037	-0.039	-0.035
D4a	+0.023	+0.036	+0.042	+0.044	+0.030
D1b	+0.031	+0.023	+0.012	+0.005	+0.008
D2b	-0.047	-0.046	-0.048	-0.046	-0.035
D3b	-0.031	-0.023	-0.015	-0.006	+0.003
D4b	+0.031	+0.039	+0.049	+0.035	+0.016
D1c	+0.022	+0.028	+0.033	+0.031	+0.021
D2c	-0.020	-0.024	-0.025	-0.020	-0.009
D3c	-0.009	-0.010	-0.009	-0.006	-0.002
D4c	-0.013	-0.008	-0.016	-0.021	-0.023
D1d	+0.005	+0.016	+0.022	+0.016	+0.001
D2d	+0.013	-0.005	-0.012	-0.011	-0.003
D3d	-0.022	-0.027	-0.026	-0.024	-0.024
D4d	-0.001	-0.001	+0.001	+0.006	+0.021
D1e	-0.006	-0.007	-0.010	-0.008	0.000
D2e	+0.013	+0.010	+0.013	+0.005	-0.001
D3e	+0.014	+0.019	+0.023	+0.022	+0.016
D4e	-0.025	-0.025	-0.027	-0.024	-0.023
D1f	-0.011	+0.004	+0.008	+0.006	+0.006
D2f	-0.002	-0.008	-0.005	-0.004	-0.008
D3f	+0.001	0.000	-0.001	0.000	+0.005
D4f	+0.001	-0.006	-0.011	-0.009	-0.010
D1g	+0.008	+0.016	+0.014	+0.006	-0.001
D2g	-0.015	-0.019	-0.015	-0.010	-0.005
D3g	-0.010	-0.021	-0.021	-0.015	-0.007
D4g	+0.009	+0.015	+0.015	+0.010	+0.005

A.4 Initial Inspection of Canisters

The exterior of each of the canisters was inspected for straightness and diameter.

The diameters were measured at tangential locations D1 (between points D1 and D3) and D2 (between points D2 and D4) for each of the seven canisters labeled "a" through "g." at five evenly spaced longitudinal locations spaced ~6.25 in. apart (Figure A4). The PMI was determined to be ± 0.002 in. The diametrical measurements for the initial inspection are listed in Table A7.

The straightness of each canister's outside diameter was measured at longitudinal locations L1 through L5 for each tangential location D1 through D4. Positive or negative values were recorded to indicate a point radially greater or less than the Reference Datum defined as the outside diameter at the extreme ends of the canister length. In Figure A4, Reference Datum "C" is the outside diameter, and reference locations "A" and "B" are 2 in. from the extreme ends of the canisters. The PMI was determined to be ± 0.002 in. The straightness measurements for the initial inspection are listed in Table A8.

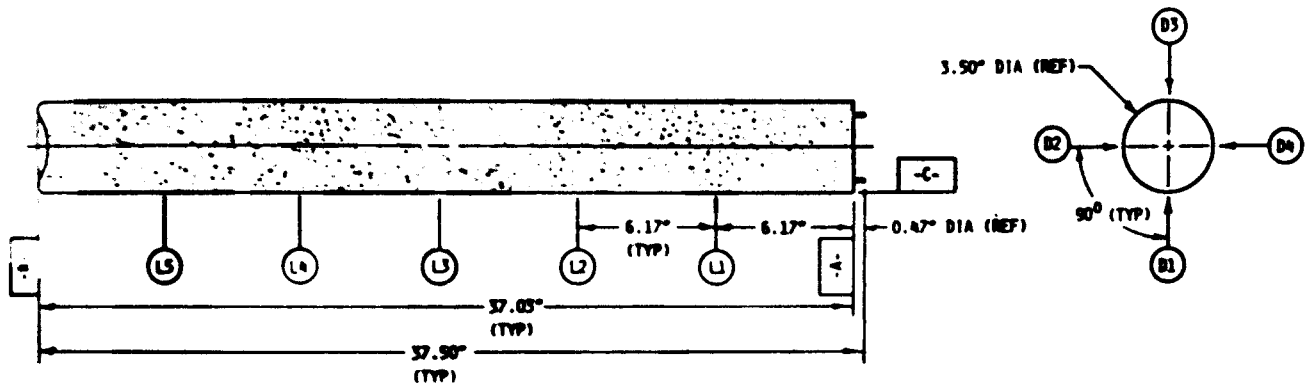


Figure A4. Canister External Inspection Geometry. (Because of material deformation, reference locations "A" and "B" are taken 2 in. from each end.)

Table A7. Diametrical Measurements (in.) of the Canisters for the Initial Inspection

Tangential Location	Longitudinal Location				
	L1	L2	L3	L4	L5
D1a	3.503	3.507	3.507	3.503	3.508
D2a	3.521	3.518	3.510	3.508	3.500
D1b	3.517	3.517	3.513	3.515	3.508
D2b	3.506	3.507	3.513	3.512	3.510
D1c	3.512	3.513	3.512	3.511	3.513
D2c	3.512	3.511	3.512	3.514	3.512
D1d	3.513	3.514	3.515	3.511	3.509
D2d	3.514	3.514	3.512	3.515	3.517
D1e	3.520	3.518	3.521	3.515	3.510
D2e	3.508	3.506	3.508	3.512	3.516
D1f	3.512	3.514	3.515	3.514	3.515
D2f	3.514	3.513	3.514	3.513	3.510
D1g	3.507	3.511	3.513	3.513	3.511
D2g	3.520	3.512	3.510	3.510	3.516

Table A8. Straightness Measurements (in.) of the Canisters for the Initial Inspection

Tangential Location	Longitudinal Location				
	L1	L2	L3	L4	L5
D1a	-0.0015	+0.0015	0.0000	-0.0020	+0.0040
D2a	+0.0090	+0.0115	+0.0125	+0.0145	+0.0080
D3a	-0.0010	-0.0015	-0.0010	-0.0035	-0.0035
D4a	-0.0025	-0.0020	-0.0060	-0.0060	-0.0015
D1b	+0.0040	+0.0085	+0.0090	+0.0110	+0.0075
D2b	0.0000	+0.0030	+0.0060	+0.0035	-0.0005
D3b	+0.0005	-0.0005	-0.0010	+0.0050	+0.0050
D4b	-0.0015	-0.0050	-0.0040	-0.0025	-0.0020
D1c	+0.0010	-0.0015	-0.0005	-0.0025	-0.0010
D2c	-0.0015	-0.0010	-0.0010	-0.0010	-0.0005
D3c	+0.0015	+0.0030	0.0000	+0.0005	+0.0005
D4c	-0.0005	-0.0020	-0.0020	0.0000	-0.0010
D1d	-0.0010	+0.0020	+0.0030	+0.0010	-0.0005
D2d	-0.0010	-0.0055	-0.0070	-0.0040	-0.0020
D3d	+0.0010	+0.0010	+0.0030	+0.0045	+0.0045
D4d	0.0000	+0.0015	0.0000	-0.0025	-0.0035
D1e	+0.0060	+0.0040	+0.0060	-0.0020	+0.0015
D2e	+0.0010	+0.0030	+0.0010	+0.0010	+0.0010
D3e	-0.0010	+0.0005	+0.0035	+0.0030	+0.0010
D4e	-0.0030	-0.0090	-0.0060	-0.0055	-0.0055
D1f	-0.0030	-0.0005	-0.0020	-0.0040	-0.0010
D2f	+0.0005	-0.0005	-0.0015	-0.0015	-0.0025
D3f	+0.0015	+0.0010	+0.0030	+0.0030	+0.0015
D4f	-0.0010	-0.0020	0.0000	-0.0005	-0.0010
D1g	-0.0020	+0.0030	+0.0045	+0.0025	+0.0050
D2g	-0.0010	-0.0035	-0.0070	-0.0050	-0.0025
D3g	+0.0010	0.0000	+0.0015	+0.0040	+0.0005
D4g	+0.0005	-0.0030	0.0000	-0.0030	+0.0010

A.5 Initial Inspection of Cask Lid, Cask Bottom, and Inner Vessel Lid

The cask lid, cask bottom, and inner vessel lids were inspected for flatness. The flatness of each surface was measured at five radial locations R1 through R5 for each orientation A through D (Figure A5). Positive or negative values were recorded to indicate a position above or below the intersection of Reference Datum "E" and the outside diameter of the surface. The PMI was determined to be ± 0.002 in.

The flatness measurements are given in Tables A9, A10, and A11 for the cask lid, cask bottom, and inner vessel lid, respectively.

A.6 Initial Inspection of Internal Impact Limiters

The length of each internal impact limiter was measured at four tangential locations L1 through L4 (Tables A12 and A13). Tangential location L1 corresponds to the alignment datum marked on each impact limiter. The PMI was determined to be ± 0.002 in.

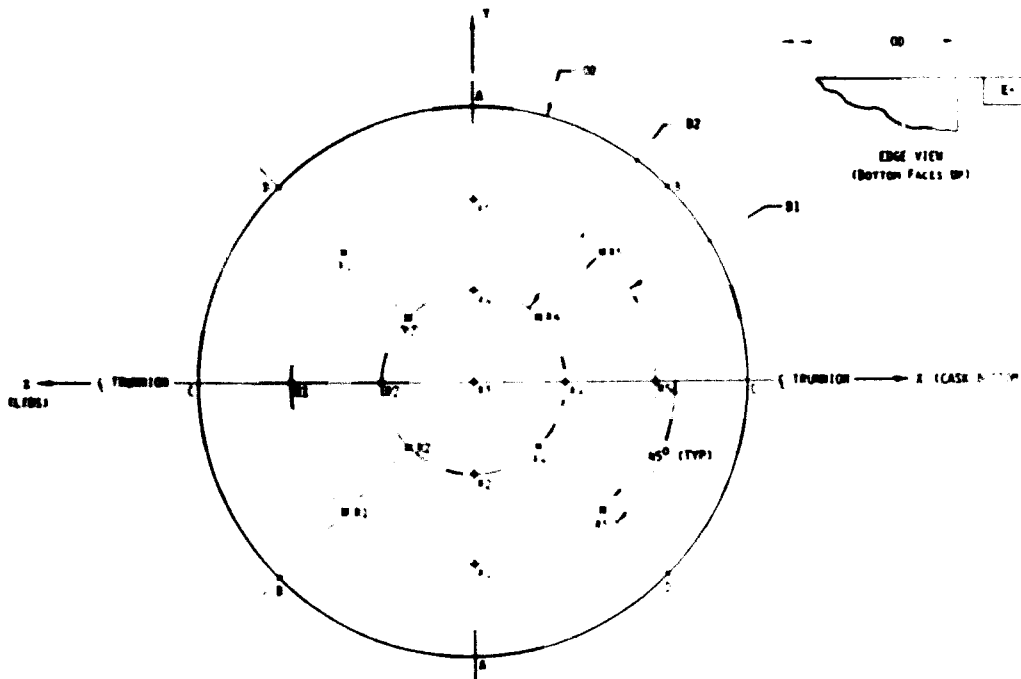


Figure A5. Cask Lid, Cask Bottom, and Inner Vessel Lid Inspection Geometry

Table A9. Flatness Measurements (in.) of the Cask Lid for the Initial Inspection

Tangential Location	Radial Location				
	R1	R2	R3	R4	R5
A	(set) 0	0	-0.0001	+0.0001	(set) 0
B	+0.0001	-0.0001	-0.0001	+0.0001	+0.0001
C	-0.0002	-0.0001	-0.0001	0	-0.0002
D	-0.0003	-0.0001	-0.0001	-0.0001	-0.0002

Table A10. Flatness Measurements (in.) of the Cask Bottom for the Initial Inspection

Tangential Location	Radial Location				
	R1	R2	R3	R4	R5
A	(set) 0	+0.008	+0.010	+0.0075	(set) 0
B	-0.006	+0.005	+0.010	+0.005	-0.0065
C	-0.012	+0.003	+0.010	+0.004	-0.0115
D	-0.0055	+0.005	+0.010	+0.0065	-0.005

Table A11. Flatness Measurements (in.) of the Inner Vessel Lid for the Initial Inspection

Tangential Location	Radial Location				
	R1	R2	R3	R4	R5
A	(set) 0	-0.0003	+0.0006	-0.0002	(set) 0
B	-0.0004	-0.0004	+0.0006	-0.0003	-0.0005
C	-0.0009	-0.0005	+0.0006	-0.0005	-0.0010
D	-0.0005	-0.0003	+0.0006	-0.0005	-0.0006

Table A12. Length Measurements (in.) of the Upper Internal Impact Limiters

Upper Impact Limiter	Tangential Location			
	L1	L2	L3	L4
a	5.240	5.238	5.245	5.248
b	5.252	5.247	5.236	5.238
c	5.246	5.238	5.239	5.248
d	5.241	5.244	5.255	5.250
e	5.261	5.263	5.257	5.256
f	5.239	5.239	5.231	5.233
g	5.242	5.246	5.251	5.248

Table A13. Length Measurements (in.) of the Lower Internal Impact Limiters

Lower Impact Limiter	Tangential Location			
	L1	L2	L3	L4
a	2.761	2.767	2.771	2.764
b	2.765	2.768	2.764	2.762
c	2.763	2.767	2.770	2.765
d	2.771	2.768	2.763	2.767
e	2.768	2.768	2.767	2.773
f	2.767	2.772	2.769	2.767
g	2.767	2.767	2.765	2.768

A.7 Weights of Model Components

All of the model components were weighed. The weights of major model components are listed in Table A14. The weights of the internal impact limiters are listed in Table A15, and the weights of the canisters are listed in Table A16. Total assembled weight was 2830 lb. The inner vessel assembly weight was 904 lb.

Table A14. Weights of Major Model Components

Component	Weight (lb)
Upper overpack	205
Lower overpack	205
Cask body (w/o lid)	1437
Cask lid	79.9
Inner vessel body (w/o lid)	475
Inner vessel lid	41.6

Table A15. Weights of Internal Impact Limiters

Location	Weight (lb)	
	Upper	Lower
a	8.3	0.85
b	8.3	0.85
c	8.35	0.85
d	8.35	0.85
e	8.35	0.85
f	8.40	0.90
g	8.40	0.85

Table A16. Weights of Canisters

Location	Weight (lb)
a	46.15
b	46.40
c	45.65
d	45.75
e	46.50
f	46.15
g	46.40

APPENDIX B1

Accelerometer and Strain Gage Data for the 30-ft Bottom End Drop Test Filtered at 1000 Hz

Figures

B1-1	Acceleration vs Time for Gage AZ1 for 30-ft Bottom End Drop Test	158
B1-2	Acceleration vs Time for Gage AX2 for 30-ft Bottom End Drop Test	158
B1-3	Acceleration vs Time for Gage AY3 for 30-ft Bottom End Drop Test	159
B1-4	Acceleration vs Time for Gage AZ4 for 30-ft Bottom End Drop Test	159
B1-5	Acceleration vs Time for Gage AX5 for 30-ft Bottom End Drop Test	160
B1-6	Acceleration vs Time for Gage AY6 for 30-ft Bottom End Drop Test	160
B1-7	Acceleration vs Time for Gage AZ7 for 30-ft Bottom End Drop Test	161
B1-8	Acceleration vs Time for Gage AX8 for 30-ft Bottom End Drop Test	161
B1-9	Microstrain vs Time for Gage SR1-Y for 30-ft Bottom End Drop Test	162
B1-10	Microstrain vs Time for Gage SR1-YZ for 30-ft Bottom End Drop Test	162
B1-11	Microstrain vs Time for Gage SR1-Z for 30-ft Bottom End Drop Test	163
B1-12	Microstrain vs Time for Gage SR2-Y for 30-ft Bottom End Drop Test	163
B1-13	Microstrain vs Time for Gage SR2-YZ for 30-ft Bottom End Drop Test	164
B1-14	Microstrain vs Time for Gage SR2-Z for 30-ft Bottom End Drop Test	164
B1-15	Microstrain vs Time for Gage SR3-Y for 30-ft Bottom End Drop Test	165
B1-16	Microstrain vs Time for Gage SR3-YZ for 30-ft Bottom End Drop Test	165
B1-17	Microstrain vs Time for Gage SR3-Z for 30-ft Bottom End Drop Test	166
B1-18	Microstrain vs Time for Gage SR4-Y for 30-ft Bottom End Drop Test	166
B1-19	Microstrain vs Time for Gage SR4-YZ for 30-ft Bottom End Drop Test	167
B1-20	Microstrain vs Time for Gage SR4-Z for 30-ft Bottom End Drop Test	167
B1-21	Microstrain vs Time for Gage SR5-Y for 30-ft Bottom End Drop Test	168
B1-22	Microstrain vs Time for Gage SR5-YZ for 30-ft Bottom End Drop Test	168
B1-23	Microstrain vs Time for Gage SR5-Z for 30-ft Bottom End Drop Test	169

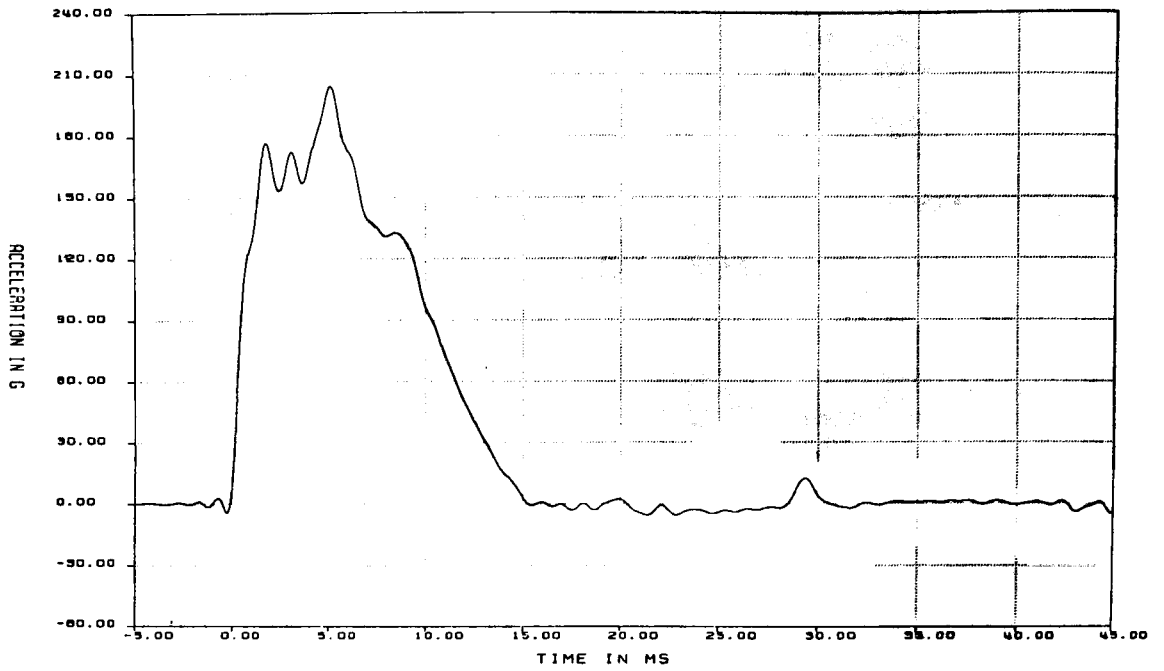


Figure B1-1. Acceleration vs Time for Gage AZ1 for 30-ft Bottom End Drop Test (filtered at 1000 Hz)

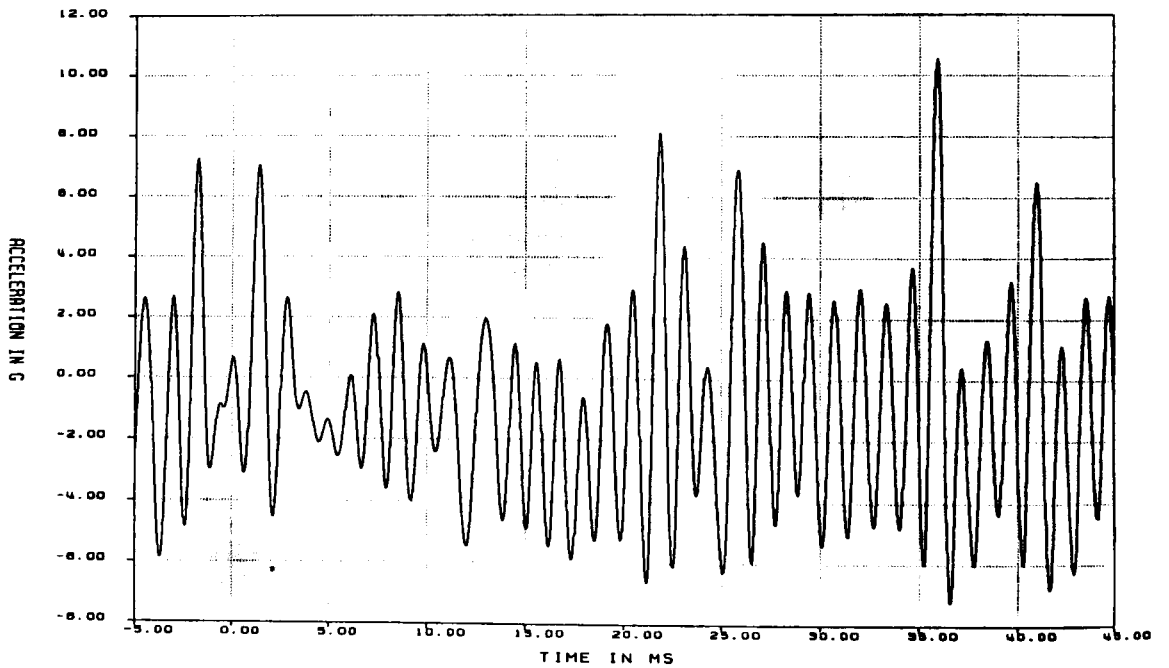


Figure B1-2. Acceleration vs Time for Gage AX2 for 30-ft Bottom End Drop Test (filtered at 1000 Hz)

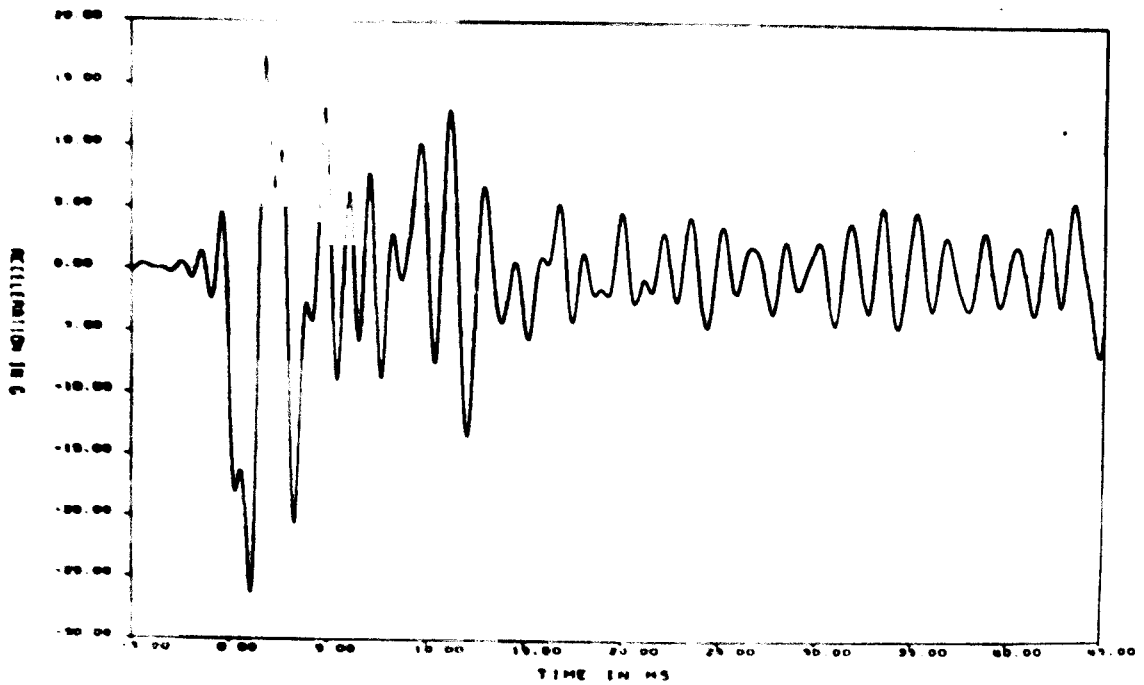


Figure B1-3. Acceleration vs Time for Gage AY3 for 30-ft Bottom End Drop Test (filtered at 1000 Hz)

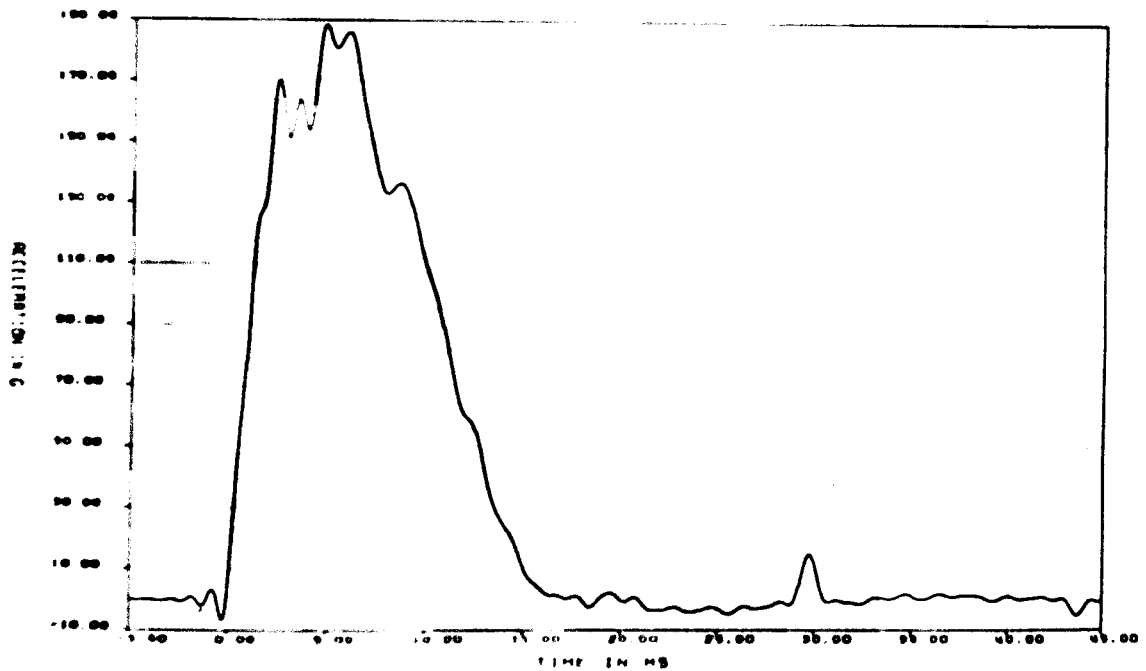


Figure B1-4. Acceleration vs Time for Gage AZ4 for 30-ft Bottom End Drop Test (filtered at 1000 Hz)

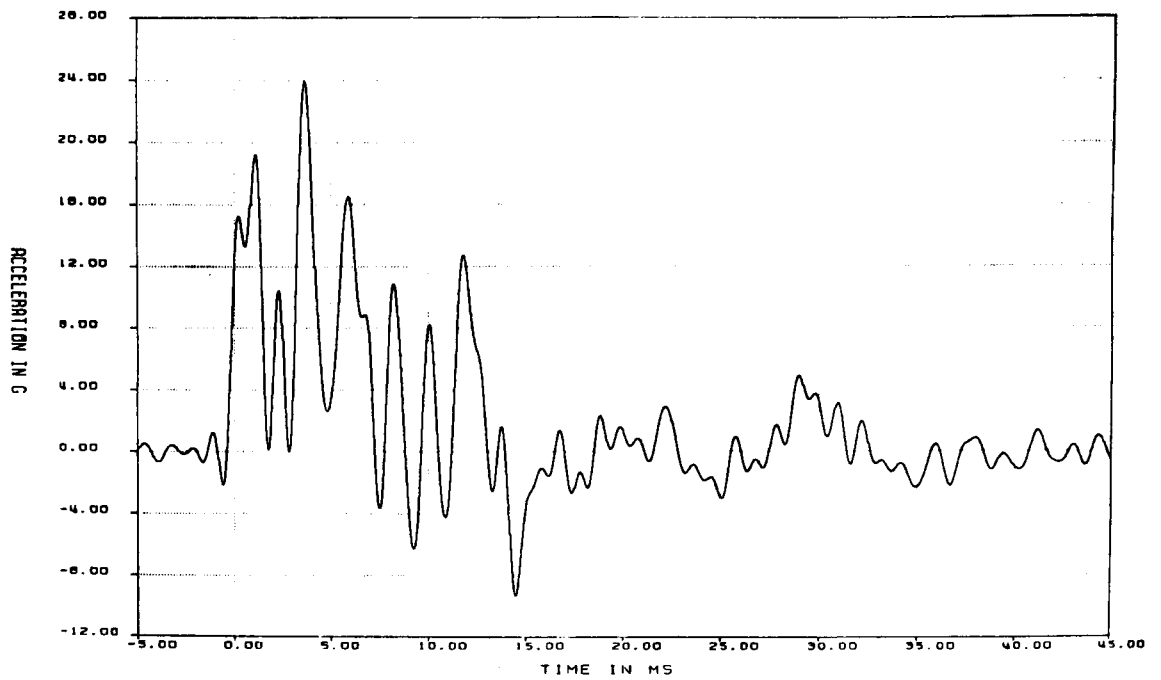


Figure B1-5. Acceleration vs Time for Gage AX5 for 30-ft Bottom End Drop Test (filtered at 1000 Hz)

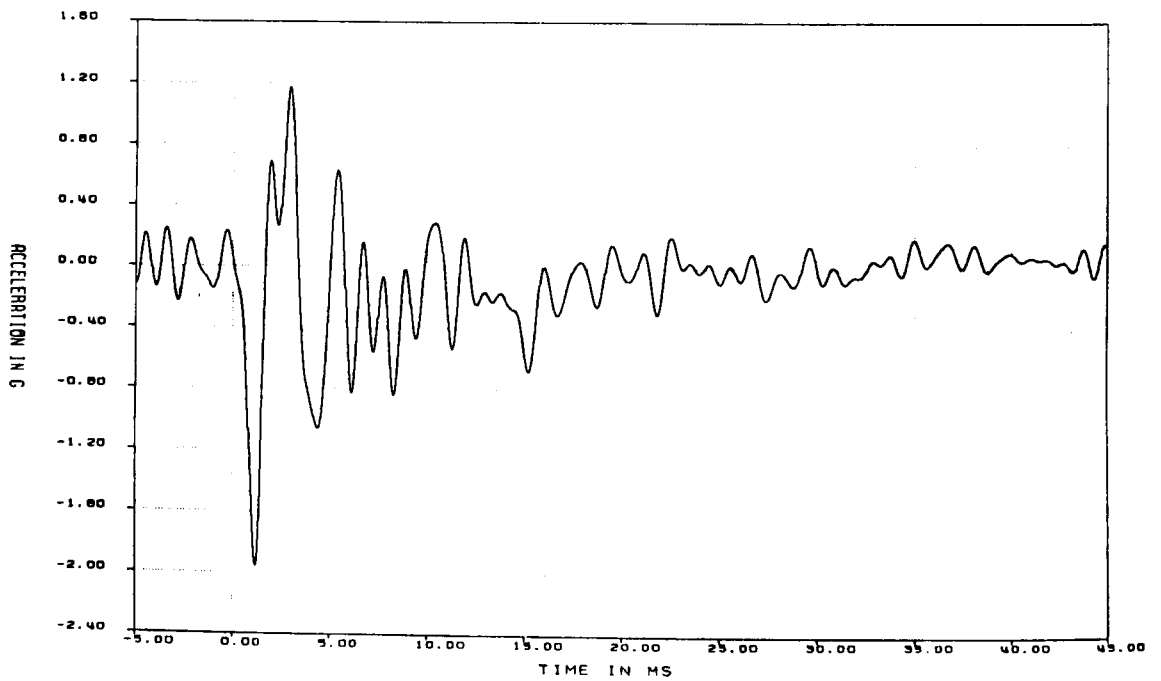


Figure B1-6. Acceleration vs Time for Gage AY6 for 30-ft Bottom End Drop Test (filtered at 1000 Hz)

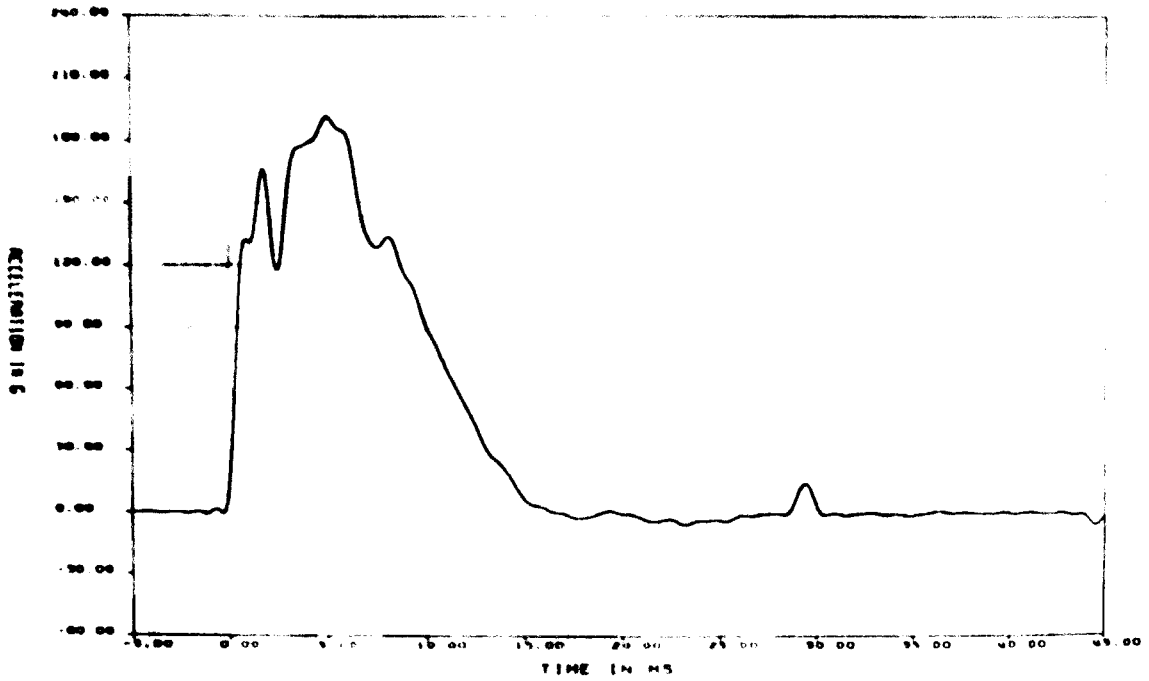


Figure B1-7. Acceleration vs Time for Gage AZ7 for 30-ft Bottom End Drop Test (filtered at 1000 Hz)

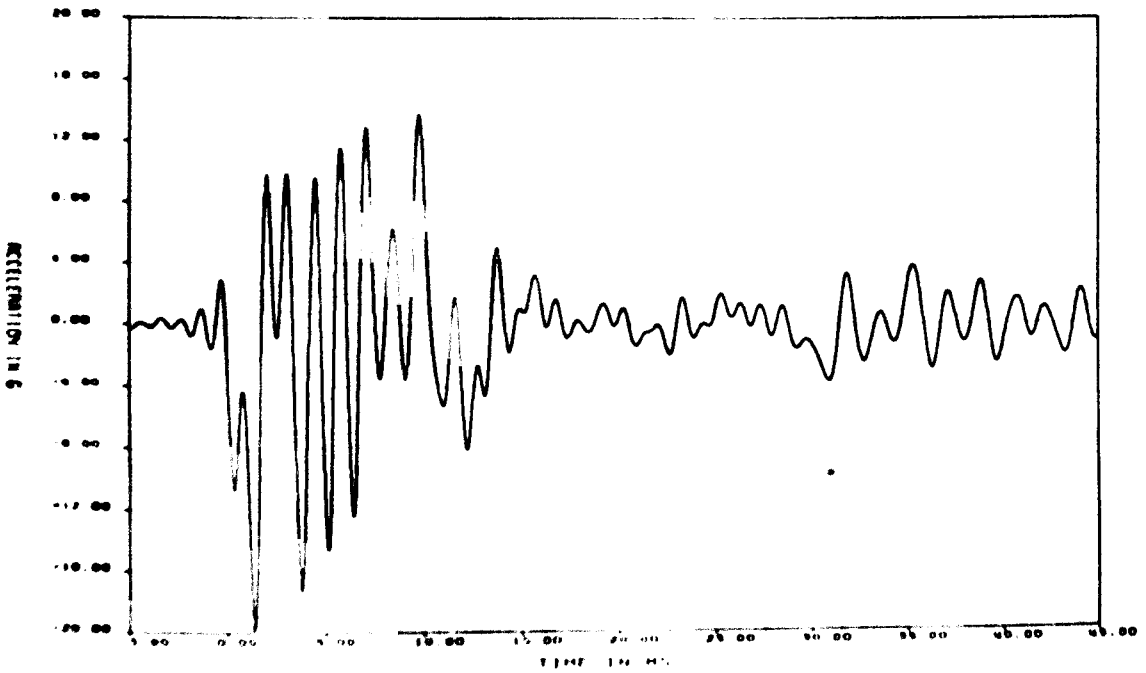


Figure B1-8. Acceleration vs Time for Gage AX8 for 30-ft Bottom End Drop Test (filtered at 1000 Hz)

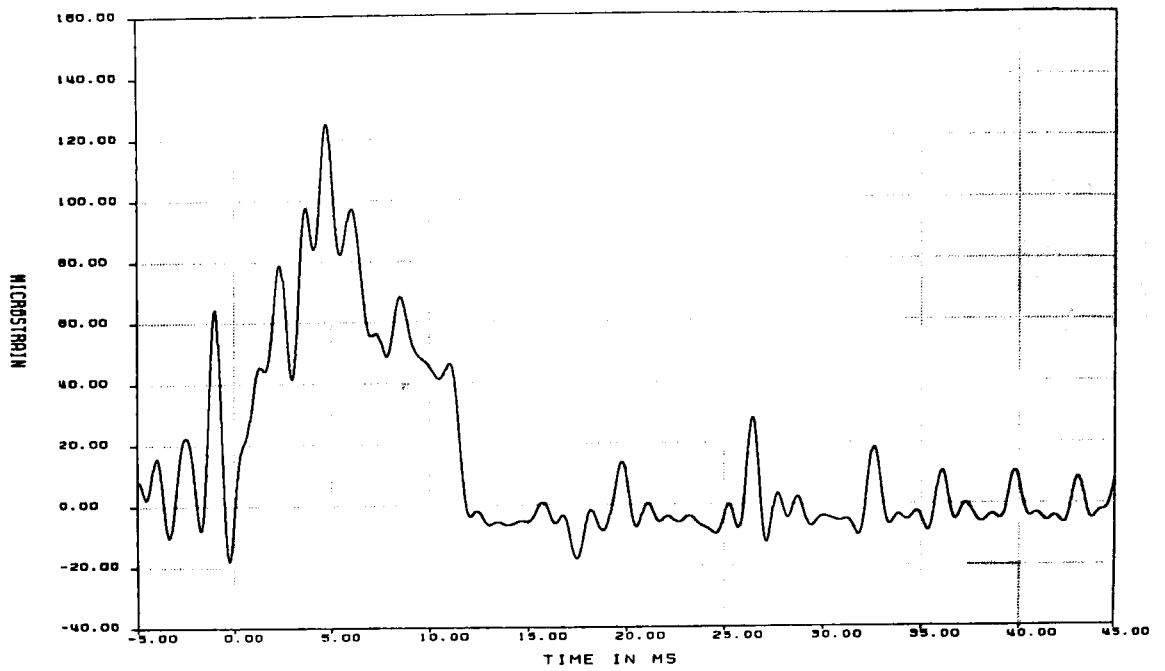


Figure B1-9. Microstrain vs Time for Gage SR1-Y for 30-ft Bottom End Drop Test (filtered at 1000 Hz)

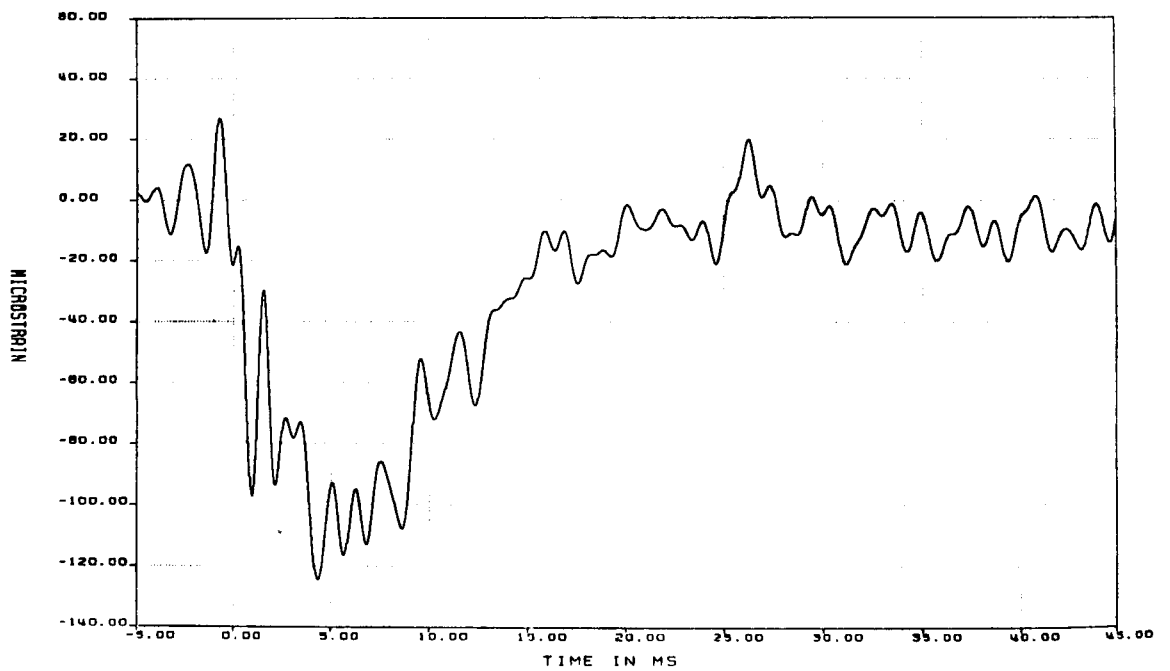


Figure B1-10. Microstrain vs Time for Gage SR1-YZ for 30-ft Bottom End Drop Test (filtered at 1000 Hz)

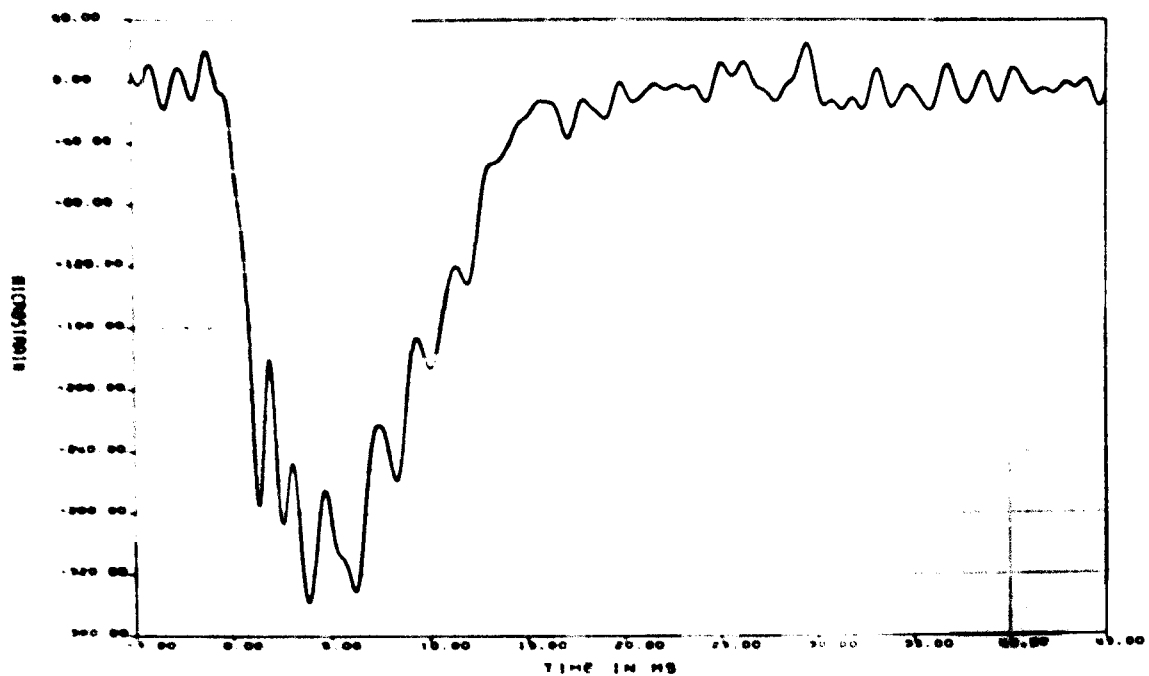


Figure B1-11. Microstrain vs Time for Gage SR1-Z for 30-ft Bottom End Drop Test (filtered at 1000 Hz)

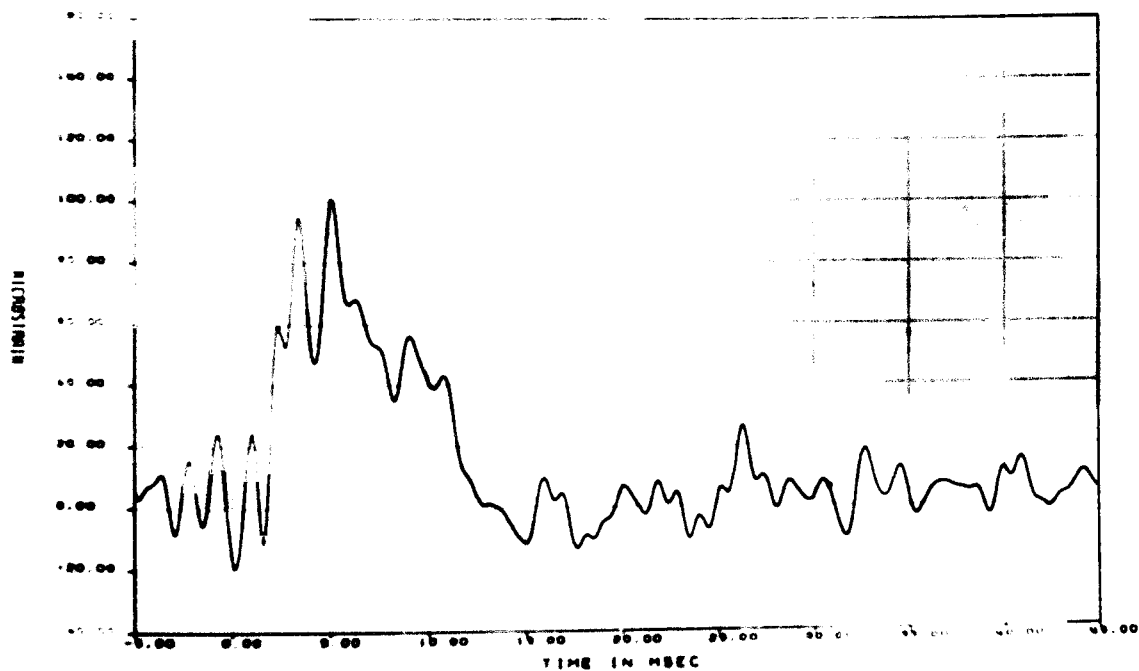


Figure B1-12. Microstrain vs Time for Gage SR2-Y for 30-ft Bottom End Drop Test (filtered at 1000 Hz)

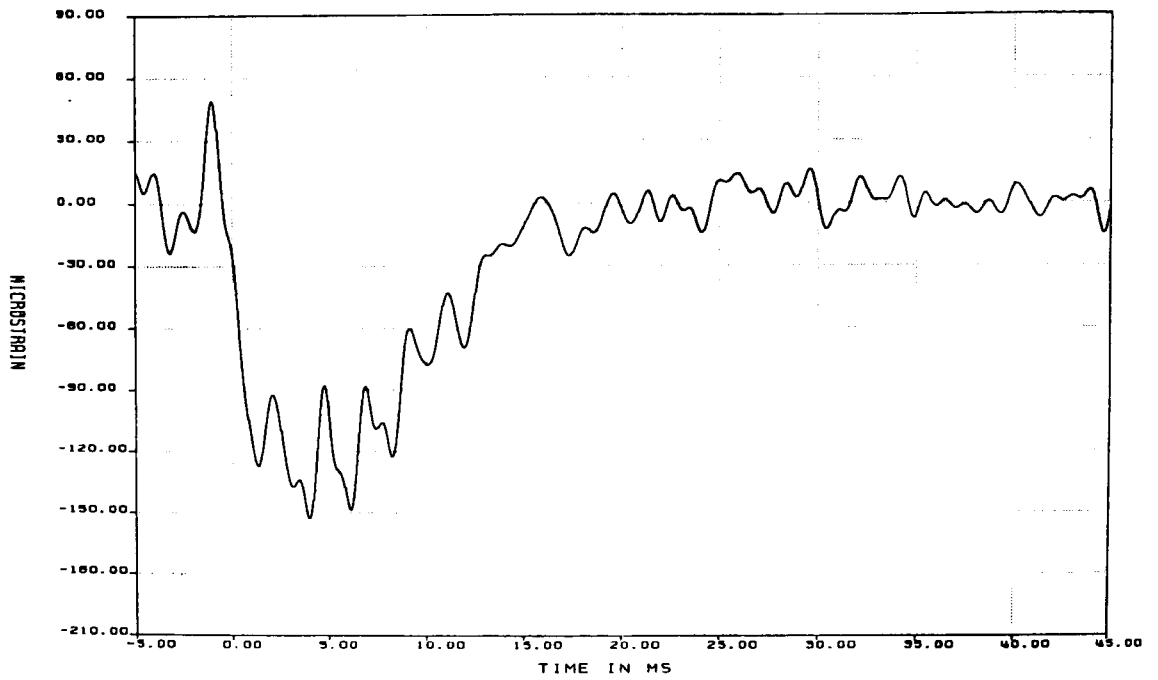


Figure B1-13. Microstrain vs Time for Gage SR2-YZ for 30-ft Bottom End Drop Test (filtered at 1000 Hz)

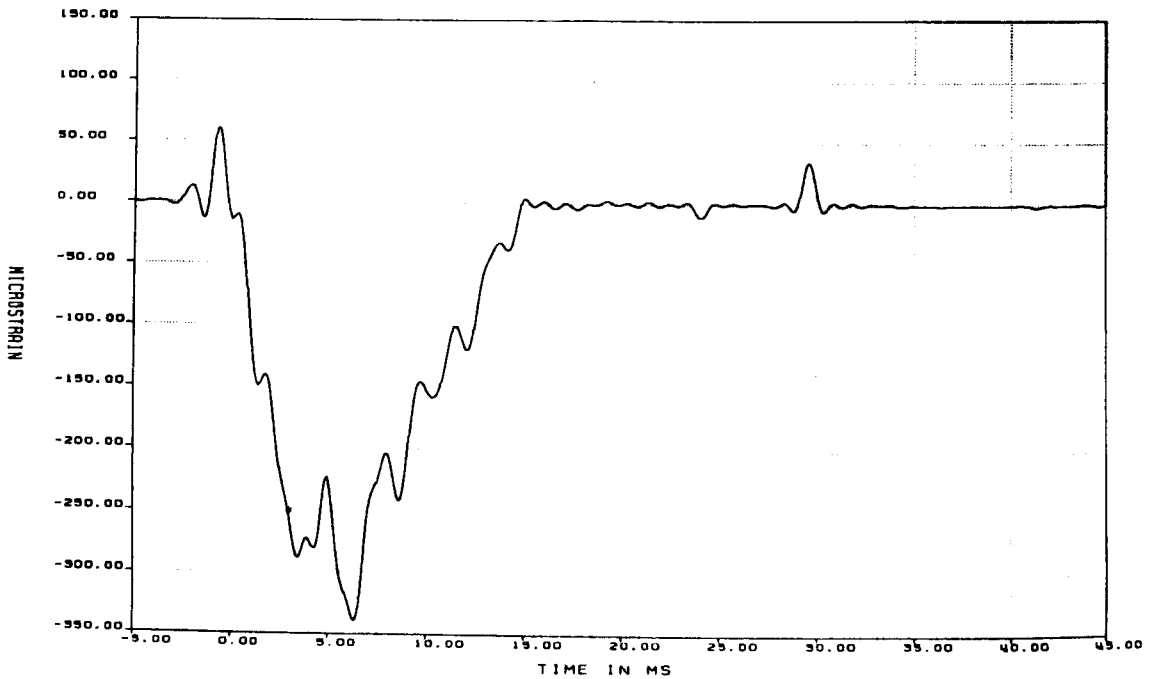


Figure B1-14. Microstrain vs Time for Gage SR2-Z for 30-ft Bottom End Drop Test (filtered at 1000 Hz)

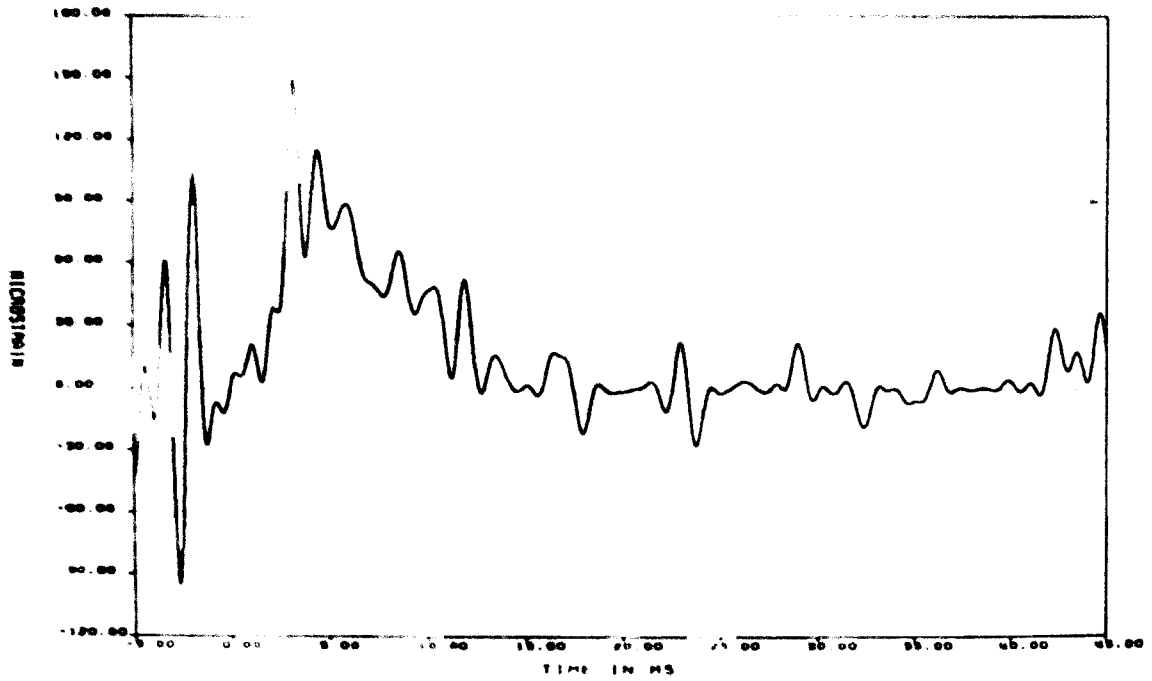


Figure B1-15. Microstrain vs Time for Gage SR3-Y for 30-ft Bottom End Drop Test (filtered at 1000 Hz)

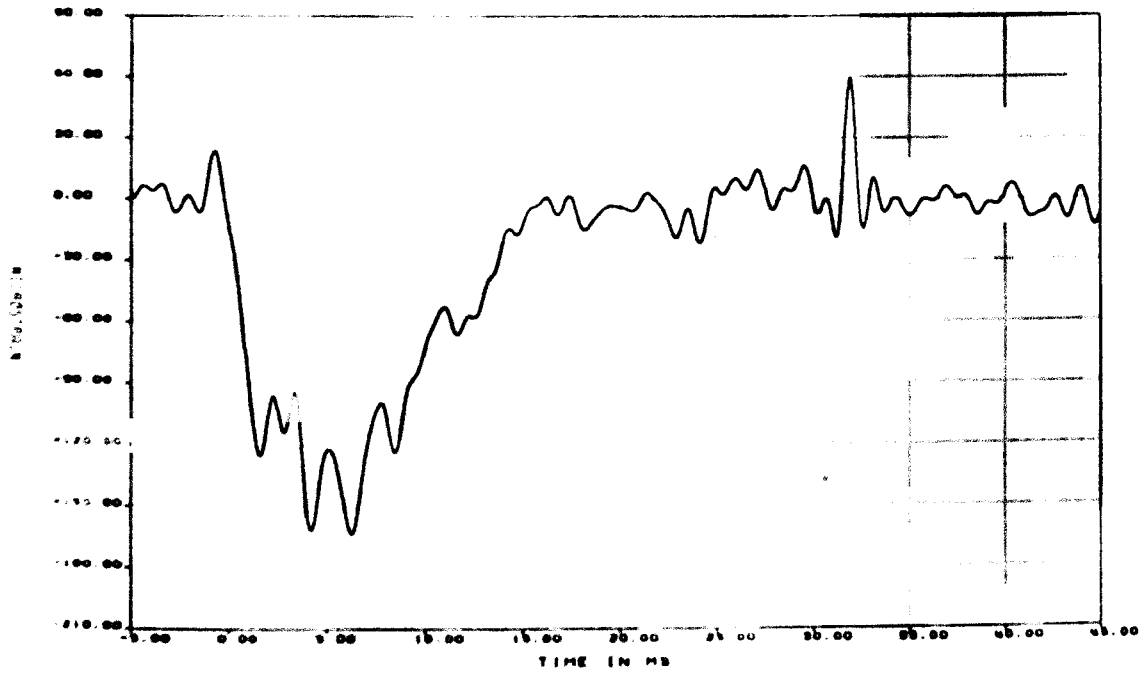


Figure B1-16. Microstrain vs Time for Gage SR3-YZ for 30-ft Bottom End Drop Test (filtered at 1000 Hz)

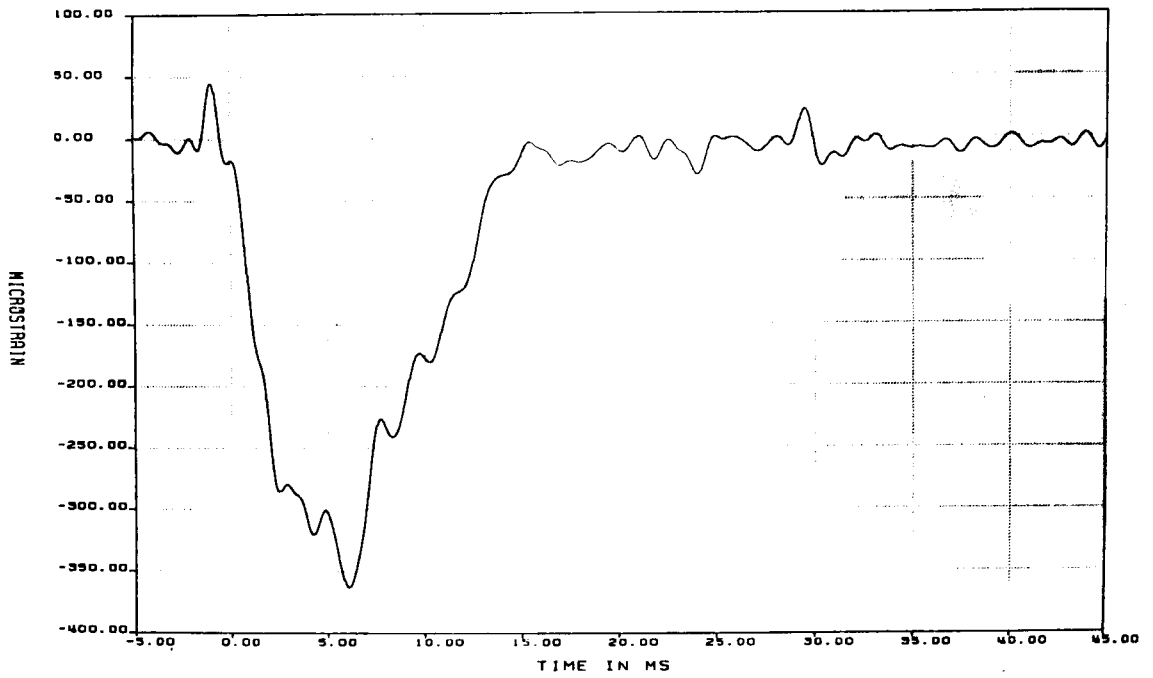


Figure B1-17. Microstrain vs Time for Gage SR3-Z for 30-ft Bottom End Drop Test (filtered at 1000 Hz)

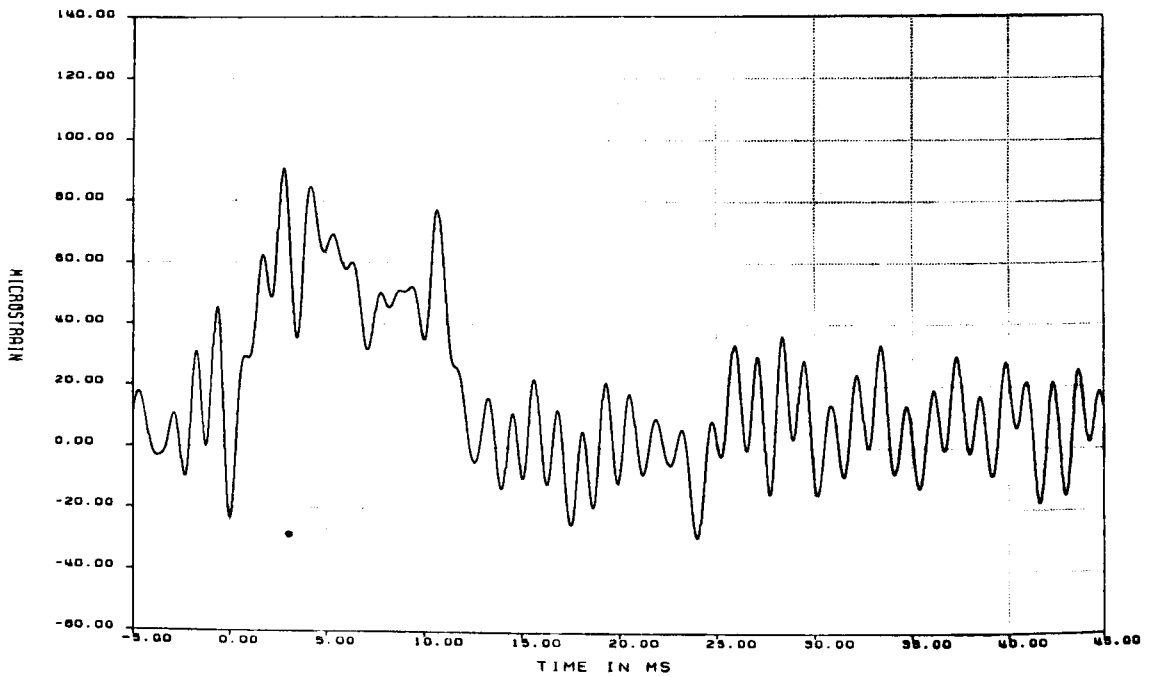


Figure B1-18. Microstrain vs Time for Gage SR4-Y for 30-ft Bottom End Drop Test (filtered at 1000 Hz)

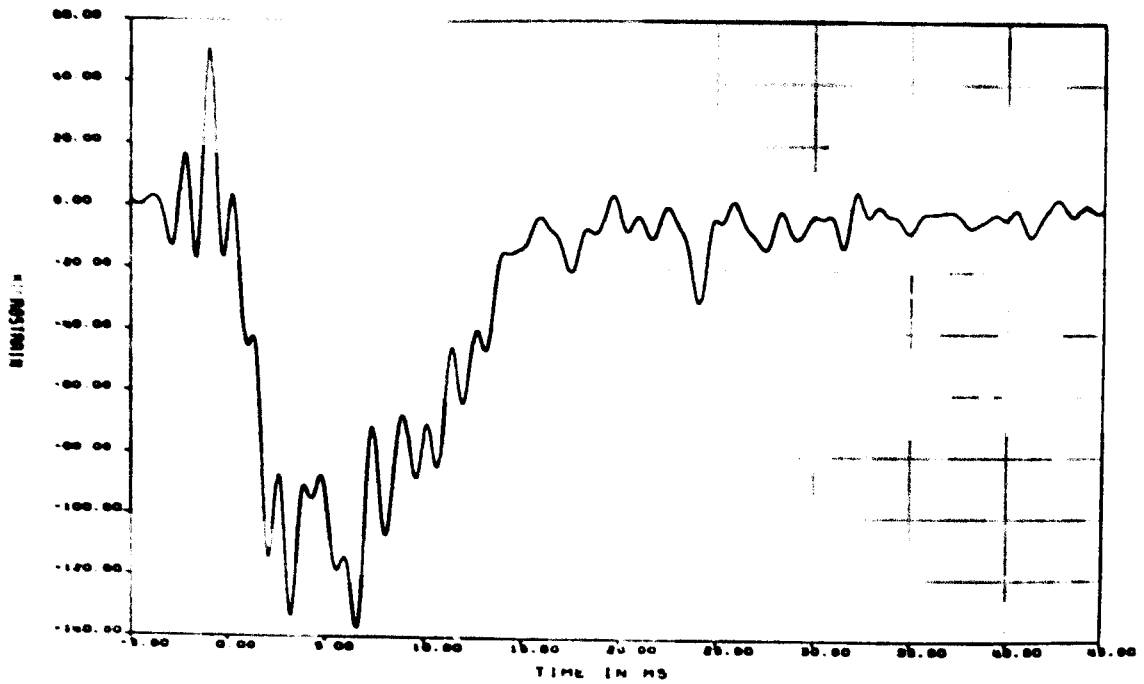


Figure B1-19. Microstrain vs Time for Gage SR4-YZ for 30-ft Bottom End Drop Test (filtered at 1000 Hz)

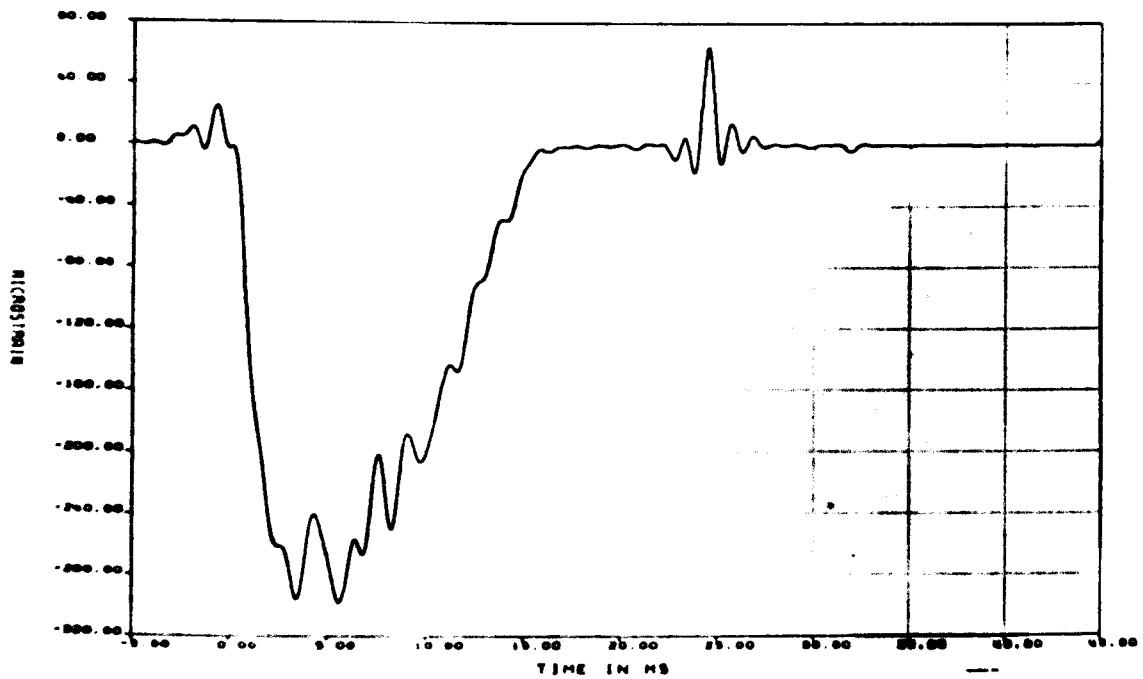


Figure B1-20. Microstrain vs Time for Gage SR4-Z for 30-ft Bottom End Drop Test (filtered at 1000 Hz)

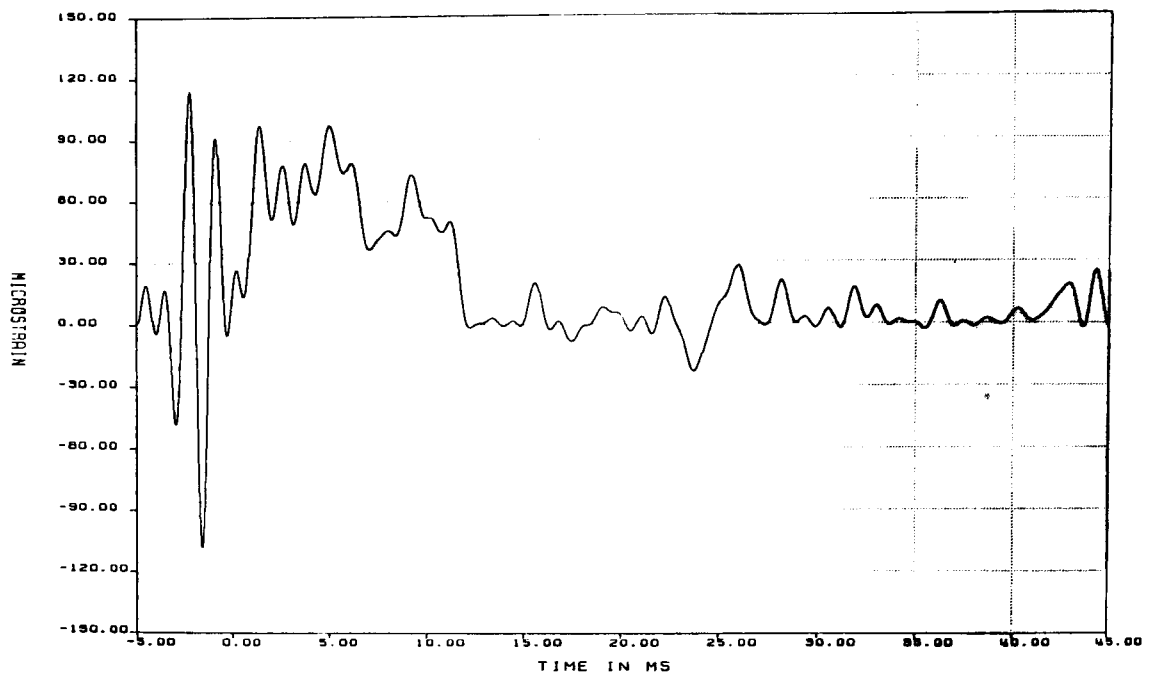


Figure B1-21. Microstrain vs Time for Gage SR5-Y for 30-ft Bottom End Drop Test (filtered at 1000 Hz)

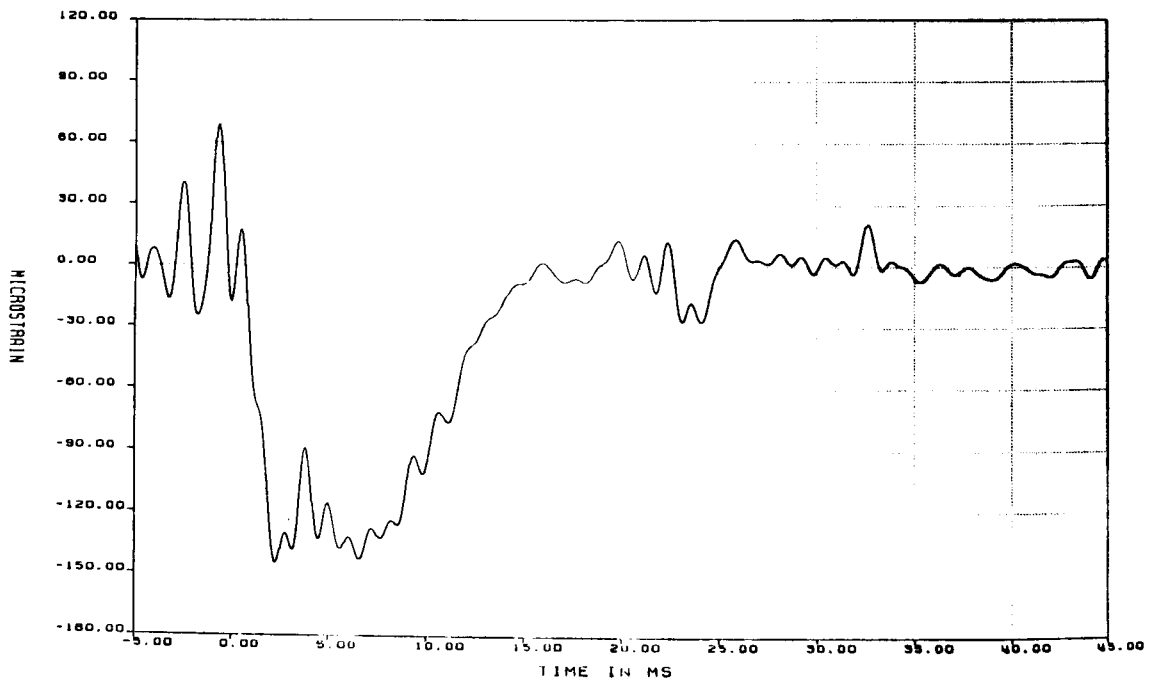


Figure B1-22. Microstrain vs Time for Gage SR5-YZ for 30-ft Bottom End Drop Test (filtered at 1000 Hz)

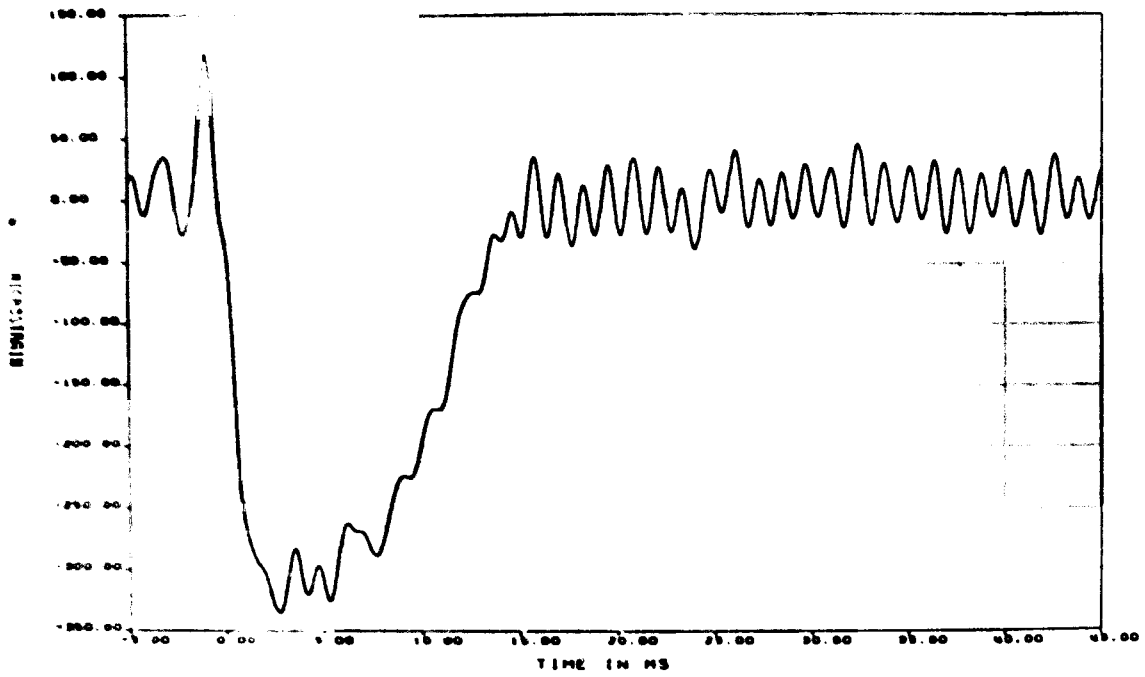


Figure B1-23. Microstrain vs Time for Gage SR5-Z for 30-ft Bottom End Drop Test (filtered at 1000 Hz)

APPENDIX B2

Fast Fourier Transforms of Raw Accelerometer Data for the 30-ft Bottom End Drop Test

Figures

B2-1	Fast Fourier Transform of Raw Data From Gage AZ1 for 30-ft Bottom End Drop Test: 0-50 kHz.....	172
B2-2	Fast Fourier Transform of Raw Data From Gage AZ1 for 30-ft Bottom End Drop Test: 0-10 kHz.....	172
B2-3	Fast Fourier Transform of Raw Data From Gage AX2 for 30-ft Bottom End Drop Test: 0-50 kHz.....	173
B2-4	Fast Fourier Transform of Raw Data From Gage AX2 for 30-ft Bottom End Drop Test: 0-10 kHz.....	173
B2-5	Fast Fourier Transform of Raw Data From Gage AY3 for 30-ft Bottom End Drop Test: 0-50 kHz.....	174
B2-6	Fast Fourier Transform of Raw Data From Gage AY3 for 30-ft Bottom End Drop Test: 0-10 kHz.....	174
B2-7	Fast Fourier Transform of Raw Data From Gage AZ4 for 30-ft Bottom End Drop Test: 0-50 kHz.....	175
B2-8	Fast Fourier Transform of Raw Data From Gage AZ4 for 30-ft Bottom End Drop Test: 0-10 kHz.....	175
B2-9	Fast Fourier Transform of Raw Data From Gage AX5 for 30-ft Bottom End Drop Test: 0-50 kHz.....	176
B2-10	Fast Fourier Transform of Raw Data From Gage AX5 for 30-ft Bottom End Drop Test: 0-10 kHz.....	176
B2-11	Fast Fourier Transform of Raw Data From Gage AY6 for 30-ft Bottom End Drop Test: 0-50 kHz.....	177
B2-12	Fast Fourier Transform of Raw Data From Gage AY6 for 30-ft Bottom End Drop Test: 0-10 kHz.....	177
B2-13	Fast Fourier Transform of Raw Data From Gage AZ7 for 30-ft Bottom End Drop Test: 0-50 kHz.....	178
B2-14	Fast Fourier Transform of Raw Data From Gage AZ7 for 30-ft Bottom End Drop Test: 0-10 kHz.....	178
B2-15	Fast Fourier Transform of Raw Data From Gage AX8 for 30-ft Bottom End Drop Test: 0-50 kHz.....	179
B2-16	Fast Fourier Transform of Raw Data From Gage AX8 for 30-ft Bottom End Drop Test: 0-10 kHz.....	179

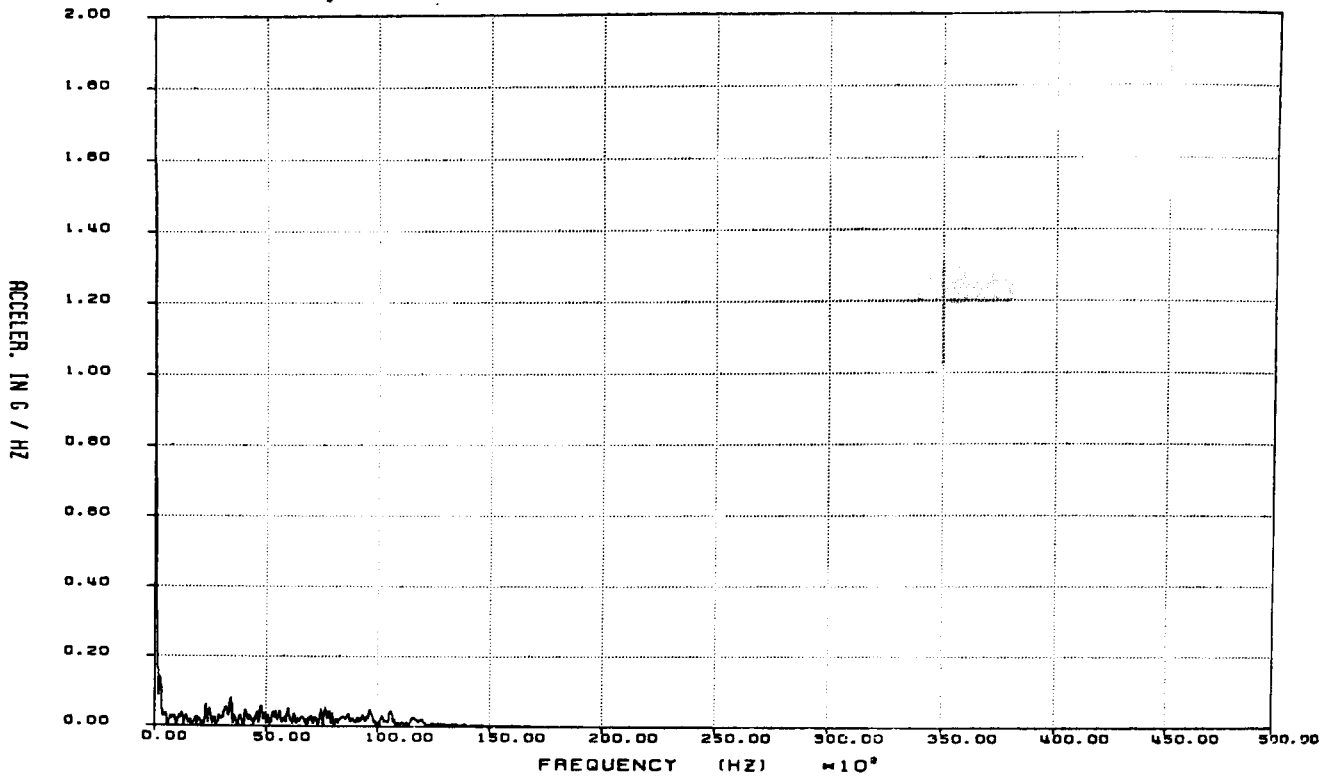


Figure B2-1. Fast Fourier Transform of Raw Data From Gage AZ1 for 30-ft Bottom End Drop Test: 0-50 kHz

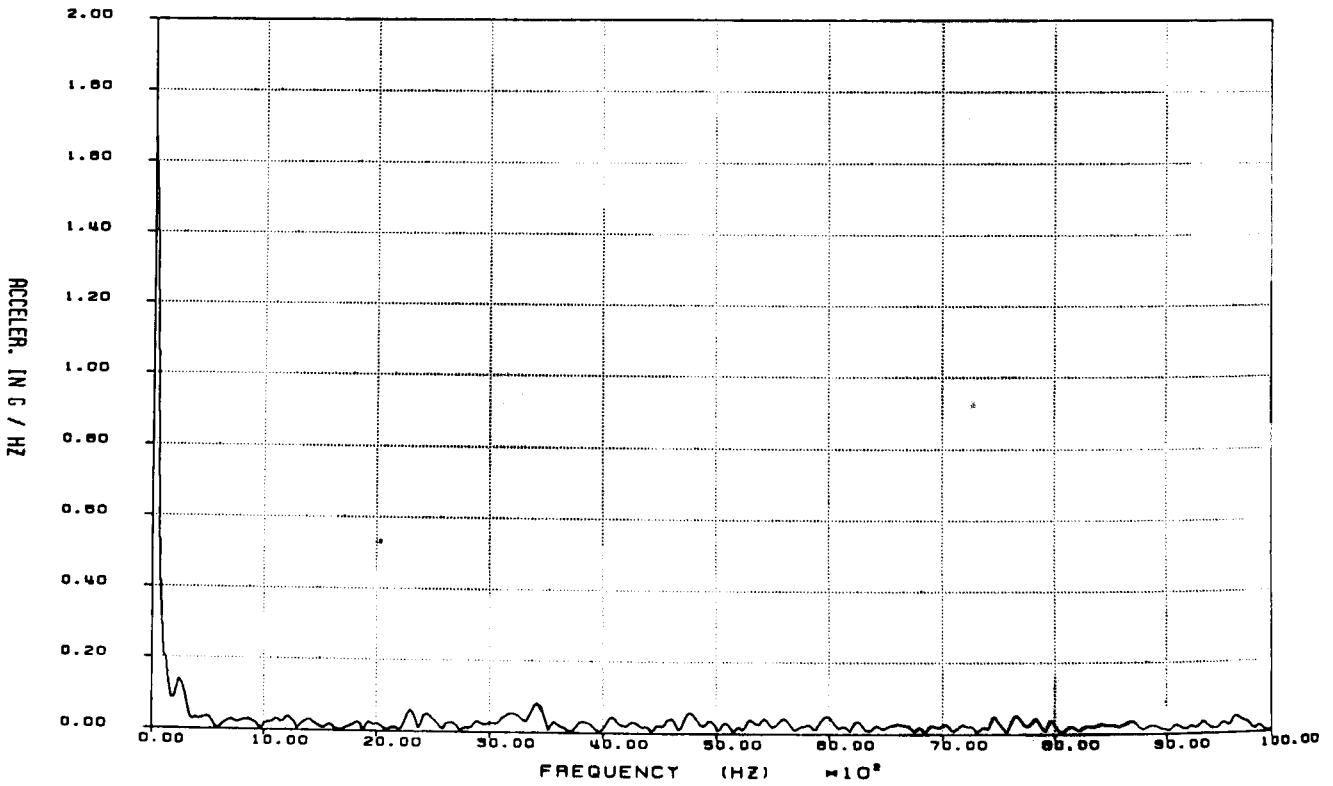


Figure B2-2. Fast Fourier Transform of Raw Data From Gage AZ1 for 30-ft Bottom End Drop Test: 0-10 kHz

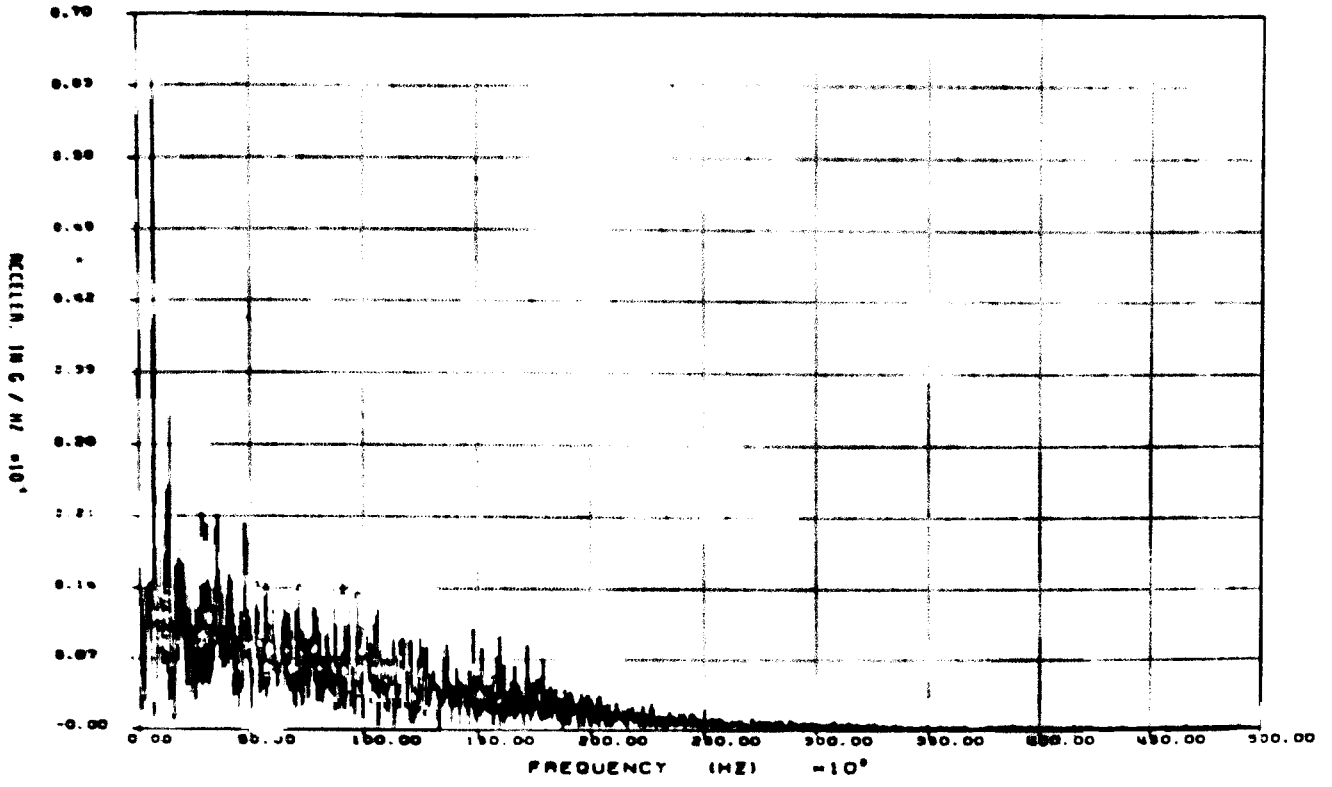


Figure B2-3. Fast Fourier Transform of Raw Data From Gage AX2 for 30-ft Bottom End Drop Test: 0-50 kHz

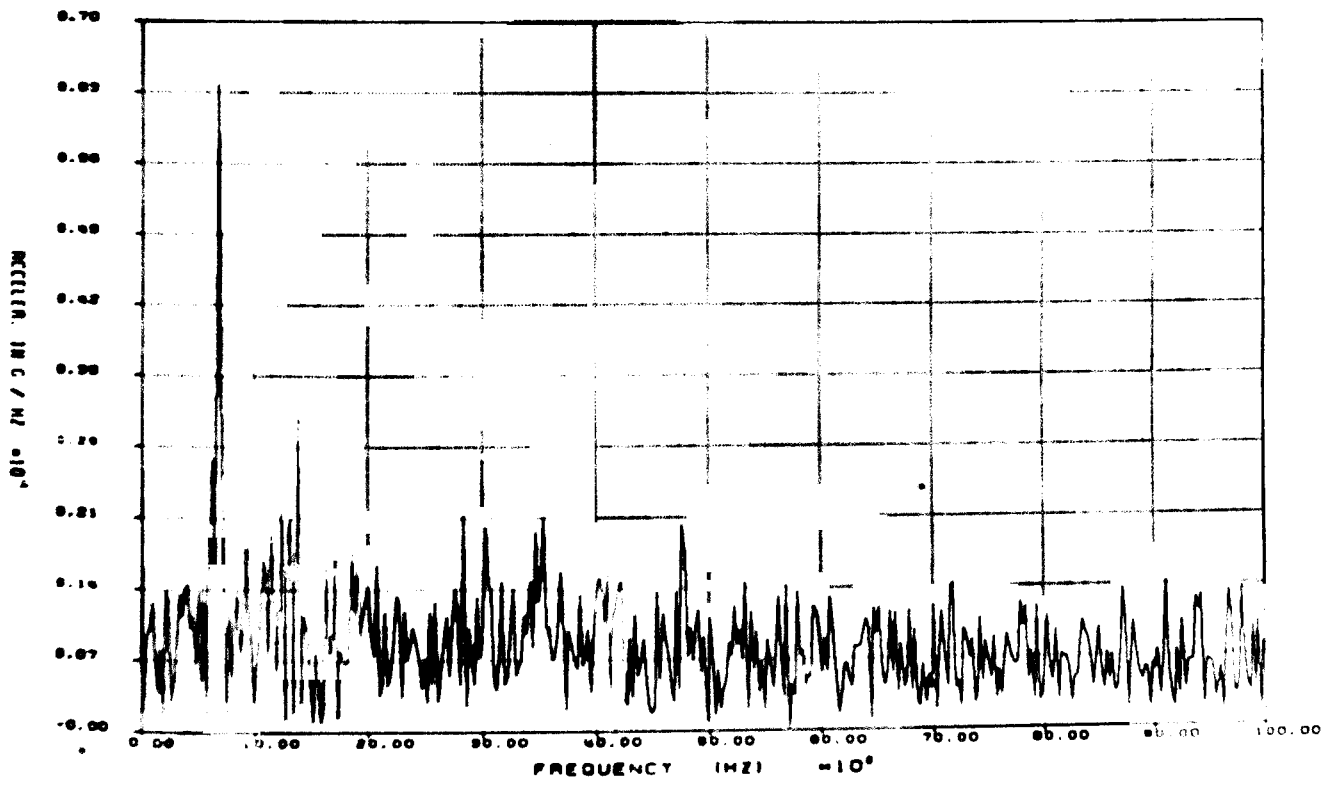


Figure B2-4. Fast Fourier Transform of Raw Data From Gage AX2 for 30 ft Bottom End Drop Test: 0-10 kHz

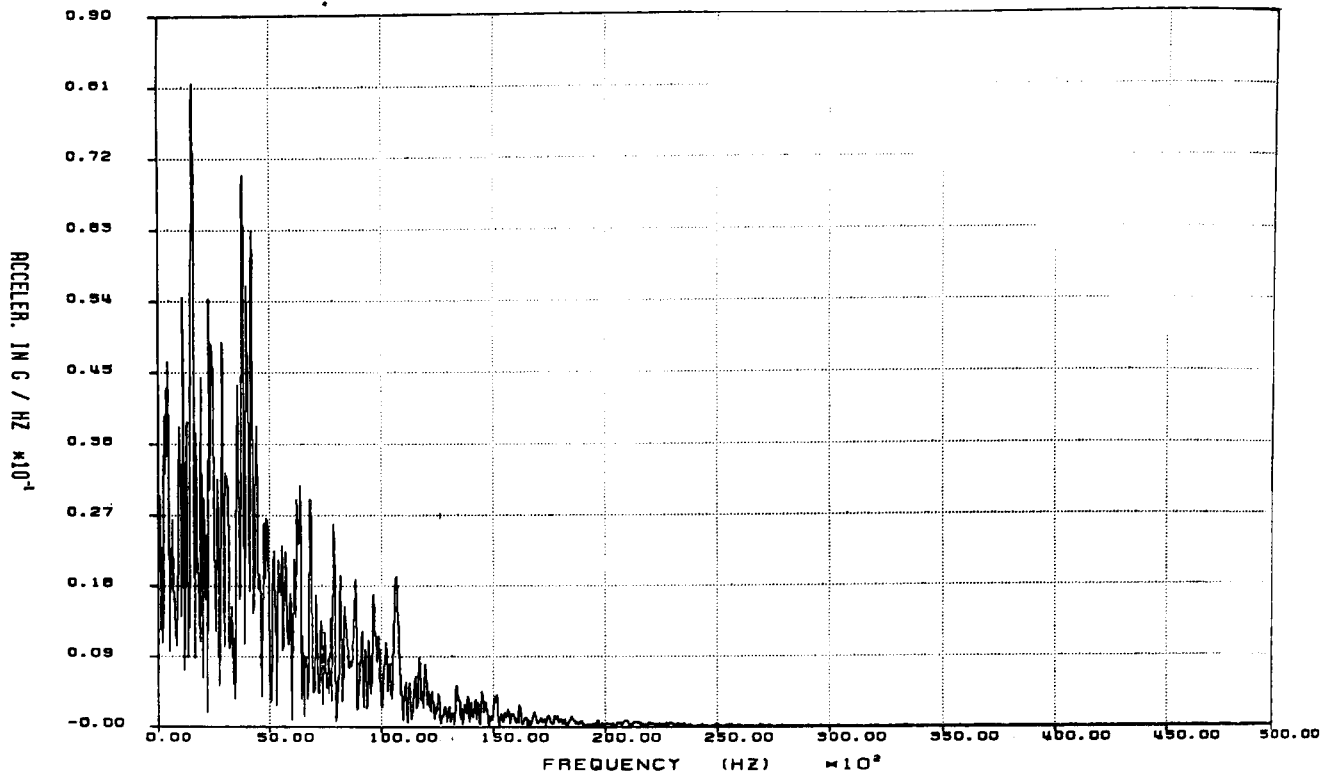


Figure B2-5. Fast Fourier Transform of Raw Data From Gage AY3 for 30-ft Bottom End Drop Test: 0-50 kHz

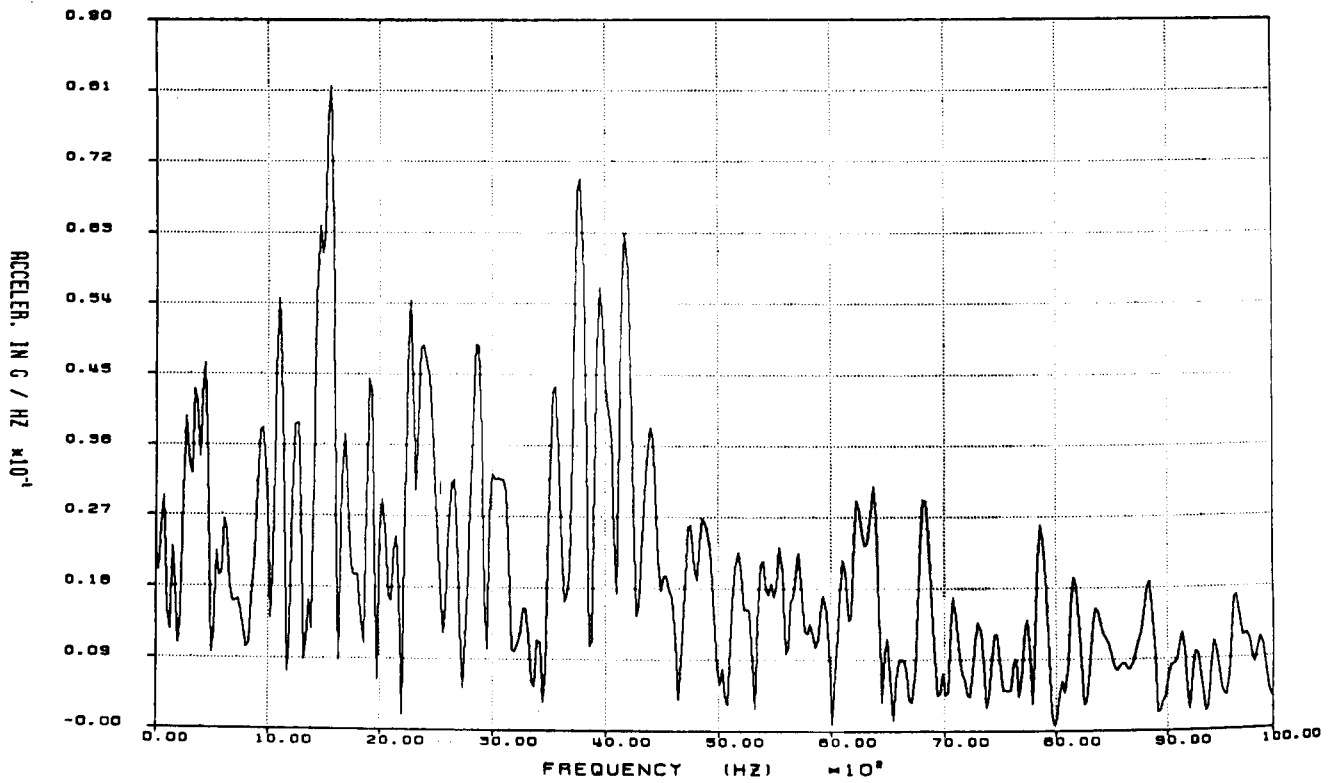


Figure B2-6. Fast Fourier Transform of Raw Data From Gage AY3 for 30-ft Bottom End Drop Test: 0-10 kHz

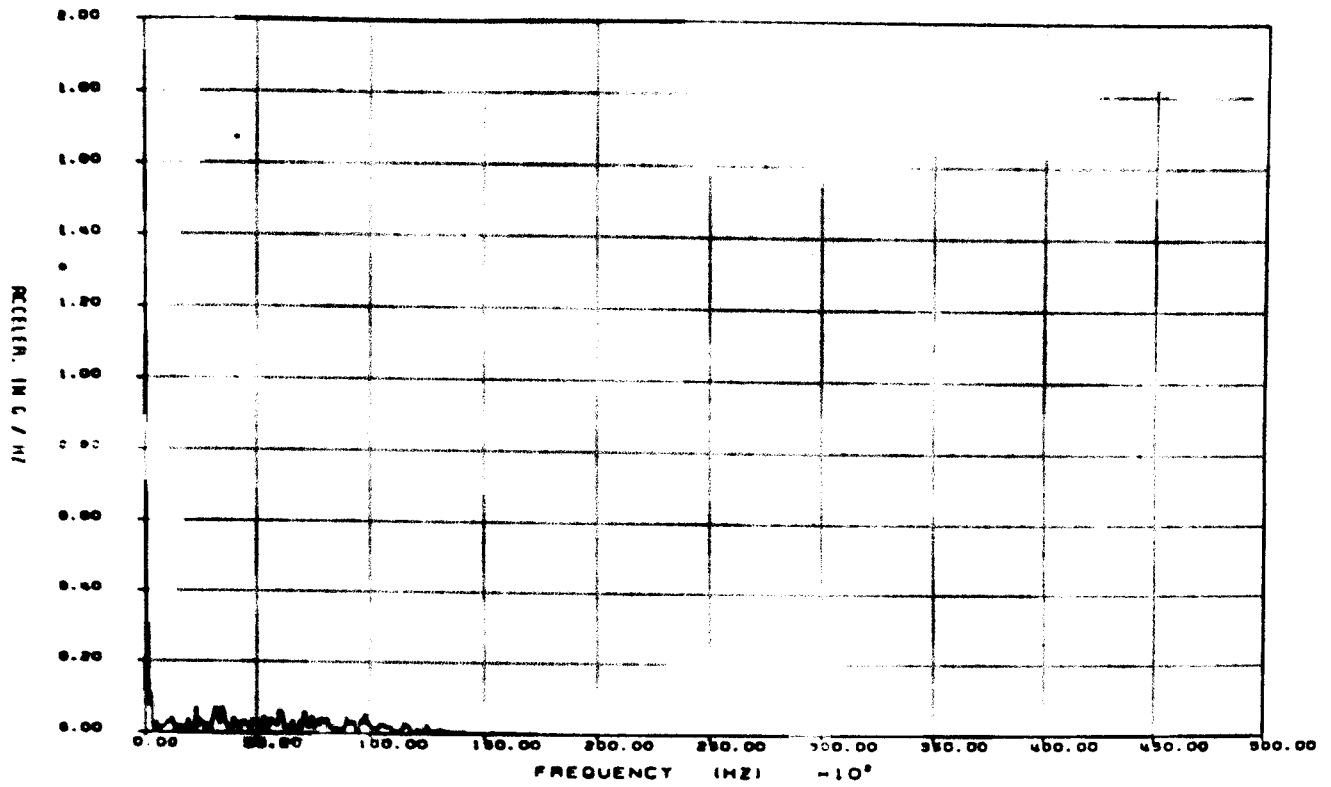


Figure B2-7. Fast Fourier Transform of Raw Data From Gage AZ4 for 30-ft Bottom End Drop Test: 0-50 kHz

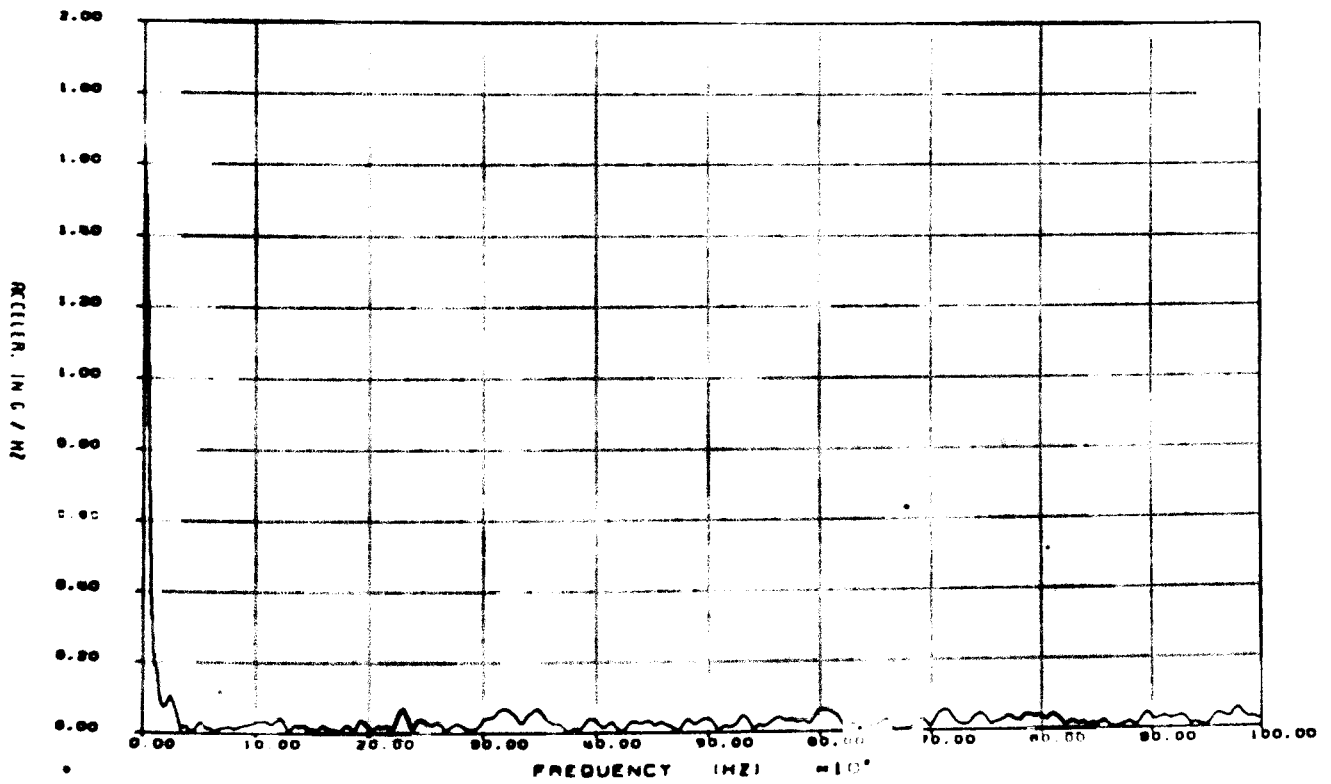


Figure B2-8. Fast Fourier Transform of Raw Data From Gage AZ4 for 30-ft Bottom End Drop Test: 0-10 kHz

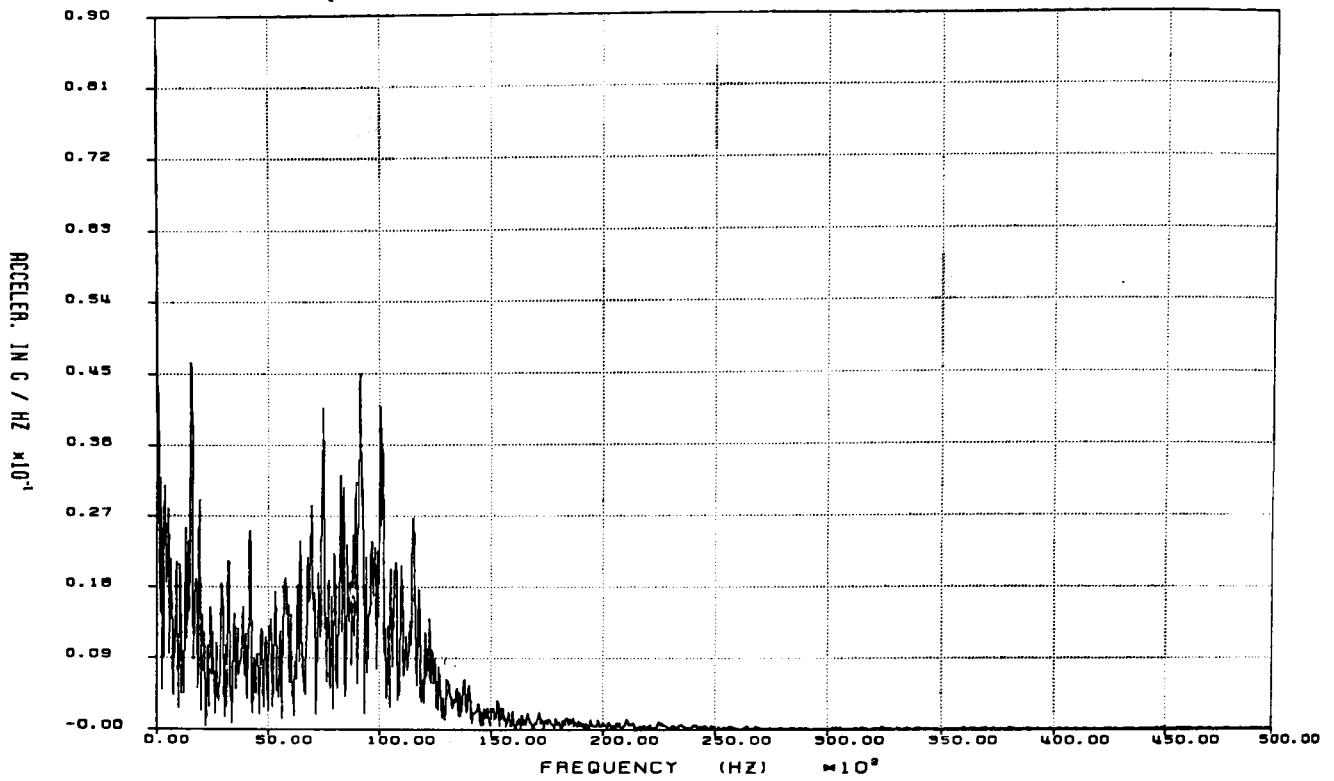


Figure B2-9. Fast Fourier Transform of Raw Data From Gage AX5 for 30-ft Bottom End Drop Test: 0-50 kHz

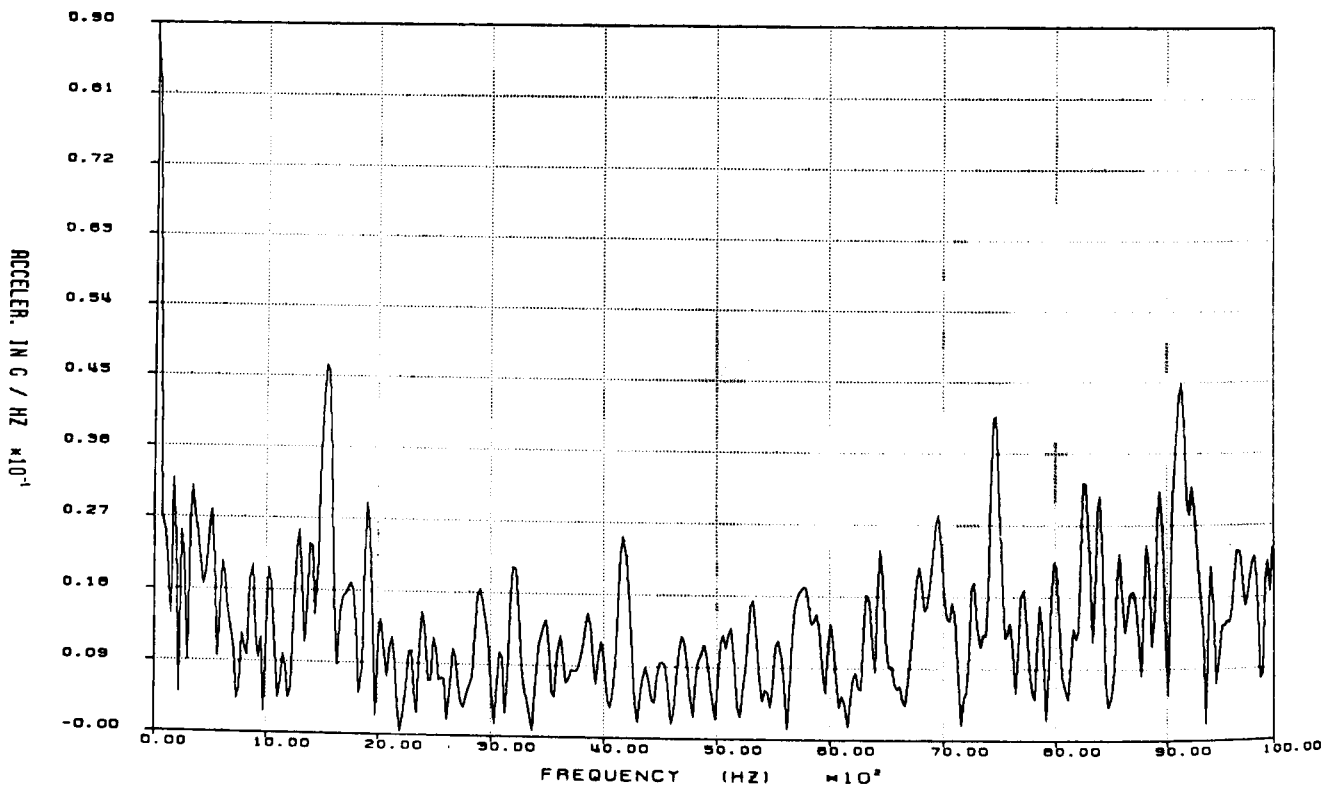


Figure B2-10. Fast Fourier Transform of Raw Data From Gage AX5 for 30-ft Bottom End Drop Test: 0-10 kHz

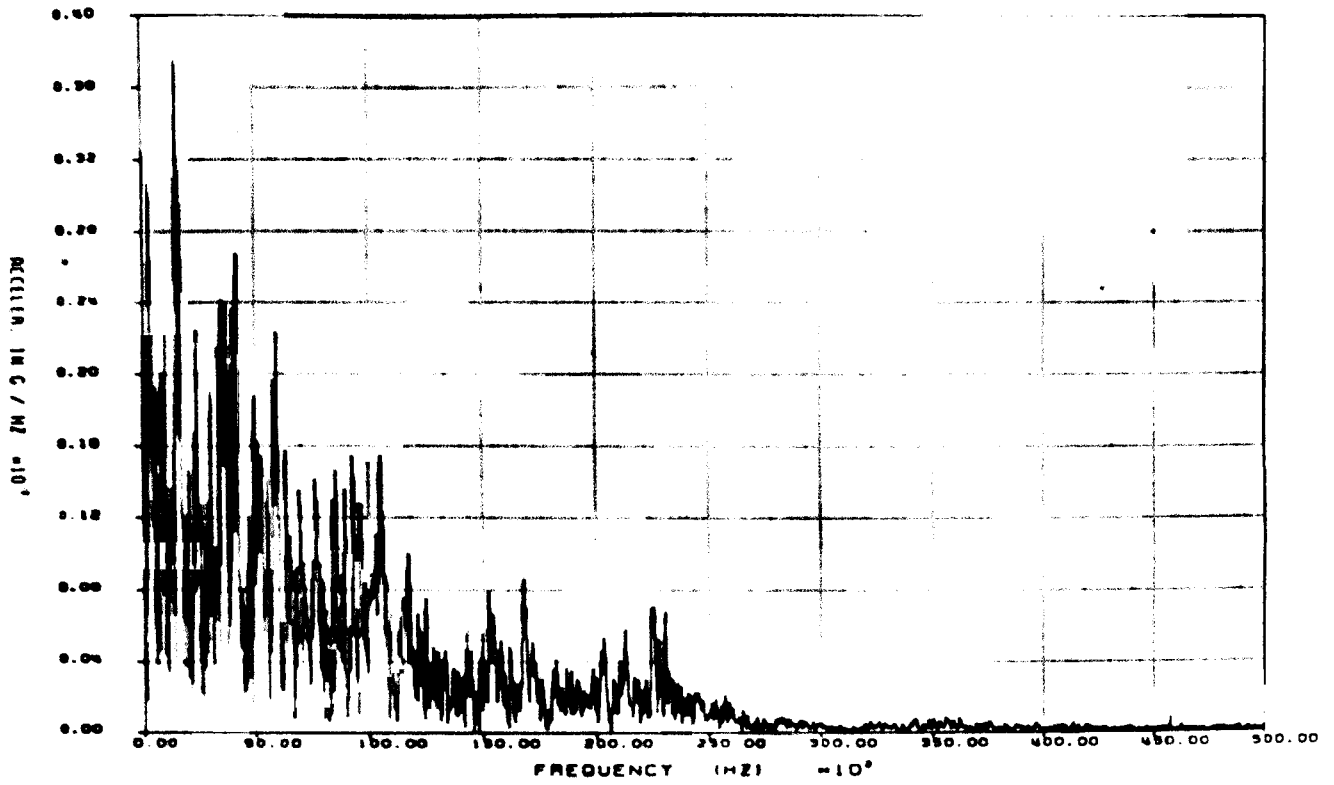


Figure B2-11. Fast Fourier Transform of Raw Data From Gage AY6 for 30-ft Bottom End Drop Test: 0-50 kHz

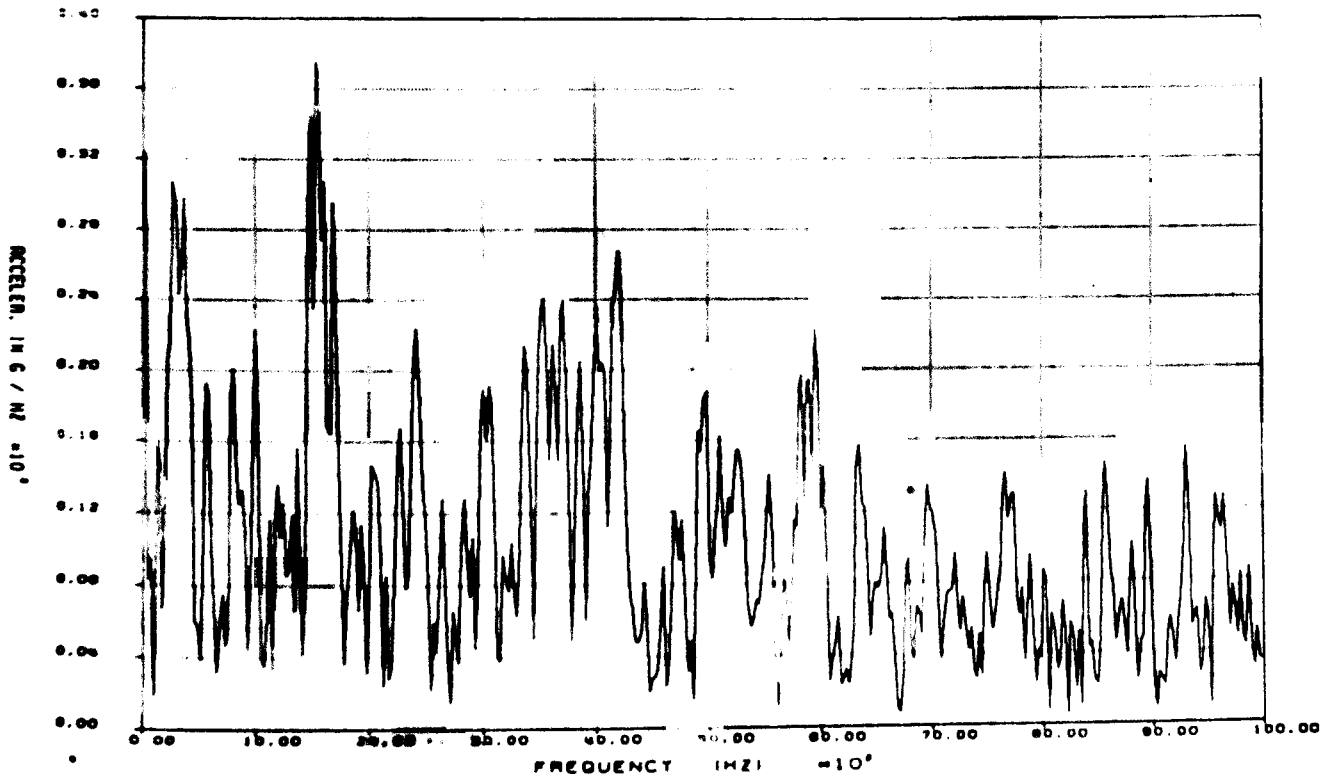


Figure B2-12. Fast Fourier Transform of Raw Data From Gage AY6 for 30-ft Bottom End Drop Test: 0-10 kHz

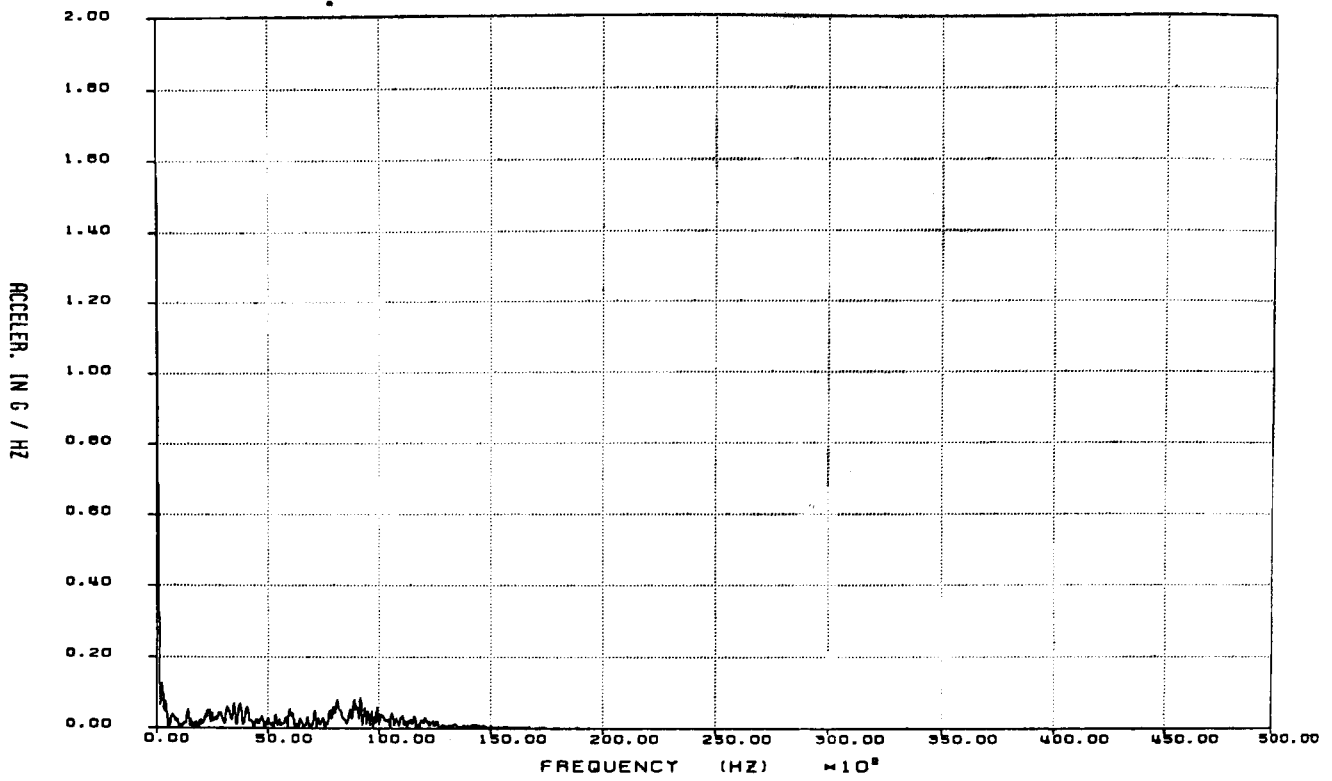


Figure B2-13. Fast Fourier Transform of Raw Data From Gage AZ7 for 30-ft Bottom End Drop Test: 0-50 kHz

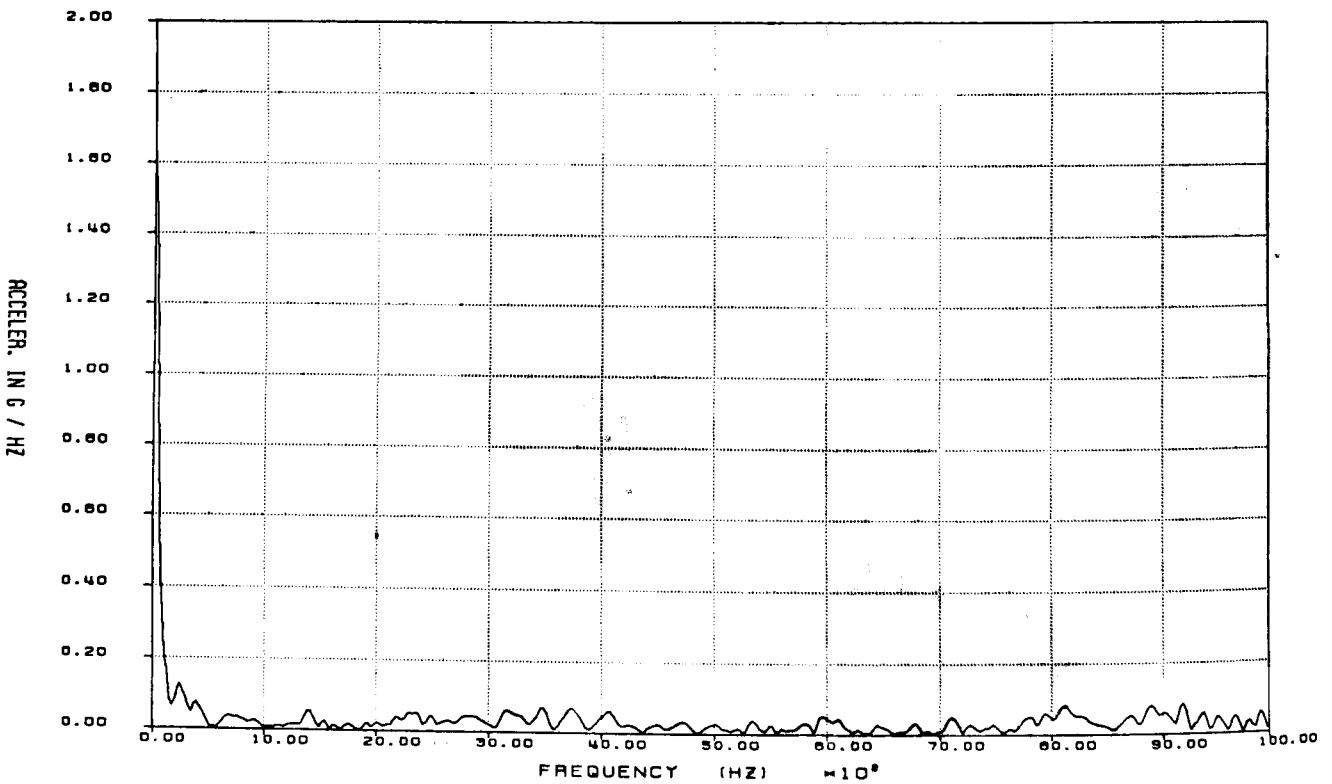


Figure B2-14. Fast Fourier Transform of Raw Data From Gage AZ7 for 30-ft Bottom End Drop Test: 0-10 kHz

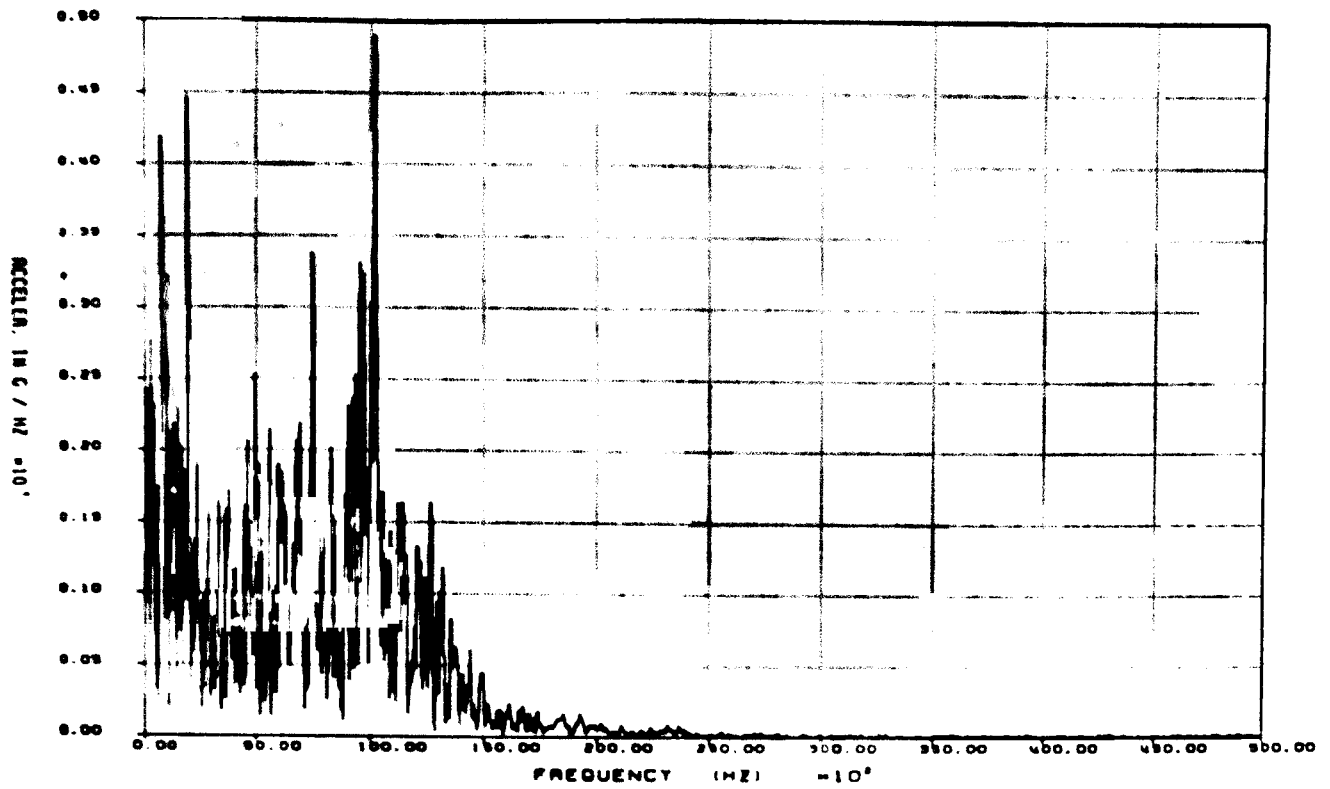


Figure B2-15. Fast Fourier Transform of Raw Data From Gage AX8 for 30 ft Bottom End Drop Test: 0-50 kHz

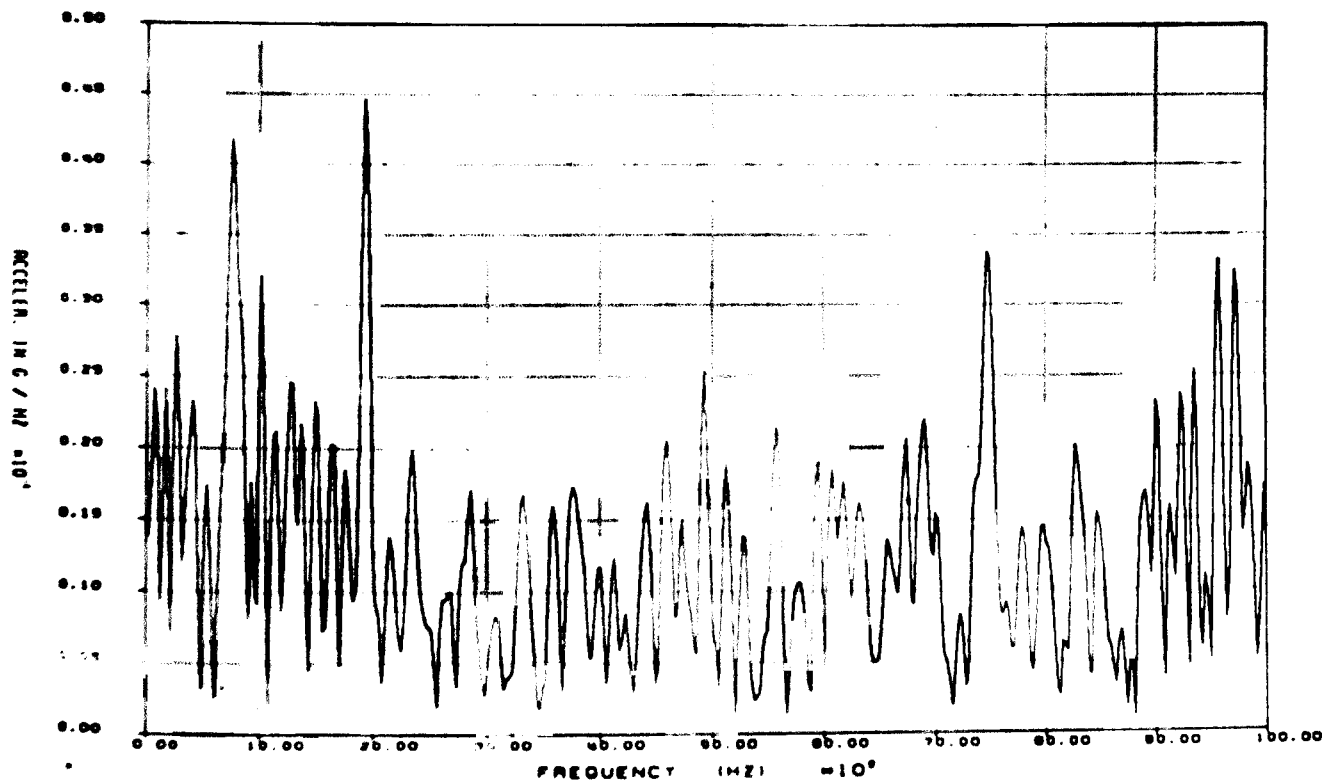


Figure B2-16. Fast Fourier Transform of Raw Data From Gage AX8 for 30 ft Bottom End Drop Test: 0-10 kHz

APPENDIX C1

Accelerometer and Strain Gage Data for the 30-ft Oblique Drop Test Filtered at 1000 Hz

Figures

C1-1	Acceleration vs Time for Gage AZ1 for 30-ft Oblique Drop Test	182
C1-2	Acceleration vs Time for Gage AX2 for 30-ft Oblique Drop Test	182
C1-3	Acceleration vs Time for Gage AY3 for 30-ft Oblique Drop Test	183
C1-4	Acceleration vs Time for Gage AZ4 for 30-ft Oblique Drop Test	183
C1-5	Acceleration vs Time for Gage AX5 for 30-ft Oblique Drop Test	184
C1-6	Acceleration vs Time for Gage AY6 for 30-ft Oblique Drop Test	184
C1-7	Acceleration vs Time for Gage AZ7 for 30-ft Oblique Drop Test	185
C1-8	Acceleration vs Time for Gage AX8 for 30-ft Oblique Drop Test	185
C1-9	Microstrain vs Time for Gage SR1-Y for 30-ft Oblique Drop Test	186
C1-10	Microstrain vs Time for Gage SR1-YZ for 30-ft Oblique Drop Test	186
C1-11	Microstrain vs Time for Gage SR1-Z for 30-ft Oblique Drop Test	187
C1-12	Microstrain vs Time for Gage SR2-Y for 30-ft Oblique Drop Test	187
C1-13	Microstrain vs Time for Gage SR2-YZ for 30-ft Oblique Drop Test	188
C1-14	Microstrain vs Time for Gage SR2-Z for 30-ft Oblique Drop Test	188
C1-15	Microstrain vs Time for Gage SR3-Y for 30-ft Oblique Drop Test	189
C1-16	Microstrain vs Time for Gage SR3-YZ for 30-ft Oblique Drop Test	189
C1-17	Microstrain vs Time for Gage SR3-Z for 30-ft Oblique Drop Test	190
C1-18	Microstrain vs Time for Gage SR4-Y for 30-ft Oblique Drop Test	190
C1-19	Microstrain vs Time for Gage SR4-YZ for 30-ft Oblique Drop Test	191
C1-20	Microstrain vs Time for Gage SR4-Z for 30-ft Oblique Drop Test	191
C1-21	Microstrain vs Time for Gage SR5-Y for 30-ft Oblique Drop Test	192
C1-22	Microstrain vs Time for Gage SR5-YZ for 30-ft Oblique Drop Test	192
C1-23	Microstrain vs Time for Gage SR5-Z for 30-ft Oblique Drop Test	193
C1-24	Acceleration vs Time for Gage AZ1 for 30-ft Oblique Drop Test, Including Primary and Secondary Impacts	193

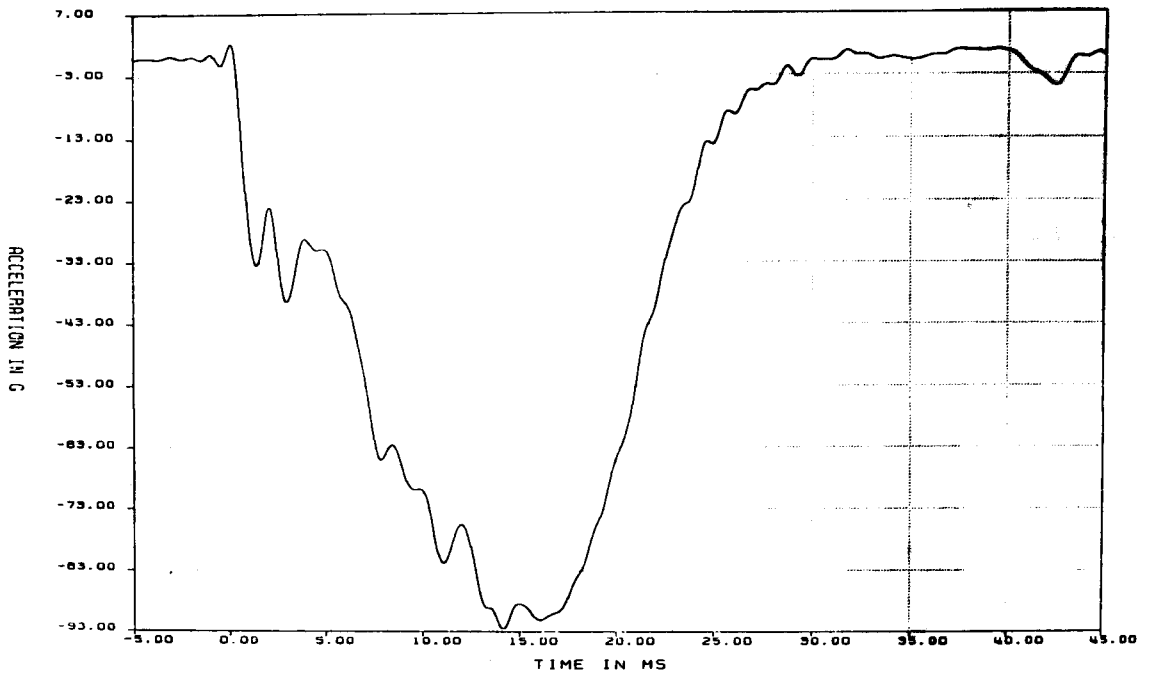


Figure C1-1. Acceleration vs Time for Gage AZ1 for 30-ft Oblique Drop Test (filtered at 1000 Hz)

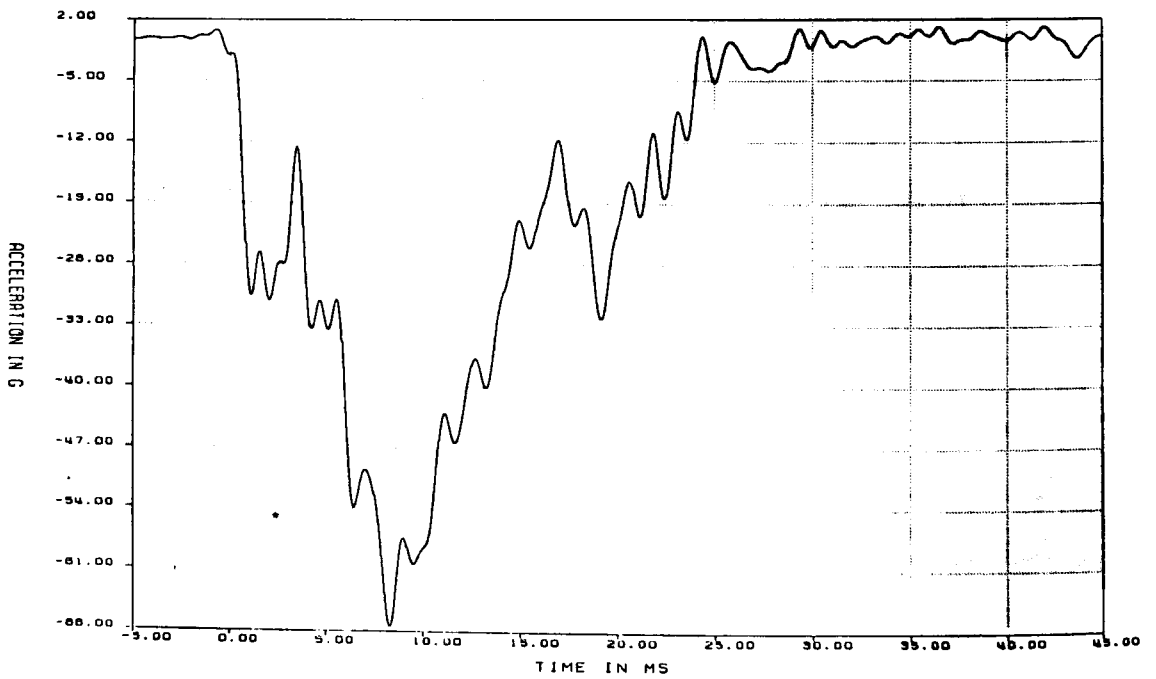


Figure C1-2. Acceleration vs Time for Gage AX2 for 30-ft Oblique Drop Test (filtered at 1000 Hz)

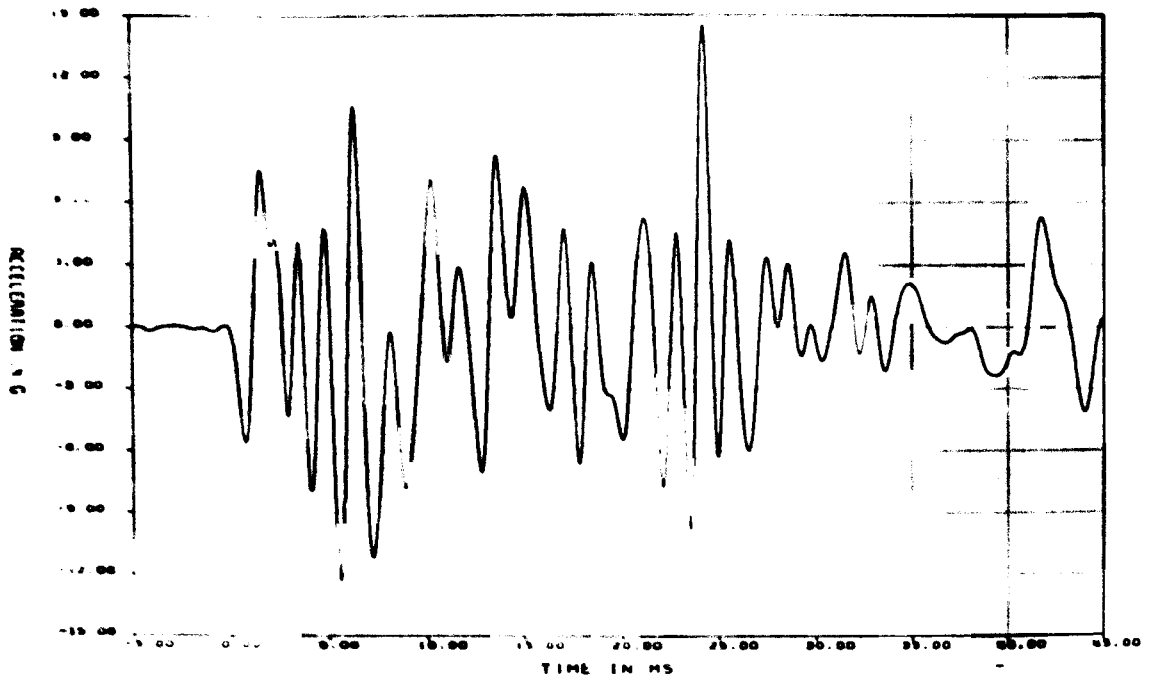


Figure C1-3. Acceleration vs Time for Gage AY3 for 30-ft Oblique Drop Test (filtered at 1000 Hz)

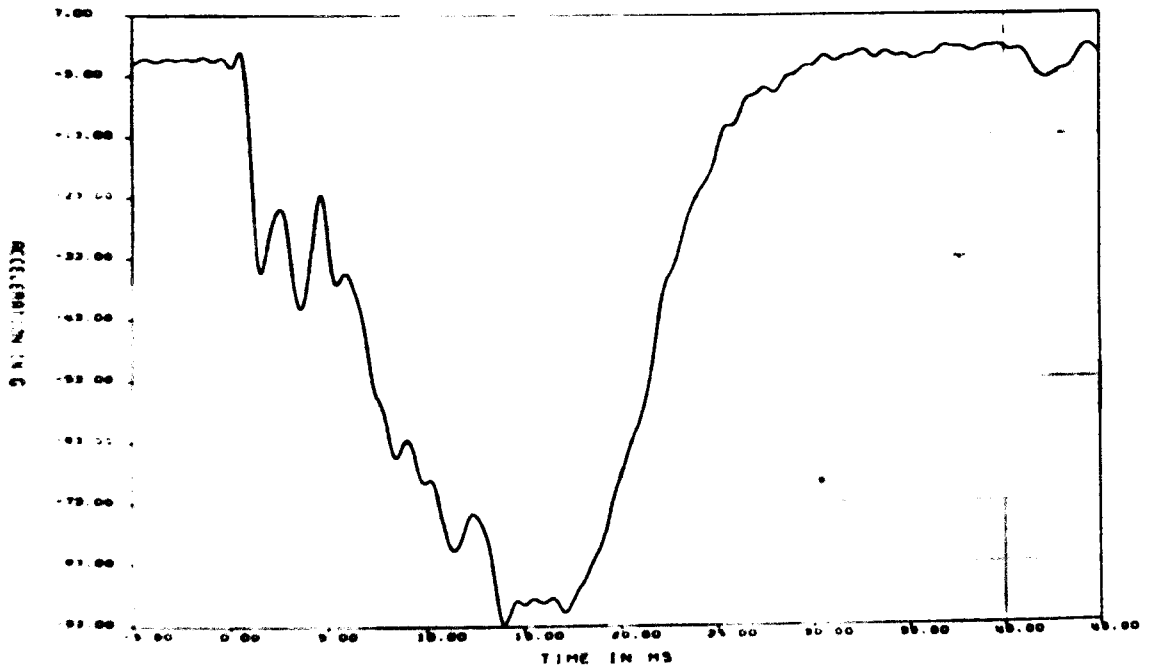


Figure C1-4. Acceleration vs Time for Gage AZ4 for 30-ft Oblique Drop Test (filtered at 1000 Hz)

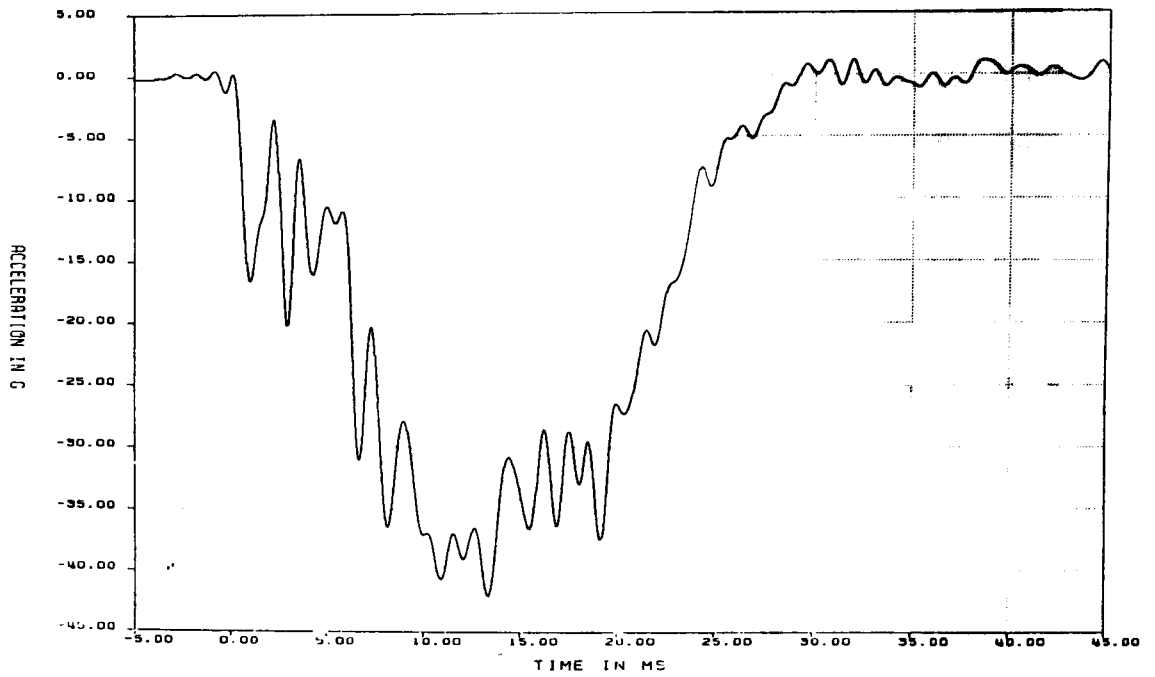


Figure C1-5. Acceleration vs Time for Gage AX5 for 30-ft Oblique Drop Test (filtered at 1000 Hz)

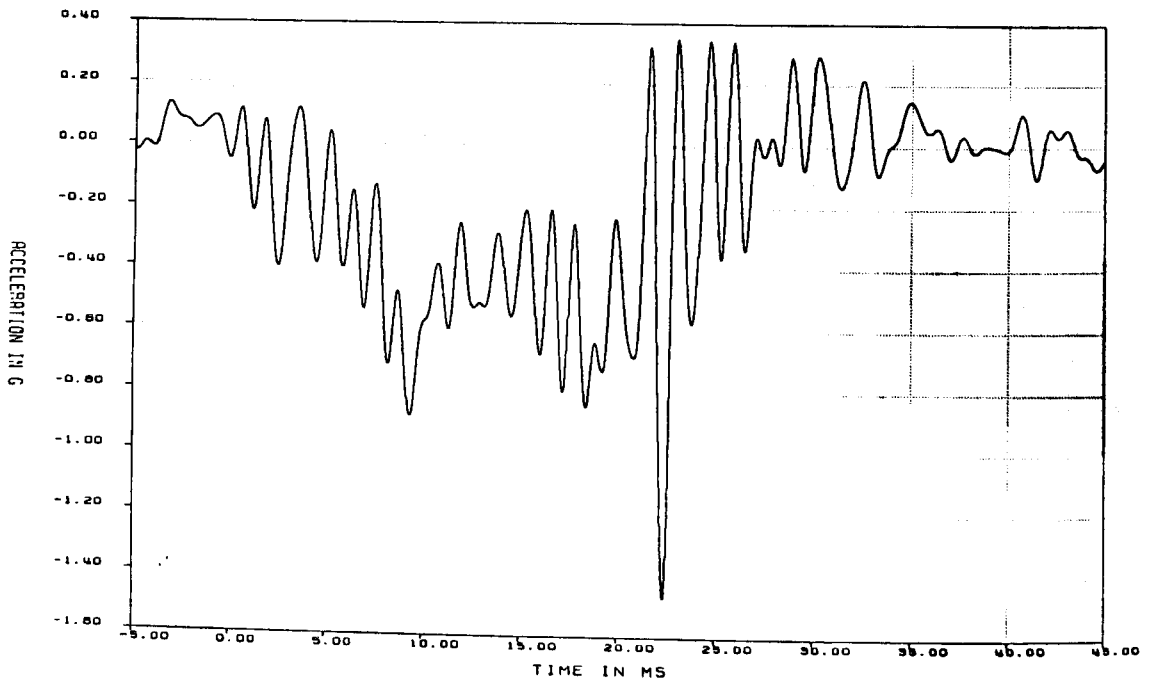


Figure C1-6. Acceleration vs Time for Gage AY6 for 30-ft Oblique Drop Test (filtered at 1000 Hz)

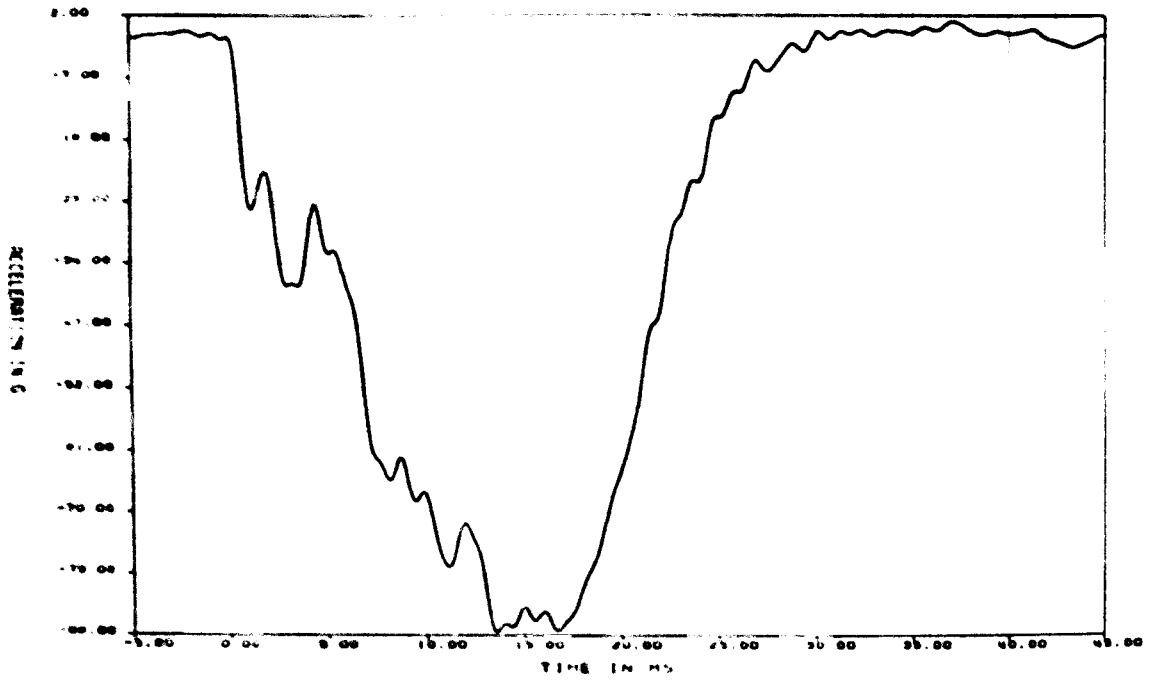


Figure C1-7. Acceleration vs Time for Gage AZ7 for 30-ft Oblique Drop Test (filtered at 1000 Hz)

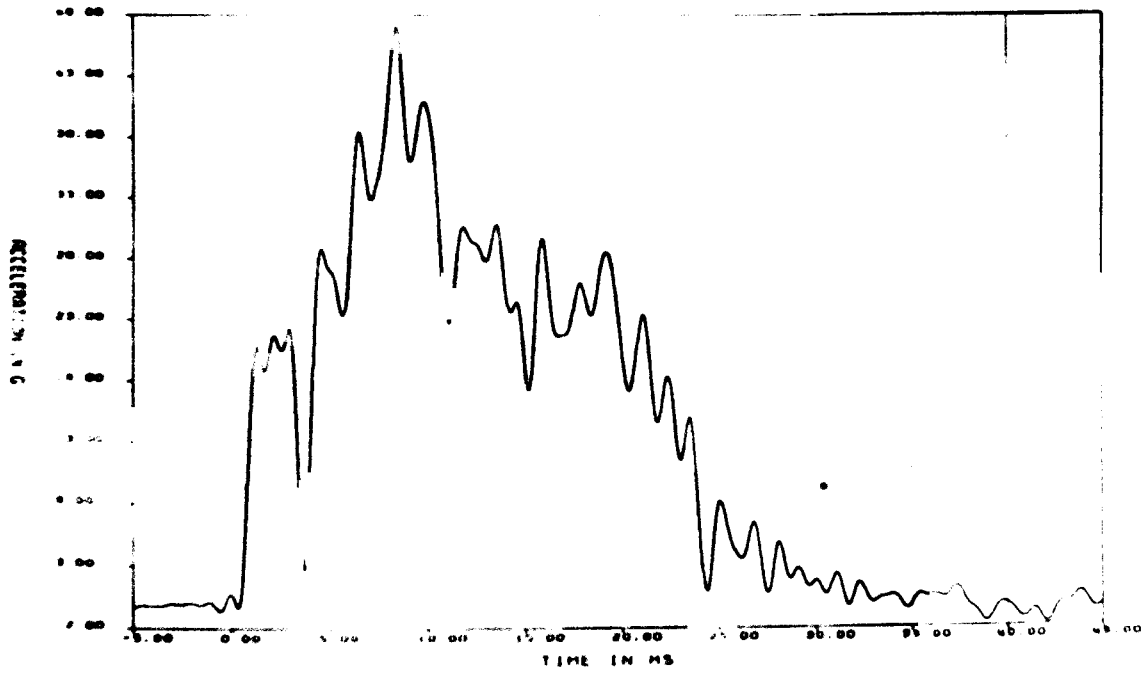


Figure C1-8. Acceleration vs Time for Gage AX8 for 30 ft Oblique Drop Test (filtered at 1000 Hz)

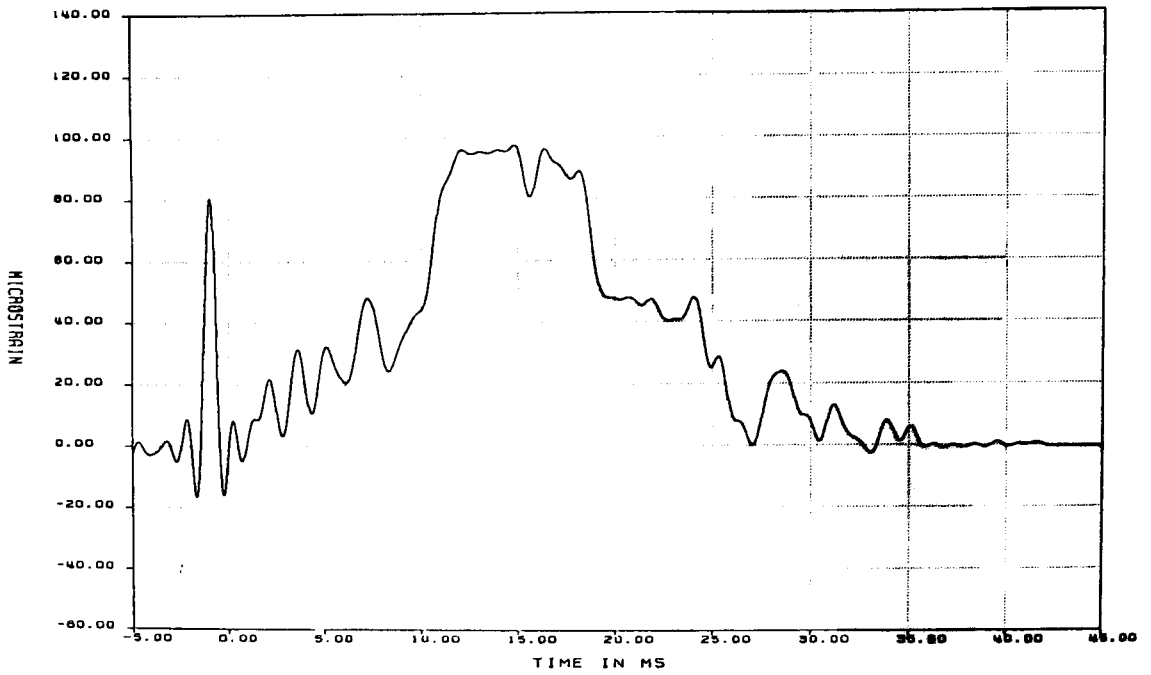


Figure C1-9. Microstrain vs Time for Gage SR1-Y for 30-ft Oblique Drop Test (filtered at 1000 Hz)

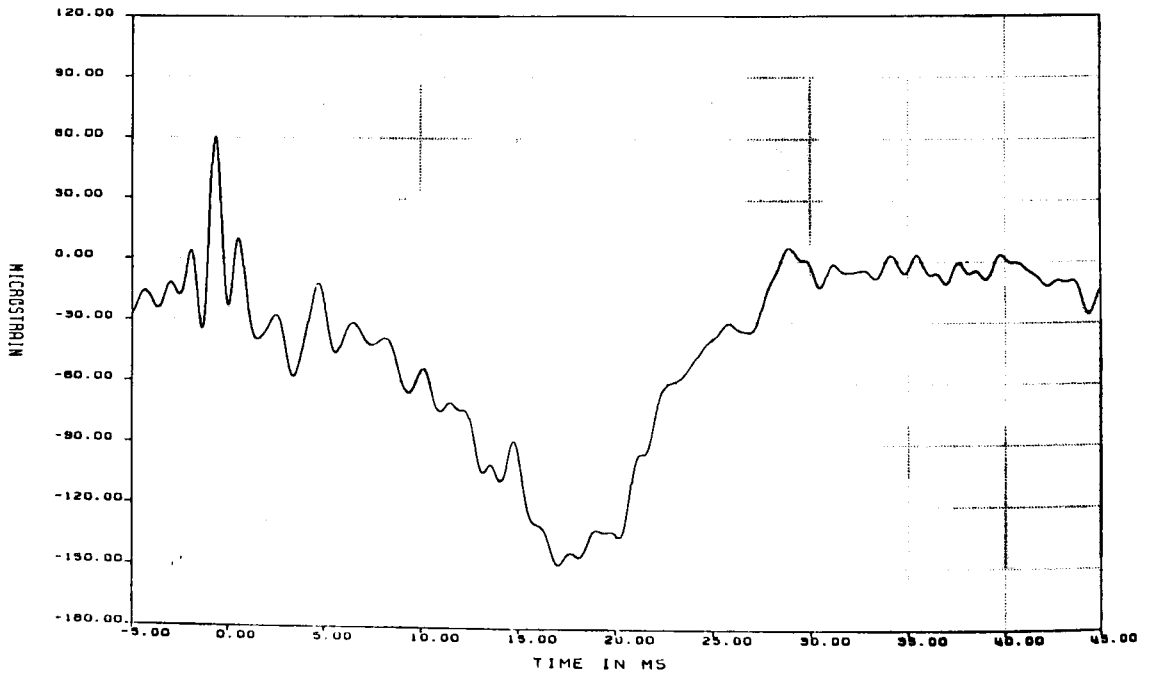


Figure C1-10. Microstrain vs Time for Gage SR1-YZ for 30-ft Oblique Drop Test (filtered at 1000 Hz)

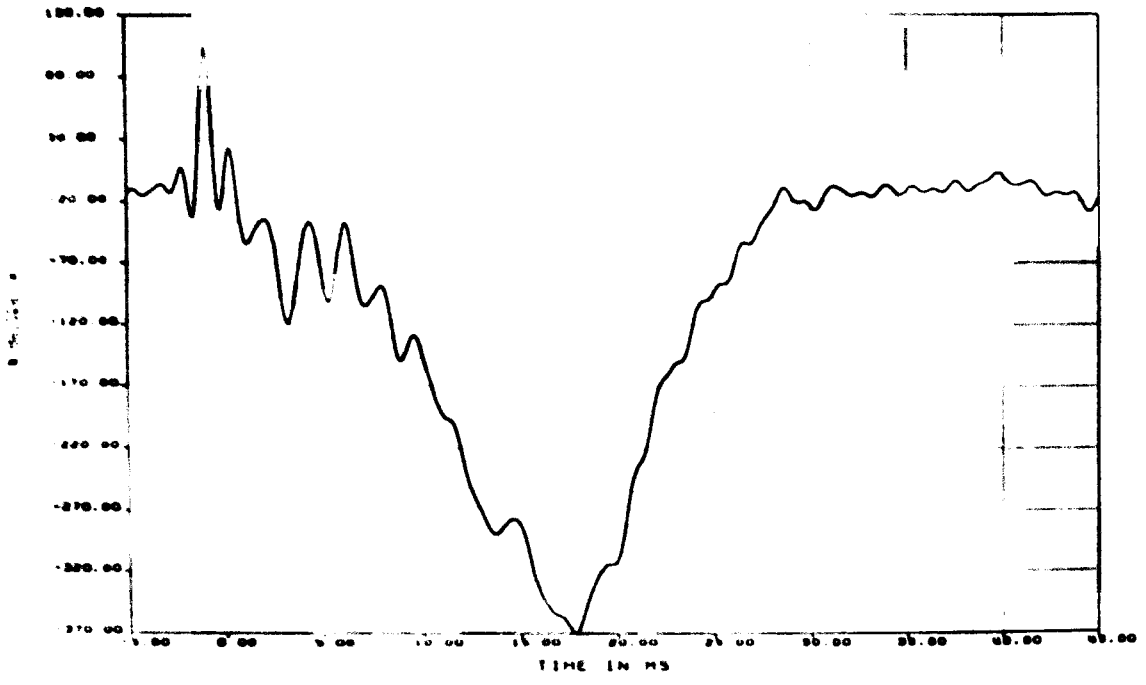


Figure C1-11. Microstrain vs Time for Gage SR1-Z for 30-ft Oblique Drop Test (filtered at 1000 Hz)

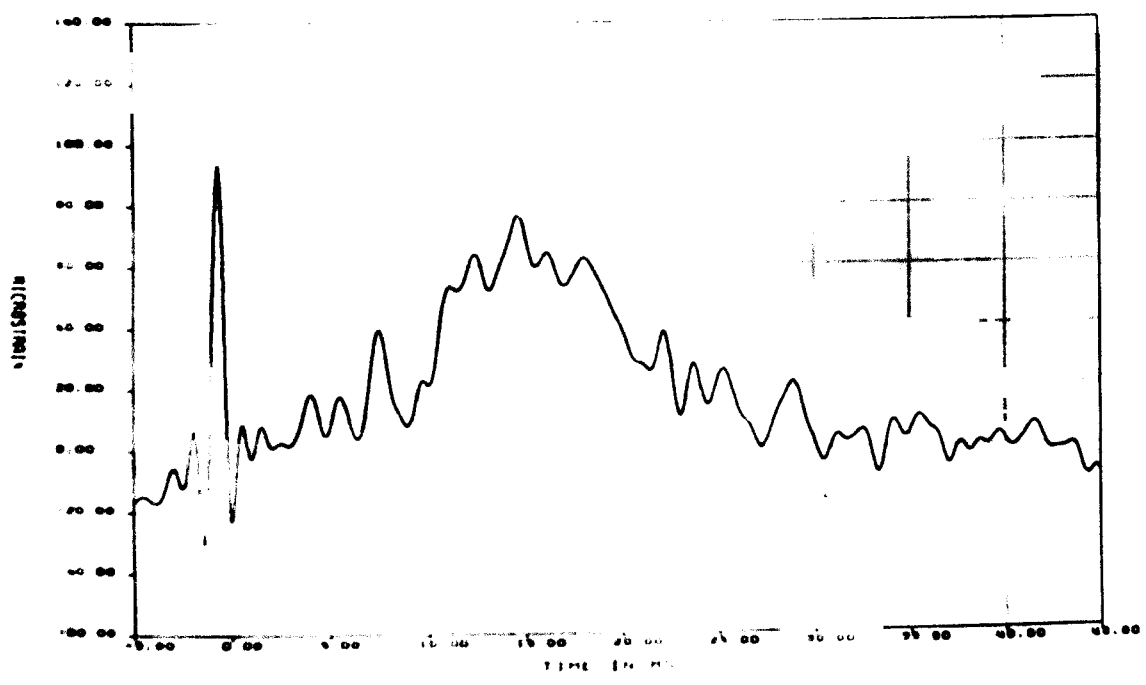


Figure C1-12. Microstrain vs Time for Gage SR2-Y for 30-ft Oblique Drop Test (filtered at 1000 Hz)

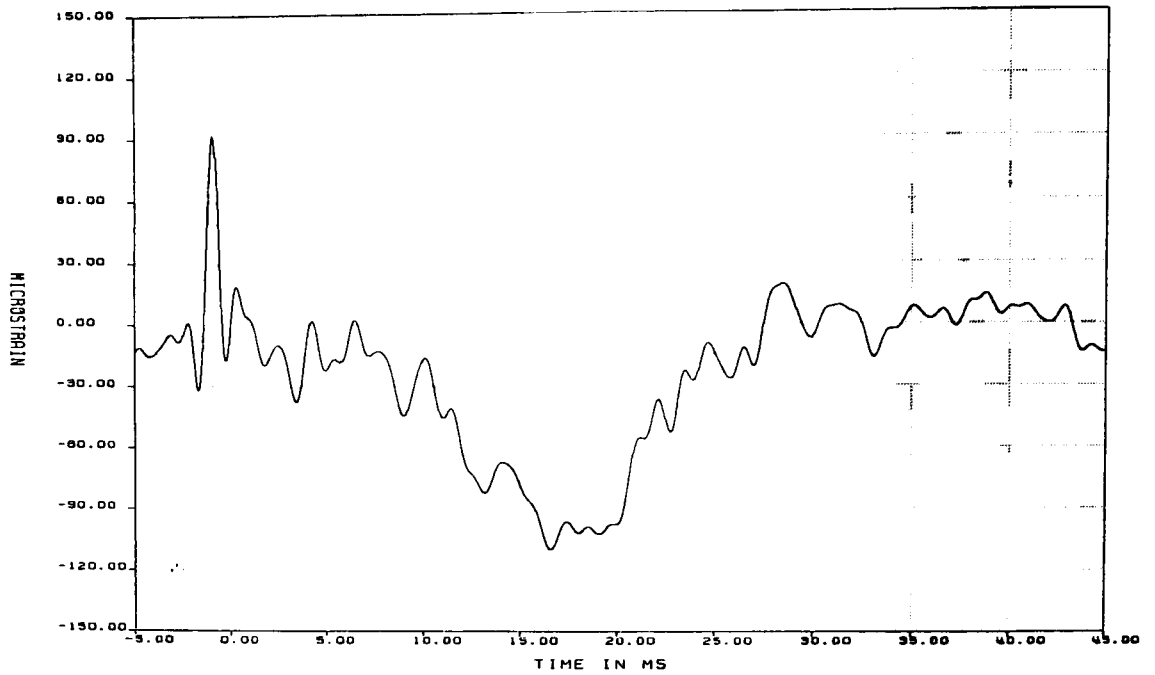


Figure C1-13. Microstrain vs Time for Gage SR2-YZ for 30-ft Oblique Drop Test (filtered at 1000 Hz)

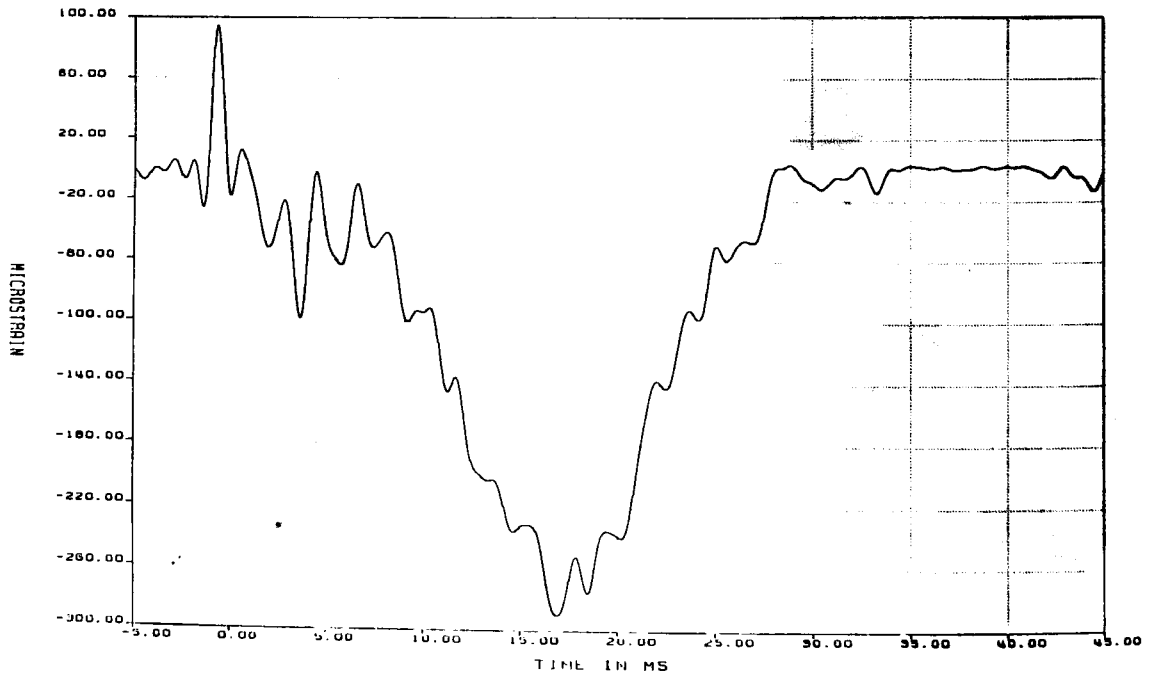


Figure C1-14. Microstrain vs Time for Gage SR2-Z for 30-ft Oblique Drop Test (filtered at 1000 Hz)

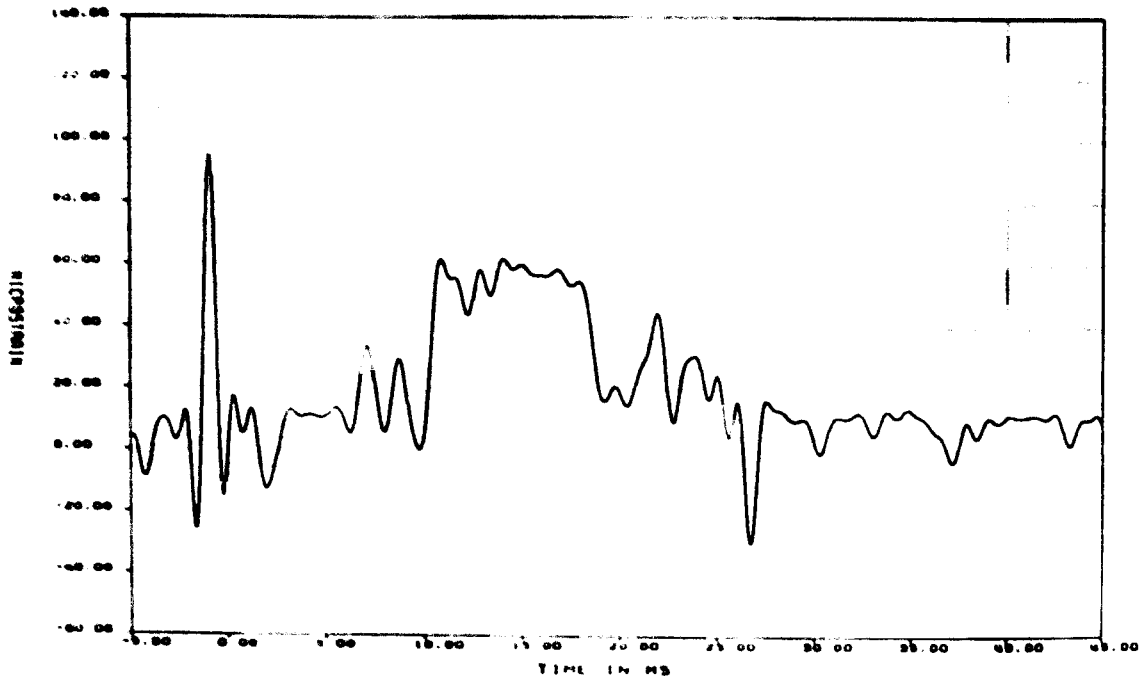


Figure C1-15. Microstrain vs Time for Gage SR3 Y for 30 ft Oblique Drop Test (filtered at 1000 Hz)

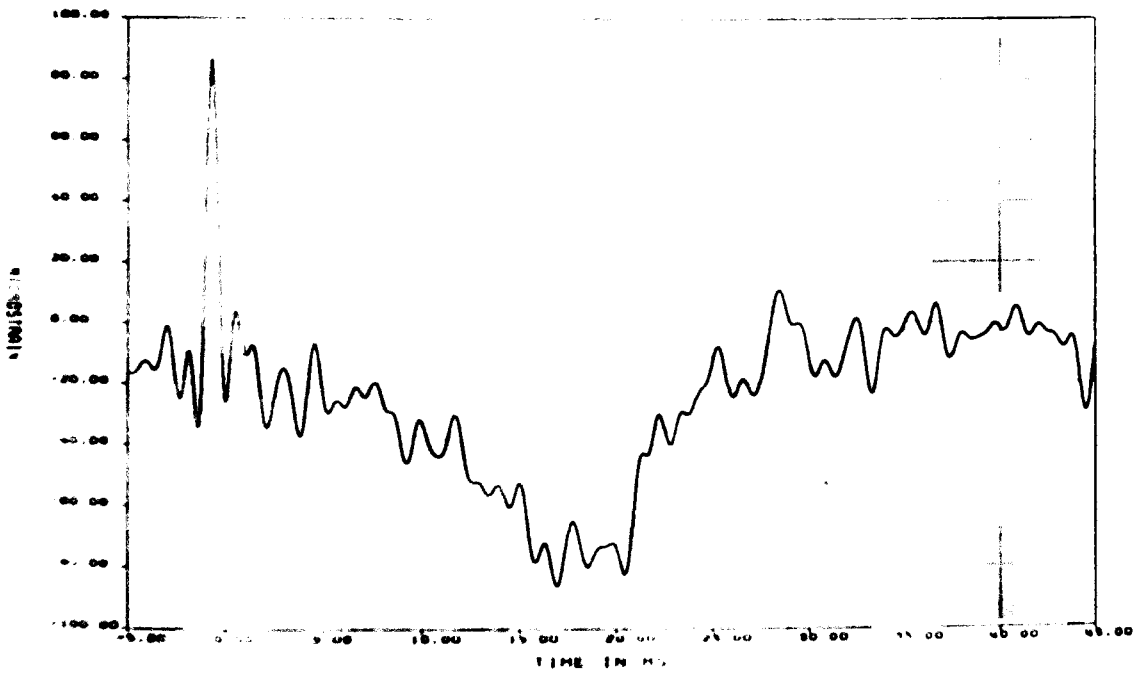


Figure C1-16. Microstrain vs Time for Gage SR3 YZ for 30 ft Oblique Drop Test (filtered at 1000 Hz)

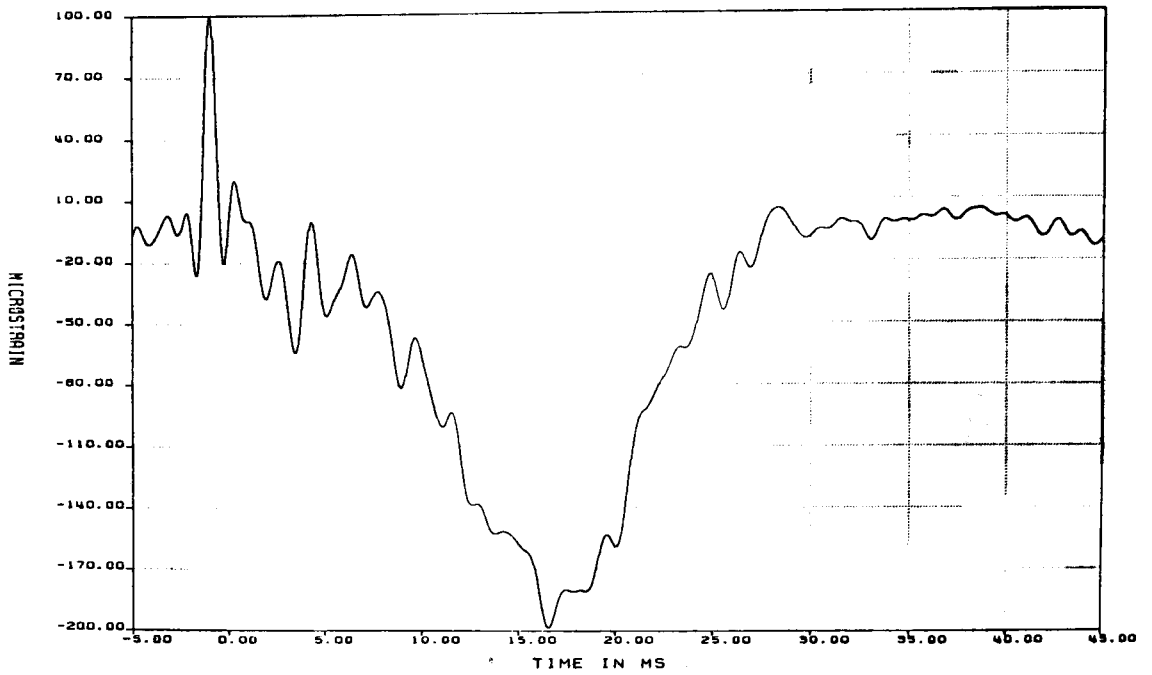


Figure C1-17. Microstrain vs Time for Gage SR3-Z for 30-ft Oblique Drop Test (filtered at 1000 Hz)

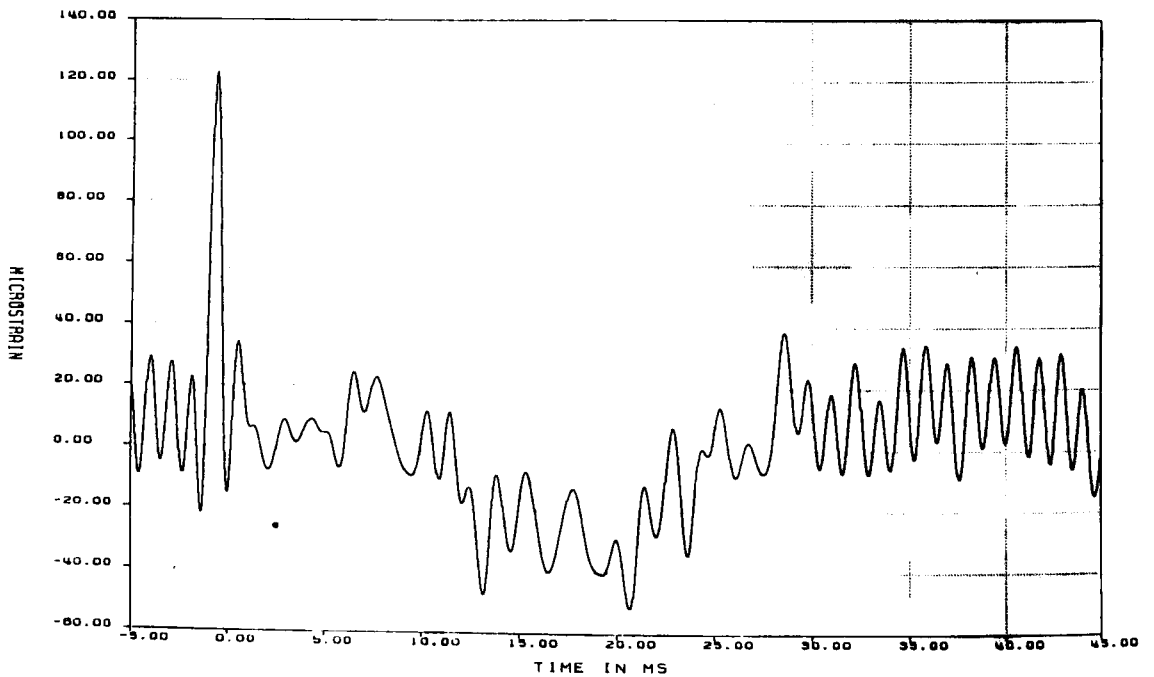


Figure C1-18. Microstrain vs Time for Gage SR4-Y for 30-ft Oblique Drop Test (filtered at 1000 Hz)

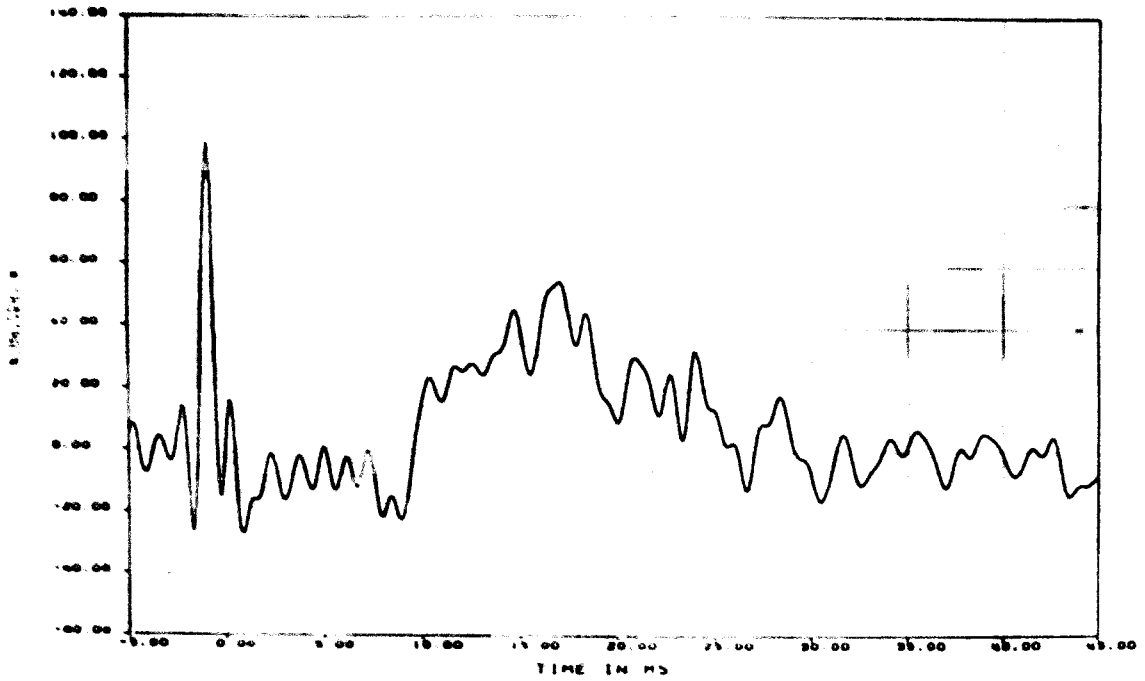


Figure C1-19. Microstrain vs Time for Gage SR4-YZ for 30-ft Oblique Drop Test (filtered at 1000 Hz)

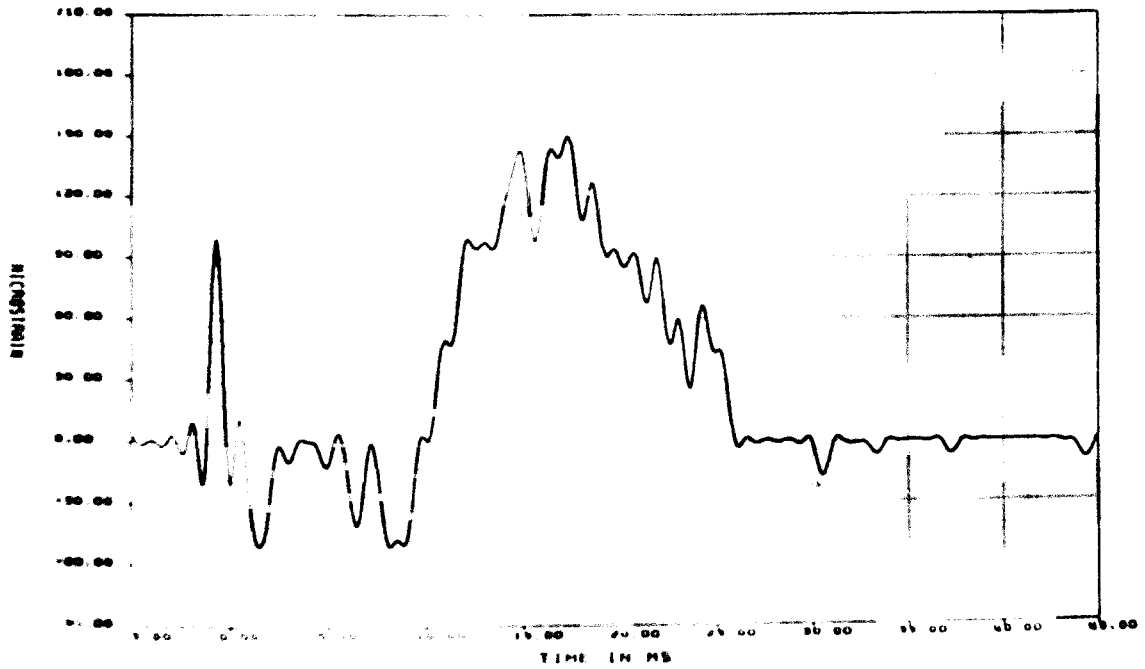


Figure C1-20. Microstrain vs Time for Gage SR4-Z for 30-ft Oblique Drop Test (filtered at 1000 Hz)

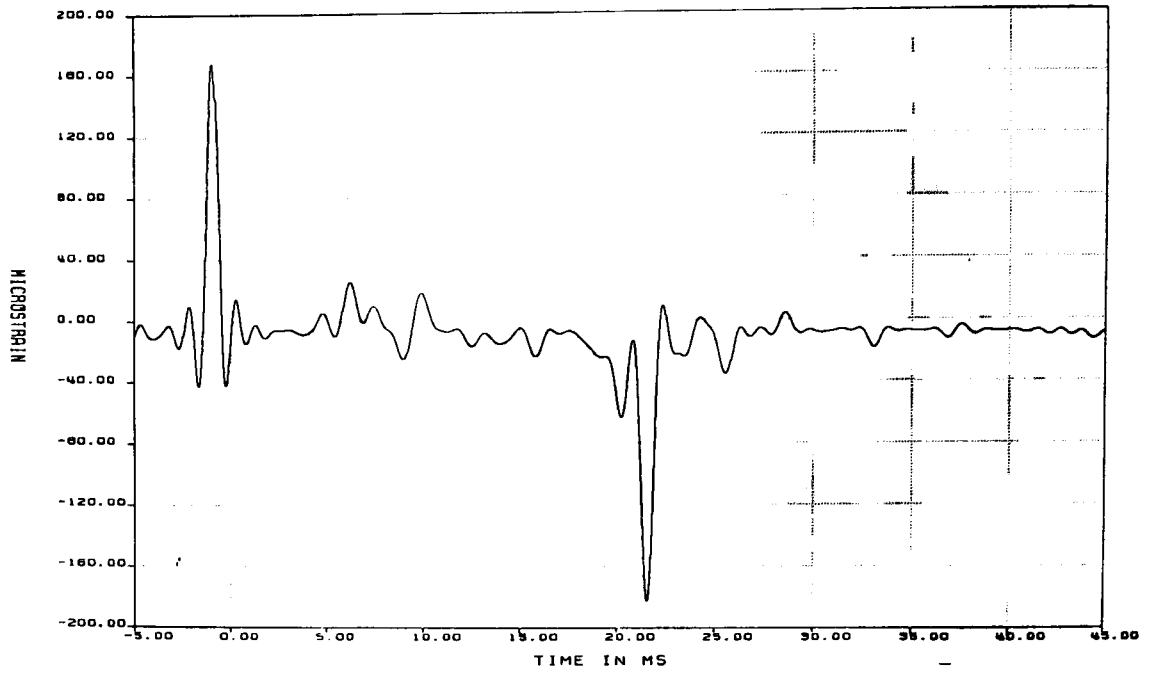


Figure C1-21. Microstrain vs Time for Gage SR5-Y for 30-ft Oblique Drop Test (filtered at 1000 Hz)

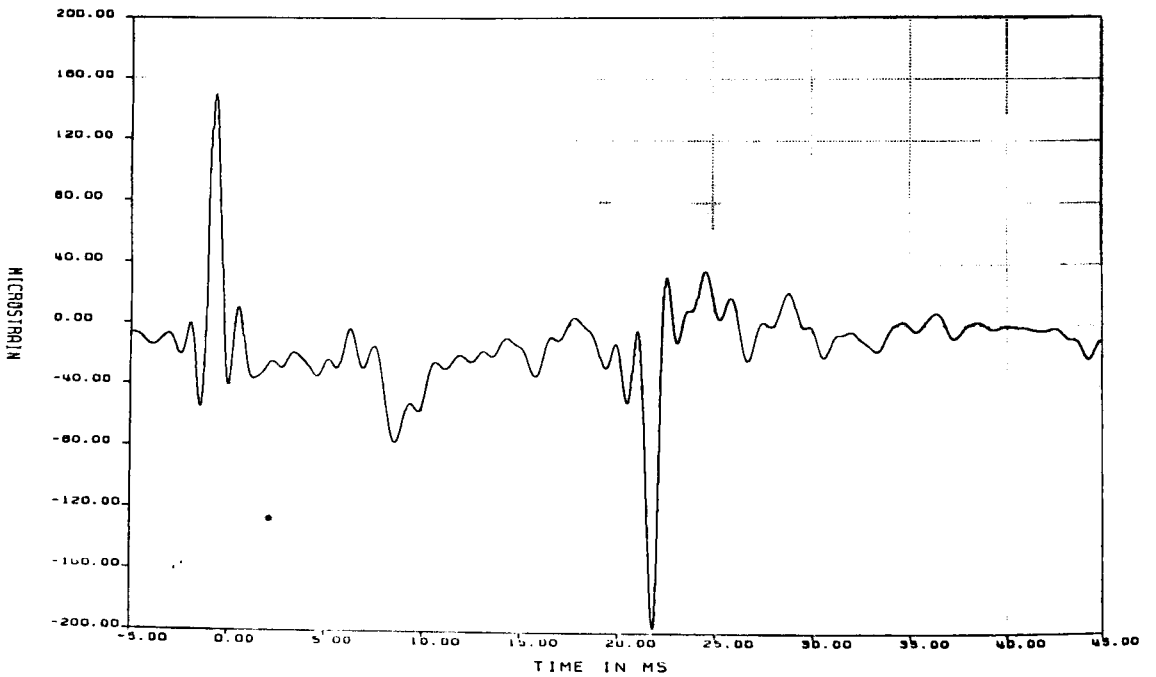


Figure C1-22. Microstrain vs Time for Gage SR5-YZ for 30-ft Oblique Drop Test (filtered at 1000 Hz)

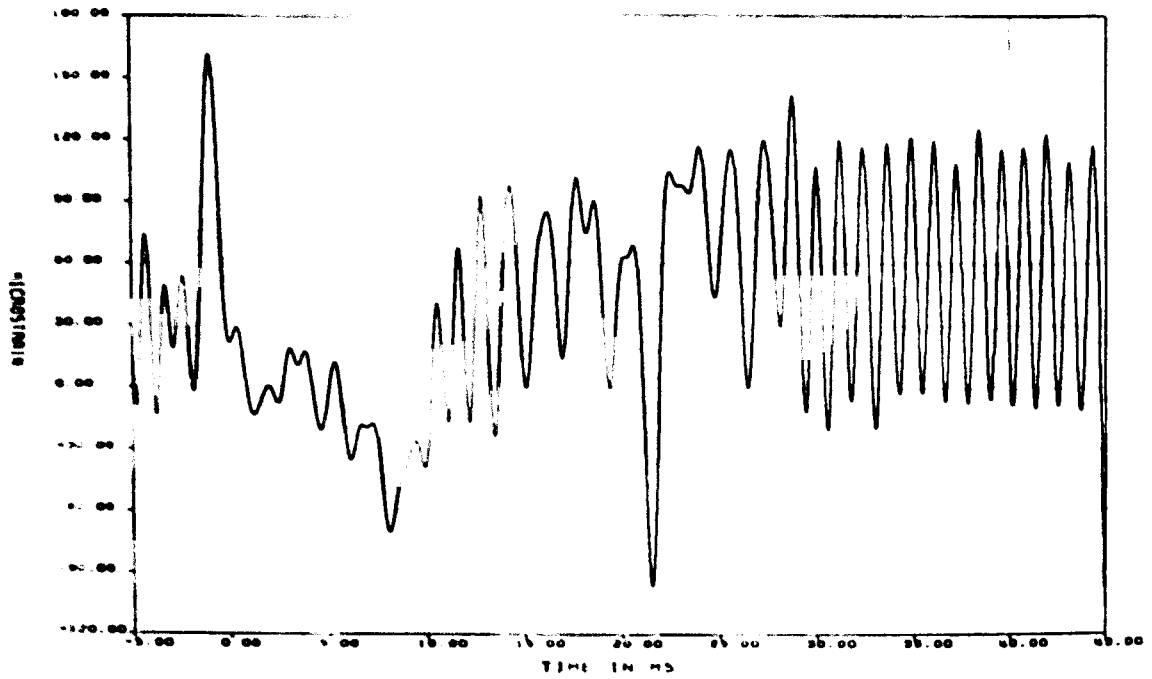


Figure C1-23. Microstrain vs Time for Gage SR5 Z for 30-ft Oblique Drop Test (filtered at 1000 Hz)

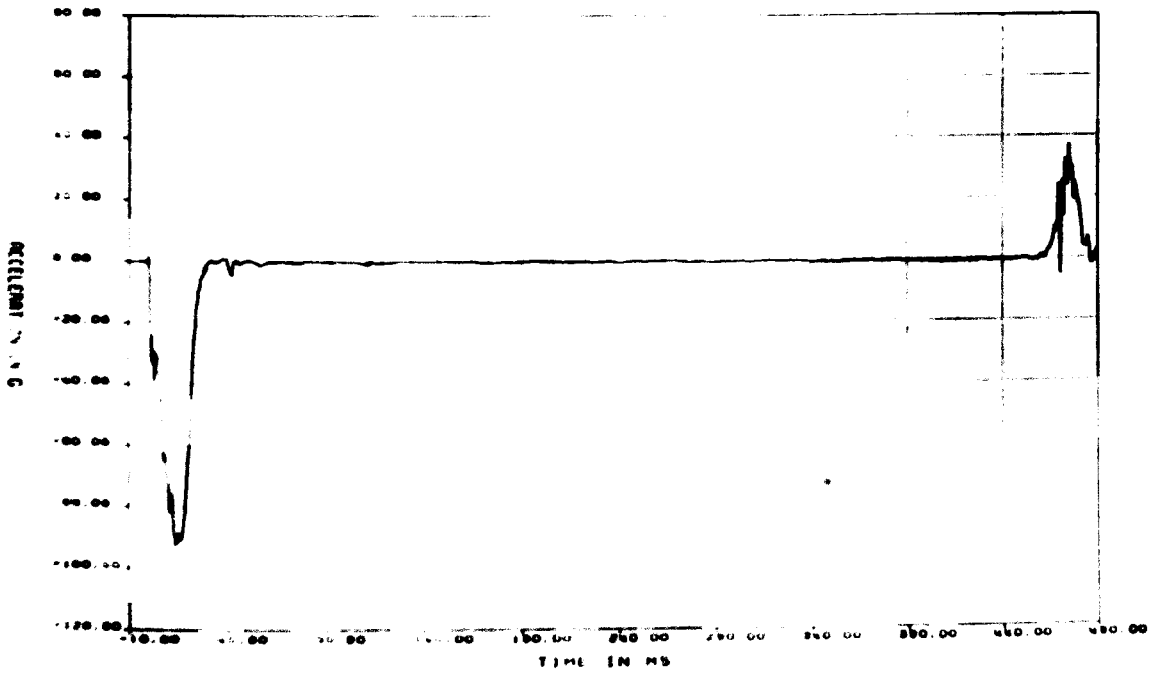


Figure C1-24. Acceleration vs Time for Gage AZ1 for 30-ft Oblique Drop Test, Including Primary and Secondary Impacts

APPENDIX C2

Fast Fourier Transforms of Raw Accelerometer Data for the 30-ft Oblique Drop Test

Figures

C2-1	Fast Fourier Transform of Raw Data From Gage AZ1 for 30-ft Oblique Drop Test: 0-50 kHz.....	196
C2-2	Fast Fourier Transform of Raw Data From Gage AZ1 for 30-ft Oblique Drop Test: 0-10 kHz.....	196
C2-3	Fast Fourier Transform of Raw Data From Gage AX2 for 30-ft Oblique Drop Test: 0-50 kHz.....	197
C2-4	Fast Fourier Transform of Raw Data From Gage AX2 for 30-ft Oblique Drop Test: 0-10 kHz.....	197
C2-5	Fast Fourier Transform of Raw Data From Gage AY3 for 30-ft Oblique Drop Test: 0-50 kHz.....	198
C2-6	Fast Fourier Transform of Raw Data From Gage AY3 for 30-ft Oblique Drop Test: 0-10 kHz.....	198
C2-7	Fast Fourier Transform of Raw Data From Gage AZ4 for 30-ft Oblique Drop Test: 0-50 kHz.....	199
C2-8	Fast Fourier Transform of Raw Data From Gage AZ4 for 30-ft Oblique Drop Test: 0-10 kHz.....	199
C2-9	Fast Fourier Transform of Raw Data From Gage AX5 for 30-ft Oblique Drop Test: 0-50 kHz.....	200
C2-10	Fast Fourier Transform of Raw Data From Gage AX5 for 30-ft Oblique Drop Test: 0-10 kHz.....	200
C2-11	Fast Fourier Transform of Raw Data From Gage AY6 for 30-ft Oblique Drop Test: 0-50 kHz.....	201
C2-12	Fast Fourier Transform of Raw Data From Gage AY6 for 30-ft Oblique Drop Test: 0-10 kHz.....	201
C2-13	Fast Fourier Transform of Raw Data From Gage AZ7 for 30-ft Oblique Drop Test: 0-50 kHz.....	202
C2-14	Fast Fourier Transform of Raw Data From Gage AZ7 for 30-ft Oblique Drop Test: 0-10 kHz.....	202
C2-15	Fast Fourier Transform of Raw Data From Gage AX8 for 30-ft Oblique Drop Test: 0-50 kHz.....	203
C2-16	Fast Fourier Transform of Raw Data From Gage AX8 for 30-ft Oblique Drop Test: 0-10 kHz.....	203

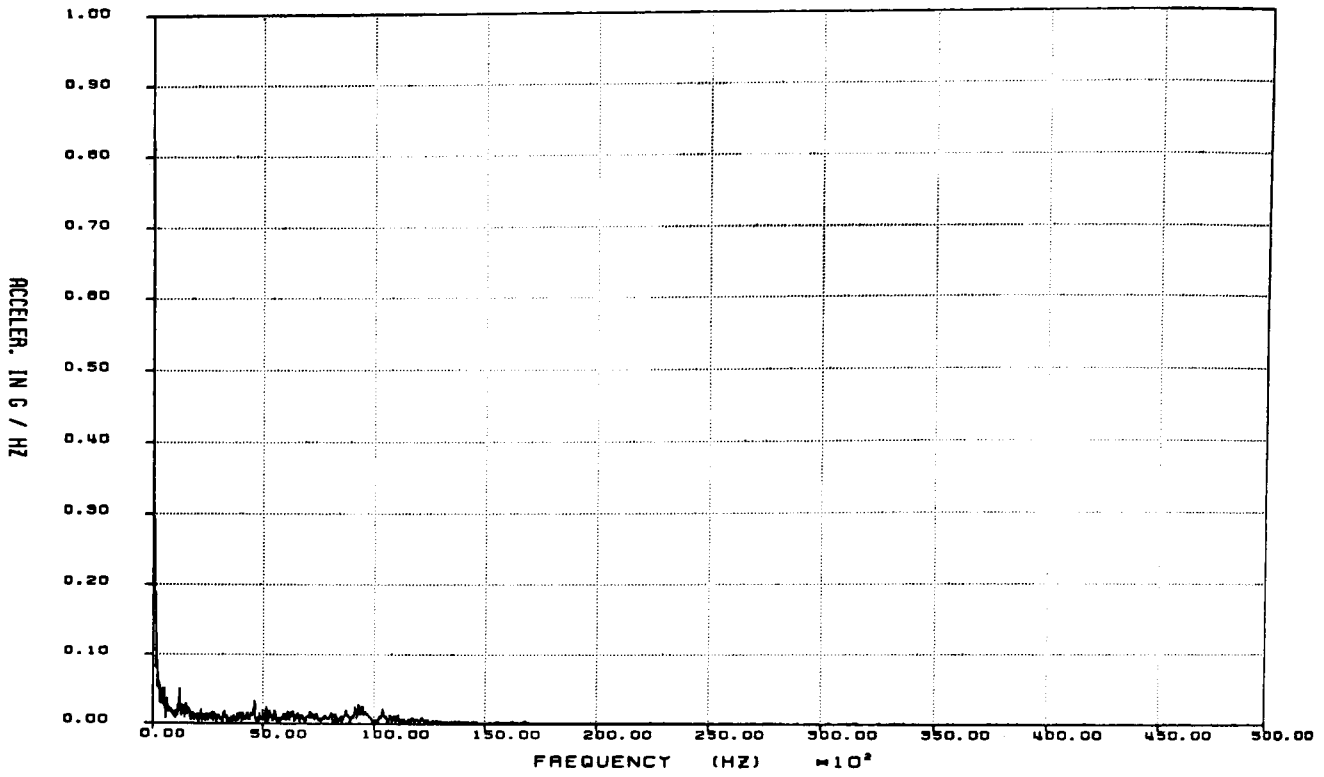


Figure C2-1. Fast Fourier Transform of Raw Data From Gage AZ1 for 30-ft Oblique Drop Test: 0-50 kHz

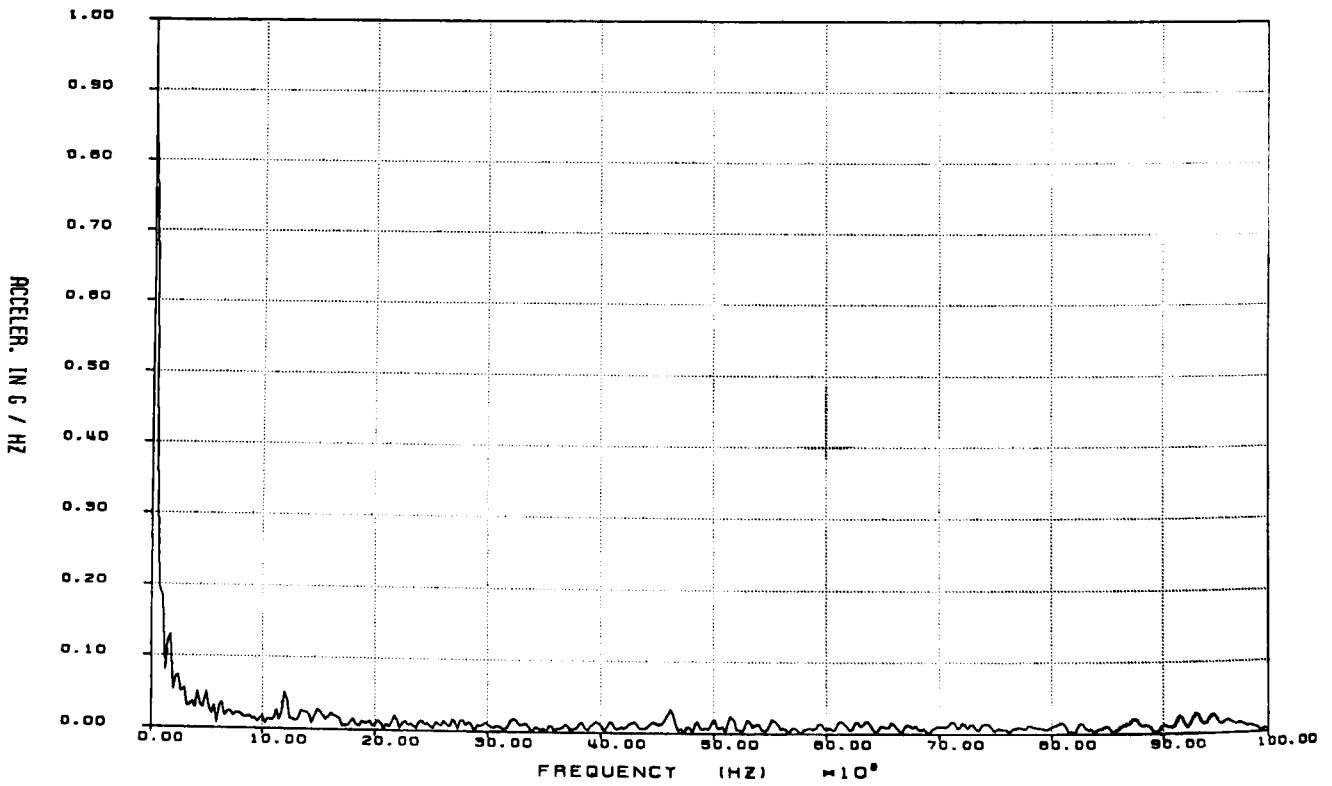


Figure C2-2. Fast Fourier Transform of Raw Data From Gage AZ1 for 30-ft Oblique Drop Test: 0-10 kHz

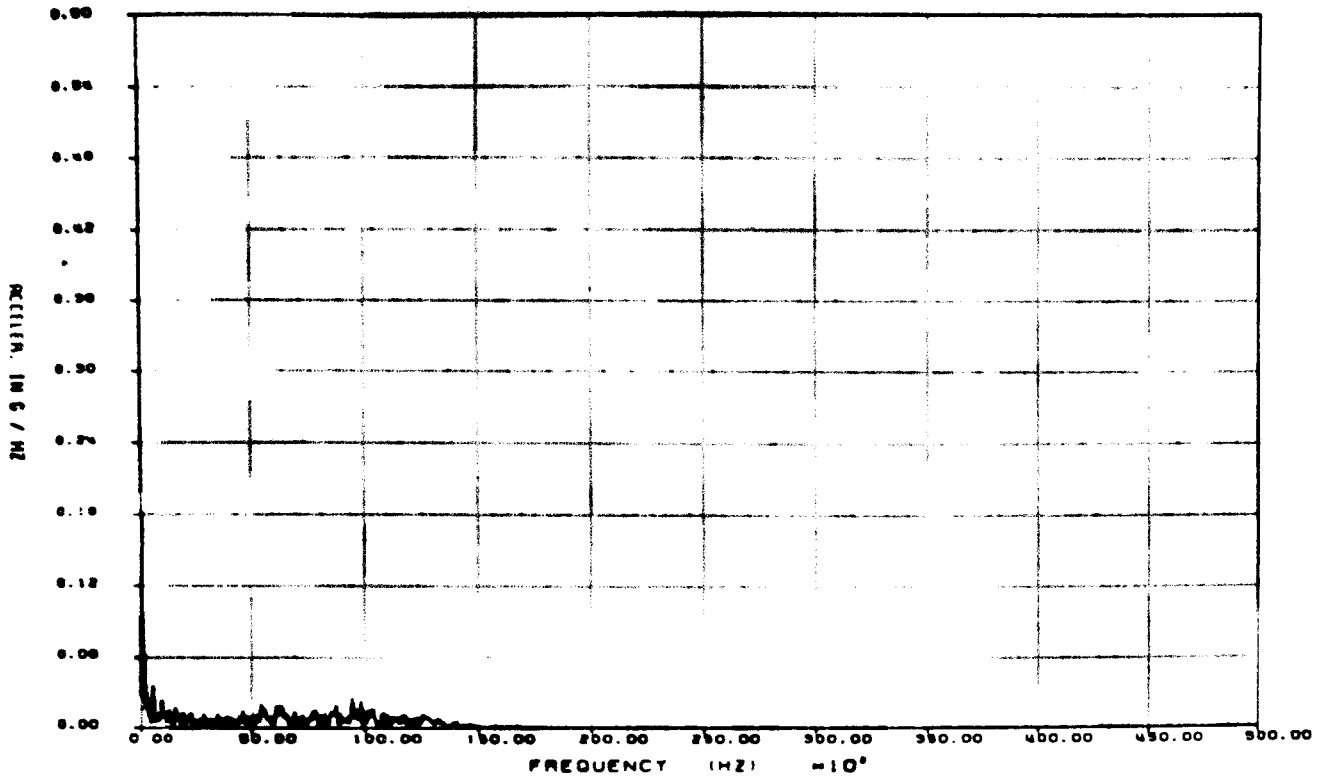


Figure C2-3. Fast Fourier Transform of Raw Data From Gage AX2 for 30-ft Oblique Drop Test: 0-50 kHz

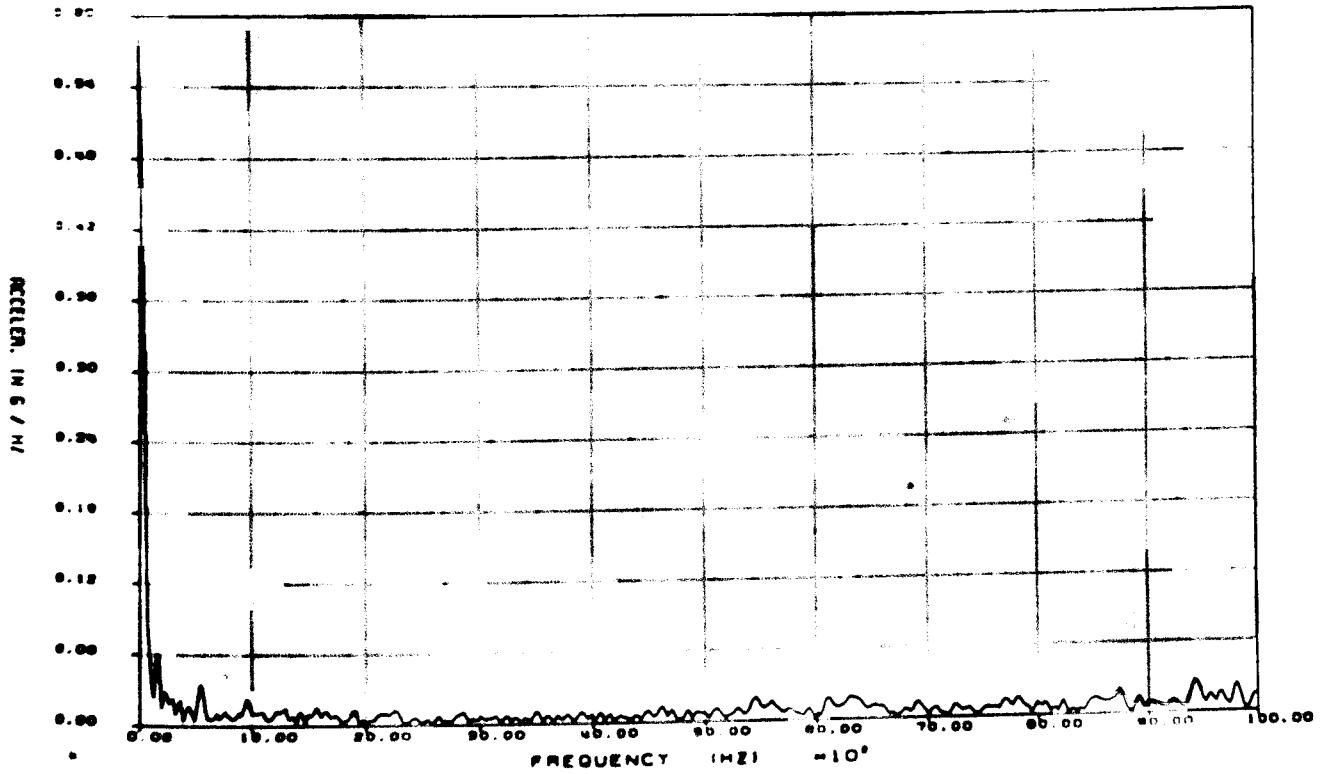


Figure C2-4. Fast Fourier Transform of Raw Data From Gage AX2 for 30-ft Oblique Drop Test: 0-10 kHz

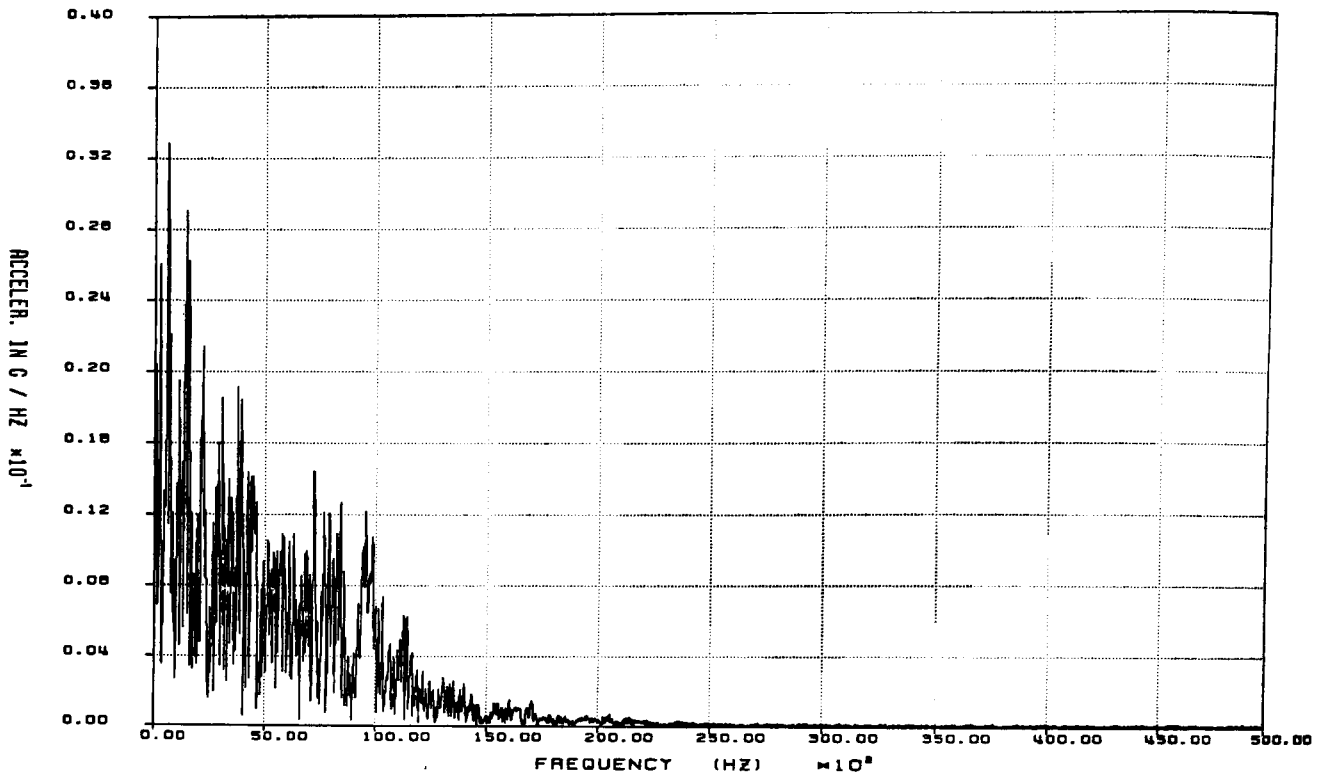


Figure C2-5. Fast Fourier Transform of Raw Data From Gage AY3 for 30-ft Oblique Drop Test: 0-50 kHz

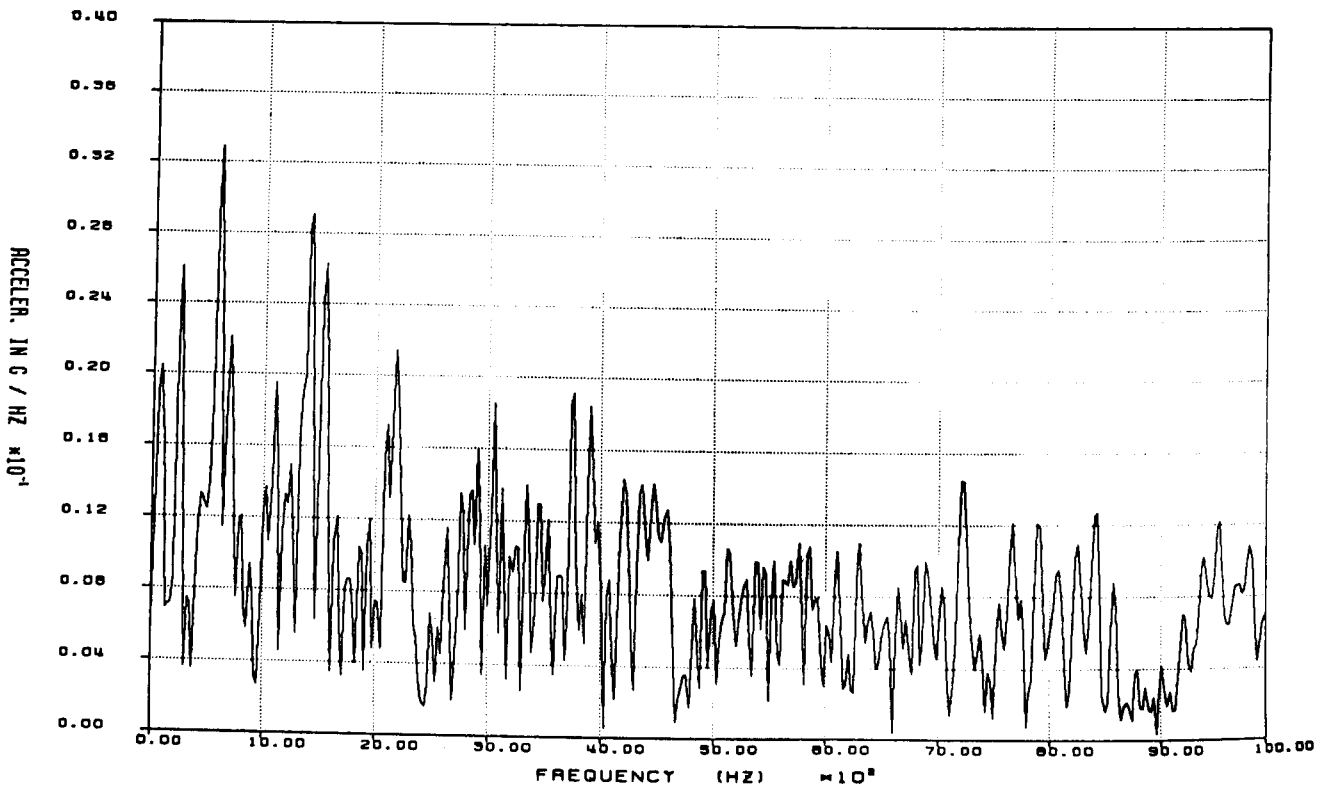


Figure C2-6. Fast Fourier Transform of Raw Data From Gage AY3 for 30-ft Oblique Drop Test: 0-10 kHz

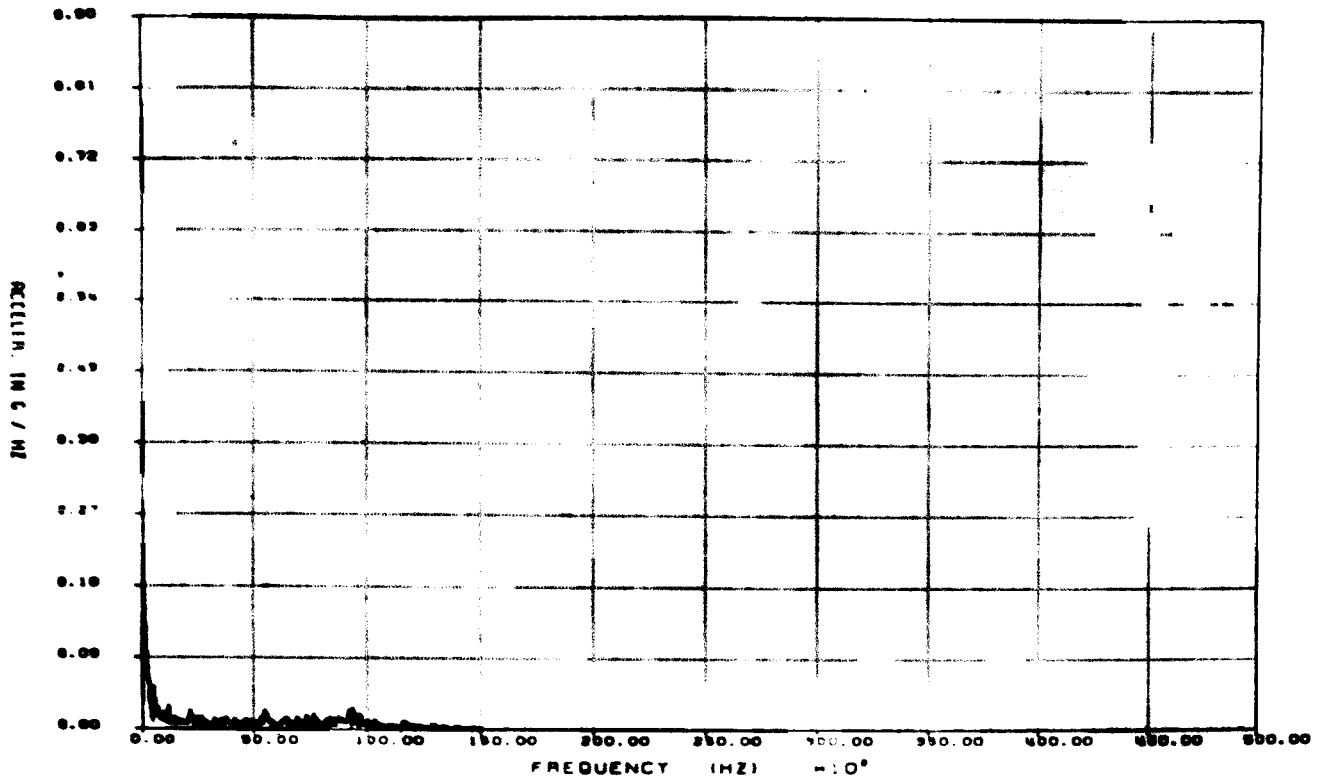


Figure C2-7. Fast Fourier Transform of Raw Data From Gage AZ4 for 30-ft Oblique Drop Test: 0-50 kHz

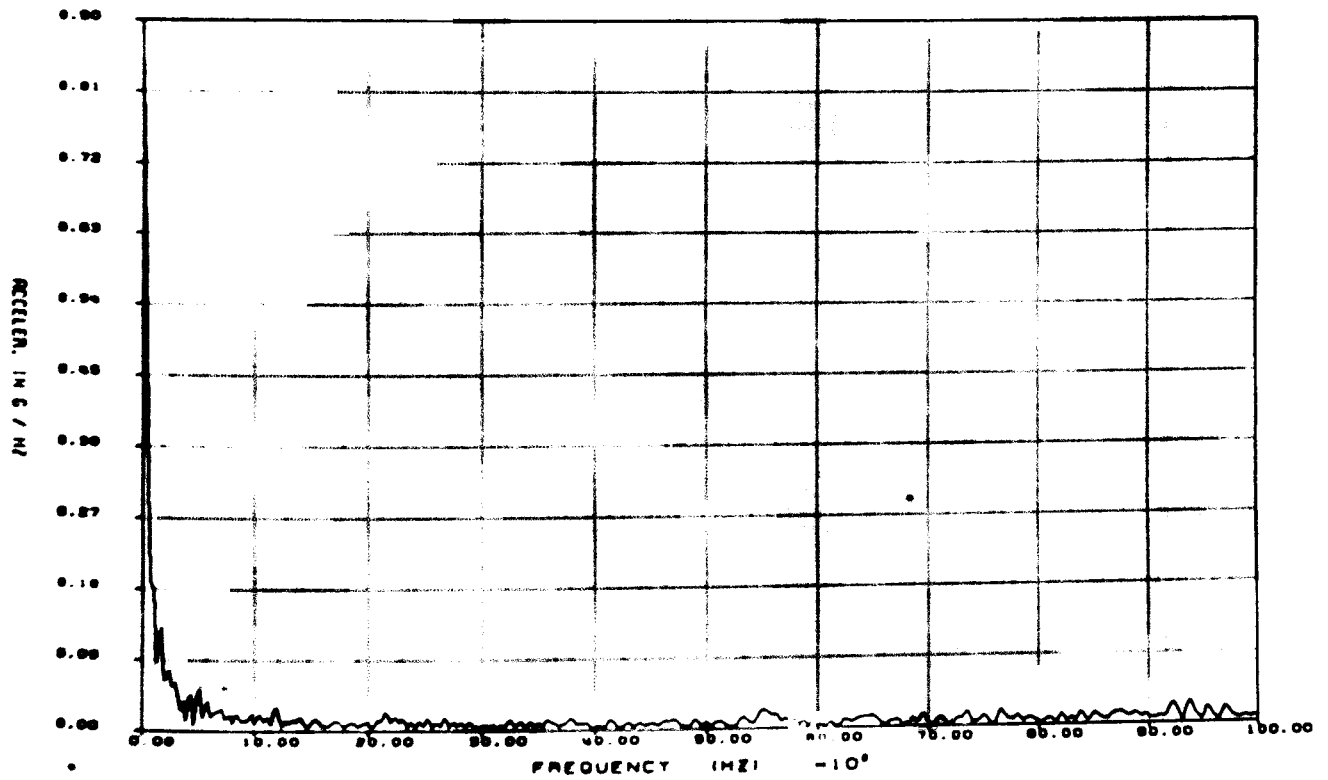


Figure C2-8. Fast Fourier Transform of Raw Data From Gage AZ4 for 30-ft Oblique Drop Test: 0-10 kHz

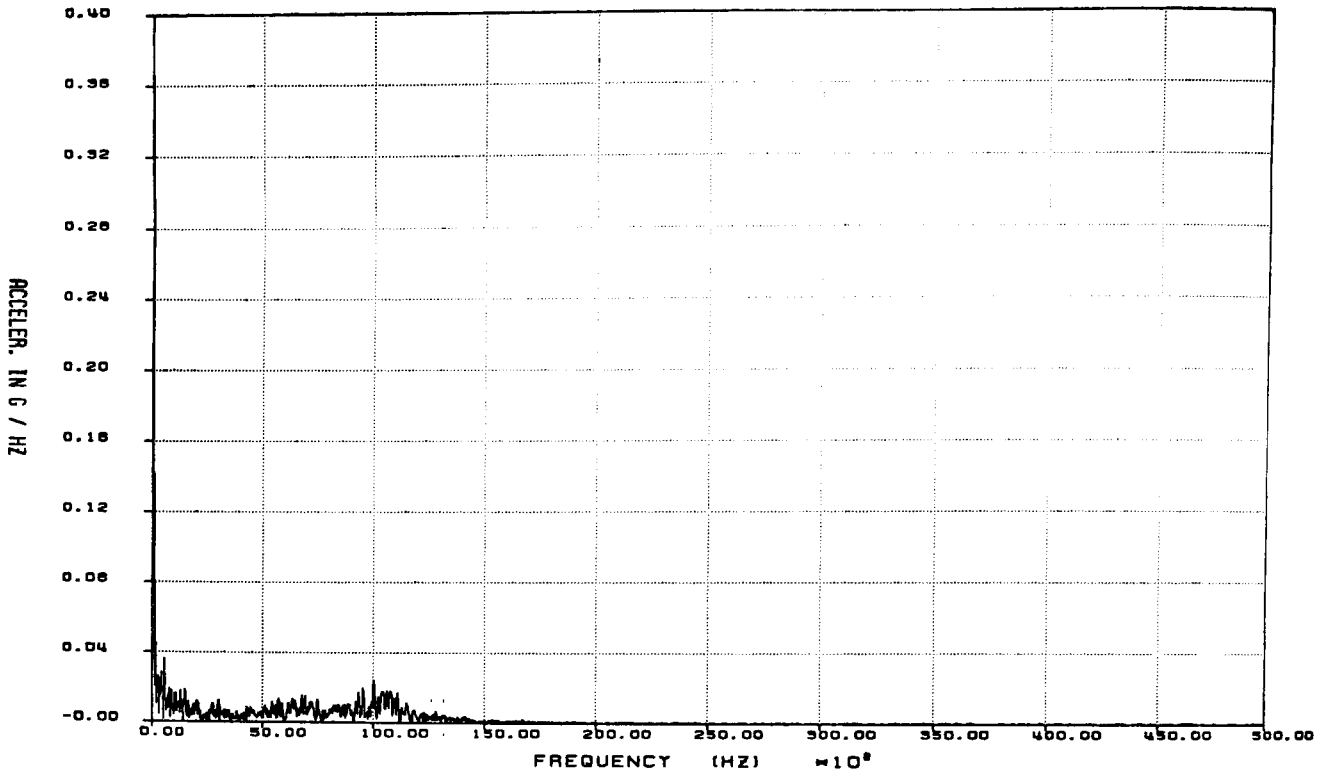


Figure C2-9. Fast Fourier Transform of Raw Data From Gage AX5 for 30-ft Oblique Drop Test: 0-50 kHz

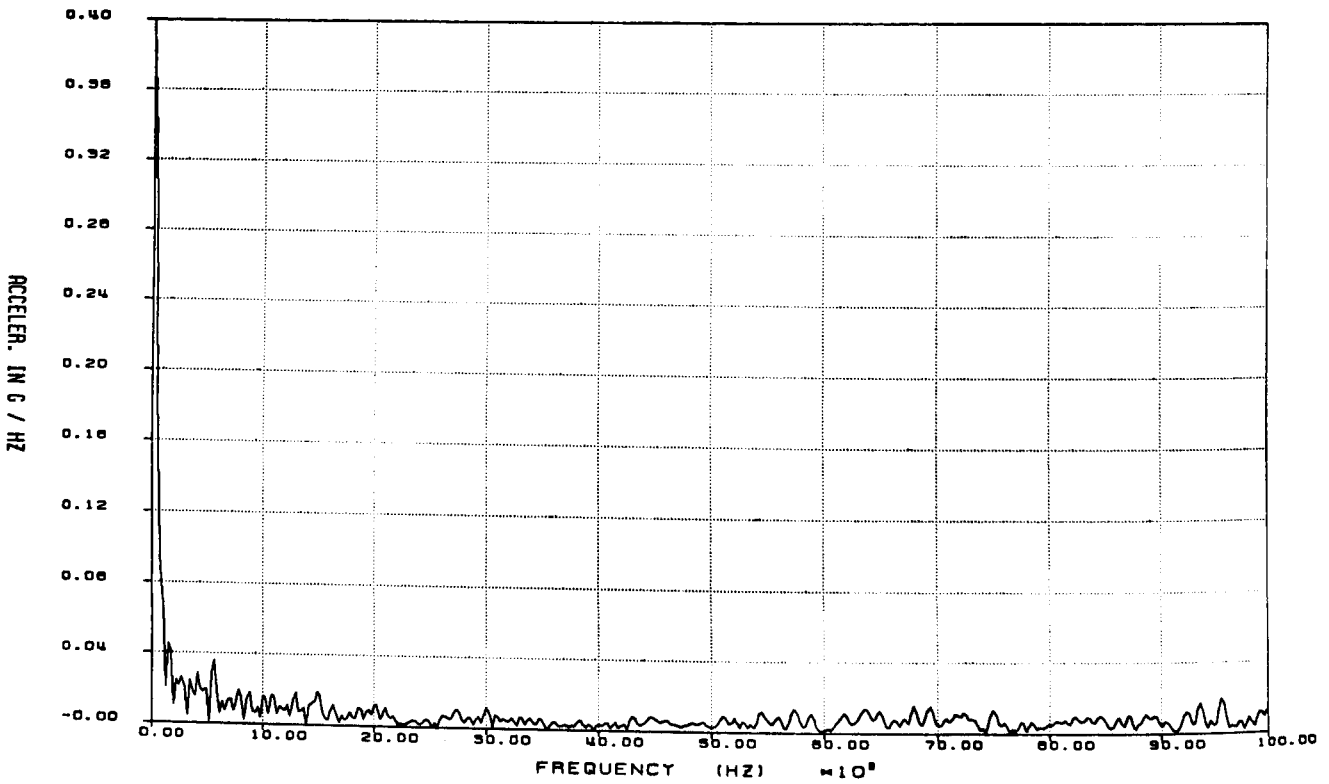


Figure C2-10. Fast Fourier Transform of Raw Data From Gage AX5 for 30-ft Oblique Drop Test: 0-10 kHz

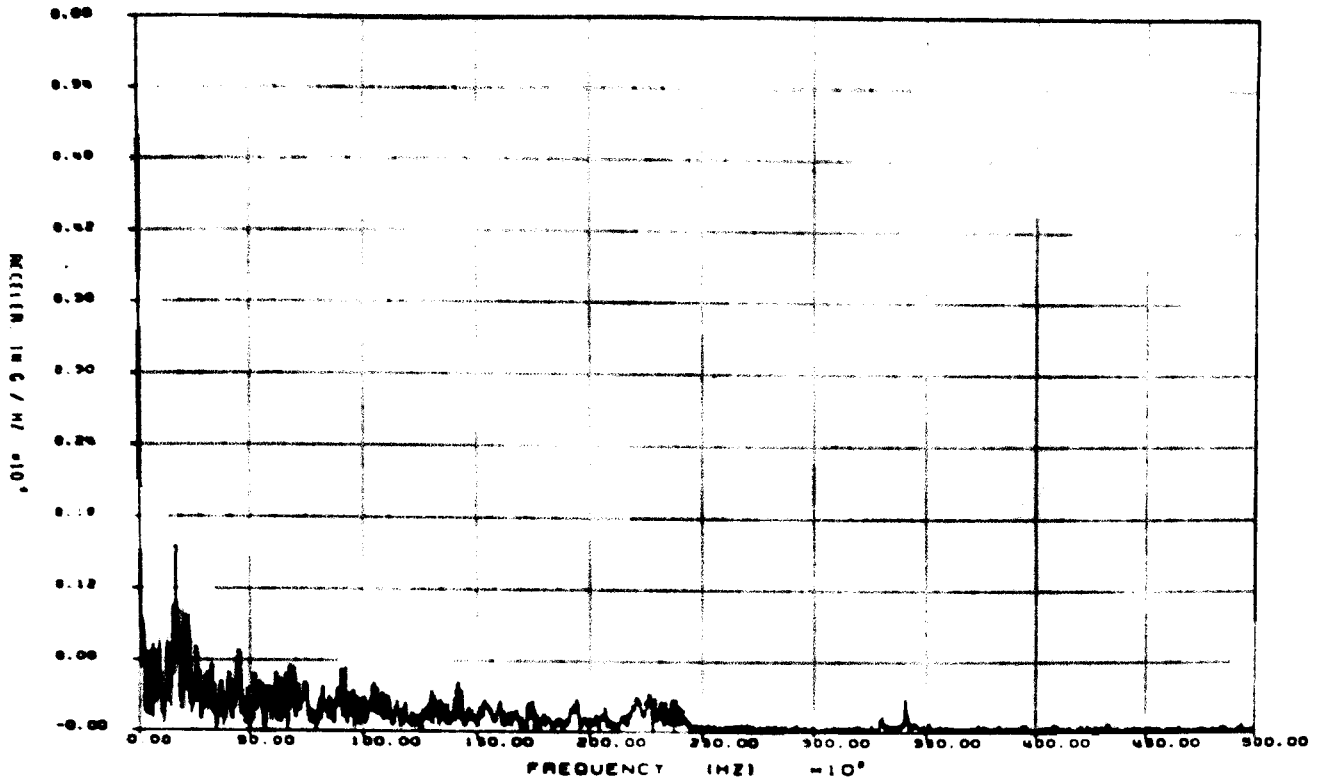


Figure C2-11. Fast Fourier Transform of Raw Data From Gage AY6 for 30-ft Oblique Drop Test: 0.50 kHz

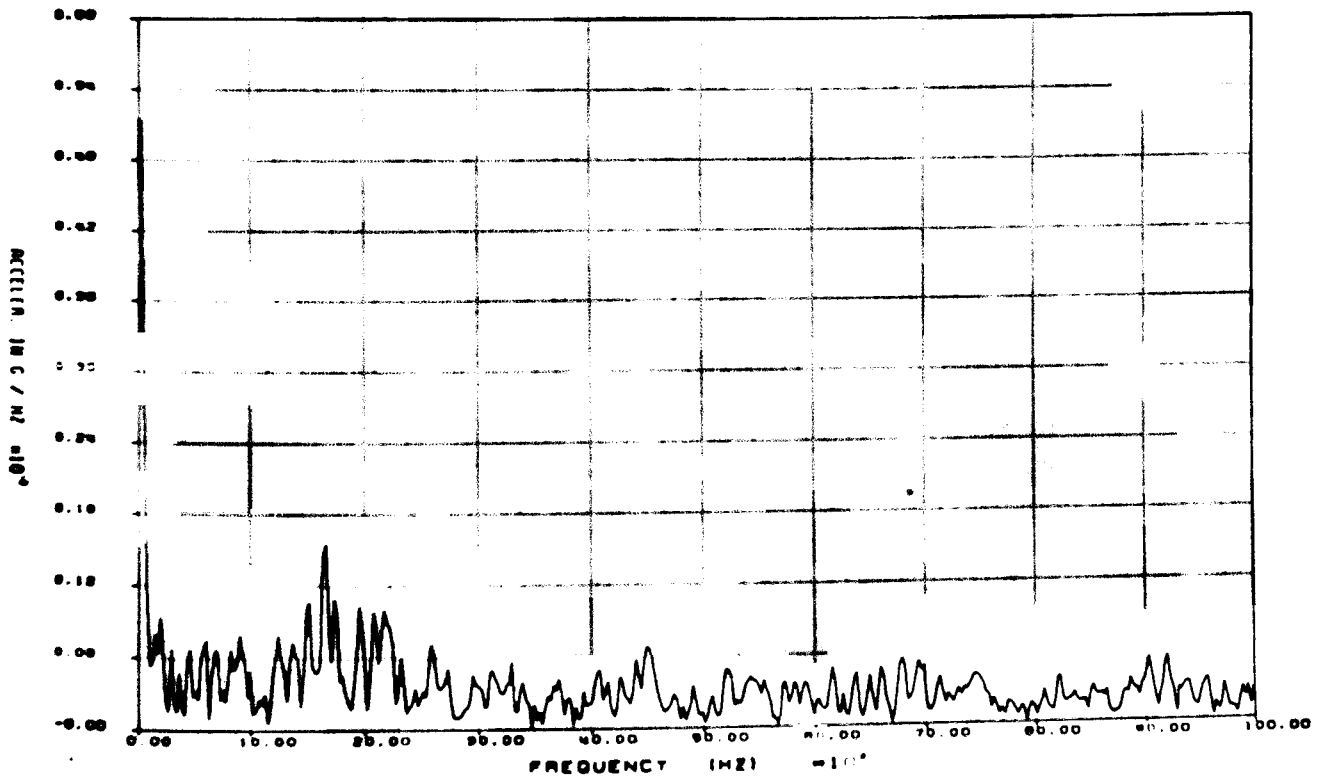


Figure C2-12. Fast Fourier Transform of Raw Data From Gage AY6 for 30-ft Oblique Drop Test: 0.10 kHz

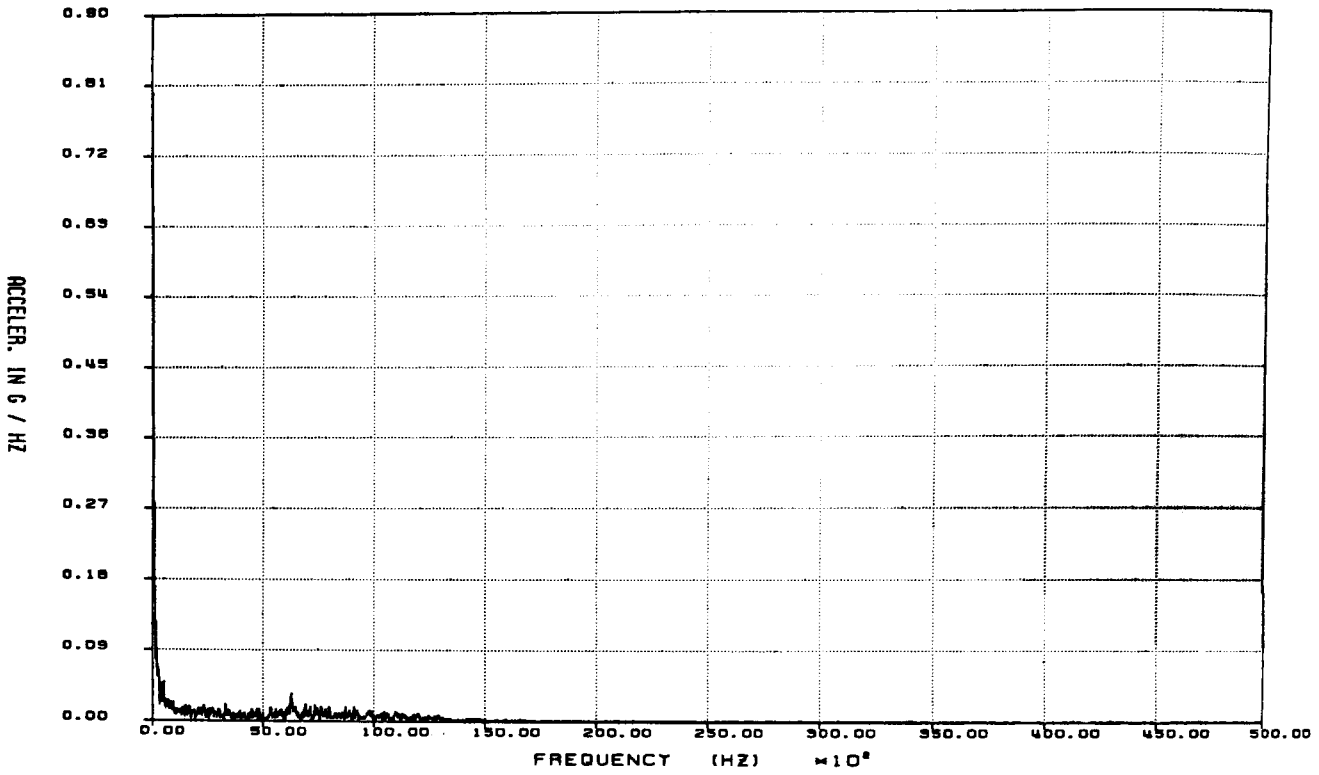


Figure C2-13. Fast Fourier Transform of Raw Data From Gage AZ7 for 30-ft Oblique Drop Test: 0-50 kHz

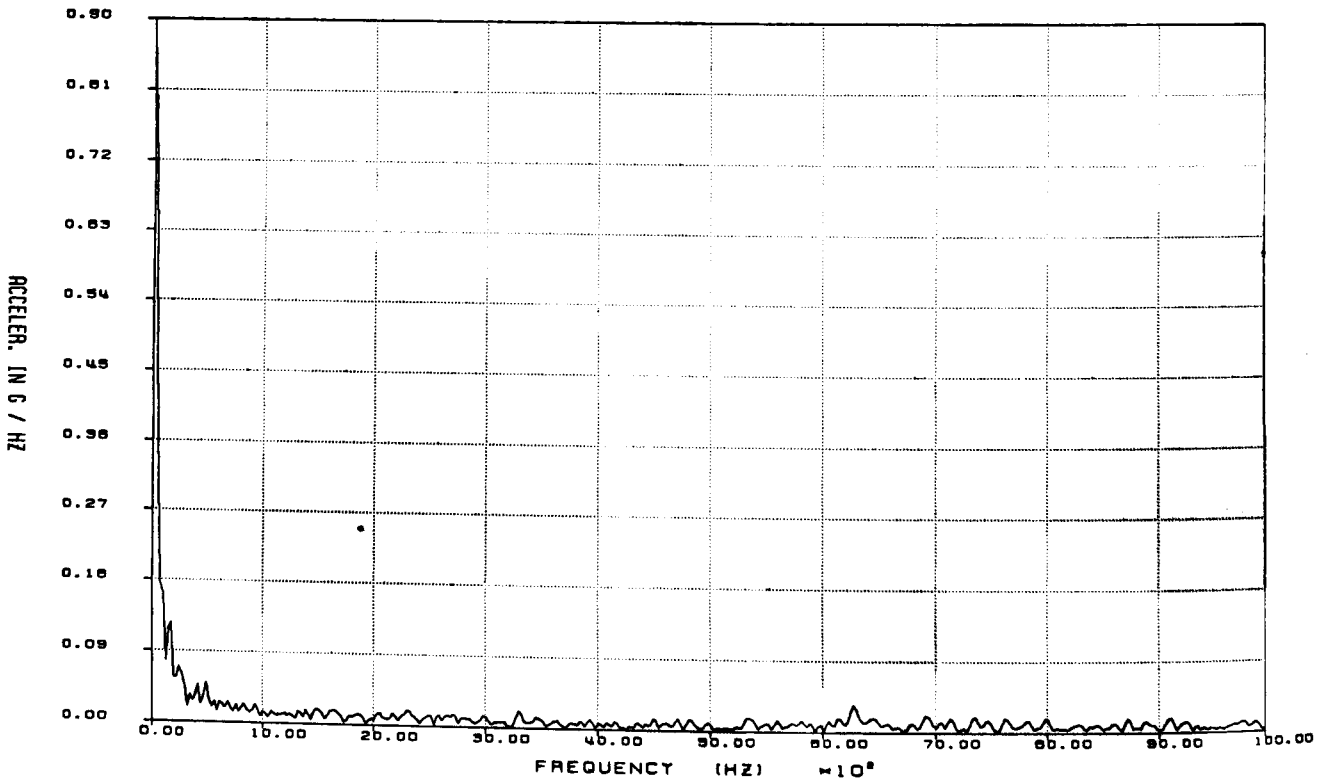


Figure C2-14. Fast Fourier Transform of Raw Data From Gage AZ7 for 30-ft Oblique Drop Test: 0-10 kHz

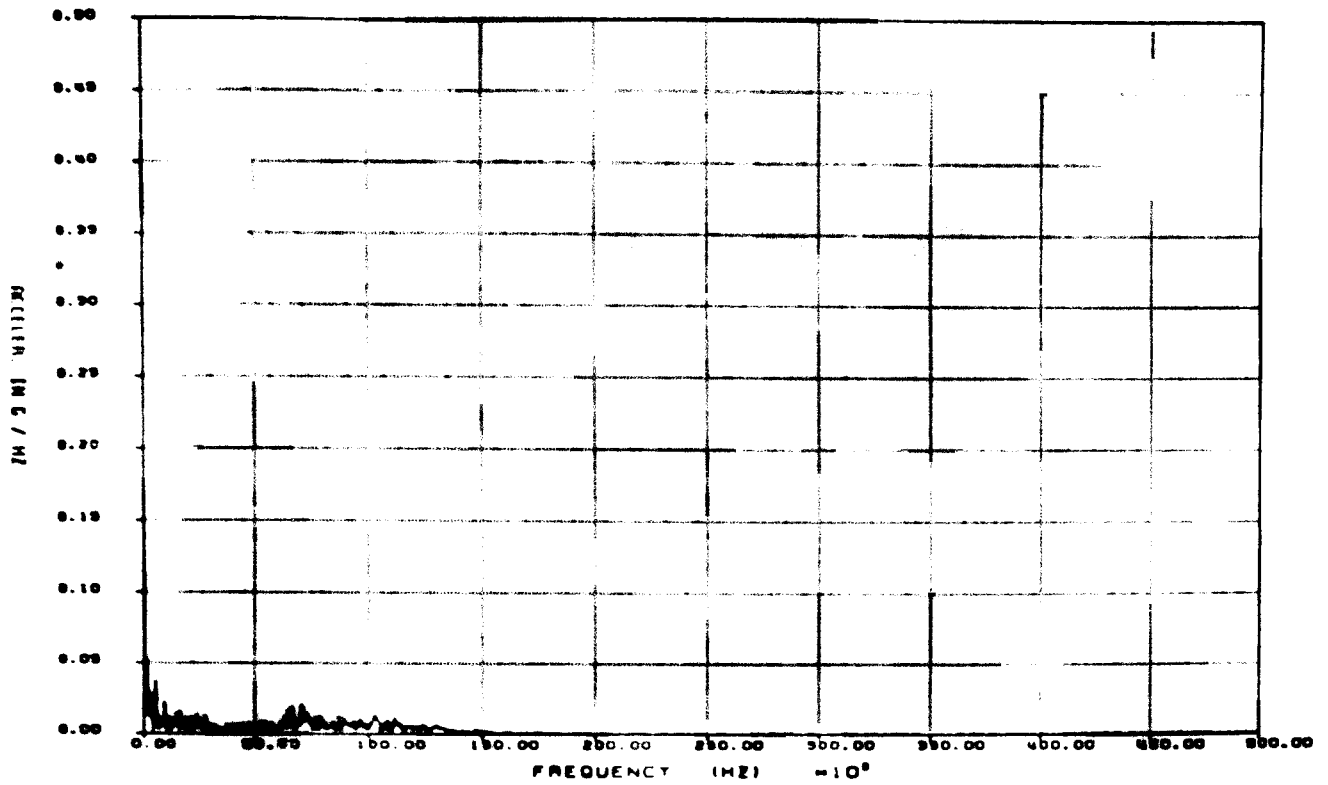


Figure C2-15. Fast Fourier Transform of Raw Data From Gage AX8 for 30-ft Oblique Drop Test: 0-50 kHz

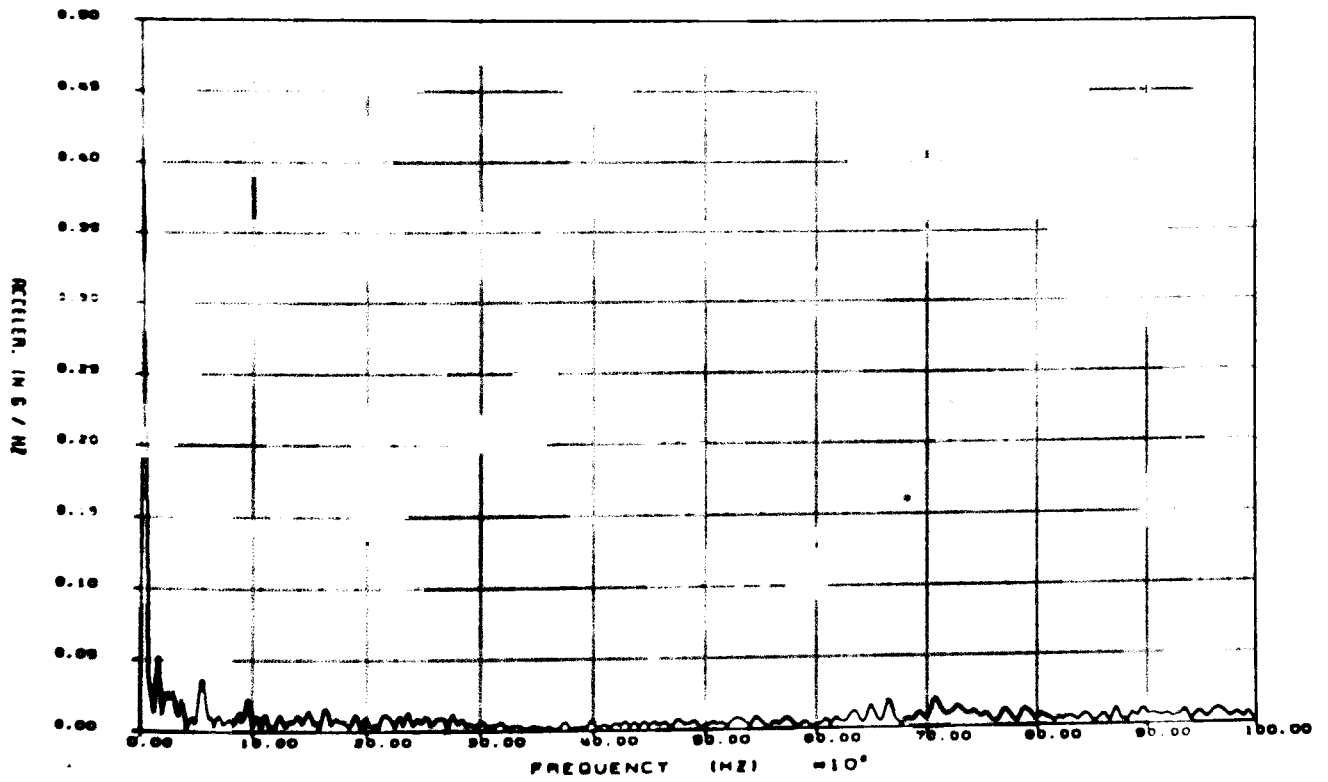


Figure C2-16. Fast Fourier Transform of Raw Data From Gage AX8 for 30-ft Oblique Drop Test: 0-10 kHz

APPENDIX D1

Accelerometer and Strain Gage Data for the 30-ft Side Drop Test Filtered at 1000 Hz

Figures

D1-1	Acceleration vs Time for Gage AZ1 for 30-ft Side Drop Test	206
D1-2	Acceleration vs Time for Gage AX2 for 30-ft Side Drop Test	206
D1-3	Acceleration vs Time for Gage AY3 for 30-ft Side Drop Test	207
D1-4	Acceleration vs Time for Gage AZ4 for 30-ft Side Drop Test	207
D1-5	Acceleration vs Time for Gage AX5 for 30-ft Side Drop Test	208
D1-6	Acceleration vs Time for Gage AY6 for 30-ft Side Drop Test	208
D1-7	Acceleration vs Time for Gage AZ7 for 30-ft Side Drop Test	209
D1-8	Acceleration vs Time for Gage AX8 for 30-ft Side Drop Test	209
D1-9	Acceleration vs Time for Gage AX9 for 30-ft Side Drop Test	210
D1-10	Acceleration vs Time for Gage AX10 for 30-ft Side Drop Test	210
D1-11	Acceleration vs Time for Gage AX11 for 30-ft Side Drop Test	211
D1-12	Microstrain vs Time for Gage SR1-Y for 30-ft Side Drop Test	211
D1-13	Microstrain vs Time for Gage SR1-YZ for 30-ft Side Drop Test	212
D1-14	Microstrain vs Time for Gage SR1-Z for 30-ft Side Drop Test	212
D1-15	Microstrain vs Time for Gage SR2-Y for 30-ft Side Drop Test	213
D1-16	Microstrain vs Time for Gage SR2-YZ for 30-ft Side Drop Test	213
D1-17	Microstrain vs Time for Gage SR2-Z for 30-ft Side Drop Test	214
D1-18	Microstrain vs Time for Gage SR3-Y for 30-ft Side Drop Test	214
D1-19	Microstrain vs Time for Gage SR3-YZ for 30-ft Side Drop Test	215
D1-20	Microstrain vs Time for Gage SR3-Z for 30-ft Side Drop Test	215
D1-21	Microstrain vs Time for Gage SR4-Y for 30-ft Side Drop Test	216
D1-22	Microstrain vs Time for Gage SR4-YZ for 30-ft Side Drop Test	216
D1-23	Microstrain vs Time for Gage SR4-Z for 30-ft Side Drop Test	217
D1-24	Microstrain vs Time for Gage SR5-Y for 30-ft Side Drop Test	217
D1-25	Microstrain vs Time for Gage SR5-YZ for 30-ft Side Drop Test	218
D1-26	Microstrain vs Time for Gage SR5-Z for 30-ft Side Drop Test	218

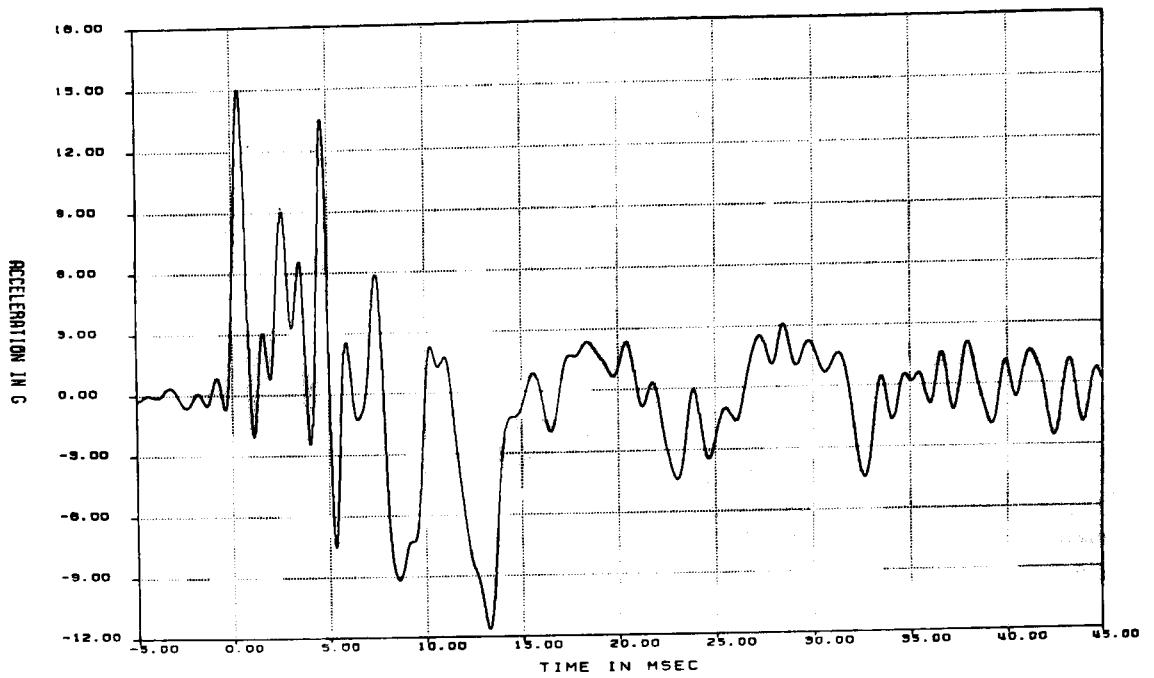


Figure D1-1. Acceleration vs Time for Gage AZ1 for 30-ft Side Drop Test (filtered at 1000 Hz)

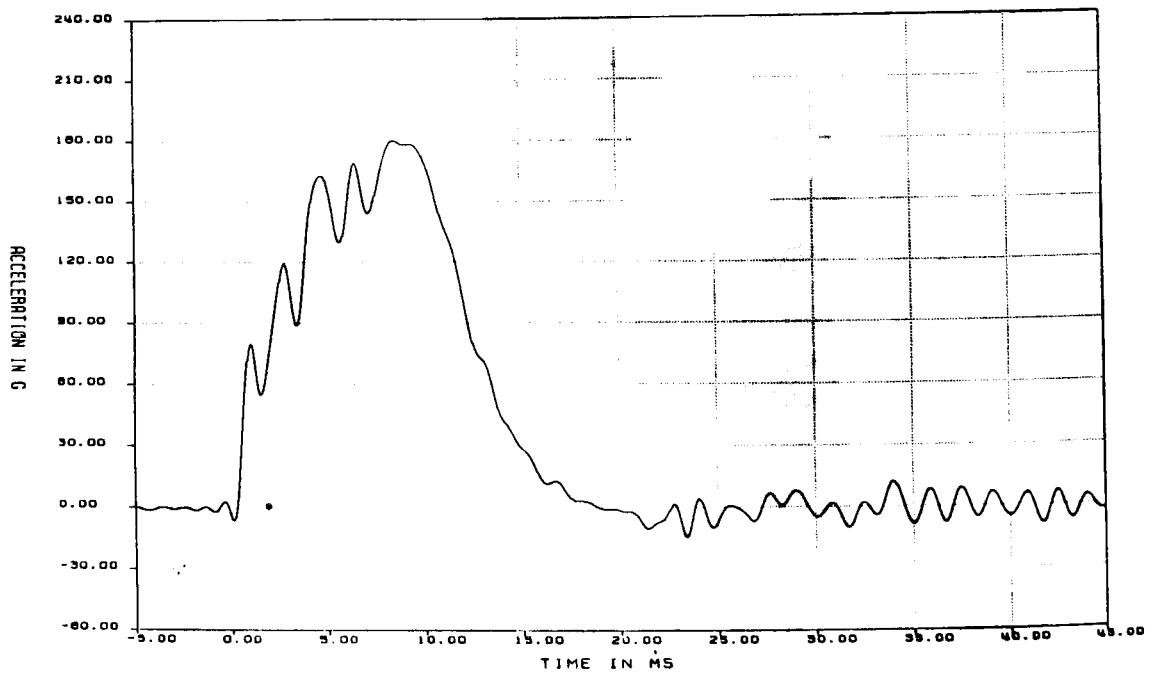


Figure D1-2. Acceleration vs Time for Gage AX2 for 30-ft Side Drop Test (filtered at 1000 Hz)

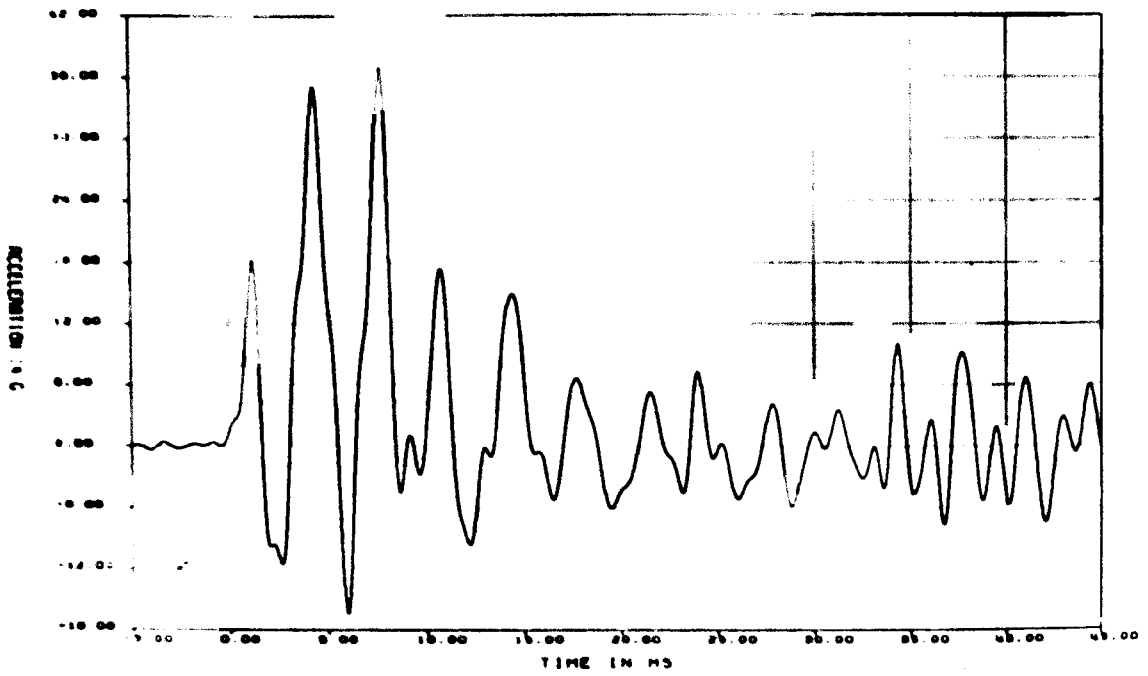


Figure D1-3. Acceleration vs Time for Gage AY3 for 30-ft Side Drop Test (filtered at 1000 Hz)

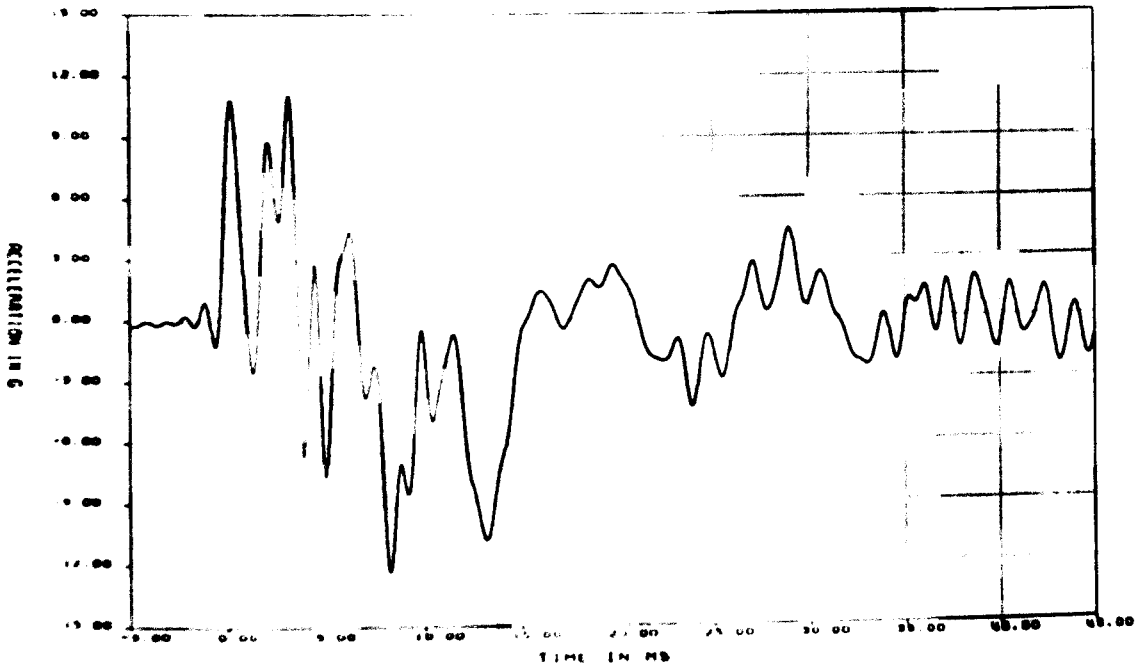


Figure D1-4. Acceleration vs Time for Gage AZ4 for 30-ft Side Drop Test (filtered at 1000 Hz)

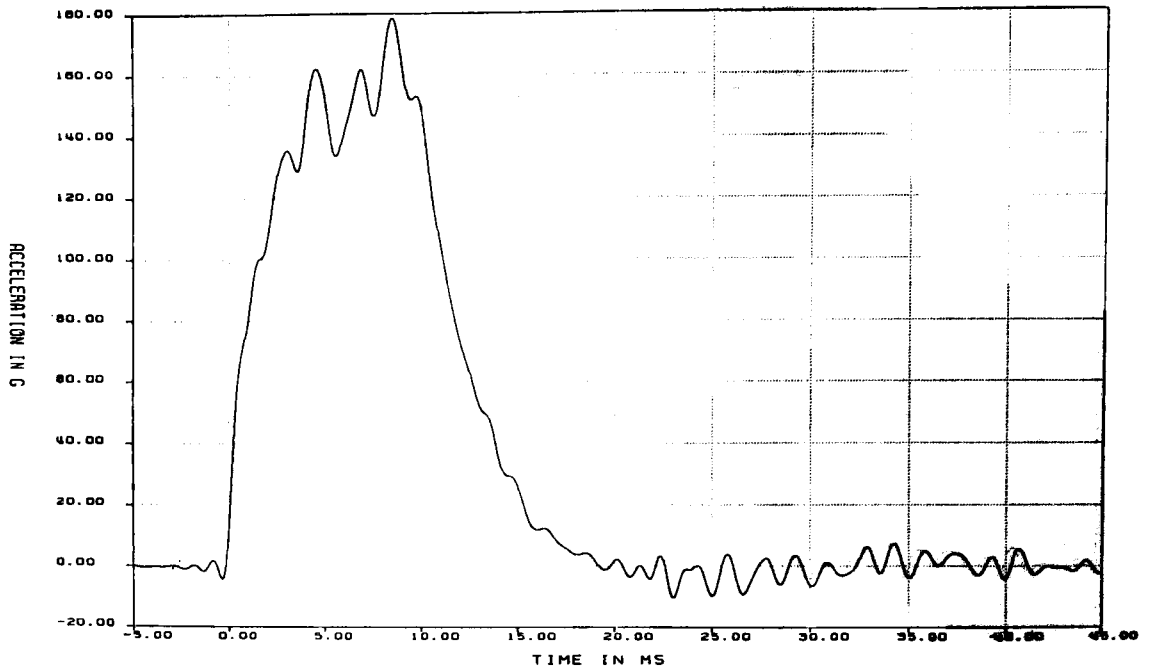


Figure D1-5. Acceleration vs Time for Gage AX5 for 30-ft Side Drop Test (filtered at 1000 Hz)

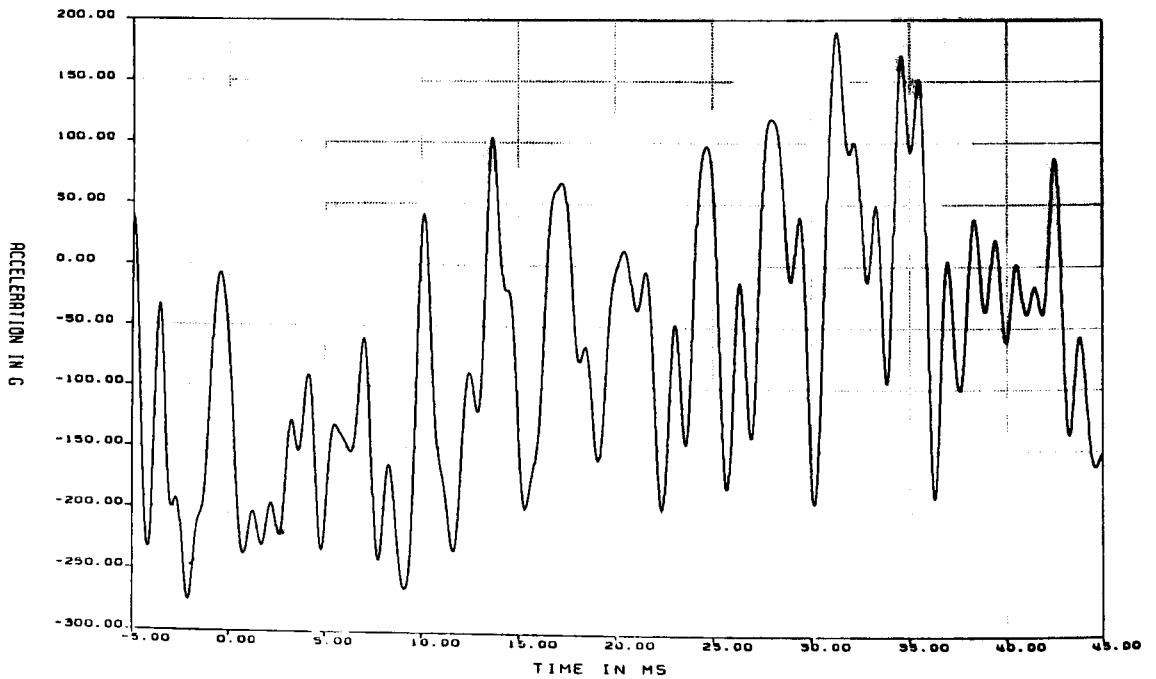


Figure D1-6. Acceleration vs Time for Gage AY6 for 30-ft Side Drop Test (filtered at 1000 Hz)

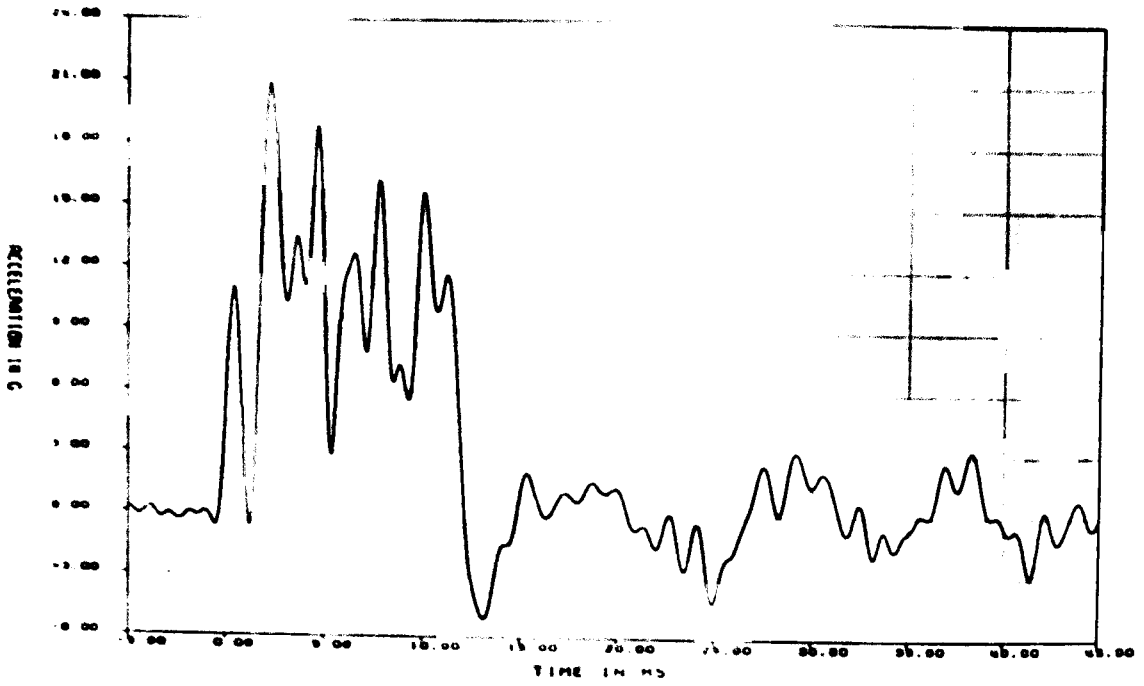


Figure D1-7. Acceleration vs Time for Gage AZ7 for 30-ft Side Drop Test (filtered at 1000 Hz)

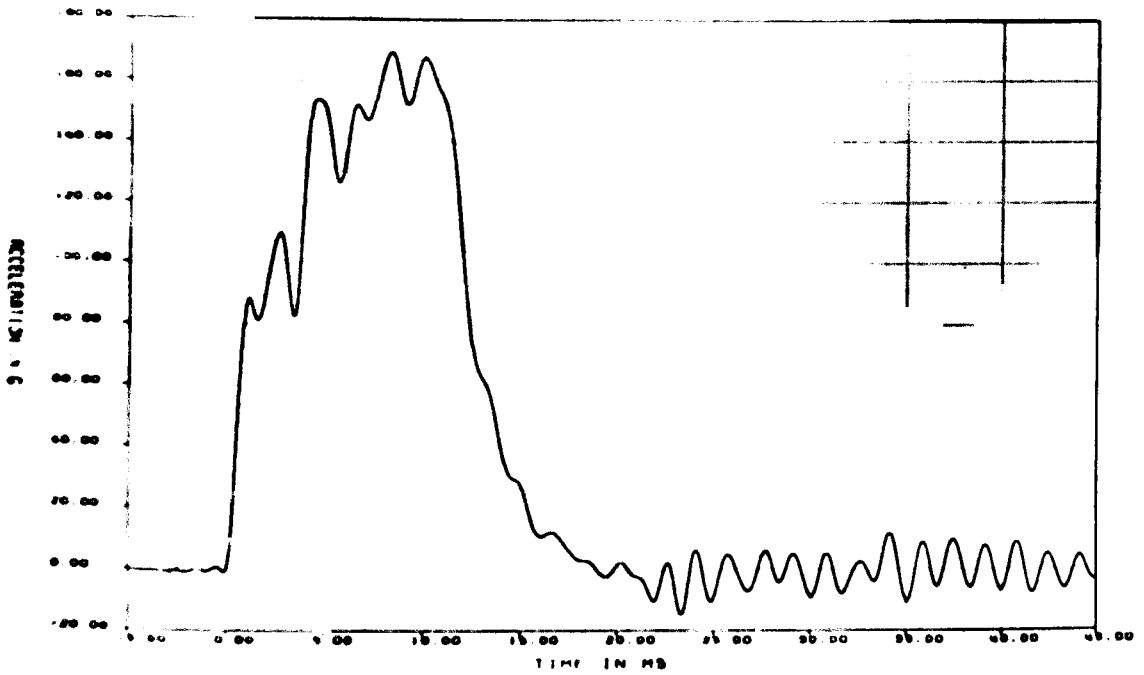


Figure D1-8. Acceleration vs Time for Gage AX8 for 30-ft Side Drop Test (filtered at 1000 Hz)

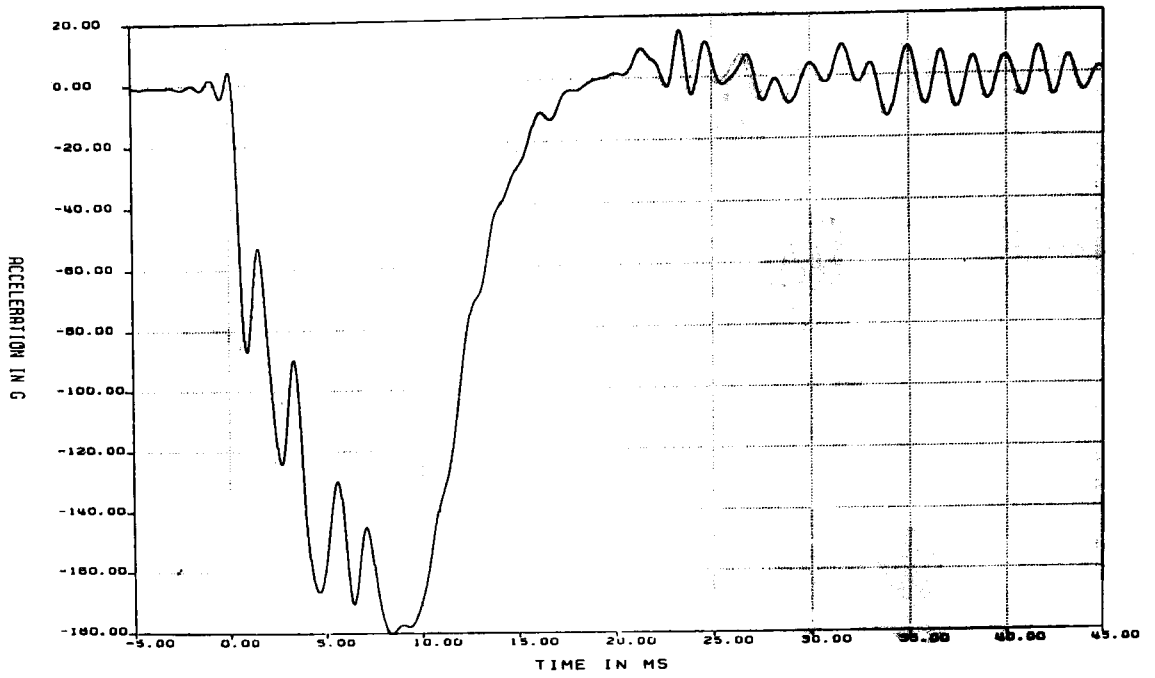


Figure D1-9. Acceleration vs Time for Gage AX9 for 30-ft Side Drop Test (filtered at 1000 Hz)

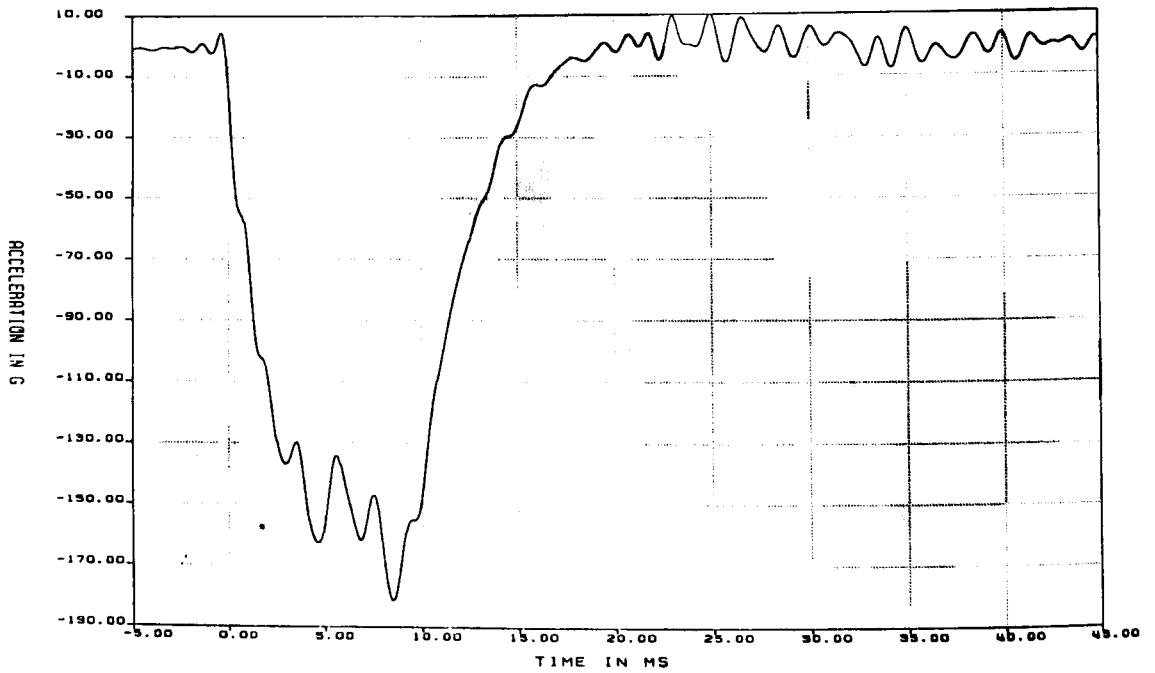


Figure D1-10. Acceleration vs Time for Gage AX10 for 30-ft Side Drop Test (filtered at 1000 Hz)

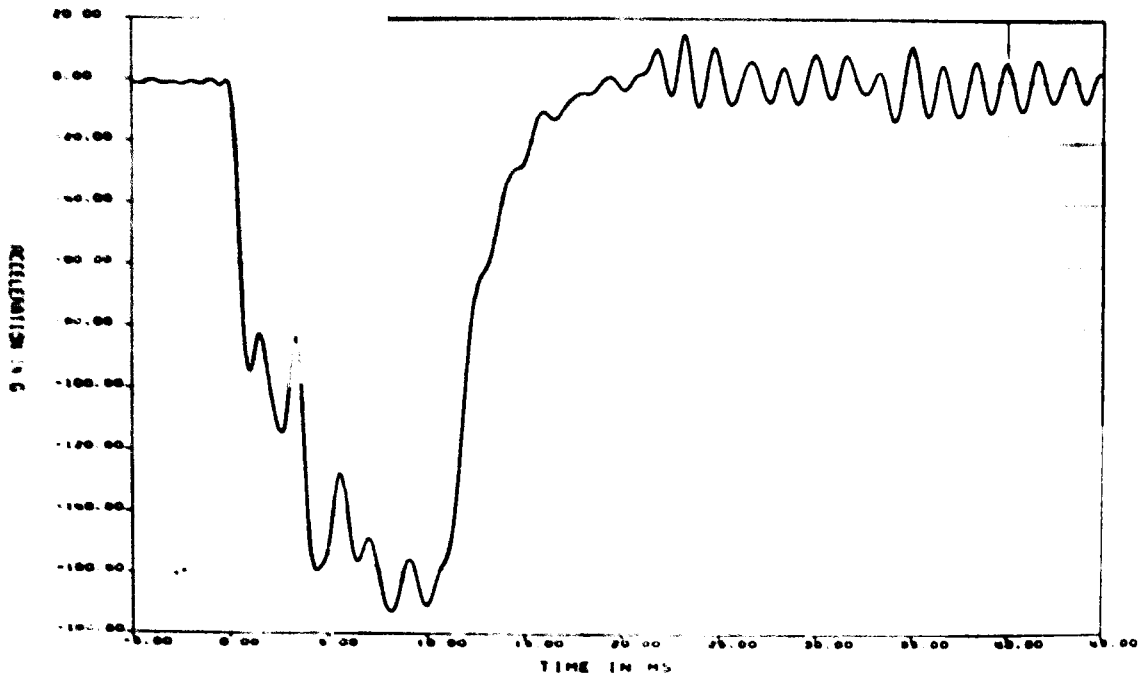


Figure D1-11. Acceleration vs Time for Gage AX11 for 30-ft Side Drop Test (filtered at 1000 Hz)

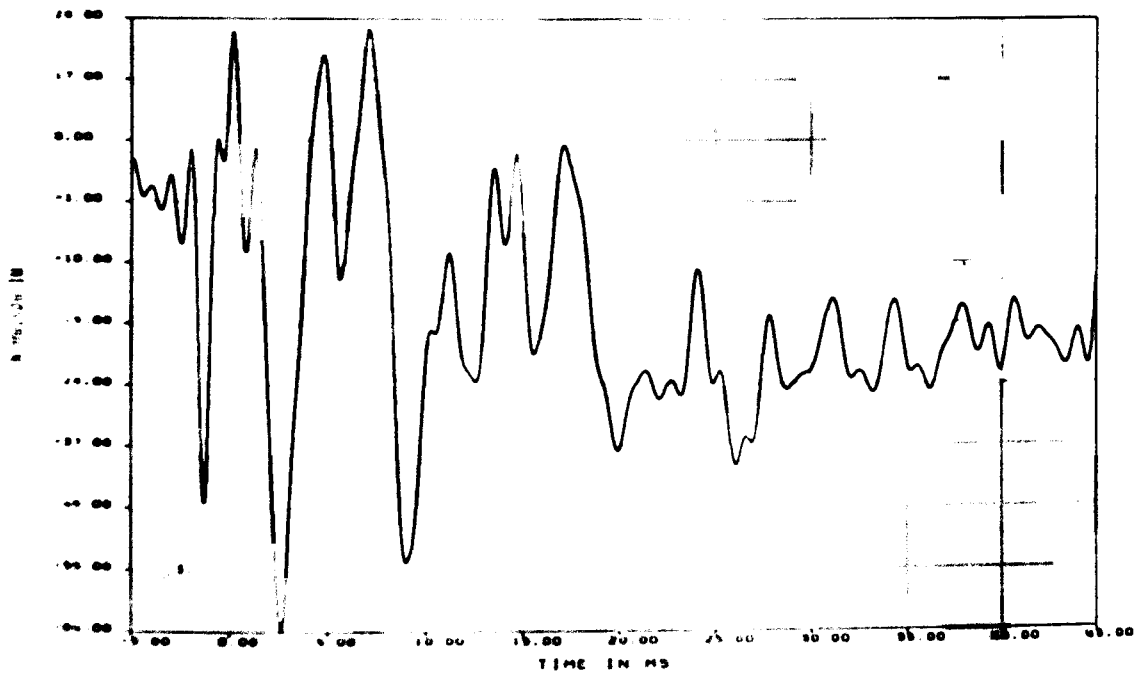


Figure D1-12. Microstrain vs Time for Gage SR1 Y for 30-ft Side Drop Test (filtered at 1000 Hz)

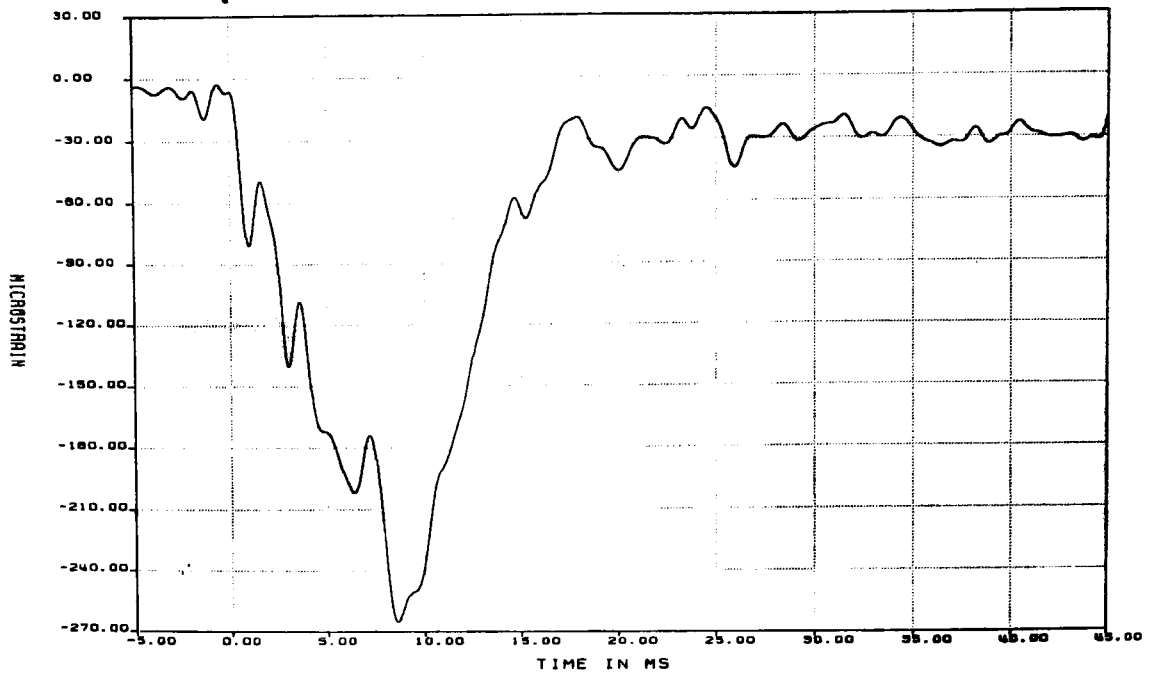


Figure D1-13. Microstrain vs Time for Gage SR1-YZ for 30-ft Side Drop Test (filtered at 1000 Hz)

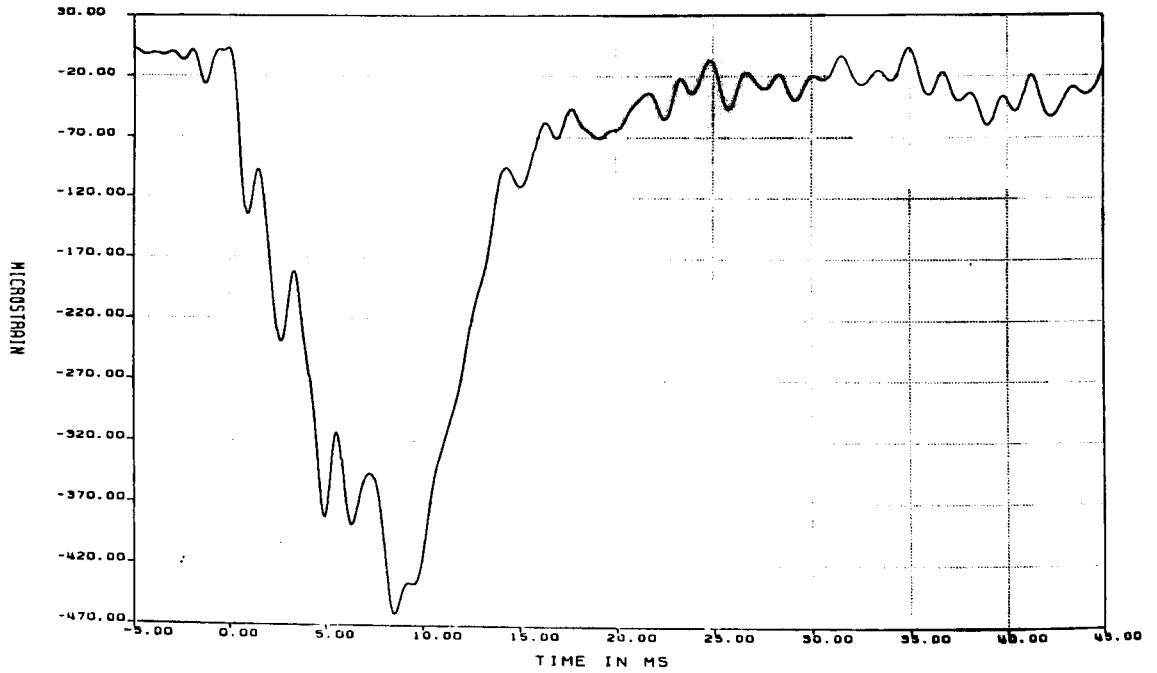


Figure D1-14. Microstrain vs Time for Gage SR1-Z for 30-ft Side Drop Test (filtered at 1000 Hz)

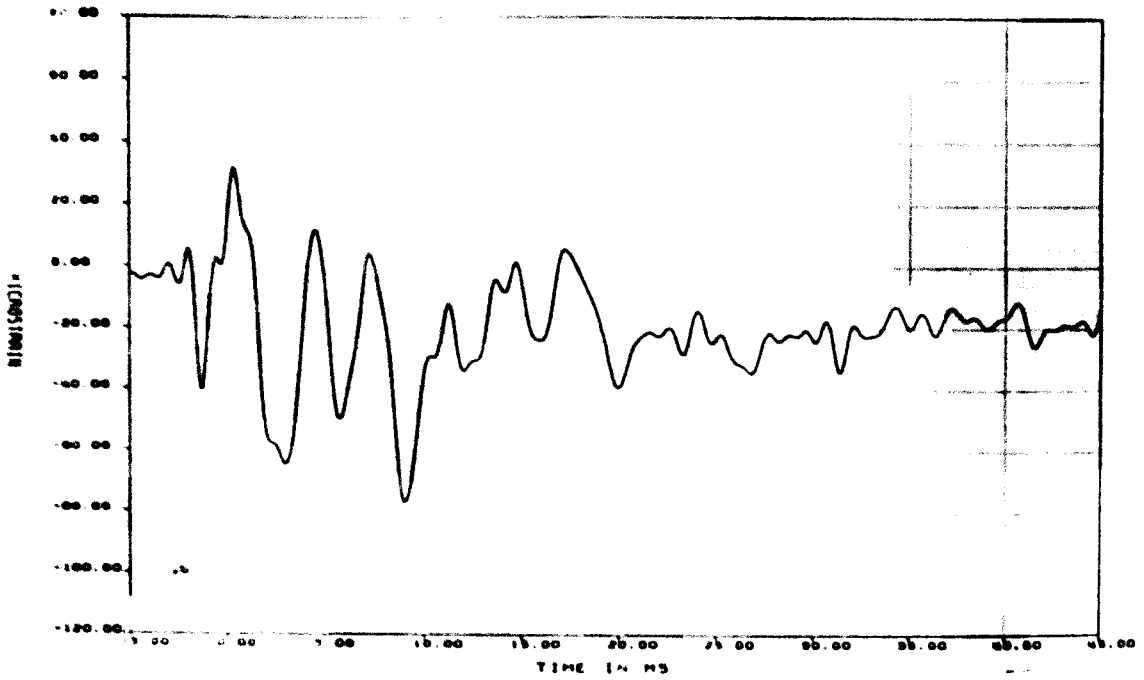


Figure D1-15. Microstrain vs Time for Gage SR2-Y for 30-ft Side Drop Test (filtered at 1000 Hz)

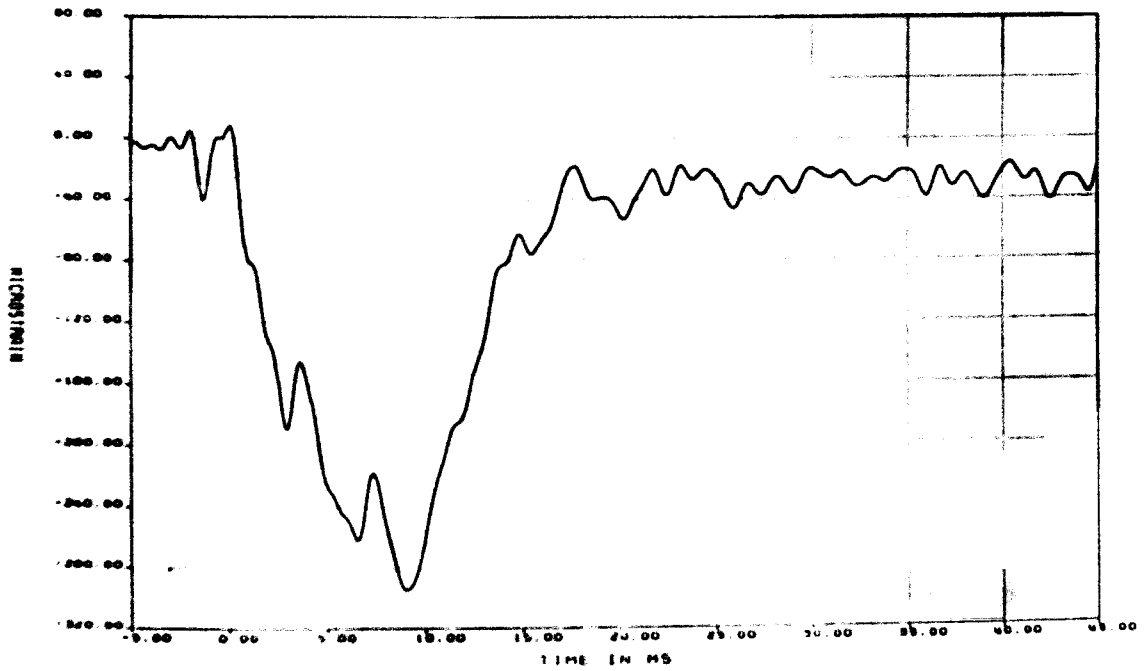


Figure D1-16. Microstrain vs Time for Gage SR2-YZ for 30-ft Side Drop Test (filtered at 1000 Hz)

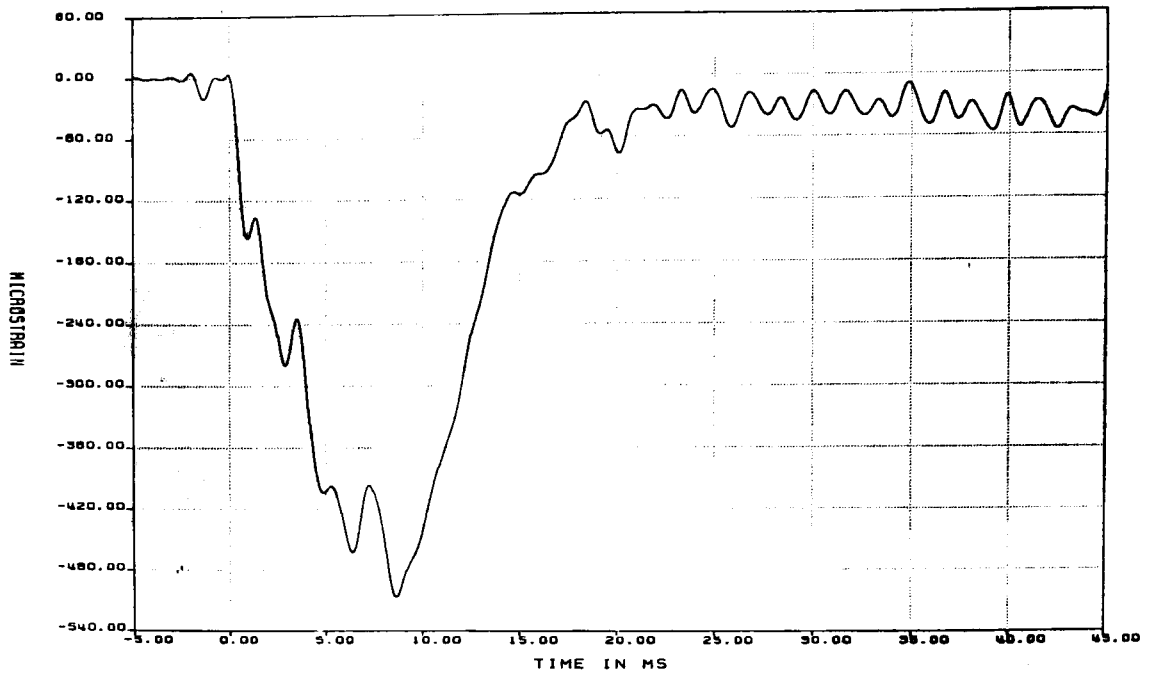


Figure D1-17. Microstrain vs Time for Gage SR2-Z for 30-ft Side Drop Test (filtered at 1000 Hz)

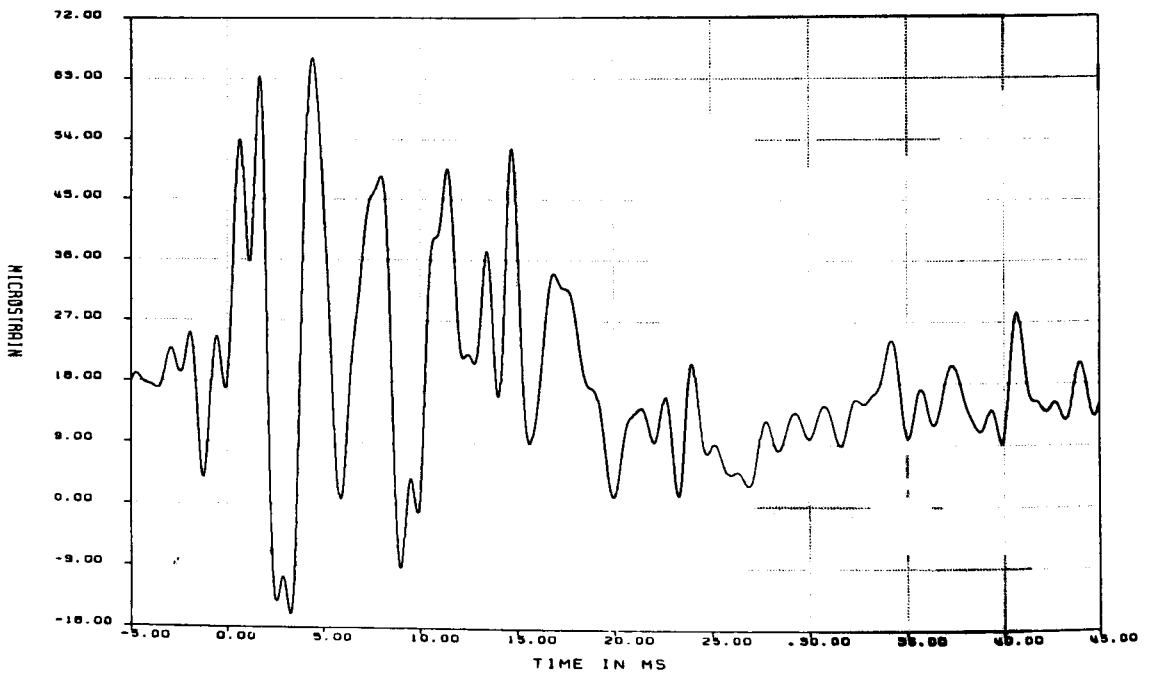


Figure D1-18. Microstrain vs Time for Gage SR3-Y for 30-ft Side Drop Test (filtered at 1000 Hz)

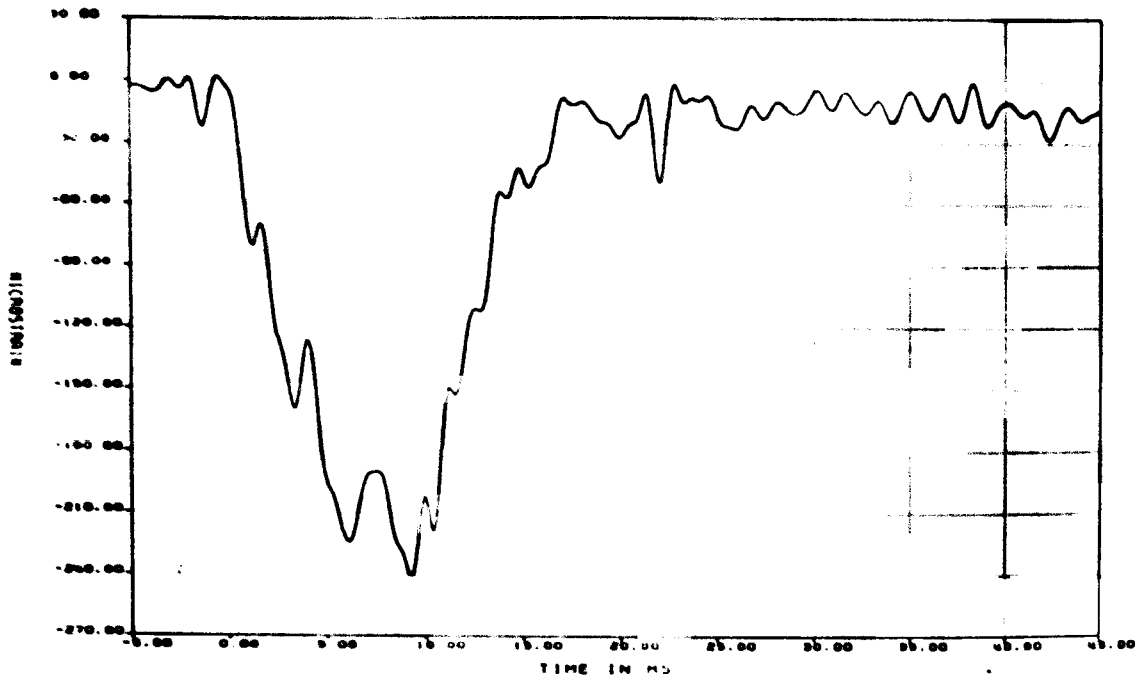


Figure D1-19. Microstrain vs Time for Gage SR3-YZ for 30-ft Side Drop Test (filtered at 1000 Hz)

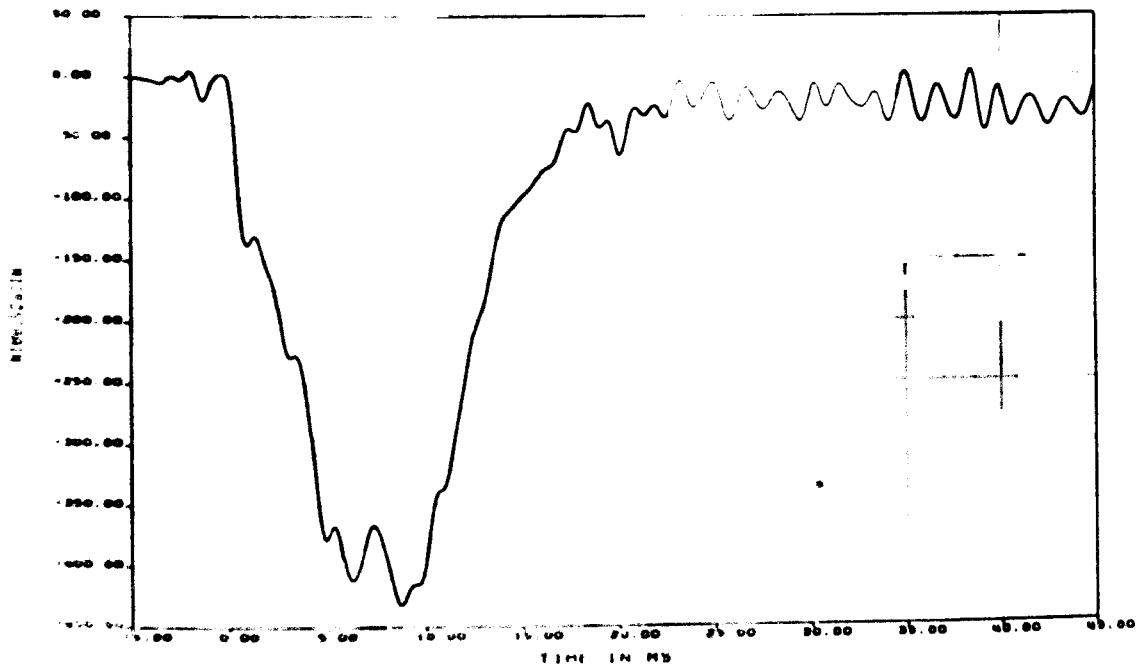


Figure D1-20. Microstrain vs Time for Gage SR3-Z for 30 ft Side Drop Test (filtered at 1000 Hz)

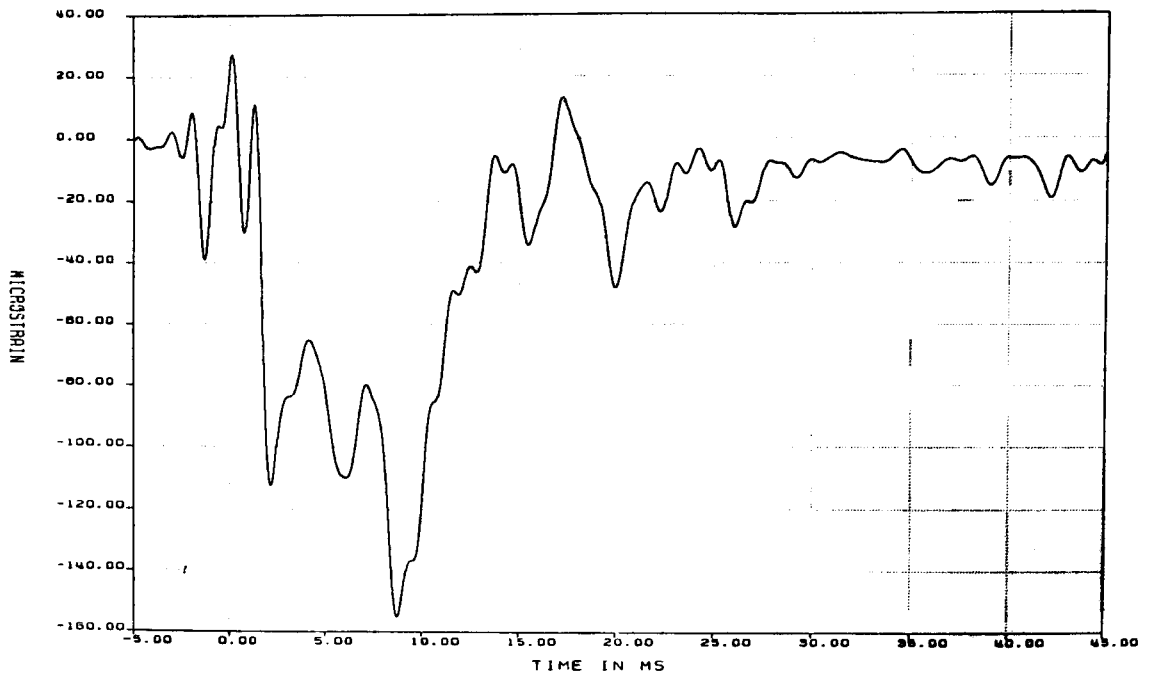


Figure D1-21. Microstrain vs Time for Gage SR4-Y for 30-ft Side Drop Test (filtered at 1000 Hz)

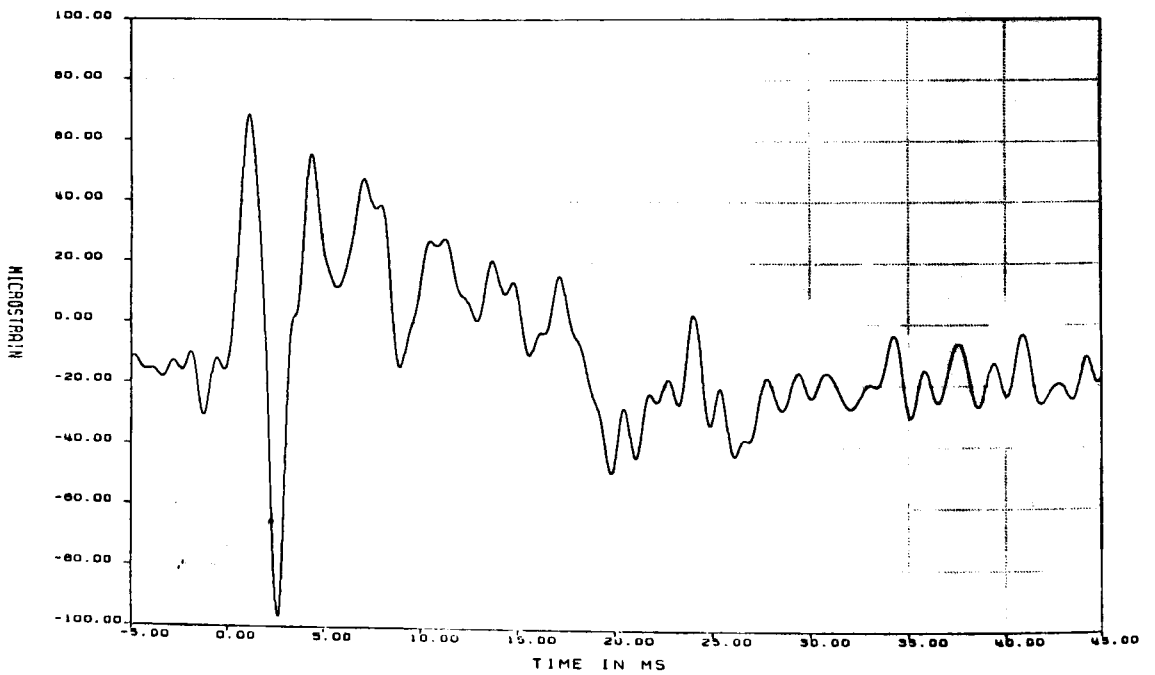


Figure D1-22. Microstrain vs Time for Gage SR4-YZ for 30-ft Side Drop Test (filtered at 1000 Hz)

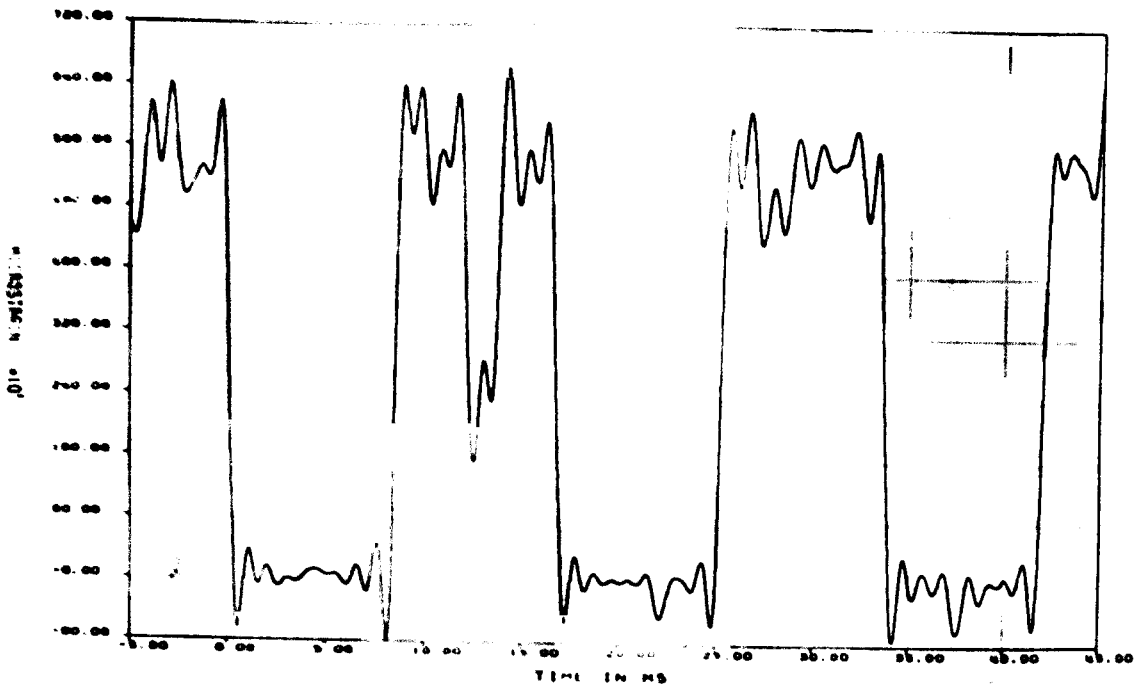


Figure D1-23. Microstrain vs Time for Gage SR4-Z for 30-ft Side Drop Test (filtered at 1000 Hz)

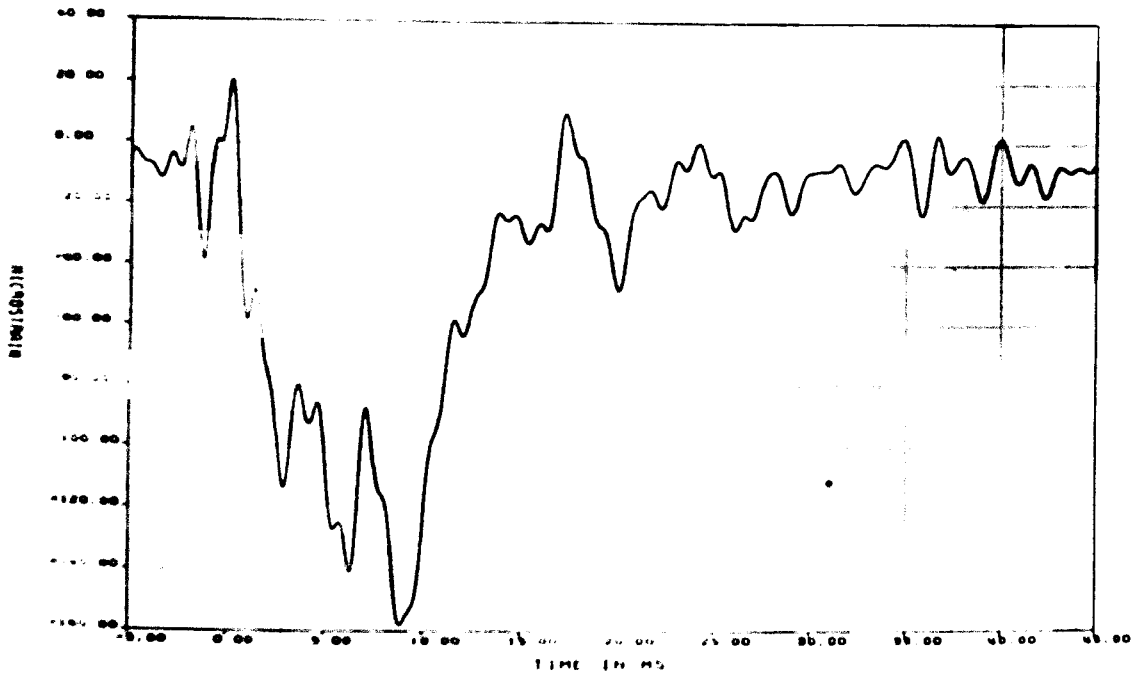


Figure D1-24. Microstrain vs Time for Gage SR5-Y for 30-ft Side Drop Test (filtered at 1000 Hz)

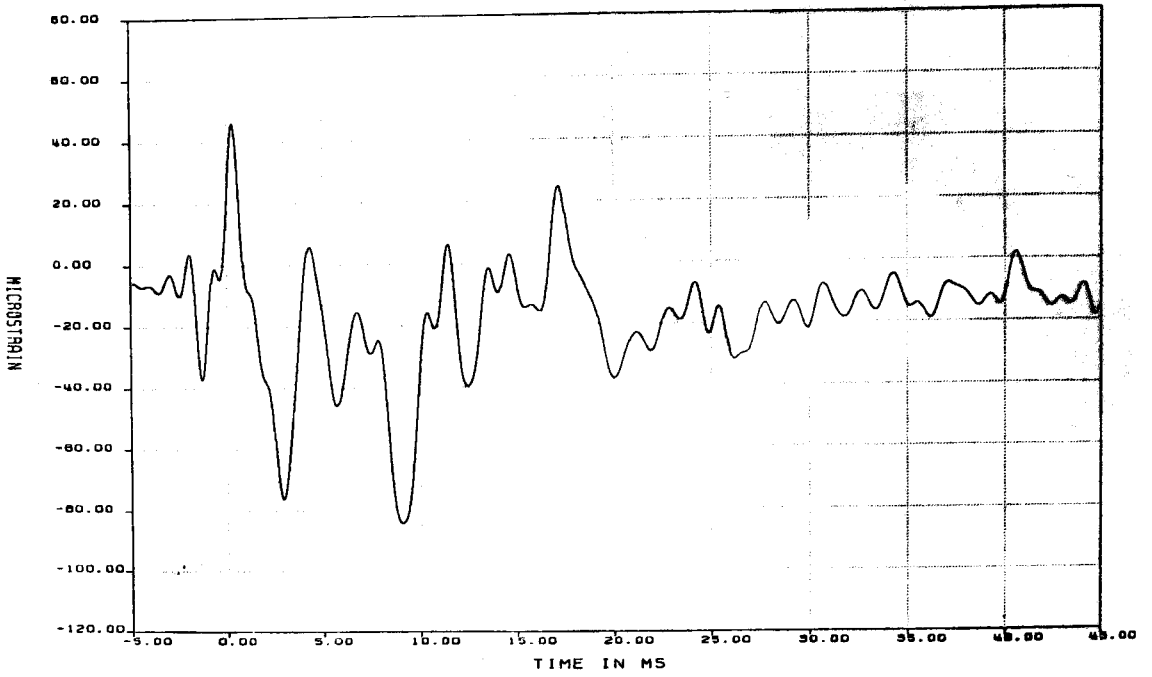


Figure D1-25. Microstrain vs Time for Gage SR5-YZ for 30-ft Side Drop Test (filtered at 1000 Hz)

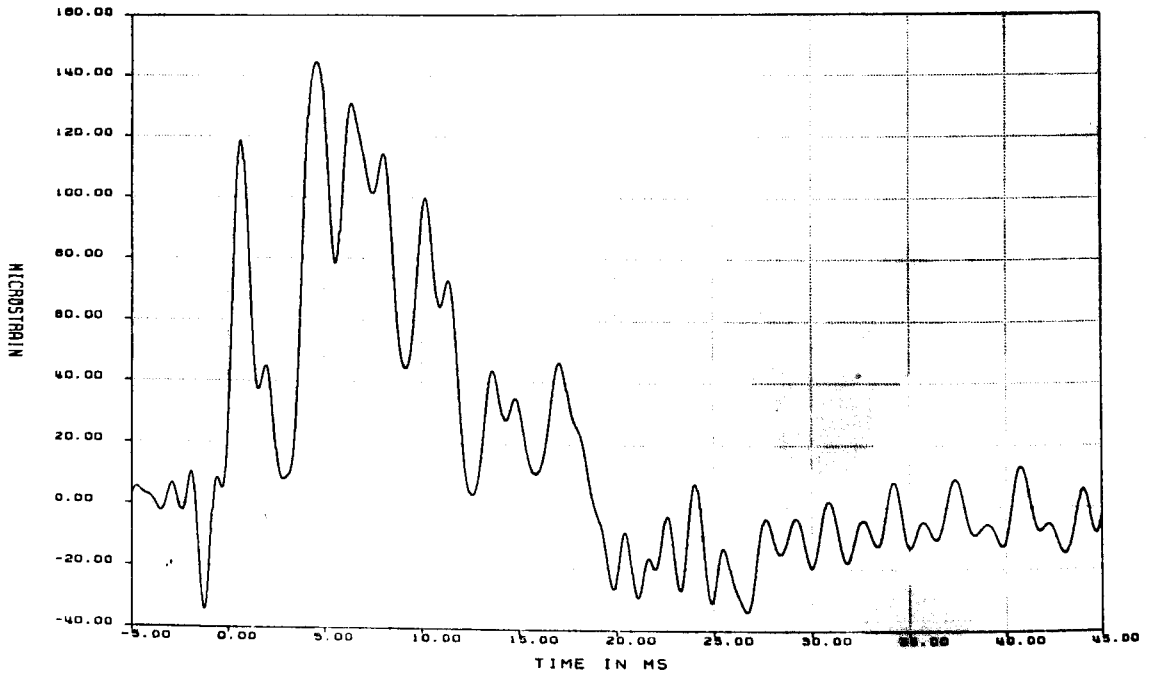


Figure D1-26. Microstrain vs Time for Gage SR5-Z for 30-ft Side Drop Test (filtered at 1000 Hz)

APPENDIX D2

Fast Fourier Transforms of Raw Accelerometer Data for the 30-ft Side Drop Test

Figures

D2-1	Fast Fourier Transform of Raw Data From Gage AZ1 for 30-ft Side Drop Test: 0-50 kHz.....	220
D2-2	Fast Fourier Transform of Raw Data From Gage AZ1 for 30-ft Side Drop Test: 0-10 kHz.....	220
D2-3	Fast Fourier Transform of Raw Data From Gage AX2 for 30-ft Side Drop Test: 0-50 kHz.....	221
D2-4	Fast Fourier Transform of Raw Data From Gage AX2 for 30-ft Side Drop Test: 0-10 kHz.....	221
D2-5	Fast Fourier Transform of Raw Data From Gage AY3 for 30-ft Side Drop Test: 0-50 kHz.....	222
D2-6	Fast Fourier Transform of Raw Data From Gage AY3 for 30-ft Side Drop Test: 0-10 kHz.....	222
D2-7	Fast Fourier Transform of Raw Data From Gage AZ4 for 30-ft Side Drop Test: 0-50 kHz.....	223
D2-8	Fast Fourier Transform of Raw Data From Gage AZ4 for 30-ft Side Drop Test: 0-10 kHz.....	223
D2-9	Fast Fourier Transform of Raw Data From Gage AX5 for 30-ft Side Drop Test: 0-50 kHz.....	224
D2-10	Fast Fourier Transform of Raw Data From Gage AX5 for 30-ft Side Drop Test: 0-10 kHz.....	224
D2-11	Fast Fourier Transform of Raw Data From Gage AY6 for 30-ft Side Drop Test: 0-50 kHz.....	225
D2-12	Fast Fourier Transform of Raw Data From Gage AY6 for 30-ft Side Drop Test: 0-10 kHz.....	225
D2-13	Fast Fourier Transform of Raw Data From Gage AZ7 for 30-ft Side Drop Test: 0-50 kHz.....	226
D2-14	Fast Fourier Transform of Raw Data From Gage AZ7 for 30-ft Side Drop Test: 0-10 kHz.....	226
D2-15	Fast Fourier Transform of Raw Data From Gage AX8 for 30-ft Side Drop Test: 0-50 kHz.....	227
D2-16	Fast Fourier Transform of Raw Data From Gage AX8 for 30-ft Side Drop Test: 0-10 kHz.....	227
D2-17	Fast Fourier Transform of Raw Data From Gage AX9 for 30-ft Side Drop Test: 0-50 kHz.....	228
D2-18	Fast Fourier Transform of Raw Data From Gage AX9 for 30-ft Side Drop Test: 0-10 kHz.....	228
D2-19	Fast Fourier Transform of Raw Data From Gage AX10 for 30-ft Side Drop Test: 0-50 kHz.....	229
D2-20	Fast Fourier Transform of Raw Data From Gage AX10 for 30-ft Side Drop Test: 0-10 kHz.....	229
D2-21	Fast Fourier Transform of Raw Data From Gage AX11 for 30-ft Side Drop Test: 0-50 kHz.....	230
D2-22	Fast Fourier Transform of Raw Data From Gage AX11 for 30-ft Side Drop Test: 0-10 kHz.....	230

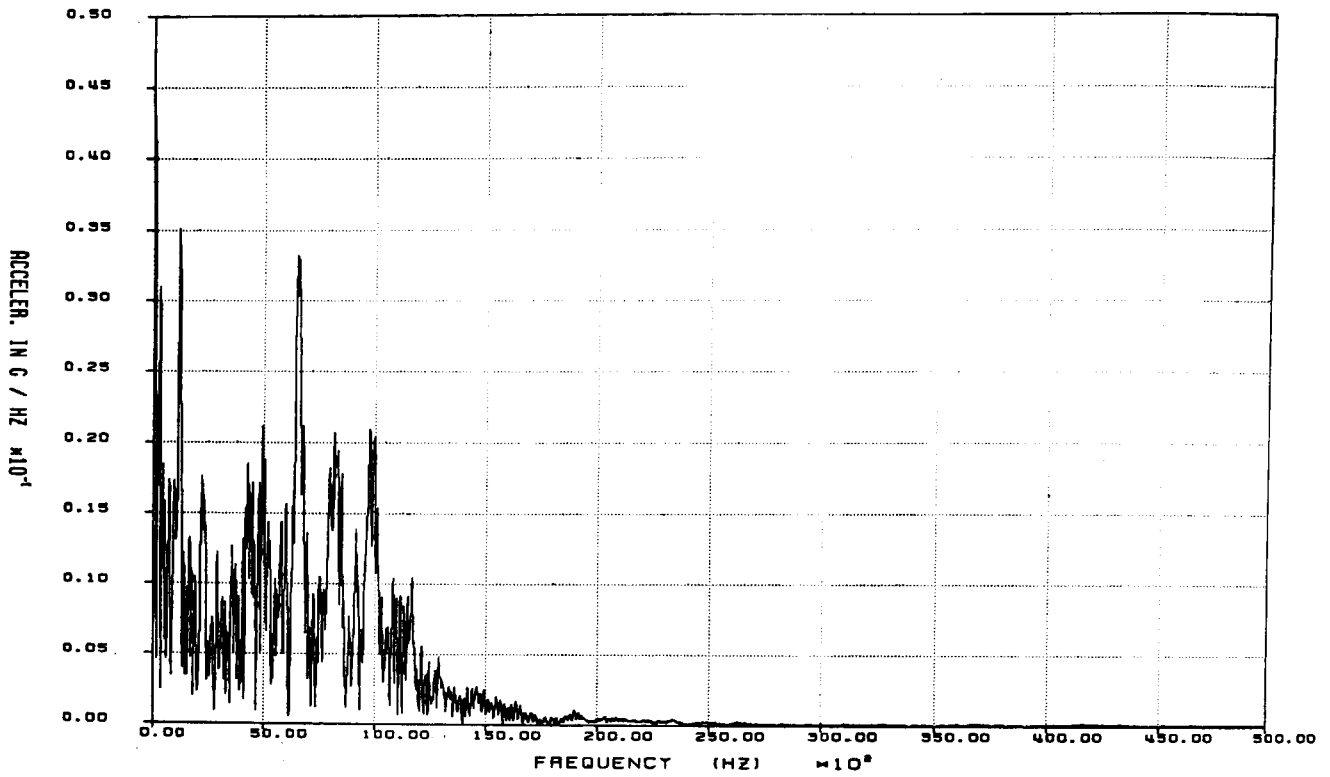


Figure D2-1. Fast Fourier Transform of Raw Data From Gage AZ1 for 30-ft Side Drop Test: 0-50 kHz

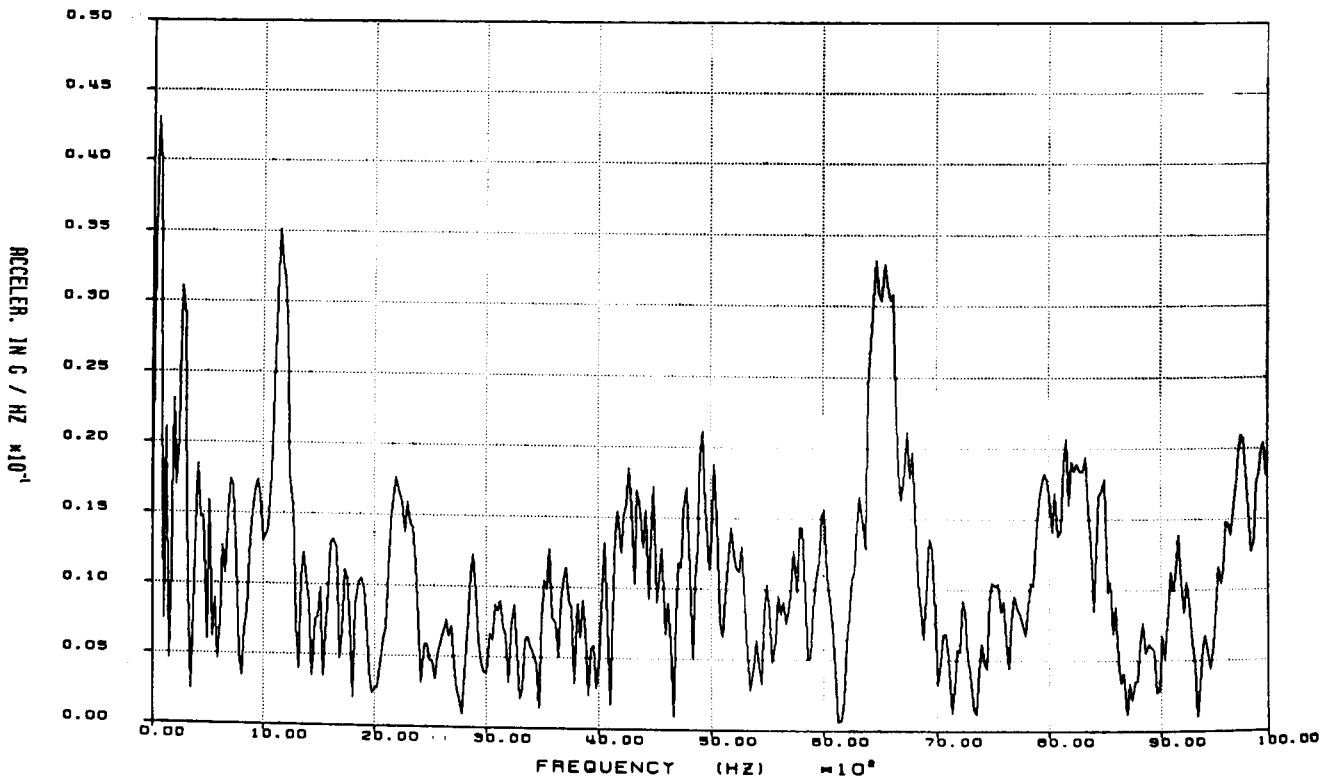


Figure D2-2. Fast Fourier Transform of Raw Data From Gage AZ1 for 30-ft Side Drop Test: 0-10 kHz

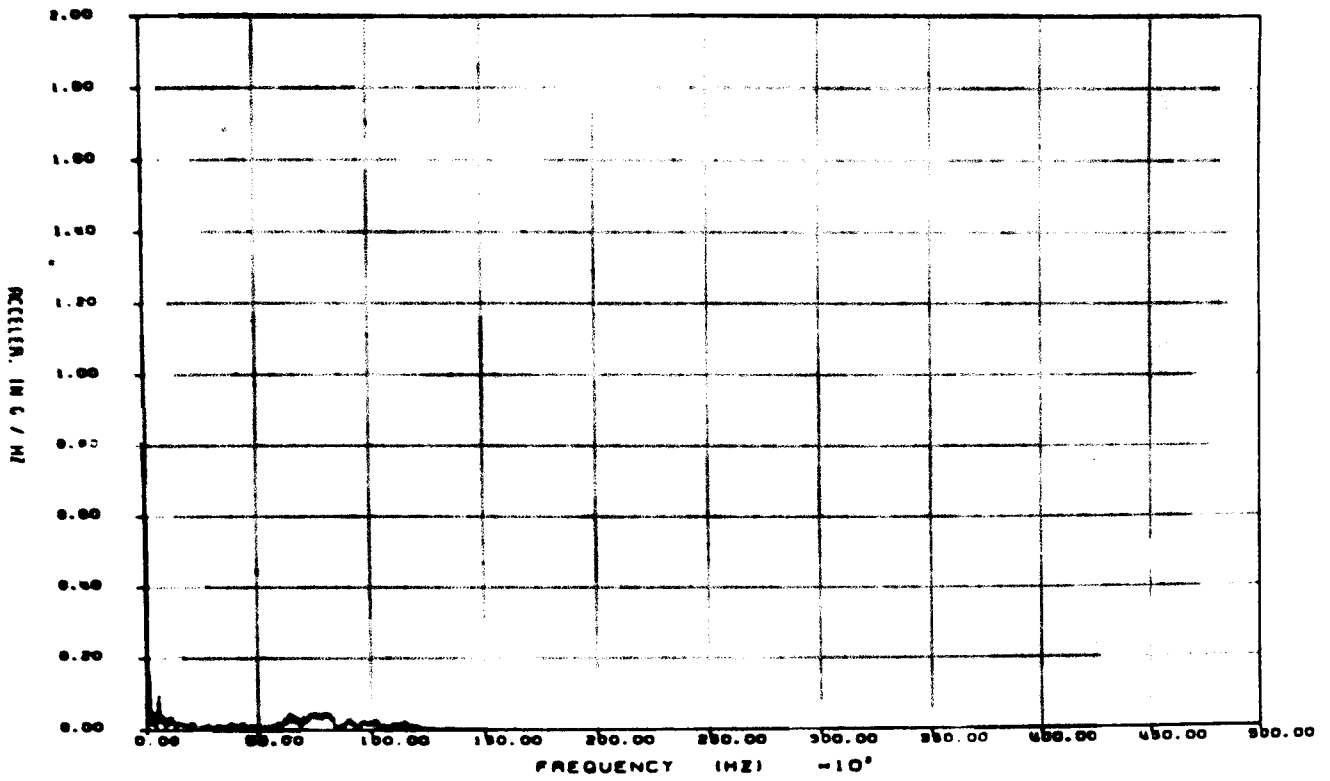


Figure D2-3. Fast Fourier Transform of Raw Data From Gage AX2 for 30-ft Side Drop Test: 0-50 kHz

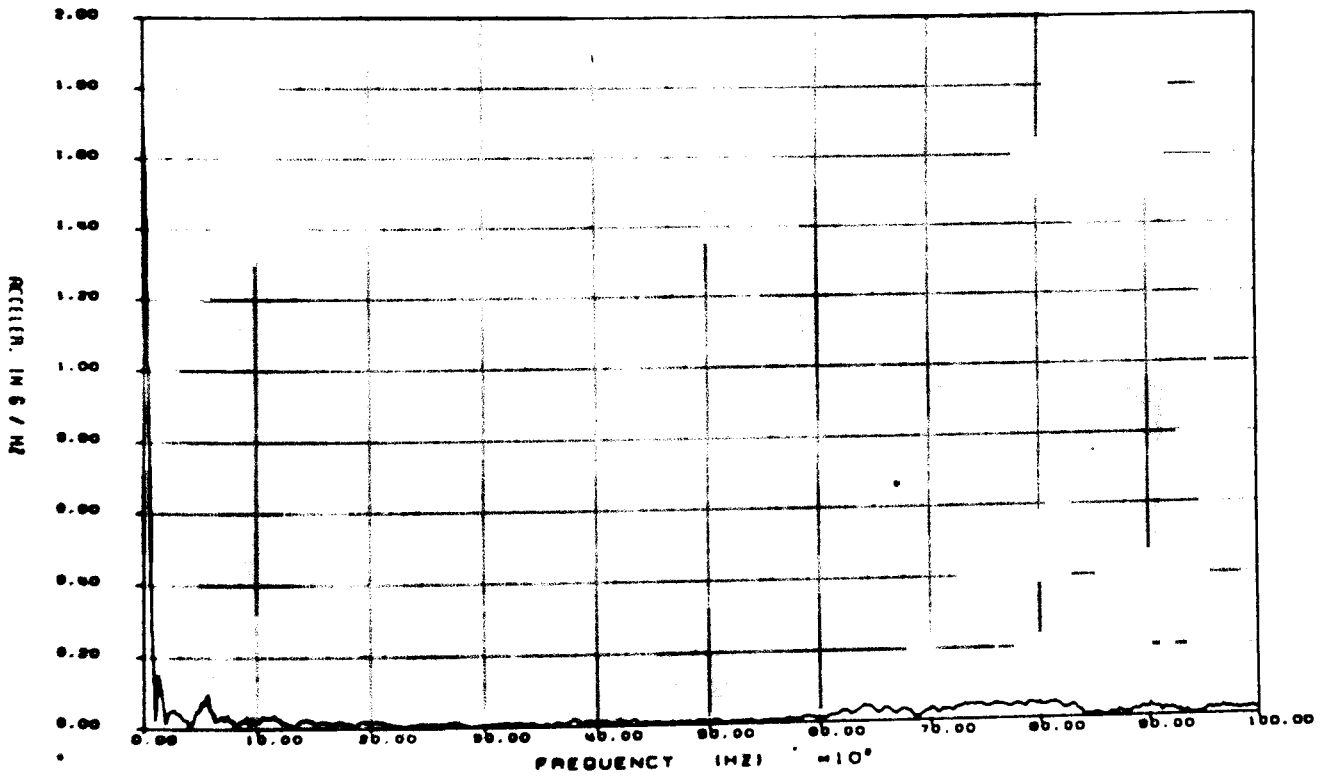


Figure D2-4. Fast Fourier Transform of Raw Data From Gage AX2 for 30-ft Side Drop Test: 0-100 kHz

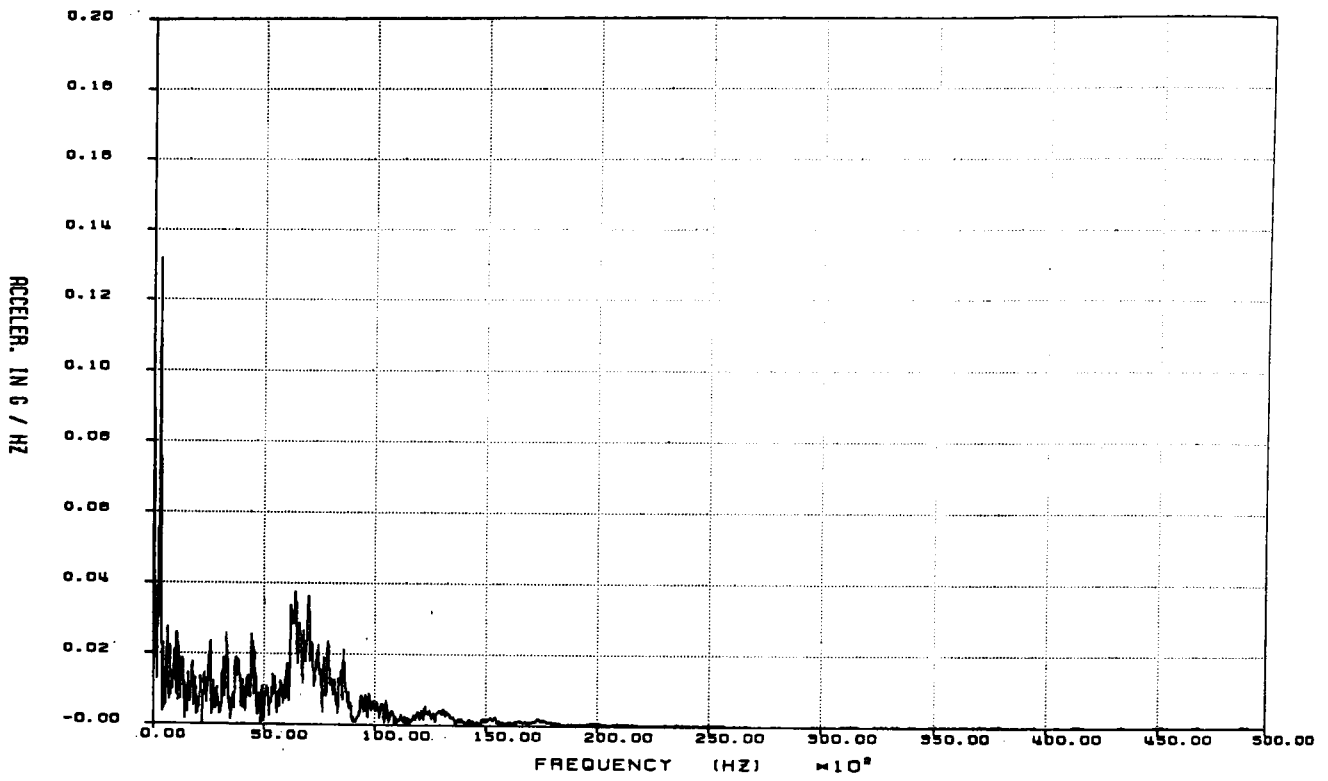


Figure D2-5. Fast Fourier Transform of Raw Data From Gage AY3 for 30-ft Side Drop Test: 0-50 kHz

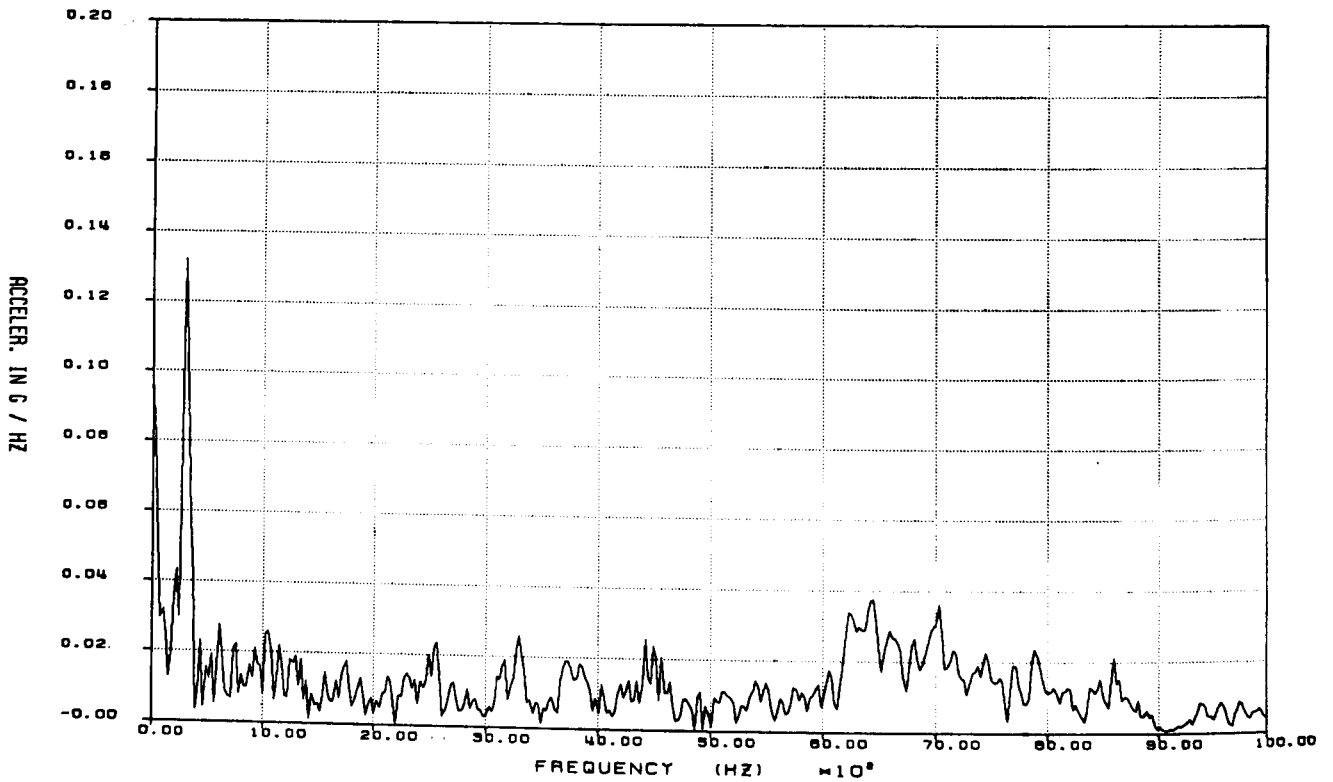


Figure D2-6. Fast Fourier Transform of Raw Data From Gage AY3 for 30-ft Side Drop Test: 0-10 kHz

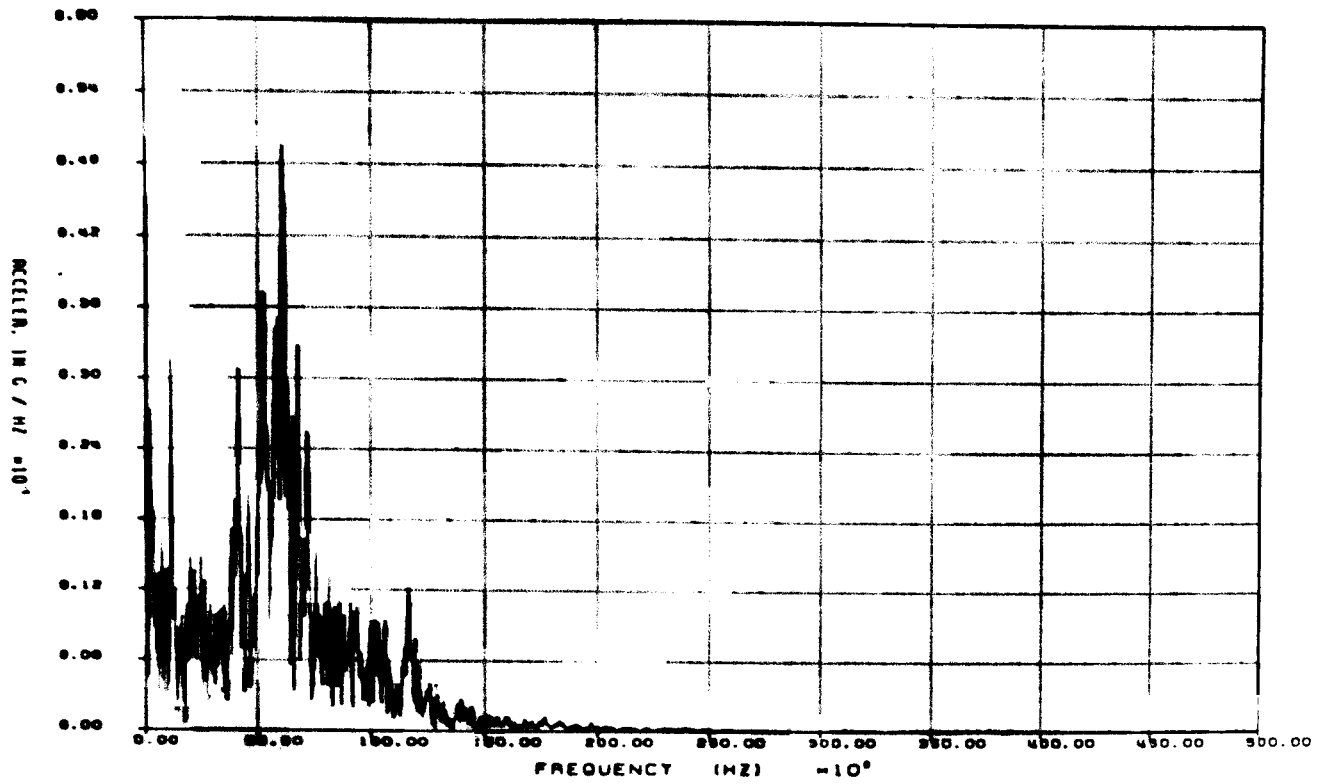


Figure D2-7. Fast Fourier Transform of Raw Data From Gage AZ4 for 30-ft Side Drop Test: 0-50 kHz

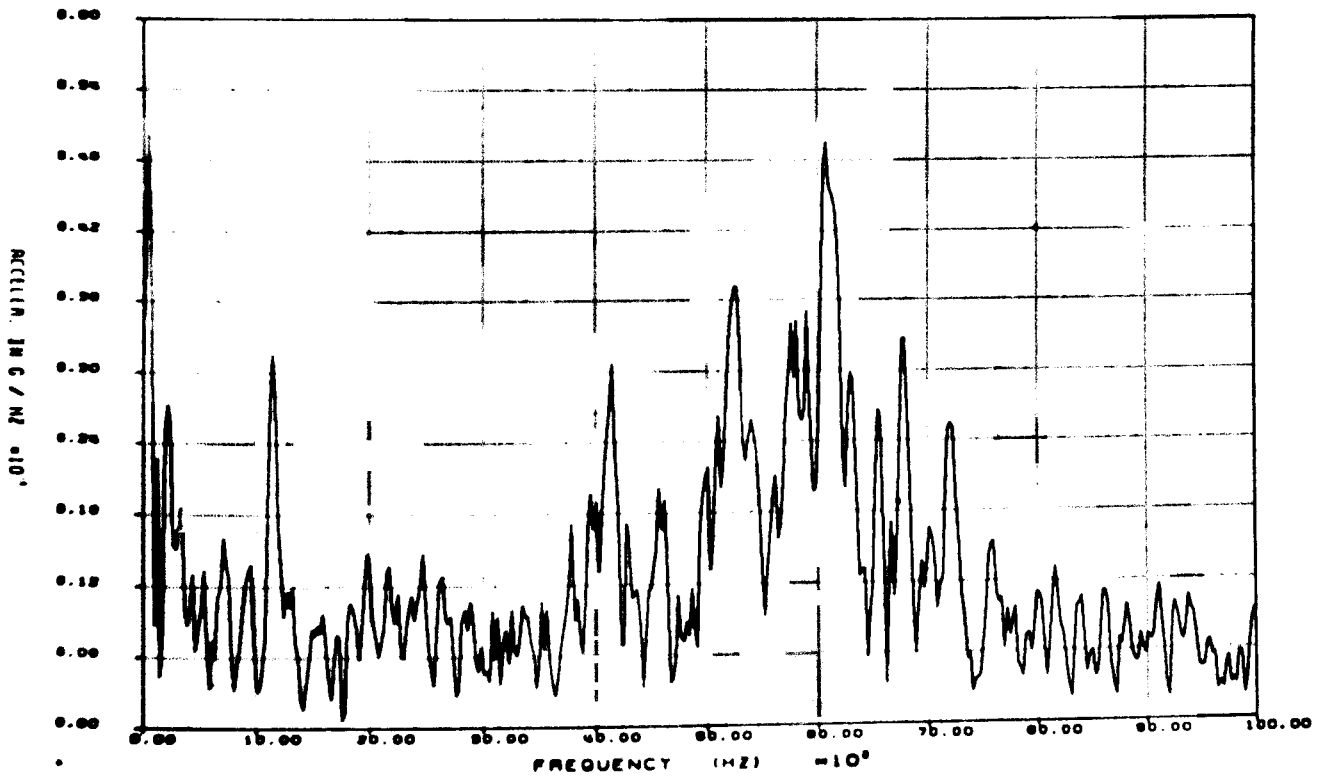


Figure D2-8. Fast Fourier Transform of Raw Data From Gage AZ4 for 30-ft Side Drop Test: 0-10 kHz

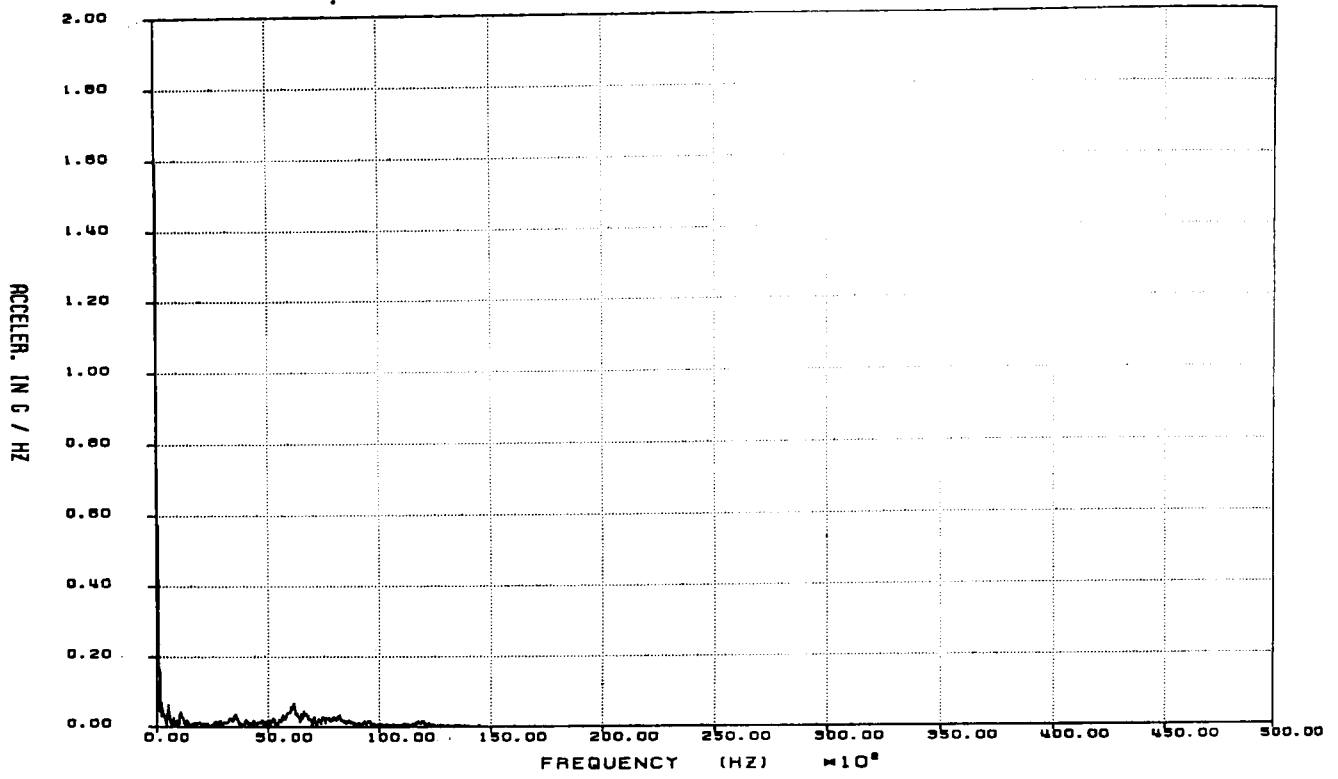


Figure D2-9. Fast Fourier Transform of Raw Data From Gage AX5 for 30-ft Side Drop Test: 0-50 kHz

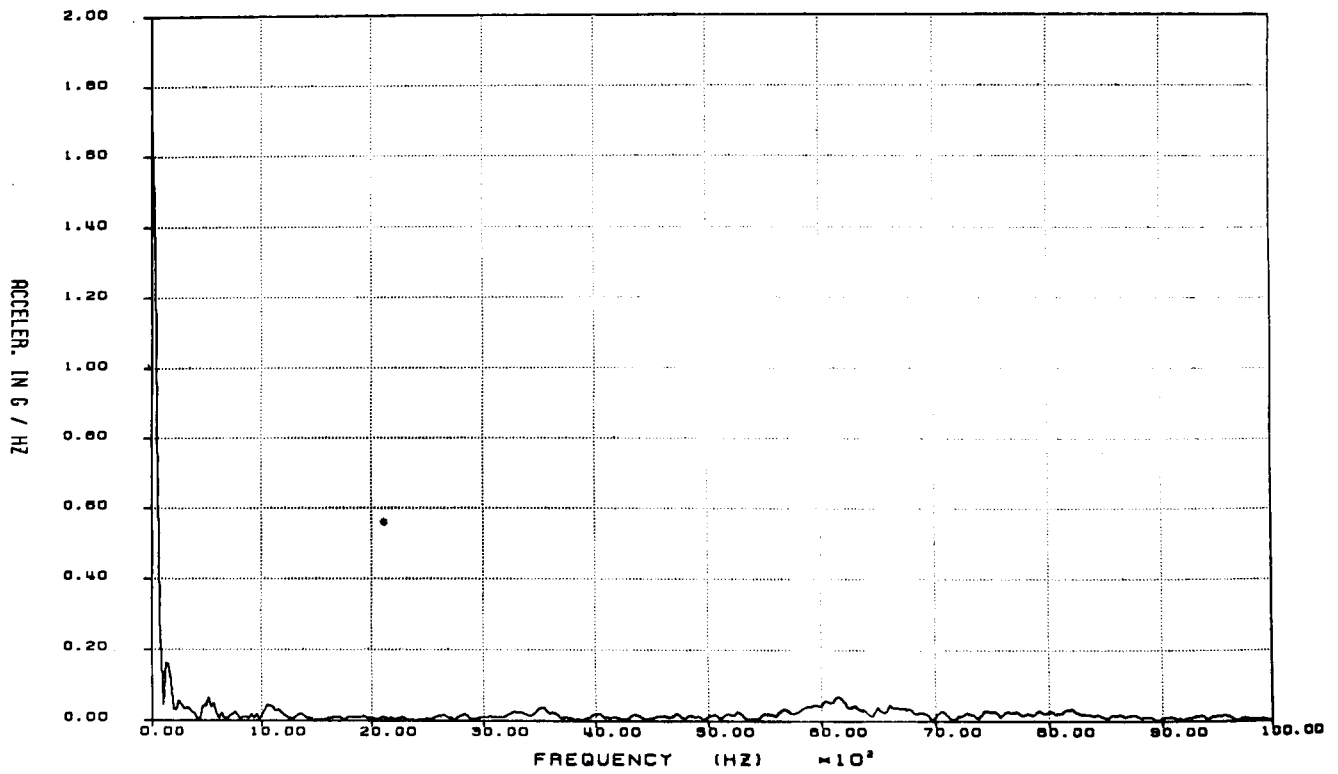


Figure D2-10. Fast Fourier Transform of Raw Data From Gage AX5 for 30-ft Side Drop Test: 0-10 kHz

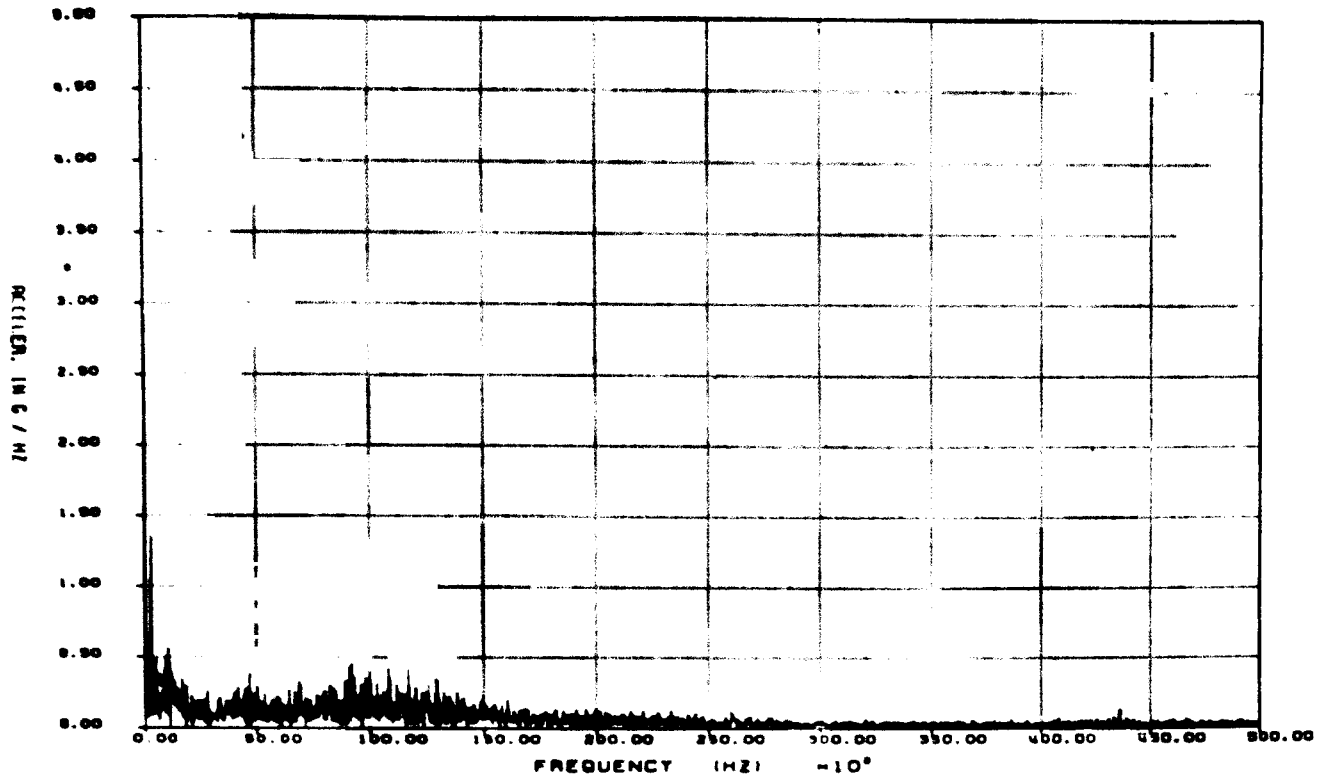


Figure D2-11. Fast Fourier Transform of Raw Data From Gage AY6 for 30 ft Side Drop Test: 0-50 kHz

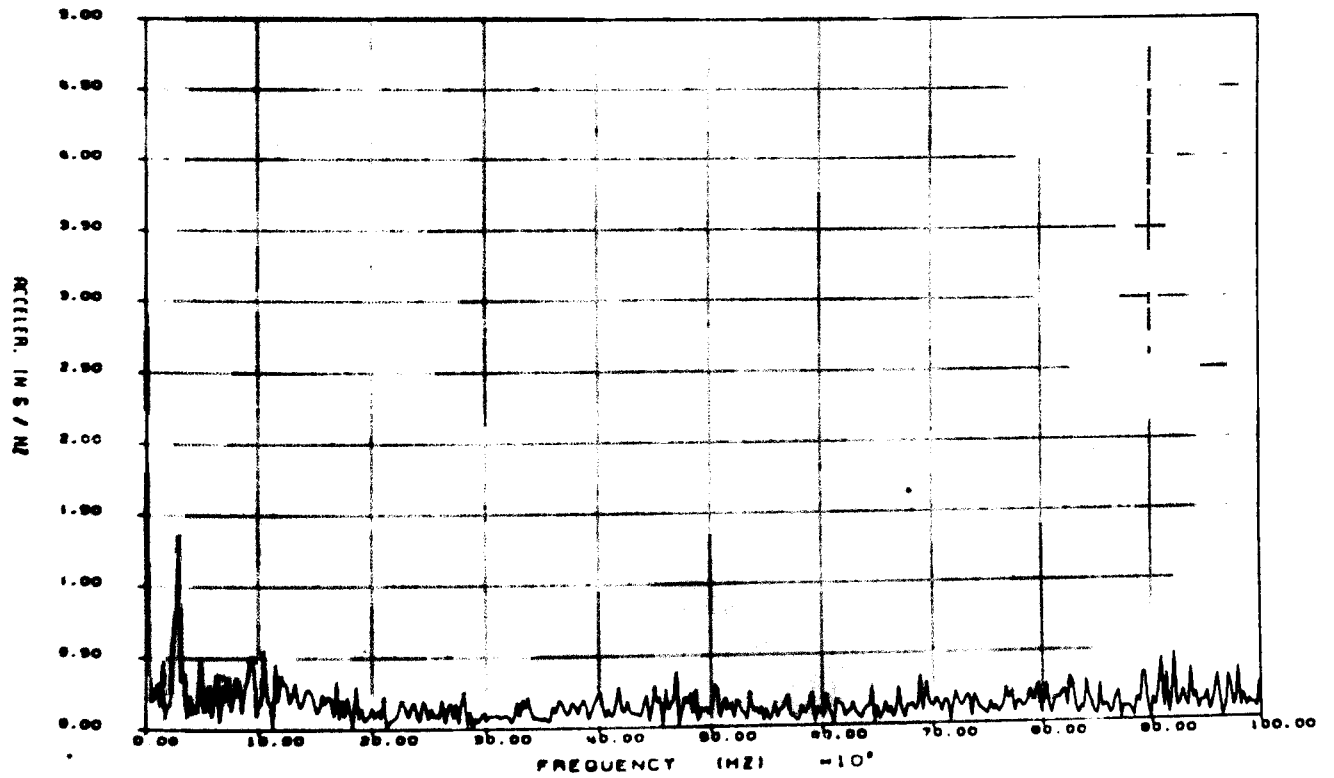


Figure D2-12. Fast Fourier Transform of Raw Data From Gage AY6 for 30 ft Side Drop Test: 0-10 kHz

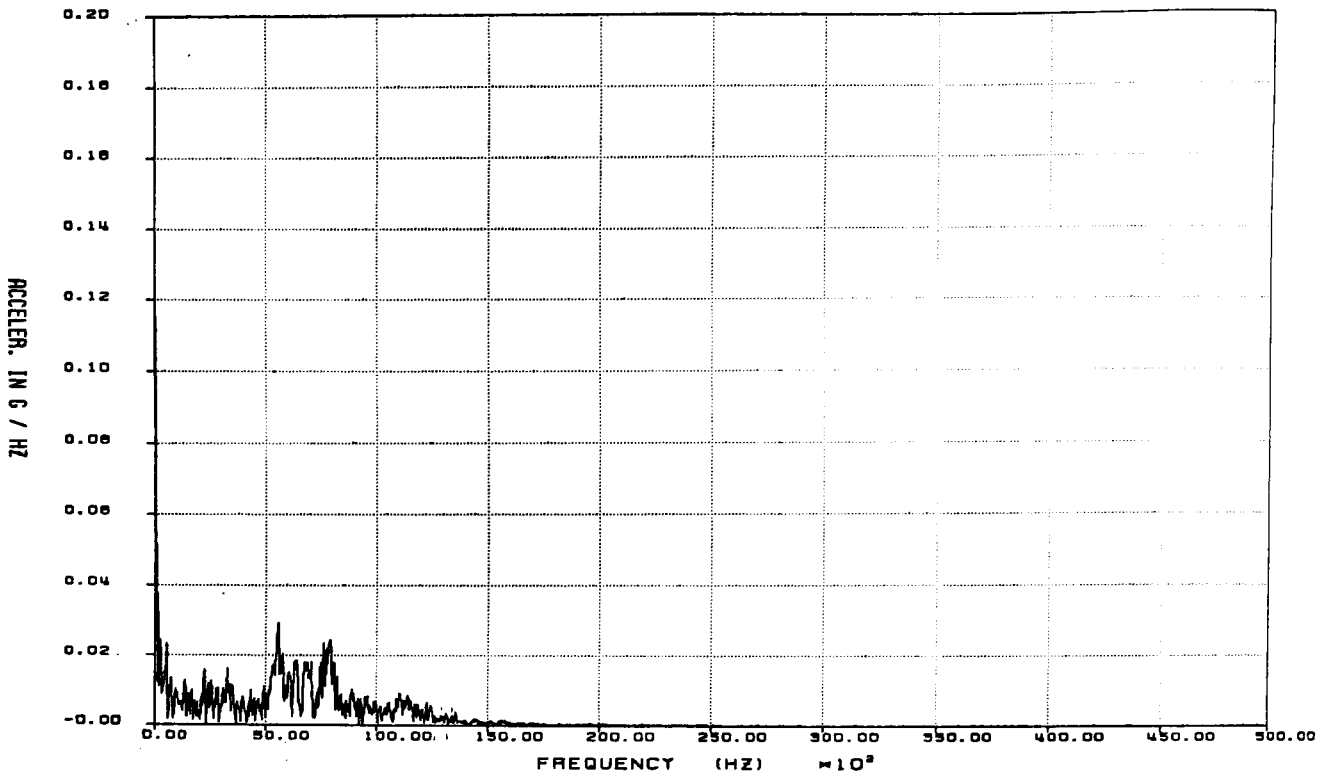


Figure D2-13. Fast Fourier Transform of Raw Data From Gage AZ7 for 30-ft Side Drop Test: 0-50 kHz

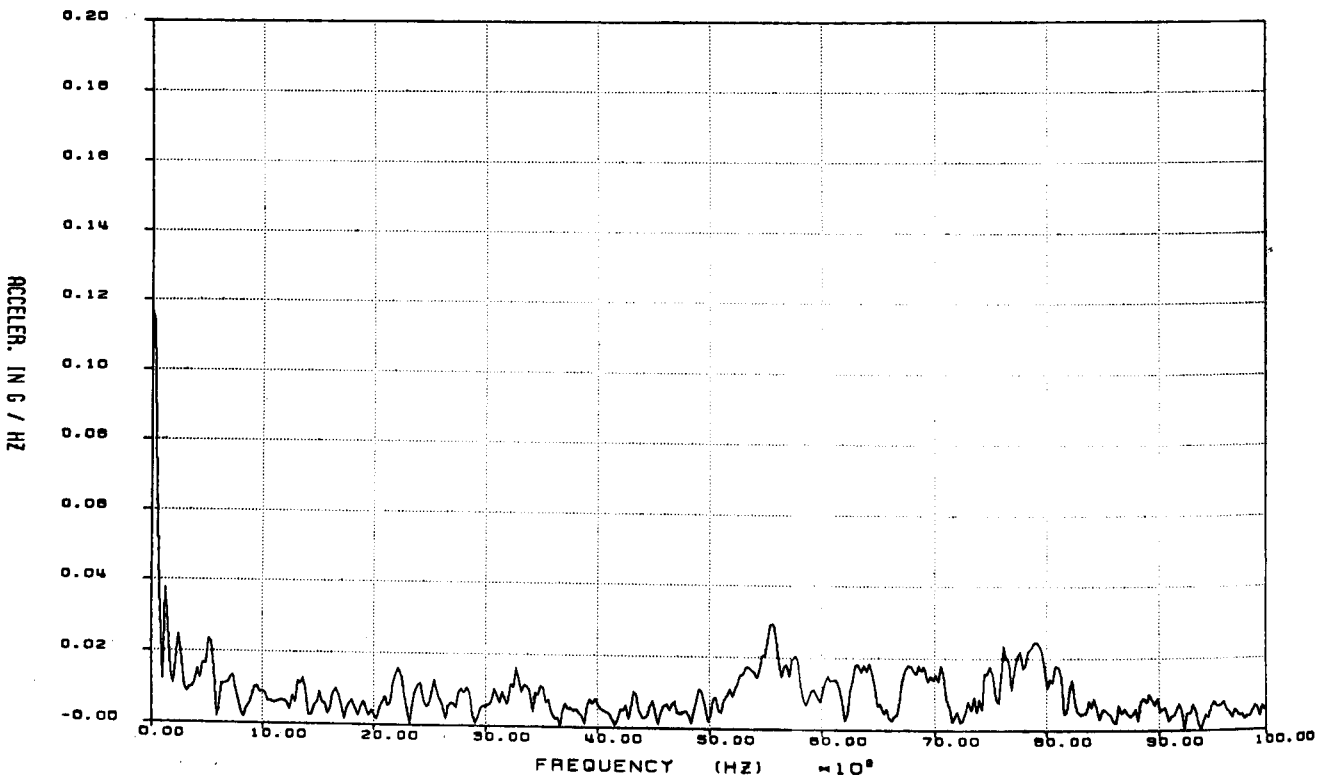


Figure D2-14. Fast Fourier Transform of Raw Data From Gage AZ7 for 30-ft Side Drop Test: 0-10 kHz

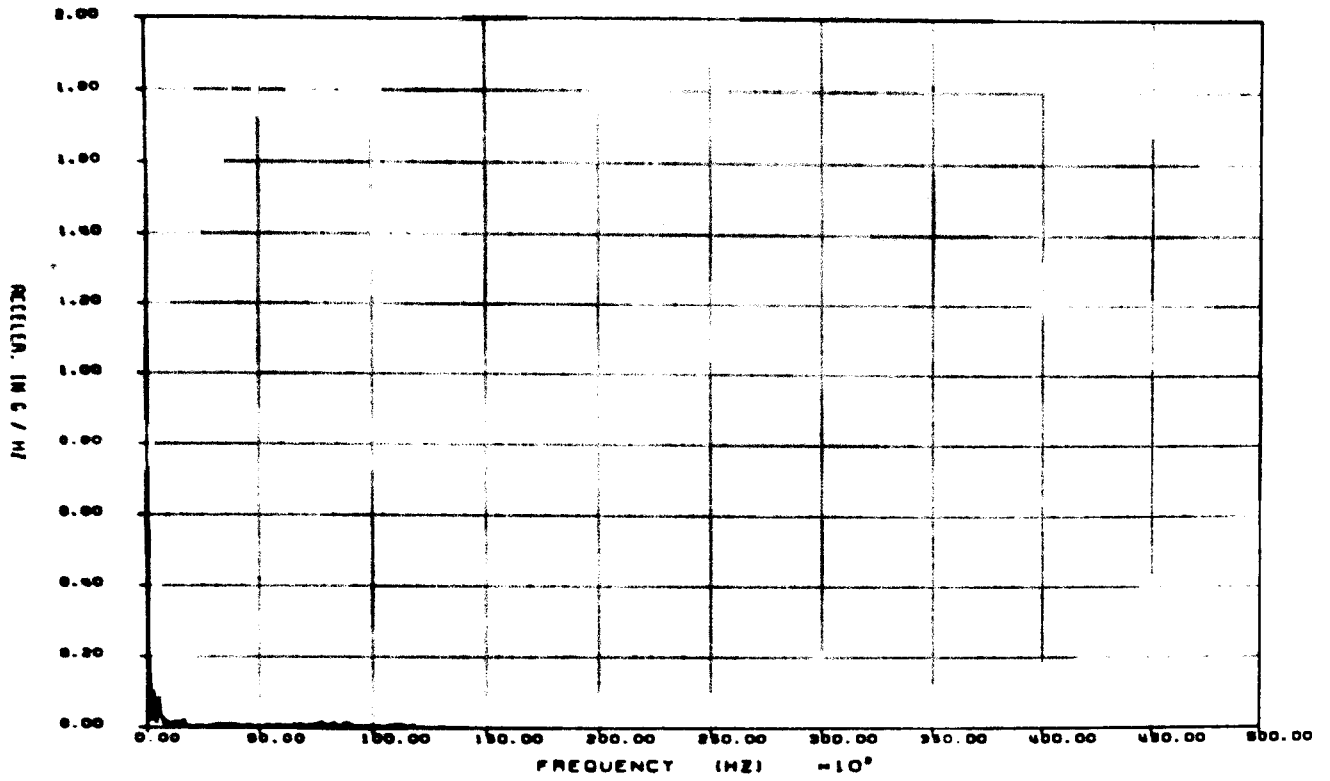


Figure D2-15. Fast Fourier Transform of Raw Data From Gage AX8 for 30-ft Side Drop Test: 0-50 kHz

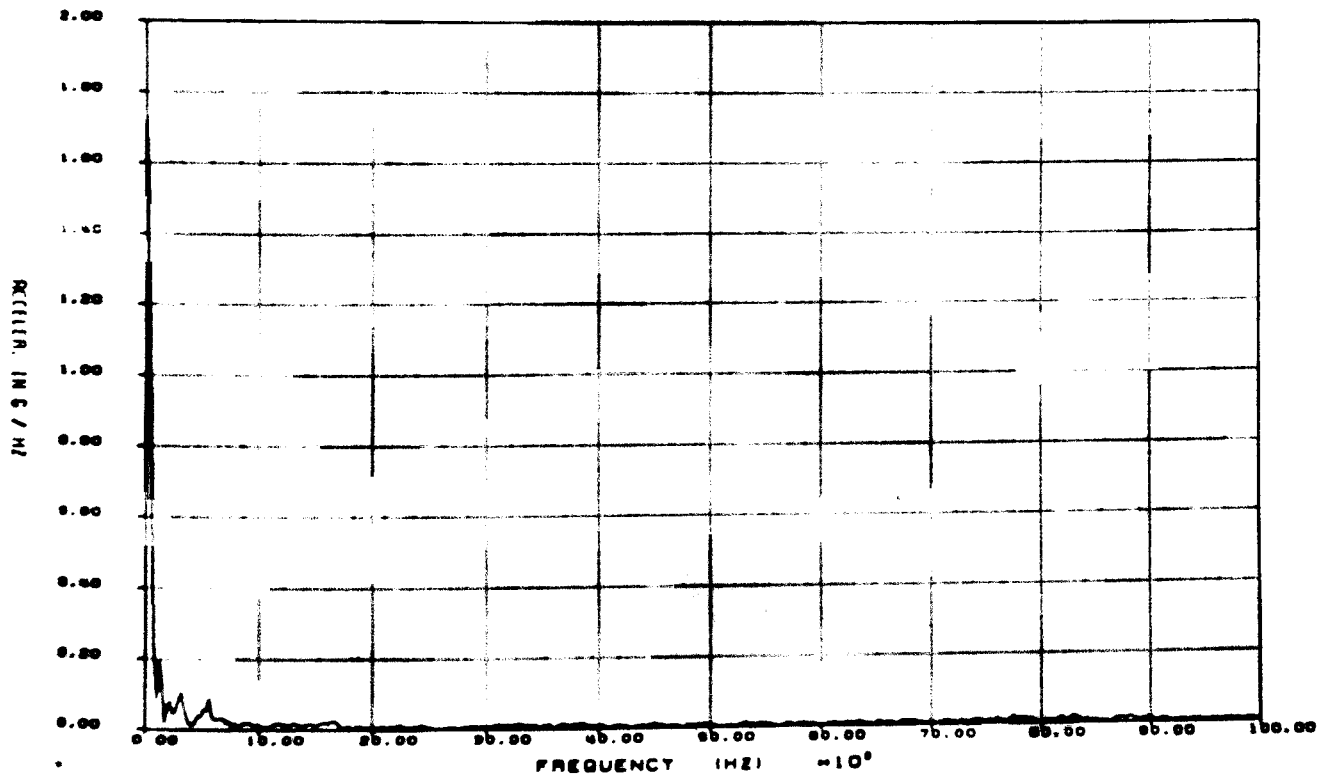


Figure D2-16. Fast Fourier Transform of Raw Data From Gage AX8 for 30-ft Side Drop Test: 0-10 kHz

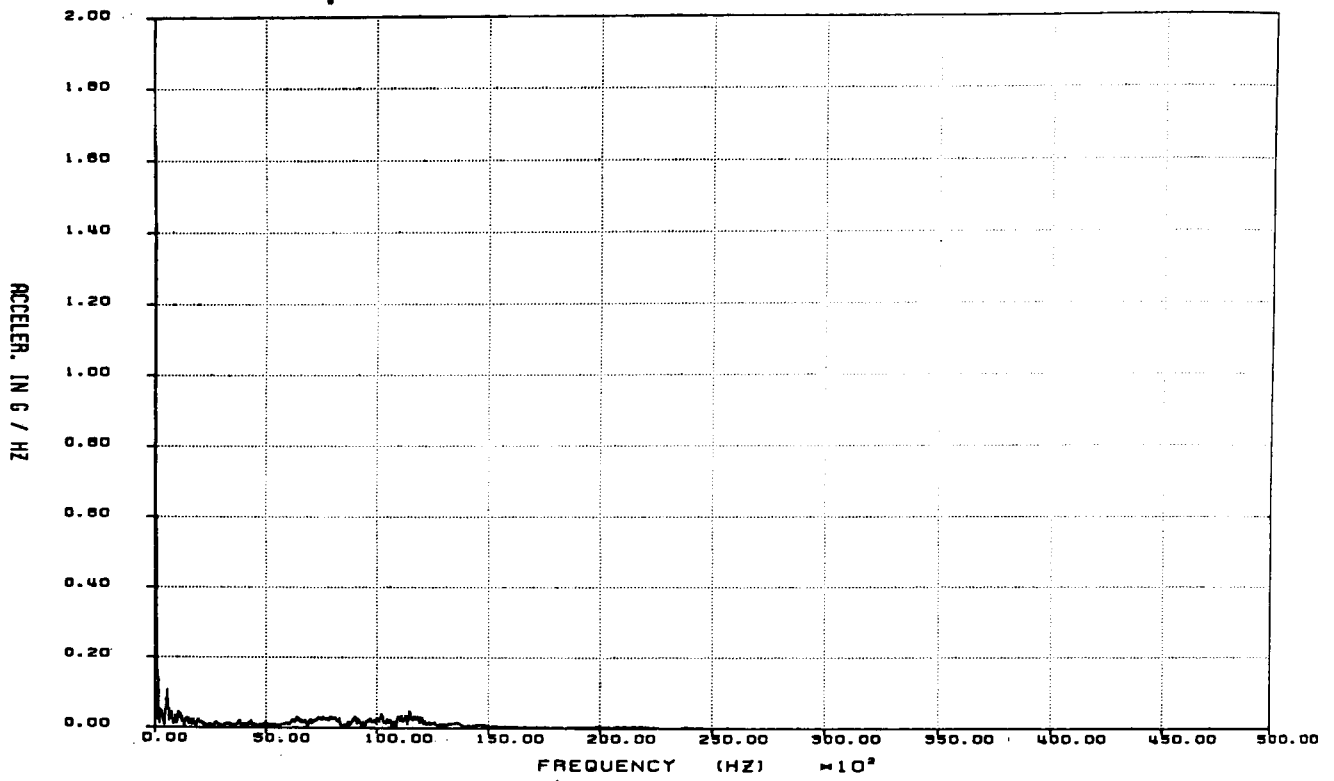


Figure D2-17. Fast Fourier Transform of Raw Data From Gage AX9 for 30-ft Side Drop Test: 0-50 kHz

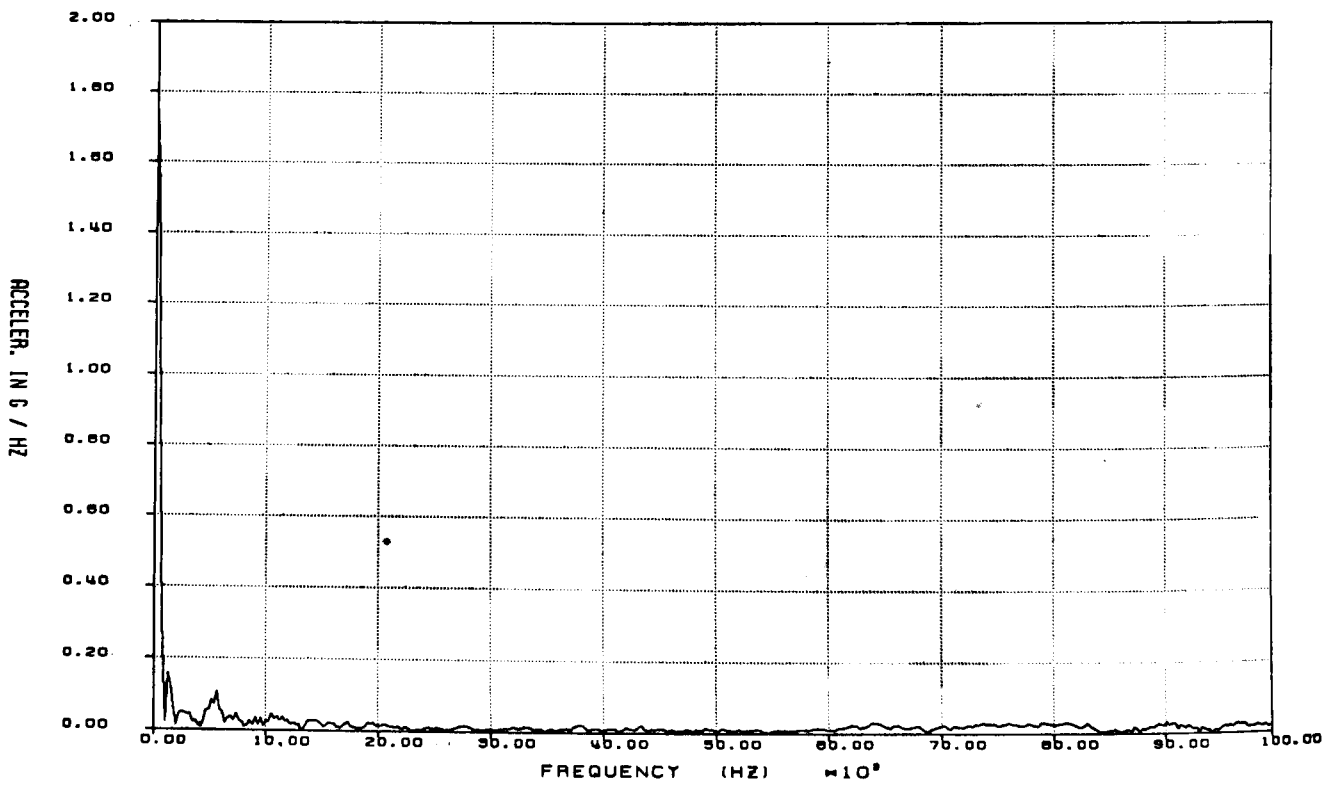


Figure D2-18. Fast Fourier Transform of Raw Data From Gage AX9 for 30-ft Side Drop Test: 0-10 kHz

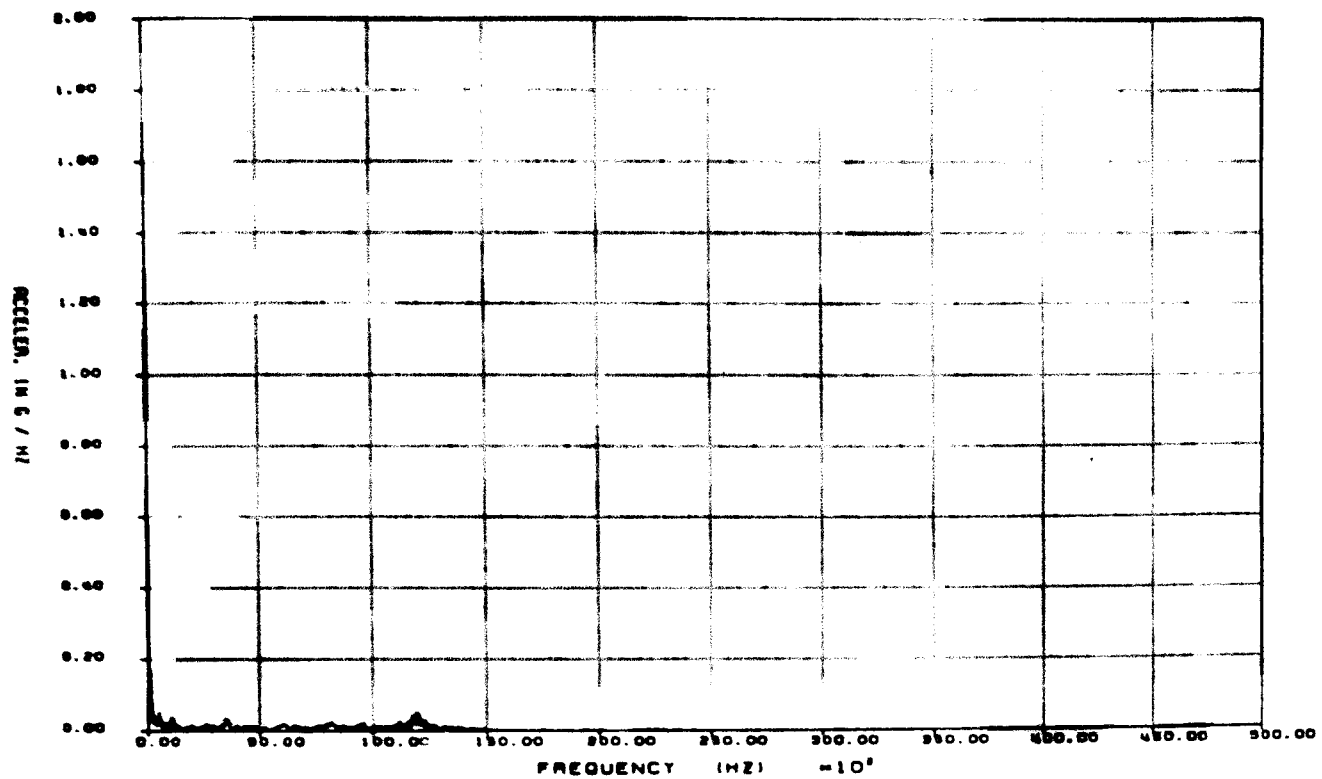


Figure D2-19. Fast Fourier Transform of Raw Data From Gage AX10 for 30-ft Side Drop Test: 0-50 kHz

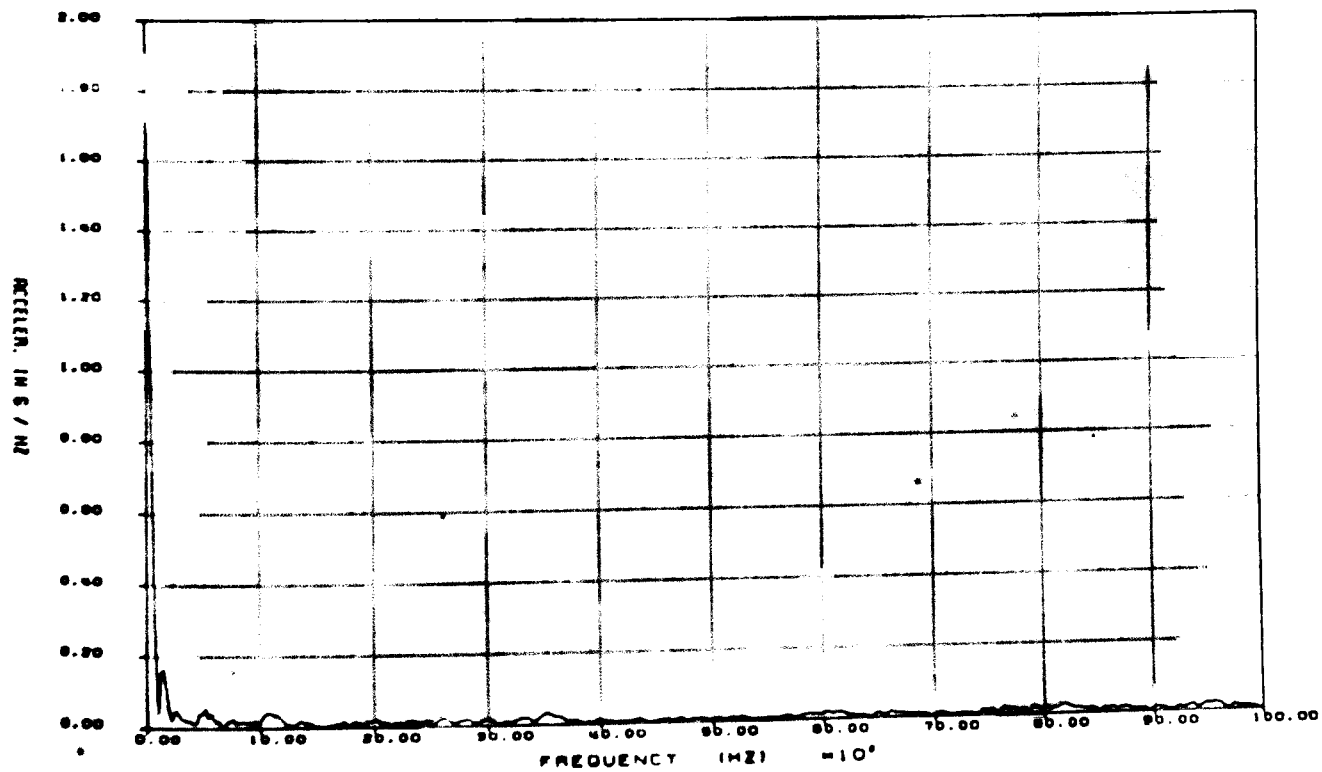


Figure D2-20. Fast Fourier Transform of Raw Data From Gage AX10 for 30-ft Side Drop Test: 0-10 kHz

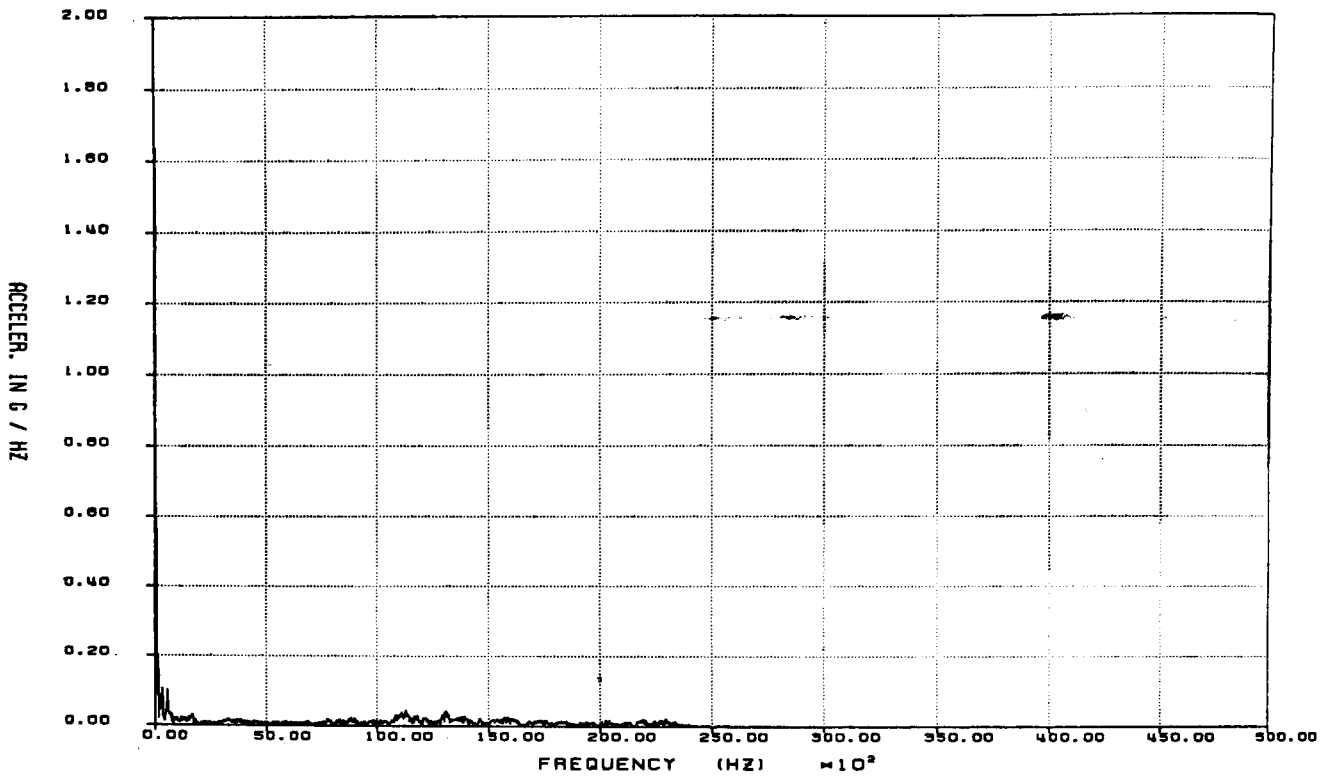


Figure D2-21. Fast Fourier Transform of Raw Data From Gage AX11 for 30-ft Side Drop Test: 0-50 kHz

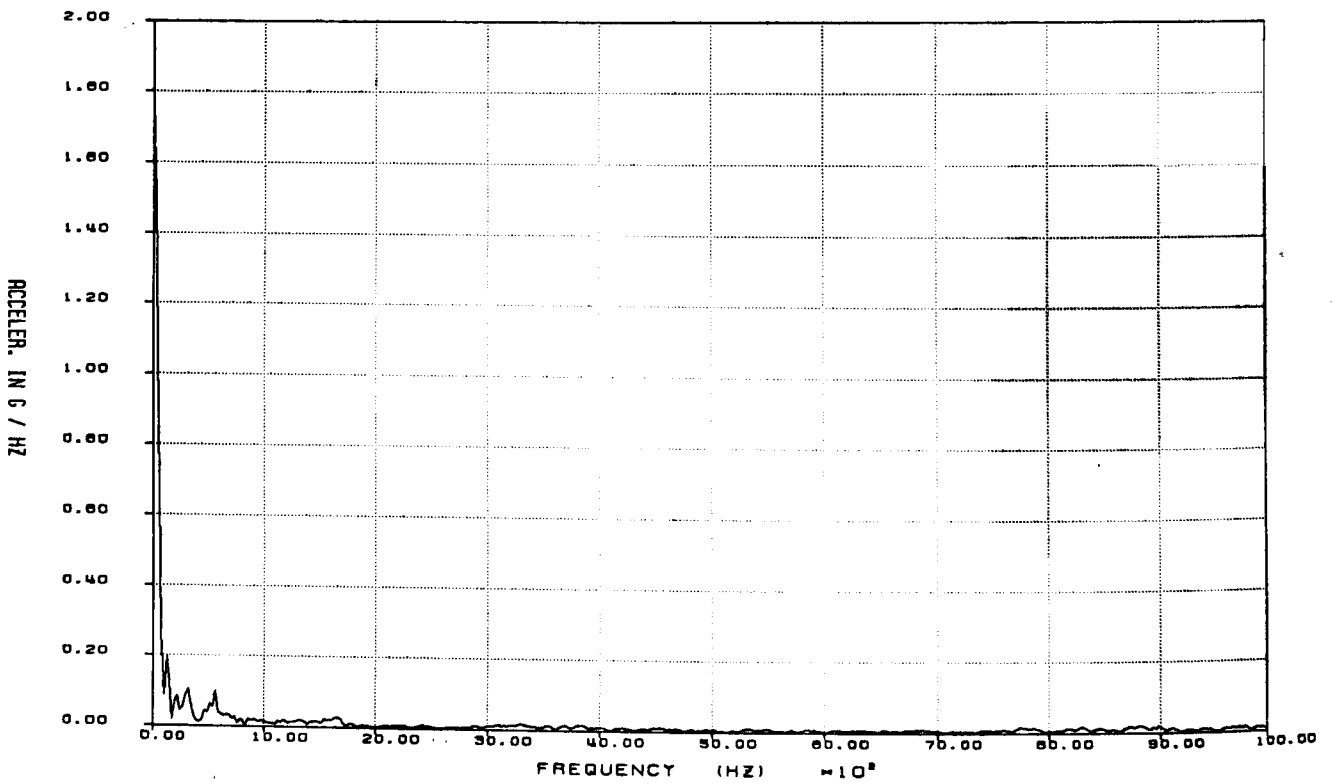


Figure D2-22. Fast Fourier Transform of Raw Data From Gage AX11 for 30-ft Side Drop Test: 0-10 kHz

APPENDIX E1

Accelerometer and Strain Gage Data for the 40-in. Side Puncture Test Filtered at 1000 Hz

Figures

E1-1	Acceleration vs Time for Gage AZ1 for 40-in. Side Puncture Test	232
E1-2	Acceleration vs Time for Gage AX2 for 40-in. Side Puncture Test	232
E1-3	Acceleration vs Time for Gage AY3 for 40-in. Side Puncture Test	233
E1-4	Acceleration vs Time for Gage AZ4 for 40-in. Side Puncture Test	233
E1-5	Acceleration vs Time for Gage AX5 for 40-in. Side Puncture Test	234
E1-6	Acceleration vs Time for Gage AY6 for 40-in. Side Puncture Test	234
E1-7	Acceleration vs Time for Gage AZ7 for 40-in. Side Puncture Test	235
E1-8	Acceleration vs Time for Gage AX8 for 40-in. Side Puncture Test	235
E1-9	Acceleration vs Time for Gage AX9 for 40-in. Side Puncture Test	236
E1-10	Acceleration vs Time for Gage AX10 for 40-in. Side Puncture Test	236
E1-11	Acceleration vs Time for Gage AX11 for 40-in. Side Puncture Test	237
E1-12	Microstrain vs Time for Gage SR1-Y for 40-in. Side Puncture Test	237
E1-13	Microstrain vs Time for Gage SR1-YZ for 40-in. Side Puncture Test	238
E1-14	Microstrain vs Time for Gage SR1-Z for 40-in. Side Puncture Test	238
E1-15	Microstrain vs Time for Gage SR2-Y for 40-in. Side Puncture Test	239
E1-16	Microstrain vs Time for Gage SR2-YZ for 40-in. Side Puncture Test	239
E1-17	Microstrain vs Time for Gage SR2-Z for 40-in. Side Puncture Test	240
E1-18	Microstrain vs Time for Gage SR3-Y for 40-in. Side Puncture Test	240
E1-19	Microstrain vs Time for Gage SR3-YZ for 40-in. Side Puncture Test	241
E1-20	Microstrain vs Time for Gage SR3-Z for 40-in. Side Puncture Test	241
E1-21	Microstrain vs Time for Gage SR4-Y for 40-in. Side Puncture Test	242
E1-22	Microstrain vs Time for Gage SR4-YZ for 40-in. Side Puncture Test	242
E1-23	Microstrain vs Time for Gage SR4-Z for 40-in. Side Puncture Test	243
E1-24	Microstrain vs Time for Gage SR5-Y for 40-in. Side Puncture Test	243
E1-25	Microstrain vs Time for Gage SR5-YZ for 40-in. Side Puncture Test	244
E1-26	Microstrain vs Time for Gage SR5-Z for 40-in. Side Puncture Test	244

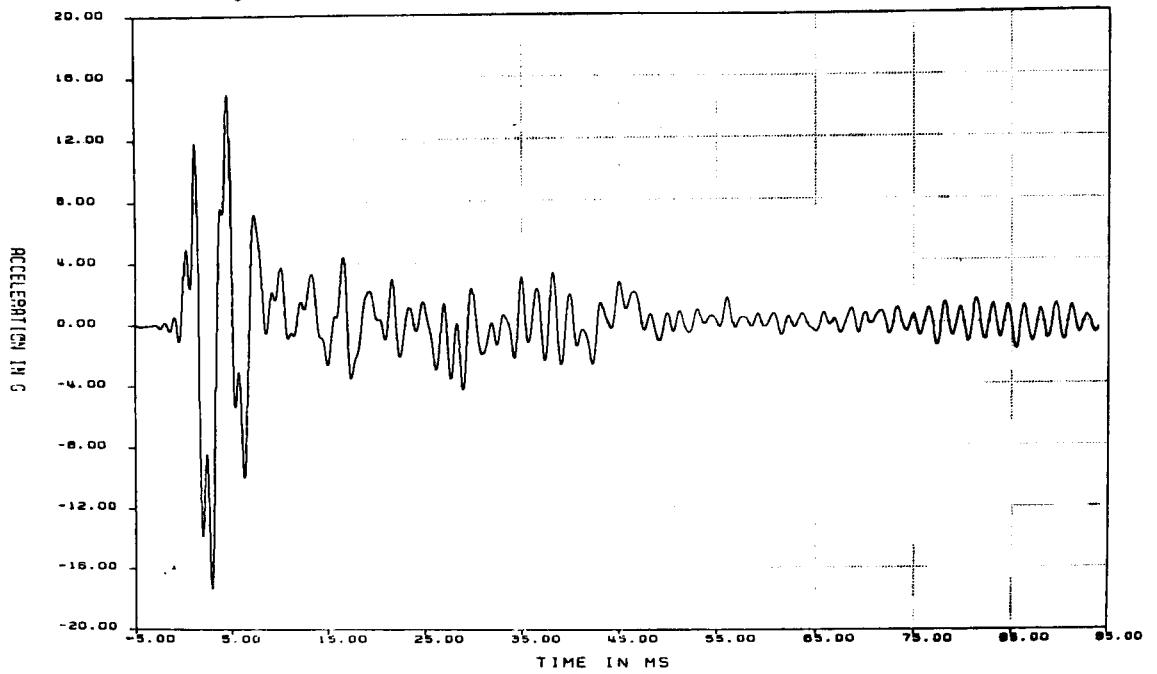


Figure E1-1. Acceleration vs Time for Gage AZ1 for 40-in. Side Puncture Test (filtered at 1000 Hz)

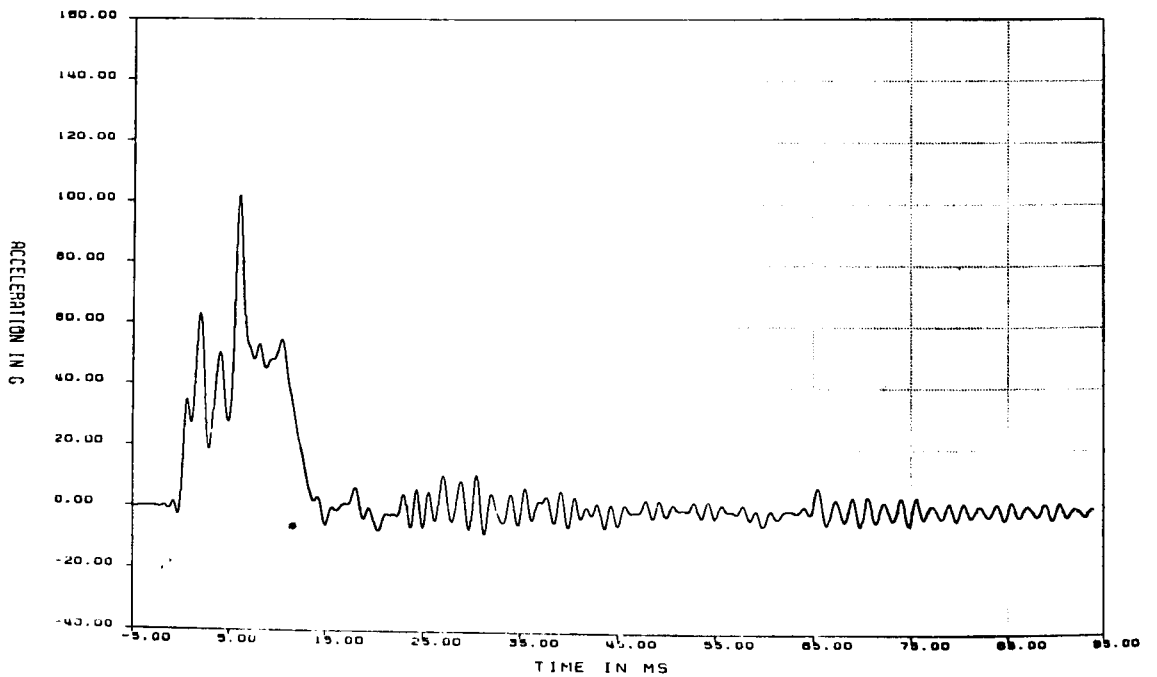


Figure E1-2. Acceleration vs Time for Gage AX2 for 40-in. Side Puncture Test (filtered at 1000 Hz)

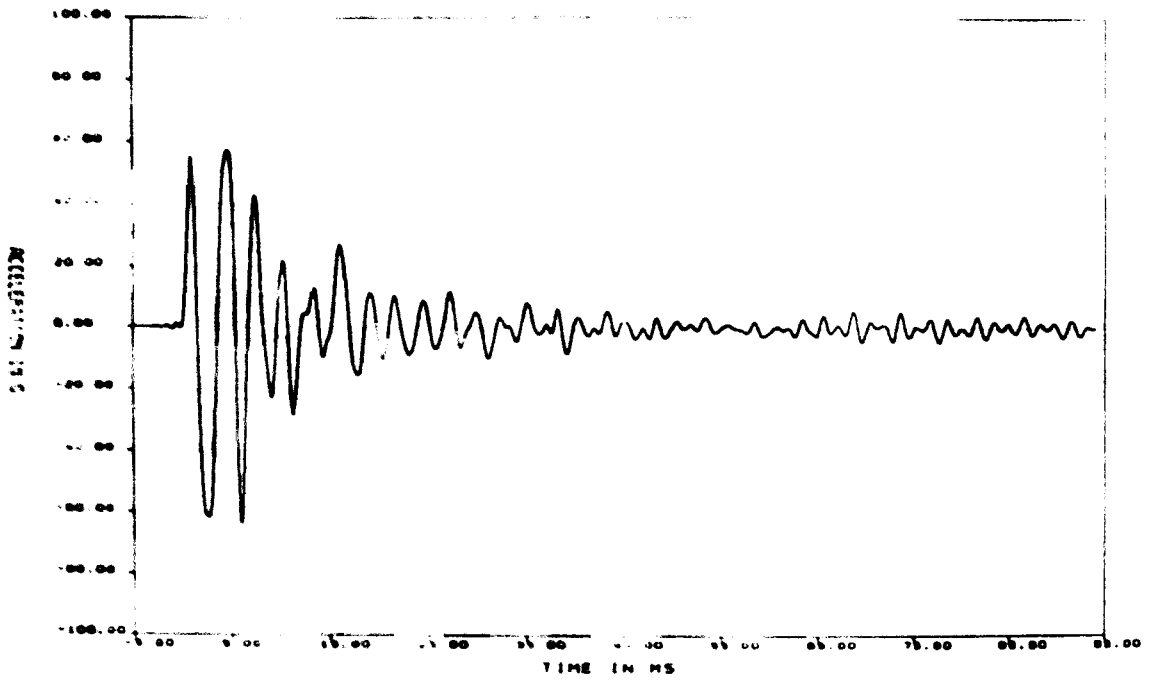


Figure E1-3. Acceleration vs Time for Gage AY3 for 40-in. Side Puncture Test (filtered at 1000 Hz)

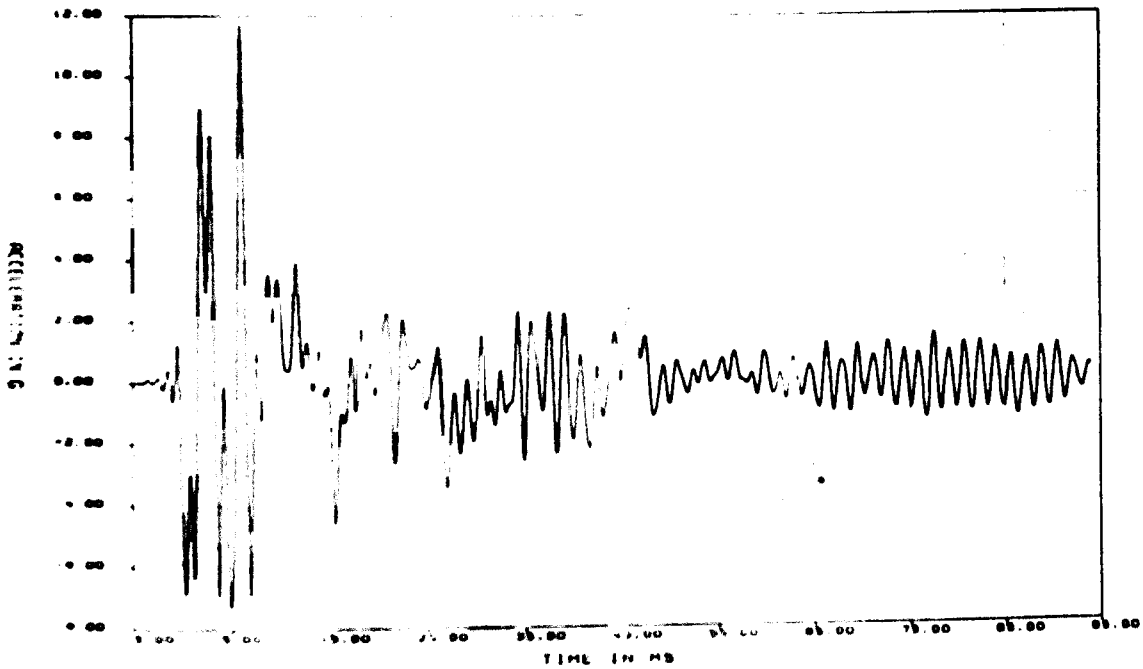


Figure E1-4. Acceleration vs Time for Gage AZA for 40 in. Side Puncture Test (filtered at 1000 Hz)

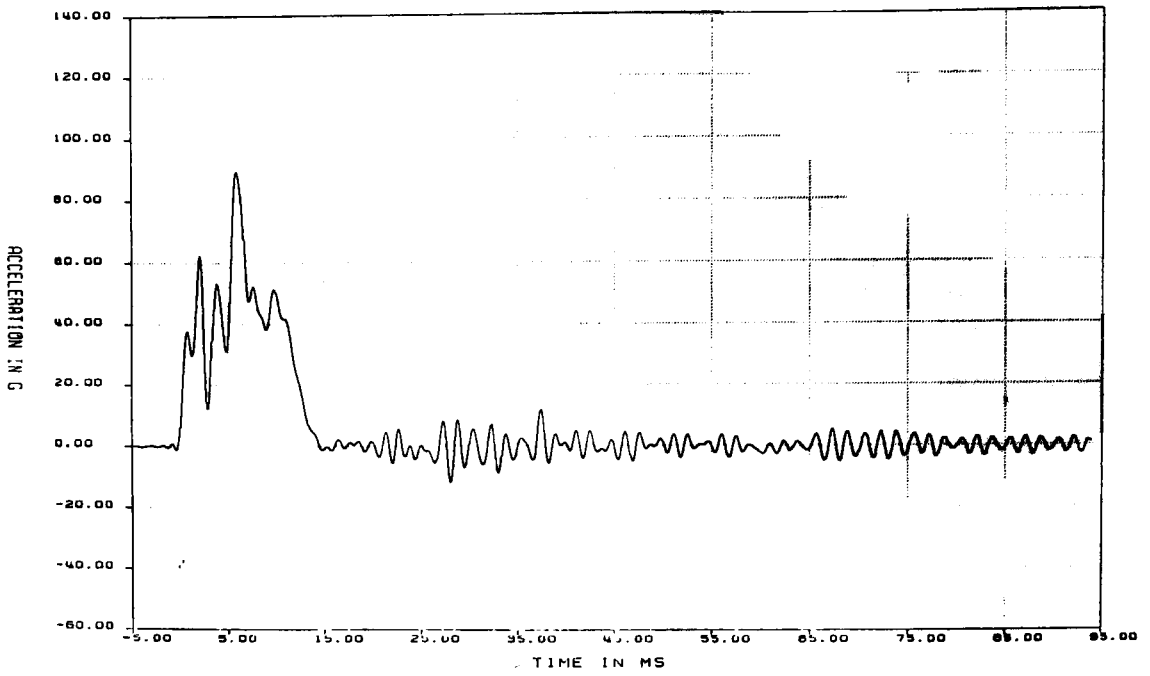


Figure E1-5. Acceleration vs Time for Gage AX5 for 40-in. Side Puncture Test (filtered at 1000 Hz)

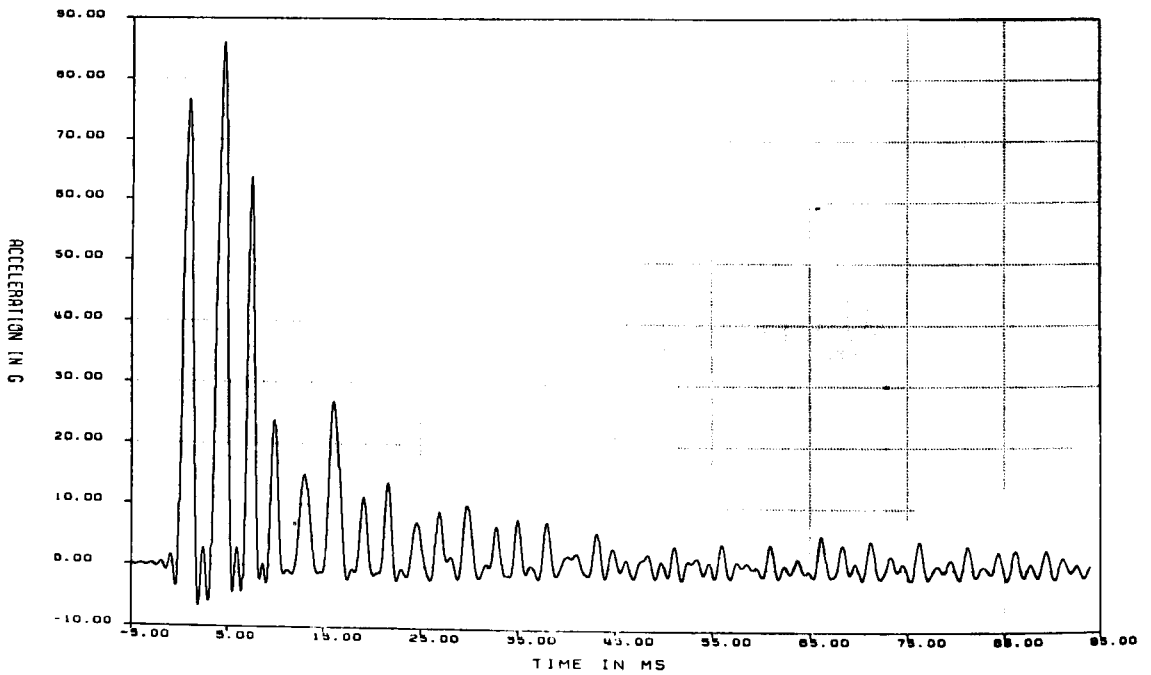


Figure E1-6. Acceleration vs Time for Gage AY6 for 40-in. Side Puncture Test (filtered at 1000 Hz)

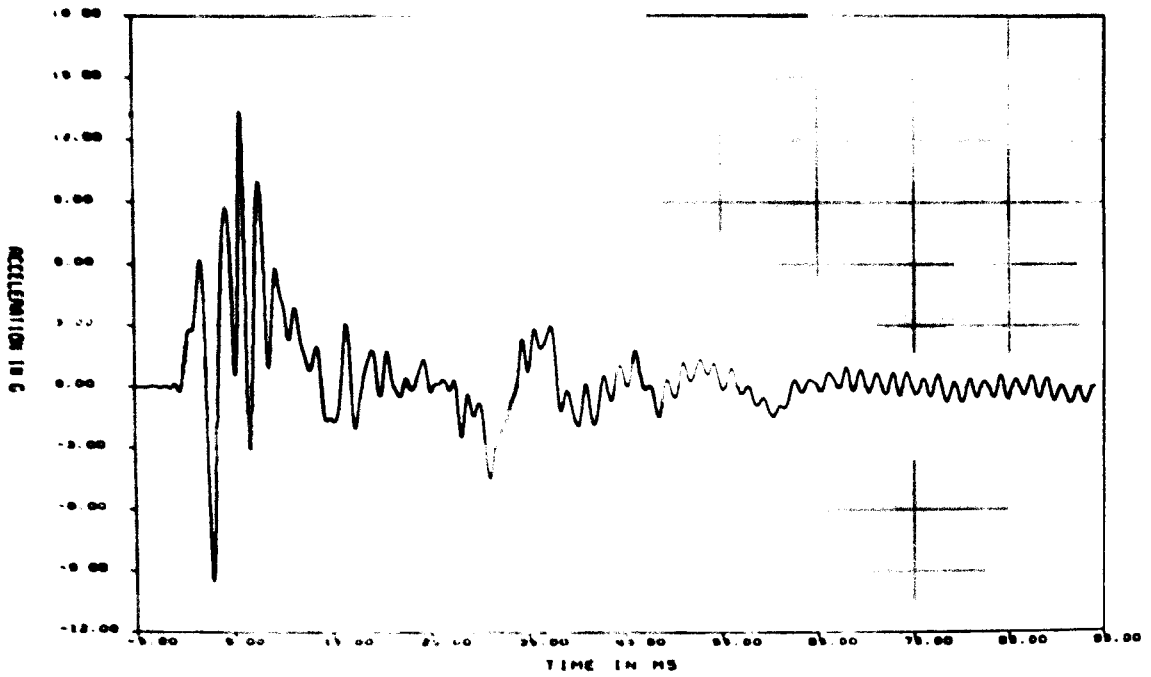


Figure E-1-7. Acceleration vs Time for Gage AZ7 for 40-in. Side Puncture Test (filtered at 1000 Hz)

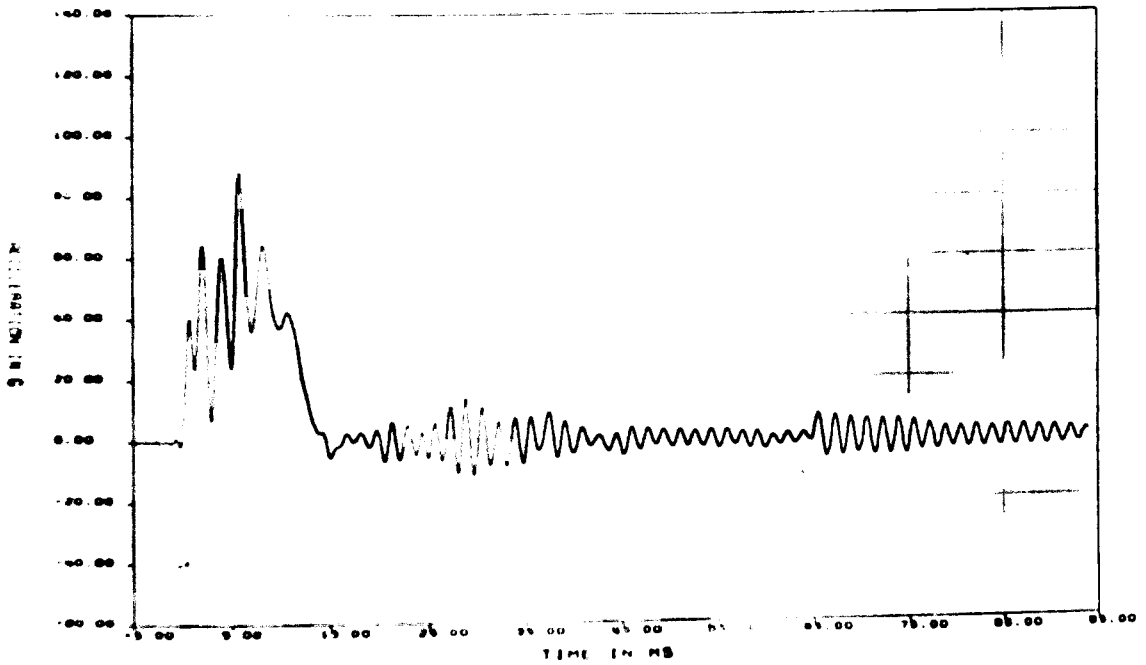


Figure E-1-8. Acceleration vs Time for Gage AX8 for 40-in. Side Puncture Test (filtered at 1000 Hz)

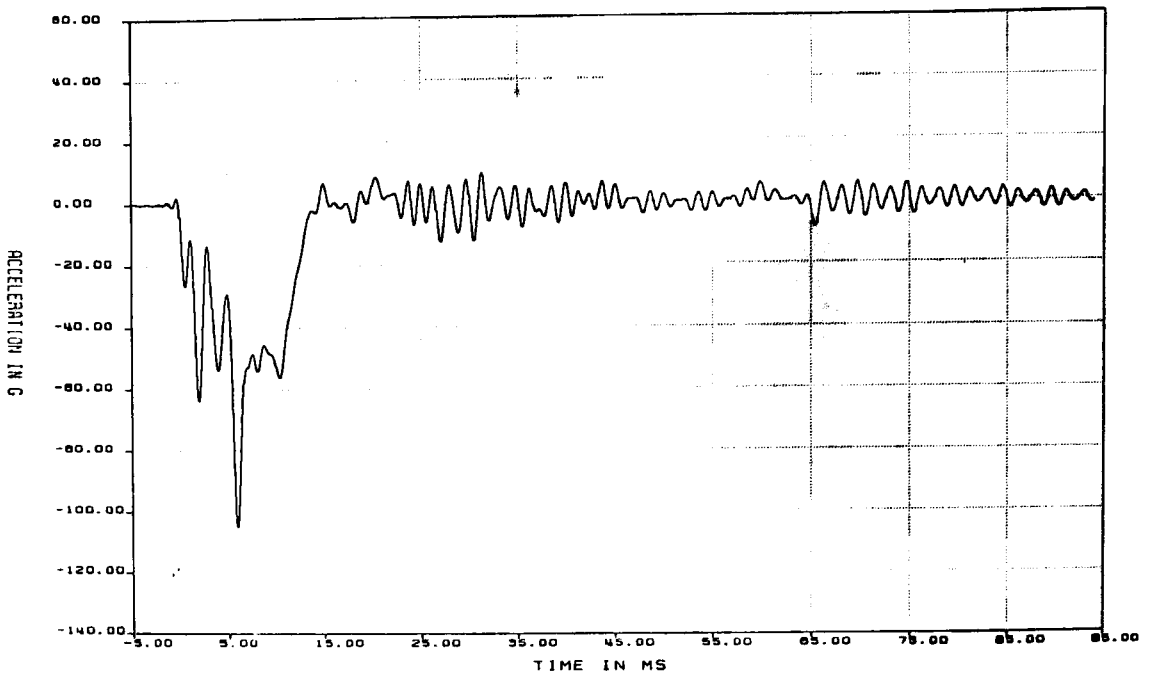


Figure E1-9. Acceleration vs Time for Gage AX9 for 40-in. Side Puncture Test (filtered at 1000 Hz)

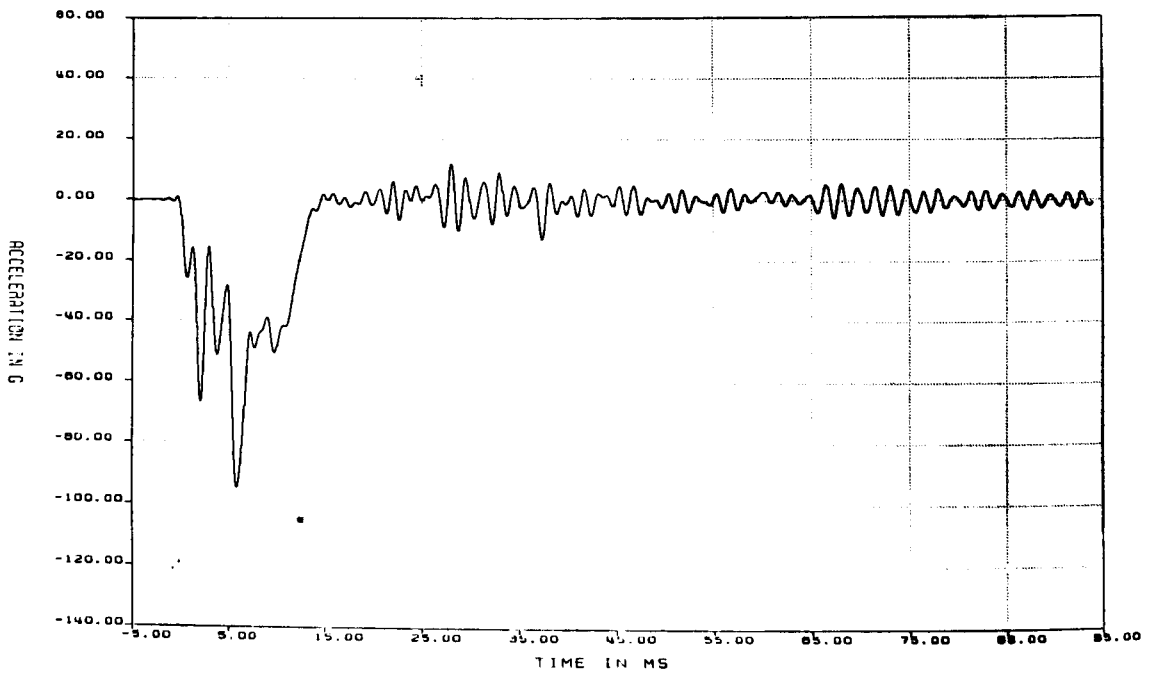


Figure E1-10. Acceleration vs Time for Gage AX10 for 40-in. Side Puncture Test (filtered at 1000 Hz)

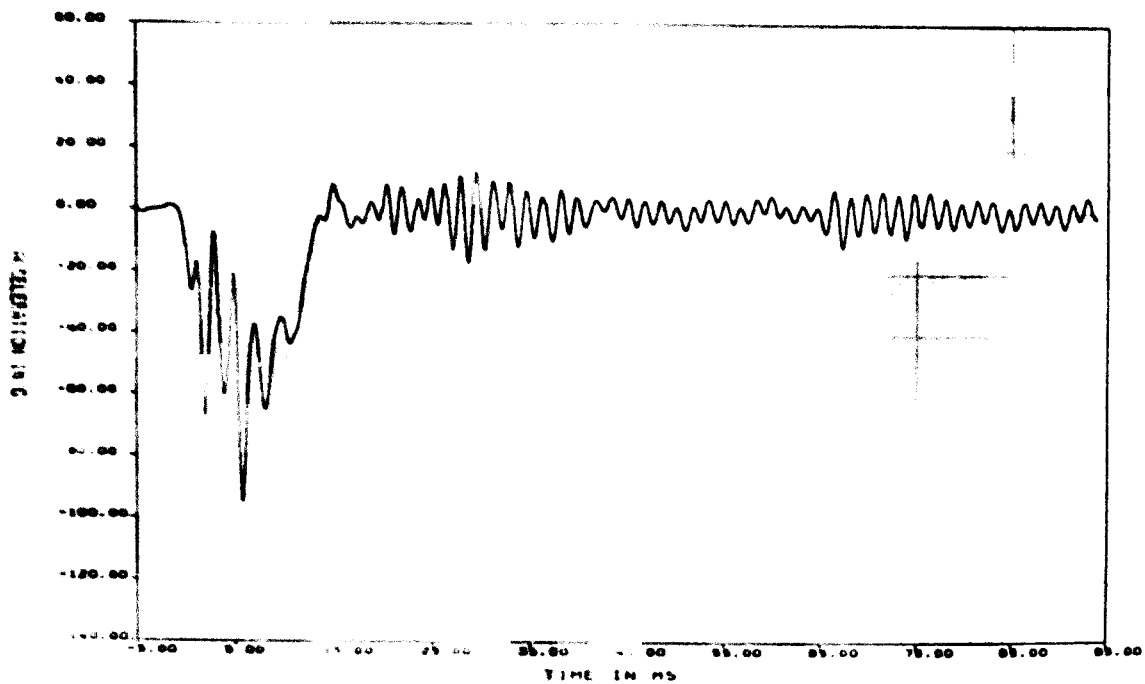


Figure E1-11. Acceleration vs Time for Gage AX11 for 40 in. Side Puncture Test (filtered at 1000 Hz)

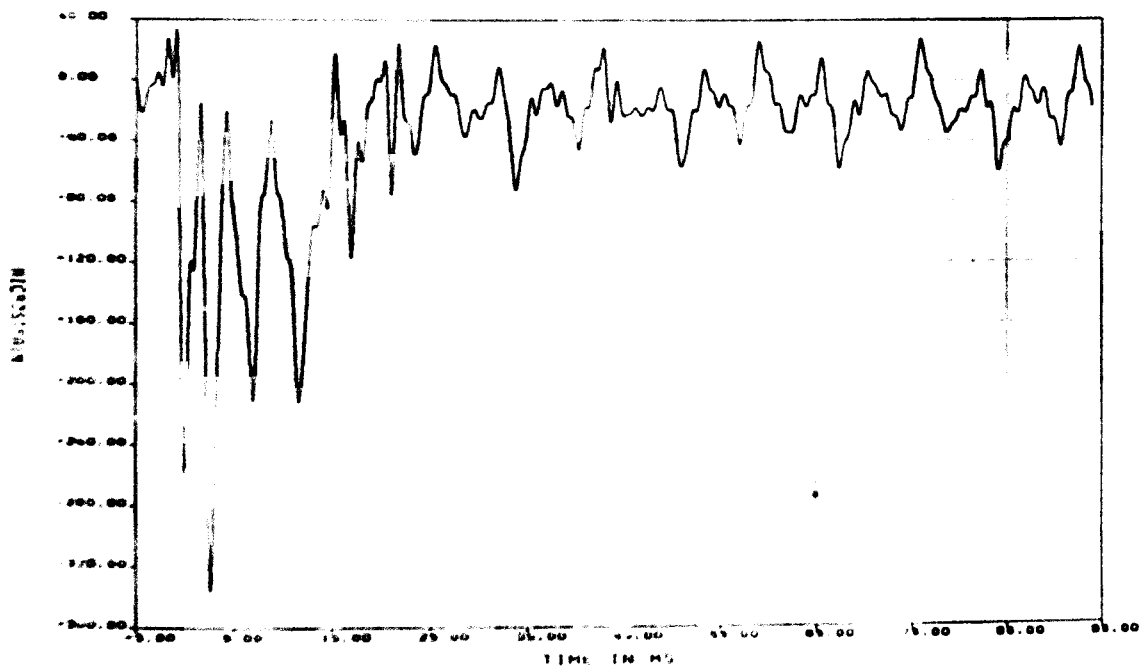


Figure E1-12. Microstrain vs Time for Gage SR1-Y for 40 in. Side Puncture Test (filtered at 1000 Hz)

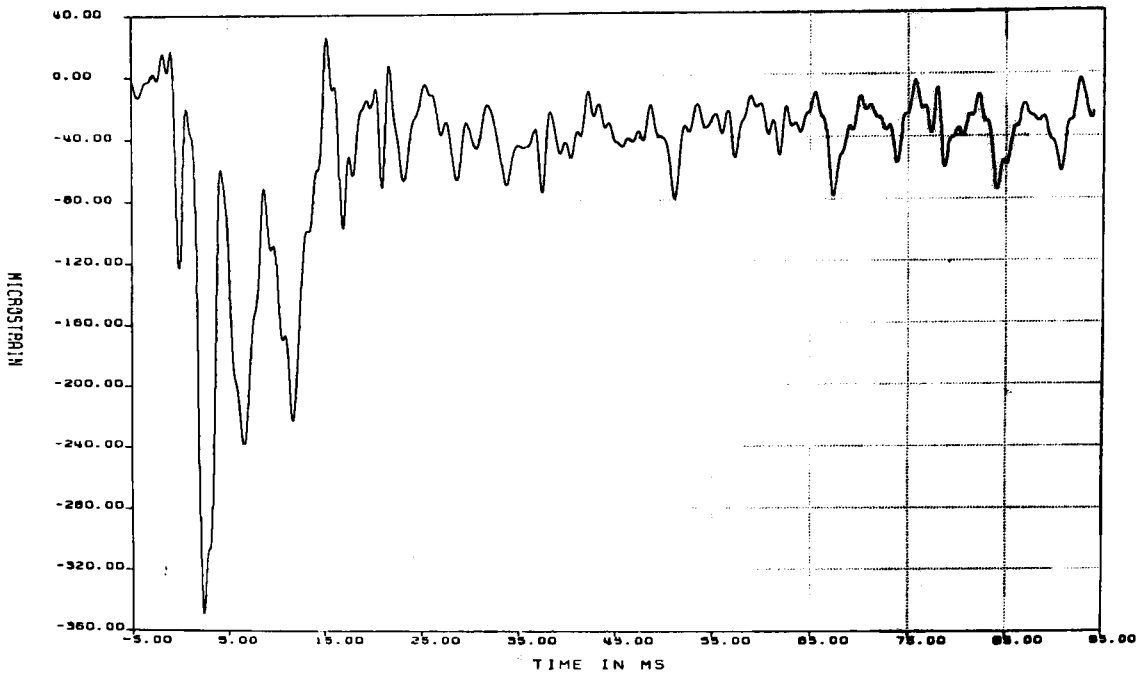


Figure E1-13. Microstrain vs Time for Gage SR1-YZ for 40-in. Side Puncture Test (filtered at 1000 Hz)

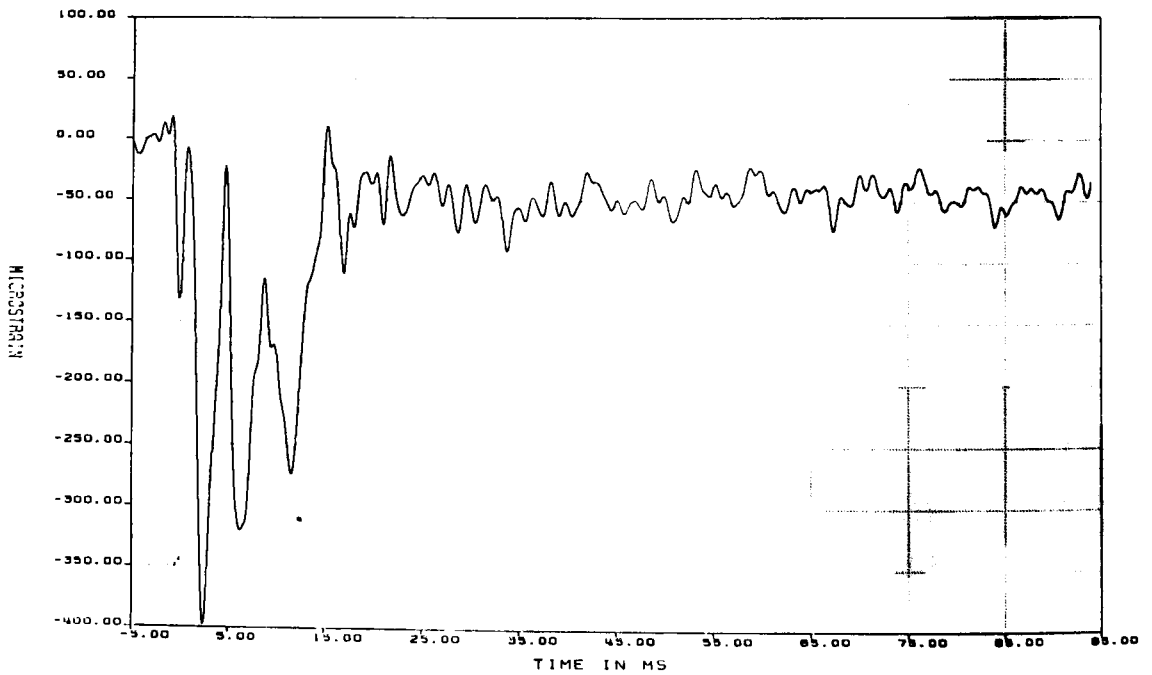


Figure E1-14. Microstrain vs Time for Gage SR1-Z for 40-in. Side Puncture Test (filtered at 1000 Hz)

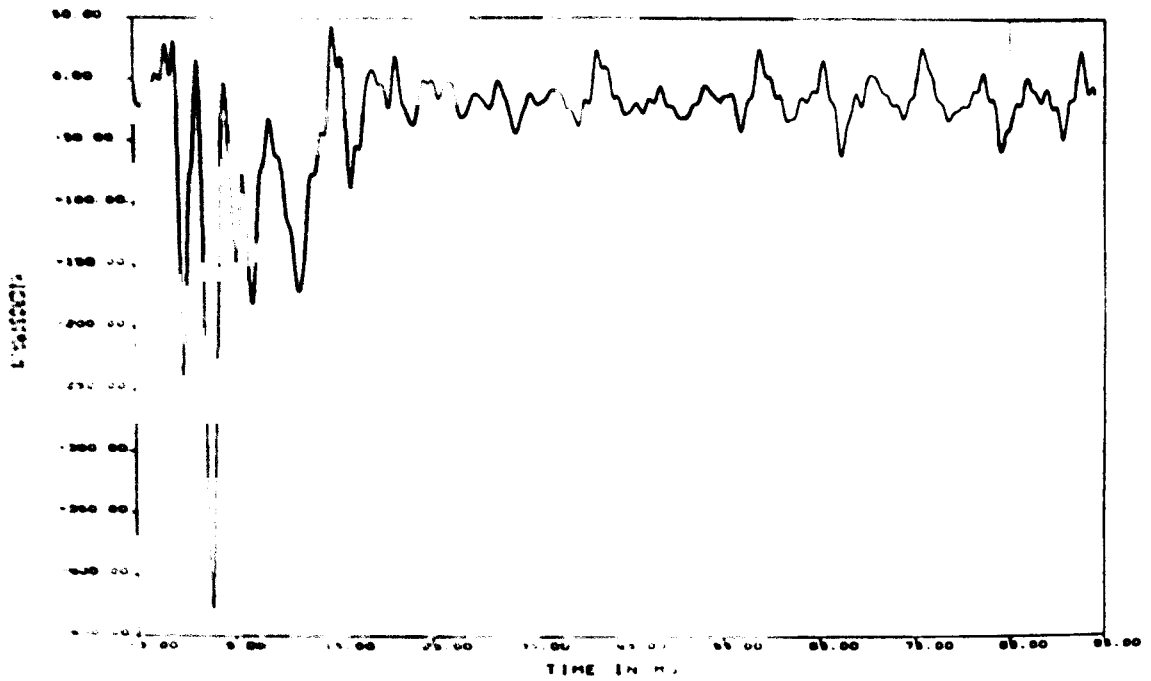


Figure E1-15. Microstrain vs Time for Gage SR2-Y for 40-in. Side Puncture Test (filtered at 1000 Hz)

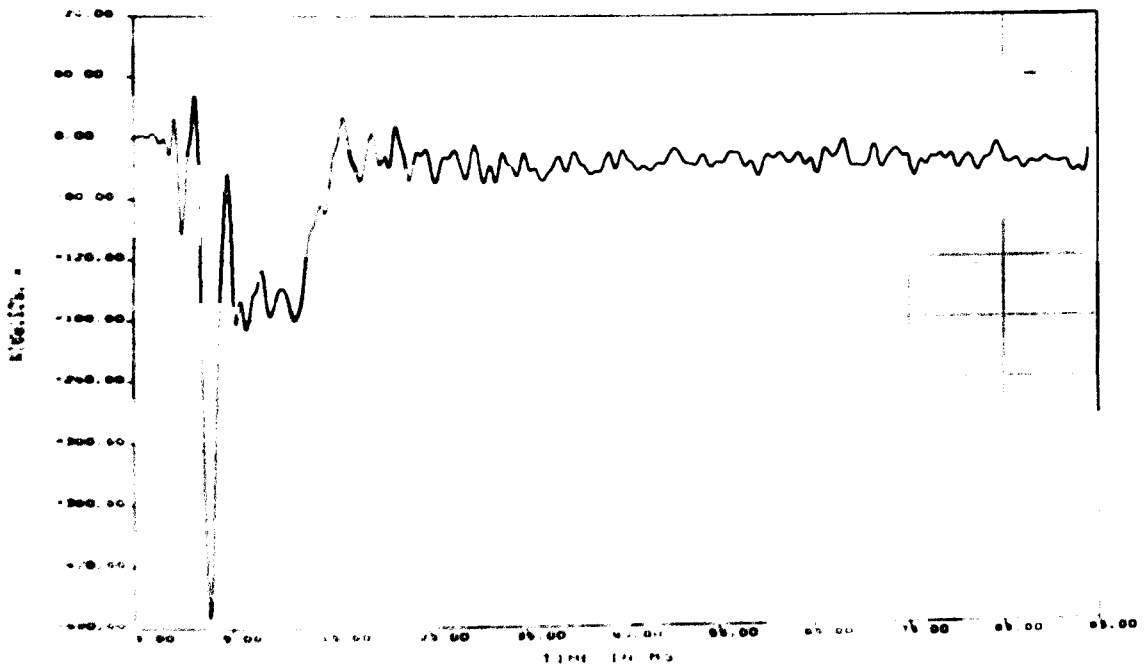


Figure E1-16. Microstrain vs Time for Gage SR2-YZ for 40 in. Side Puncture Test (filtered at 1000 Hz)

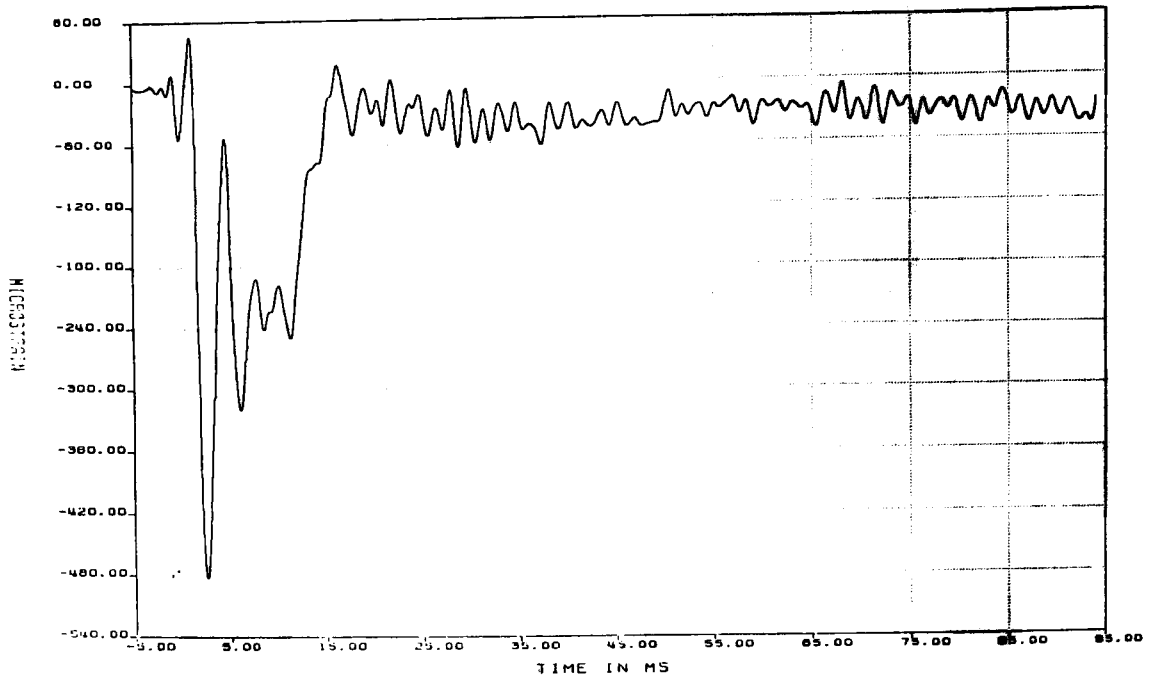


Figure E1-17. Microstrain vs Time for Gage SR2-Z for 40-in. Side Puncture Test (filtered at 1000 Hz)

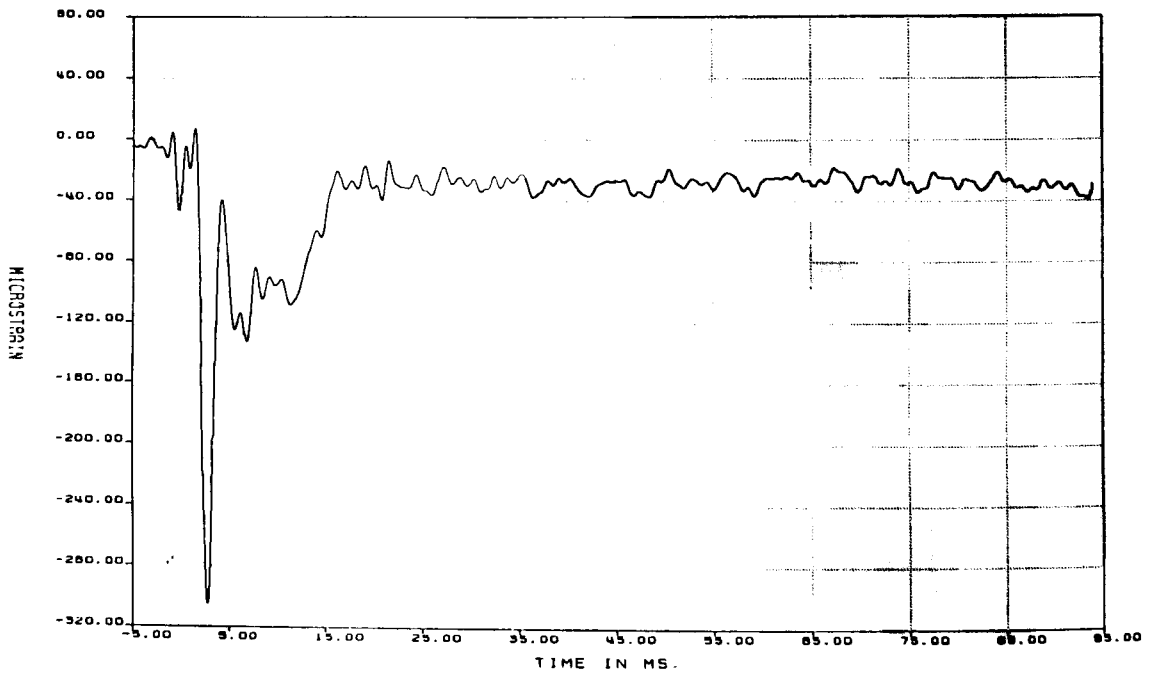


Figure E1-18. Microstrain vs Time for Gage SR3-Y for 40-in. Side Puncture Test (filtered at 1000 Hz)

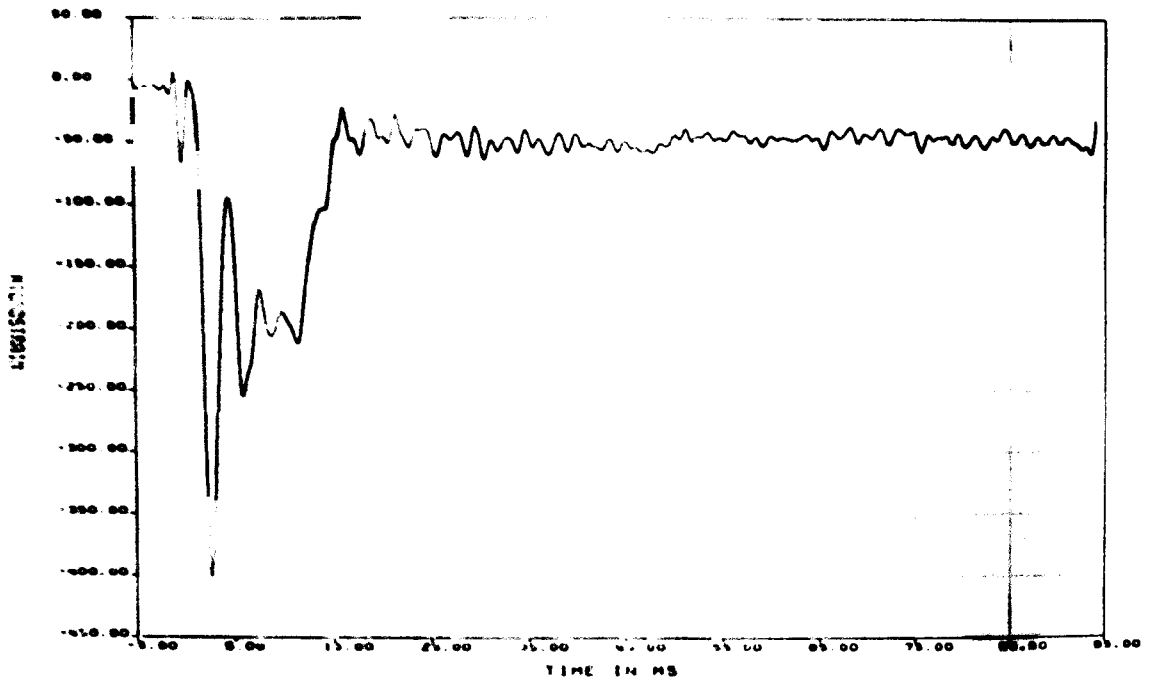


Figure E1-19. Microstrain vs Time for Gage SR3-YZ for 40-in. Side Puncture Test (filtered at 1000 Hz)

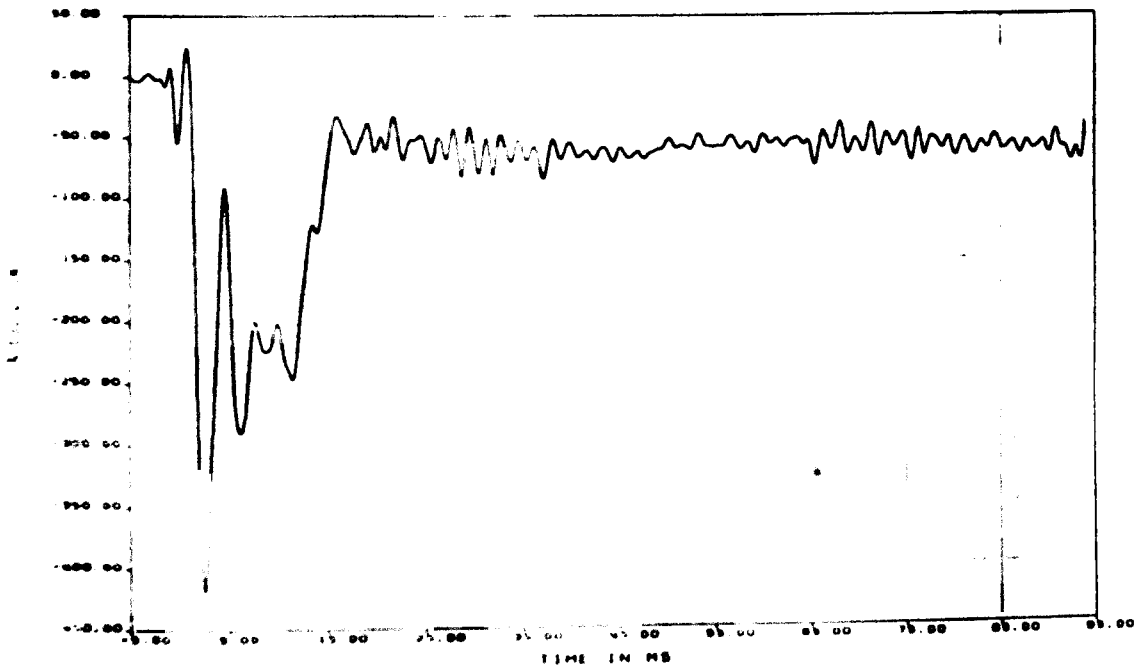


Figure E1-20. Microstrain vs Time for Gage SR3-Z for 40-in. Side Puncture Test (filtered at 1000 Hz)

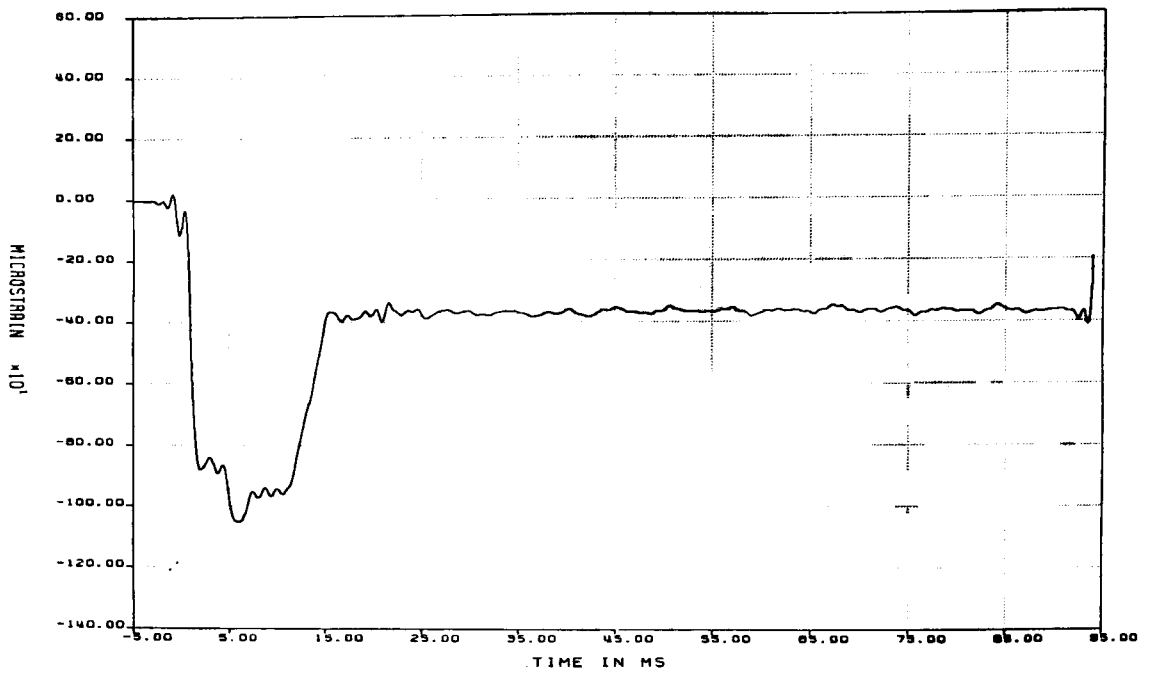


Figure E1-21. Microstrain vs Time for Gage SR4-Y for 40-in. Side Puncture Test (filtered at 1000 Hz)

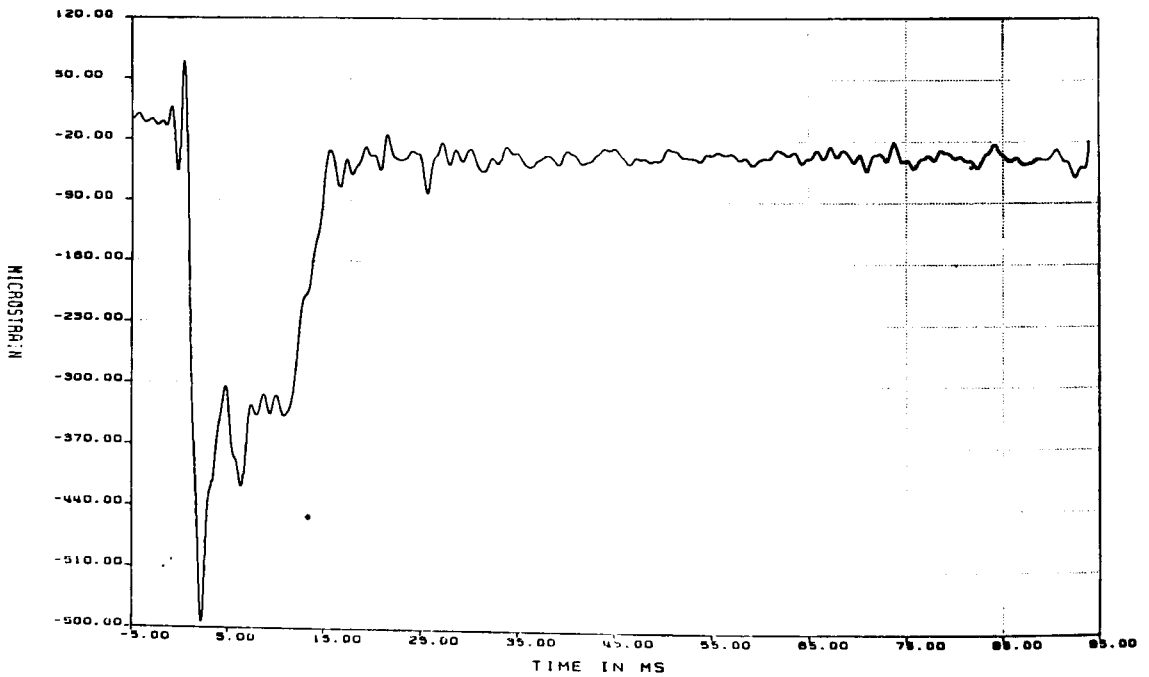


Figure E1-22. Microstrain vs Time for Gage SR4-YZ for 40-in. Side Puncture Test (filtered at 1000 Hz)

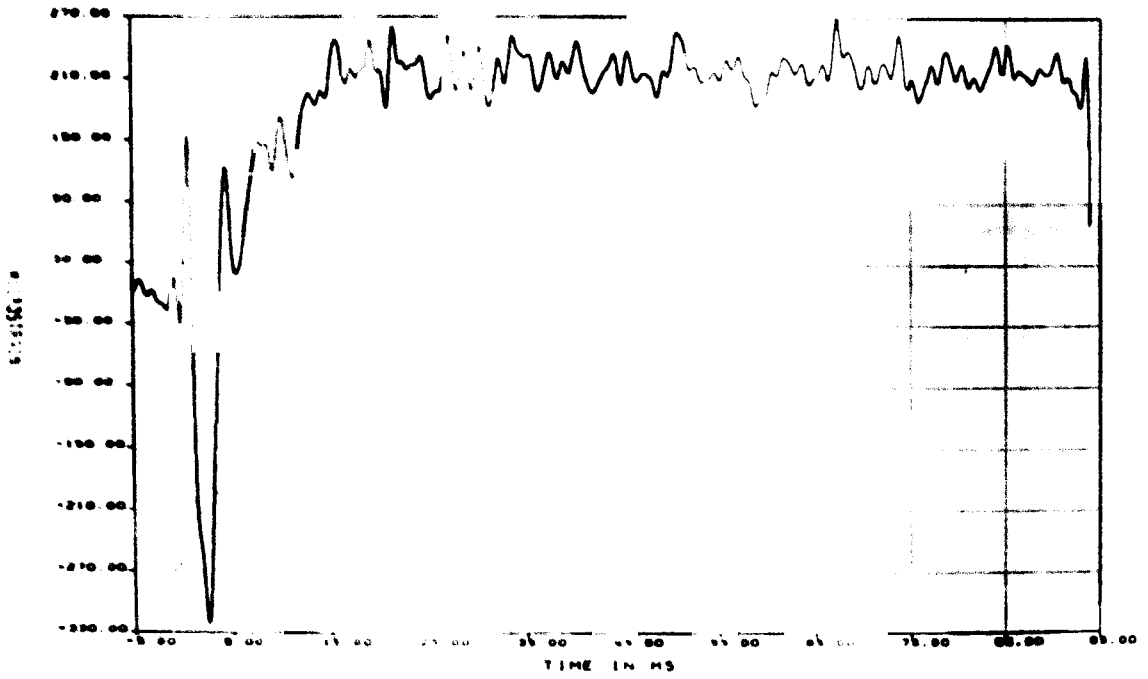


Figure E 1-23. Microstrain vs Time for Gage SR4-Z for 40-in. Side Puncture Test (filtered at 1000 Hz)

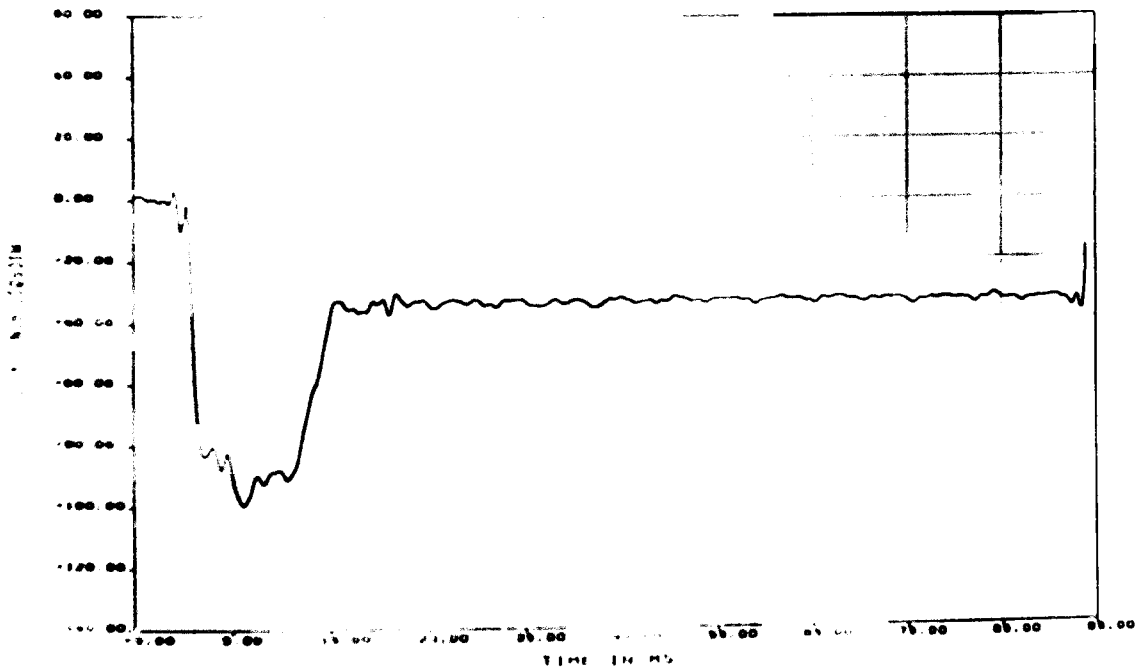


Figure E 1-24. Microstrain vs Time for Gage SR5-Y for 40-in. Side Puncture Test (filtered at 1000 Hz)

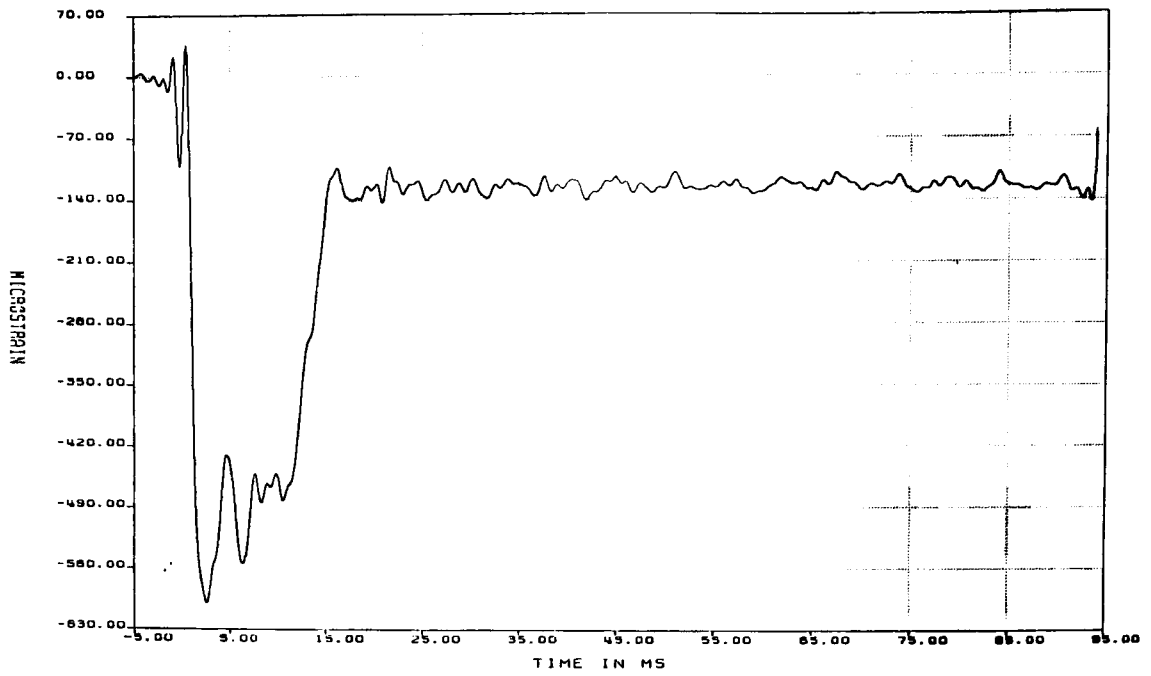


Figure E1-25. Microstrain vs Time for Gage SR5-YZ for 40-in. Side Puncture Test (filtered at 1000 Hz)

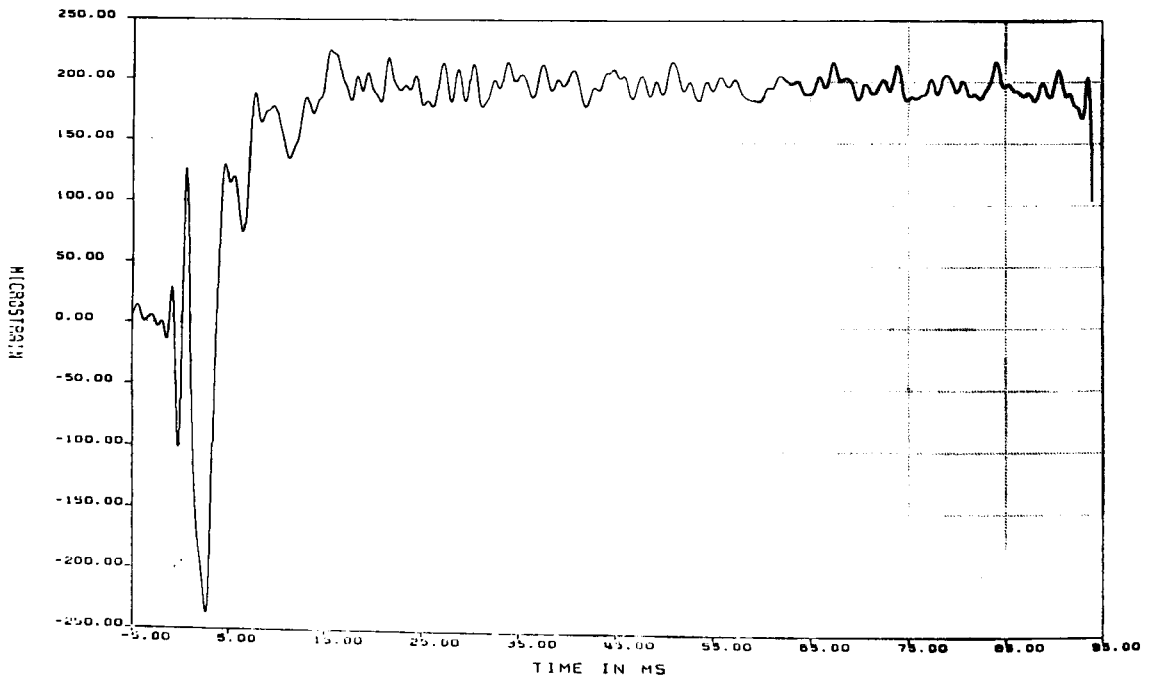


Figure E1-26. Microstrain vs Time for Gage SR5-Z for 40-in. Side Puncture Test (filtered at 1000 Hz)

APPENDIX E2

Fast Fourier Transforms of Raw Accelerometer Data for the 40-in. Side Puncture Test

Figures

E2-1	Fast Fourier Transform of Raw Data From Gage AZ1 for 40-in. Side Puncture Test: 0-50 kHz	246
E2-2	Fast Fourier Transform of Raw Data From Gage AZ1 for 40-in. Side Puncture Test: 0-10 kHz	246
E2-3	Fast Fourier Transform of Raw Data From Gage AX2 for 40-in. Side Puncture Test: 0-50 kHz	247
E2-4	Fast Fourier Transform of Raw Data From Gage AX2 for 40-in. Side Puncture Test: 0-10 kHz	247
E2-5	Fast Fourier Transform of Raw Data From Gage AY3 for 40-in. Side Puncture Test: 0-50 kHz	248
E2-6	Fast Fourier Transform of Raw Data From Gage AY3 for 40-in. Side Puncture Test: 0-10 kHz	248
E2-7	Fast Fourier Transform of Raw Data From Gage AZ4 for 40-in. Side Puncture Test: 0-50 kHz	249
E2-8	Fast Fourier Transform of Raw Data From Gage AZ4 for 40-in. Side Puncture Test: 0-10 kHz	249
E2-9	Fast Fourier Transform of Raw Data From Gage AX5 for 40-in. Side Puncture Test: 0-50 kHz	250
E2-10	Fast Fourier Transform of Raw Data From Gage AX5 for 40-in. Side Puncture Test: 0-10 kHz	250
E2-11	Fast Fourier Transform of Raw Data From Gage AY6 for 40-in. Side Puncture Test: 0-50 kHz	251
E2-12	Fast Fourier Transform of Raw Data From Gage AY6 for 40-in. Side Puncture Test: 0-10 kHz	251
E2-13	Fast Fourier Transform of Raw Data From Gage AZ7 for 40-in. Side Puncture Test: 0-50 kHz	252
E2-14	Fast Fourier Transform of Raw Data From Gage AZ7 for 40-in. Side Puncture Test: 0-10 kHz	252
E2-15	Fast Fourier Transform of Raw Data From Gage AX8 for 40-in. Side Puncture Test: 0-50 kHz	253
E2-16	Fast Fourier Transform of Raw Data From Gage AX8 for 40-in. Side Puncture Test: 0-10 kHz	253
E2-17	Fast Fourier Transform of Raw Data From Gage AX9 for 40-in. Side Puncture Test: 0-50 kHz	254
E2-18	Fast Fourier Transform of Raw Data From Gage AX9 for 40-in. Side Puncture Test: 0-10 kHz	254
E2-19	Fast Fourier Transform of Raw Data From Gage AX10 for 40-in. Side Puncture Test: 0-50 kHz	255
E2-20	Fast Fourier Transform of Raw Data From Gage AX10 for 40-in. Side Puncture Test: 0-10 kHz	255
E2-21	Fast Fourier Transform of Raw Data From Gage AX11 for 40-in. Side Puncture Test: 0-50 kHz	256
E2-22	Fast Fourier Transform of Raw Data From Gage AX11 for 40-in. Side Puncture Test: 0-10 kHz	256

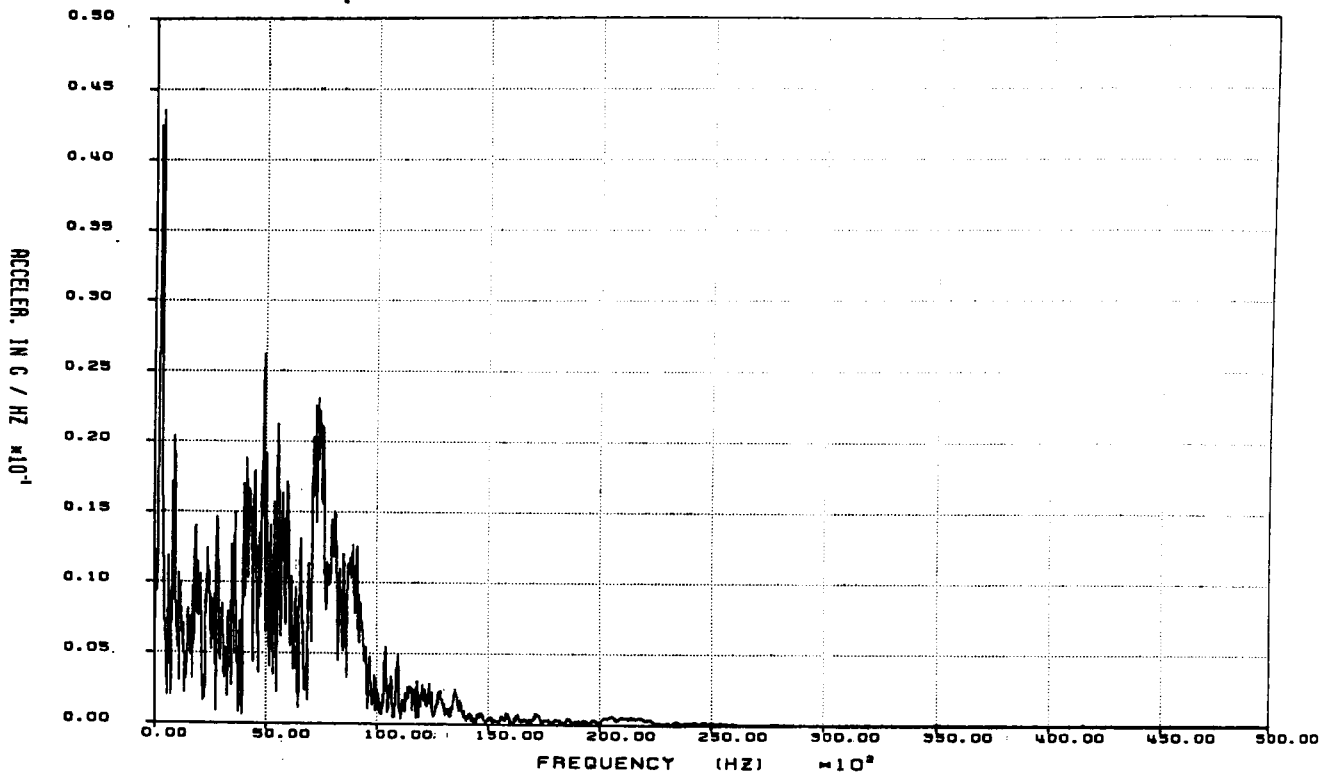


Figure E2-1. Fast Fourier Transform of Raw Data From Gage AZ1 for 40-in. Side Puncture Test: 0-50 kHz

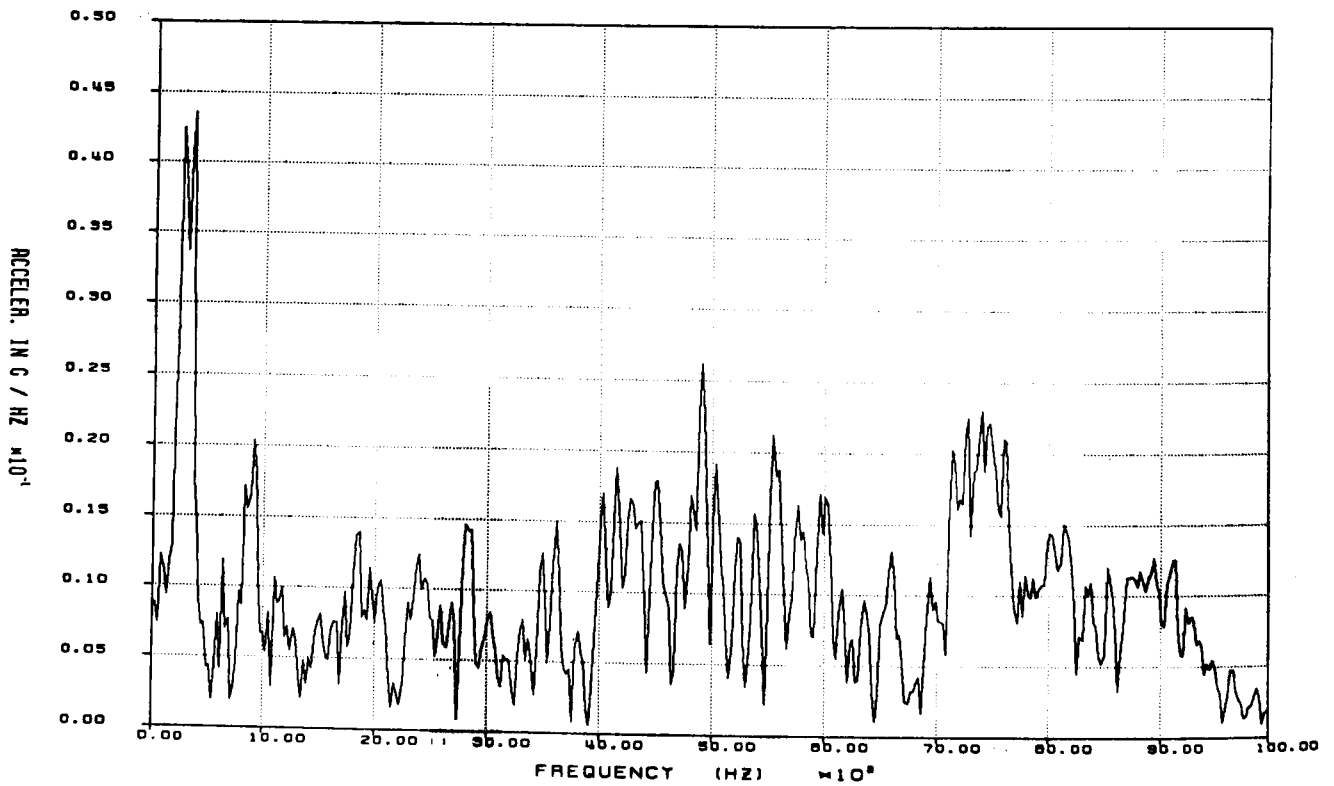


Figure E2-2. Fast Fourier Transform of Raw Data From Gage AZ1 for 40-in. Side Puncture Test: 0-10 kHz

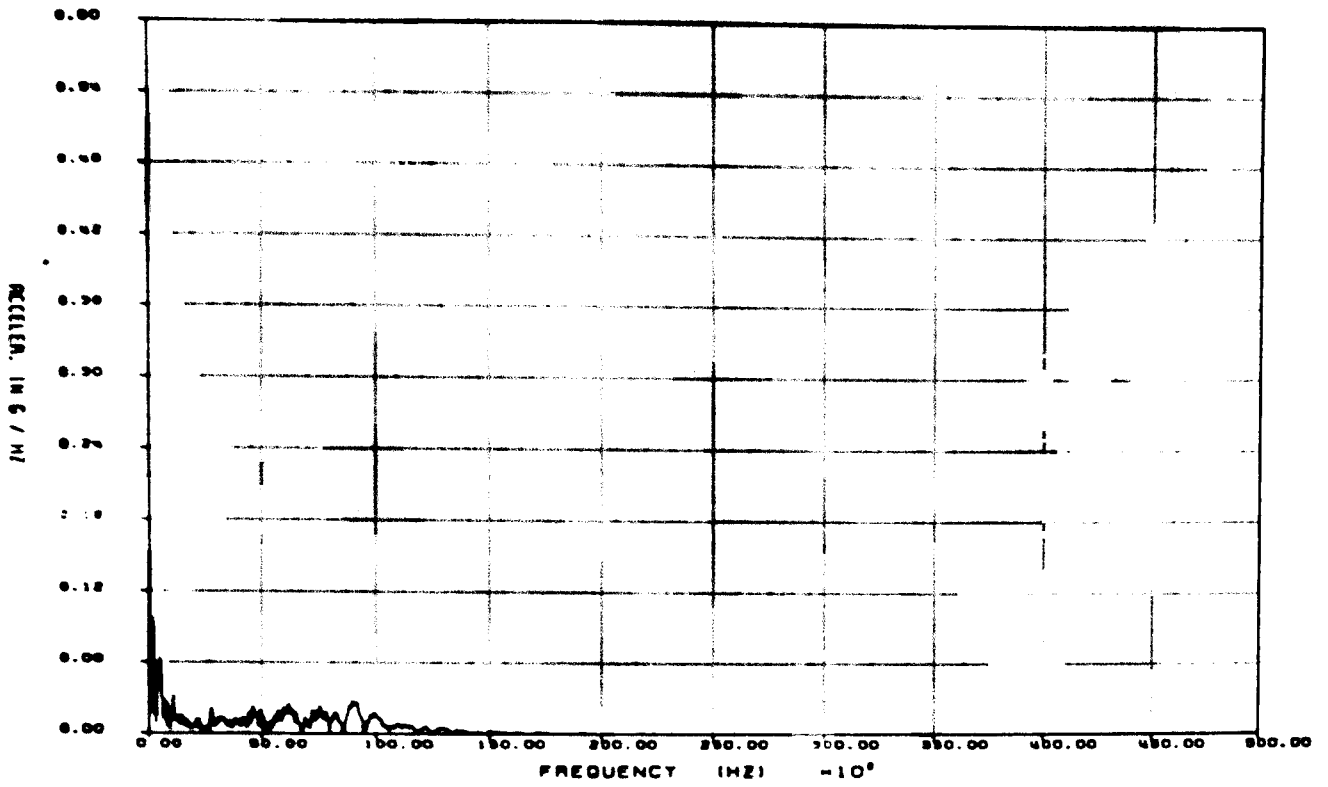


Figure E2-3. Fast Fourier Transform of Raw Data From Gage AX2 for 40-in. Side Puncture Test: 0-50 kHz

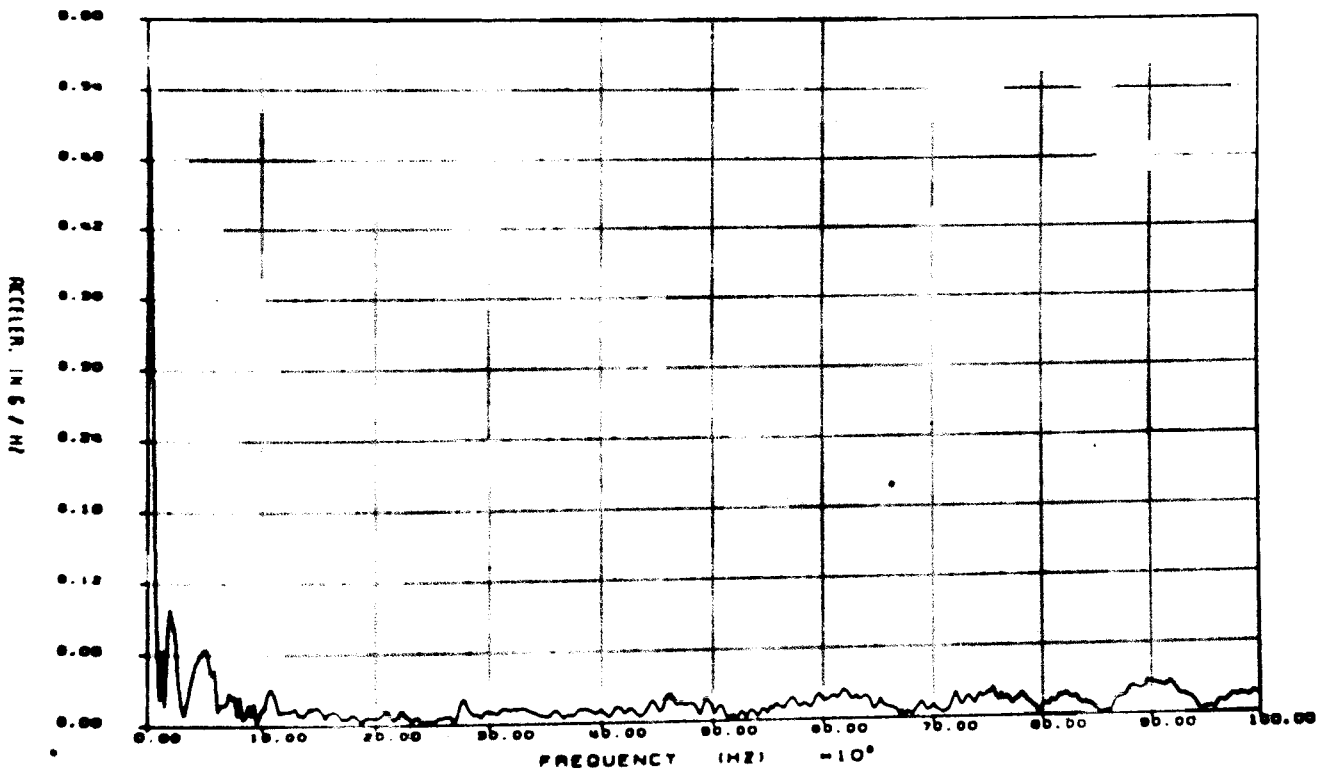


Figure E2-4. Fast Fourier Transform of Raw Data From Gage AX2 for 40 in. Side Puncture Test: 0-10 kHz

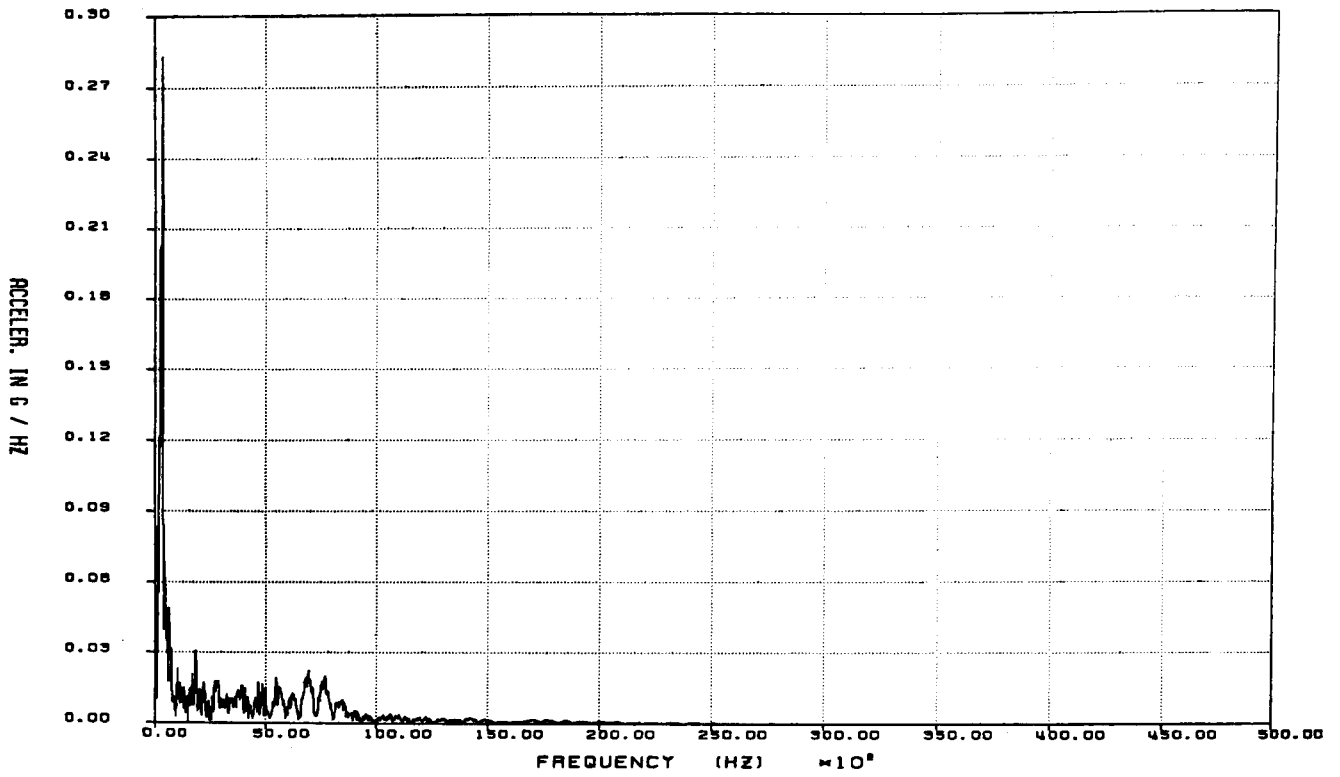


Figure E2-5. Fast Fourier Transform of Raw Data From Gage AY3 for 40-in. Side Puncture Test: 0-50 kHz

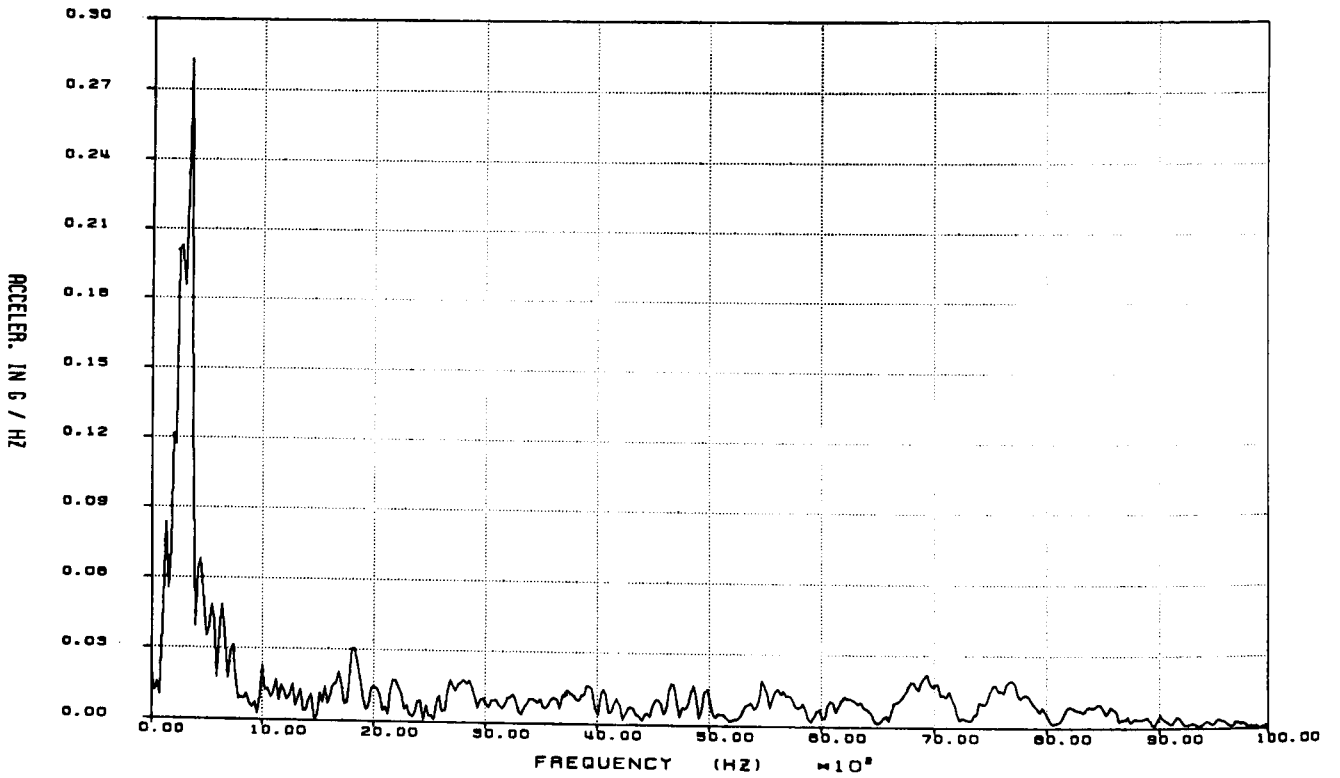


Figure E2-6. Fast Fourier Transform of Raw Data From Gage AY3 for 40-in. Side Puncture Test: 0-10 kHz

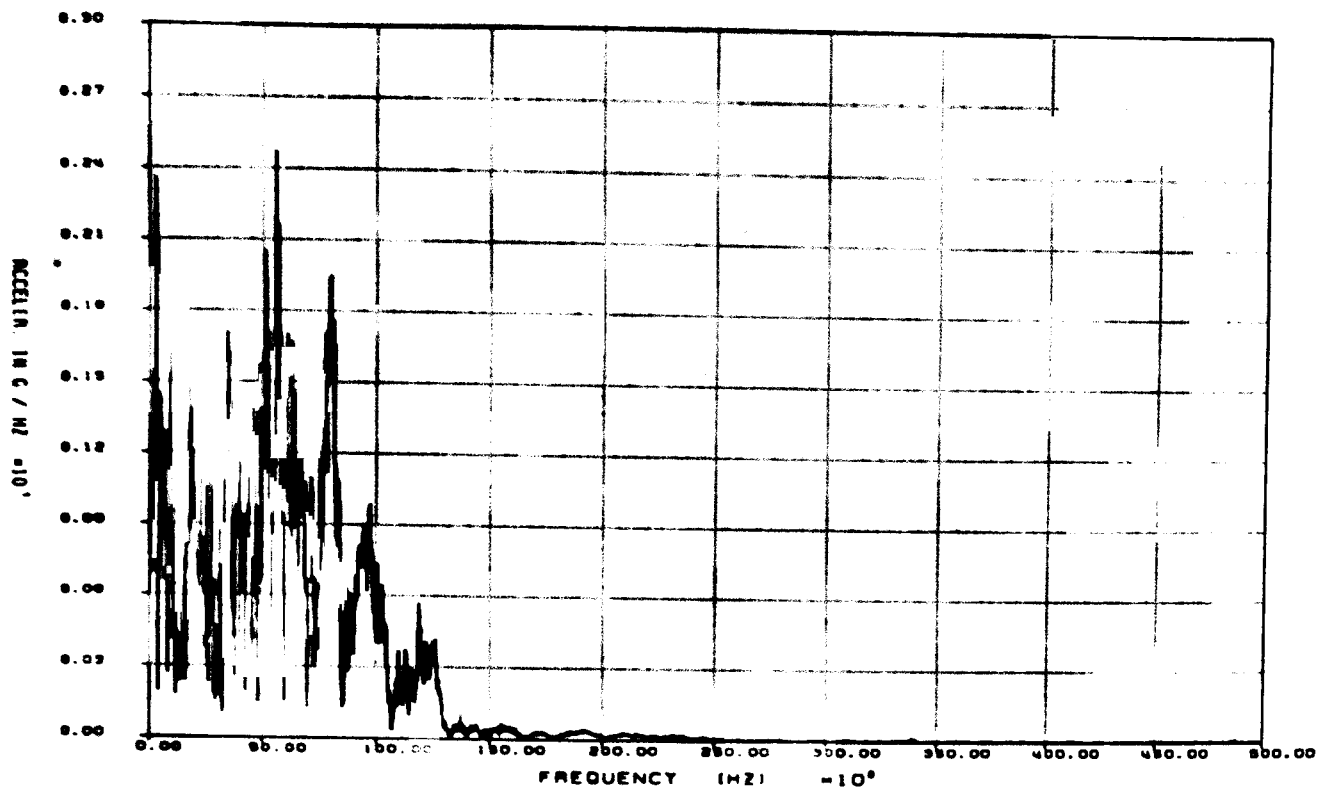


Figure E2-7. Fast Fourier Transform of Raw Data From Gage AZ4 for 40-in. Side Puncture Test: 0-50 kHz

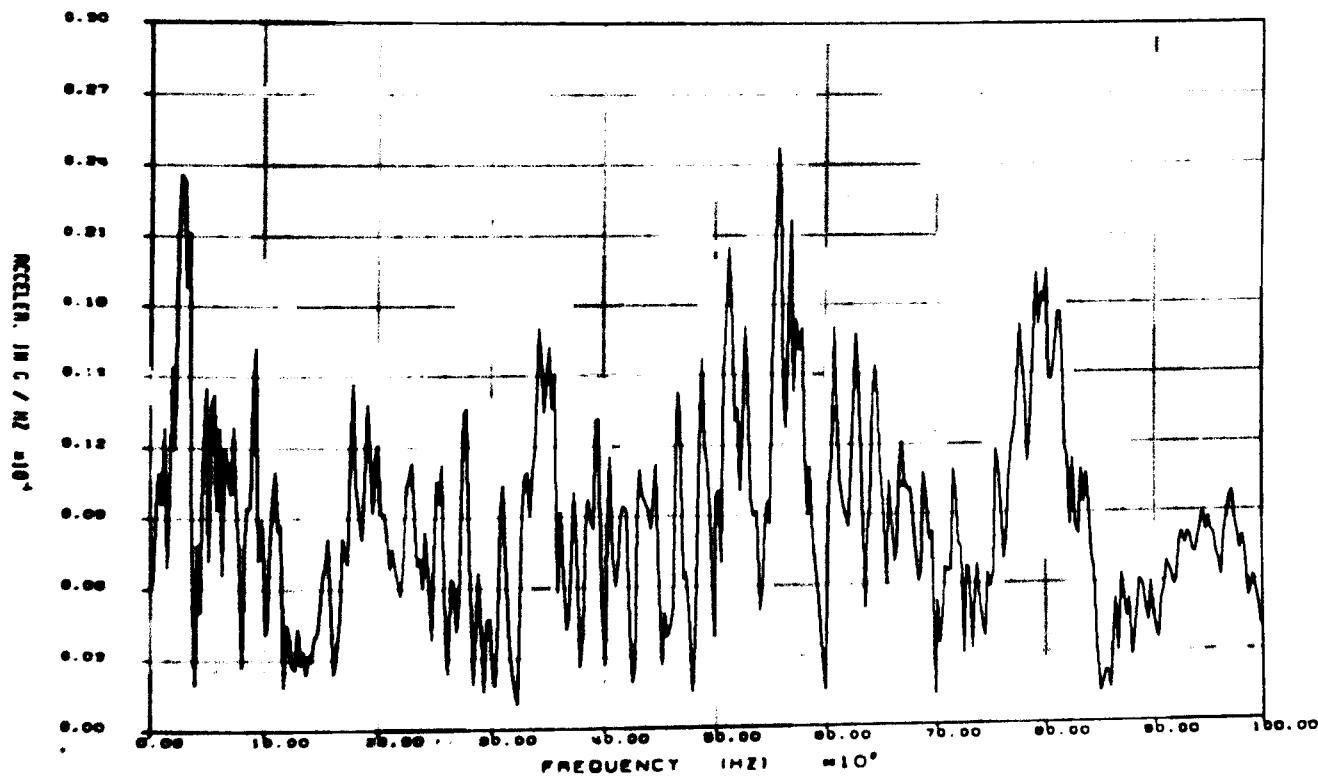


Figure E2-8. Fast Fourier Transform of Raw Data From Gage AZ4 for 40-in. Side Puncture Test: 0-10 kHz

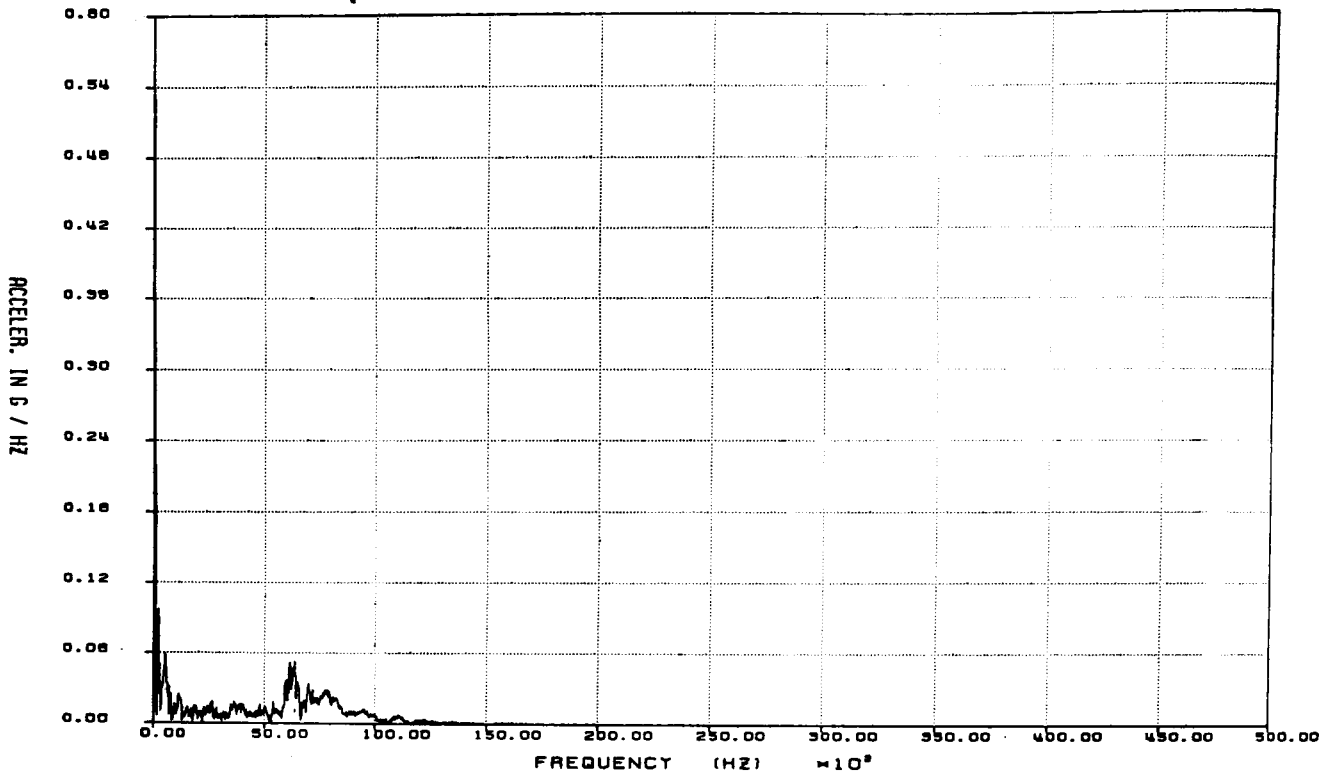


Figure E2-9. Fast Fourier Transform of Raw Data From Gage AX5 for 40-in. Side Puncture Test: 0-50 kHz

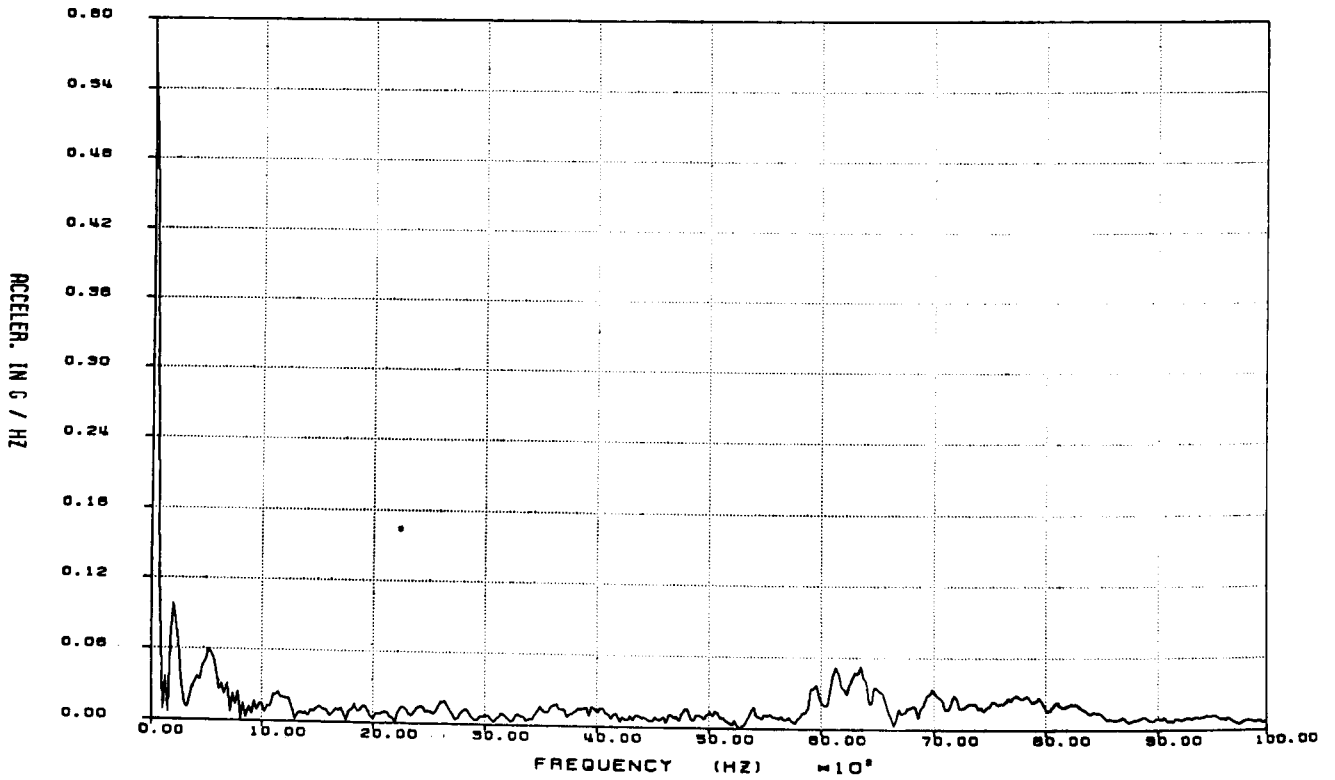


Figure E2-10. Fast Fourier Transform of Raw Data From Gage AX5 for 40-in. Side Puncture Test: 0-10 kHz

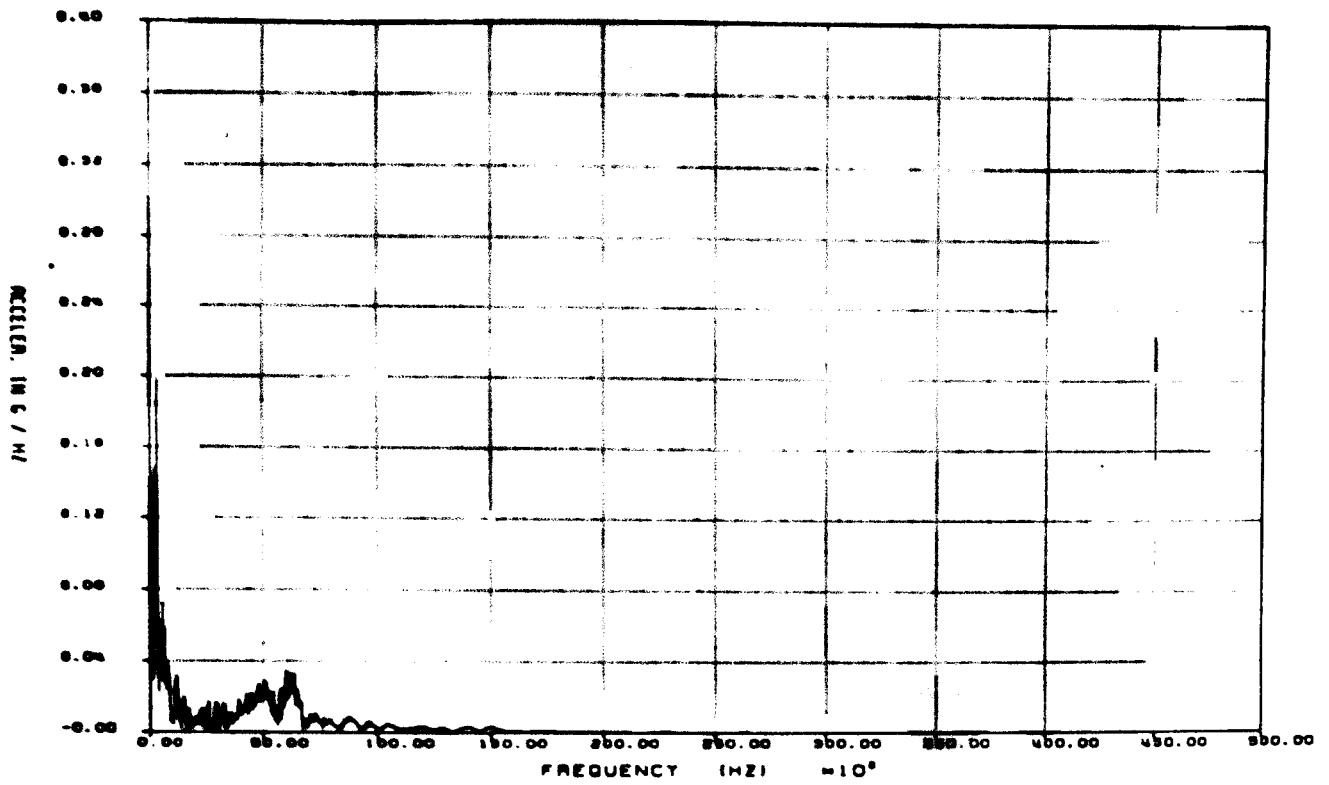


Figure E2-11. Fast Fourier Transform of Raw Data From Gage AY6 for 40-in. Side Puncture Test: 0-50 kHz

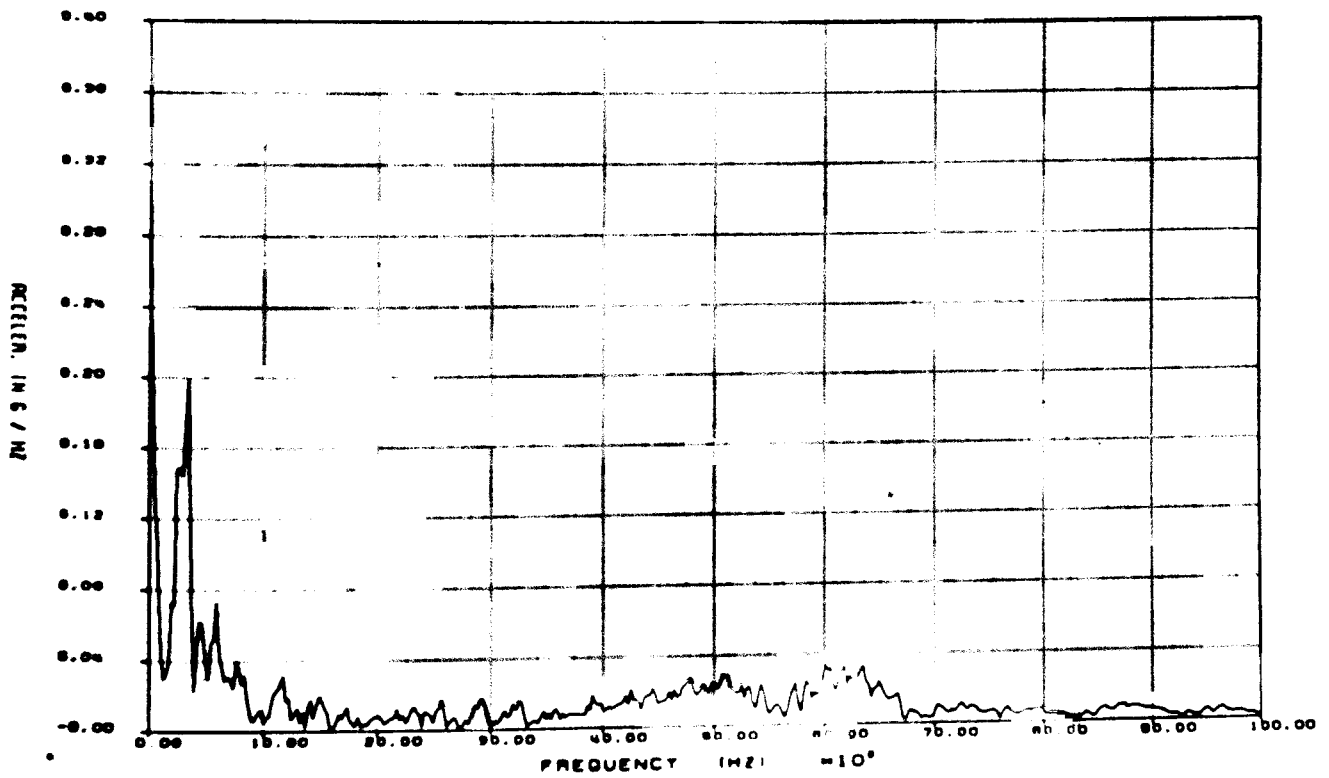


Figure E2-12. Fast Fourier Transform of Raw Data From Gage AY6 for 40 in. Side Puncture Test: 0-10 kHz

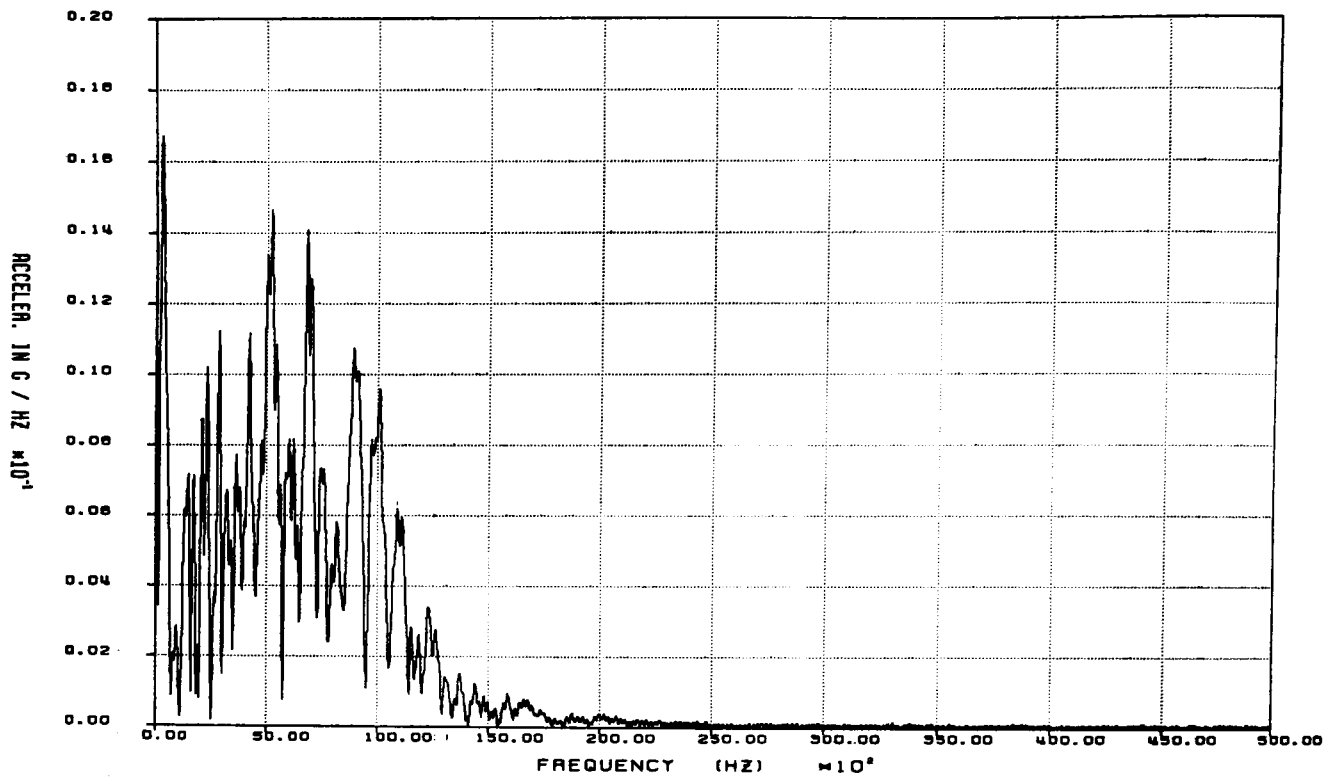


Figure E2-13. Fast Fourier Transform of Raw Data From Gage AZ7 for 40-in. Side Puncture Test: 0-50 kHz

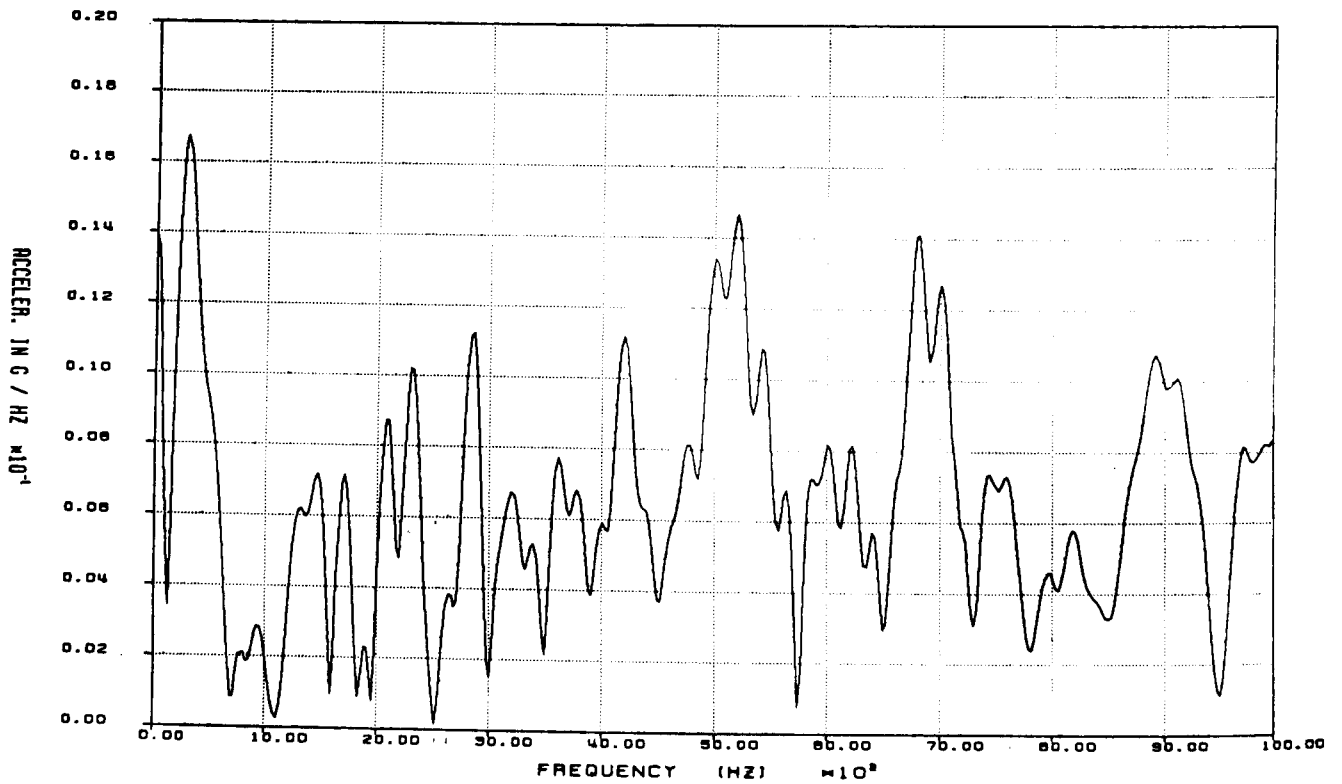


Figure E2-14. Fast Fourier Transform of Raw Data From Gage AZ7 for 40-in. Side Puncture Test: 0-10 kHz

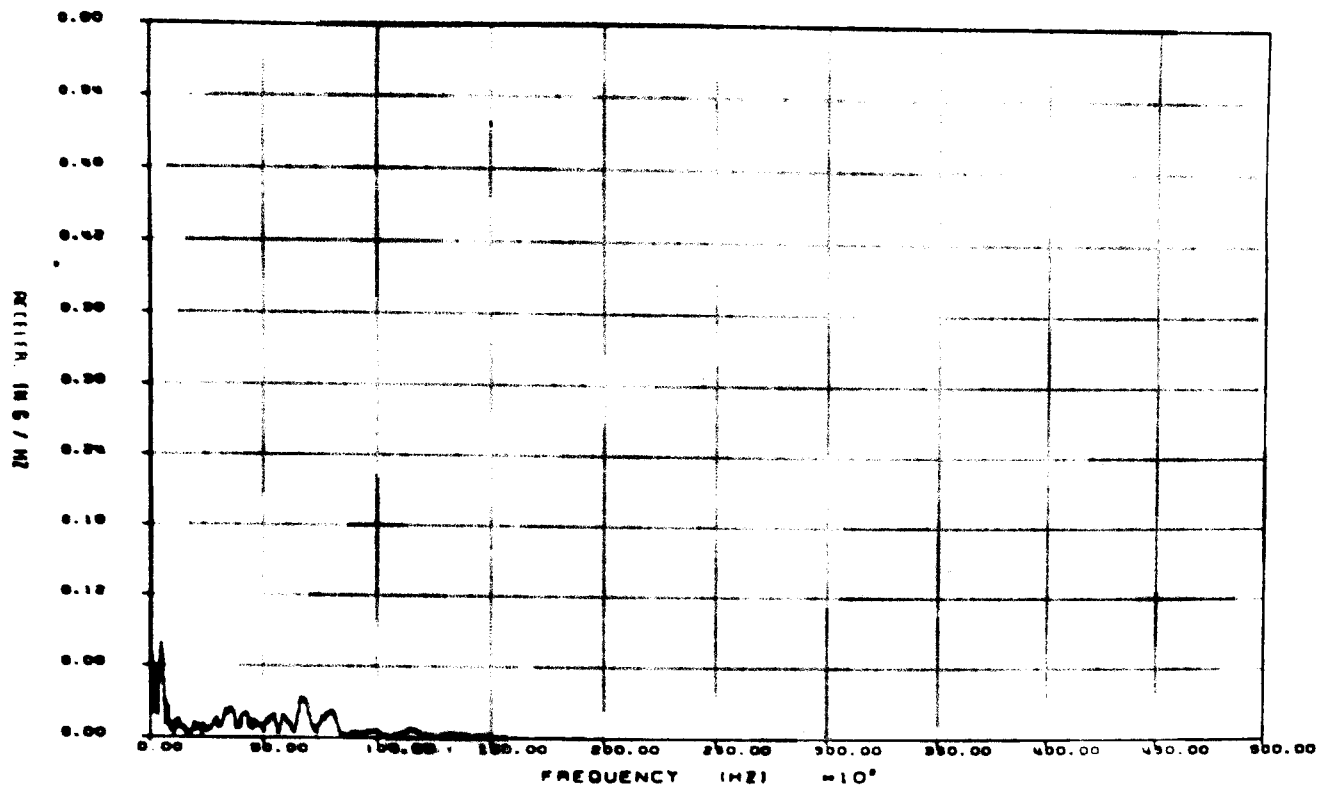


Figure E2-15. Fast Fourier Transform of Raw Data From Gage AX8 for 40-in. Side Puncture Test: 0-50 kHz

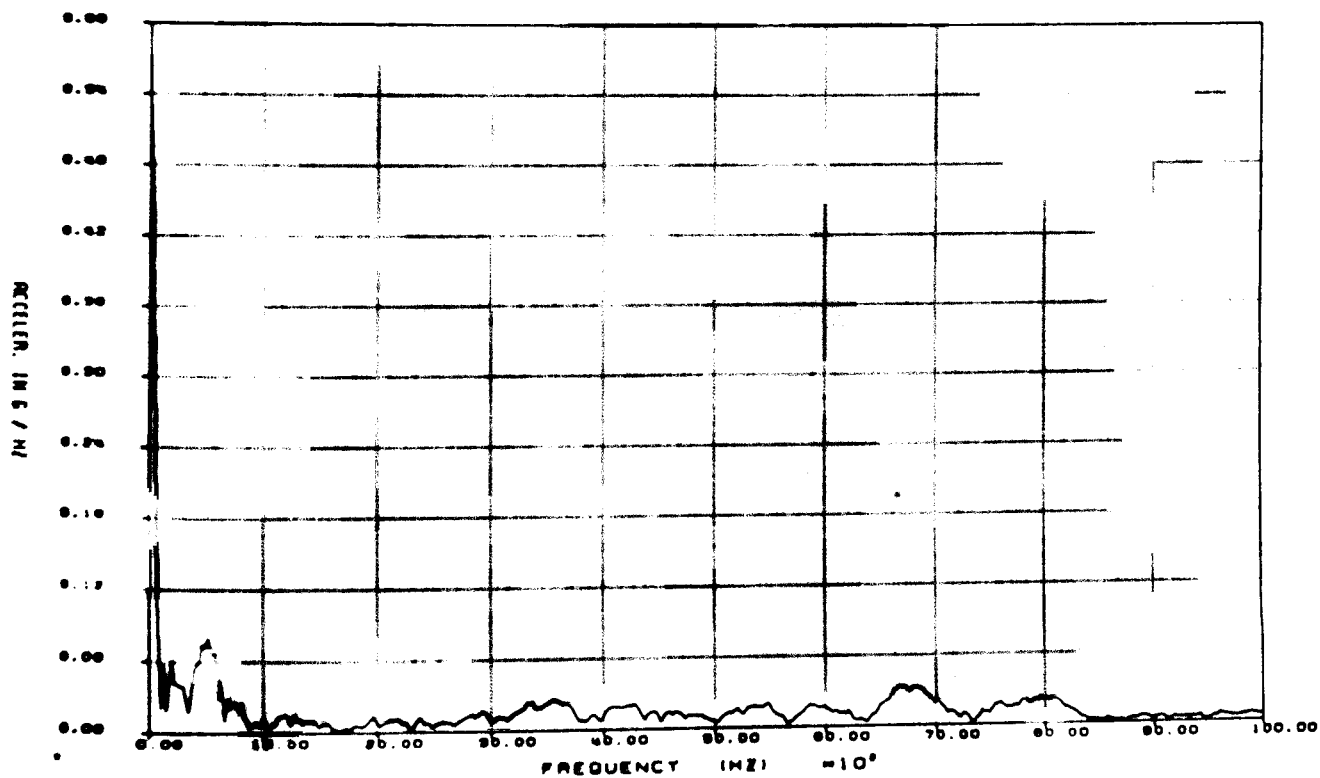


Figure E2-16. Fast Fourier Transform of Raw Data From Gage AX8 for 40 in. Side Puncture Test: 0-10 kHz

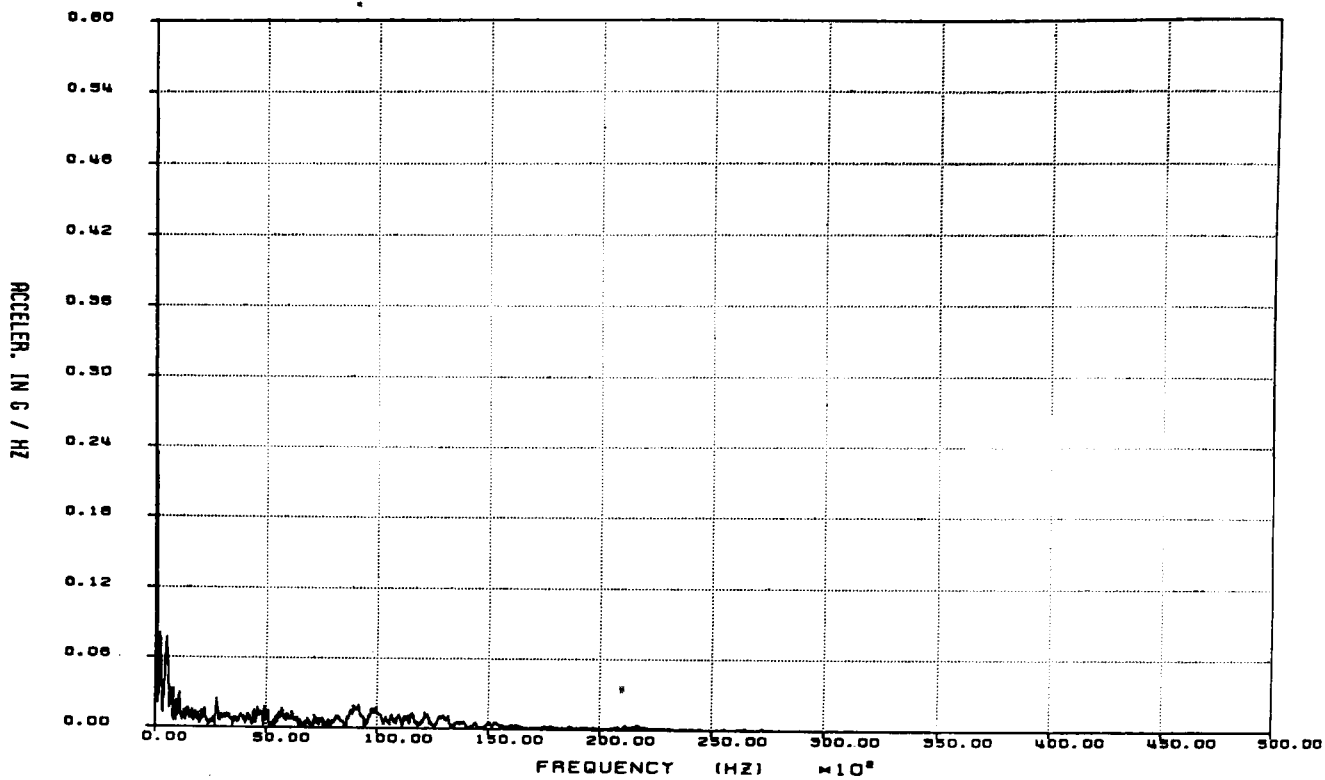


Figure E2-17. Fast Fourier Transform of Raw Data From Gage AX9 for 40-in. Side Puncture Test: 0-50 kHz

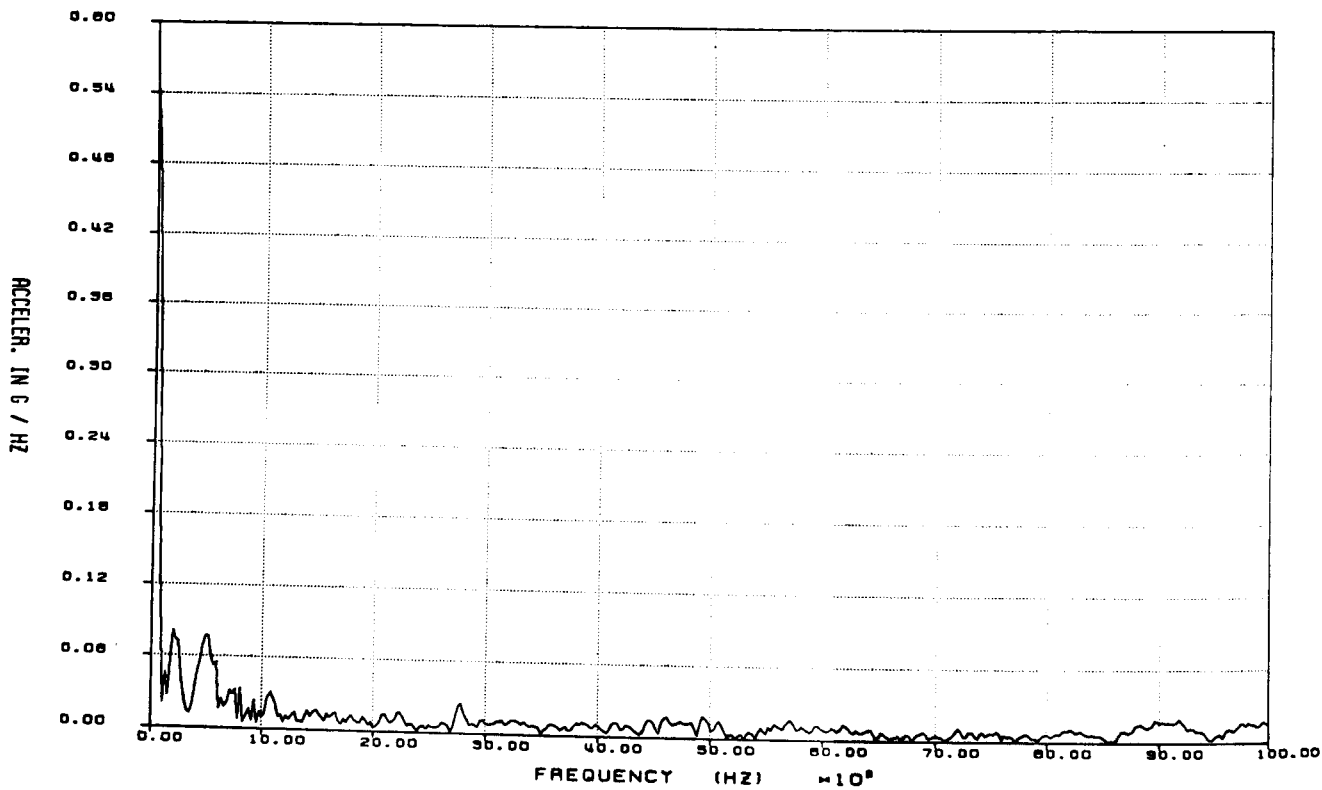


Figure E2-18. Fast Fourier Transform of Raw Data From Gage AX9 for 40-in. Side Puncture Test: 0-10 kHz

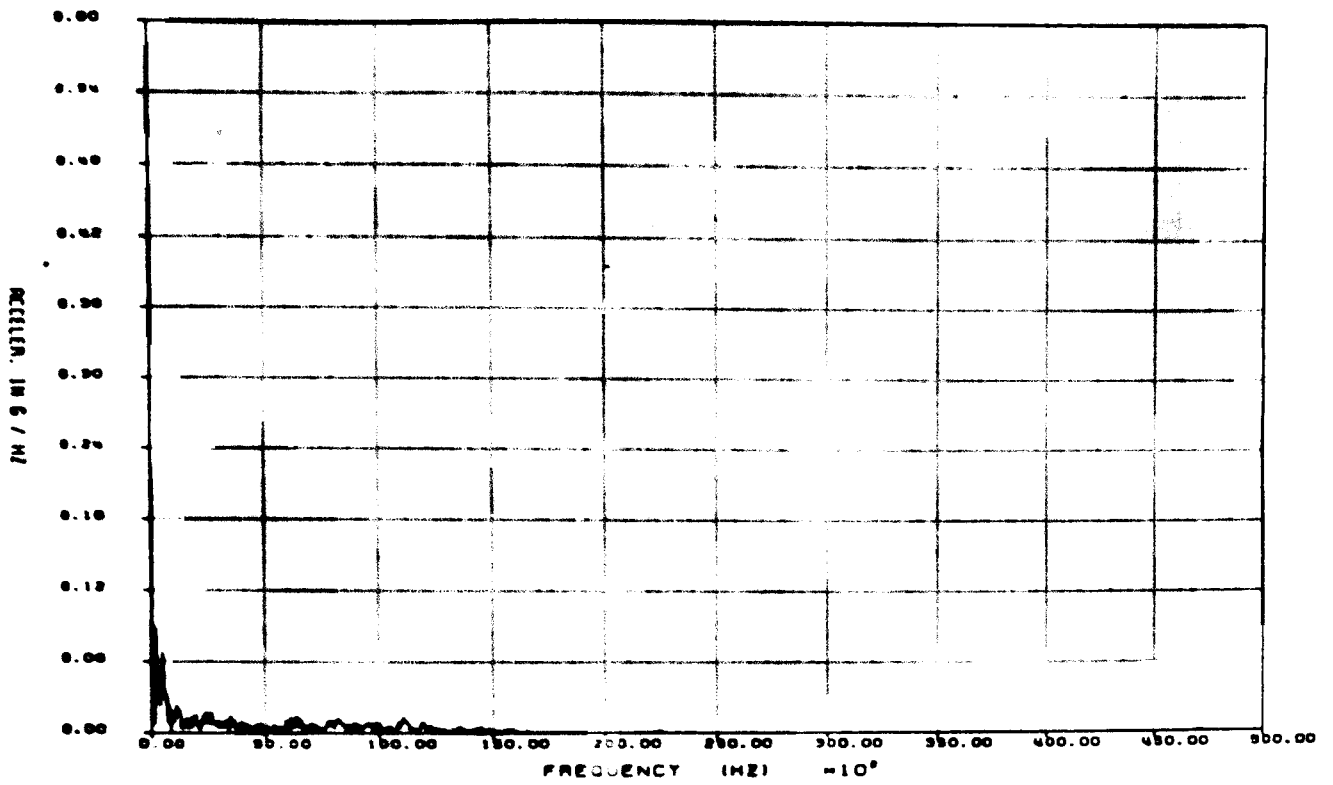


Figure E2-19. Fast Fourier Transform of Raw Data From Gage AX10 for 40-in. Side Puncture Test: 0-50 kHz

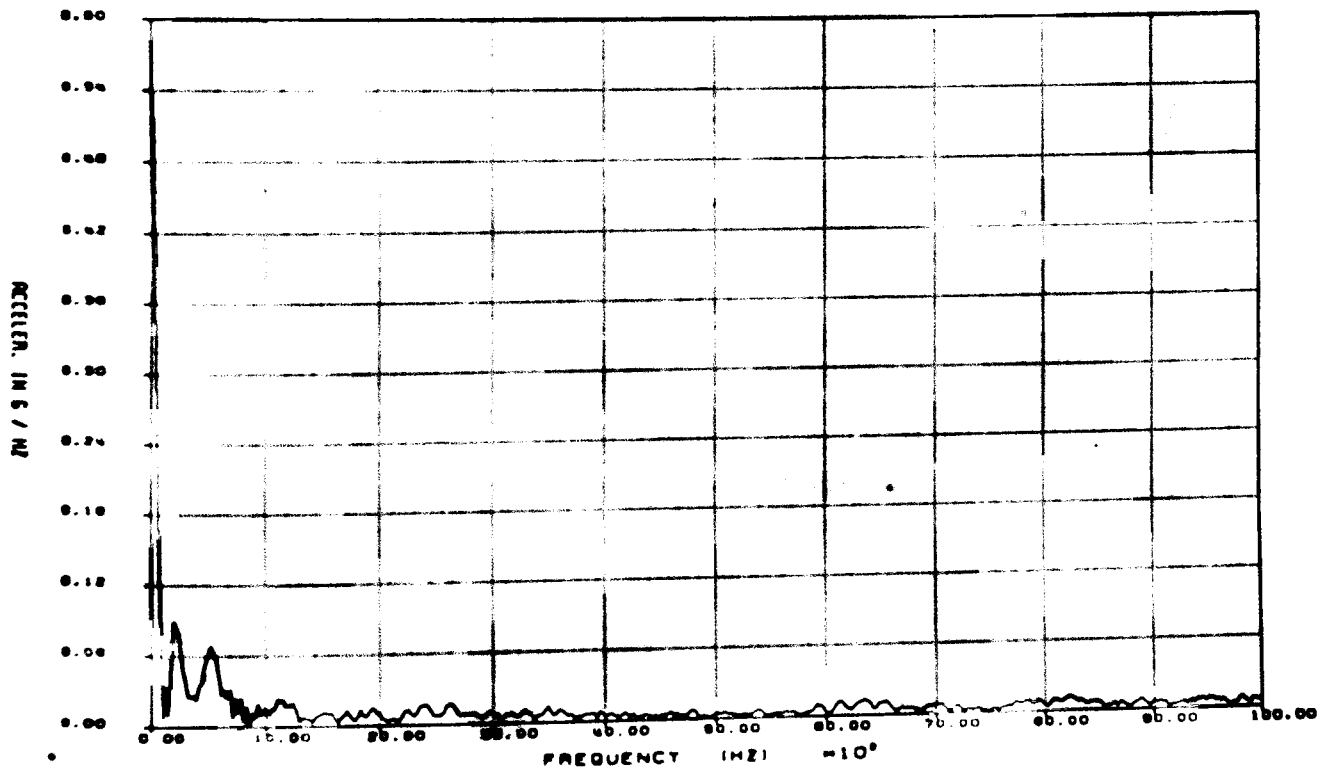


Figure E2-20. Fast Fourier Transform of Raw Data From Gage AX10 for 40-in. Side Puncture Test: 0-10 kHz

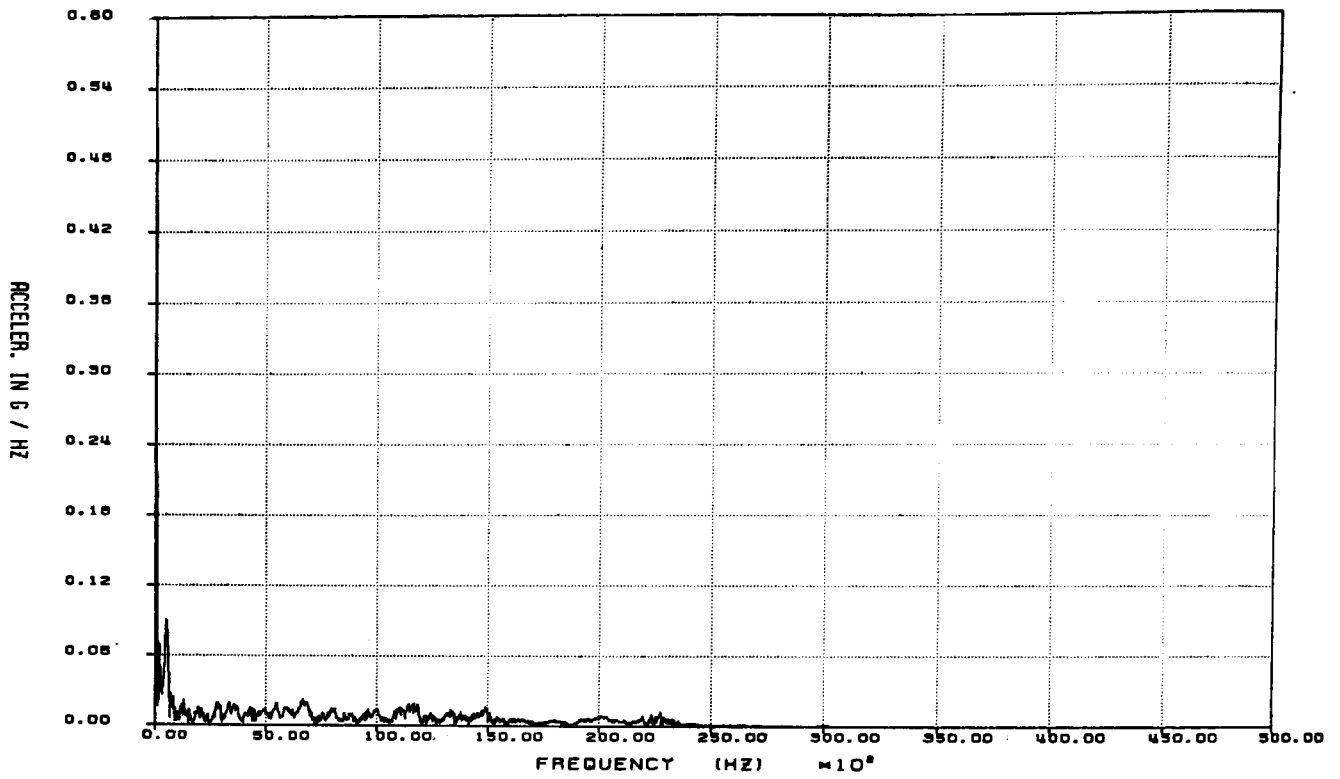


Figure E2-21. Fast Fourier Transform of Raw Data From Gage AX11 for 40-in. Side Puncture Test: 0-50 kHz

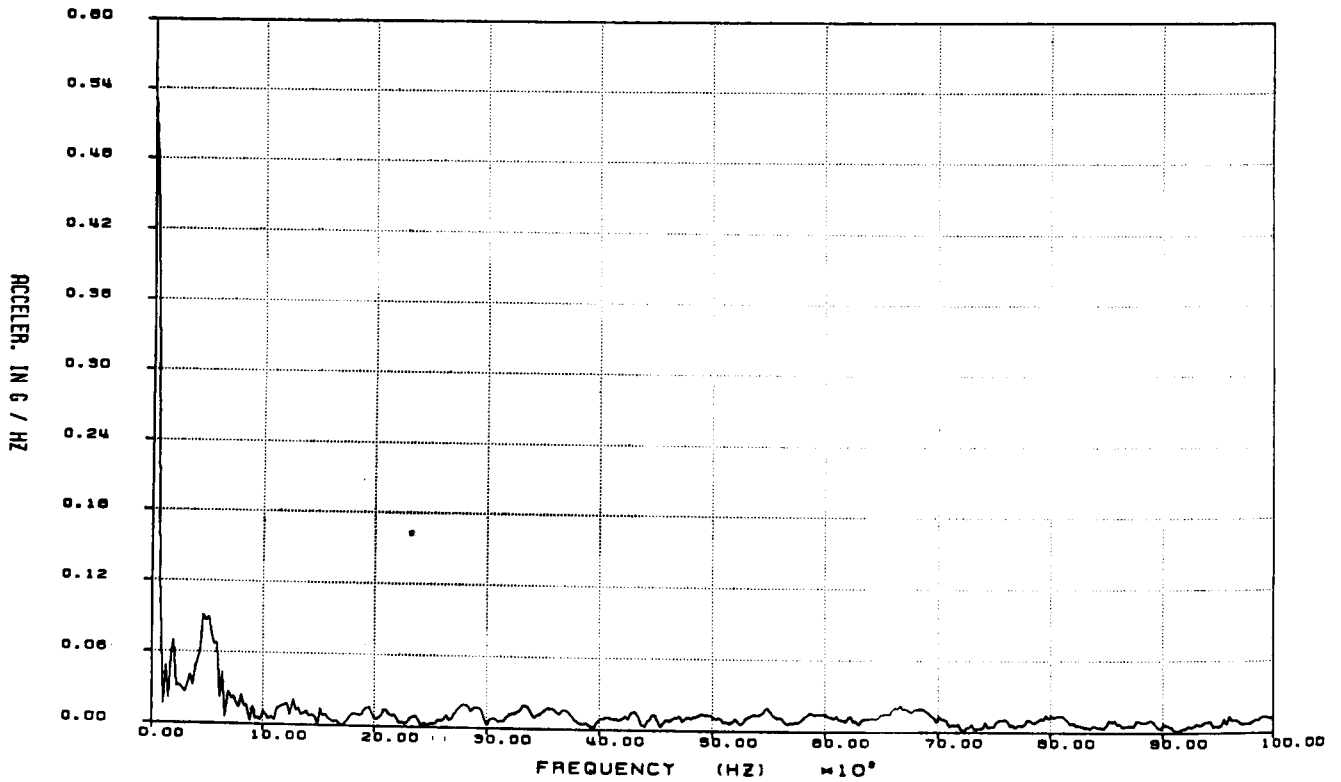


Figure E2-22. Fast Fourier Transform of Raw Data From Gage AX11 for 40-in. Side Puncture Test: 0-10 kHz

APPENDIX F1

Accelerometer and Strain Gage Data for the 40-in. Closure End Puncture Test Filtered at 1000 Hz

Figures

F1-1	Acceleration vs Time for Gage AZ1 for 40-in. Closure End Puncture Test	258
F1-2	Acceleration vs Time for Gage AX2 for 40-in. Closure End Puncture Test	258
F1-3	Acceleration vs Time for Gage AY3 for 40-in. Closure End Puncture Test	259
F1-4	Acceleration vs Time for Gage AZ4 for 40-in. Closure End Puncture Test	259
F1-5	Acceleration vs Time for Gage AX5 for 40 in. Closure End Puncture Test	260
F1-6	Acceleration vs Time for Gage AY6 for 40-in. Closure End Puncture Test	260
F1-7	Acceleration vs Time for Gage AZ7 for 40-in. Closure End Puncture Test	261
F1-8	Acceleration vs Time for Gage AX8 for 40-in. Closure End Puncture Test	261
F1-9	Acceleration vs Time for Gage AX9 for 40-in. Closure End Puncture Test	262
F1-10	Acceleration vs Time for Gage AX10 for 40 in. Closure End Puncture Test	262
F1-11	Acceleration vs Time for Gage AX11 for 40-in. Closure End Puncture Test	263
F1-12	Microstrain vs Time for Gage SR1-Y for 40-in. Closure End Puncture Test	263
F1-13	Microstrain vs Time for Gage SR1-YZ for 40-in. Closure End Puncture Test	264
F1-14	Microstrain vs Time for Gage SR1-Z for 40-in. Closure End Puncture Test	264
F1-15	Microstrain vs Time for Gage SR2-Y for 40-in. Closure End Puncture Test	265
F1-16	Microstrain vs Time for Gage SR2-YZ for 40-in. Closure End Puncture Test	265
F1-17	Microstrain vs Time for Gage SR2-Z for 40-in. Closure End Puncture Test	266
F1-18	Microstrain vs Time for Gage SR3-Y for 40-in. Closure End Puncture Test	266
F1-19	Microstrain vs Time for Gage SR3-YZ for 40-in. Closure End Puncture Test	267
F1-20	Microstrain vs Time for Gage SR3-Z for 40-in. Closure End Puncture Test	267
F1-21	Microstrain vs Time for Gage SR4-Y for 40-in. Closure End Puncture Test	268
F1-22	Microstrain vs Time for Gage SR4-YZ for 40-in. Closure End Puncture Test	268
F1-23	Microstrain vs Time for Gage SR4-Z for 40-in. Closure End Puncture Test	269
F1-24	Microstrain vs Time for Gage SR5-Y for 40-in. Closure End Puncture Test	269
F1-25	Microstrain vs Time for Gage SR5-YZ for 40 in. Closure End Puncture Test	270
F1-26	Microstrain vs Time for Gage SR5-Z for 40-in. Closure End Puncture Test	270
F1-27	Force vs Time for Gage F-1 on Puncture Bar for 40-in. Closure End Puncture Test (raw data)	271
F1-28	Force vs Time for Gage F-2 on Puncture Bar for 40-in. Closure End Puncture Test (raw data)	271

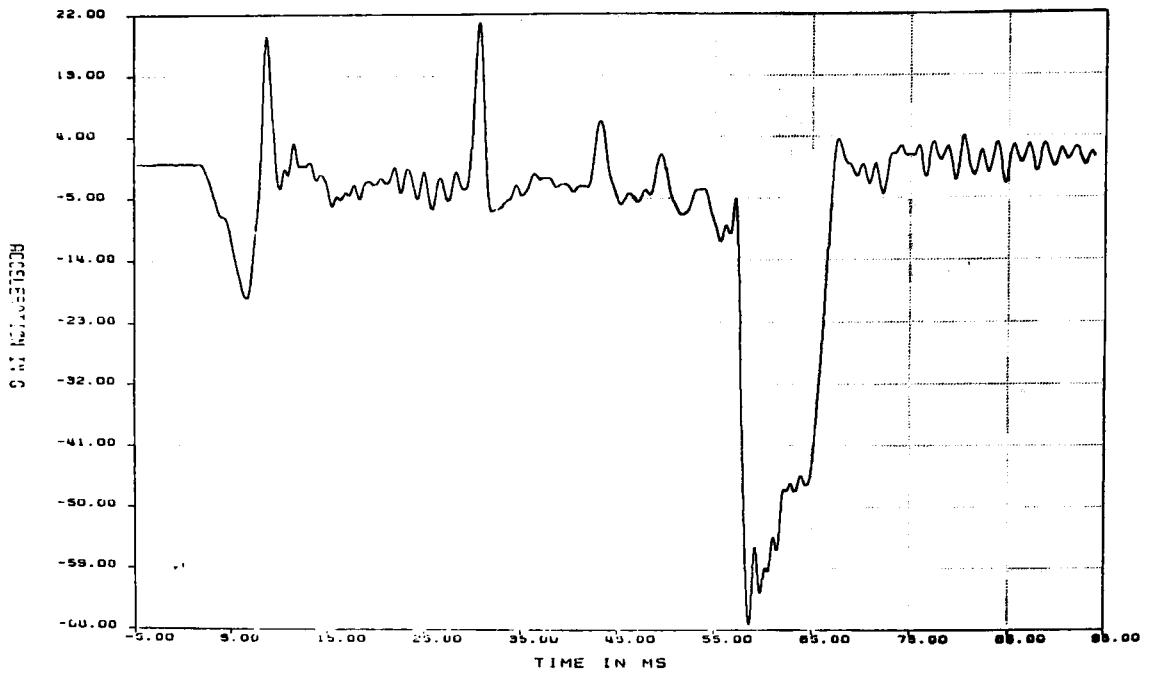


Figure F1-1. Acceleration vs Time for Gage AZ1 for 40-in. Closure End Puncture Test (filtered at 1000 Hz)

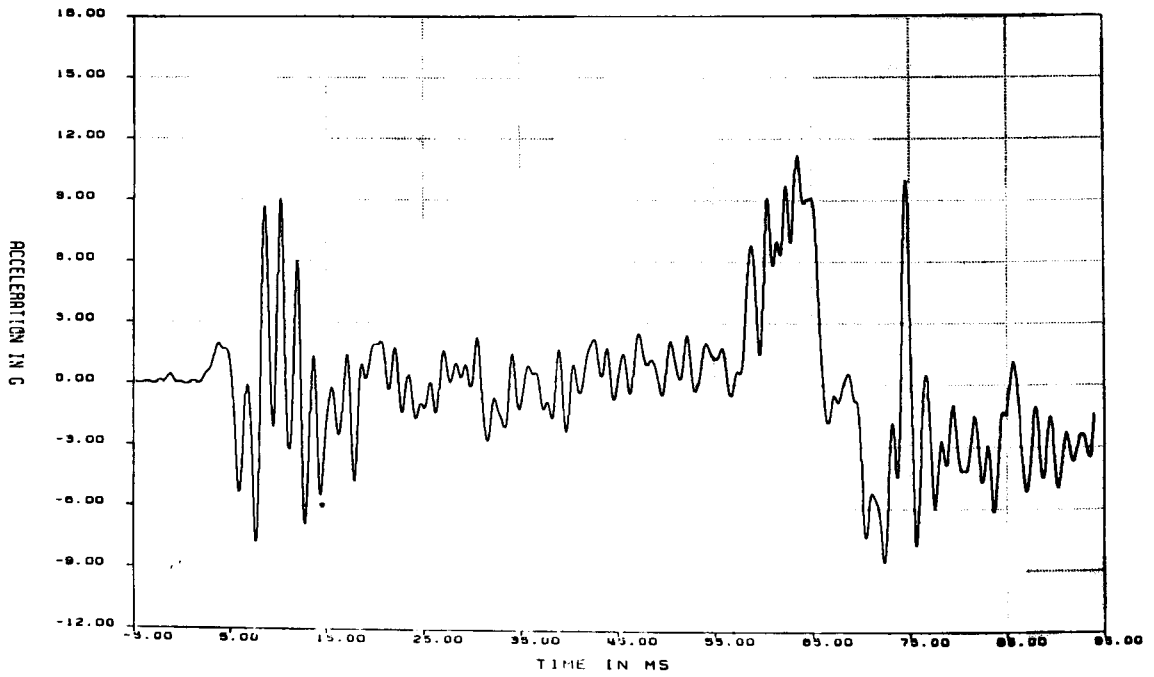


Figure F1-2. Acceleration vs Time for Gage AX2 for 40-in. Closure End Puncture Test (filtered at 1000 Hz)

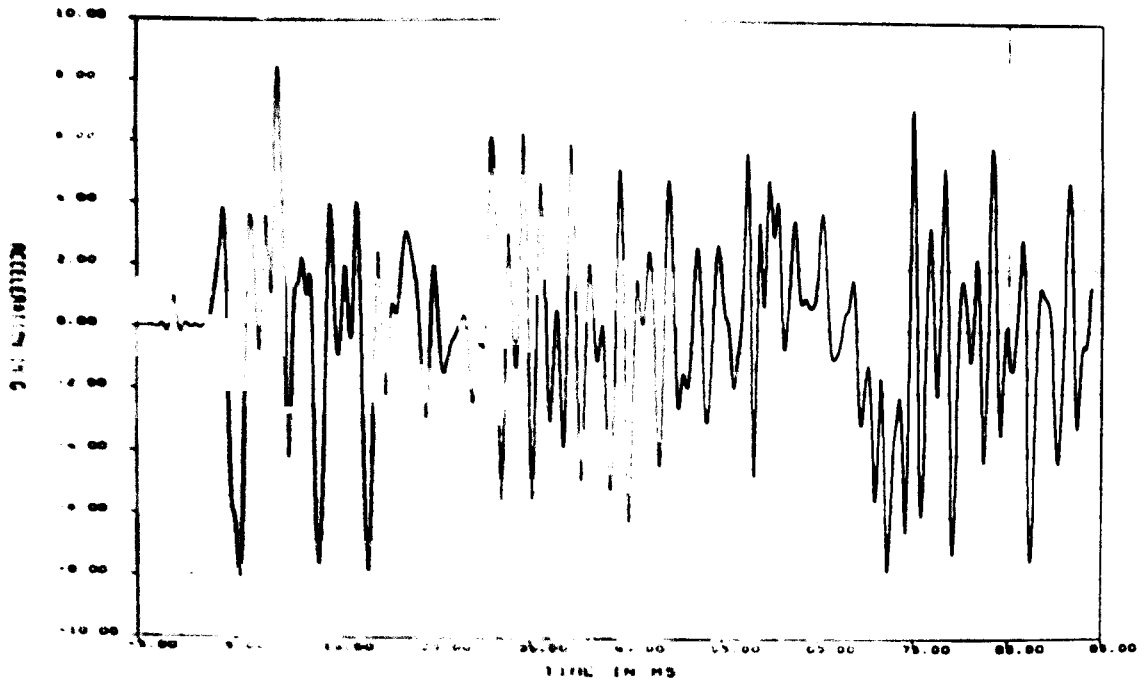


Figure F1-3. Acceleration vs Time for Gage AY3 for 40-in. Closure End Puncture Test (filtered at 1000 Hz)

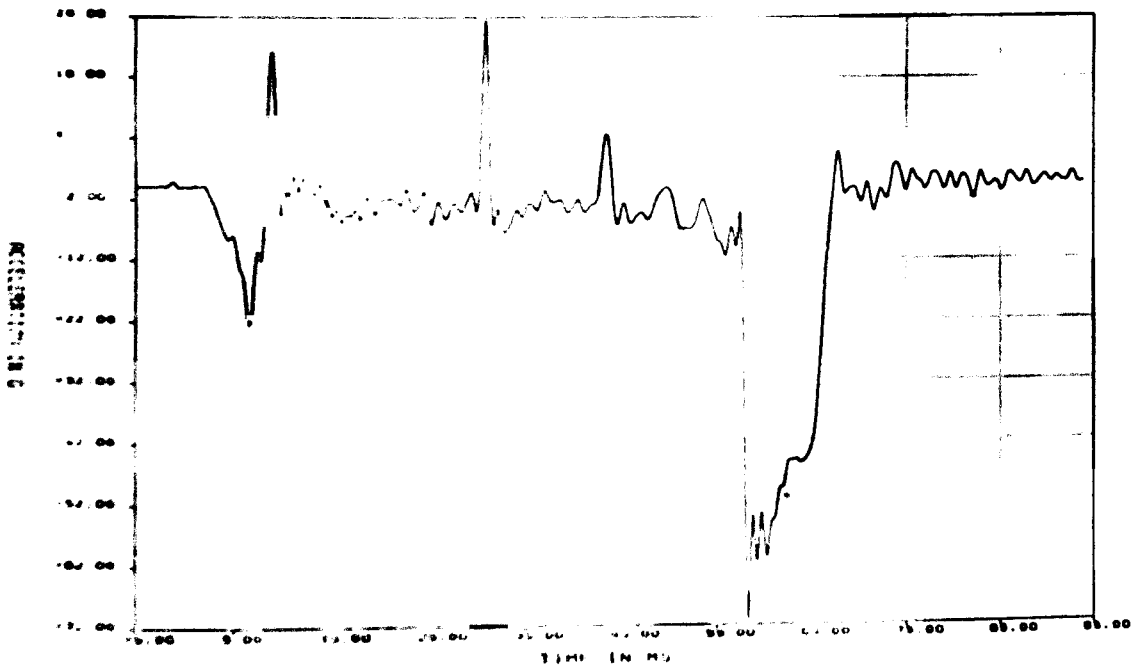


Figure F1-4. Acceleration vs Time for Gage AZ4 for 40-in. Closure End Puncture Test (filtered at 1000 Hz)

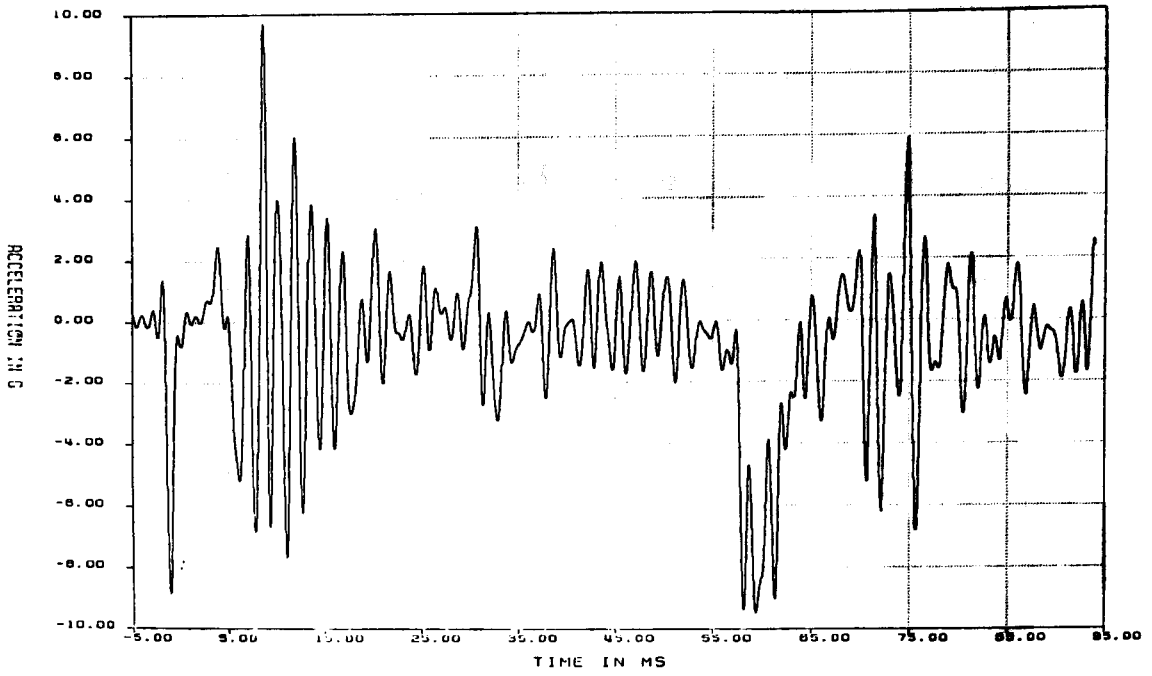


Figure F1-5. Acceleration vs Time for Gage AX5 for 40-in. Closure End Puncture Test (filtered at 1000 Hz)

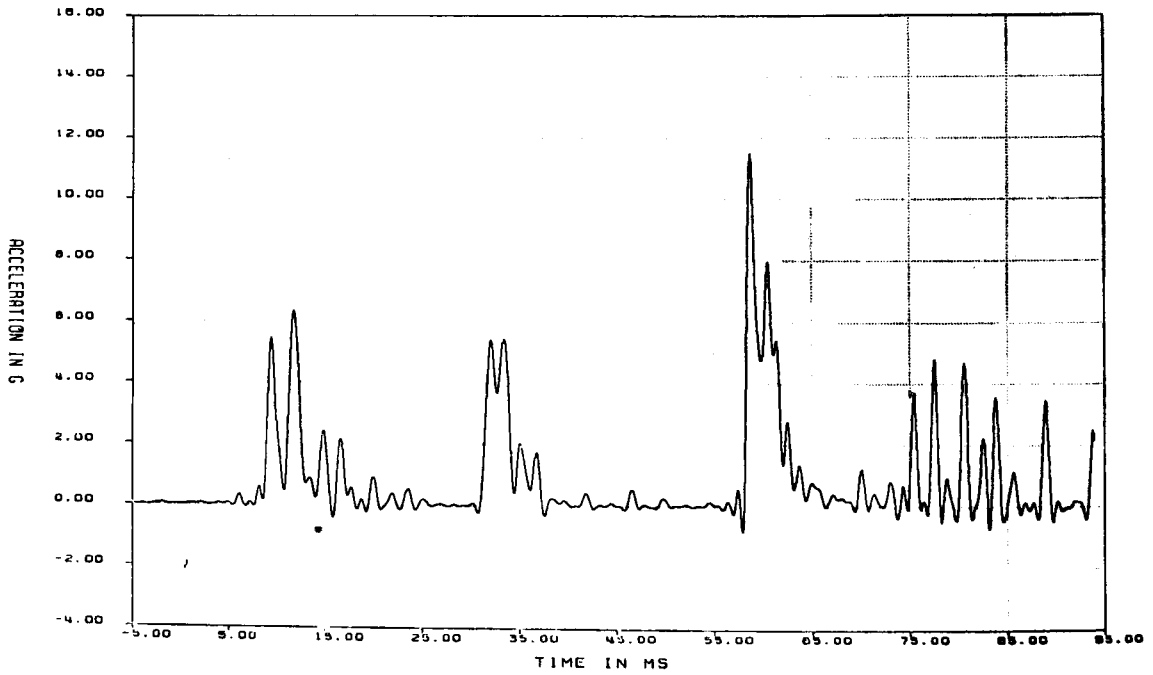


Figure F1-6. Acceleration vs Time for Gage AY6 for 40-in. Closure End Puncture Test (filtered at 1000 Hz)

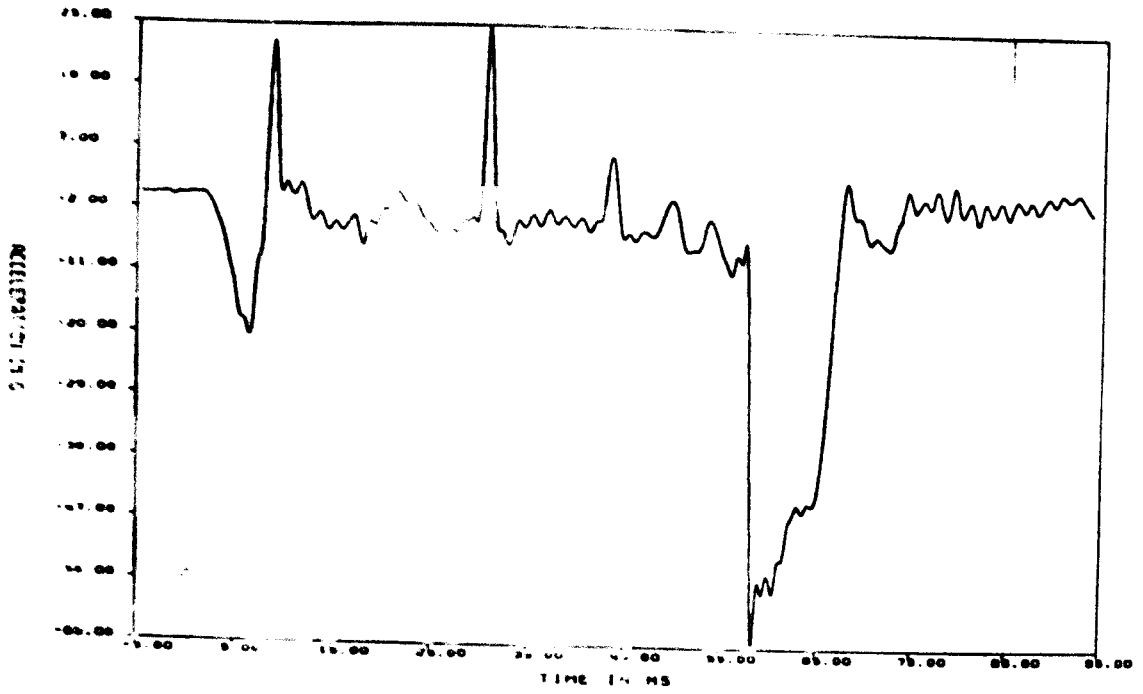


Figure F1-7. Acceleration vs Time for Gage AZ7 for 40-in. Closure End Puncture Test (filtered at 1000 Hz)

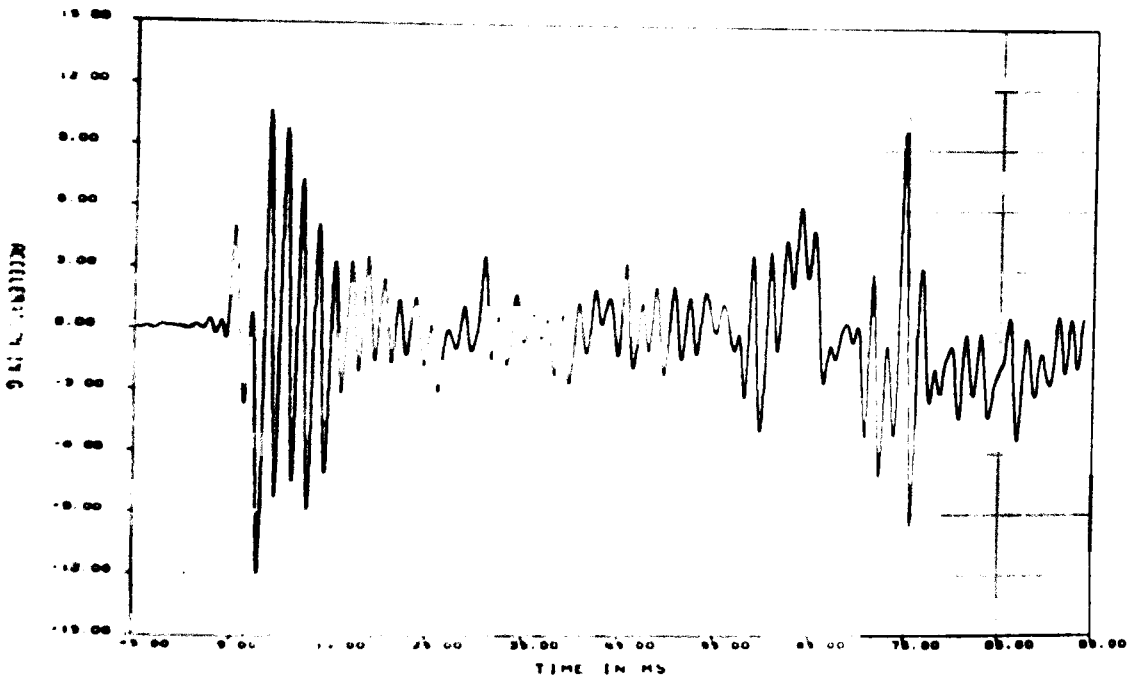


Figure F1-8. Acceleration vs Time for Gage AX8 for 40-in. Closure End Puncture Test (filtered at 1000 Hz)

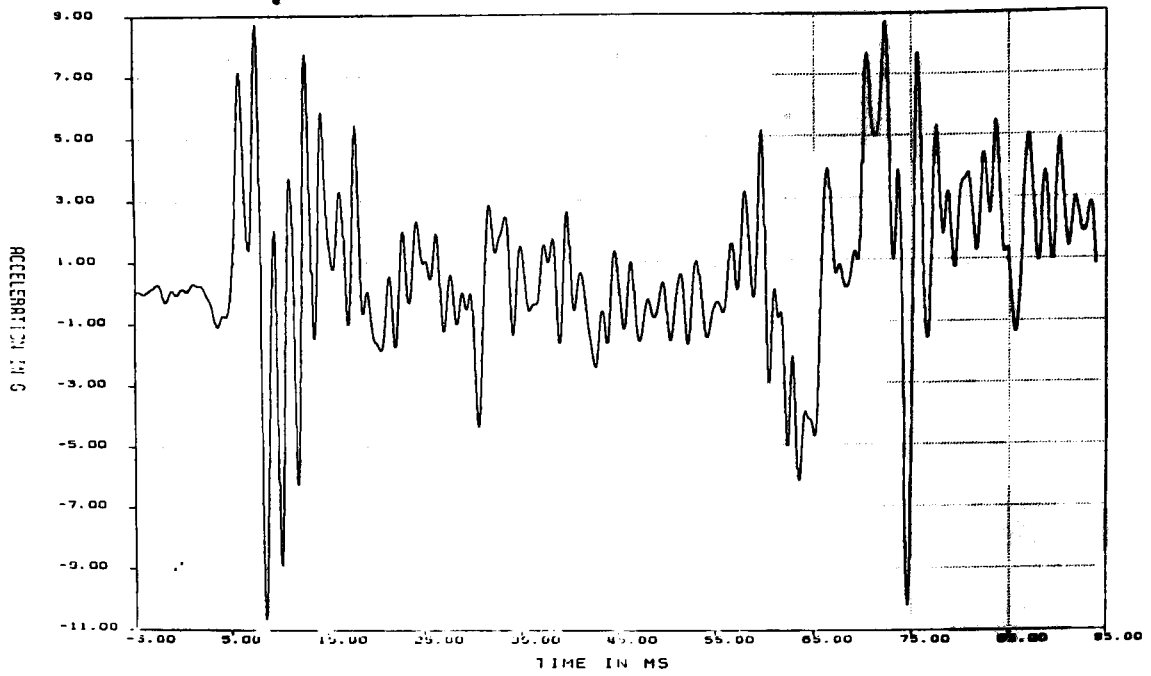


Figure F1-9. Acceleration vs Time for Gage AX9 for 40-in. Closure End Puncture Test (filtered at 1000 Hz)

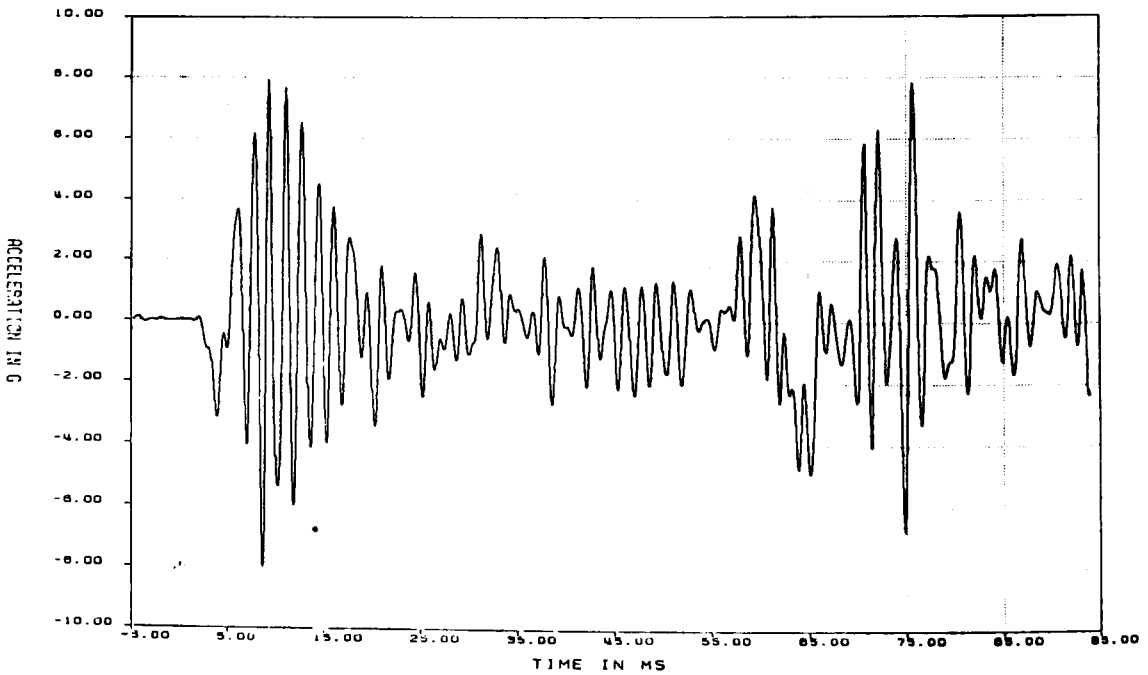


Figure F1-10. Acceleration vs Time for Gage AX10 for 40-in. Closure End Puncture Test (filtered at 1000 Hz)

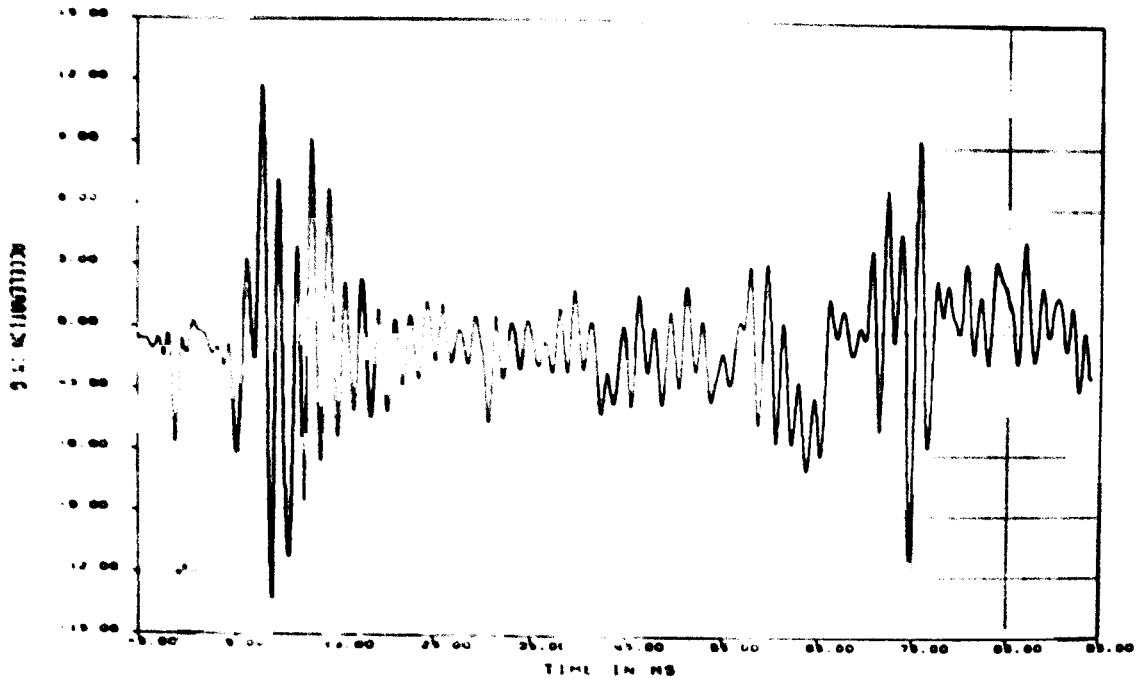


Figure F1-11. Acceleration vs Time for Gage AX11 for 40-in. Closure End Puncture Test (filtered at 1000 Hz)

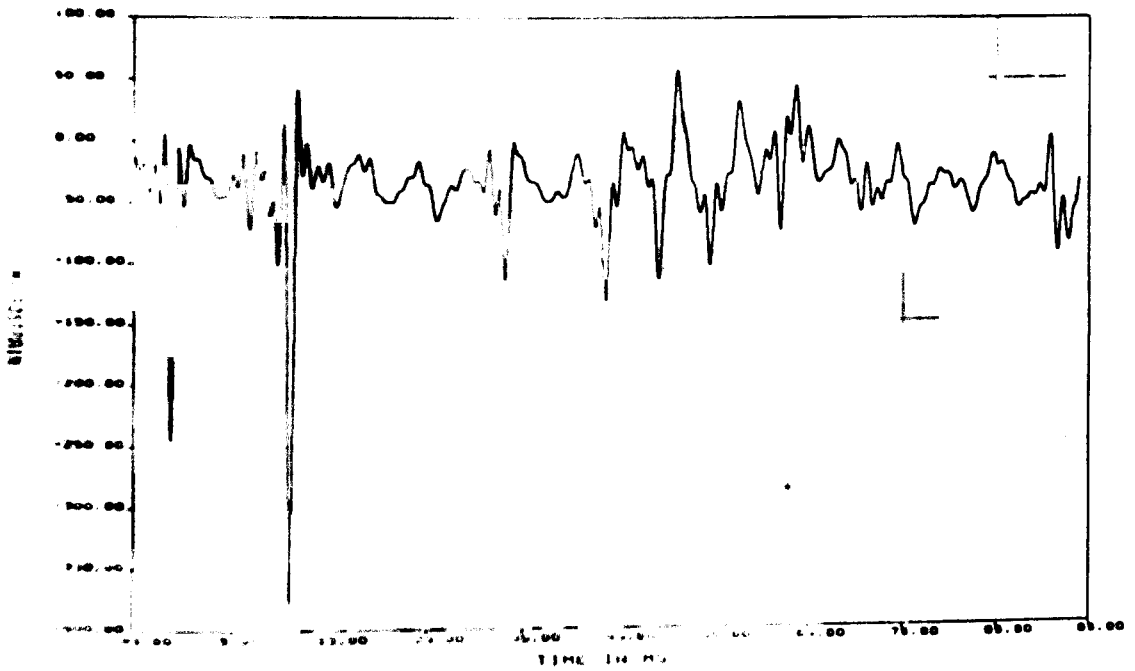


Figure F1-12. Microstrain vs Time for Gage SR1-Y for 40-in. Closure End Puncture Test (filtered at 1000 Hz)

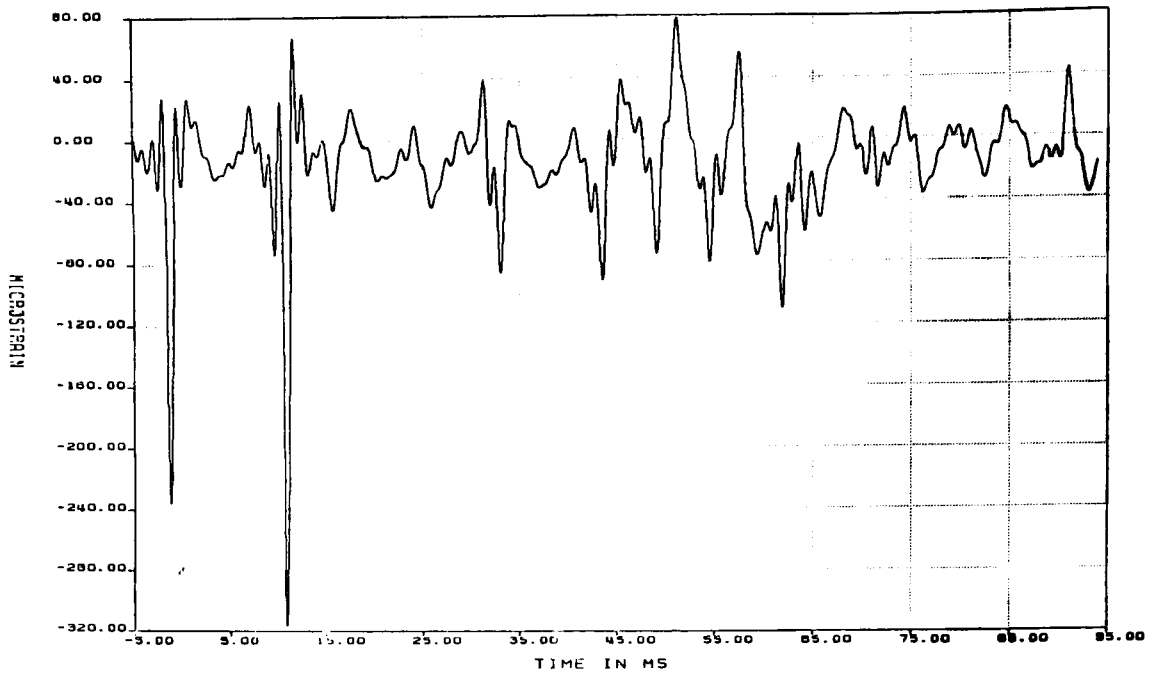


Figure F1-13. Microstrain vs Time for Gage SR1-YZ for 40-in. Closure End Puncture Test (filtered at 1000 Hz)

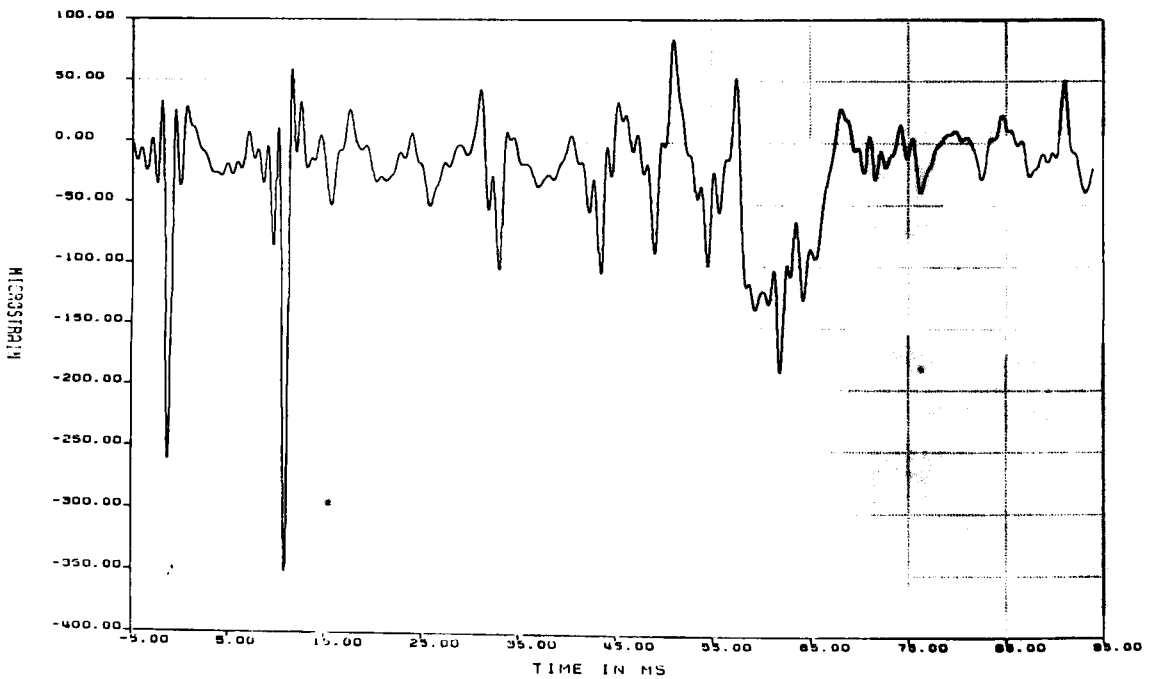


Figure F1-14. Microstrain vs Time for Gage SR1-Z for 40-in. Closure End Puncture Test (filtered at 1000 Hz)

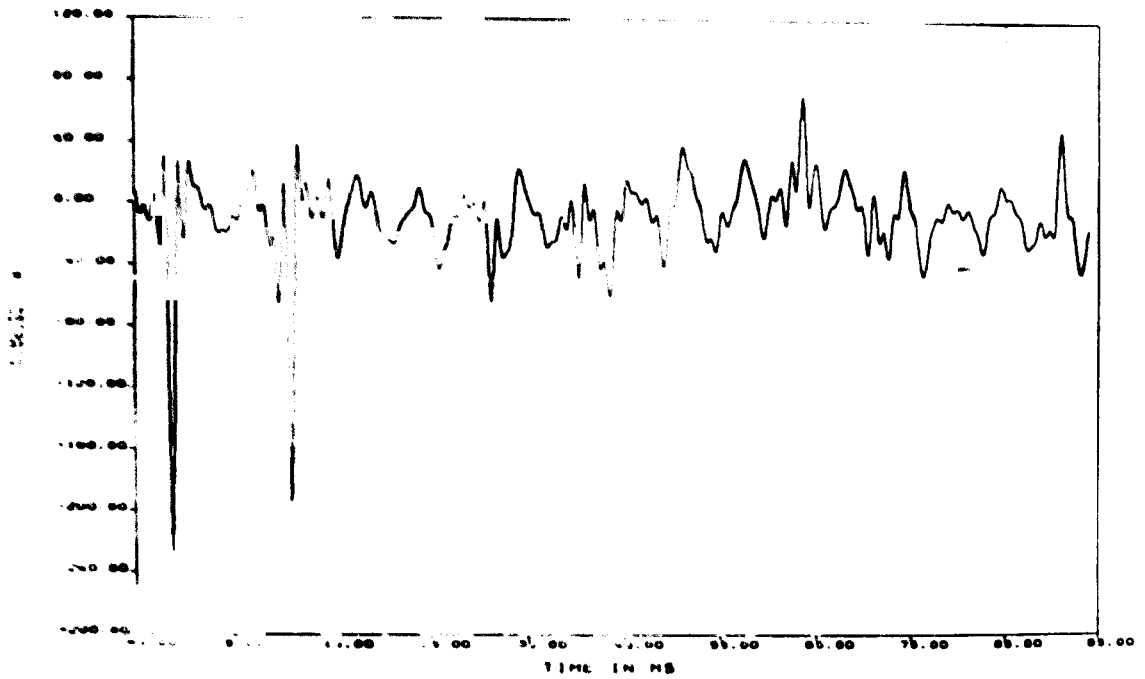


Figure F 1-15. Microstrain vs Time for Gage SR2 Y for 40-in. Closure End Puncture Test (filtered at 1000 Hz)

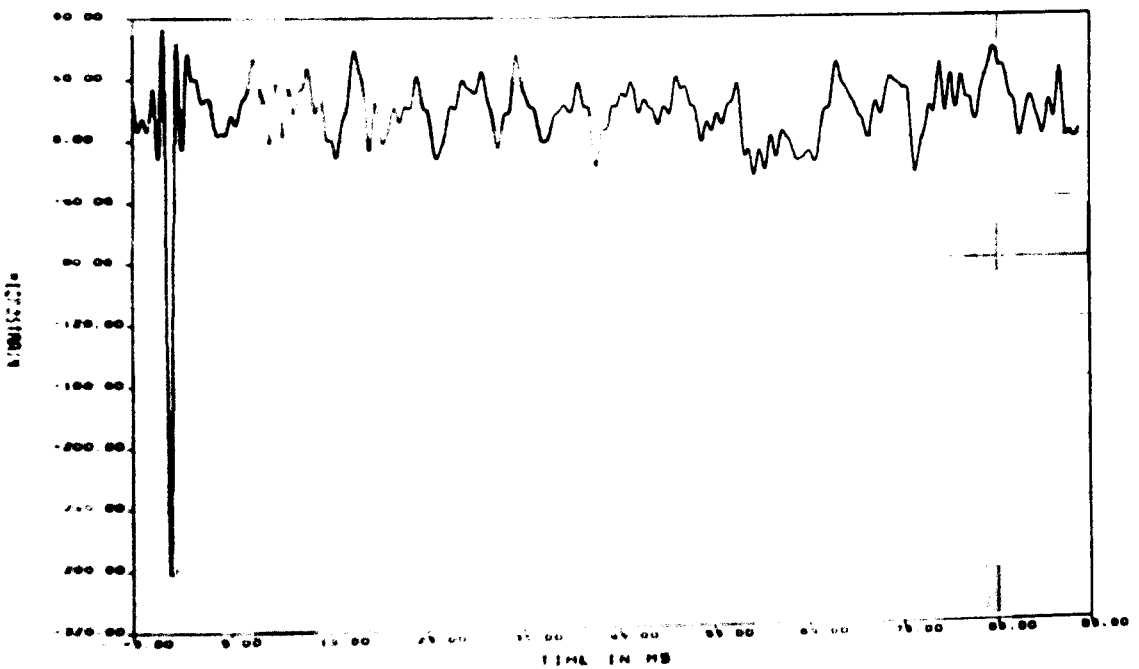


Figure F 1-16. Microstrain vs Time for Gage SR2 YZ for 40-in. Closure End Puncture Test (filtered at 1000 Hz)

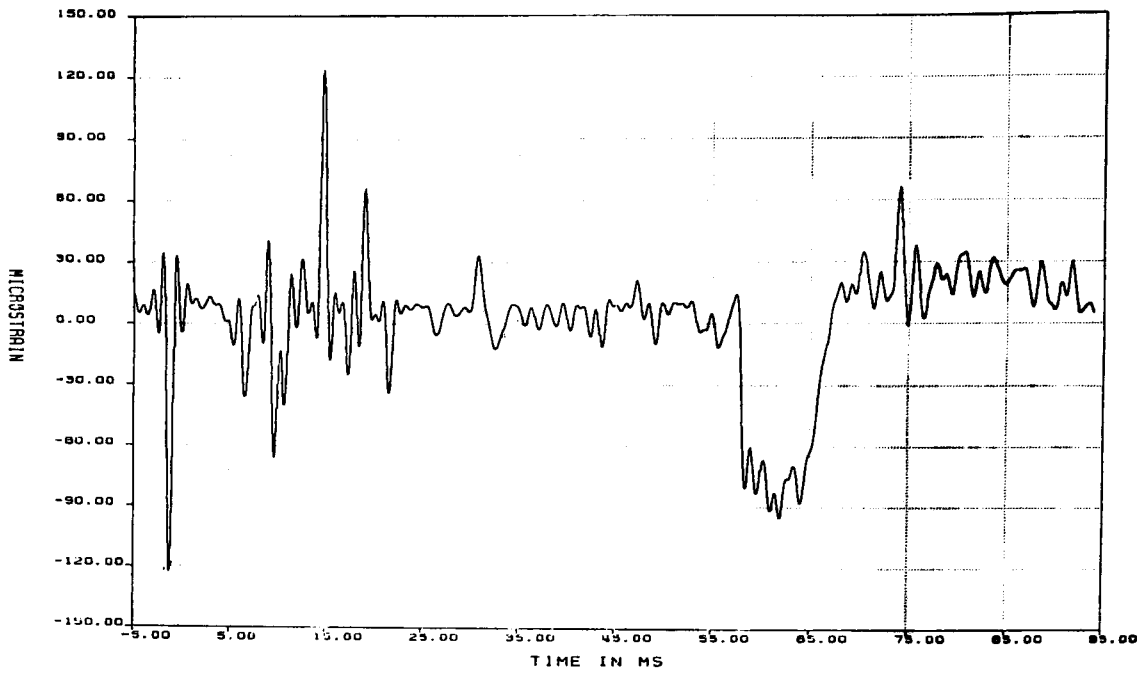


Figure F1-17. Microstrain vs Time for Gage SR2-Z for 40-in. Closure End Puncture Test (filtered at 1000 Hz)

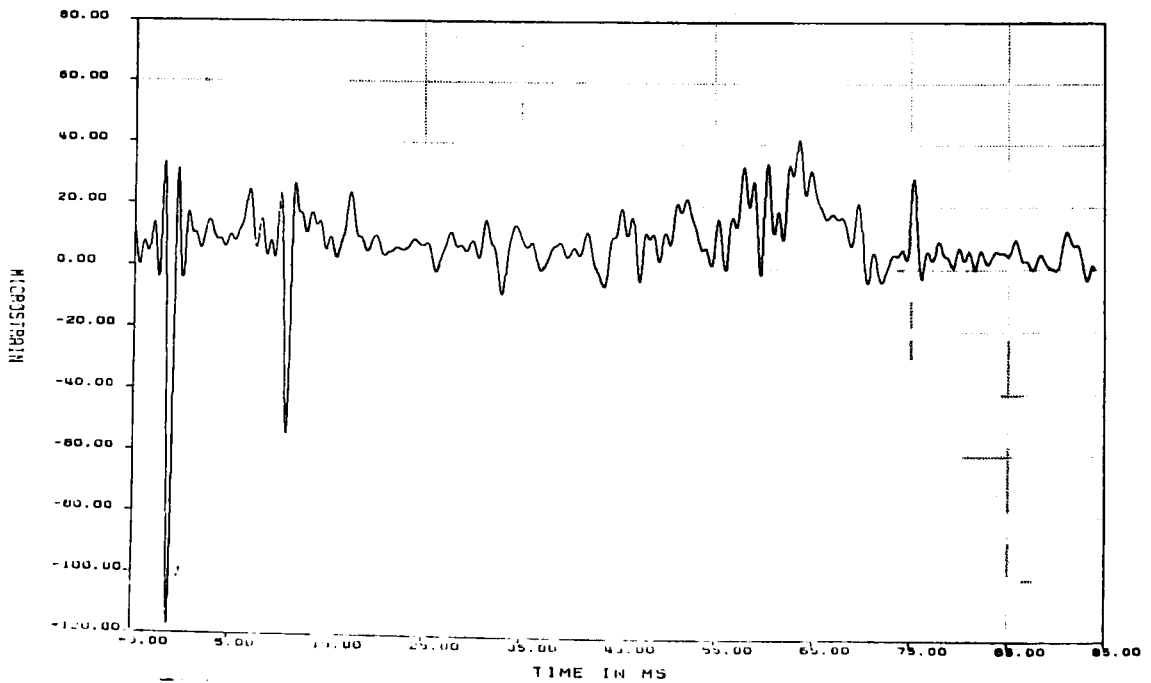


Figure F1-18. Microstrain vs Time for Gage SR3-Y for 40-in. Closure End Puncture Test (filtered at 1000 Hz)

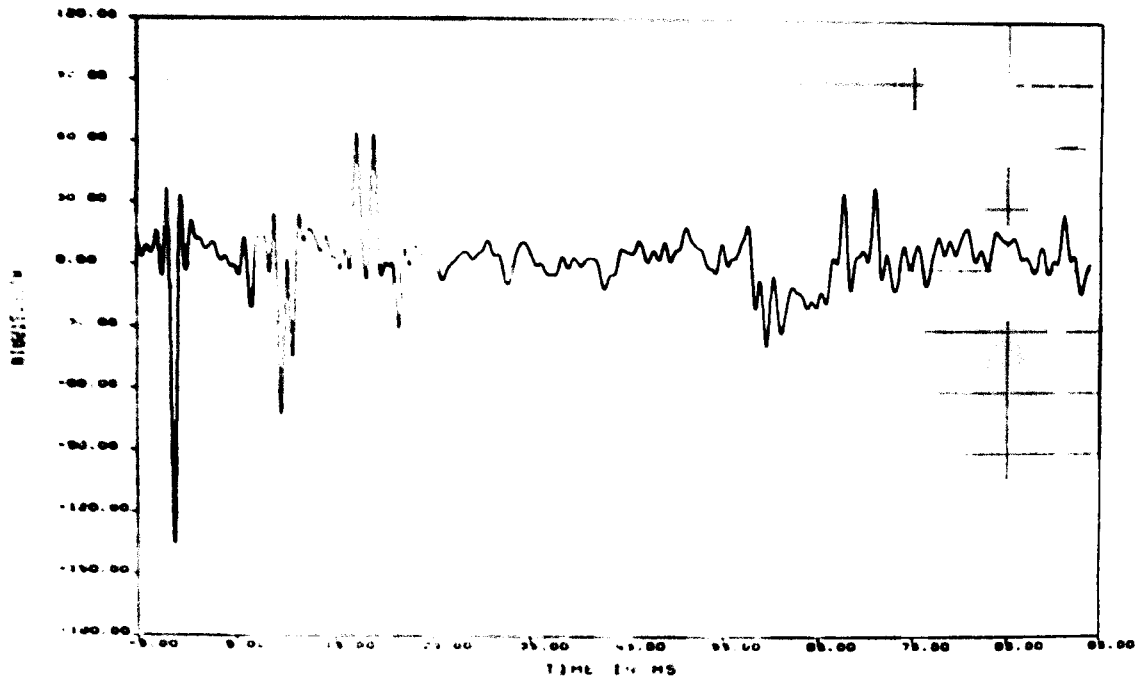


Figure F 1-19. Microstrain vs Time for Gage SR3-YZ for 40-in. Closure End Puncture Test (filtered at 1000 Hz)

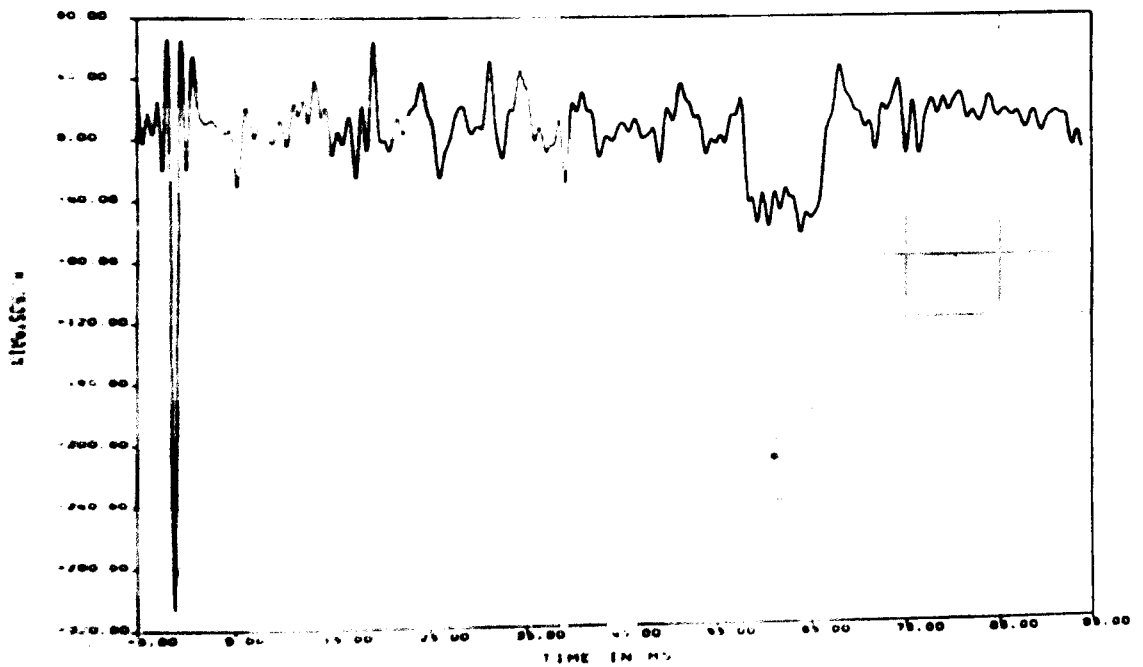


Figure F 1-20. Microstrain vs Time for Gage SR3-Z for 40-in. Closure End Puncture Test (filtered at 1000 Hz)

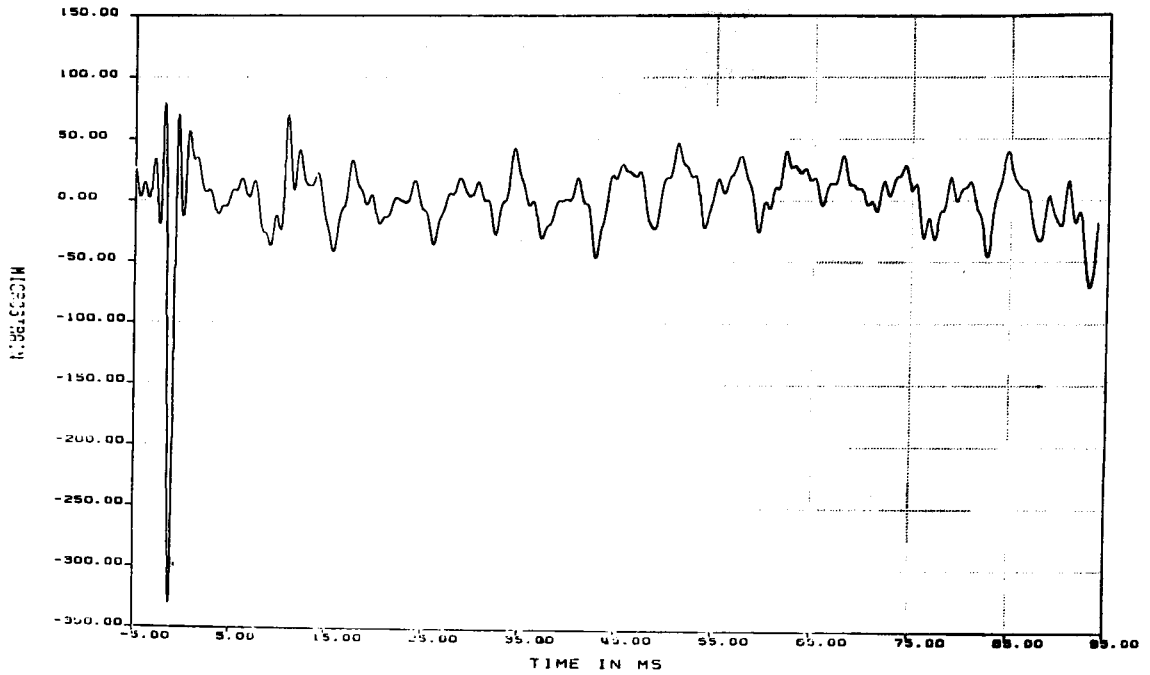


Figure F1-21. Microstrain vs Time for Gage SR4-Y for 40-in. Closure End Puncture Test (filtered at 1000 Hz)

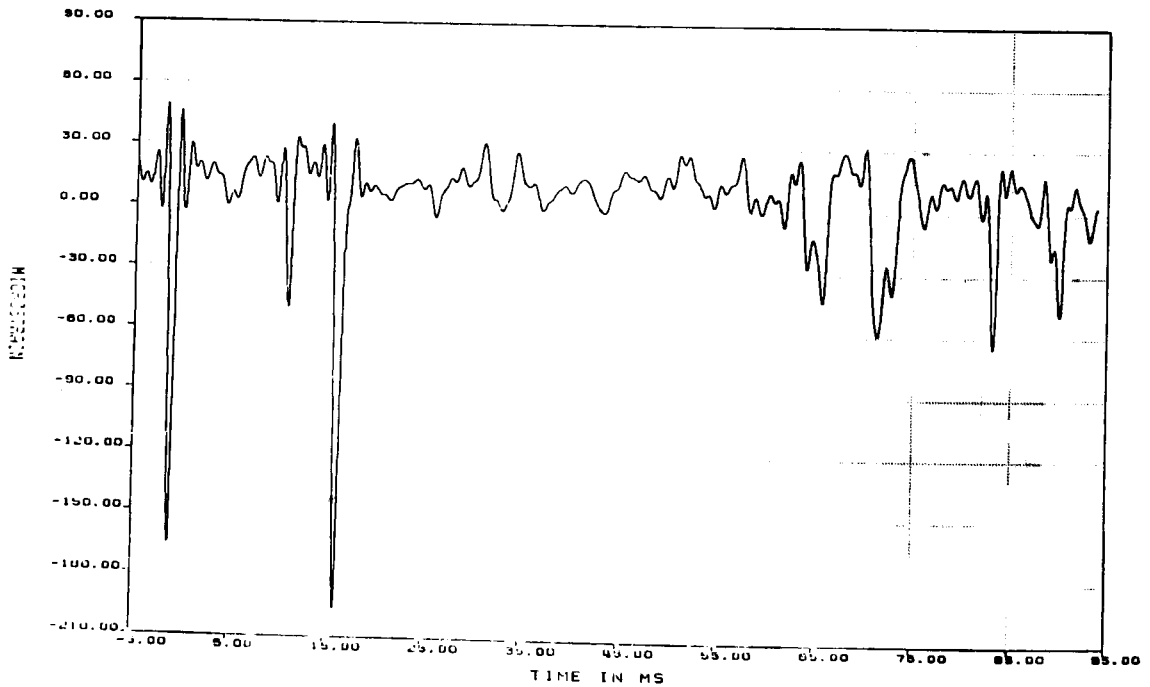


Figure F1-22. Microstrain vs Time for Gage SR4-YZ for 40-in. Closure End Puncture Test (filtered at 1000 Hz)

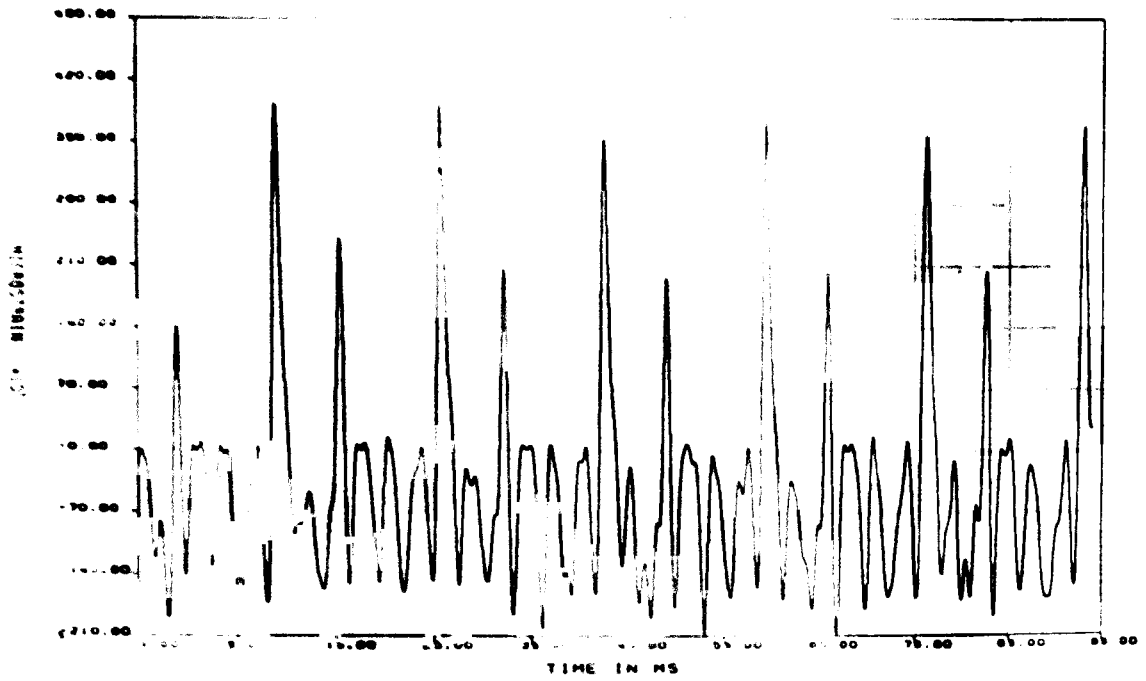


Figure F 1-23. Microstrain vs Time for Gage SR4-Z for 40-in. Closure End Puncture Test (filtered at 1000 Hz)

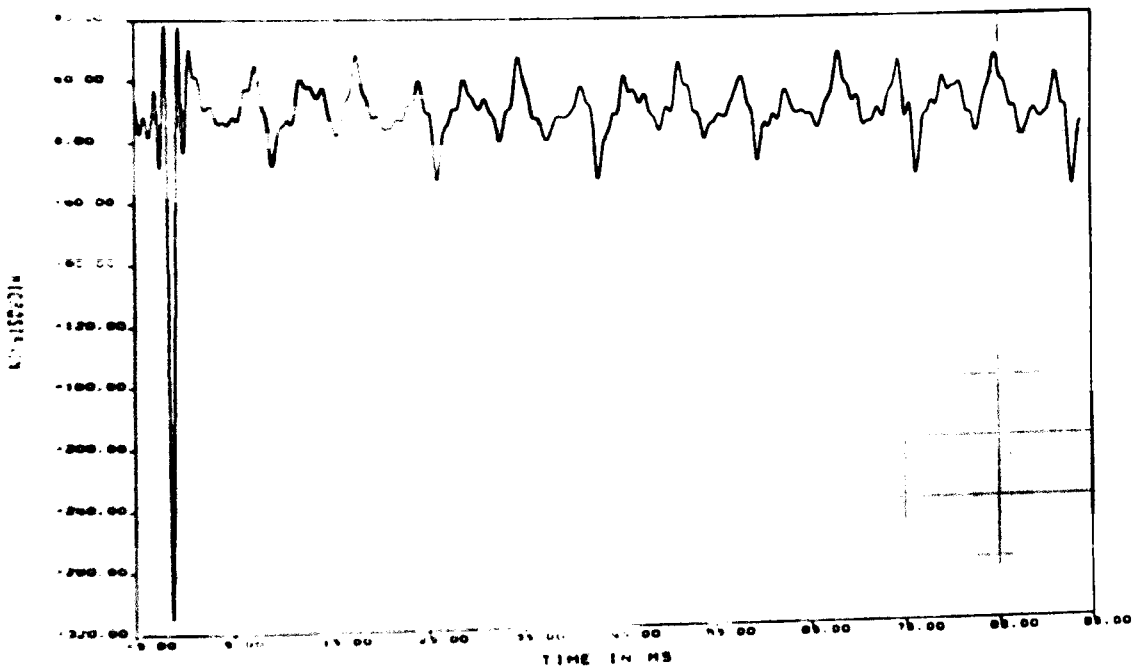


Figure F 1-24. Microstrain vs Time for Gage SR5-Y for 40-in. Closure End Puncture Test (filtered at 1000 Hz)

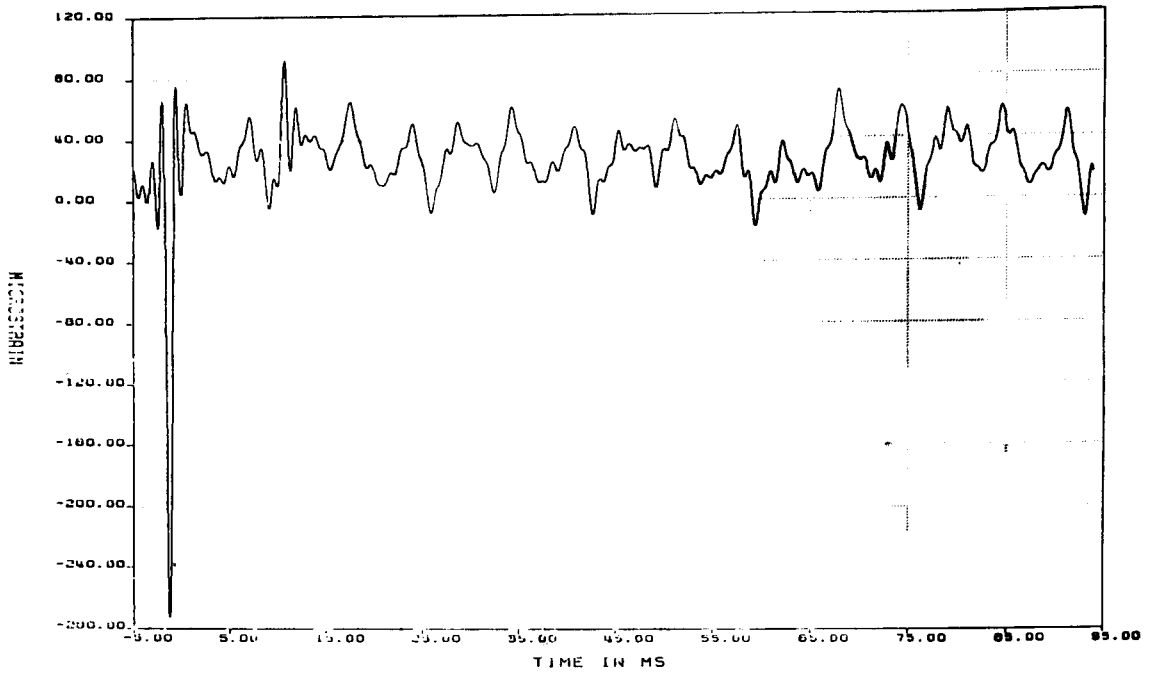


Figure F1-25. Microstrain vs Time for Gage SR5-YZ for 40-in. Closure End Puncture Test (filtered at 1000 Hz)

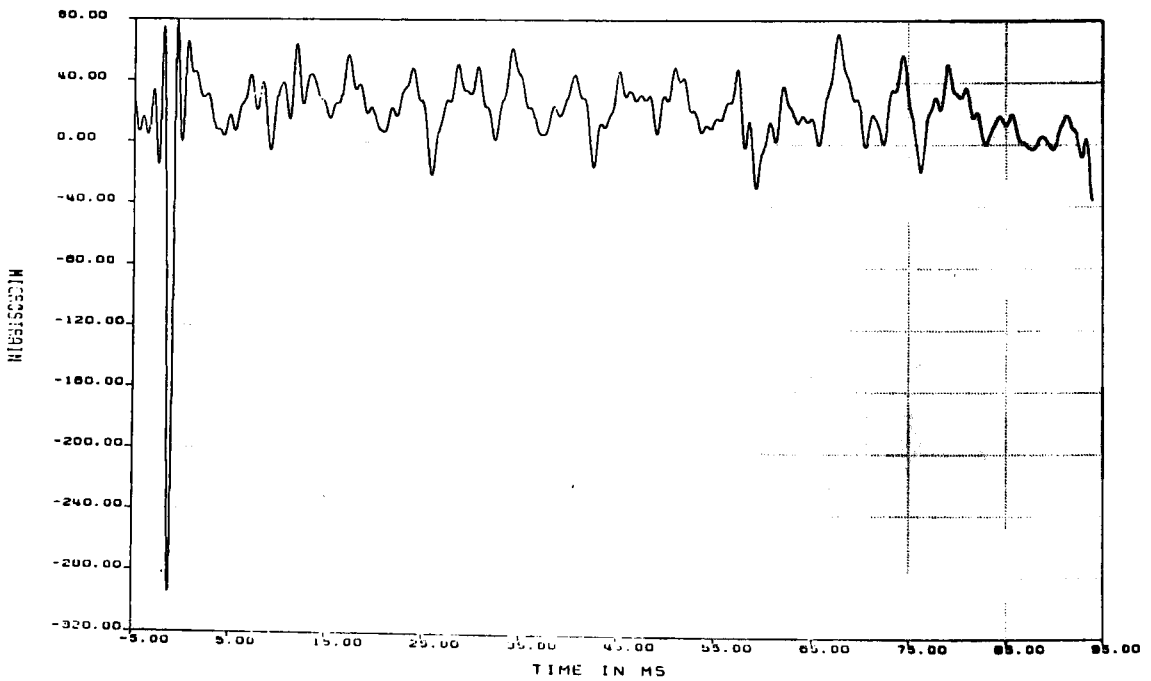


Figure F1-26. Microstrain vs Time for Gage SR5-Z for 40-in. Closure End Puncture Test (filtered at 1000 Hz)

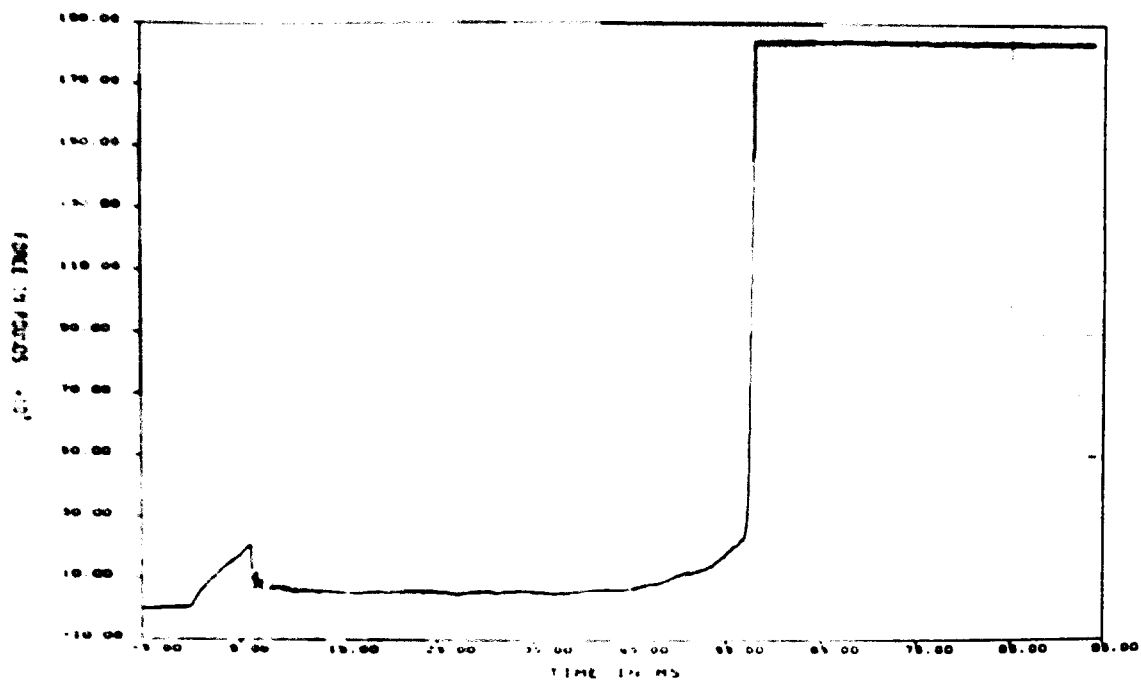


Figure F-1-27. Force vs Time for Gage F-1 on Puncture Bar for 40-in. Closure End Puncture Test (raw data)

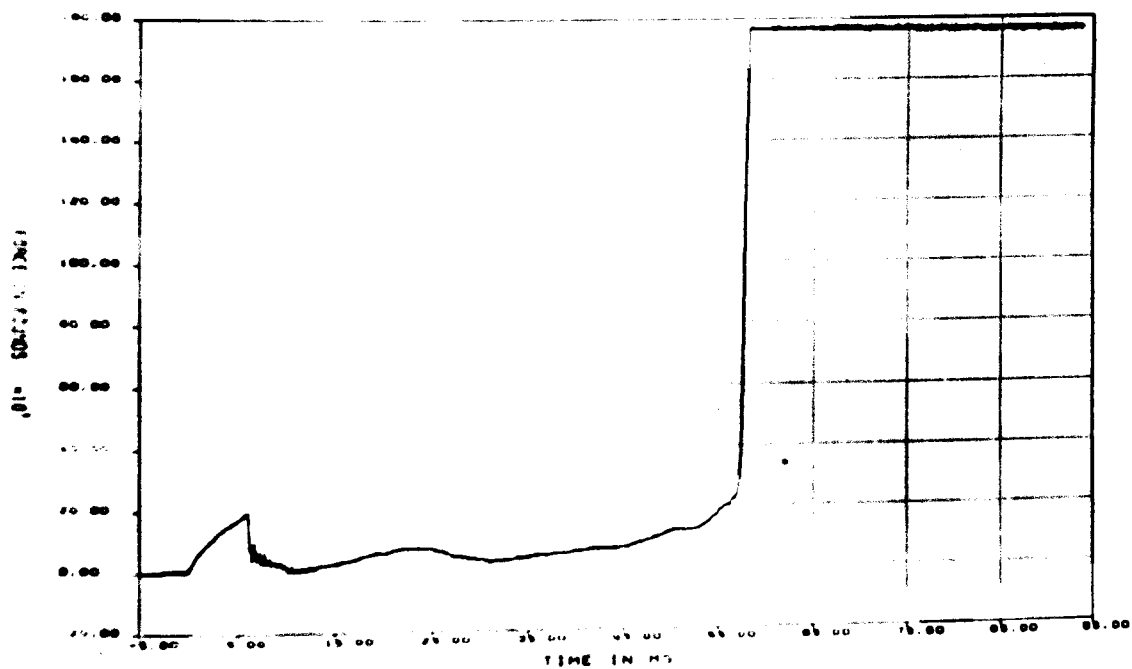


Figure F-1-28. Force vs Time for Gage F-2 on Puncture Bar for 40-in. Closure End Puncture Test (raw data)

APPENDIX F2

Fast Fourier Transforms of Raw Accelerometer Data for the 40-in. Closure End Puncture Test

Figures

F2-1	Fast Fourier Transform of Raw Data From Gage AZ1 for 40-in. Closure End Puncture Test: 0-50 kHz	274
F2-2	Fast Fourier Transform of Raw Data From Gage AZ1 for 40-in. Closure End Puncture Test: 0-10 kHz	274
F2-3	Fast Fourier Transform of Raw Data From Gage AX2 for 40-in. Closure End Puncture Test: 0-50 kHz	275
F2-4	Fast Fourier Transform of Raw Data From Gage AX2 for 40-in. Closure End Puncture Test: 0-10 kHz	275
F2-5	Fast Fourier Transform of Raw Data From Gage AY3 for 40-in. Closure End Puncture Test: 0-50 kHz	276
F2-6	Fast Fourier Transform of Raw Data From Gage AY3 for 40-in. Closure End Puncture Test: 0-10 kHz	276
F2-7	Fast Fourier Transform of Raw Data From Gage AZ4 for 40-in. Closure End Puncture Test: 0-50 kHz	277
F2-8	Fast Fourier Transform of Raw Data From Gage AZ4 for 40-in. Closure End Puncture Test: 0-10 kHz	277
F2-9	Fast Fourier Transform of Raw Data From Gage AX5 for 40-in. Closure End Puncture Test: 0-50 kHz	278
F2-10	Fast Fourier Transform of Raw Data From Gage AX5 for 40-in. Closure End Puncture Test: 0-10 kHz	278
F2-11	Fast Fourier Transform of Raw Data From Gage AY6 for 40-in. Closure End Puncture Test: 0-50 kHz	279
F2-12	Fast Fourier Transform of Raw Data From Gage AY6 for 40-in. Closure End Puncture Test: 0-10 kHz	279
F2-13	Fast Fourier Transform of Raw Data From Gage AZ7 for 40-in. Closure End Puncture Test: 0-50 kHz	280
F2-14	Fast Fourier Transform of Raw Data From Gage AZ7 for 40-in. Closure End Puncture Test: 0-10 kHz	280
F2-15	Fast Fourier Transform of Raw Data From Gage AX8 for 40-in. Closure End Puncture Test: 0-50 kHz	281
F2-16	Fast Fourier Transform of Raw Data From Gage AX8 for 40-in. Closure End Puncture Test: 0-10 kHz	281
F2-17	Fast Fourier Transform of Raw Data From Gage AX9 for 40-in. Closure End Puncture Test: 0-50 kHz	282
F2-18	Fast Fourier Transform of Raw Data From Gage AX9 for 40-in. Closure End Puncture Test: 0-10 kHz	282
F2-19	Fast Fourier Transform of Raw Data From Gage AX10 for 40-in. Closure End Puncture Test: 0-50 kHz	283
F2-20	Fast Fourier Transform of Raw Data From Gage AX10 for 40-in. Closure End Puncture Test: 0-10 kHz	283
F2-21	Fast Fourier Transform of Raw Data From Gage AX11 for 40-in. Closure End Puncture Test: 0-50 kHz	284
F2-22	Fast Fourier Transform of Raw Data From Gage AX11 for 40-in. Closure End Puncture Test: 0-10 kHz	284

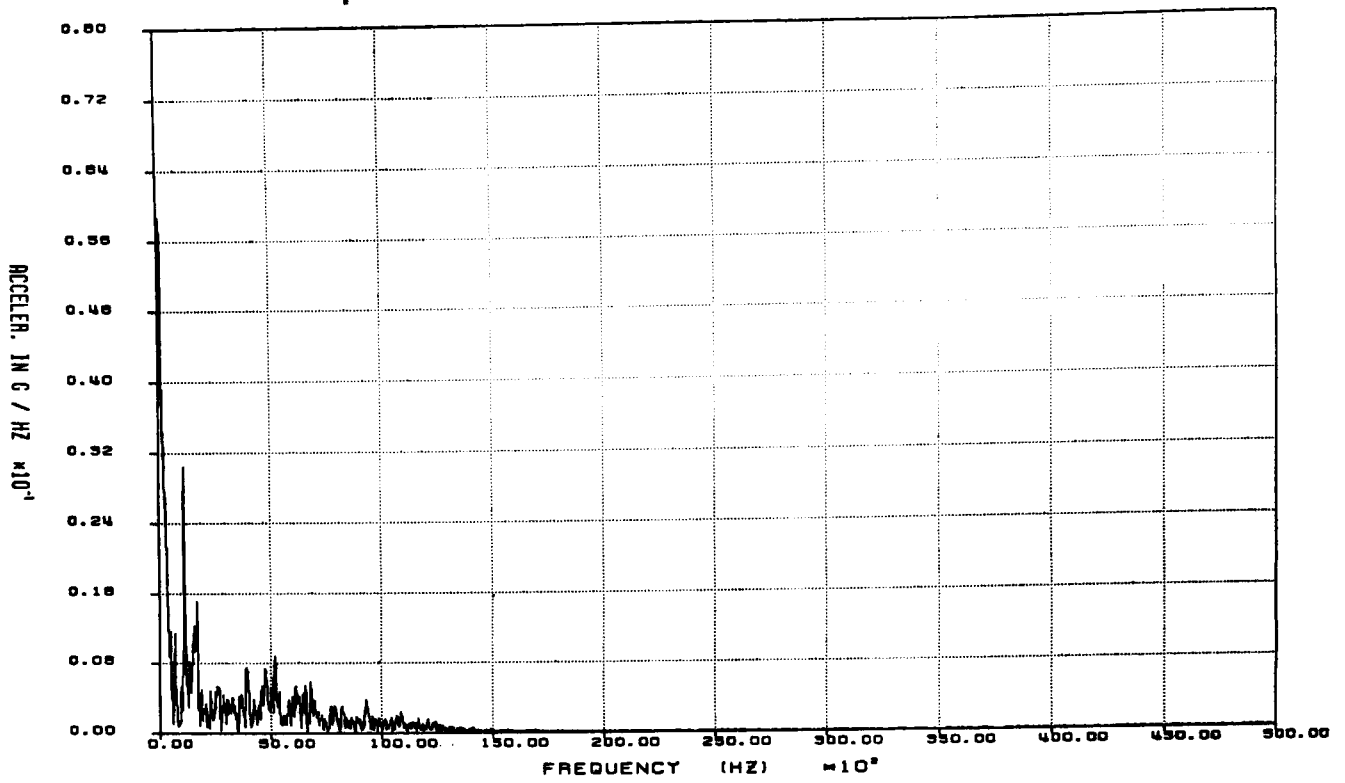


Figure F2-1. Fast Fourier Transform of Raw Data From Gage AZ1 for 40-in. Closure End Puncture Test: 0-50 kHz

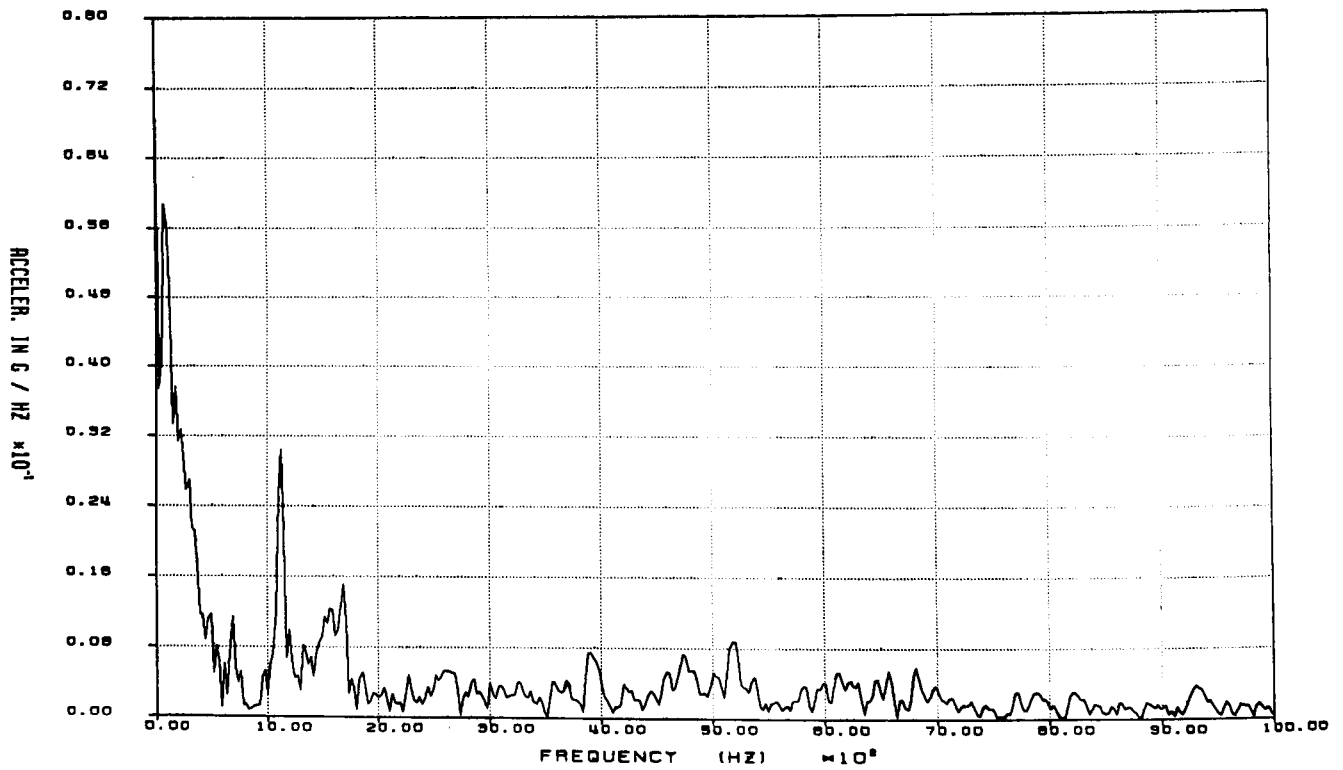


Figure F2-2. Fast Fourier Transform of Raw Data From Gage AZ1 for 40-in. Closure End Puncture Test: 0-10 kHz

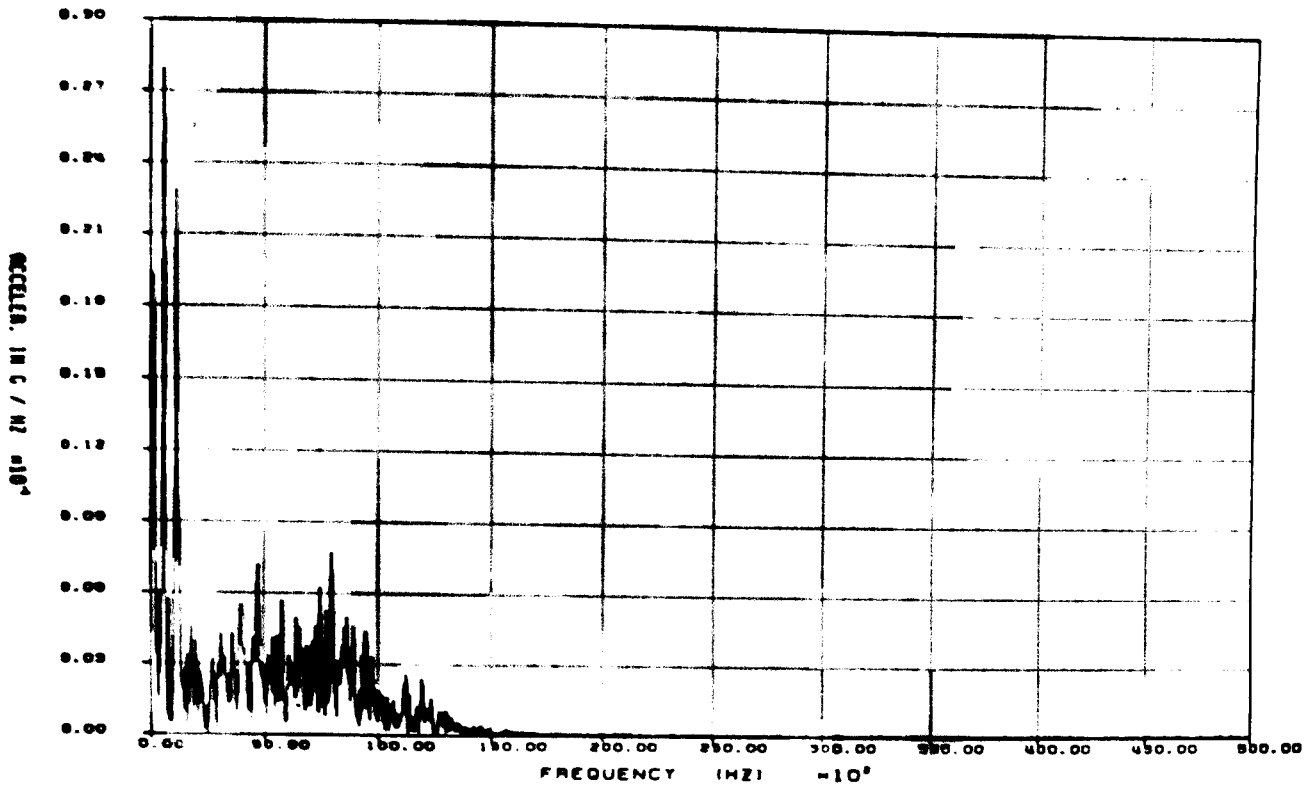


Figure F2-3. Fast Fourier Transform of Raw Data From Gage AX2 for 40-in. Closure End Puncture Test: 0-50 kHz

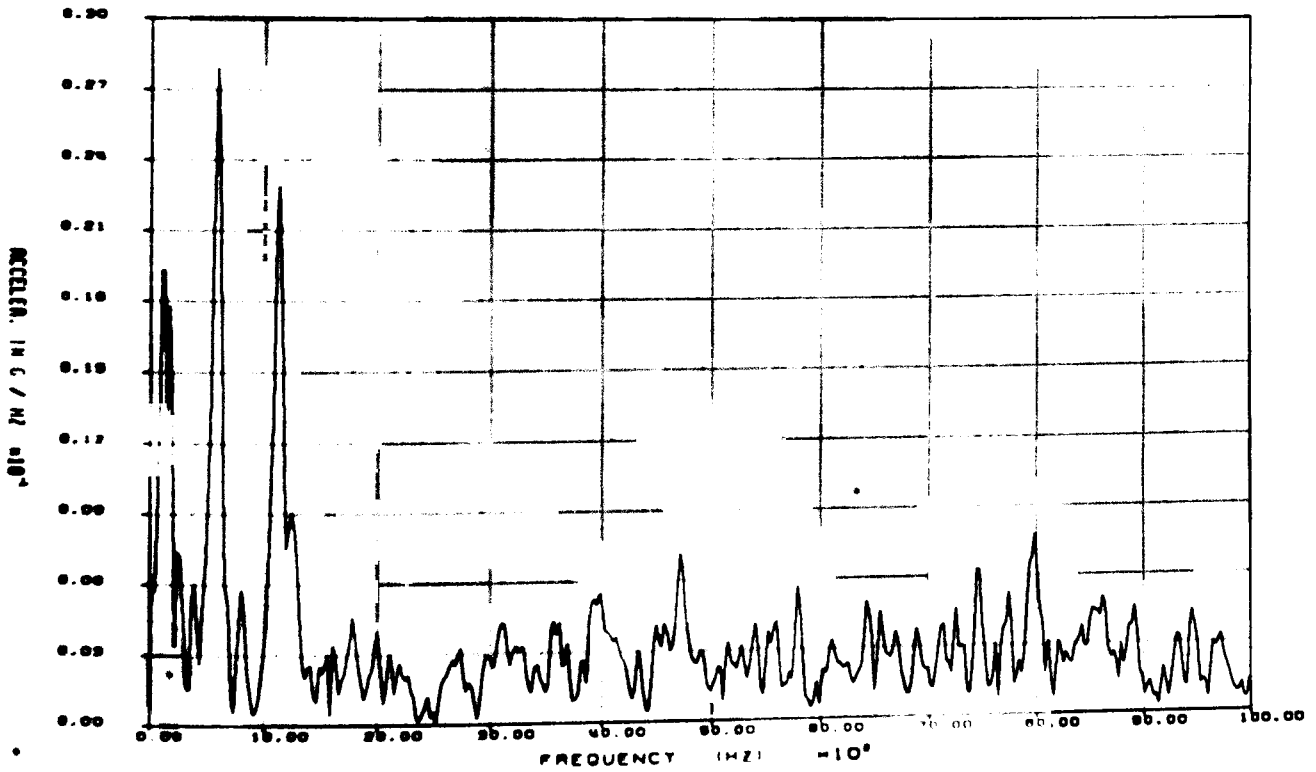


Figure F2-4. Fast Fourier Transform of Raw Data From Gage AX2 for 40-in. Closure End Puncture Test: 0-10 kHz

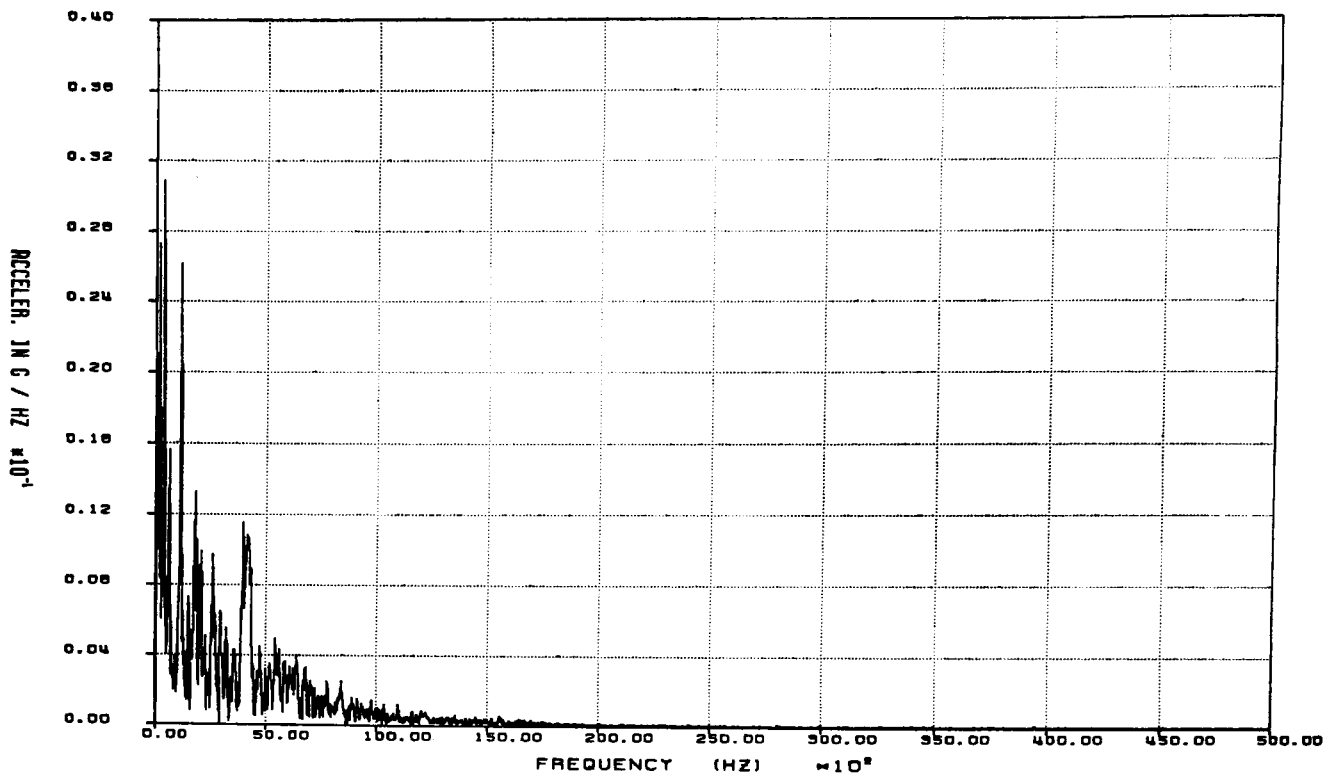


Figure F2-5. Fast Fourier Transform of Raw Data From Gage AY3 for 40-in. Closure End Puncture Test: 0-50 kHz

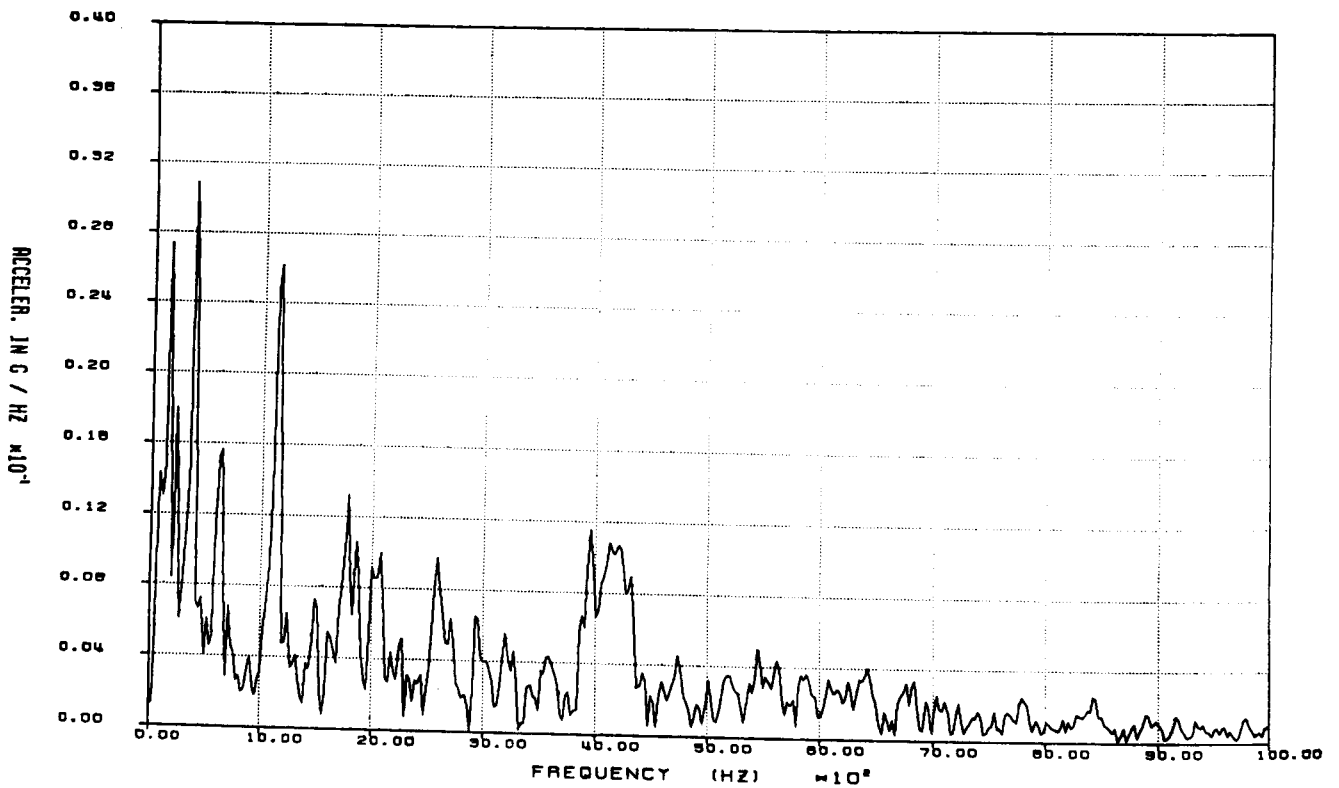


Figure F2-6. Fast Fourier Transform of Raw Data From Gage AY3 for 40-in. Closure End Puncture Test: 0-10 kHz

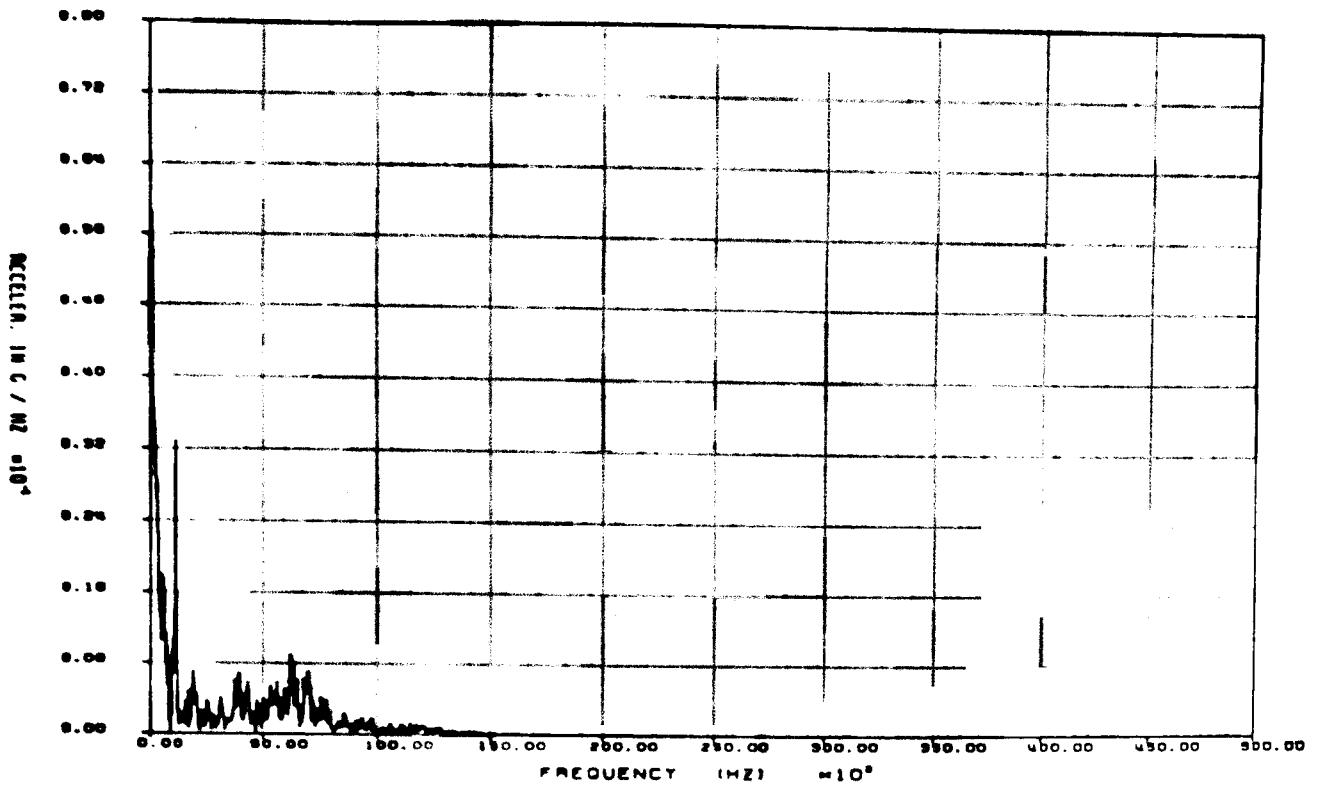


Figure F2-7. Fast Fourier Transform of Raw Data From Gage AZ4 for 40-in. Closure End Puncture Test: 0-50 kHz

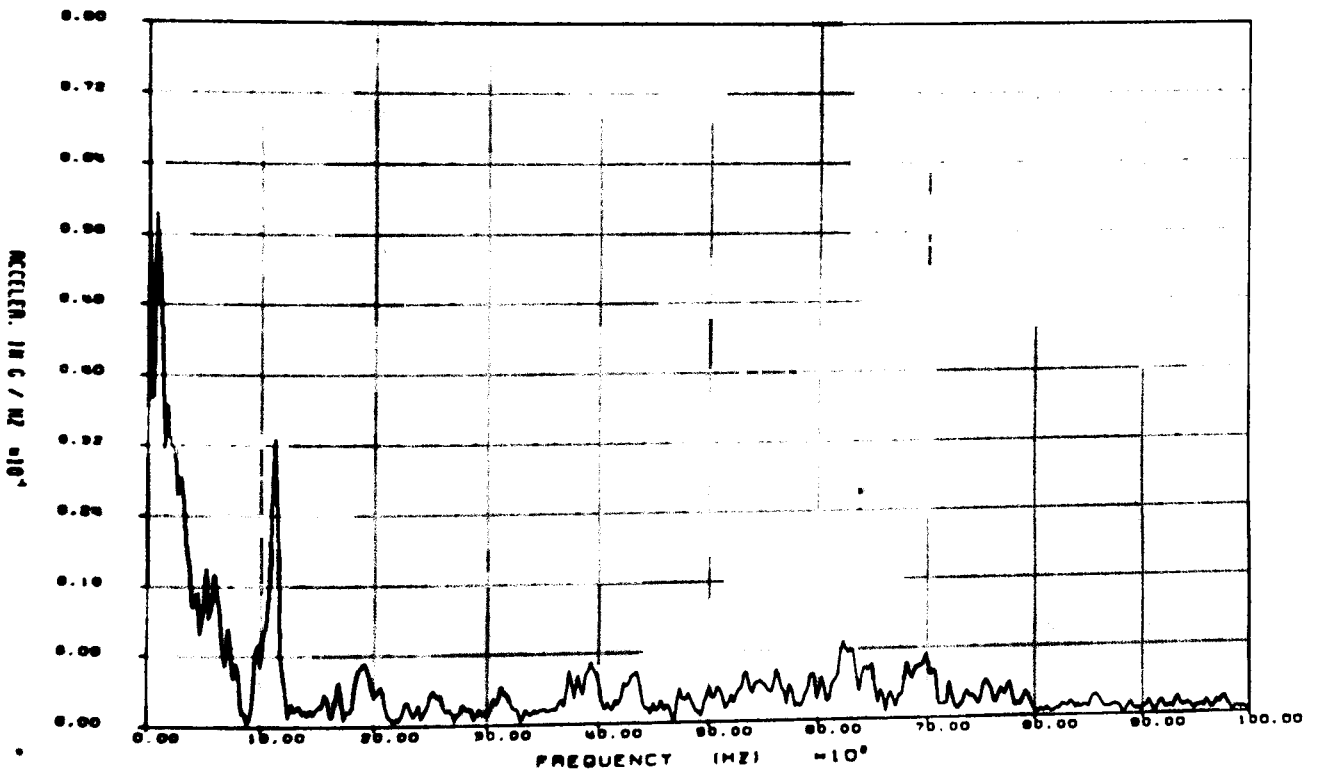


Figure F2-8. Fast Fourier Transform of Raw Data From Gage AZ4 for 40-in. Closure End Puncture Test: 0-10 kHz

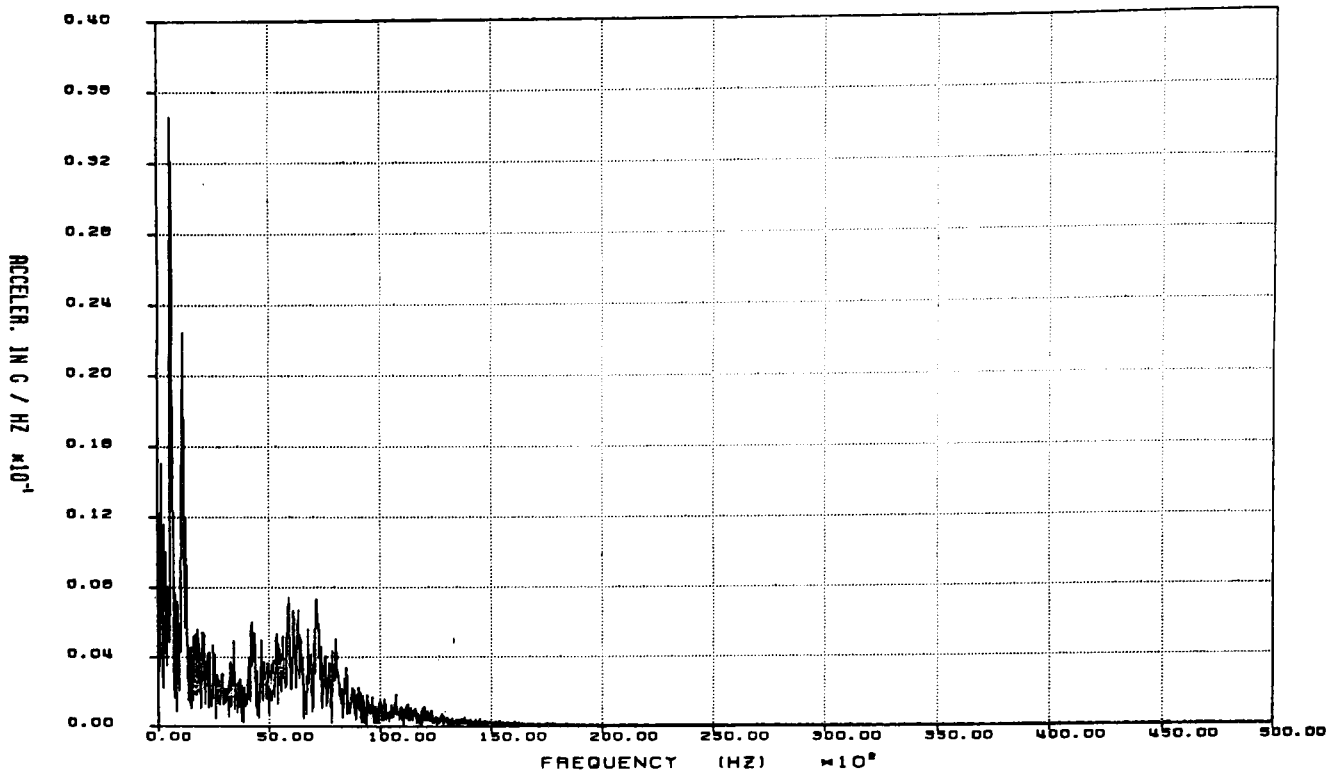


Figure F2-9. Fast Fourier Transform of Raw Data From Gage AX5 for 40-in. Closure End Puncture Test: 0-50 kHz

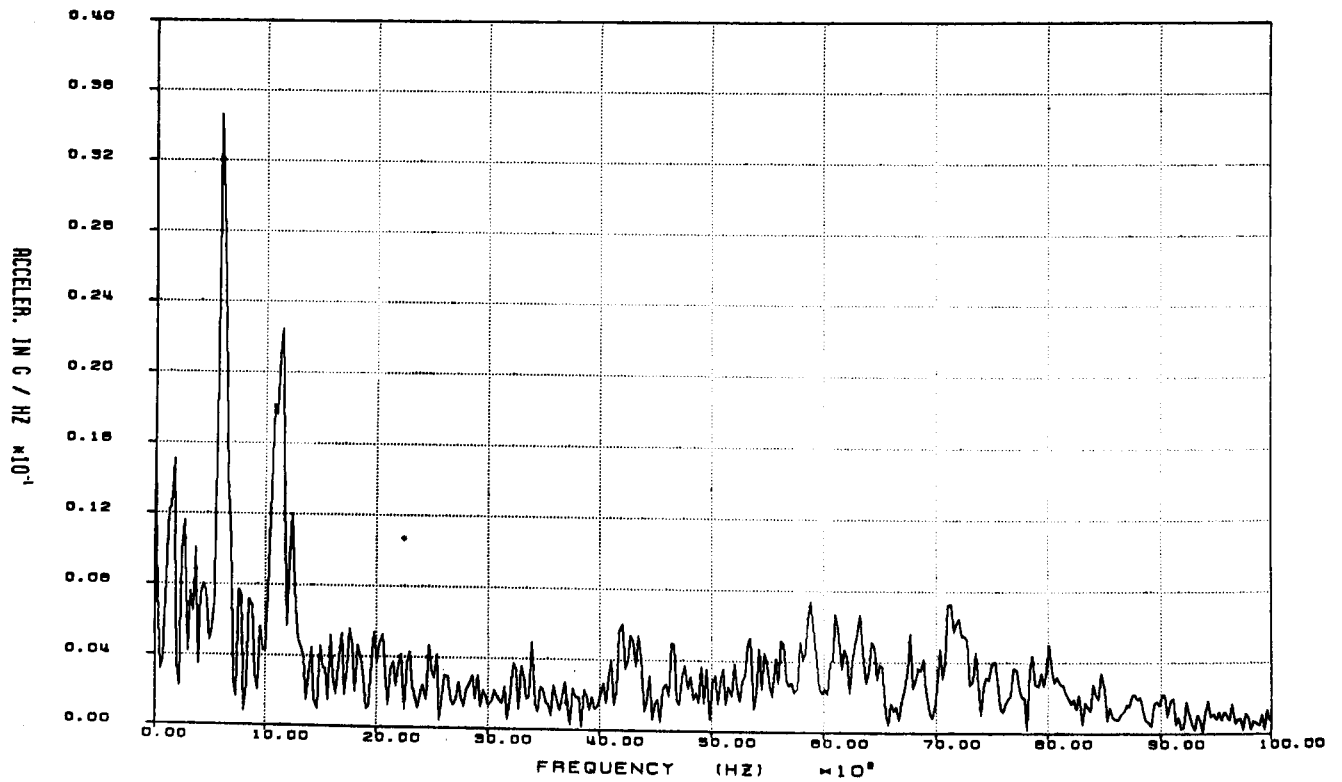


Figure F2-10. Fast Fourier Transform of Raw Data From Gage AX5 for 40-in. Closure End Puncture Test: 0-10 kHz

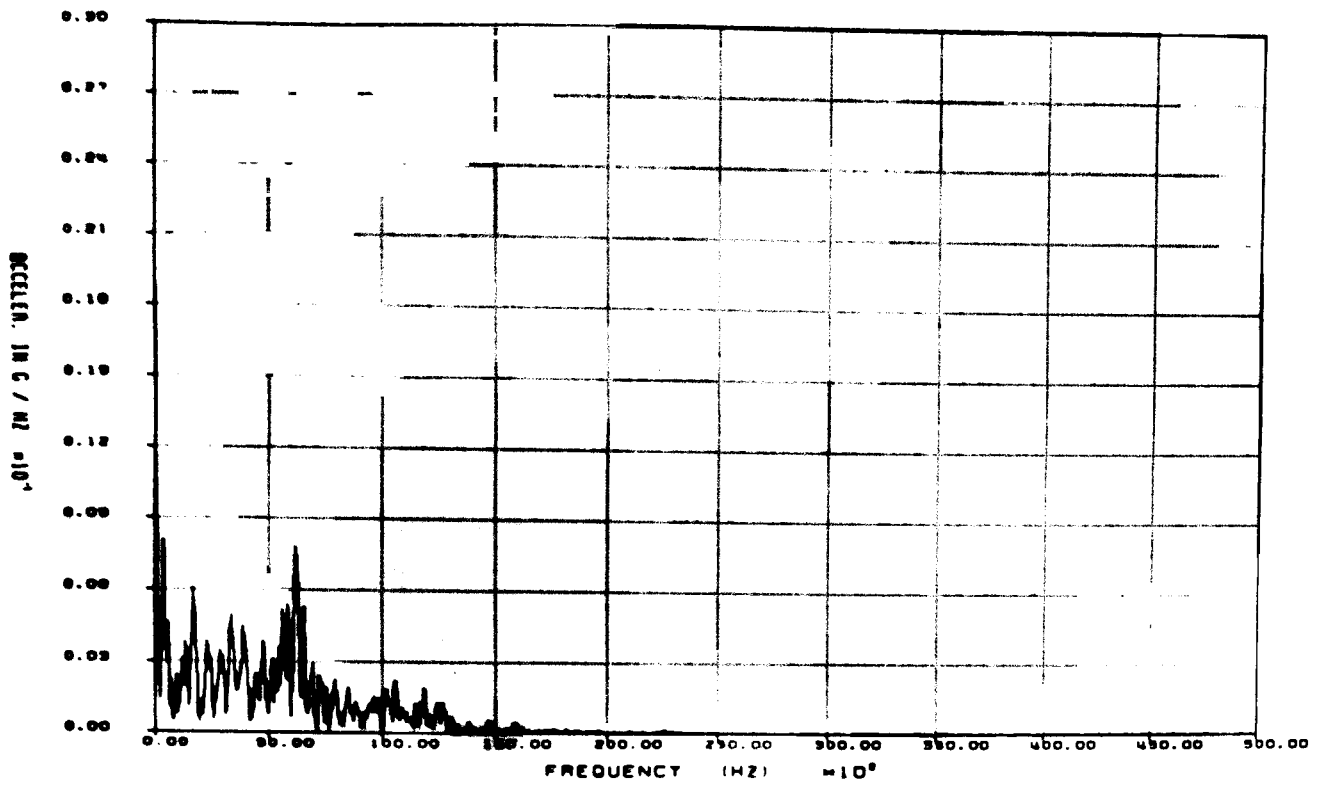


Figure F2-11. Fast Fourier Transform of Raw Data From Gage AY6 for 40-in. Closure End Puncture Test: 0-50 kHz

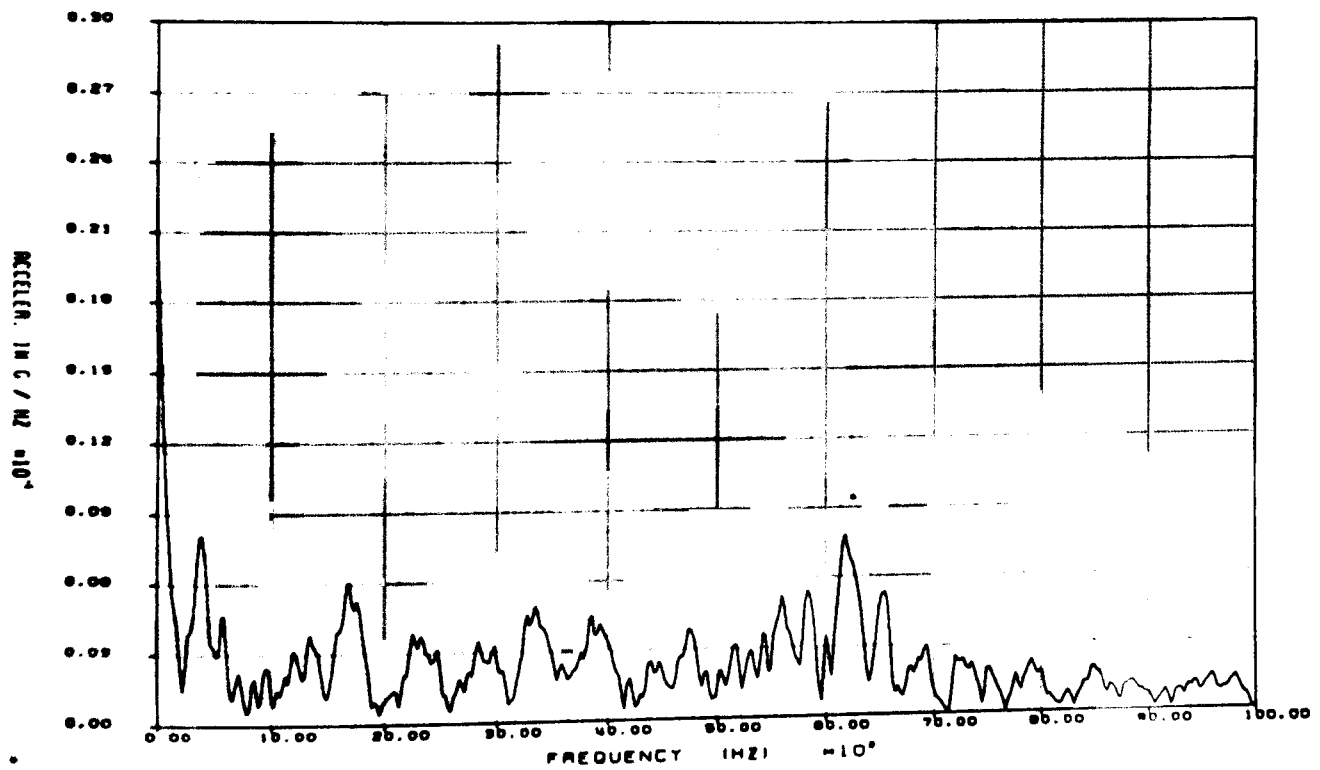


Figure F2-12. Fast Fourier Transform of Raw Data From Gage AY6 for 40-in. Closure End Puncture Test: 0-10 kHz

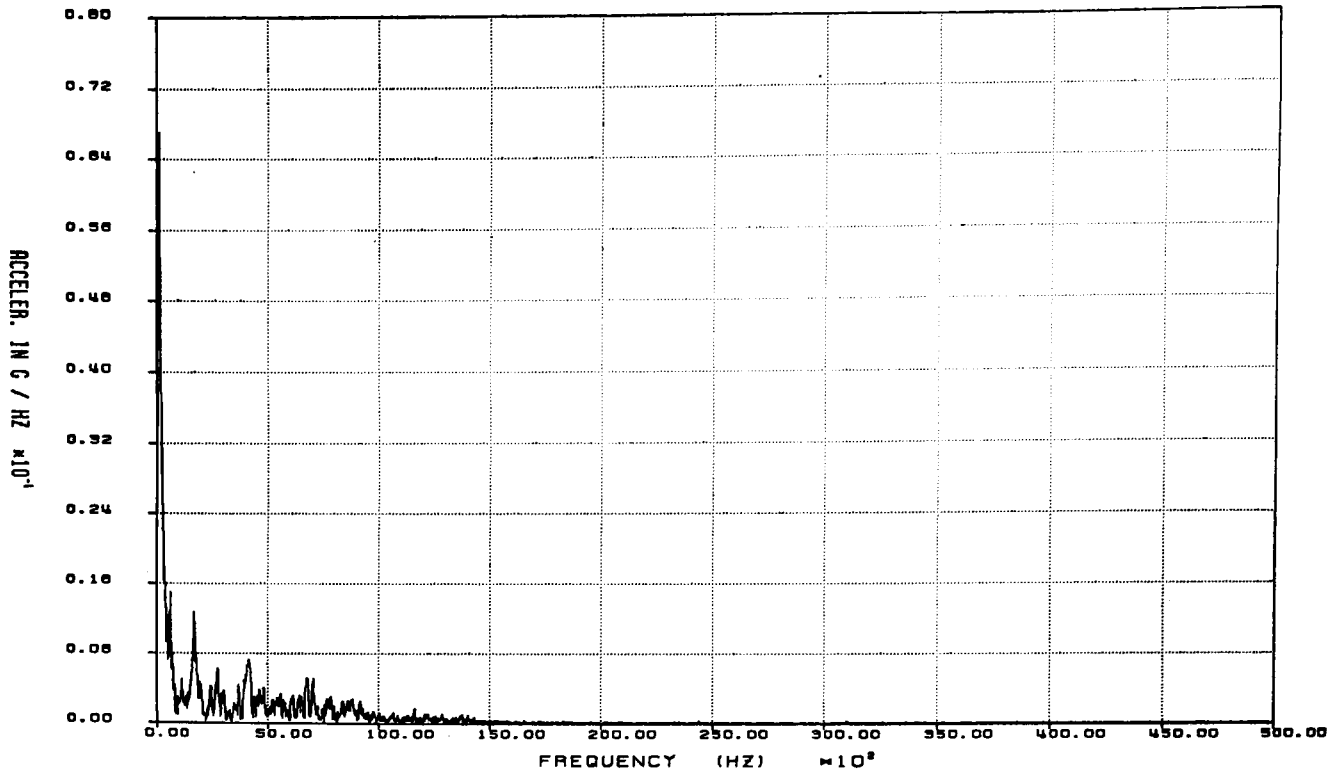


Figure F2-13. Fast Fourier Transform of Raw Data From Gage AZ7 for 40-in. Closure End Puncture Test: 0-50 kHz

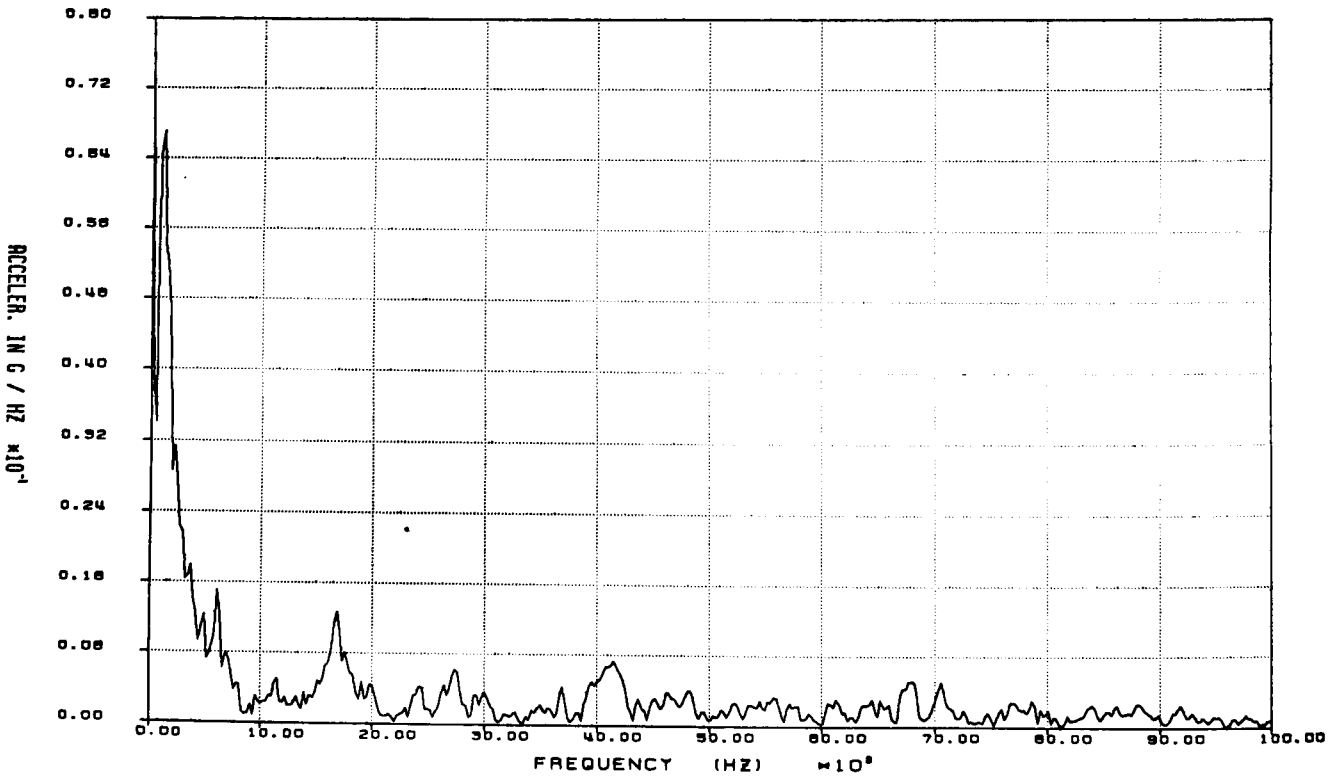


Figure F2-14. Fast Fourier Transform of Raw Data From Gage AZ7 for 40-in. Closure End Puncture Test: 0-10 kHz

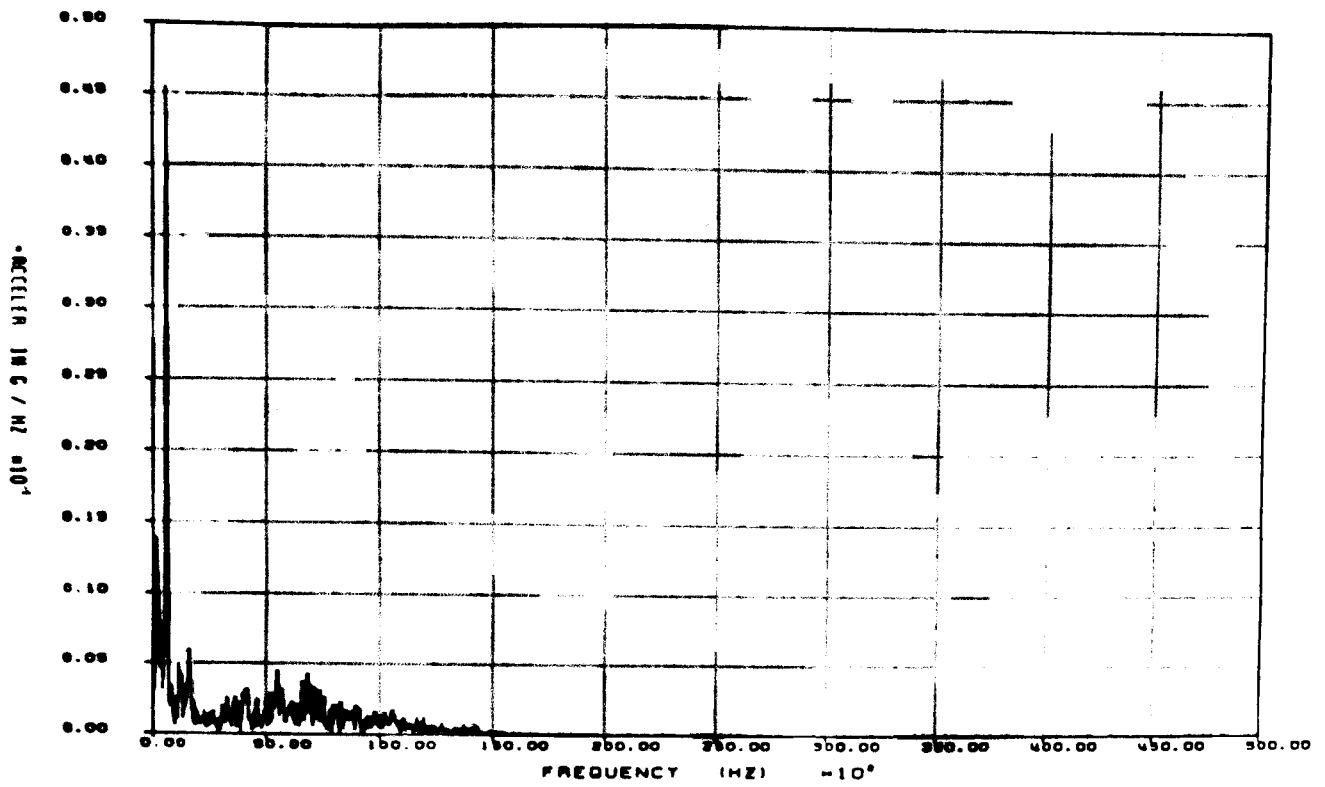


Figure F2-15. Fast Fourier Transform of Raw Data From Gage AX8 for 40-in. Closure End Puncture Test: 0-50 kHz

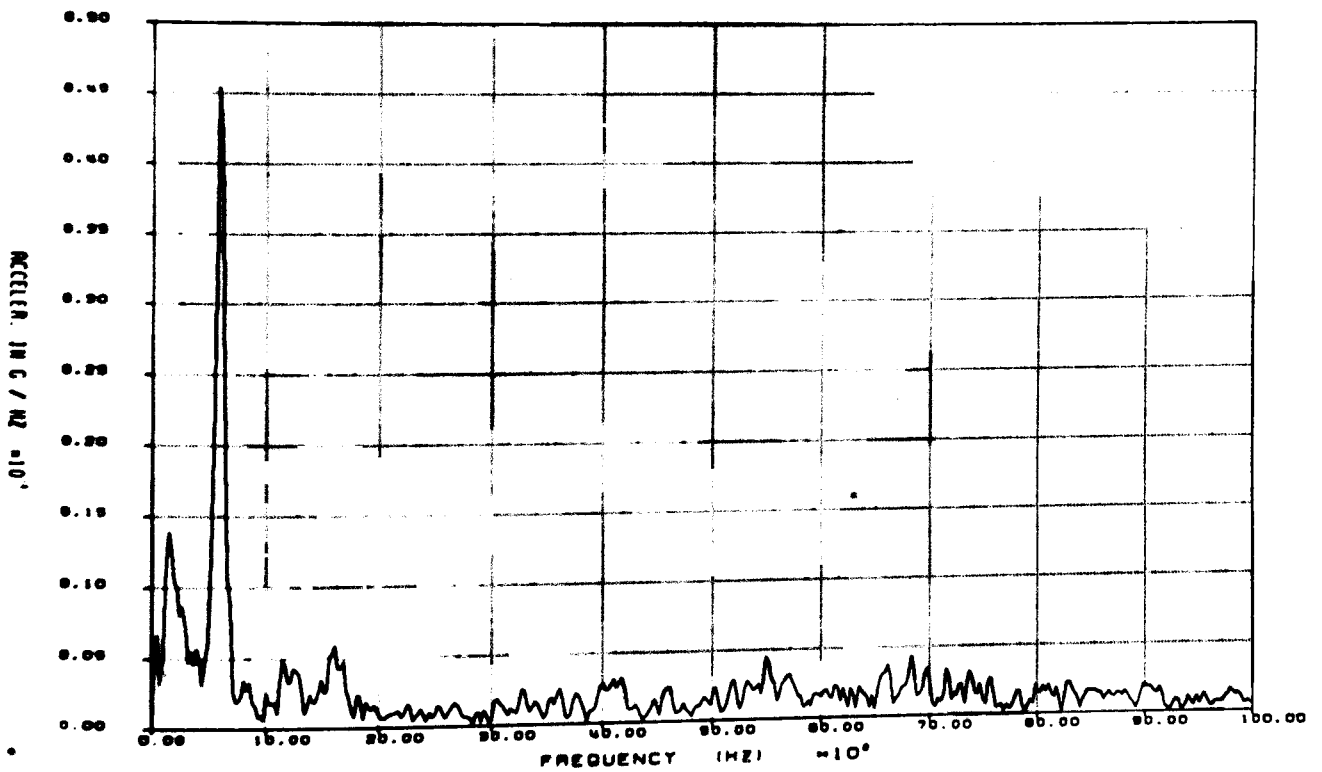


Figure F2-16. Fast Fourier Transform of Raw Data From Gage AX8 for 40-in. Closure End Puncture Test: 0-10 kHz

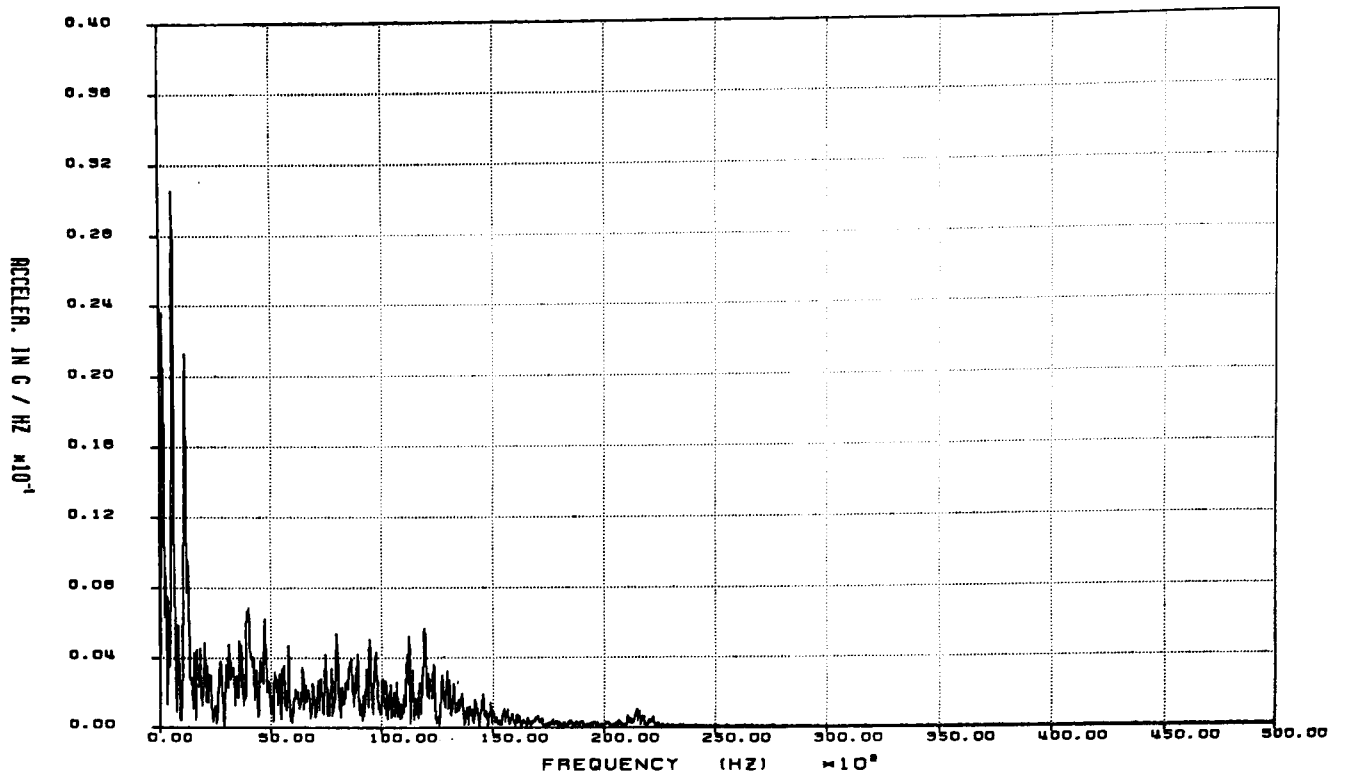


Figure F2-17. Fast Fourier Transform of Raw Data From Gage AX9 for 40-in. Closure End Puncture Test: 0-50 kHz

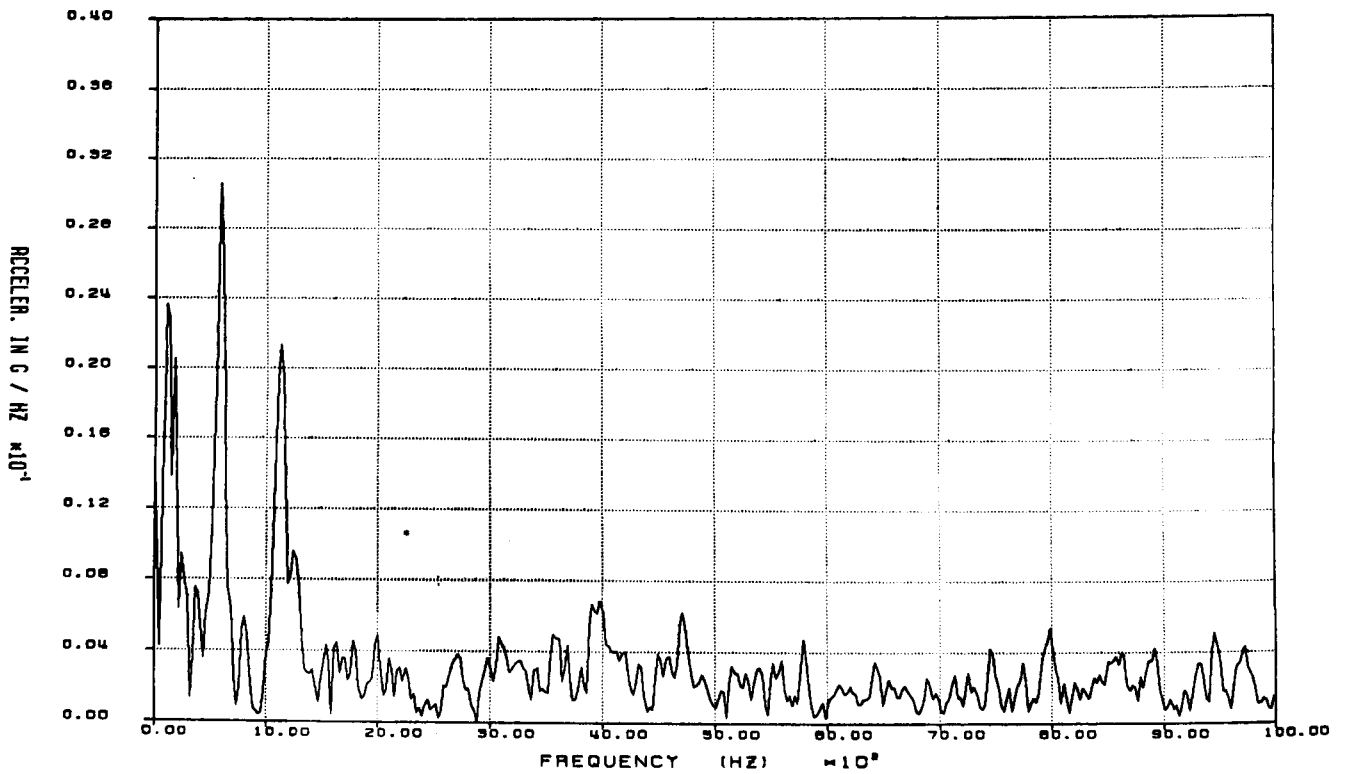


Figure F2-18. Fast Fourier Transform of Raw Data From Gage AX9 for 40-in. Closure End Puncture Test: 0-10 kHz

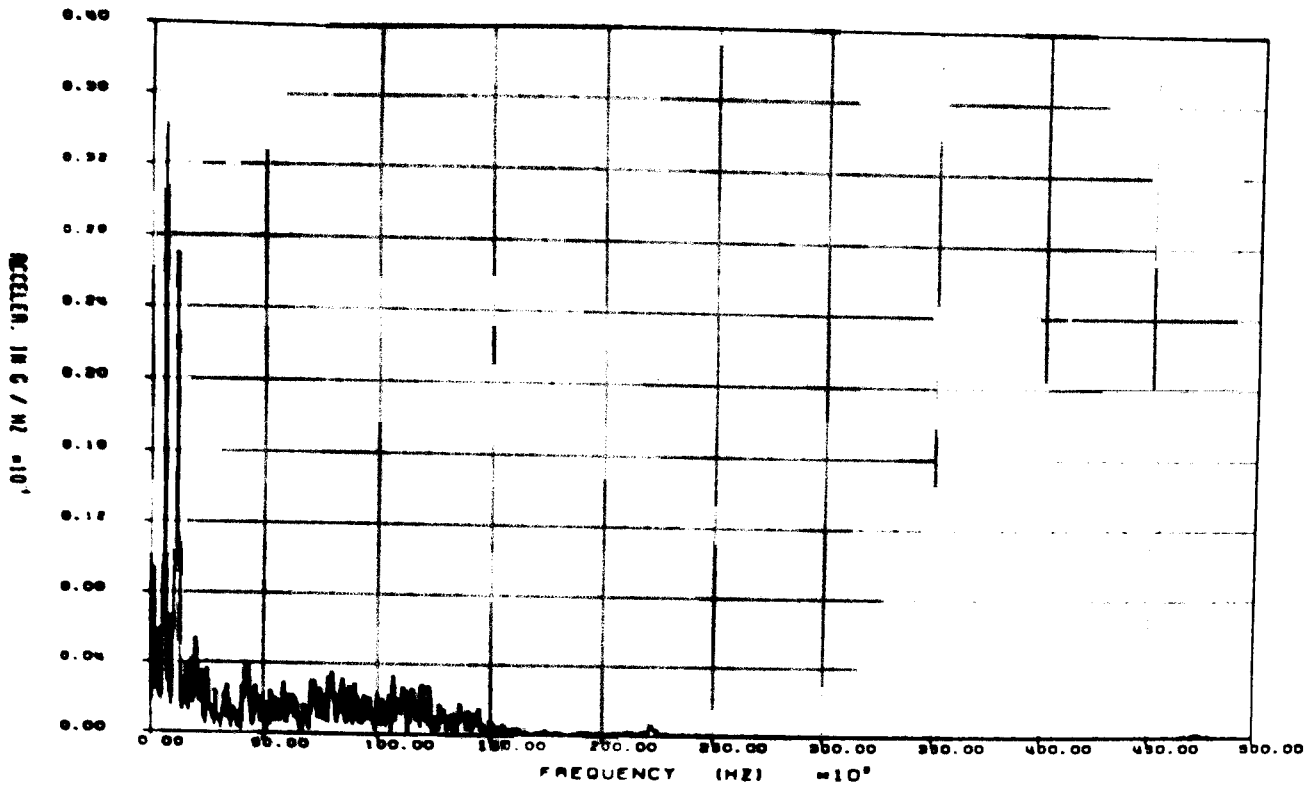


Figure F2-19. Fast Fourier Transform of Raw Data From Gage AX10 for 40-in. Closure End Puncture Test: 0-50 kHz

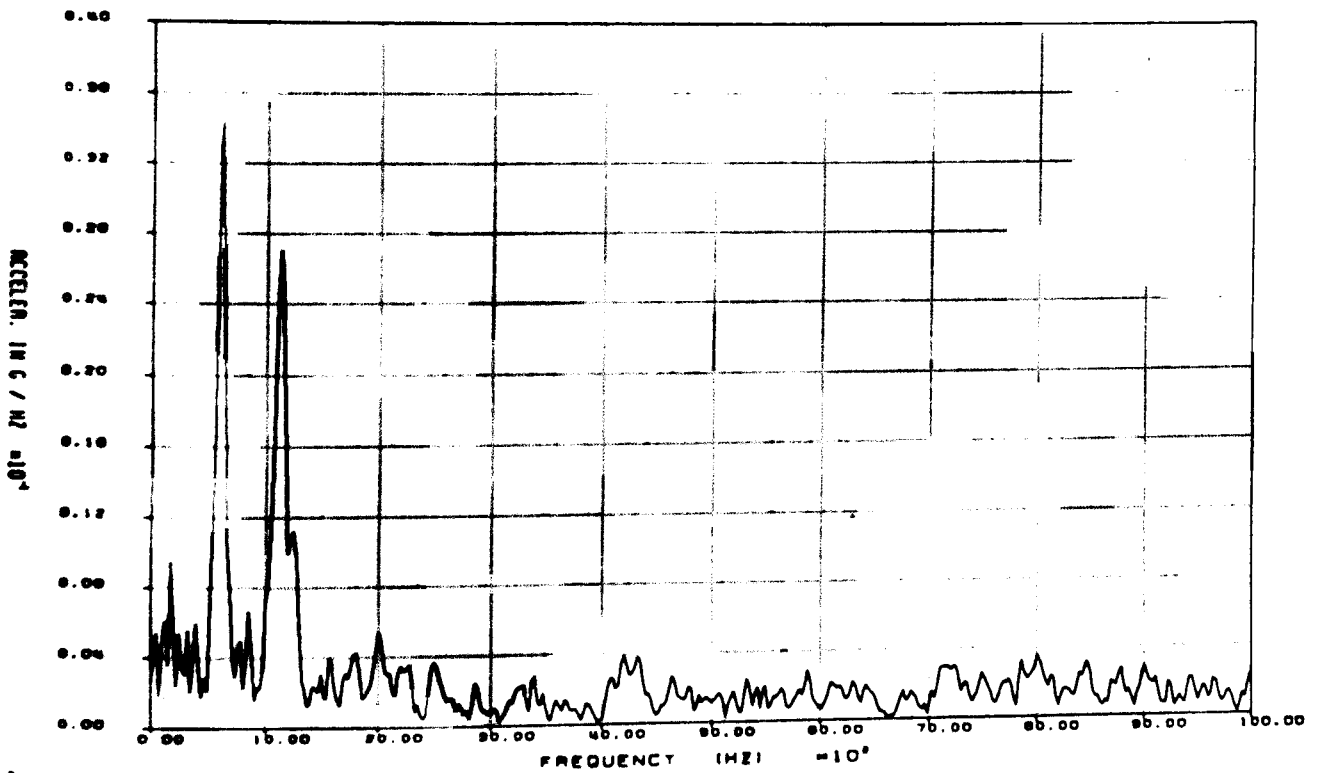


Figure F2-20. Fast Fourier Transform of Raw Data From Gage AX10 for 40-in. Closure End Puncture Test: 0-10 kHz

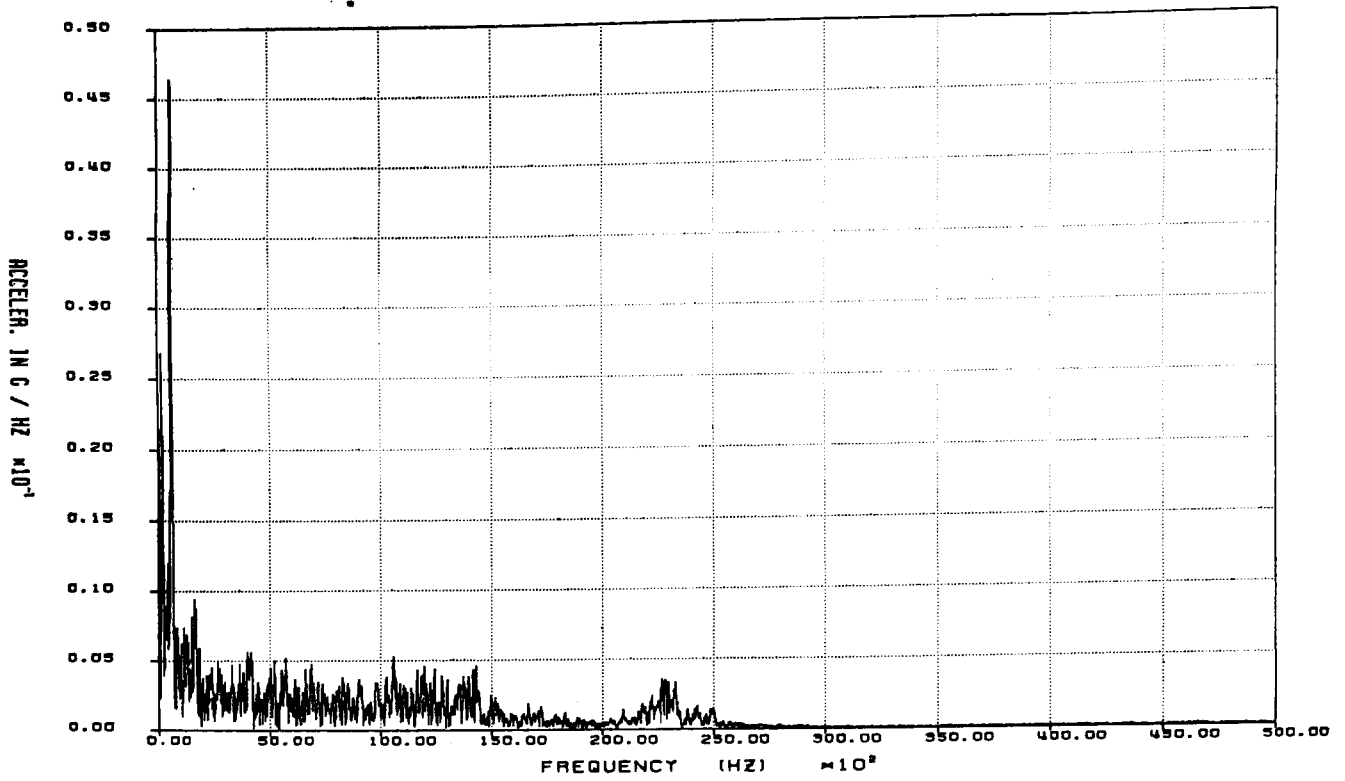


Figure F2-21. Fast Fourier Transform of Raw Data From Gage AX11 for 40-in. Closure End Puncture Test: 0-50 kHz

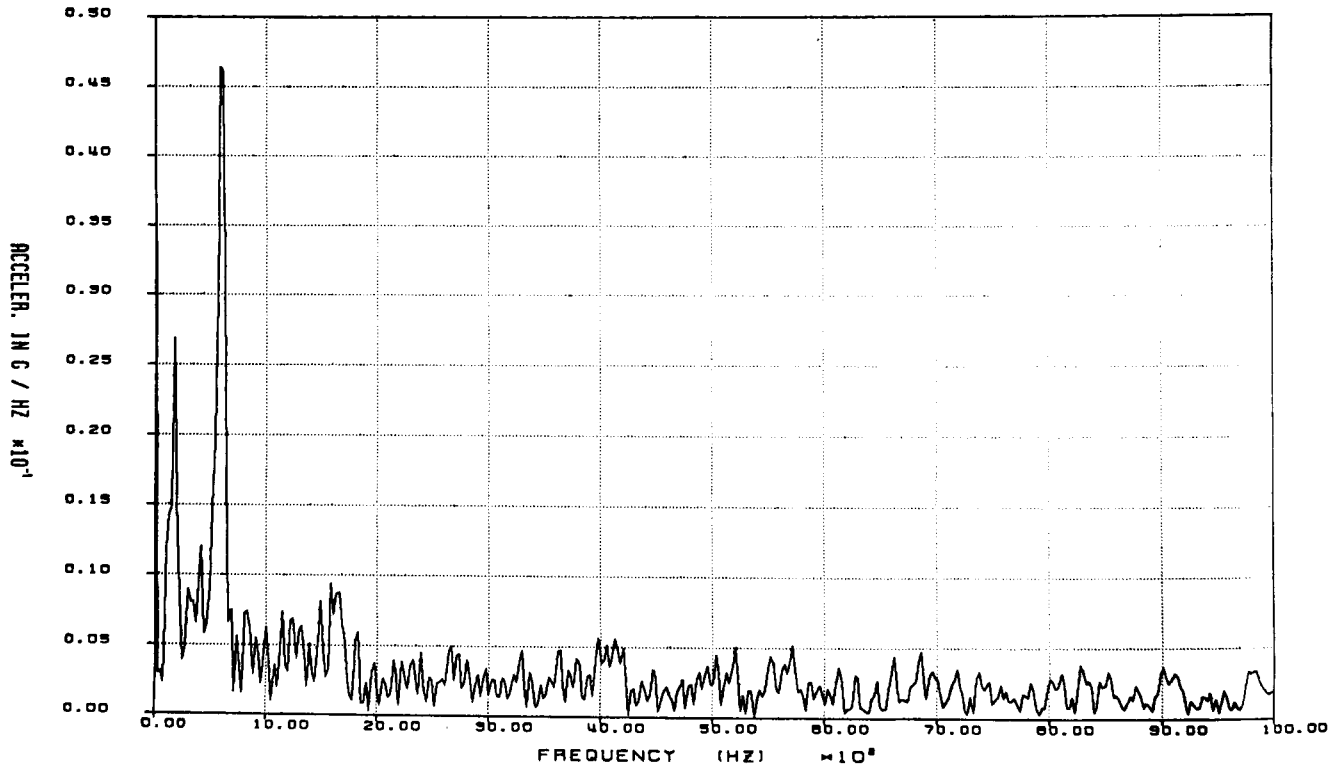


Figure F2-22. Fast Fourier Transform of Raw Data From Gage AX11 for 40-in. Closure End Puncture Test: 0-10 kHz

